INDIAN AGRICULTURAL
RESEARCH INSTITUTE, NEW DELHI

I. A. R. I. 6.
MGIPC—S4—10 AR—21-6-49—1,000.

PROCEEDINGS

OF THE

ROYAL SOCIETY OF LONDON

SERIES A. MATHEMATICAL AND PHYSICAL SCIENCES

VOL 174

LONDON
Printed and published for the Royal Society
By the Cambridge University Press
Bentley House, N.W.1

8 March 1940

PRINTED IN GREAT BRITAIN BY
WALTER LEWIS, M.A.
AT THE CAMBRIDGE UNIVERSITY PRESS

CONTENTS

SERIES A VOL 174

No. A 956. 12 January 1940

PAGE

The thermal capacity of pure iron. By J. H. Awberry and E. Griffiths, F.R.S. 1

A new derivation of the quadratic equation for the masses of the proton and electron. By Sir Arthur Eddington, F.R.S. 16

The masses of the neutron and mesotron. By Sir Arthur Eddington, F.R.S. 41

Kinetics of the thermal decomposition of fully deuterated diethyl ether. By J. G. Davoud and C. N. Hinshelwood 50

The lamellar structure of potash-soda felspars. By S. H. Chao and W. H. Taylor 57

The scattering of mesotrons in metal plates. By J. G. Wilson. (Plate 1) 73

The photodisintegration of the deuteron in the meson theory. By H. Fröhlich, W. Heitler and B. Kahn 85

Critical and co-operative phenomena. V. Specific heats of solids and liquids. By A. F. Devonshire 102

The emission spectrum of hydrocarbon flames. By E. C. W. Smith. (Plates 2, 3) 110

On the production of radium E and polonium by deuteron bombardment of bismuth. By D. G. Hurst, R. Latham and W. B. Lewis . . . 126

The torsional flexibility of aliphatic chain molecules. By A. Müller . 137

No. A 957. 1 February 1940

Wave form, energy and reflexion by the ionosphere, of atmospherics. By T. H. Laby, F.R.S., J. J. McNeill, F. G. Nicholls and A. F. B. Nickson. (Plates 4, 5) 145

Determinations of the Rydberg constants, e/m, and the fine structures of H_α and D_α by means of a reflexion echelon. By J. W. Drinkwater, Sir Owen Richardson, F.R.S., and W. E. Williams. (Plates 6, 7) . 164

Statistical thermodynamics of super-lattices. By R. H. Fowler, F.R.S., and E. A. Guggenheim 189

PAGE

The absorption spectra of ethylene, deutero-ethylene and some alkyl-substituted ethylenes in the vacuum ultra-violet. By W. C. Price and W. T. Tutte. (Plates 8, 9) 207

The absorption spectra of conjugated dienes in the vacuum ultra-violet (1). By W. C. Price and A. D. Walsh. (Plates 10, 11) . . . 220

Investigations of infra-red spectra (2·5–7·5μ). Absorption of water. By *J. J. Fox and A. E. Martin* 234

The specific heat of superconducting mercury, indium and thallium. By A. D. Misener 262

The molecular spectrum of iodine excited by fluorescence (in the presence of nitrogen) and by active nitrogen. By A. Elliott. (Plates 12, 13) . 273

No. A 958. 21 February 1940

Adsorption of lauryl sulphonic acid in the surface of its aqueous solution, and the Gibbs theorem. By J. W. McBain, F.R.S., and L. A. Wood 286

The association of meteorological changes with variations of ionization in the F_2 region of the ionosphere. By J. Bannon, A. J. Higgs, D. F. Martyn and G. H. Munro. (Plate 14) 298

Behaviour of the crystalline structure of brass under slow and rapid cyclic stresses. By W. A. Wood *and* P. L. Thorpe. (Plates 15, 16) . . 310

The equilibrium of grains on the bed of a stream. By C. M. White . 322

The neutrons from the disintegration of fluorine by deuterons. By T. W. Bonner. (Plate 17) 339

The transfer of excitation energy from uranium ions in solution. By A. H. Carter and J. Weiss 351

Rotational analysis of the first negative band spectrum of oxygen. II. By T. E. Nevin 371

The combustion of aromatic and alicyclic hydrocarbons. III. Ignition and cool-flame characteristics. By J. H. Burgoyne, T. L. Tang and D. M. Newitt 379

The combustion of aromatic and alicyclic hydrocarbons. IV. The kinetics of the slow combustion of benzene and its mono-alkyl derivatives at low temperatures. By J. H. Burgoyne 394

The thermal decomposition of nitrogen iodide. By F. R. Meldrum . . 410

The heat of formation of nitrogen iodide. By F. R. Meldrum . . 424

No. A 959. 8 March 1940

PAGE
On the natural frequencies of vibrating systems. By R. V. Southwell, F.R.S. 433
The lattice spacings of the primary solid solutions of silver, cadmium and indium in magnesium. By G. V. Raynor. 457
The equilibrium and lattice-spacing relations in the system magnesium-cadmium. By W. Hume-Rothery, F.R.S., and G. V. Raynor . . 471
The dehydration of crystals of chrome alum. By J. A. Cooper and W. E. Garner, F.R.S. (Plate 18) 487
The repulsive forces between isotopic molecules. By R. P. Bell . . 504
On the statistical method in nuclear theory. By K. Fuchs . . . 509
Calculation of nuclear energies and stability by the statistical method. By B. Spain 523
Some measurements of γ-ray energies. By S. C. Curran, P. I. Dee and J. E. Strothers. 546
Reciprocity failure of photographic materials at short exposure times. By W. F. Berg 559
Index 569

The thermal capacity of pure iron

By J. H. Awbery, B.A., B.Sc. and Ezer Griffiths, D.Sc., F.R.S.
Physics Department, The National Physical Laboratory, Teddington, Middlesex

(*Received* 25 *August* 1939)

INTRODUCTION

Although the heat capacity of iron at different temperatures has been the subject of a number of investigations in the past, it is only recently that iron of purity greater than 99·9 % has been available. Furthermore, in most previous determinations the property actually measured has been the total heat over a relatively large temperature range. Specific heats deduced from such measurements are liable to appreciable error, since if the total heat curve is smoothed, small fluctuations in the specific heat will be concealed, whereas if the actual observations are retained without smoothing, fluctuations which have no physical existence may appear in the result. Thus, suppose that the total heat is measured from 50 to 145 and from 50 to 155° C, the former being in error by 1 part in 1000 in excess and the latter the same amount in defect, the error in the specific heat over the range 145–155° C will be almost 2 %. Evidently a real variation of 1 or 2 % would be liable to pass unnoticed if any smoothing is undertaken, and conversely, fluctuations of this order may be introduced spuriously if the observations are used without smoothing. In general, calorimetry from high temperatures cannot be carried out to an accuracy of 1 part in 1000, and in any case, even this accuracy is insufficient at temperatures of the order of 1000° C.

Iron of high purity having been prepared at the Laboratory, it was decided to determine the specific heat by an electrical method in which the thermal capacity is measured over ranges of 5° C or less. It is found in the present work that the specific heat rises fairly regularly from a value of 0·113 cal./g. at 50° C to the "magnetic point", which occupies a range of more than 100° C, with a sharp peak at 755° C, where the specific heat is 0·28 cal./g. The abrupt discontinuities which have been reported by some authors (see for example, Naeser (1935) who gives details of the earlier work) at temperatures below 450° C were not found. There is, however, a broad band centred about 200° C in which the specific heat rises to a maximum of about 2 % higher than it would do if the variation with temperature were linear.

The α-γ transformation occupies a total temperature range of about 10° C, with the main absorption of heat at 903–908° C. The most striking point is that it is found to be double; at 903° C, the specific heat is infinite, since heat can be added without any temperature rise occurring, and after the specific heat has fallen to about 0·37 cal./g. at 907° C, it rises again to about 0·45, before falling to the value 0·13–0·14 for γ iron.

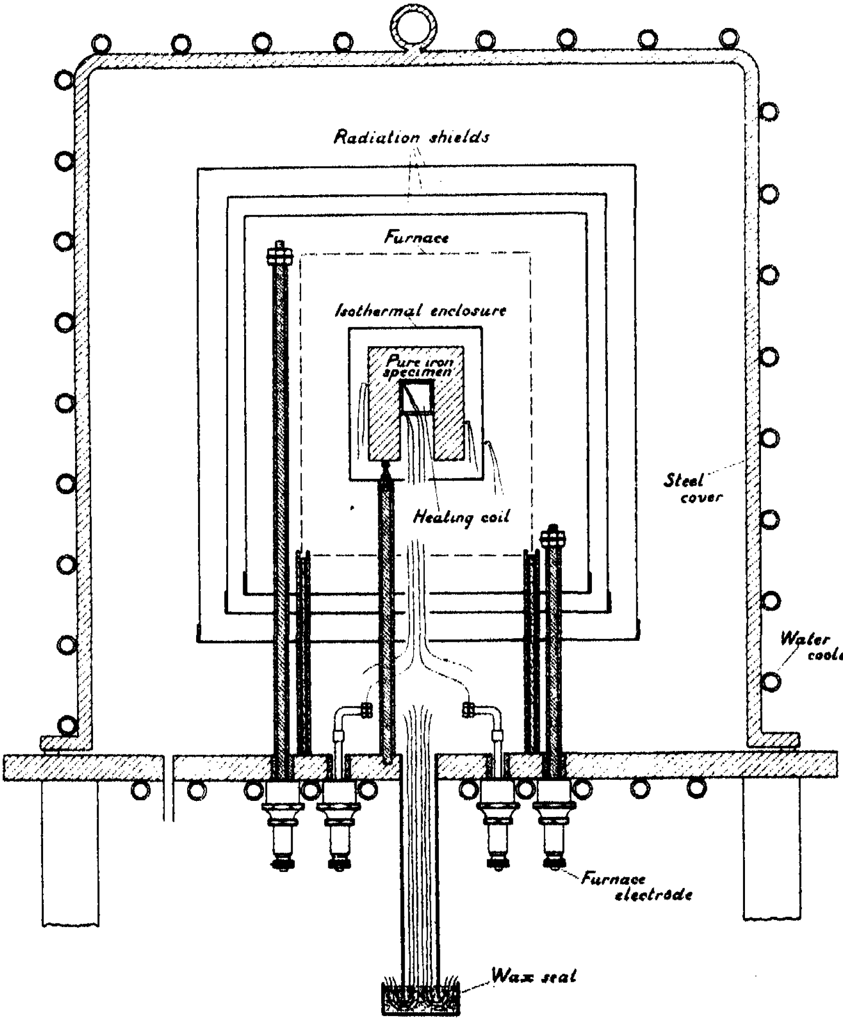

FIGURE 1. Apparatus assembly.

METHOD OF MEASUREMENT

The specific heat was determined on a cylindrical specimen weighing about 1200 g. prepared in the Metallurgy Department of the Laboratory by Dr F. Adcock. The purity was higher than that of the 99·99 % iron of which an analysis is given in the N.P.L. pamphlet *Physical constants of pure metals* (1936).*

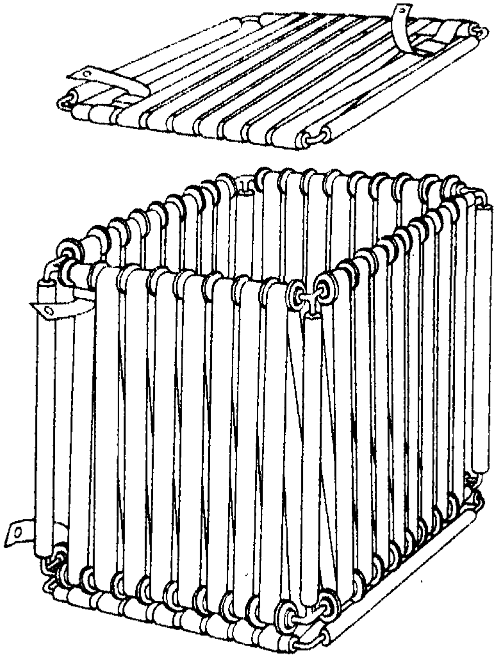

FIGURE 2. Furnace of small thermal inertia.

The specimen was drilled out for the reception of a heater of nichrome wire wound on a steatite former, as shown in figure 1. The resistance of the heater was approximately 80 Ω, and the lower part of the hole into which it was inserted was plugged with asbestos wool. The specimen was surrounded by a light metal jacket heated by radiation from a furnace of Kanthal strip built around it (figure 2). By means of two thermocouples, one attached to the surface of the specimen and the other to the jacket and connected to a galvanometer of special design, it was possible to have as scale reading the difference of temperature between the specimen and jacket. In practice, the current in the furnace was continuously adjusted by hand so that the jacket and specimen were always at the same temperature, and consequently there was no net loss of heat from the specimen throughout the experiment. The specific heat was thus obtained directly by measurement of the energy supplied by means of the internal heater and of the temperature rise of the specimen, as given by base-metal thermocouples plugged into the surface.

---

* See also Adcock (1940).

It has been found in preliminary work that at high temperatures it was essential to insulate the thermocouples from each other in order to avoid errors due to parasitic currents, and a galvanometer was therefore used having two windings insulated from each other but so arranged as to have the same magnetic moment for the same current. The couples on the specimen and jacket were connected to the two coils of the galvanometer so as to be in opposition to each other. With such an arrangement, there is no natural "zero" when the two junctions of the thermocouple are at the same temperature, and further, the balance of the two coils is not quite perfect. The "zero" position was therefore determined at the commencement of a run and also half-way through by finding the condition under which there was no change of temperature of the specimen when no heat was being generated in the internal heater, although the specimen and the jacket were hotter than their surroundings. At the end of an experiment, after switching off the current in the internal heater, the galvanometer spot was maintained on this "zero" for some time, and the temperature drift of the specimen measured. Owing to the imperfect match of the coils of the galvanometer, and to unavoidable slight differences in the e.m.f. of different thermocouples, this drift was not usually negligible. A correction was applied to all the results on the basis that the drift had grown uniformly throughout the experiment, and that at any time when the drift was a fall of n degrees per second, if the observed rise was $N°$ in t sec., the corrected rise was $(N+nt)$ degrees in the same time.

In order to reduce heat loss and avoid thermal lag in the response of the enclosure to the adjustment of furnace current, radiation shields of stainless steel were used outside the furnace, but without any other insulation. The whole apparatus was enclosed in a large steel bell-jar, which was cooled by water flowing in a pipe spot-welded to it as shown in figure 1. The bell-jar stood on a massive steel base plate, and the whole apparatus was evacuated to a pressure of about 0·1 mm., the joint between the bell-jar and base plate being made with a rubber ring and sealed with de Khotinsky cement. The thermocouple wires were brought out through a tube through the base plate, sealed with wax. The electrical connexions to the furnace and to the internal heating coil were made through six sparking plugs with heavy copper electrodes, screwed into the base plate. The specimen was supported on rods of high-speed steel, capped with steatite to prevent heat loss.

When the current in the internal heater is first switched on, the temperature of the specimen does not appear to rise instantaneously, since a temperature gradient has to be established in the specimen. Similarly, after switching off the current, there is a further rise before the temperature becomes steady. The net heat input of course corresponds to the total temperature rise, and it would be possible to explore the curve of specific heat against temperature by a series of such isolated experiments, each covering a range of say 5° C, though it would be difficult in the neighbourhood of a transformation point. It is preferable, however, to put the internal heater in action continuously, and to observe the time taken for the specimen to rise through determined temperature ranges. By this procedure, the temperature gradient in the specimen causes no error in the temperature rise, unless the gradient itself is changing, though the temperature measured at the surface is slightly below the mean temperature of the volume of the specimen. A simple calculation shows that it is unlikely to be in error by as much as 3° C under the conditions prevailing throughout the greater part of the temperature range. The change in specific heat for a change of 3° C in mean temperature is negligible. Near the magnetic and α-γ points, where the specific heat increases greatly, the specimen rises much more slowly in temperature, and the gradient of temperature between the inside and outside is greatly reduced, so that again there is no serious error introduced by it. In practice, the specimen was heated at two different rates (the heat input being 50 and 35 W in the two cases) and the time was observed for each successive rise of 200 or 400 μV (about 5 or 10° C) in the thermocouple reading, by stopping one stop-watch and starting another as the galvanometer spot crossed the zero line. The potentiometer was then set for the next temperature, and the second stop-watch stopped as the spot again reached the zero line, the first watch being started at the same time, to read the time for the next period. When the transformation temperatures were approached, the temperature intervals were reduced sometimes to as little as $\frac{1}{2}$°, i.e. 20 μV. In this case, since three scale-divisions (occupying 5 mm.) corresponded to 1 μV, an error of one-fifth division in the position of the spot when the watch was stopped would introduce an error of $\frac{1}{3}$ %. Such an error would correspond to rather more than half a second of time.

RESULTS

A curve (figure 3) is given showing the specific heat as a function of temperature up to about 950° C, as a mean of all the experiments carried out, but it is necessarily on too small a scale to show much detail. The results over different temperature ranges are therefore discussed individually below.

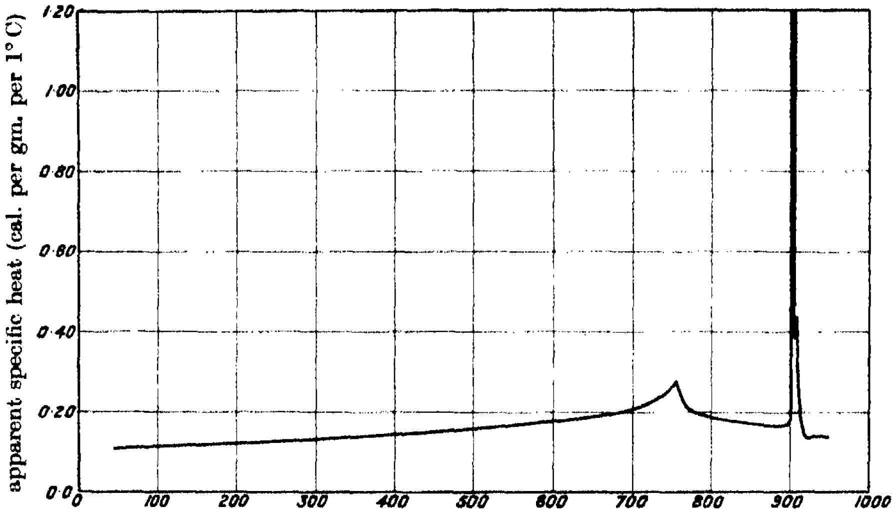

FIGURE 3. Apparent specific heat of pure iron.

(*a*) *Temperatures up to* 300° C

It is in this range that various experimenters have claimed to detect large variations, and even discontinuities, in the specific heat curve. Our own experiments do not reveal these, though, as mentioned above, they do show an increased absorption of heat in the range from about 120 to 280° C, reaching a maximum of about 1½ % at a temperature in the neighbourhood of 200° C. Most of the experiments were carried out with chromel-alumel thermocouples, which are the most suitable base-metal couples for temperatures up to 1000° C. They have, however, the defect that there is a sharp change in slope in the calibration curve at about 150° C, and it was thought desirable to verify that the local increase in specific heat was not a spurious effect introduced by slight errors in the calibration curve. Over this part of the temperature range, therefore, two sets of observations were taken using nichrome-constantan thermocouples. These gave a specific heat which was slightly lower than that obtained with the chromel-alumel couples, though the general features of the curve were confirmed. It was also found that the results were the same whether the energy input was at the rate of 50 or 35 W. Altogether, ten out of the various series of experiments covered all or part of the range up to 300° C, and a figure showing all the observations would be too confused. The mean curve is given in figure 4. It was noted that the first and last sets carried out with chromel-alumel couples agreed, showing that there had been no change in the specific heat with time or with

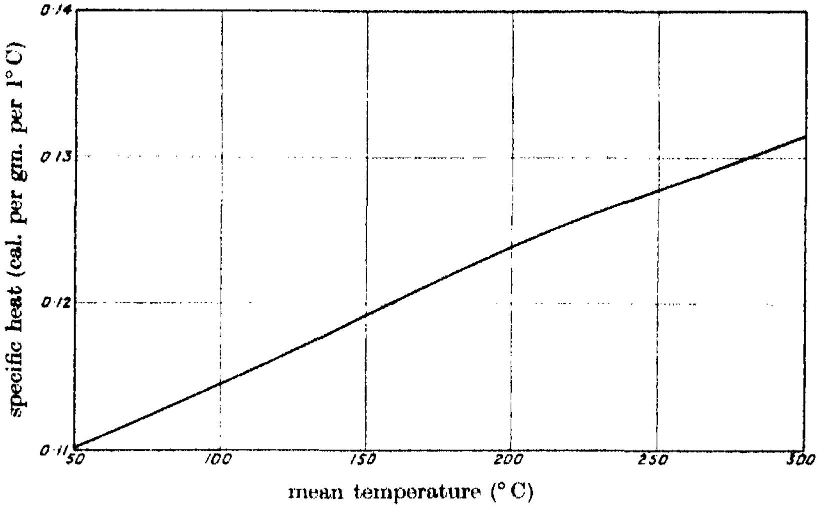

FIGURE 4. Specific heat of alpha iron (mean of 10 experiments).

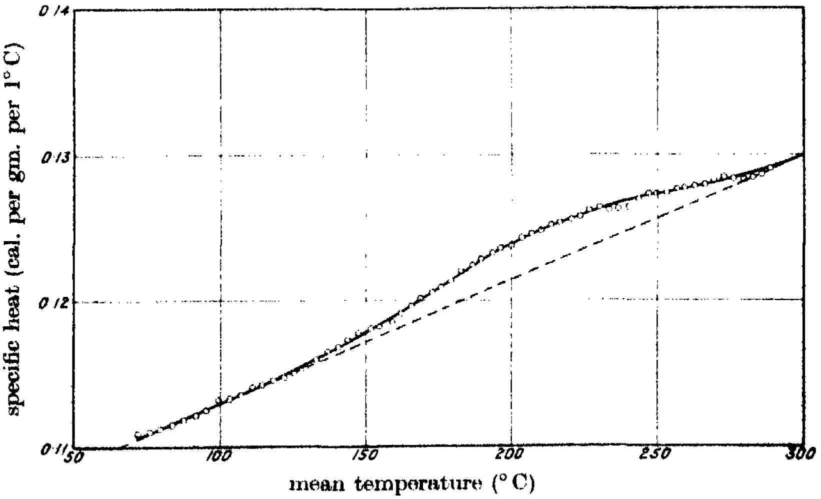

FIGURE 5. Specific heat of alpha iron (nichrome-constantan thermocouples).

the successive heatings and coolings of the specimen. In figure 5 are shown the data obtained as the mean of the two series of observations using nichrome-constantan thermoelements.

There are inherent limitations to the use of thermoelements for the measurement of small differences of temperature on account of low sensitivity and calibration difficulties. If absolute values of high accuracy were required over this range of temperature, a modification of the method would be made as the present apparatus was designed primarily for high temperature work.

(*b*) *From* 300 *to* 900° C (*the commencement of the* α-γ *transformation*)

The main feature in this region is the magnetic point, which was found to have its peak at 755° C. Its effect, however, appears to spread over a very large temperature range on each side of this peak; so much so that the limits can hardly be defined, and the question as to the heat absorption associated with the magnetic point is not susceptible of a definite answer.* The specific heat curve in this region, the mean of five sets of experiments, is given in figure 6, on which the individual observations of one set only are given, in order to avoid confusion. It was noted that, in general, the later experiments gave slightly higher values than the earlier ones in the range 400–750° C, though this was probably fortuitous since the last experiment of all gave lower values than the one which preceded it.

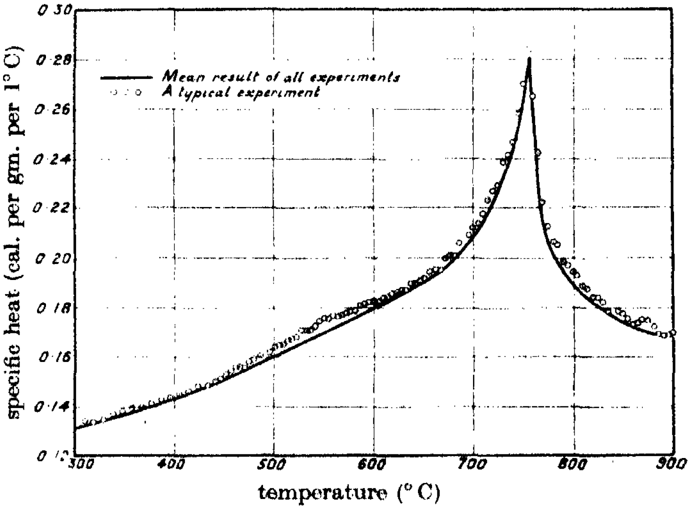

FIGURE 6. Specific heat of alpha iron (300—900° C).

---

* [*Note added* 6 *December* 1939.] Experiments on steels which have since been carried out suggest that the contribution to the specific heat which is independent of the magnetic latent heat can be separated from the total by means of Grüneisen's law, if the expansion coefficient of the same material is known.

(*c*) *The α-γ transformation*

Immediately above 900° C, the specific heat commences to rise rapidly, so that under the circumstances of these experiments, in which the heat input is constant, the temperature rises less and less rapidly, until the rise ceases altogether. In practice, it was usually found that the temperature fell slightly below its maximum, and returned to it again in a time of the order to 60 sec. The peak of the transformation was taken to be this maximum but the value observed varied by about 1° C. It is manifestly impossible to average curves which tend to infinity at different temperatures, but the best-defined curve is given in figure 7. It shows, as mentioned earlier, that after the specific heat has begun to decrease, it rises again to a minor maximum before finally falling. This effect is not a peculiarity of this particular experiment, but was found also in all the others, except in one case where no observations happened to fall between the main and the subsidiary peak; in order to show this in the same figure, the observations in the remaining experiments are also plotted, with a shift of the temperature scale so as to bring the peak to the same place in each set.

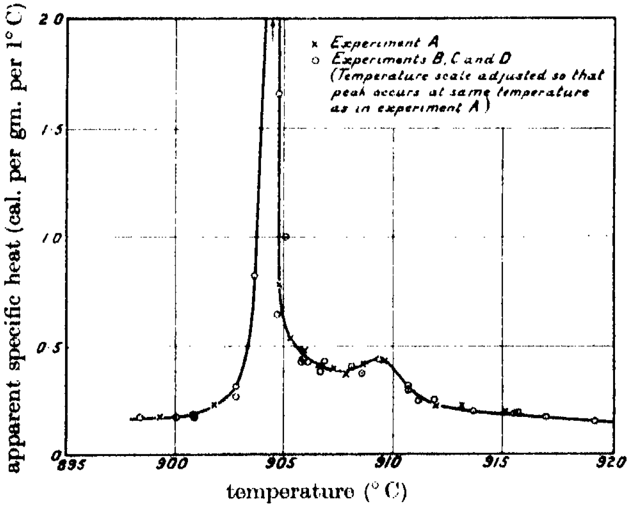

FIGURE 7. Alpha-gamma transformation in pure iron.

The precise values of the specific heat at the different temperatures within this range of 20° C are probably subject to some error owing to the annihilation and subsequent rebuilding of the temperature gradient in the specimen, but the curve must be correct in its main features.

The quantity which is of most interest is the heat absorption associated with the transformation. This has been calculated from each of the four experiments, as follows: The total time occupied by the specimen in rising from a temperature corresponding to an e.m.f. of 37,300 μV to that corresponding to 38,100 μV was taken from the observation record, and the total energy input in this time was computed. The heat necessary to raise the temperature of the specimen from the lower fixed temperature to the observed transformation point, and through a temperature interval corresponding to the natural fall of temperature (interpolated from the observed rate of drift before and after the experiment), was subtracted from this input, and a similar correction applied for the heat necessary to raise the specimen from the transformation temperature to the upper limit. For these corrections, the specific heats below and above the transformation range were extrapolated from the results of the particular experiment, though the results would not have been appreciably affected if a mean value had been used.

The results of the experiments are set out below:

Experiment	Gross heat input (cal./g.)	Correction	Heat absorption at the α-γ transformation cal./g.
A	6·91	3·22	3·69
B	7·70	3·78	3·92
C	7·47	3·59	3·88
D	6·48	2·32	4·16
		Mean	3·91

(d) From 910 *to* 950° C (γ *iron*)

The data above the α-γ transformation are shown on an open scale in figure 8.

DISCUSSION OF RESULTS

The specific heat of iron has been the subject of at least twenty researches, but of these all save a few recent ones can be disregarded, either because they were carried out on iron of low purity, or because of the uncertainty of the temperature scale used, or, most frequently, because the difficulties of deducing the specific heat from measurements of total heat over considerable ranges led to large errors. These difficulties are enormously greater in a material like iron, where the specific heat is subject to rapid changes at different temperatures, than in a material of which the specific heat rises gradually and uniformly with temperature. The whole of the literature prior to 1935 was surveyed in a book entitled *The metal iron* published in that year by Cleaves and Thompson, and earlier work calls for no further comment.

Below room temperature, the results of recent work are fairly concordant, and the values given by Austin (1932), who reviewed the literature with great care, are probably still the most reliable. They are given in table 1.

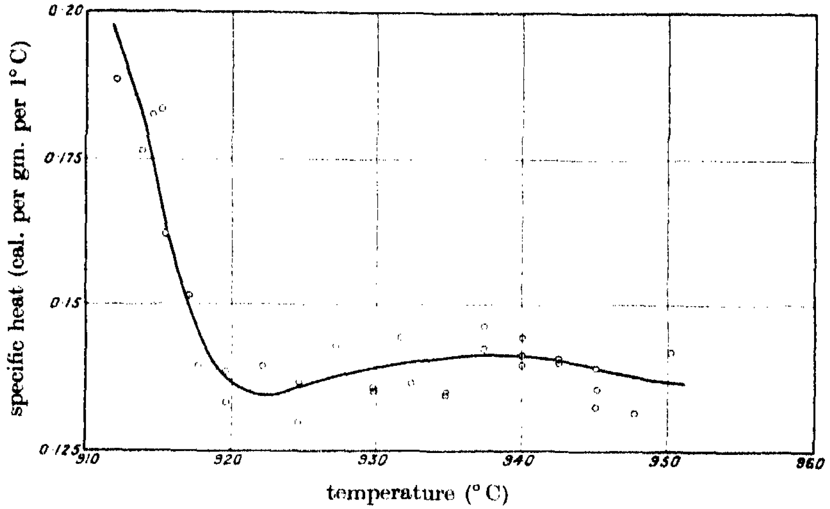

FIGURE 8. Specific heat of gamma iron.

TABLE 1. SPECIFIC HEAT OF IRON BELOW 0° C (VALUES SELECTED BY AUSTIN 1932)

Temp. ° K	Specific heat (cal./g.)
20	0·00009
30	0·003
40	0·007
50	0·013
75	0·032
100	0·051
125	0·065
150	0·077
175	0·086
200	0·092
225	0·097
250	0·101
273·1	0·104

From 0° C to the magnetic point at 750° C, the results of the more recent investigators are in fair agreement. These investigators include Oberhoffer and Grosse (1927), Wüst, Meuthen and Durrer (1918), Klinkhardt (1927), Umino (1926, 1929) and Baerlecken (1933). Of these the most interesting work is that of Klinkhardt (1927), who was the first to use a "point" method *of determining the specific heat, instead of deducing it from heat capacities* over large ranges. He heated the specimen through small temperature intervals by electron bombardment, and measured the corresponding temperature rise. His results are compared with our own in table 2 below. Three workers since 1933 have reported the results of measurements on true specific heat, viz. Mlle Lapp (1936), Baerlecken (1933) and Sykes and Evans (1938). Their results are included in table 2, as also are those of Jaeger, Rosenbohm and Zuithoff (1938), which were determined by the method of mixtures.

TABLE 2. SPECIFIC HEAT OF IRON BELOW THE MAGNETIC POINT

Temp. ° C	Klinkhardt (iron melted *in vacuo* and chemically pure) (1927)	Lapp (Heraeus iron) (1936)	Sykes (electrolytic iron) (1938)	Jaeger and colleagues (electrolytic iron) (1938)	Baerlecken (electrolytic iron) (1933)	Present authors (iron melted *in vacuo* and chemically pure)
100	0·115	0·106	0·115	0·112	0·114	0·114
200	0·128	0·124	0·126	0·123	0·126	0·124
300	0·140	0·138	0·135	0·136	—	0·132
400	0·151	0·161	0·144	0·146	0·146	0·143
500	0·163	0·176	—	0·160	0·161	0·160
600	0·188	0·194	—	0·175	0·180	0·180
700	0·230	0·222	—	0·213	0·227	0·209
760	0·320	0·230	—	0·288	0·261	0·249

The temperature of the magnetic transformation (the so-called Curie point) had been found by earlier writers as 780–785° C, and was stated to vary little with the state of purity of the iron. Klinkhardt (1927), however, using the electron bombardment method, found that the thermal effect associated with this point extends over a wide range of temperature on both sides of the maximum, and the latter occurred at 760° C. He explains this lowering as due in fact to the residual impurities, to which he says the Curie *point is very sensitive. We ourselves find the peak at 755° C, Jaeger and his* colleagues (1938) give 760° C, and Mlle Lapp (1936) locates it at 758° C. It would appear, therefore, that the thermal effect reaches its maximum at a much lower temperature than has usually been cited as the Curie point, and it is possible that, at high purity, it falls as the impurities are reduced.

From the magnetic point to the α-γ transformation

Results in the region above the magnetic transformation, at the time of the publication of Cleaves and Thompson's book (1935), were very discordant. The present position may be gauged from table 3 below, which compares the results of the same authors as were considered in table 2, with the exception of Sykes (1938), who made no measurements in this temperature range.

TABLE 3. SPECIFIC HEAT OF IRON FROM 760 TO 900° C

Temp. °C	Klinkhardt (1927)	Lapp (1936)	Jaeger and colleagues (1938)	Baerlecken (1933)	Present authors
760	0·320	0·231	0·288	0·261	0·249
780	—	0·202	0·250	0·223	0·200
800	0·209	0·203	0·213	0·219	0·189
820	—	0·189	0·199	0·207	0·181
840	—	0·176	0·192	0·203	0·176
860	—	0·168	0·188	0·201	0·172
880	—	0·163	0·185	0·200	0·169
900	0·186	0·160	0·182	—	0·190

Temperature of the transformation from α to γ iron

As stated above, we find that the specific heat commences to rise at about 900° C, becoming infinite at about 903° C and immediately falling, after which it rises again to a subsidiary maximum at 908° C. The initial rise before 903° C is probably not characteristic of iron, but an effect due to the impossibility of instantaneously annulling the temperature gradient in the specimen. It is probable, therefore, that the centre of the specimen reaches the transformation temperature, 903° C, before the outer layers, and that actually the transformation is very sharp. The shape of the curve suggests that the subsidiary maximum is less sharp, though it probably only occupies a few degrees. Klinkhardt (1927) stated that the specific heat begins to rise at 904° C, passes through a very high maximum at 911° C and then returns to the normal value. His curve, however, does not show the rise, since he has extrapolated it smoothly to the transformation temperature at 908° C. Jaeger, Rosenbohm and Zuithoff (1938) give the transformation temperature as 906° C, with no comment as to possible spreading over a range, and Mlle Lapp (1936) states that it occurred at 910° C. Her observations, however, were made at 885, 910, 913, 914·4 and 918° C and were thus clearly insufficient to locate the point accurately; the highest value which she gives for the specific heat in this range is 0·175 at 914·4° C.

Above the α-γ transformation

For the specific heat of γ iron, our own results are less reliable than at lower temperatures, since the difficulties of securing equality of temperature between the outer jacket and the specimen increased rapidly above 900° C. In figure 8 the results are shown on an open scale. Again, the specific heat of γ iron is subject to no discontinuities until the A_4 point is reached, at which α iron again became the stable form. The method of mixtures is therefore entitled to weight in this region, and in table 4 we include therefore the results of Umino (1926), who has used this method up to the melting point of iron.

TABLE 4. SPECIFIC HEAT OF γ IRON

Temp. ° C	Umino (1926)	Klinkhardt (1927)	Lapp (1936)	Jaeger (1938)	Baerlecken (1933)	Present authors
910	0·227	0·160	—	—	—	0·268
920	—	0·160	0·142	0·137	0·173	0·137
930	—	0·160	0·142	0·138	0·175	0·139
940	0·134	0·161	0·142	0·139	0·176	0·141
950	0·150	0·161	0·142	0·140	0·177	0·137
960	0·163	0·161	0·142	0·141	0·177	—
970	0·164	0·161	—	0·142	0·177	—
980	0·163	0·162	—	0·142	0·177	—
990	—	0·162	—	0·143	0·177	—
1000	—	0·162	—	0·144	0·177	—

We have to thank Dr F. Adcock, of the Metallurgy Department of the Laboratory, for supplying the specimen of very pure iron to the size and shape required for this work, and for helpful discussion. Mr A. R. Challoner gave great help at each stage of the experiments.

SUMMARY

The energy changes associated with the Curie point of iron are not concentrated closely around that point, but influence the specific heat curve over a wide range. In the range from 50° C to the Curie point, which was found to occur at 755° C, the specific heat rises fairly regularly except that there is a slight increase above the regular increment, amounting to rather less than 2 % at its maximum, over a broad band of temperature centred around 200° C.

Above the magnetic point, the specific heat falls rapidly, but the thermal effect of the magnetic transformation is still visible when the α-γ transformation sets in. At this point, iron changes from a body-centred to a face-centred lattice. It was found that the transformation is at least in part a true phase-change involving a latent heat, since energy could be added for a considerable time without any rise of temperature. The latent heat associated with the change was measured as $3{\cdot}9_1$ cal./g. It was further

found that the transformation is double; the main peak occurs at 903° C, but after the specific heat has fallen to 0·37 cal./g., it rises again to a smaller but definite peak at 908° C, before finally falling to the value for the face-centred variety, known usually as γ iron. The specific heat of the latter was found to be approximately 0·14 cal./g.

REFERENCES

Adcock, F. 1940 *Trans. Soc. Chem. Ind.* (in the press).

Austin, J. B. 1932 *Industr. Engng Chem.* **24**, 1225.

Baerlecken, H. 1933 Dissertation, Aachen.

Cleaves, H. E. and Thompson, J. G. 1935 *The metal iron.* New York: Chemical Catalog Co.

Jaeger, F. M., Rosenbohm, E. and Zuithoff, A. J. 1938 *Rec. Trav. chim. Pays-Bas,* **57**, 1313.

Klinkhardt, H. 1927 *Ann. Phys., Lpz.,* **84**, 167.

Lapp, Mlle. 1936 *Ann. Phys., Paris,* **6**, 826.

Naeser, G. 1935 *Mitt. K.-Wilh.-Inst. Eisenforsch.* **17**, 185.

National Physical Laboratory 1936 *Physical constants of pure metals,* **5**. London: H.M. Stationery Office.

Oberhoffer, P. and Grosse, W. 1927 *Stahl. u. Eisen, Düsseldorf,* **47**, 576.

Sykes, C. and Evans, H. 1938 *J. Iron Steel Inst.* **138**, 125*P*.

Umino, S. 1926 *Sci. Rep. Tôhoku Univ.* **15**, 97.

— 1929 *Sci. Rep. Tôhoku Univ.* **18**, 91.

Wüst, F., Meuthen, A. and Durrer, R. 1918 *ForschArb. IngWes.* **204**, 1.

A new derivation of the quadratic equation for the masses of the proton and electron

By Sir Arthur Eddington, F.R.S.

(*Received* 10 *October* 1939)

1. In this paper I introduce some improvements of method which will, I think, bring about a considerable simplification of most of the physical problems treated in Part II of my book, *Relativity theory of protons and electrons* (hereinafter referred to as *P. and E.*). They also facilitate the extension of the theory to other problems awaiting solution. Here I confine myself to one of the problems, namely, the derivation of the fundamental quadratic $10m^2 - 136mm_0 + m_0^2 = 0$ for the mass m of a proton or electron. The derivation in *P. and E.* is, I believe, valid, though it now appears clumsy. But a proof giving more physical insight was greatly to be desired, since a thorough understanding of the underlying meaning of this relation is the first condition for a general advance.

A general acquaintance with the relativistic theory in *P. and E.* must be presumed; but, as it happens, there is little occasion to refer to the more specialized parts of the theory.

2. In relativity theory *density* is a component T_{44} of a tensor $T_{\mu\nu}$; on the other hand, *mass* (or its equivalent *energy*) is not normally part of a tensor. If the mass of a body is defined as the integral of T_{44} over a three-dimensional volume, the result is not a component of a tensor unless the space is assumed to be flat; but to assume flat space in treating $T_{\mu\nu}$ is inconsistent with the fundamental equation $-8\pi\kappa T_{\mu\nu} = G_{\mu\nu} - \frac{1}{2}g_{\mu\nu}G$ which determines the curvature in terms of $T_{\mu\nu}$. A more significant quantity is obtained by defining the mass of a system to be that of an equivalent point-particle which would produce the same gravitational field at great distances. This is found to be equal to the integral of $T_{44} + t_{44}$, where t_{44} is the potential energy; but the expression $t_{\mu\nu}$ (the potential energy pseudo-tensor) of which t_{44} is a component is not a tensor.

This difficulty associated with integration is especially pronounced in applications to quantum theory, because "the mass of a particle" is first introduced as a density distribution over a large (nominally infinite) wave front.

Accordingly, in extending relativity theory to microscopic physics, our starting-point must be the representation of density in wave mechanics rather than the representation of mass or energy. By the general principles of wave analysis the whole density of the system is considered to be the sum of contributions from a set of elementary wave functions. By a survival of classical terminology we often describe the density associated with a particular wave function as due to a particle occupying the state which the wave function describes. This circumlocution is difficult to avoid, though it often involves using the term "particle" in a sense remote from ordinary conception. If we assign the density and other physical characteristics directly to the wave function, we have to reword the exclusion principle appropriately. The density contributed by an elementary wave function has a saturation value which cannot be exceeded; the actual contribution may be any fraction p $(0 \leqslant p \leqslant 1)$ of the saturation value. A wave function will be said to be "fully occupied" if the density has the saturation value; and p will be called the "degree of occupation" or "occupation factor".

Our point of entry into wave mechanics is therefore the *density of a fully occupied wave function* in contrast to elementary quantum theory which begins with the *mass* (or *energy*) *of a particle*.

Many of the wave functions in current quantum theory are self-normalizing; that is to say, the functions themselves define a saturated density distribution which, if collected together, amounts to the mass of the particle. Quite early in the development of quantum theory it is customary to restrict wave functions by this condition. But the condition is not made retrospective, and the most elementary wave functions are not self-normalizing. Moreover, self-normalizing wave functions, when they are used, account for only part of the energy of the system; the remainder is left to be represented by functions of the elementary type. Thus we cannot evade the problem of normalizing functions which are not self-normalizing.

The functions which cause the difficulty are the "infinite plane waves". Quantum theory assigns a mass to the particle associated with the wave, but does not indicate any particular saturation density. This gap must be filled before we can connect the relativistic description of matter by an energy tensor with the quantum description of it by masses and momenta of so-called particles; and the form of treatment which follows is largely determined by this requirement. Clearly we must find for these unbounded functions a "natural normalization volume" such that the mass of the particle divided by the volume gives the saturation density. This would be a straightforward matter were it not for *degeneracy*—a complication due to symmetrical conditions and therefore the more liable to occur the more we simplify the system under consideration. Degeneracy is treated rigorously in current quantum theory when it arises in the course of its developments;

but current theory does not seem to have found occasion to study the degeneracy brought into it at the beginning by the simplest elements with which it deals.

The work thus falls into two stages. We first develop the theory of the natural normalization volume for non-degenerate unbounded wave functions. In § 10 we begin the discussion of degeneracy.

3. We shall use a "natural system" of units of length, time and mass chosen so that

$$c = 1, \quad \kappa h^2 = 1, \tag{1}$$

where κ is the constant of gravitation. The former is a common convention which eliminates the troublesome and unnecessary distinction between mass and energy; the latter is chosen primarily to simplify the relation between mass and density, which is the problem that will occupy us. Although the particular conventions are arbitrary, the fixing of definite relations between the units of length, time and mass by two such conventions is not an arbitrary procedure; and it is rather important to understand why the retention of triply-variable units in this branch of physics would be obstructive.

The purpose of the conditions (1) is to reduce the redundant fluidity of description of a physical system occasioned by referring it to three independent standards; it is *redundant* because, in so far as fluidity of description is advantageous, physics nowadays employs a much more comprehensive transformation theory (tensor calculus, etc.) better adapted to theoretical needs. The meaning of conditions such as (1) is that we employ in our formulae the numerical ratio of a physical magnitude to another comparable physical magnitude *covered by the theory* instead of its ratio to a physical magnitude outside the theory. It is clearly necessary to make a distinction in theory between a standard defined by a theoretical description and a standard (such as the kilogram) defined by pointing at it. Reference to the latter kind of standard means that we have come to the end of coherent speech and can only gesticulate. When we ascribe the dimensions ML^2T^{-2} to energy the symbols M, L, T stand for gesticulations. We cannot sacrifice the development of physics to the curious tradition that at the end of any statement it is necessary to point three times to make clear what we mean. Normally, in relativity theory and quantum theory what we want to say is of a form which makes it only necessary to point once. We retain *one* extrinsic standard because that corresponds to the conditions postulated in the problems usually treated; for, so long as the system is supposed to be observed from outside, the "observables" contain reference to something not comprised in the theoretical description of the system.

The extrinsic standard may be taken to be length, time or mass, or indeed any physical quantity which implies reference to a standard. We shall here take it to be mass, since that is the standard most directly concerned in our problem. By the conditions (1) every physical quantity will have a dimension-index specifying the way in which it varies with the extrinsic unit of mass.

By the formula $G = 8\pi\kappa T = 8\pi\kappa\rho_0$, $\kappa\rho$ has the same dimensions as G, namely L^{-2}. (The condition $c = 1$ is understood to be already employed, so that L stands for length *or* time.) By the quantum expression for momentum $(-ih/2\pi)\,\partial/\partial x$, M/h has dimensions L^{-1}. Hence, eliminating L, $\kappa h^2\rho$ has the dimensions M^2. Then, since $\kappa h^2 = 1$, ρ has the dimensions M^2.

We shall accordingly write the density of a fully occupied wave function in the form

$$\rho = m_1 m_2 f(x, y, z, t), \tag{2}$$

where m_1, m_2 are masses, and $f(x, y, z, t)$ is a pure number.

It may be noted that in our units length has the dimensions $M^{-\frac{1}{2}}$, so that the reciprocal of a volume is a mass. The ordinary definition of density is obtained by interpreting the second mass in (2) as the reciprocal of a volume. But we shall proceed with the investigation of (2) unprejudiced by this interpretation.

4. Since all components of the energy tensor have the same dimension-index, (2) can be extended to

$$T_{\mu\nu} = m_1 m_2 f_{\mu\nu}(x, y, z, t), \tag{3}$$

where $f_{\mu\nu}$ is a purely numerical tensor function.

By the theory of the relation of space tensors and wave tensors a symmetrical tensor of the second rank $f_{\mu\nu}$ is derived from double wave vectors (*P. and E.* § 10·2); that is to say, the components of $f_{\mu\nu}$ are the appropriate matrix components of the product $\Psi_{\alpha\beta} X_{\gamma\delta}$ of two double wave vectors, or of a sum of such products. The wave tensor $\Psi_{\alpha\beta} X_{\gamma\delta}$ has other components besides those which form the energy tensor; their interpretation is treated in *P. and E.* § 11·4, where it is shown that the Riemann-Christoffel tensor is also included. Only one of the double vectors Ψ, X need be specified, the other being derivable from it by the reality conditions of the theory; this is well known in Dirac's theory which employs Hermitic reality conditions, and H. T. Corben (in an unpublished investigation) has shown that the form of reality conditions obtained in my own relativistic theory yields the same result.

We can now see the appropriateness of the *two* masses in (3). In special cases $\Psi_{\alpha\beta}$ may be a product $\psi_\alpha \phi_\beta$, and the reality conditions then show that $X_{\gamma\delta}$ will also be a product $\chi_\gamma \omega_\delta$. The complete space tensor is then the outer product of two complete space vectors $J_1 = \psi_\alpha \chi_\gamma$ and $J_2 = \phi_\beta \omega_\delta$. Thus, when the numerical tensor $f_{\mu\nu}$ is the product of two *numerical* vectors J_1, J_2, the energy tensor is the product of two *mass-like* vectors $M_1 = m_1 J_1$ and $M_2 = m_2 J_2$, which may be regarded as the momentum vectors of two particles of proper masses m_1, m_2. In this way our approach to quantum theory via the density or energy tensor begins to be connected with the usual elementary treatment which starts with masses or momentum vectors. I shall call the entity analysed in this way into two particles a *bi-particle*.

No serious difference is made when Ψ is not factorizable so long as we confine attention to the case $f_{\mu\nu}$ = constant. If Ψ is not a simple product it can be represented as the sum of products, and elementary quantum theory has provided for this by recognizing that a "particle" need not have an exact momentum vector, but may be in a number of superposed states with different momentum vectors; and similarly the bi-particle represented by a double vector need not be an exact pair of particles, but may be a superposition of exact pairs of particles. But a *function* $\Psi_{\alpha\beta}(x, y, z, t)$ cannot in general be represented as the sums of products of functions $\psi_\alpha(x, y, z, t)$, $\phi_\beta(x, y, z, t)$; and in this respect the attempt to establish a universal association of density with particles characterized by momentum vectors, exact or inexact, breaks down.

This fulfils our anticipations in § 2 where we saw that integration destroys the tensor character of $T_{\mu\nu}$, so that either mass is not rigorously the component of a vector (and accordingly the entity possessing it is not characterized by a momentum vector) or it is not exactly the integral of density. The introduction of field energy (potential energy), not localizable in individual particles, is part of the complication ensuing from this breakdown of elementary conceptions.

We shall find that the functions $f_{\mu\nu}$ required for our purposes are constant over the domain to which they apply, so that the complication will not arise. Nor does it arise if $f_{\mu\nu}$ is an algebraic wave function (*P. and E.* p. 120).

5. That two particles are concerned in an element of density is obvious from the principle of relativity. What we observe is, not the particles, but relations between the particles. An observable, such as density, can therefore only be associated with the relations between pairs of particles, which

are contained in the double wave functions specifying their combined probability distributions. But alongside the relativistic outlook we have to keep in mind the ordinary conception of density as made up of contributions of individual particles. The principle of this change of conception is that, of the two particles which furnish the contribution, m_2 is understood to be a standard comparison particle providing a reference frame for the "object-particle" m_1 to which the density is attributed. In order to connect with relativity theory the quantities (such as the masses of the proton and electron) which appear in the ordinary treatment, we must follow the conventions of the ordinary treatment where they are permissible, and we shall therefore distinguish the two masses m_1, m_2 as the masses of an object-particle and a comparison particle. The ordinary treatment goes further and treats the physical reference frame furnished by the comparison particle as a purely geometrical Galilean frame, ignoring the combined uncertainty of position and velocity dependent on m_2; so that m_2 is forgotten about except in so far as it reappears in the empirical values of the constants of nature. Naturally we cannot follow the conventions of the ordinary treatment which are unpermissible—the mistakes—so we shall take due account of the mass m_2 of the comparison particle.

We shall now examine more closely the way in which one particle furnishes a reference frame for another.

Considering the co-ordinates x_1, y_1, z_1, t_1 and x_2, y_2, z_2, t_2 of two particles, let

$$\left.\begin{array}{c} \mathrm{X} = \dfrac{m_1x_1+m_2x_2}{m_1+m_2}, \quad \mathrm{Y} = \dfrac{m_1y_1+m_2y_2}{m_1+m_2}, \quad \mathrm{Z} = \dfrac{m_1z_1+m_2z_2}{m_1+m_2}, \quad \mathrm{T} = \dfrac{m_1t_1+m_2t_2}{m_1+m_2}, \\ \xi = x_1-x_2, \quad \eta = y_1-y_2, \quad \zeta = z_1-z_2, \quad \tau = t_1-t_2. \end{array}\right\} \tag{4}$$

Then a function $\Psi_{\alpha\beta}$ of $x_1, y_1, z_1, t_1, x_2, y_2, z_2, t_2$ can also be expressed as a function $\Phi_{\alpha\beta}$ of $\mathrm{X}, \mathrm{Y}, \mathrm{Z}, \mathrm{T}, \xi, \eta, \zeta, \tau$. The formal theory of Φ is the same as the formal theory of Ψ in § 4; that is to say, we can (under the same conditions) represent the energy tensor as the product of the momentum vectors of two particles associated respectively with the co-ordinates $\mathrm{X}, \mathrm{Y}, \mathrm{Z}, \mathrm{T}$ and ξ, η, ζ, τ which we call the *external particle* and the *internal particle*. The proper masses of the internal and the external particle are well known to be

$$\mu_1 = m_1m_2/(m_1+m_2), \quad \mu_2 = m_1+m_2.$$

Hence

$$\mu_1\mu_2 = m_1m_2. \tag{5}$$

The internal and external particles are commonly said to be fictitious; but it is difficult to say in what sense one circumlocution can be more fictitious than another.

6. The internal wave function specifies the probability distribution of the *relative* co-ordinates ξ, η, ζ, τ. Since these co-ordinates express spatio-temporal relations between two ordinary physical particles, we usually regard the observable properties of a system as concentrated in its internal wave function. But in saying that the co-ordinates ξ, η, ζ of m_1 measured from a comparison particle m_2 are observable, whereas the co-ordinates x_1, y_1, z_1 measured from a geometrical origin are not, we pay attention only to the origin. An origin does not suffice to define a frame of co-ordinates. In substituting ξ, η, ζ, τ for x_1, y_1, z_1, t_1 we eliminate only the part of the unobservability of the reference frame which refers to the origin, and not the part which refers to the orientation of the axes. In particular the orientation of the time-axis which determines the velocity of the frame is not replaced by anything observable. Now in practice in studying internal wave functions, e.g. those of a hydrogen atom, we choose a frame such that the momentum of the system as a whole is zero; that is to say, the time-axis is chosen to coincide with the external momentum vector. When therefore we ascribe an observable energy to an internal wave function, our reference frame is (so far as four-dimensional orientation is concerned) not a Galilean frame but the physical frame defined by the momentum vector of the external particle. Relative to a Galilean frame the physical frame has the same uncertainty of velocity as the external particle.

Just as the position vector of the particle m_2 provides a physical origin from which positions of the object-particle m_1 can be measured, so the momentum vector of the external particle μ_2 provides a physical time-axis or standard of rest from which the momenta of the internal particle μ_1 can be measured. Properly the resulting momentum should be considered to belong equally to the internal and external particles; but the same kind of convention which leads us to assign the observable co-ordinates to m_1, treating m_2 as a comparison particle, leads us to assign the observable momenta to μ_1 treating μ_2 as a comparison particle.

Since we are here concerned with momentum vectors, we must adopt the resolution into external and internal particles which provides for the reference of one momentum vector to a standard of rest provided by the other. That we cannot provide simultaneously for the reference of the position of one particle to an origin provided by the other is intelligible; because, when the momentum vectors are exact, the positions are entirely uncertain and there is nothing more to be said about them.

7. A certain conflict of conception must be noticed. We have just seen that the object-particles to which the observed mechanical characteristics are transferred are internal particles, the external particles constituting the physical reference frame. This gives us the ordinary picture of matter as a collection of particles with mass and momentum. But in the ordinary picture these are *genuine* particles—protons and electrons—whereas internal particles are generally labelled *fictitious*. This conflict merely emphasizes that the terms "genuine" and "fictitious" do not mean anything in particular as applied to particles in quantum theory. What we have shown is that in the present approach, via the energy tensor, the elementary mass-bearing particles appear as internal particles. Elementary quantum theory starts with these as its ordinary particles; so that the internal particles occurring in it (e.g. the particle associated with the internal wave function of a hydrogen atom) are, as it were, doubly internal.

In transferring the mechanical characteristics of matter from the relations between particles to the particles themselves we necessarily modify the concept of a particle, since we attribute to the particle characteristics which, according to the primary concept, it could not possibly possess. We shall call this modified concept the *secondary concept*, and the corresponding particles *secondary particles*.

We cannot simultaneously transfer the geometrical characteristics of the relations between particles to individual particles, since that would involve converting m_1, m_2 instead of μ_1, μ_2 into secondary particles. It is this incoherency which makes the secondary particles an unsuitable starting-point for theory, and drives us back to the primary particles for enlightenment.

To embody the conclusions of § 6 we should rewrite (3) as

$$T_{\mu\nu} = \mu_1 \mu_2 f_{\mu\nu}(\mathrm{X}, \mathrm{Y}, \mathrm{Z}, \mathrm{T}). \tag{6}$$

By (5), $f_{\mu\nu}$ is not altered, but it is now made clear that its arguments are those of the comparison (external) particle μ_2. The object-particle μ_1, abstracted from its comparison particle, ***has no position in space or time.*** Its co-ordinates ξ, η, ζ, τ do not associate it with one region of space-time rather than another. What they signify as applied to a particle is difficult to describe, since we have transferred to a particle properties which cannot be pictured without invoking two particles, but we may perhaps call it a ***polarization***. The distribution over ξ, η, ζ, τ may be called the ***internality*** of the object-particle. It is only connected with the energy tensor as an integrated whole.* If the internal wave function is self-normalizing, its

---

* Including integration over τ—an important point, but not required in the present discussion.

"density" is integrated into a mass; then, by associating the object-particle with its comparison particle, the mass is distributed along with the comparison particle over the co-ordinates X, Y, Z, T in space-time. For infinite wave functions a natural normalization volume must exist in both sets of co-ordinates; otherwise there is no systematic way of collecting density from one set and distributing it over the other set, and the link with the energy tensor is broken.

The whole energy tensor of a piece of matter is made up of a number of contributions such as we have been analysing. We shall speak of the comparison particles collectively as the *comparison fluid* (*P. and E.* § 11·1) and the object-particles as the *object-system*. Current theory concerns itself solely with the object-system, the comparison fluid being represented partly in the empirical constants and partly by the mistakes which become prominent when it attempts to deal with energies of the order of magnitude of the mass of a comparison particle ($136mc^2$). We are concerned especially with two of the empirical constants (the masses of the proton and electron) which are no longer empirical when the comparison fluid is studied as part of the system.

8. Comparison particles and object-particles play an unsymmetrical part in the description of phenomena. We shall now formulate this difference mathematically. Consider the momentum vectors $\mu_1 J_1$, $\mu_2 J_2$ of an internal and external particle. When the latter is adopted as comparison particle, so that its momentum vector defines the time-axis, J_2 automatically becomes the matrix E_{45} associated with the time-direction. Thus the form of the momentum vector of a comparison particle is limited to $\mu_2 E_{45}$; whereas in the momentum vector $\mu_1 J_1$ of an object-particle (an "ordinary" particle of current theory) J_1 may be any unitary matrix.

I present here a rather cut-and-dried picture of the comparison fluid, because I have a definite problem in hand, and the requirement in this (as in a large class of problems) is that the comparison fluid shall provide a definite standard of rest from which momentum can be measured. Various modifications of the scheme of separation into an object-system and comparison fluid can be made to meet the requirements in other problems. The point that we have to notice is that, whereas an object-particle can have a multiply infinite variety of relationship to a comparison particle, a comparison particle has only one possible relationship to itself—that of identity. They have therefore different numbers of degrees of freedom in the reference frame furnished by the comparison particle. We shall find later that this difference is expressed in the statement that the phase space of an object-particle is ten-dimensional and the phase space of a comparison particle is one-dimensional.

We have seen that a different separation of comparison particles and object-particles is needed according as we require the former to furnish an origin for the measurement of position or a standard of rest for the measurement of momentum. This scarcely exhausts the possibilities; and it may well be that other types of problems will arise in which the requirement is a standard of non-rotation for the measurement of angular momentum. For this we should require "spin-comparison-particles". In a general way one would expect nuclear problems to be of this type.

9. As initially derived the comparison particles have exact momentum vectors $\mu_2 E_{45}$ and therefore complete uncertainty of position. Each particle fills all space. But the particles have no individuality (the term "particle" being an epithet associated with a fully occupied wave function), so that the analysis of the comparison fluid into individual particles follows the analysis into eigenfunctions and is changed if the system of eigenfunctions is changed. By this generalization the term "comparison particle" means "as much comparison fluid as would amount to one of the original particles if distributed in the same way". The simplest reanalysis is to divide the comparison fluid into non-overlapping volumes V, each containing one comparison particle. We shall call this *vertical section* in contrast to the original *horizontal section* into particles each extending over all space. It should be added that (except in horizontal section) the comparison particles are delineated in, not detached from, the comparison fluid; for, if detached, they would have uncertainty of momentum corresponding to their limitation of extension. This is expressed more formally by noticing that the momentum vector $\mu_2 E_{45}$ has ceased to be a true vector, since by nominating its particle as a comparison particle we have made it impossible for it to have a component in any direction other than E_{45}. Thus what we are really reanalysing is a scalar which gives no field of application for the uncertainty principle.

The functional factor in $f_{\mu\nu}$ belongs primarily to the comparison particle, its arguments X, Y, Z, T being the co-ordinates of that particle. But as the object-particle acquires position in space by its association with a comparison particle, so it acquires a distribution of position by association with a comparison particle which has that distribution of position. Thus the "delineation" of the comparison particle referred to in the preceding paragraph is also the distribution of the object-particle associated with it; and in practice it is more conveniently handled in the latter aspect. Naturally, current quantum theory before proceeding to neglect the comparison particles transfers as much as possible of their attributes to the object-system; accordingly, the functional factor is attached to the object-vector instead of to the comparison vector when the two factors of the double vector are separated. The comparison particle must retain its momentum vector (since the object-particle has one already and cannot take over another); except for this, the comparison fluid has only those qualities which exist also in the geometrical frame of space-time for which it is commonly mistaken.

The consideration of functional factors, however, takes us beyond the point at which we wish to make contact with current quantum theory. We are concerned with plane waves for which the momentum vector is constant; so there is no functional factor to be transferred. The waves are nominally infinite, but in actual application normalized so that there is one object-particle in a prescribed volume. It is important to remember that the condition is one particle in a given volume, say q^{-1}, not (as is sometimes loosely stated) q particles per unit volume; for it is an elementary principle that q particles are represented by a q-tuple wave function. The wave front is therefore divided into cells, each cell containing one particle uniformly distributed. Since the positional distribution of an object-particle is that of the comparison particle to which it belongs, this corresponds to the "vertical section" of the comparison fluid in which the comparison particles occupy non-overlapping volumes V. Thus the volume V is the natural normalization volume, and the formally infinite wave function is applicable only within the volume V.

Since vertical section seems a very artificial device, I would point out that our reason for considering it is that the formulae of elementary quantum theory (which we have to connect with our own relativistic formulae) are expressed in terms of vertical section, since it is unable to deal with overlapping particles except by multiple wave functions.

By extending the same wave function over a number of cells, we should represent a number of particles having the same characteristics. This is forbidden by the exclusion principle. The continuation can only be approximate, and the complete momentum vector for each particle must be slightly different. This difference is evidently the quantum representation of the curvature introduced into space when it is occupied by mass and momentum. The exclusion principle is in fact a quantum adaptation of the equation $G_{\mu\nu} - \frac{1}{2} g_{\mu\nu} G = -8\pi\kappa T_{\mu\nu}$. The cellular division gives a polyhedral space closely approximating to the continuously curved space contemplated in relativity theory. The so-called cosmological developments of relativistic quantum theory transform the unnatural vertical section, imposed by the limitations of elementary quantum theory, into a more nearly horizontal section associated with the eigenfunctions of spherical space. The corresponding development within quantum theory itself is the introduction of *second quantization* which enables us to treat particles overlapping in space without multiple wave functions.

When we decide the curvature of the space in which this cellular arrangement is to be constructed, we make provision for a density corresponding to the curvature. "Full occupation" normally means that the density is that for which provision has been made. We here encounter a feature of quantum theory which has no counterpart in relativity theory. Quantum theory erects a skeleton frame of eigenfunctions, leaving itself free to settle and vary afterwards the extent to which they are occupied. The framework is supposed to be there before anything is put into it. That is a survival of the classical outlook. Relativity theory admits no such flexibility; we cannot put anything into space without remodelling its curvature. This makes its problems so difficult that the exact solution, even of the problem of two bodies, has not yet been found. The more flexible method of quantum theory is, of course, an approximation—sometimes a bad approximation—but it is the beginning of a systematic method of successive approximation (the method of the "self-consistent field") so that ultimately it fulfills its purpose. When applied to a system of many particles, it avoids a vast number of individual adjustments most of which would in practice cancel out. The difference is that, if the content of the system differs from that for which provision has been made, relativity theory demands immediate readjustment of the reference frame, whereas quantum theory postpones it to a second approximation. Thus an exact comparison of the formulae of the two theories can only be based on the content for which provision has been made, i.e. for full occupation.

If our physical reference frame (the comparison fluid) is uniform, the volumes V of the comparison particles will all be equal. If the physical frame is non-uniform, the geometrical frame will be correspondingly non-uniform and represent a space of non-uniform curvature; but it will remain true that equal natural volumes correspond to equal numbers of comparison particles, for otherwise volumes which are observationally congruent according to relativity theory would not be observationally congruent according to quantum theory. The natural normalization volume V is thus a universal constant; its evaluation in terms of better known constants belongs to the cosmological branch of the theory.

10. I return now to the concept of a fully occupied wave function. This presents no difficulty when the eigenstates are discrete, but a complication

arises when they form a continuum. We have to distinguish continuity which arises from symmetry or indistinguishability (degenerate continuity) from continuity which arises as the limit of close packing (non-degenerate continuity). Broadly speaking, we can trust commonsense to deal with continuity from close packing, but continuity from symmetry is likely to be a pitfall. *Degeneracy*, which is the continuity arising from symmetry, does not signify a close packing of the eigenstates, in any one complete set of eigenstates, but a multiplicity of the admissible systems of analysis into complete sets of eigenstates. Thus if in unsymmetrical conditions we have two eigenstates associated correspondingly with an x-axis and a y-axis, when there is circular symmetry these will become similar (except for direction) and will be connected by a continuum of eigenstates associated with every direction in the xy plane, since there are now no distinctive directions in that plane. We call the number of original eigenstates amalgamated by symmetry into a continuum the *degree of degeneracy*. Evidently an $(n-1)$-dimensional continuum corresponds to the degree of degeneracy n.

Degeneracy is especially prominent in ideal elementary systems, because they are abstracted from the environment which in actual physical systems would always be in some degree asymmetrical. Current quantum theory (through a mistaken analogy with macroscopic systems) regards them as having *no* environment other than a geometrical frame of space-time. This idealization goes too far, since it leaves the system without observable properties. The ideal environment (for which the elementary equations and definitions are valid) is a physical environment, but it has the same symmetry as a space-time frame.

The local symmetry of space-time (which includes also *uniformity*, i.e. symmetry about a centre of curvature) is described by the group of its relativistic transformations. These will also apply to the idealized physical environment which has the same symmetry. The wave functions of a system in this environment will therefore have a degree of degeneracy ascertainable from a study of the group of relativistic rotations of the vectors or tensors defining the system. If the tensor has $n-1$ independent relativity rotations, the eigenstates will fill an $(n-1)$-dimensional continuum, and the degree of degeneracy will be n. A full analytical study of the relativity rotations of wave vectors and tensors (and of the corresponding complete space vectors and tensors) is contained in my development of wave tensor calculus, where n appears as the number of dimensions of the "phase space" (*P. and E.* §§ 7·2, 10·6). I am now able to add in § 17 some further explanation, which I think will render this part of the subject less obscure from the physical point of view. Meanwhile I shall use the results of the analytical investigation, namely that n is 10 for a simple wave tensor and 136 for a double wave tensor. The wave tensor of a comparison particle is necessarily non-degenerate, being restricted as explained in § 8; hence for a comparison particle $n = 1$.

One of the most striking achievements of ordinary quantum theory is the device by which it is able to employ rigorously these conceptions of elementary particles and systems, which by their definition require symmetrical environment (or, as it mistakenly supposes, no environment at all), in problems which postulate unsymmetrical conditions. Relativity theory provides no means of describing the perturbation of a system by its environment except as a change of its structure; but quantum theory describes small perturbations as changes of the degree of occupation of the various eigenstates, the structure and tensor characteristics of the eigenstates themselves remaining unchanged. This fundamental difference in the treatment of unsymmetrical environment makes it impossible to correlate the formulae of relativity theory and quantum theory except in the most symmetrical conditions, i.e. in uniform space (spherical or flat). Here we should notice that, according to the method of quantum theory, a degenerate wave vector or tensor does not cease to exist in unsymmetrical conditions; it becomes non-uniformly occupied. In certain cases new wave functions are introduced to describe permanent or semi-permanent non-uniformity of occupation.

Besides varying in orientation by relativistic rotation, a momentum vector $M = mJ$ can vary in magnitude. Since J is understood to be normalized, this is provided for by varying m. The eigenvalues of m can only become continuous by close packing; there is no question of degeneracy, since change of m is not a relativistic transformation. We shall take the eigenvalues of m to be discrete; the continuous case can then be included (if necessary) by forming the limit in the usual way.

Although cosmological considerations are outside the scope of this paper, it will be useful to have in mind the results of the cosmological theory in this connexion. There must, of course, be a vast number of possible values of m for an elementary object-particle; if there were only two eigenvalues, there could be at most twenty particles in the universe. But the values are extremely close packed, so that unless we treat aggregations of particles on an astronomical scale the differences from the standard values are insignificant. In very large systems, in order to provide enough particles, we have to include eigenvalues of m sensibly lower than the standard value for small systems. This is the quantum representation of gravitational potential energy, which makes the total energy or mass of a system sensibly lower than the sum of the standard values of the masses of its particles.

11. Although current quantum theory does not concern itself with the degeneracy of its ultimate particles, it deals with degeneracy in other connexions. In radiation problems it is found that the degeneracy factor represents the *weight* of an oscillator for the purpose of calculating the intensity of the emitted radiation. This is a problem which connects atomic quantities, described by momentum vectors, with field quantities (electromagnetic waves), described by an energy tensor; and it is not difficult to verify that in our problem, which also connects atomic quantities with the energy tensor, degeneracy has the same effect as a weight. Thus we can treat degenerate particles as simple particles provided that we multiply their contributions to the energy tensor by the weight n. This rule is all that we require for the calculations later in this paper. But the degeneracy factors have so wide an importance in all branches of relativistic quantum theory that it is desirable at the outset to remove all obscurity connected with them.

In the radiation problem a degenerate state is capable of occupation by n particle-units. But here we are dealing with the initial degeneracy of the vector wave functions by which elementary particles are defined. That which fully occupies a complete momentum vector is called an electron (or proton). To square with the practice in later applications of degeneracy, we should say rather that it is a union of ten sub-electrons (or sub-protons). This is a mere formalism; but it is useful to remember that, according to the same system, the bi-particle is a union of 136 sub-bi-particles, and the comparison particle is just one comparison sub-particle. It is the three kinds of sub-particle that have the most simple analytical connexion with one another, since they (if they existed) would be free from degeneracy and would be represented by discrete wave functions.

The degenerate wave function replaces n discrete wave functions amalgamated by symmetry. The amalgamation is different from ordinary combination, because wave functions combine by multiplication. Instead of a discrete n-tuple wave function occupying a $3n$-dimensional volume, we have a simple degenerate wave function occupying a space volume V, *but also extended over a continuum of orientation*. The volume is V because references to the "object-particle" in our previous work must be understood to mean the *whole* particle occupying the momentum vector M_1.

The important point to notice is that the amalgamation involves a partial replacement of the usual multiplicative occupation factors (or probabilities) by additive occupation factors. The occupation factor of the multiple wave function is the product $p_1 p_2 \dots p_n$ of the occupation factors of the n discrete wave functions composing it. This is now replaced by a simple degenerate wave function whose total occupation is distributed *additively* over the continuum of orientation. The original set of n discrete wave functions is obtained by concentrating the distribution at n orthogonal points in the continuum; but the occupation factors are now such that the total occupation or probability is $p_1 + p_2 + \dots + p_n$. Thus if discrete wave functions are regarded as having an occupation factor 1 when fully occupied, the degenerate wave function must be regarded as having an occupation factor n when fully occupied. This would be a departure from the original conception of degree of occupation; so we prefer to call n a "weight factor", recognizing, however, that it has the same effect as an occupation factor.

A case of special importance is when the probability distribution of the degenerate wave function is limited to a very small solid angle of orientation, so that the corresponding vector or tensor is "almost exact"; we shall call this a *pseudo-discrete* wave function. There is no sensible difference between a pseudo-discrete and a discrete wave function except that the former has a weight n—as if it were a discrete function occupied n times over.

Thus if we calculate the contribution to the energy tensor as if the momentum vector were discrete and fully occupied, we must multiply the result by n to obtain the contribution of the fully occupied pseudo-discrete momentum vector. This is the rule already given at the beginning of this section.

It will be noticed that in the pseudo-discrete wave function the concentration of the probability in orientation is greater than that obtainable from a set of n orthogonal discrete functions; and it might perhaps be thought that such excessive concentration would be forbidden. But the degenerate function represents a physical particle or bi-particle, and there is certainly nothing to forbid the allocation of its whole probability to a single eigenstate. In saying that the degenerate wave function replaces n discrete wave functions, we do not mean that it is merely a mathematical substitution. The replacement is occasioned by the fact that symmetry of environment affects the nature of our observational knowledge of a system, so that a new form of description must be introduced. Owing to the absence of landmarks for the determination of orientation, the simple direct method of measurements of the characteristics of a system (postulated in the most elementary quantum formulae) is inapplicable. A change in the method of observation implies a different system of separation into object-system and comparison fluid (see § 15).

It is worth noticing explicitly that a bi-particle (which fully occupies a double vector) yields one object-particle and a comparison particle; but, expressed in terms of sub-particles, 136 sub-bi-particles yield 10 object-sub-particles and a comparison particle. Thus a weight-transformation factor 13·6 commonly appears in passing from the primary to the secondary concept of particles.

To see how degeneracy affects the problem on which we are engaged, we must return to the factorization of the original double vector $\Psi_{\alpha\beta}X_{\gamma\delta}$ into two complete vectors M_1 and M_2. We have identified them as the momentum vectors of certain particles, but that only means that our terminology has introduced particles ("genuine" or "fictitious") for them to belong to. Primarily they are wave functions which happen to be constant over the domain to which they apply. We have treated the double vector as discrete; for otherwise we could not have factorized it without taking account of the element of solid angle over which its orientation is distributed. In my earlier derivation of the masses of the proton and electron I have taken account of the elements of solid angle associated with the double vector and with M_1 (M_2 being discrete). Progress was difficult because the solid angles are in domains with different numbers of dimensions; but the difficulty was not insuperable. Now, however, we have a much simpler method of dealing with "almost exactness". The double vector and the object-vector are pseudo-discrete, but we may continue treating them as discrete provided that we multiply their contributions to the energy tensor by their respective degeneracy factors in accordance with the rule stated.

12. We began with the expression for the energy tensor in terms of primary particles. We have now to examine its constitution in terms of secondary particles. We consider an *elementary* object-particle, i.e. an entity fully specified by one complete momentum vector $M = mJ$. Its contribution to the energy tensor is required to be a space tensor of the second rank. In principle there is only one way of forming such a tensor; we must take the outer square $M \times M$. For if another vector M' were introduced, the contribution would be jointly associated with particles specified by M and M'. It would, in fact, be a reversion to the primary concept which associates each element of density with two particles.

For accuracy it must be stated that the reality conditions of the theory may require that the second factor is not M but a vector uniquely determined by M, e.g. its complex conjugate. This, however, is merely a convention of symbolism. To guard ourselves formally, it must be understood that the operator × includes the transformation (if any) imposed by the reality conditions.

The most general expression for the contribution of the fully occupied wave function of an elementary particle to the energy tensor is accordingly $a(M \times M)$, where a is a pure number. Since there are no pure numbers included in the specification of the particle, a must be a constant of nature.

This step in the argument is of great importance, because we shall find that there are two kinds of elementary secondary particles (protons and electrons), and it shows that a must be the same for both. Elementary theory seems to suggest that they ought to have different coefficients a_p and a_ϵ proportional to the reciprocals of their masses; but this is excluded by the fact that we cannot work a_p and a_ϵ into the specification of these particles. If we try to introduce the same difference solely in terms of the momentum vectors specifying the particles by taking the density equal to

$$(M \times M) \div \text{quarterspur } M,$$

we obtain a quantity of the wrong dimensions. We do not say that there can be no physical entity whose specification requires a pure number in addition to a momentum vector; but such an entity does not fulfil the definition of an elementary object-particle.

A comparison particle is an example of an entity whose specification includes a pure number as well as a momentum vector; for we have to qualify the momentum vector by the epithet "discrete", which means that it has only $\frac{1}{10}$ the degeneracy factor of a true vector. Thus if the momentum vector of a comparison particle is M_0, we must not assume that its contribution to the energy tensor is $a(M_0 \times M_0)$. But we have learned in § 11 the precise way in which the pure number $\frac{1}{10}$ appears in the energy tensor. Writing $a = 10b$, so as to show the degeneracy coefficient explicitly, the energy tensors of the comparison particle and object-particle are respectively

$$b(M_0 \times M_0), \quad 10b(M \times M). \tag{7}$$

The original expression for the energy tensor (according to the primary concept of particles) was the product $M \times M_0$ of the two momentum vectors (§ 4). In order to postpone the discussion of the scale in which this is expressed, we shall write it more generally as

$$136c(M \times M_0), \tag{8}$$

since we already know that it includes the degeneracy factor 136 of a double vector.

The expression of the energy tensor of a secondary particle as the square of its momentum vector accords in principle with macroscopic relativity theory which sets the part of $T_{\mu\nu}$ due to a particle of proper mass m equal to

$p_\mu p_\nu/m$, where $p_\mu = m\,dx_\mu/ds$ is the momentum vector. We have already remarked that our result omits the divisor m. The macroscopic expression is, of course, no definite guide to the individual contributions of protons and electrons, and the difference is not to be looked upon as a discordance.

13. We can now express the condition that in the replacement of the bi-particles by secondary object-particles and comparison particles the energy tensor is not altered. The sum of the energy tensors of the object-particles and comparison particles must be equal to the sum of the energy tensors of the bi-particles. Accordingly, by (7) and (8),

$$\Sigma\{b(M_0 \times M_0) + 10b(M \times M)\} = \Sigma 136c(M \times M_0). \tag{9}$$

If a double vector is partially occupied, the occupation factor p is attached to the vector of the object-particle in the factorization, the comparison particle being understood to be a permanent constituent of the physical reference frame and therefore incapable of reduced occupation. Thus the factor p would appear in two of the terms of (9) but not in the term $b(M_0 \times M_0)$. Clearly the equation (9), corresponding to full occupation, will not remain satisfied when arbitrary occupation factors are inserted. This was to be expected, because we have seen that the difference in method of relativity and quantum theory in treating variation of the content of the reference frame makes it essential to connect their respective formulae on the basis of full occupation (§ 9).

When we come to consider how it is possible to satisfy equation (9) certain difficulties appear. But it is necessary to remember that our discussion has been confined to the most elementary material of quantum theory—independent elementary particles in uniform motion—and the equation applies to object-systems composed solely of such material. Interaction energy, field energy, reaction at the boundary of the volume considered, would introduce extra terms whose form we have not yet discussed. Nor have we considered how a variation of the degrees of occupation of a wave function would affect the energy tensor, except in so far as a quasi-static approximation is sufficient.

The most conspicuous difficulty is that, whereas the left-hand side of (9) will generally yield a pressure component T_{11}, there is no provision for pressure components on the right. But a little reflexion shows that this was to be expected. If pressure is treated in the usual elementary way as a boundary effect, it corresponds to exchange of particles between the region W considered and the region outside W, and the corresponding exchange-energy must be introduced to represent it. If the pressure is treated as an internal distribution, it is represented by the collision forces between the particles which are also a variety of exchange effect. Finally, if there are no collisions and no boundary exchange, so that the system is dispersing freely, terms representing the progressive evacuation dp/dt must be inserted.

To avoid a long incursion into other branches of relativistic quantum theory in which these matters are treated, we must find a simple application of (9) which steers clear of them. With this limitation the only problem we can tackle is that of particles at rest, since motion immediately raises the evacuation problem.* We can omit the summation, since there is now no advantage in considering more than one double vector and its factors.

Accordingly, taking the object-particle at rest and considering the double-time component T_{44} of the tensor, (9) gives

$$bm_0^2+10bm^2 = 136cmm_0, \qquad (10)$$

where m, m_0 are the proper masses of the object-particle and comparison particle.

It is already clear from (10) that there will be two possible values of the ratio m/m_0, so that there are elementary particles of two different masses.

14. The factors 1, 10, 136 in the three terms of (10) are the degeneracy factors of the respective wave tensors. By omitting them we obtain

$$b(m_0^2+m^2) = cmm_0, \qquad (11)$$

which would have been the result if degeneracy had been neglected. In order to find the ratio b/c, we examine how this simplified equation would be interpreted, weight factors being disregarded. We are considering a normalization volume V in which from the ordinary point of view there is only one particle whose mass is m. The two sides of the equation give two expressions for the density. The right-hand side corresponds to the ordinary expression $\rho = m/V$, so that we must have

$$cm_0 = 1/V. \qquad (12)$$

The reciprocal of a three-dimensional volume is a vector normal to the volume; and, since in our units it has the dimensions of a mass, it has appeared in our analysis as the vector cM_0 which has a time-component cm_0, as expressed in (12).

Relativity theory, however, insists that an observable such as density cannot be associated with one particle in empty space; so that the second vector, whether written as cM_0 or V^{-1}, must represent a physical system and not a mere geometrical abstraction. Accordingly, the left-hand side of (11) exhibits the same density divided between the particle which we recognize and a comparison particle. It shows that if the ordinary particle were removed, so that the space became technically empty, there would still be a density bm_0^2 and therefore a mass bm_0^2V in the volume. Since this must be the mass m_0 of the comparison particle, we have

---

* We should have to express in terms of occupation factors the condition (obvious from relativity considerations) that a space component of the momentum vector causes a particle to "move", i.e. become associated progressively with different elements of the comparison fluid.

$$m_0 = bm_0^2V = bm_0^2/cm_0$$

by (12). Hence $b = c$.

Using this result, (10) becomes

$$m_0^2 + 10m^2 = 136mm_0, \tag{13}$$

which is the equation for the masses of the proton and electron (Eddington 1931). It equates the density of the *mutual energy* of particles (on the right) to that of the equivalent *self-energies* of particles (on the left).

15. If m_1, m_2 are the masses of the proton and electron, i.e. the roots of equation (13), the masses μ, M of the internal and external particles of the hydrogen atom are

$$\left.\begin{aligned} \mu &= m_1m_2/(m_1+m_2) = m_0/136, \\ \mathrm{M} &= m_1+m_2 = 136m_0/10. \end{aligned}\right\} \tag{14}$$

It is instructive to see how these masses can be derived directly instead of via the proton and electron. If the foregoing arguments were applicable to internal and external particles without modification, we should have had

$$m_0^2 + (10\mu^2) = 136\mu m_0, \tag{15}$$

$$(m_0^2) + 10\mathrm{M}^2 = 136\mathrm{M}m_0. \tag{16}$$

The brackets show the terms which must be omitted to agree with (14), and therefore call attention to the points at which the argument becomes modified.

A peculiar feature of the internal particle is that it has no rest-mass. The proper mass of the system is M, not $\mathrm{M} + \mu$. Alternatively, we can say that the particle has a rest-mass equal to its mass-constant μ, but the zero of energy-reckoning has been lowered by a constant μ. Thus the density $10\mu^2$, corresponding to a mass μ, is either absent or cancelled, and must be omitted on the left-hand side of (15).

For the external particle the term m_0^2 is omitted. The argument for inserting this term was that when the self-energy of the object-particle is removed there remains the self-energy of the comparison particle. This no longer applies, because the self-energy of the comparison particle is provided out of the internal mutual energy $136\mu m_0$ as shown in equation (15). The difference is that when we remove the self-energy of a proton we have to remember to make provision for the energy of the comparison particle; but when we remove the self-energy of an external particle we leave an internal particle which undertakes the provision of the energy of the comparison particle.

It will be seen that when internal and external wave functions are employed there is only one comparison particle instead of two. We have reached this conclusion by deduction; but the physical reason for it should also be considered. It turns on the fact that ξ is not the difference of two co-ordinates measured from the physical origin, but a direct measurement of one particle from the other as origin. The transformation to internal and external wave functions is not simply an analytical transformation but a change of the method of observation, the new method being one which *causes less disturbance to the physical frame*; for every measurement from the physical origin communicates an uncertain momentum to the physical frame just as it does to the particle that is being located. This lessened disturbance is represented by providing one comparison particle instead of two to take up the reaction from the measurements.

16. We are now in a position to treat more fully the transformation (4). In § 5 it was applied to primary particles; but we here consider the same transformation applied to object-particles so as to replace the wave functions of a proton and electron by internal and external wave functions. Being an initial step towards other developments, the transformation is limited to field-free non-interacting particles represented by "infinite plane waves". After this step has been taken, interaction can be introduced in the internal wave function, which then fulfils its normal practical purpose of specifying the *correlation* of the proton and electron distributions. The transformation, like any mathematical substitution, is always valid, but its utility is limited to uncorrelated distributions.

A well-known property of (4) is that the Jacobian $\partial(\xi, \mathrm{x})/\partial(x_1, x_2)$ is unity; this has the effect of eliminating any difference between polarization space ξ, η, ζ and ordinary space as regards normalization volumes.

Another well-known result is

$$\frac{1}{m_1}\frac{\partial^2}{\partial x_1^2}+\frac{1}{m_2}\frac{\partial^2}{\partial x_2^2}=\frac{1}{\mathrm{M}}\frac{\partial^2}{\partial \mathrm{x}^2}+\frac{1}{\mu}\frac{\partial^2}{\partial \xi^2}, \tag{17}$$

with similar equations for the other three co-ordinates. Hence

$$m_1^{-1}\Box_1 + m_2^{-1}\Box_2 = \mathrm{M}^{-1}\Box_x + \mu^{-1}\Box_\xi. \tag{18}$$

The second order (relativistic) wave equation for a field-free particle is

$$\{(-ih/2\pi)^2\Box - m'^2\}\psi = 0, \tag{19}$$

where m' is considered to be the proper mass of the particle. Hence, for discrete eigenfunctions, (18) reduces to

$$m_1'^2/m_1 + m_2'^2/m_2 = \mathrm{M}'^2/\mathrm{M} + \mu'^2/\mu. \tag{20}$$

This reduction is not quite so simple as it seems, because the four $\Box$ operators do not usually reduce to eigenvalues simultaneously. But it is justified by the familiar theory of invariance of the density of the eigenstates in different modes of analysis, provided that the eigenstates are non-degenerate. When, however, non-scalar wave functions are employed, we must take account of their innate degeneracy. If in (19) ψ is a wave vector, it describes an amalgamation of ten discrete states and only $\frac{1}{10}$ of the eigenvalue m'^2 can be allotted to one discrete state. Thus the general form of (20) is

$$m_1'^2/m_1 n_1 + m_2'^2/m_2 n_2 = \mathrm{M}'^2/\mathrm{MN} + \mu'^2/\mu\nu, \tag{21}$$

where n_1, n_2, N, ν are the degeneracy factors. When, as in the formation of a hydrogen atom, the wave functions are all simple wave vectors, all four factors are 10 and we regain equation (20); but the form (21) should be kept in reserve for future developments.

Equation (20) or (21) expresses the condition that the pairs of wave systems ψ_1, ψ_2 and ψ_{M}, ψ_μ, satisfying wave equations of the form (19), describe the same object-system. We can use it in two ways: (1) to show how the eigen-masses M', μ' must be chosen in order that the condition may be satisfied, or (2) if M', μ' are assigned by convention in a way which does not satisfy the condition, we can find the nominal change of the energy of the object-system in passing from one mode of description to the other.

We must adopt $m_1' = m_1$, $m_2' = m_2$, since that is essentially the definition of the transformation we are applying. The practice of quantum theory commits us to the identification $\mu' = \mu$. Then if the condition (20) is satisfied, we have

$$\mathrm{M}'^2 = \mathrm{M}(\mathrm{M} - \mu). \tag{22}$$

It is not impracticable to accord the external wave function the exceptional treatment which (22) demands, but it is confusing in conception. But a more illuminating point of view is obtained by following up alternative (2). We then adopt $\mathrm{M}' = \mathrm{M}$, making no distinction between the external particle and the other particles. Condition (20) is then not satisfied, but the discrepancy is regarded as a change μ in the zero-point of our reckoning of energy when we pass from a description of the object-system in terms of ordinary particles to a description in terms of internal and external particles.

A change of zero-point is justified physically by the fact that the transformation is not merely analytical but implies a different procedure of observation—a procedure which introduces one comparison particle instead of two (§ 15), so that a different separation of the object-system from the comparison fluid is involved. I may add that the change of zero-point is not the direct result of the elimination of a comparison particle (for our method of analysis has provided for that); it is due to the elimination of its *interchange energy* with the comparison particle which is retained (*P. and E.* § 15·8).

17. The derivation of the numbers 10 and 136, representing degree of degeneracy or number of dimensions of phase space, is given in *P. and E.* pp. 95, 165. The following is a more elementary physical derivation.* The mechanical characteristics of a particle consist of its energy, momentum and spin-momentum. The momentum and energy constitute a 4-vector $(m_{15}, m_{25}, m_{35}, m_{45})$ and the spin momentum is a 6-vector $(m_{23}, m_{31}, m_{12}, m_{14}, m_{24}, m_{34})$, so that ten quantities are required to specify the mechanical characteristics. If, however, we are considering the possible variations of the characteristics of a particle of *fixed* proper mass m, there are only nine independent variations. In the postulated symmetrical conditions these form a nine-dimensional continuum of degeneracy; hence the degree of degeneracy is 10.

It is commonly assumed that the spin-momentum has only three components m_{23}, m_{31}, m_{12}; but this assumes that the particle is at rest, since a Lorentz transformation would introduce the other components of the 6-vector. Bearing in mind that the particle is in general a superposition of elementary states with different momenta, we see that the full 6-vector must be specified, and each component is capable of independent variation. This applies even when we are dealing with a single elementary state as ordinarily understood, because the momentum vector is not exact (discrete) but almost exact (pseudo-discrete).

To exhibit the connexion of this treatment with phase space, we have to consider the strain vectors corresponding to the above space vectors. These are $(S_{14}, S_{24}, S_{34}, S_{16})$ and $(S_1, S_2, S_3, S_{15}, S_{25}, S_{35})$, together forming the ten space-like components of the complete strain vector. Starting with $S_{16} = m$, the other components being 0, infinitesimal variations of the other components give nine dimensions of phase space. To these we have to add the algebraic phase conjugate to S_{16}, making ten dimensions in all (*P. and E.* § 7·3).

---

* This is the result of discussions with H. T. Corben as to the physical identification of the components of a strain vector.

An interesting point is that only *mechanical* characteristics of the particle are taken into account. The electromagnetic characteristics (distinguished by their change of sign in passing from a right-handed to a left-handed frame) correspond to the six time-like components of the complete strain vector, and are not represented in phase-space. The meaning of this is that electromagnetic characteristics have no physical significance if the particle is alone in a Riemannian frame; on the other hand mechanical characteristics have a significance, since the $g_{\mu\nu}$ constitute an inertial frame.

Passing to the bi-particle, the ten mechanical characteristics of each component form 100 combinations. These are all capable of independent variation, because the bi-particle is not necessarily in one separable state; it may be a superposition of separable states. In addition, electromagnetic characteristics of one particle in combination with those of another particle have a physical significance. The six dormant electromagnetic characteristics of each particle give 36 combinations representing electric stresses, etc., in the bi-particle. Naturally, the specification is more complicated than that of a macroscopic electromagnetic field which is much simplified by averaging. The total number of significant characteristics is $100 + 36 = 136$. There are also 120 combinations of mechanical characteristics of one particle with electromagnetic characteristics of the other which are not physically significant when the bi-particle is isolated in space; these are distinguished analytically as time-like components of the double strain vector.

Strictly speaking, one more degree of degeneracy is introduced into the bi-particle when we nominate one of the two components as the comparison particle. Exchange of the nomination is clearly a relativistic transformation, so that it forms an additional dimension of the continuum of degeneracy. I have taken no account of this in the foregoing discussion, because the subject of interchange is better treated as a whole. If we neglect interchange in this derivation of primitive material, and then hand over the material to current quantum theory which continues to neglect interchange, we obtain a consistent theory into which the complicated effect of interchange can be introduced systematically. But if we take account of interchange in the preliminary stages and then join our results to current theory, we obtain a mixture which is not only incorrect but difficult to amend. I consider therefore that the non-interchange masses in equation (13) should be regarded as the standard masses of the proton and electron. It appears from the theory of interchange that the mass of the internal particle of a hydrogen atom (and therefore approximately the mass of an electron) derived by applying the formulae of current quantum theory to observation is 137/136 times the standard mass (*P. and E.* § 15·8).

In many other parts of my theory the formulae are more easily derived and understood when we interpret the numerical coefficients as degrees of degeneracy. Besides the coefficients 10, 136, 137 the coefficients most frequently occurring are 4 expressing the degeneracy of an ordinary (not a *complete*) space vector, and 3 for the three-dimensional vectors in static problems. But other combinations can arise according to the circumstances of the problem under consideration.

REFERENCES

Eddington, A. S. 1931 *Proc. Roy. Soc.* A, **134**, 524.
— 1933 *Proc. Roy. Soc.* A, **143**, 327.
— 1936 *Relativity theory of protons and electrons.* Camb. Univ. Press.

The masses of the neutron and mesotron

BY SIR ARTHUR EDDINGTON, F.R.S.

(*Received* 10 *October* 1939)

THE NEUTRON

1. The development of relativistic wave mechanics in the preceding paper makes it possible to calculate the mass of the neutron. References, unless otherwise stated, are to the sections of that paper. We have only to express the fact that a proton and electron by emitting a neutrino yield a neutron.

We consider the proton and electron initially without interaction, since the interaction energy would in any case have to be recalculated after the emission of the neutrino. They are equivalent to an external and an internal particle of masses $M = m_1 + m_2$, $\mu = m_1 m_2/(m_1 + m_2)$. These, like the electron and proton, are specified by complete momentum vectors having the full degree of degeneracy 10. I take it that the emission of a neutrino is a way of saying that one of the particles loses its spin. Accordingly its complete momentum vector, which (leaving aside the six dormant electrical components) consists of an ordinary momentum 4-vector and a spin 6-vector (§ 17), is reduced to a momentum 4-vector, and its degree of degeneracy is changed from 10 to 4. The particle which undergoes the modification is clearly the internal particle, for the neutron in its external relations resembles a hydrogen atom; indeed a spinless external momentum vector would represent a particle capable of existing only in one Lorentz frame and therefore immobile, since the spin 6-vector is necessary for a Lorentz transformation as Dirac's pioneer investigation demonstrated.

The reduction of the degeneracy factor from 10 to 4 increases the energy of the internal particle in the ratio 10 to 4, i.e. from μ to $2{\cdot}5\mu$. This follows from § 16, equation (21), bearing in mind that it is the generalized form of equation (20) whose significance is followed up later in the section. The last term $\mu'^2/\mu\nu$ is the energy of the internal particle, which is increased in the ratio 2·5 by the change of the degeneracy factor ν from 10 to 4.

To satisfy ourselves that the change is effective—that it adds $1{\cdot}5\mu$ to the whole mass and is not merely a formal change of reckoning—we must recall that (21) is not imposed as a condition to be satisfied unless we intend the system referred to on the right-hand side to be merely an alternative description of the dissociated proton and electron referred to on the left; in other cases the discrepancy of the two sides indicates the excess of energy of the system represented by the internal and external wave functions over the proton-electron system. By changing ν from 10 to 4 this discrepancy is increased by $1{\cdot}5\mu$; that accordingly is the increase of mass necessitated by the emission of a neutrino. The point to notice is that although we start with a discrepancy μ between the two sides of the equation, attributable to a formal change of reckoning in the transition from an absolute to a relative description, variations of the discrepancy are not formal changes.

Accordingly the mass of a neutron exceeds the mass of a hydrogen atom by $1{\cdot}5\mu$, or very nearly 1·5 electron masses.

This result has already been obtained in an investigation by H. O. W. Richardson* based on the theory as given in *Relativity theory of protons and electrons*. Richardson's work has been known to me for a year; and, although it did not profess to give a complete proof (some details being left obscure), I could feel no doubt as to its substantial truth. By indicating a new direction in which advance was undoubtedly possible if certain parts of my theory were brought into better order, it has greatly helped me in these developments.

---

* Owing to incompleteness, Mr Richardson has withheld publication of the investigation.

2. There can be no internal angular momentum in the neutron. Although spin momentum is normally only part of the whole angular momentum, relativistic conditions make it impossible to attribute angular momentum to a spinless particle (*P. and E.* § 8·3). The neutron therefore does not possess an internal structure with negative energy-levels analogous to those of a hydrogen atom. I think that the only possible form of internal motion open to it would be pulsation, but no solutions of the wave equation are of that form. It seems clear therefore that the neutron has only one state, namely, that in which the momentum vector of the internal particle is directed along the τ-axis. Thus there will be no correction for internal energy, and the result found above is the true mass of the neutron.

The magnetic moment of a free neutron is easily determined. Since there is no internal angular momentum, the magnetic moment is that of the external wave function only, which is identical with the external wave function of a hydrogen atom. This moment is

$$2{\cdot}5eh/4\pi c\mathrm{M}, \qquad (1)$$

that is to say, it is the moment erroneously attributed to the proton in current quantum theory. A derivation of (1) is given in *P. and E.* § 12·8, but this could now be considerably improved. It may be noted that (1) applies to the neutron as it stands, *not* with the mass of the neutron substituted for M.

THE MESOTRON

3. The mesotron is more difficult to treat, and the following determination of its mass may not be so definitive as the corresponding investigation for the neutron. We have to express the fact that a mesotron by emitting a neutrino becomes an electron, or, more conveniently, that an electron by combining with a neutrino becomes a mesotron.

The complete momentum vector representing an electron cannot *absorb* a neutrino in the sense in which it can emit one; it can lose the spin 6-vector incorporated in it, but it cannot be extended to accommodate an additional 6-vector. Thus we can only represent the association of an electron and neutrino as a *combination*, their respective vectors being combined into a double vector occupied by a bi-particle. The 10-fold degeneracy of the electron vector coupled with the 6-fold degeneracy of the neutrino spin-vector gives a double vector with degeneracy 60. Since the pure spin-vector contains no electrical components to combine with the electrical components of the electron vector, there are no additional dimensions of degeneracy.

I conclude that a mesotron is a bi-particle with degree of degeneracy 60.

One of the very few possibilities that present themselves for consideration is that the mesotron bi-particle includes what will ultimately be the comparison particle; so that the actual transformation is

mesotron − neutrino → electron + comparison particle.

This seems probable when we consider the origin of the mesotron. The nucleus appears to be a region of intense angular momentum. The ordinary macroscopic theory of Riemannian space, which assumes that microscopic vorticity cancels out on the average, ceases to apply even approximately; so that both the geometrical frame and the physical comparison fluid which materializes it require the fuller specification explained in *P. and E.* § 11·4. We noticed (§ 8) that the ordinary comparison particles do not provide a standard of non-rotation, and that special spin-comparison particles might be required in certain types of problem. It seems reasonable to suppose that in the nucleus we have a certain number of ordinary comparison particles furnishing a standard of rest for the measurement of momentum, and a certain number of spin-comparison particles furnishing a standard of non-rotation for the measurement of angular momentum. The number and nature of the comparison particles is, of course, determined by the nature of the ideal measurements which we must suppose ourselves to have made in order to be in possession of the knowledge which we should regard as a full description of the system.

When an electron emerges from the nucleus it may bring with it an ordinary comparison particle or a spin-comparison particle, depending on the nature of the measurements required to obtain full knowledge of the transformed nucleus. In the first case the comparison particle merges at once into the comparison fluid, and we observed only an ordinary electron in undisturbed environment. In the second case the combination remains for some time a distinct bi-particle—an electron existing in a vortex. The vorticity is gradually dissipated; that is to say there is a probability of transition into an ordinary electron and comparison particle. The transition is described as emission of a neutrino, but it is an altogether different process from the emission of a neutrino in forming a neutron. I suppose that a physical picture of what happens is that, when released from the constraint of the nucleus, the bi-particle has new degrees of freedom which, by non-commutation with the neutrino spin, cause a precession which ultimately makes the original plane of spin untraceable. When it is necessary to distinguish the two ways of losing spin, I shall describe the mesotron process as emission of an *anti-neutrino*. The *anti*-ness lies in the fact that the spin is in the comparison part of the bi-particle instead of in the object part.

We have therefore to consider the conversion of a pseudo-discrete double vector of degeneracy 60 into the corresponding pseudo-discrete double vector of full degeneracy 136 which is immediately replaceable by an electron and comparison particle. In the case of the neutron we found that the change of degeneracy alters the mass in inverse ratio, and the same rule applies here; but the argument requires restating since we are now considering a bi-particle.

As in the case of the neutron, the key-condition is that energy must be gained or lost in the transition in such a way as to preserve a one-to-one correspondence of the particles. This requires that the mesotron wave function shall have the same normalization volume V as the electron and comparison particle.

Each double vector consists of a mass-product multiplied by a unitary double matrix. The transformation of the double matrix of a mesotron into the double matrix of an electron + comparison particle is merely a relativity rotation of the double frame $E_\mu F_\nu$; thus apart from degeneracy, a mesotron in one frame would actually be an electron + comparison particle in another equivalent frame. The effect of degeneracy is contained in the formula relating the density to the mass-product (§ 12, formula (8)); the relation $\rho = 136 c m_0 m_e$ must be replaced in the mesotron by $\rho' = 60 c m_0' m_e'$. Treating this as a change of scale of energy, we must change ρ in the same ratio as m_0 and m_e, since the normalization volume has to be kept constant. Setting

$$m_0' = a m_0, \quad m_e' = a m_e, \quad \rho' = a\rho,$$

the conditions $\rho = 136 c m_0 m_e$, $\rho' = 60 c m_0' m_e'$ give

$$a = 136/60.$$

Thus if we build an electron + comparison particle system on 136/60 times the ordinary scale of energy, the result is equivalent to a mesotron; and conversely the transformation of a mesotron into an electron + comparison particle is a deflation of this system to the normal scale by emission of the surplus energy.

It may be noticed that the presence of the additional mass of the mesotron in the volume V must alter the curvature of space. This is represented in our formulae by the increase of the mass m_0 of the physical reference frame. The fact that *both* m_0 and m_e have to be altered follows from the relativistic condition that we cannot alter what is put into the frame without altering the frame itself (§ 9). The ordinary approximation of quantum theory which neglects the alteration of the frame would be hopelessly in error in this type of problem.

The mass $\frac{136}{60}(m_0+m_e)$ of the mesotron is measured from a zero-level $-m_0$; for, after the emission of the excess energy, we are left with the mass (m_0+m_e) of which only m_e counts as object-mass. The actual object-mass of the mesotron is therefore

$$M=\tfrac{136}{60}(m_0+m_e)-m_0. \tag{2}$$

Since $m_0 = 135{\cdot}93m_e$, this gives

$$M = 174{\cdot}44 \text{ standard electron masses}$$
$$= 173{\cdot}17 \text{ current electron masses,}$$

the mass currently assigned to the electron being 137/136 times the standard mass.

Presumably there can exist also "heavy mesotrons" which change into protons (or negatrons). Their mass, obtained by substituting m_p for m_e in (2), is 2·36 proton masses.

4. A very rough idea of the lifetime of a mesotron is obtained in the following way. We have first to find a basal time t, or equivalently a length $l = ct$, which is naturally connected with the mass-product m_1m_2 which characterizes the mesotron or the system into which it is transformed. One of the two mass factors is usually replaced by the reciprocal of the natural normalization volume V; and the most relevant association of length and mass is obtained by identifying V^{-1} with the mass of one of the simple particles which can occupy it. Then V^{-2} is identified with the mass-product of two such masses. Accordingly for the most simple double vector the characteristic length l is $V^{\frac{1}{6}}$. Since we have left vague the particular mass $(m_e, m_0$ or $m_p)$ associated with V^{-1}, we cannot define more closely the l corresponding to the mass-product m_em_0 of the mesotron; but since l varies only as the sixth root of the mass-product the indefiniteness is comparatively small.

By cosmological theory the volume V is found to be 250 cm.^{3} (*P. and E.* § 14·9). Hence $l = 6$ cm., and $t = 2\times10^{-10}$ sec. We cannot expect this basal time to be a close guide to the lifetime of the mesotron, because rather large factors, such as 60 and 136, will appear in the precise calculation of the transition probability. It seems clear that the basal time would apply most directly to a structure which offers no resistance to collapse. The fact that a neutrino is emitted would seem to place the mesotron transformation in the category of forbidden transitions. It is therefore not surprising that metastability prolongs the lifetime of a mesotron to 10^4 times the basal time.

NUCLEAR STRUCTURE

5. One or two points preliminary to an understanding of nuclear structure appear to be settled by the foregoing results, coupled with an earlier investigation of the non-Coulombian force between protons (Eddington 1937). Perhaps the most interesting conclusion is that mesotrons have no connexion with the so-called Yukawa particles.

The elementary material to be combined in the nucleus consists of protons (p), electrons (e), ordinary comparison particles (c) and spin-comparison particles (s). The comparison particles are virtual particles; they are not in the nucleus until we make the measurements necessary to obtain the knowledge which forms the quantum description of the nucleus. This material yields four possible kinds of bi-particles p_c, e_c, p_s, e_s. Owing to the large rest-energy ($2{\cdot}36m_p$) of the heavy mesotron p_s, the tendency will be to form the combinations p_c, e_s rather than the opposite combinations p_s, e_c. Provisionally we may suppose that an electron can only be inside the nucleus if it is attached to a spin-comparison particle; then if the number of electrons exceeds the number of spin-comparison particles, the electrons with ordinary comparison particles will remain outside as satellite electrons. This reduces the nuclear constituents to protons with ordinary comparison particles p_c and mesotrons e_s, the former being in excess.

We can advance one step in investigating the fusion of this material by complex interaction. Consider a combination of one p_c with one e_s. In a combination of p_c with e_c, p and e combine into the internal and external particles of a hydrogen atom and the two comparison particles reduce to one. To obtain the same combination of p_c and e_s, we must make e_s convert itself into e_c by emitting an anti-neutrino; this (presumably) will be cancelled if at the same time we make the internal particle of the hydrogen atom emit a neutrino, thereby converting the hydrogen atom into a neutron. Thus the result of the combination of p_c and e_s is a neutron with an ordinary comparison particle n_c.

We cannot suppose that the mesotrons are selectively combined each with a particular p_c; but it is not unlikely that the condition can be represented with sufficient approximation as combination with a p_c whose identity is being continually varied by interchange. But leaving aside the question whether it is the best starting-point for detailed investigation, we can see why the analysis of the nucleus into protons and neutrons (p_c, n_c) has seemed so much simpler than the analysis into protons and electrons (p_c, e_s). In the proton-neutron analysis all the comparison particles are ordinary, so that the protons and neutrons are represented in a physical frame corresponding to ordinary Riemannian space; the proton-electron analysis requires spin-comparison particles and cannot be represented in Riemannian space.

The ordinary comparison particle was chosen so as to provide an exact reference frame for momentum; individually it provides no reference origin for position and no standard of non-rotation for the determination of angular momentum. But when we pass from horizontal to vertical section (§ 9), so that the volume V contains a mean of a large number of the original comparison particles, we obtain a fairly good standard of position and of non-rotation provided that the conditions are such that the law of chance is applicable. For example, different parts of the comparison fluid will (by averaging) furnish nearly the same standard of non-rotation unless we deliberately select a permanently disturbed region such as a vortex. The nucleus occupies such an exceptional region. It is well known that this occasional failure of averaging depends on the existence of integrals of the dynamical equations. There appears to be no integral which could cause a failure of positional averaging; and in any case the nucleus is not an exceptional region in this respect. The uncertainty of the origin provided by the comparison fluid (or by a single comparison particle in vertical section) is found to be e^{-r^2/k^2}, where (in terms of cosmical constants)

$$k = \sqrt{(R^2/2N)} = 1{\cdot}56 \times 10^{-13} \text{ cm}.$$

(Eddington 1937, equation (7·2))[*]. By this uncertainty a point in the physical reference frame corresponds to a Gaussian distribution in the geometrical reference frame and *vice versa*. It is this Gaussian spread which provides the "range of nuclear forces" between protons.

It is therefore the comparison particle attached to the proton or neutron which (by the uncertainty of its position relative to a Galilean frame) determines the range of nuclear forces. The "Yukawa particles" introduced by nuclear physicists to account for this range are therefore identical with the comparison particles already familiar in extra-nuclear theory. They are neutral spinless particles of mass $m_0 = 136m_e$.

When the mesotron was discovered experimentally it was assumed to be identical with the Yukawa particle. I found this very puzzling because the comparison particle is essentially a virtual particle; and it was difficult to see how it could be turned into an object particle and lose its electrically neutral character. We see now that the mesotron is an altogether different particle. If we adopt the analysis p_c, e_s of the nucleus, the Yukawa or comparison particles c and the mesotrons e_s are exhibited as distinct constituents. Since the mesotrons have an altogether different type of wave function from the comparison particles, the present tendency to confuse them is likely to hamper the progress of nuclear physics.

---

[*] This is one of the investigations which can be simplified by the degeneracy method of treatment. A note by H. M. Thaxton and the author (not yet published) suggests that there will probably be a small change of k in the revised investigation.

Our conclusions may be summarized as follows: In its normal state the nucleus may be taken to consist of protons and neutrons each with a comparison (Yukawa) particle (p_c, n_c). When a transition is about to occur the neutron is to be regarded as a combination of p_c and e_s. If the transition is spontaneous, the available energy is insufficient to provide for the emission of a mesotron e_s. Accordingly e_s is transformed into e_c before emission, by the process described as emission of an anti-neutrino, and we have the ordinary β-ray disintegration. If the transition is a consequence of the entry into the nucleus of a large amount of energy sufficient to provide the rest-mass $173m_e$ of the mesotron, direct emission of e_s becomes possible and the second transition $e_s \rightarrow e_c$ is deferred until the end of the natural lifetime of the mesotron in free spaee.

REFERENCES

Eddington, A. S. 1936 *Relativity theory of protons and electrons.* Camb. Univ. Press.
— 1937 *Proc. Roy. Soc.* A, **162**, 155.

Kinetics of the thermal decomposition of fully deuterated diethyl ether

By J. G. Davoud and C. N. Hinshelwood

(*Received* 28 *October* 1939)

This paper describes an experimental study of the thermal decomposition of fully deuterated diethyl ether. In discussing the results it is assumed for brevity that reference will be made to the two most recent papers dealing with the reaction of the hydrogen ether, namely that of Davoud and Hinshelwood (1939) and Hobbs (1938).

The experimental method was to observe with a mercury manometer or bourdon gauge the change of pressure with time when the ether decomposed in a silica bulb kept at a temperature constant to 0·5°. Pressure-time readings were corrected by numerous analyses of the aldehydes formed (Davoud and Hinshelwood 1939). The heavy ether was obtained from the Norsk Hydro and was 99·0 % pure. All measurements with the heavy ether were repeated with light ether within a short time and under identical conditions: comparisons are therefore independent of temperature errors, which in any case are small. The principal results are given consecutively below with the comments on each immediately following.

(A) The presence of increasing small quantities of nitric oxide causes the rate of decomposition of ether to fall to a well-defined limit. According to the hypothesis of Staveley and Hinshelwood (1936, 1937) this is due to the suppression of reaction chains: the fully inhibited reaction represents the chain free molecular reaction of the ether, and the ratio of the normal rate, ρ_0, to that of the fully inhibited reaction, ρ_∞, measures the proportion of chain reaction occurring in the absence of nitric oxide. This ratio is called the apparent chain length.

Table 1 shows that the ratio $\rho_{\infty(\mathrm{H})}/\rho_{\infty(\mathrm{D})}$ has a mean value of 1·78: $\rho_{0(\mathrm{H})}/\rho_{0(\mathrm{D})}$ the rather greater value of 2·14. The proportion of chain reaction is therefore somewhat greater with the light ether, the apparent chain length averaging 3·7 for the light ether, 3·0 for heavy ether. The ratios 1·78 and 2·14 are, absolutely, of the order of magnitude to be expected. The primary process of the chain reaction depends upon the breaking of a carbon-carbon or of a carbon-oxygen bond and is therefore not likely to be much slower for the deuterium compound. This would in itself tend to make the proportion of chain reaction higher for the deuterium compound, since the total rate for the deuterium compound is less than that for the hydrogen compound. The observed results, therefore, probably mean that the introduction of deuterium slows down some later stage in the chain process more than it does the molecular reaction. This is consistent with the idea that one of the chain steps involves complete rupture of a C—H or C—D bond (Rice and Teller 1938).

TABLE 1. REACTION RATES AND APPARENT CHAIN LENGTHS FOR H- AND D-ETHERS. TEMPERATURE 550° C. ρ_0 IS RATE FOR COMPLETELY UNINHIBITED REACTION. ρ_∞ IS RATE FOR FULLY INHIBITED REACTION

Initial pressure mm.	$\left(\frac{\rho_0}{\rho_\infty}\right)_H$	$\left(\frac{\rho_0}{\rho_\infty}\right)_D$	$\frac{\rho_{0(H)}}{\rho_{0(D)}}$	$\frac{\rho_{\infty(H)}}{\rho_{\infty(D)}}$
(1) Rates estimated from 25 % pressure increase				
100	3·96	2·99	2·17	1·63
200	3·54	2·95	2·10	1·79
300	3·65	3·18	1·94	1·72
(2) Rates estimated from 50 % pressure increase				
100	3·71	3·02	2·25	1·83
200	3·61	2·93	2·22	1·80
300	3·73	3·21	2·18	1·87

(B) Table 2 shows the influence of the initial ether pressure on the rate of the maximally inhibited reactions. There is little difference in behaviour between the two compounds except that the variation with initial pressure seems to be a little slower with the deuterium ether.

TABLE 2. INFLUENCE OF INITIAL PRESSURE ON REACTION RATE FOR H- AND D-ETHERS. REACTION INHIBITED BY 5 MM. OF NITRIC OXIDE. TEMPERATURE 550° C. RATE WITH 100 MM. INITIAL PRESSURE TAKEN AS UNITY

Initial pressure (mm.)		100	200	300	400
H-ether:	25 % increase	1·00	1·42	1·79	1·93
	50 % increase	1·00	1·29	1·55	1·73
	Mean	1·00	1·35	1·67	1·83
D-ether:	25 % increase	1·00	1·27	1·42	1·48
	50 % increase	1·00	1·22	1·37	1·41
	Mean	1·00	1·24	1·40	1·45

(C) Table 3 shows that the maximum aldehyde produced is nearly the same for the D- and H-compounds. This means that, under the conditions prevailing in the respective systems, replacement of hydrogen by deuterium changes the reaction rate to nearly the same extent for the aldehyde and for the ether. In the previous paper (Davoud and Hinshelwood 1939) it was shown that radicals from the ether reaction intervene in the decomposition of the light aldehyde and cause it to react 2·9 times as rapidly as it would in their absence. A similar calculation for the heavy ether gives the value 1·93, which is not very accurate, since it depends upon the drawing of a tangent to a curve, but which is certainly less than the value for the hydrogen compound: the result is consistent with the conclusion already reached that the proportion of chain reaction is somewhat smaller with the deuterium ether.

TABLE 3. INTERMEDIATE FORMATION OF ALDEHYDE, FOR H- AND D-ETHERS. PRESSURE 300 MM. TEMPERATURE 550° C

H-ether

	Max. pressure of aldehyde mm.	Time for $p_{\max.}$ sec.
Normal reaction	59·5	220
Inhibited reaction	53·5	1000

Ratio $\frac{t_{\max.}(\text{normal})}{t_{\max.}(\text{inhibited})}$ 0·220 Ratio $\frac{F_a(\text{normal})}{F_a(\text{inhibited})}$ 2·9

D-ether

	Max. pressure of aldehyde mm.	Time for $p_{\max.}$ sec.
Normal reaction	58·2	530
Inhibited reaction	52·2	1400

Ratio $\frac{t_{\max.}(\text{normal})}{t_{\max.}(\text{inhibited})}$ 0·379 Ratio $\frac{F_a(\text{normal})}{F_a(\text{inhibited})}$ 1·93

(D) The amount of nitric oxide required to produce a given degree of inhibition is independent of the initial pressure of the ether (Hobbs 1938; Davoud and Hinshelwood 1939). This has been explained by supposing that the nitric oxide reacts chiefly with a complex radical which does not propagate chains itself until it has suffered a thermal decomposition to give a simple alkyl radical—an assumption independently made to explain other kinetic properties of the reaction (Rice and Herzfeld 1934). The longer the life of the complex radical the more it is exposed to nitric oxide and the smaller the amount of this gas required to produce a given degree of inhibition. Table 4 shows that in this respect there is rather little difference between the two ethers, but that slightly less nitric oxide is required to inhibit the reaction of the D-compound; this means that the life of the complex radical which has to suffer the spontaneous decomposition is slightly increased by putting deuterium in place of hydrogen. One might have expected a rather greater difference.

TABLE 4. AMOUNT OF NITRIC OXIDE REQUIRED TO PRODUCE A GIVEN DEGREE OF INHIBITION. TEMPERATURE 550° C

$\frac{p-p_\infty}{p_0-p_\infty}$	mm. of nitric oxide	
	H-ether	D-ether
0·1	1·90	1·67
0·2	1·07	1·05
0·3	0·70	0·675
0·4	0·47	0·43
0·5	0·32	0·26
0·6	0·20	0·15

(E) Activation energies are given in table 5. They differ from all previously published values in that they are derived from reaction rates corrected in the manner explained in a previous paper (Davoud and Hinshelwood 1939).

TABLE 5. ACTIVATION ENERGIES FOR H- AND D-ETHERS, CORRECTED THROUGHOUT FOR ALDEHYDE FORMATION. REACTION INHIBITED BY PRESENCE OF 5 MM. OF NITRIC OXIDE

	Initial pressure mm.	E (from t_{50})	E (from t_{25})
H-ether:	400	64,100	62,700
	200	62,800	61,500
	100	62,000	61,000
D-ether:	400	69,900	67,800
	200	67,300	67,400
	100	68,200	69,500

The figures show that there is little change in E with initial pressure of ether—a fact not previously established for the inhibited reaction—and that the value of E for the D-compound is several thousand calories greater than that for the H-compound. The difference amounts to several times the probable value of the difference in zero-point energy of C—H and C—D bonds: this is not in itself surprising, since the compounds contain ten H- or D-atoms. But the difference is also greater than is needed to explain the difference in reaction rate. If this is correct, then it means that the decomposition probability of the activated deuterium compound is somewhat greater than that of the hydrogen compound. Such a result is not inexplicable: in the unimolecular reaction of a complex molecule a correct internal phase is necessary for transformation: the frequency of this depends upon the *difference* of other frequencies. If the introduction of deuterium lowers the frequencies themselves to varying extents, certain differences may be changed in either direction. If the experimental data were clearer cut and the whole system a simpler one, this result might indeed be taken as evidence of the internal complexity of the transformation process. In the circumstances the result and its possible meaning are mentioned without insistence.

Discussion and summary

On the basis of the current hypothesis that the total decomposition consists of the two consecutive molecular reactions I and II, and the chain reactions 1, 2, 3 and 4 (modified in accordance with the views of Rice and Teller (1938) that radicals attack hydrogen rather than carbon), it will be of interest to see whether a rough sequence can be established showing which are most and which least affected when hydrogen is replaced by deuterium.

I $C_2H_5.O.C_2H_5 = CH_3.CHO + C_2H_6$.

II $CH_3.CHO = CH_4 + CO$.

1 $C_2H_5.O.C_2H_5 = CH_3 + CH_2O.C_2H_5$.

2 $CH_3 + C_2H_5.O.C_2H_5 = CH_4 + CH_2.CH_2.O.C_2H_5$.

3 $CH_2.CH_2.O.C_2H_5 = CH_3.CHO + C_2H_5$.

4 $C_2H_5 + C_2H_5.O.C_2H_5 = C_2H_6 + CH_2.CH_2.O.C_2H_5$.

The probable order of decreasing effect appears to be 2 and/or 4, I and II, 3, 1.

Placing 1 last is an initial assumption based upon the fact that no C—H or C—D bond is involved. Next comes 3 which is little influenced, the estimate being based upon the conclusions of section (D). Given that 1 and 3 are low in the series, 2 and/or 4 must come above I and II, since the chain reaction is more sensitive than the molecular reaction to D/H replacement (section (A)). We are not in a position to deal separately with 2 and 4. Under the conditions of the experiments I and II are about equally sensitive (section (C)).

The influence of deuterium

Hydrogen has a specific effect in maintaining the unimolecular rate constant in the thermal decomposition of diethyl ether at low pressures

(Mitchell and Hinshelwood 1937). To further a comparison between ordinary and fully deuterated ethers, the influence of deuterium on the latter has been investigated.

The measurements were made at 550° C.

Pressure changes were followed with a bourdon, employing an optical lever for magnification.

Reaction chains were eliminated by 5 mm. of nitric oxide.

The initial pressure of ether was 20 mm.

Deuterium was prepared by the action of sodium on heavy water.

The results, given in table 6*a*, show clearly that the presence of 500 mm. of deuterium increases the rate to the value found for an initial ether pressure of 500 mm.

TABLE 6*a*. VARIATION OF t_{25} FOR FULLY DEUTERATED ETHER, WITH PRESSURE OF ADDED DEUTERIUM, IN THE PRESENCE OF 5 MM. OF NITRIC OXIDE. TEMPERATURE 550° C. INITIAL ETHER PRESSURE 20 MM.

mm. of deuterium	t_{25} sec.	mm. of deuterium	t_{25} sec.
0	915 930	300	514 529
187	618 657	400	475
		500	475 508

TABLE 6*b*. VARIATION OF t_{25} FOR HYDROGEN ETHER, WITH PRESSURE OF ADDED DEUTERIUM, IN THE PRESENCE OF 5 MM. OF NITRIC OXIDE. TEMPERATURE 520° C. INITIAL ETHER PRESSURE 20 MM.

mm. of deuterium	t_{25} sec.	mm. of deuterium	t_{25} sec.
0	3500 3280	200	2340
		216	2370
100	2907 3040	330	1540
		400	1480 1410

It was thought worth while to investigate again the influence of deuterium on ordinary ether at low pressure, in the temperature region 520–525° C. Mitchell and Hinshelwood (1937) had concluded from their results that deuterium had no effect on the rate of reaction; whereas the present work leads to the conclusion that deuterium has a marked effect in increasing the rate of reaction—as indeed might have been expected.

The results are given, in tables 6*b*, *c*, along with the earlier results. There is no question that both sets, as experimental measurements of what actually occurred, are equally valid. There is therefore an unknown factor which influences the energy exchanges. The nature of this must be more fully explored. Further work on the subject being impracticable for the present, we think it more correct to record than to withhold these observations.

TABLE 6c. VARIATION OF t_{50} FOR HYDROGEN ETHER, WITH PRESSURE OF ADDED DEUTERIUM, IN THE PRESENCE OF 5 MM. OF NITRIC OXIDE. TEMPERATURE 525° C. INITIAL ETHER PRESSURE 50 MM.

Results found by Mitchell and Hinshelwood (1937)		Results of present investigation	
mm. of deuterium	t_{50} sec.	mm. of deuterium	t_{50} sec.
0	1940 1870	0	3265 3146
200	1953	66	2700
300	1985	175	2460
400	1973	307	2230
500	1945	388	2285
		508	2120

SUMMARY

A detailed study of the kinetics of the decomposition of fully deuterated diethyl ether has been made. The results are discussed and compared with those (already published in the Proceedings) on the hydrogen ether.

REFERENCES

Davoud and Hinshelwood 1939 *Proc. Roy. Soc.* A, **171**, 39.
Hobbs 1938 *Proc. Roy. Soc.* A, **167**, 456.
Mitchell and Hinshelwood 1937 *Proc. Roy. Soc.* A, **162**, 357.
Rice and Herzfeld 1934 *J. Amer. Chem. Soc.* **56**, 284.
Rice and Teller 1938 *J. Chem. Phys.* **6**, 489.
Staveley and Hinshelwood 1936 *Nature, Lond.*, **137**, 29; *Proc. Roy. Soc.* A, **154**, 335.

The lamellar structure of potash-soda felspars

By S. H. Chao and W. H. Taylor
Physics Department, College of Technology, Manchester

(*Communicated by W. L. Bragg, F.R.S.—Received* 13 *June* 1939)

1. Introduction

The structures of some typical members of the felspar group were determined by Taylor, Darbyshire and Strunz (1934), and an attempt was made to explain the characteristic twinnings and the nature of the lamellar intergrowths known as perthites and microperthites.

These authors emphasized that the Carlsbad, Manebach, and Baveno types of twin, which appear in monoclinic as well as in triclinic felspars, should be regarded as quite distinct from the albite and pericline types which are of frequent occurrence in the triclinic felspars. For in these last types the twinned triclinic individuals are merely simulating the higher symmetry of the monoclinic structures: thus for example in an albite twin the individuals are related by reflexion in the plane (010) which is actually a symmetry plane of the monoclinic crystal, while in a pericline twin the individuals are related by rotation about the *b*-axis [010] which is a digonal axis in the monoclinic structure. The formation of Carlsbad, Manebach, or Baveno twins is a consequence of certain special features of the structure, and is not due to the simulation of higher symmetry.

It was also suggested that the lamellae in structures of the microperthitic type might represent regions of segregation of the large potassium ions on the one hand, and of the small sodium ions on the other, within a tetrahedron framework which is essentially continuous throughout the crystal. This hypothesis is based on the fact that the lamellae lie nearly parallel to the crystallographic plane (100) containing the axes *b* and *c* which are nearly identical for the potash-felspar and soda-felspar, while the marked difference in length of the *a*-axes does not affect the "fit" of the different regions of the structure.

Until recently, however, no attempt appears to have been made to apply X-ray methods to a systematic survey of the various microperthitic structures. Ito and Inuzuka (1936) examined powder photographs of various potash-soda felspars, and Ito (1938) has now described an extremely interesting investigation of Korean moonstone; the second paper will be discussed in a later section of this paper. In a paper read before the Mineralogical Society in January 1939, and published in the *Mineralogical Magazine* in June 1939, the present authors with D. L. Smare (1939) reported the results of a general survey by single-crystal methods of a number of specimens of potash-soda felspars, mostly of the orthoclase-microperthite type, which were very kindly supplied by Dr Edmondson Spencer. The results of detailed chemical, optical, and thermal investigations of these materials have been described in three important papers by Spencer (1930, 1937, 1938).

The present paper contains an account of further work on three of Spencer's specimens. Although it is not yet possible to give anything like a complete picture of their constitution, we have now succeeded in introducing some apparent order in the classification of lamellar felspar structures, and hope that the consequent simplification may enable further rapid advance to be made.

The general survey (Chao, Smare and Taylor 1939) of orthoclase-microperthites containing various amounts, up to 60 %, of soda-felspar suggested the existence of three types of structure. The *first* is a simple monoclinic structure, and is found when the amount of soda-felspar is very small—not exceeding 10 % by weight. The *second* is a lamellar intergrowth of two components, one (corresponding to the potash-felspar) monoclinic with unit cell edges $a_1 b_1 c_1$ and angle β_1, the other (corresponding to the soda-felspar) with unit cell edge a_2 parallel to a_1 but of different length, and edges $b_2 c_2$ and angle β_2 identical with $b_1 c_1 \beta_1$. The *third* is also lamellar with two components: one corresponding to the potash-felspar, with monoclinic cell $a_1 b_1 c_1 \beta_1$, the other (soda-felspar) with a_2 parallel to a_1 but of different length, b_2 inclined to b_1 but of the same length, c_2 identical with c_1. The limiting composition which divides the second from the third structure-type is not fixed with certainty: specimen F with 21·5 % soda-felspar belongs to the second type, specimen I with 30·5 % belongs to the third type. [As in our previous paper (1939), all specimens are lettered and named in accordance with the lists in Spencer's *second* paper (1937, p. 455 and table 1)]. There is an apparently significant change in the length of the axis a_1 of the principal (potash-felspar) component in passing from the second type of structure to the third.

For the new investigation now to be described, specimen F was selected as representing the second structure-type, and specimen M for the third structure-type; specimen P was also examined since it is from the same locality as the moonstone used by Ito (1938) and in fact is assumed by Ito to be identical with his material.

2. EXPERIMENTAL DATA FOR UNTREATED SPECIMENS F, M, P

In our earlier work we examined the various materials both in the natural state and after prolonged heat treatment under specified conditions: the new experimental data, set out below, were obtained from the natural untreated materials. Chemical composition and optical properties of each specimen are taken from Spencer (1937, p. 455 and table 1). Principal axes $a_1 b_1 c_1$ refer to the potash-felspar component, subsidiary axes $a_2 b_2 c_2$ refer to the soda-felspar component. The angle β ($\sim 116°$) is approximately the same for all felspars, and is not measured directly in our experiments. A cylindrical film-holder was used throughout, so that when the axis of rotation of the crystal fragment is parallel to a crystallographic axis, the reflexions are arranged on a series of straight horizontal "layer-lines" and from the separations of these layer-lines the length of the crystallographic axis can be determined. Cu $K\alpha$ radiation of wave-length $\lambda = 1{\cdot}54$ A was used throughout.

Specimen F (Burma Blue, No. II)

The specimen shows blue schiller and microperthitic lamellar structure, and contains 18·5 % soda-felspar and 2·5 % lime-felspar. From rotation photographs with Mo $K\alpha$ radiation, and with rotation axis parallel to each of the principal axes $a_1 b_1 c_1$ in turn, axial lengths were deduced as follows (Chao *et al.* 1939): principal axes $a_1 = 8{\cdot}50$ A, $b_1 = 13{\cdot}07$ A, $c_1 = 7{\cdot}18$ A; subsidiary axis $a_2 = 8{\cdot}12$ A. The use of radiation of longer wave-length, and of small angle oscillation photographs as well as rotation photographs, reveals new detail as follows:

(i) *a-axis.* With rotation axis parallel to principal axis a_1, sharp reflexions due to potash-felspar lie on straight layer-lines, and are accompanied by subsidiary diffuse reflexions due to soda-felspar; the subsidiary reflexions are relatively very weak, usually (but not invariably) occur in close pairs connected by a streak of blackening and corresponding to a single principal reflexion, and lie *approximately but not exactly* upon a set of subsidiary layer-lines corresponding to an axis $a_2 \sim 8{\cdot}15$A. The subsidiary axis a_2 is not exactly parallel to a_1, and the appearance of small angle oscillation photographs is most easily explained on the assumption that there are *three* crystallographic a-axes: the principal axis a_1 is parallel to the rotation axis, and two subsidiary axes a_2 and a_2', of equal length 8·15 A, approximately, lie in a plane which makes an angle of $\sim 1°$ with the principal plane (001) containing a_1; the angle between a_2 and a_2' in this inclined plane is also $\sim 1°$ and a_2 and

a_2' are symmetrically inclined on either side of a_1. The relations of these axes are shown in figure 1. The measurements of these small angles are necessarily liable to be very inaccurate, and it should be emphasized that other alternative explanations may be possible.

(ii) *b-axis*. All reflexions lie accurately upon a single set of layer-lines corresponding to the principal axis b_1. Subsidiary reflexions are recognizable as rather diffuse and relatively weak satellites to many of the more intense principal reflexions; reflexions with indices $\{hkl\}$, where h is zero (and l not very large), are not accompanied by subsidiary satellites.

(iii) *c-axis*. With rotation axis parallel to principal axis c_1 the sharp potash-felspar reflexions lie on straight layer-lines, and are accompanied in nearly all cases by a pair of very weak subsidiary reflexions due to soda-felspar: the subsidiary reflexions in small-angle oscillation photographs are in positions which correspond to the existence of *two* subsidiary axes c_2 and c_2' of lengths identical with c_1 within the accuracy of our experimental method, lying in a plane inclined at ~ 1° to the principal plane (100), and with an angle (in this inclined plane) of ~ 5° between c_2 and c_2' which lie symmetrically on either side of c_1 (see figure 2). We may note that the two members of a satellite pair correspond to slightly different spacings, and that the reflexions are diffuse and linked by a well-marked band of blackening. Again we may stress that, in view of the complexity of the photographs, other explanations *may* be possible: that suggested appears to us to be simple and direct.

Specimen M (Ceylon Blue, No. III)

The specimen shows a blue schiller and microperthitic structure, and contains 40 % soda-felspar and 2·5 % lime-felspar. The following axial lengths and directions were deduced from rotation photographs taken with Mo $K\alpha$ radiation (Chao *et al.* 1939): $a_1 = 8{\cdot}65$ A, $b_1 = 12{\cdot}84$ A, $c_1 = 7{\cdot}18$ A, $a_2 = 8{\cdot}12$ A; axes b_2c_2 equal in length to b_1c_1 respectively; axes a_2c_2 parallel to a_1c_1 respectively, axis b_2 inclined to b_1 at an angle ~ 3°. The new experimental results are as follows:

(i) *a-axis*. With rotation axis parallel to principal axis a_1, principal reflexions lie on a single set of layer-lines, and are accompanied by weaker satellite reflexions due to soda-felspar. The satellite reflexions usually occur in pairs, are relatively diffuse, and are in positions corresponding to a *single* subsidiary axis a_2 of length 8·15 A approximately, approximately but not exactly parallel to axis a_1: both axes a_1 and a_2 lie in the (principal) plane (010), and the angle between them is ~1°.

(ii) *b-axis*. Subsidiary reflexions due to soda-felspar accompany the principal reflexions due to potash-felspar, each principal reflexion on a layer-line being accompanied, in general, by a pair of satellites lying one above, the other below, the layer line, and corresponding to slightly different spacings both of which are smaller than that of the principal reflexion: principal reflexions $\{hkl\}$ with l zero have a single satellite lying on the layer-line, those with h zero have two satellites with spacings much more nearly equal to the principal spacing than in the general case. In oscillation photographs taken with a very minute fragment of crystal, a fine-structure is clearly visible *within* each of the best-defined subsidiary reflexions: for the present we neglect this fine-structure, and consider the subsidiary reflexions as pairs linked by a faint band of blackening.*

From the arrangement of the subsidiary reflexions we deduce the existence of two subsidiary axes b_2 and b_2', each of length equal to b_1 within our experimental accuracy, inclined symmetrically on opposite sides of b_1 at angles which are $\sim 2^\circ$ and $\sim 3\frac{1}{2}^\circ$ when projected on the (principal) plane (001), and on a plane perpendicular to (001) and containing axis b_1, respectively (figure 3).

The arrangement of reflexions is such that any photograph with oscillation about the principal axis b_1 possesses a horizontal symmetry plane at right angles to the axis.

(iii) *c-axis*. Subsidiary reflexions lie upon a single set of layer-lines which are almost exactly superposed on the principal layer lines: the axes c_1 and c_2 are equal in length, both lie in the plane (010), and the angle between them does not exceed $0{\cdot}5^\circ$ approximately.

Specimen P (Korea Blue)

The crystals are glass-clear, show faint blue schiller, and have abnormally low optic axial angle for the chemical composition—51·5 % soda-felspar, 0·5 % lime-felspar—resembling *sanidine* in this respect. This specimen has not previously been examined by us.

X-ray photographs with rotation or oscillation about all three (principal) axes are identical in every respect with corresponding photographs from specimen F, except that subsidiary reflexions are relatively more intense in specimen P as would be expected in view of the greater soda-felspar content.

---

* This fine structure is also visible in one or two reflexions in *a*-axis photographs.

3. INTERPRETATION OF EXPERIMENTAL DATA FOR UNTREATED SPECIMENS F, M, P

The experimental data set out above in detail are discussed in the following paragraphs:

(i) *Comparison with previous investigation of specimens F and M*

The new data confirm in a general way the results previously obtained for specimen M, but show that principal and subsidiary axes a_1 and a_2, and c_1 and c_2, are not *exactly* parallel as was previously stated: the interaxial angles are found to be $\sim 1^\circ$ and $\sim 0{\cdot}5^\circ$ respectively. The lengths of principal axes, measured (without any attempt at great accuracy) on the new photographs, agree with the earlier measurements within the accuracy of the new determinations; they are $a_1 = 8{\cdot}65$ A, $b_1 = 12{\cdot}85$ A, $c_1 = 7{\cdot}15$ A (all $\pm 0{\cdot}05$A).

For specimen F the new experiments reveal similarly that a mean axis a_2 is inclined to a_1 at an angle of $\sim 1^\circ$, and confirm that b_2 coincides exactly in length and direction with b_1, by contrast with the corresponding inclined b axes in specimen M. It is now revealed for the first time that there are probably *two* equal subsidiary axes a_2 and a_2' which are mutually inclined at $\sim 1^\circ$, and *two* equal subsidiary axes c_2 and c_2' mutually inclined at an angle of 5–6°, and each inclined at $2\frac{1}{2}$–3° to axis c_1. [The probable reason for the failure to discover the existence of subsidiary c-axes in the previous investigation is as follows. In a-axis rotation photographs the subsidiary reflexions are concentrated in regions near a set of layer-lines corresponding to an axis a_2 of length 8·15 A (approximately) and parallel to a_1: in spite of this the subsidiary layer-lines are very weak by comparison with the principal layer-lines. In c-axis photographs, owing to the greater tilt of the subsidiary axes with respect to the principal axis, the reflexions are spread over a much wider space in the photographic film and are correspondingly harder to detect. We may say with some confidence that if the "F type" of lamellar structure had persisted in specimens I, J, etc. (which are actually of the "M type") the increased soda-felspar content would have revealed clearly the existence of the subsidiary c-axes.] The lengths of the principal axes are $a_1 = 8{\cdot}55$ A, $b_1 = 12{\cdot}95$ A, $c_1 = 7{\cdot}20$ A (all $\pm 0{\cdot}05$ A) which may be compared with 8·50, 13·07, 7·18 A, the values obtained from the earlier measurements.

(ii) *Structural relationship of the lamellae*

We have to explain two distinct sets of experimental data, given by specimens F and P, and by specimen M, respectively. In both cases it has been shown that in order to account for the disposition of the reflexions observed it is not sufficient to assume a single set of subsidiary axes $a_2b_2c_2$ in addition to a single set of principal axes $a_1b_1c_1$; for F and P we must assume axes $a_1b_1c_1$ and $a_2a_2'b_2c_2c_2'$, for M we must assume axes $a_1b_1c_1$ and $a_2b_2b_2'c_2$, at the various angles of inclination given in § 2 of this paper. It is therefore necessary to discuss two relationships: that between principal axes and subsidiary axes, and that between the two sets of subsidiary axes, within the same lamellar crystal.

All the data so far obtained* are explained if it is assumed that in all cases the potash-felspar is present as a truly monoclinic component, and that the soda-felspar is present in the form of lamellae which are triclinic and arranged in the mutual orientation characteristic of the pericline twin-law in specimens F and P, and in the orientation characteristic of the albite twin law in specimen M. The X-ray method fails to distinguish between a structure in which there is actual twinning (according to a given law) within each single lamella, and one in which each lamella is untwinned, but in which on the average equal numbers of lamellae assume the relative orientation characteristic of the given twin law. In view of Spencer's statement (1937, pp. 485, 486) that he has not obtained any optical evidence of twinning on the albite law within the soda-felspar lamellae of any microperthite, the second alternative seems more probable. The arguments which follow, with regard to the geometry of the composite structure, are the same in either case.

In the first place, it appears to be established that the potash-felspar is dimensionally and structurally monoclinic in all orthoclase structures so far examined: for the principal axes $a_1b_1c_1$ are never duplicated as the subsidiary axes are, and there is a plane of symmetry in X-ray oscillation photographs about the b_1-axis.

Secondly, when twinning takes place according to the albite law the two triclinic individuals of the twin are related by reflexion across the plane (010), so that axes a, c of the first individual are parallel to axes a', c' of the second individual, but axes b and b' are inclined at an angle calculable in terms of the crystal angles $\alpha\beta\gamma$; in the case of albite itself the angle bb' is $8\frac{1}{4}°$, which projects into $\sim 3\frac{1}{2}°$ on the mean plane (001), and into $\sim 7\frac{1}{4}°$ on the plane perpendicular to this and to the common plane (010). These relations between axial directions correspond with those observed in the ***subsidiary*** (soda-felspar) reflexions in specimen M, which are referred to single axes a_2 and c_2 and to a pair of axes b_2 and b_2', with an angle between

---

* With the exception of the fine structure observed within the subsidiary reflexions in b-axis photographs of specimen M (vide p. 61).

b_2 and b'_2 which projects into ~ 4° on the (mean) plane (001) and into ~ 7° on the perpendicular plane (figure 3).

Thirdly, triclinic crystals twinned on the pericline law are related by hemitropy about the b-axis [010], so that axes b, b' of the two individuals are parallel, axes a, a' lie in the (common) plane (001) at an angle (180°–2γ), axes c, c' lie in the (common) plane (100) at an angle (180°–2α); in the case of albite these angles are 3° 43′ in (001) and 8° 6′ in (100) respectively. The *subsidiary* reflexions in specimens F and P are arranged in precisely this way (figures 1, 2), though the observed angles differ from those of albite; thus there is a single axis b_2; axes a_2 and a'_2 lying in the (subsidiary) plane (001) and inclined at ~ 1° in that plane, and axes c_2 and c'_2 lying in the (subsidiary) plane (100) and inclined at ~ 5° in that plane.

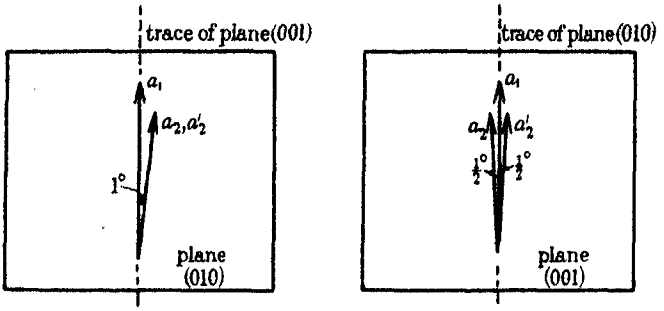

FIGURE 1. Relative orientation of principal and subsidiary a-axes in specimen F. In the left-hand diagram the axes are seen in projection on the (principal) plane (010), *in the right-hand diagram in projection on the (principal) plane (001) which is at* right angles to (010). All angles are exaggerated in the diagrams.

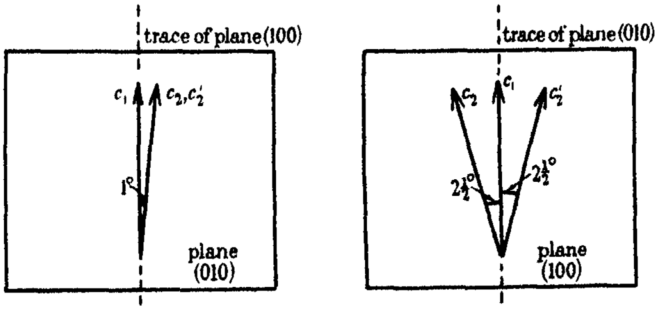

FIGURE 2. Relative orientation of principal and subsidiary c-axes in specimen F. *The axes are seen in projection on the (principal) planes (010) and (100) in the left-hand* and right-hand diagrams respectively.

The discussion of the precise relationship between the monoclinic potash-felspar and the soda-felspar is postponed to a later section.

(iii) *The soda-felspar lamellae*

The hypothesis advanced above has the merit of essential simplicity, especially if it is found that the structure of the soda-felspar lamellae is the same in both "F" and "M" types of microperthitic intergrowth with potash-felspar. At the moment we are unable to decide with certainty whether this is the case, since the only photographs available for comparison are twin photographs in which the twin laws are different, and in any case the differences (if any) between the two lamellar soda-felspar structures must be small. On general grounds we should expect only *one* soda-felspar structure, common to both "F" and "M" types of microperthite, and identical with ordinary albite. We are attempting to secure decisive experimental evidence on this point, but in the meantime we may summarize such evidence as is already available.

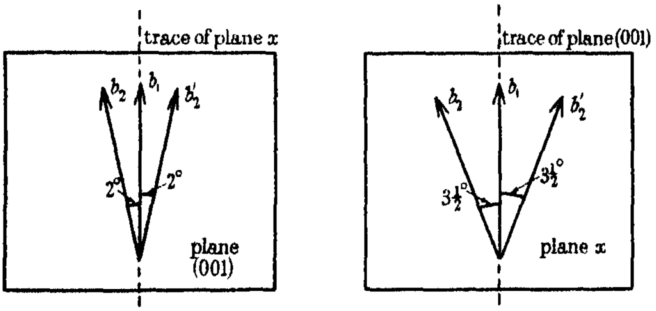

FIGURE 3. Relative orientation of principal and subsidiary b-axes in specimen M. In the left-hand diagram the axes are seen in projection on the (principal) plane (001), and in the right-hand diagram in projection on a plane x which is at right angles to (001) and contains the principal axis b_1.

First it is clear, both from our previous results (1939) and from the relative intensities of the satellite (soda-felspar) reflexions in the new photographs, that the structure of the soda-felspar lamellae is on the whole very similar to the potash-felspar structure and to the albite structure; it follows therefore that the difference between soda lamellae of the "F" type and those of the "M" type must be small if it exists. It is, however, a small difference of precisely this kind which may be significant in an attempt to discover why the F or M type of intergrowth shall be formed in a given case.

Secondly, we may note that in the M structure the projections of the angle between b_2 and b'_2 on the plane (001) and on the plane x perpendicular to it are (by observation) $\sim 4°$ and $\sim 7°$ respectively, compared with corresponding angles $\sim 3\frac{1}{2}°$ and $\sim 7\frac{1}{4}°$ for ordinary albite twinned on the albite law; whereas in the F structure the observed angles between a_2 and a_2' in the plane (001), and between c_2 and c_2' in the plane (100) are ~ 1° and ~ 5° respectively, compared with corresponding angles ~ 3½° and ~ 8° for ordinary albite twinned on the pericline law. If the observed angles are accurate within ± 1°, two conclusions may be drawn: that the F and M soda-felspar lamellae are slightly different in unit cell (angular) dimensions, and that the M structure may be identical with albite, whereas the F structure is not. It should be emphasized that we do not consider that the observed angles are measured with sufficient accuracy to establish either of these conclusions with certainty.

Thirdly, we may refer to our own earlier comparison of a rotation-photograph of pure albite about the a-axis, with the appearance of the subsidiary layer lines in a rotation photograph of an orthoclase-microperthite about the (principal) a_1-axis: it is stated (Chao *et al.* 1939, p. 341) that in layer-lines corresponding to $h = 0, 1, 2$ there are no significant differences, whereas in layer-lines for $h = 4, 5$ there are quite obvious differences. We now know that the subsidiary axis a_2 (or axes a_2 and a_2') in the microperthite are not exactly parallel to a_1 but inclined to it at ~ 1°: in the above experiment we therefore compare an albite photograph for rotation about the true a-axis, with a photograph in which the rotation axis is inclined at ~ 1° to the subsidiary axis or axes. Purely geometrical factors, due to this slight difference in orientation, *may* be responsible for the differences observed in the outer layer-lines ($h = 4, 5$), though we think it more probable, on the whole, that there is some slight but real structural difference.

(iv) *Factors which influence the soda-felspar orientation*

The earlier general survey suggested that microperthitic orthoclase felspars with more than approximately 30 % soda-felspar belong to the structure-type of which M is characteristic: we have to discuss the factors which may influence the orientation of the soda-felspar lamellae with respect to the potash-felspar, in an attempt to discover why, with the increase in soda-felspar content, the structure type changes from F to M, and why in specimen P the arrangement reverts to the low-soda F type. The following facts seem to us to have some bearing on the problem:

(*a*) Spencer's physical tests (1937) established a general difference in behaviour of an orthoclase-microperthite according as it contains less than, or more than, 30 % of soda-felspar: in particular it appears that in microperthites with less than 30 % soda-felspar, a short period of heating at ~ 800° C is sufficient to cause complete solution of the soda-felspar; with a greater percentage of soda-felspar, a longer period at a higher temperature is necessary.

(*b*) Specimen P, with ~ 50 % soda-felspar, differs from the other high-soda microperthites in that it is (like sanidine) glass clear, and has an abnormally low optic axial angle of ~ 40° compared with ~ 80° for normal microperthites of similar composition (Spencer 1937).

(*c*) Our earlier survey revealed a slight but apparently real increase in the length of the *principal* (potash-felspar) axis a_1 in passing from F to M types (Chao *et al.* 1939, figure 1). This is confirmed in the new examination by the figures given in § 3, para. (i), for the individual specimens F and M. It is highly significant that the principal axial lengths of specimen P, which contains *more* soda-felspar than specimen M, are identical with those of specimen F, within our experimental accuracy.

These data are not in themselves sufficient basis for a complete theory of the relation between the soda-felspar and the potash-felspar regions in a microperthitic orthoclase—thus, for example, we lack definite information regarding the identity or otherwise of the soda-felspar lamellae in F and M types of structure, and regarding their relationship to albite—but we venture to make the following tentative suggestion as a working hypothesis which we hope to be able to test in the course of our further work.

The pure potash-felspar structure is monoclinic. An amount of soda-felspar up to approximately 10 % can be held in solution by the monoclinic structure without any significant change in dimensions and of course without separation of lamellae.

If the amount of soda-felspar exceeds 10 % but is less than 30 %, the *excess* separates in microperthitic lamellae which are triclinic but with angles α and γ very close to 90° as in the monoclinic structure. The a_2-axis differs appreciably in length from a_1, and in order to make it possible to preserve a continuous tetrahedron framework throughout the crystal (in accordance with the hypothesis originally advanced by Taylor *et al.* (1934) it is necessary for individual soda-felspar lamellae of these dimensions to be oriented as in the pericline type of twinning. The monoclinic symmetry of the potash-felspar ground mass thus constrains the small amount of separated soda-felspar to assume a form which departs only slightly from monoclinic symmetry, although the a_2-axis assumes the shorter length apparently characteristic of all soda-felspars. At the same time the *principal* axis a_1 is slightly shortened (by about 0·05 A) under the influence of the soda-felspar. This is the F type of structure.

If the amount of soda-felspar exceeds 30 %, the *whole* of the soda-felspar separates out as lamellae; the monoclinic axis a_1 is lengthened, and the soda-felspar is present in sufficient amount to demand a triclinic structure closely resembling or identical with albite in which, in particular, angles α and γ depart appreciably from 90°. To accommodate these lamellae within the continuous tetrahedral framework, they must be oriented as in twins on the albite law. This is the M type of structure.

The case of specimen P fits naturally into this scheme. The general physical properties, and the abnormally low optic axial angle in particular (Spencer 1937) indicate that the state of this moonstone approaches that of sanidine. Now the reduced optic axial angle of sanidine is a consequence of a structural change which results in the retention of the soda-felspar in solid solution with the potash-felspar, the symmetry of the structure remaining monoclinic: it may be supposed that something like one-half of the soda-felspar is held in solution in this way in specimen P, with consequent reduction of the principal axis a_1 to the observed value (8·55 A) by contrast with the value 8·65A for normal microperthites of similar composition. The felspar is now in a state which corresponds structurally to that of specimen F, i.e. it contains a monoclinic component with axis a_1 of the same length, and an amount of soda-felspar which can be accommodated in lamellae oriented in pericline-twin orientation as in F.

Further work may enable conclusions to be drawn as to the validity of these speculations, which are, admittedly, based on incomplete experimental data.

4. THE EVIDENCE FOR THE EXISTENCE OF MONOCLINIC SODA-FELSPAR

In his very interesting paper Ito (1938) describes the results of an examination of a Korean moonstone from the same locality as Spencer's specimen P, and concludes that this crystal represents an intergrowth of sanidine with a corresponding high-temperature *monoclinic* form of soda-felspar, the *b*-axes of the two components being parallel, and the only dimensional difference being in the *a*-axis, which he quotes as 8·45 A and 7·94 A for the two components respectively.

Ito's conclusions are based on a considerable body of experimental data, and we originally undertook our examination of specimen P in the confident expectation that we should fully confirm Ito's results. As will be clear from the account given, our conclusions for specimen P differ radically from those of Ito for his material.

Two explanations of the apparent disagreement may be suggested. In the first place, the two materials may really be different. They are from the same locality, and it is implied by Ito that they are in fact identical since he quotes Spencer's analysis and applies it to his own specimens, but since neither chemical nor optical tests were applied to Ito's material, it is possible that it does differ from Spencer's; in this case there is not necessarily any difficulty in accepting both Ito's conclusions and ours, since they apply to two distinct materials.

If, however, we suppose that Ito's material and ours are substantially the same, it becomes necessary to examine whether it is possible to explain Ito's experimental data on the basis of the suggestions already advanced in this paper.

First we note that our b-axis oscillation photographs of specimen P show *single* layer-lines, but doubled reflexions on these layer-lines, exactly similar to Ito's figure 1*a* (1938, p. 298); and that reflexions of type $\{okl\}$, in a b-axis oscillation photograph of P, are single when l is small as in Ito's figure 4*a* (1938, p. 301); from this we conclude that so far it is not *necessary* to assume the soda-felspar to be present in monoclinic form, though we agree that this would be the most natural explanation of this limited amount of data.

Ito supports his conclusions by Sauter and Weissenberg photographs, with rotation about a- and b-axes respectively: we have no such photographs of specimen P for direct comparison, but it seems to be possible to apply our hypothesis to explain the appearance of Ito's published photographs. Consider first the Sauter photograph (Ito 1938, p. 303, figure 6*a*): for this the crystal rotates about the a-axis, and reflexions lying on the zero layer-line ($h = 0$) are registered on the flat circular rotating film: even with Mo $K\alpha$ radiation, only those reflexions with $k \ngtr 8$ or $l \ngtr 4$ appear to be included in the photograph. Now our measurements show that the two subsidiary axes a_2, a_2' are inclined at approximately 1° to the principal axis a_1, and as a consequence the zero layer-line of an a-axis photograph is very nearly *single*, especially in the central region which is that covered by Ito's Sauter photograph; moreover, in our oscillation photographs principal reflexions, where accompanied by close satellites, lie *between* the two satellites of a pair; we therefore consider it unlikely that the duplication of reflexions could be detected with large diffraction spots such as are shown in Ito's diagram.

Consider next Ito's Weissenberg photographs, with cobalt radiation, and rotation about the b-axis: as we have previously described, and as shown in figures 1 and 2, the subsidiary axes a_2, a_2' coincide when seen in projection along b, and so do c_2 and c_2', and the projections of these two axial directions are inclined at only 1° in each case to the axes a_1 and c_1. It follows that reflexions $\{hol\}$ from *both* triclinic components will coincide, and give the single set of subsidiary reflexions registered in Ito's figure 7; similarly *to a* *first approximation* reflexions $\{h2l\}$ from the two triclinic components will coincide, since such planes are not very steeply inclined to the b-axis (cf. Ito's figure 8).

Passing to Ito's general arguments, we may point out that he does not consider in detail the case of a crystal comprising a monoclinic component and a twinned triclinic component, except to remark (p. 303) that such a structure is impossible since it would require certain reflexions to be tripled, an effect which he does not observe. This is, however, precisely the effect which we do observe with our specimen P.

Summarizing, we may perhaps conclude that although Ito's experimental evidence for the existence of a monoclinic soda-felspar appears to be very conclusive, it may be possible to account for his data in terms of the hypothesis which explains our own data. Further work is needed to settle this point.

5. Experimental data for specimen P after heat treatment

To complete our examination of this material, we have taken oscillation photographs, about all three axes, of specimens which have been homogenized by prolonged heating at high temperatures (300 hr. at 1075° C) (Spencer 1937).

In each case the reflexions lie on single sets of layer-lines, corresponding to axial lengths $a = 8{\cdot}35\,\text{A}$, $b = 12{\cdot}95\,\text{A}$, $c = 7{\cdot}15\,\text{A}$ (all $\pm 0{\cdot}05\,\text{A}$), values which are of the order expected from our earlier investigation of heat-treated materials.

6. Conclusion

The principal members of the felspar group are pure potash-orthoclase ($KAlSi_3O_8$), the rare barium felspar celsian ($BaAl_2Si_2O_8$), albite ($NaAlSi_3O_8$), and anorthite ($CaAl_2Si_2O_8$). In addition to these, there are potassium-barium felspars (hyalophanes), sodium-calcium felspars (plagioclases), and potassium-sodium felspars (orthoclases, microclines, sanidines, anorthoclases); many of these materials contain in addition to large proportions of two of the principal members a relatively small quantity of a third member. A complete understanding of the felspar problem therefore requires the elucidation of a complex phase system, and for this it is necessary to apply all possible physical and chemical methods of enquiry.

The application of X-ray methods has, up to the present, settled two main points. It has shown (Taylor *et al.* 1934) that the potassium and barium felspars, and the mixed potassium-barium felspars, have closely similar structures because the cations are of similar sizes, while the sodium-, calcium-, and sodium-calcium felspars are also closely similar but differ from the first group to a degree which represents the difference in sizes of cations. It has also enabled the general features of the atomic arrangements in the two groups of structures to be described in some detail, proving incidentally that the main structural scheme is the same in all—as had always been assumed.

Perhaps of greater importance than these are the special problems of the two isomorphous series of sodium-calcium and potassium-sodium felspars. It has been suggested by Taylor *et al.* (1934) that the plagioclases do not form a simple isomorphous series between albite and anorthite as end-members, and further work now in progress in this laboratory confirms this view; a comprehensive classification cannot yet be attempted.

In attempting in the present paper a classification of the effects observed in the potash-soda orthoclase-microperthites, we believe that we are beginning to find in the experimental data clues to the wider problem of the constitution of potash-soda felspars in general. It is still necessary to examine the microclines, and to decide various points left unsettled by the present work—such as the identity or otherwise of the "F" and "M" types of soda-felspar lamellae, and their relationship with albite—but it should be possible to do this without very serious difficulty. It will then be necessary to face new problems, viz. the *reason* for the existence of the various structures including lamellar structures on the one hand, and homogeneous or "sanidine" structures on the other, and the factors which determine the appearance of one or other under given geological conditions. Directly connected with this is the structural interpretation of the changes observed as a consequence of specified heat treatments (Spencer 1930, 1937): a beginning has been made (Chao *et al.* 1939), and further work is now in hand.

It is clear that we are here concerned with physical problems of a type which have recently been much discussed, viz. changes within the solid state. The homogenization of potash-soda felspars which can be brought about by prolonged heating at temperatures near the melting point (Spencer 1937) probably represents both a diffusion of cations through an alumino-silicate framework, to give a disordered (random) arrangement, and another change, of unknown nature, which prevents the ordering process from taking place on cooling through the normal exsolution temperature range. (Similarly in the plagioclase series there are effects which receive their most simple explanation in terms of some kind of "superlattice" behaviour, now well known in alloy systems: our investigation of the plagioclases is not yet at the stage where generalization is possible.) It seems that the next step must be the detailed examination of the structures of the various components of the potash-soda felspars; this will confirm the hypothesis advanced in the present paper, or perhaps modify it, and will at the same time provide the data necessary for the precise investigation of the changes in atomic arrangement which accompany the changes observed externally on examination by ordinary physical (particularly *optical*) methods.

One of us (S. H. C.) is indebted to the Government of the Province of Honan, China, for the grant of a Scholarship during the tenure of which this work was carried out.

SUMMARY

A previous general survey of orthoclase-microperthites suggested the existence of different types of lamellar structure according as the proportion of soda-felspar is less than or greater than 30 % approximately. A new and more detailed examination confirms this, and suggests that the low-soda structure comprises monoclinic potash-felspar with triclinic soda-felspar lamellae in the mutual orientation characteristic of pericline twins, while the high-soda structure comprises monoclinic potash-felspar with triclinic soda-felspar lamellae oriented in accordance with the albite twin-law. The constitution of the soda-felspar, and the bearing of the new data on the general theory of microperthitic structures, are discussed.

An examination of a Korean moonstone, apparently identical with material in which Ito claims to have established the existence of *monoclinic* soda-felspar, reveals a lamellar structure of the low-soda type described above. Ito's results are discussed.

REFERENCES

Chao, Smare and Taylor 1939 *Miner. Mag.* **25**, 338.
Ito 1938 *Z. Kristallogr.* **100**, 297.
Ito and Inuzuka 1936 *Z. Kristallogr.* **95**, 404.
Spencer, E. 1930 *Miner. Mag.* **22**, 291.
— 1937 *Miner. Mag.* **24**, 453.
— 1938 *Miner. Mag.* **25**, 87.
Taylor, Darbyshire and Strunz 1934 *Z. Kristallogr.* **87**, 464.

The scattering of mesotrons in metal plates

By J. G. Wilson
University of Manchester

(*Communicated by P. M. S. Blackett, F.R.S.—Received 14 August* 1939)

[Plate 1]

1. Introduction

Measurements by Blackett and Wilson (1938) showed that the scattering of cosmic-ray particles in metal plates was in approximate agreement with the simple theory then available, at least for energies less than 2×10^9 e-volts. This result provided important evidence as to the nature of the cosmic-ray particles, for it tended to confirm the view that the penetrating particles were much heavier than electrons, rather than the alternative assumption that the particles were electrons for which radiative energy losses were suppressed at high energies.

Recently, Williams (1939) has given a critical development of the theory of scattering of very energetic particles in the atomic field. This treatment leads to a more accurate value of the theoretical Coulomb scattering and shows that, for cosmic-ray scattering experiments, a fairly sharp separation in angular range is to be expected between scattering in the Coulomb field of the scattering atom and that arising from the short-range interaction between the incident particle and the separate nuclear particles. Accurate measurements of scattering therefore offer a method of estimating the magnitude of the short-range interaction of mesotrons with neutrons or protons. Williams, for example, shows that our previous measurements indicate a mesotron-proton (neutron) interaction decidedly less than that of slow neutrons with protons.

The present work incorporates the more accurate of our previous measurements and extends these to show the close agreement of mean scattering angle, and of distribution of scattering angles, with the theory of the main electrical (Coulomb) scattering. These measurements, together with a more general survey of a large number of track photographs unsuitable for accurate measurement, also lead to an estimate of the interaction cross-section of mesotrons with the constituent nuclear particles.

2. THE MEASUREMENT OF SCATTERING

The technique of accurate measurements of scattering of cosmic ray particles at a metal plate in an expansion chamber has been described in detail in our earlier work. The upper limit of energy has been taken at 2×10^9 e-volts and so excludes the region for which our earlier measurements indicated a possible anomaly, but for which the accuracy of experiment is low.

As far as possible electrons have been excluded from the measurements. For the tracks passing through a 2 cm. plate of gold this exclusion is complete (Wilson 1939, § 4); for other scattering plates all particles with $E_c < 2 \times 10^8$ e-volts are omitted and hence the total number of electrons remaining must be negligible. Protons cannot be similarly excluded except at low energies where they ionize heavily. However, the percentage of protons in the penetrating beam is small, probably less than 10 %, and the effect of a proton component of this order of magnitude is considered in § 7 (figure 2) and is shown to be negligible. The measurements therefore refer almost exclusively to mesotrons.

The accuracy of measurement, and hence of the comparison with theory, cannot be stated with certainty. The observations of scattering angle are made to 0·1°, and the mean value for several independent settings on the same track is probably accurate to within 0·05°. Since for the majority of the tracks used the mean scattering angle is 1–2°, this corresponds to a probable random error of measurement of less than 5 %, and leads to no appreciable systematic error in the arithmetic mean scattering. The precision of the measurements is limited by residual distortions, which are largest near the scattering plate, and by the fact that the larger clusters of ionization, which are particularly conspicuous at small magnifications, lie beside, but not necessarily exactly on, the direct trajectory of a particle. These factors make it necessary to determine the direction of the trajectory over a length for which the curvature in the magnetic field is appreciable. The individual measurements of energy are subject to considerable random errors (7 % at 10^9 e-volts), but, over the energy range used, these random errors do not lead to an appreciable systematic error in the product $\beta E_c \theta$ (see § 4).

The main source of systematic error lies probably in the value of the magnetic field. The field falls off considerably towards the edge of the chamber, and the length of track lying in this peripheral region varies according to the position of the track in the chamber. The mean effective value of the field which has been used is probably uncertain to about 3 %.

The effective magnification of the photographs also varies by 3 or 4 % between tracks at the extreme front or extreme back of the illuminated part of the chamber, but the possible variation of the adopted mean value is very much smaller than the uncertainty of field.

The measured mean scattering, $\overline{\beta E_e \theta}$, is therefore probably accurate, apart from statistical errors, to within 3 %.

3. EXPERIMENTAL RESULTS

The results tabulated in table 1 give measurements for four different scattering plates—1 cm. lead, 0·3 cm. lead, 2 cm. copper, and 2 cm. gold. The tracks with the gold plate are all new measurements, while most of the remainder are taken from our previous work, having been selected for the conditions given in § 2. In the second column, the number of tracks measured is shown, and in the third, the mean value of $\beta E_e \theta$, where $E_e \equiv 300 H\rho$ is measured in 10^9 e-volts and θ, the projected angle of scattering in the plane of the chamber, is measured in degrees. The theory (§ 4) shows that it is this quantity $\beta E_e \theta$, which is the measure of the multiple scattering. The value of β used corresponds to a mesotron mass $\mu = 180 m_0$. The last two columns give the direct comparison with the theoretical mean electric scattering when the finite size of the scattering nucleus is taken into account (§ 4), and for the less exact theory in which the nucleus is treated as a point charge.

TABLE 1. MEAN ANGLE OF MULTIPLE SCATTERING OF MESOTRONS IN METAL PLATES

2×10^8 e-volts $< E_e < 2 \times 10^9$ e-volts

Scattering material	No. of particles	Mean scattering $\bar{\theta} = \overline{\beta E_e \theta}$ (degrees × 10^9 e-volts)	$\bar{\theta}/\bar{\theta}_{\text{th}}$ (finite nucleus)	$\bar{\theta}/\bar{\theta}_{\text{th}}$ (point nucleus)
1 cm. lead	55	0·91	1·01 ± 0·06	0·91 ± 0·06
0·3 cm. lead	15	0·48	1·00 ± 0·13	0·90 ± 0·12
2 cm. copper	25	0·73	0·98 ± 0·10	0·91 ± 0·09
2 cm. gold	90	1·75	1·06 ± 0·05	0·95 ± 0·05
Total	185	—	1·033 ± 0·035	0·931 ± 0·033
Total $\theta < 5\bar{\theta}$	184	—	1·003 ± 0·035	0·906 ± 0·033

The individual measurements of multiple scattering will be shown to agree closely with a Gaussian distribution, and the probable errors of table 1 are calculated accordingly (Brunt, 1931, p. 57). The last line of the table differs from the preceding one by the omission of one track traversing 1 cm. lead, for which $E_e = 1{\cdot}5 \times 10^9$ e-volts and $\theta = 4^\circ$. This track is considered to be a case of large-angle scattering (see § 5), and is certainly not relevant to the Gaussian scattering to which the theory is applicable (table 2). The result for all measured tracks (line 6) is in much better agreement with the finite nucleus theory given by Williams than with the point nucleus theory; however, it must be noted that since both measured and theoretical values are uncertain to 2 or 3 %, the accuracy of the comparison is rather lower than is indicated by the statistical error which is given in the table.

The distribution of scattering angles of all the measured tracks is given in table 2, and the observations are compared with the theoretical Gaussian scattering in figure 1.

TABLE 2. DISTRIBUTION OF ANGLE OF MULTIPLE SCATTERING —COMBINED RESULTS FOR ALL SCATTERING PLATES

Angular range $\theta/\bar{\theta}_{\text{th}}$	Observed number of tracks	Theoretical number of tracks (finite nucleus)
0–0·5	63	56
0·5–1·0	48	49
1·0–1·5	32	37
1·5–2·0	19	22
2·0–3·0	16	17
3·0–4·0	4	2·8
4·0–5·0	2	0·24
5·0–6·0	0	0·012
6·0–7·0	1	0·0004
> 7·0	0	0·000005

The observed distribution follows closely the theoretical scattering in the shielded field of a finite nucleus. Only one particle, to which reference has already been made, falls appreciably outside the main distribution.

4. THE SCATTERING OF FAST MESOTRONS—THEORY

The detailed general treatment of this problem is due to Williams (1939), and only the main features of the results which are applicable to cosmic-ray experiments will be given here.

The scattering is considered in terms of an effective impact parameter and two separate cases are distinguished according as the impact parameter is greater or less than a value r_0, which is approximately the nuclear radius. The main observed scattering arises from a range of impact parameters greater than r_0. This is effectively scattering in the Coulomb field of the nucleus, between extreme collision distances, the upper limit being determined by the shielding of the orbital electrons, and the lower limit (r_0) by the modification of the electrostatic field within the nucleus radius. These Coulomb collisions would normally lead to an angular distribution mainly due to multiple scattering, together with a "tail" of large-angle single scattering corresponding to close collisions which do not, on the average, occur as often as once per particle in the scattering layer. Williams shows that the effect of the lower (nuclear) limiting impact parameter is to suppress completely this "tail" of single scattering and to modify slightly the magnitude, but not the form, of the multiple scattering distribution. Hence the scattering due to these more distant collisions is entirely multiple, and the distribution of observed scattering angles (i.e. the projection of the true scattering angles in the plane of the photograph) should be strictly Gaussian.

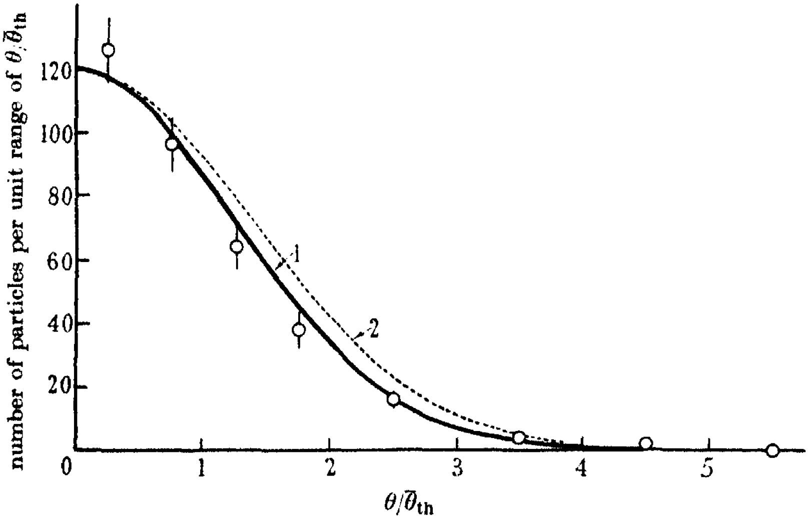

FIGURE 1. The distribution of scattering for mesotrons, $E_e < 2\times 10^9$ e-volts. (ϕ) observed number of tracks per unit range of $\theta/\bar{\theta}_{th}$, (1) theoretical curve, finite nucleus, (2) theoretical curve, point nucleus, drawn to the same maximum as (1).

We may consider the closer collisions, which correspond to a distance of approach of less than r_0, in terms of scattering due to the constituent nuclear particles. It is shown by Williams that for these collisions the scattering in the Coulomb field of separate nuclear protons is negligible, and that any scattering contribution from this region is due to the short range interaction between the scattered particle and the individual neutrons and protons in the nucleus. The short-range forces produce relatively many more large-angle deflexions than arise from the multiple Coulomb scattering. The predicted absence of a single scattering "tail" to the Gaussian of electrical scattering is thus particularly favourable to the detection of scattering due to close collisions with nuclear particles.

The mean value of the multiple electrical scattering is given by

$$\bar{\theta}_{\rm th} = (19{\cdot}5 - 3{\cdot}1 \log_{10} Z)^{\frac{1}{2}} \frac{600 Ze\sqrt{(Nt)}}{\beta E} \tag{1}$$

for scattering material of atomic number Z, thickness t and N atoms per cm.^{3}, and for a scattered particle of single charge, of electron energy $E_e \equiv 300 H\rho$ and of velocity $v = \beta c$. For 1 cm. lead, equation (1) gives the numerical value $\overline{\theta_{\rm th} E_e \beta} = 0{\cdot}90$ degrees × 10^9 e-volts. The mass of the scattered particle is effective only in so far as it determines β for a given value of E. We are not able to measure the value of β directly for the tracks used, and all of these are assumed to be mesotrons ($\mu = 180 m_0$). Protons in the energy range considered would give rise to a component of scattering of appreciably larger mean angle than that of mesotrons.

It is not possible, with the experimental data available, to discuss the *distribution* of large-angle scattering due to short range forces; in the following section an estimate of the total cross-section for this scattering is given, but the data are insufficient to give any information as to the law of force involved. These large angle collisions may conveniently be considered in terms of the energy transfer, assuming that this takes place to a single free nuclear particle.* Williams shows that for such a collision, the energy transfer ϵ is given by

$$\epsilon \sim 0{\cdot}35 \times 10^6 \, (E\phi)^2 \text{ e-volts}, \tag{2}$$

where ϕ is the deflexion at collision. The measured deflexion θ is a resultant of ϕ and the normal multiple scattering, and the most probable value of ϕ is θ.

5. EXPERIMENTAL EVIDENCE OF SHORT-RANGE MESOTRON-NEUTRON (PROTON) INTERACTION

As already mentioned, the group of accurately measured tracks (§ 3) contains only one particle falling appreciably outside the distribution of multiple scattering. For this particle the probability of occurrence as a fluctuation on the main distribution is less than 1/1000. The incident particle has an electron energy $1\cdot5 \times 10^9$ e-volts and the energy transfer to a particle of protonic mass corresponding to the whole observed deflexion is about 12×10^6 e-volts (equation (2)), an energy probably sufficient to cause disintegration of the nucleus, although there is no evidence that this has occurred.

---

* Although the mesotron collision is considered as free, the excited particle will probably lose energy to the remainder of the nucleus even if it eventually leaves the nucleus (Heitler 1938*b*).

Only one collision involving this large transfer of momentum has taken place for the traversal of about 4 cm. lead equivalent of scattering material. It follows, as has already been pointed out by Williams, that the mesotron interaction must be much less than that between protons and slow mesotrons.

A large number of additional photographs representing a total scattering layer of about 50 metres lead equivalent, but which are not suitable for accurate measurement, have also been inspected for the presence of mesotrons suffering large deflexions. It is unlikely that any deflexion as great as 10° would be undetected. Only one example of a large deflexion of this type was observed (photograph, plate 1). This shows a proton which has been ejected from the nucleus in the collision, and is considered in detail in § 6.1, where it is shown that the energy transfer is more than 10^8 e-volts. Although we have observed only one proton ejection of this type, Brode and Starr (1938), in a much larger number of traversals, observed three such events, which appear to represent a similar frequency of occurrence to our observations.

TABLE 3. ENERGY TRANSFER IN CLOSE NUCLEAR COLLISIONS BY MESOTRONS

	No. of *tracks*	Energy transfer (e-volts)	Equivalent thickness lead traversed (metres)	Cross-section per proton or neutron cm.^{2}
Wilson	1	$> 10^7$	4	4×10^{-28}
Wilson	1	$> 10^8$	50	$0\cdot3 \times 10^{-28}$
Brode and Starr	3*	$> 10^8$	~ 200	$\sim 0\cdot2 \times 10^{-28}$

* Computed from observations of proton ejection; the cross-section is that per proton and *not* per proton or neutron.

We cannot exclude the possibility that some of these particles which undergo large deflexion are protons, for although protons form only a small fraction of the whole beam, the proton-proton cross-section is probably large compared with the mesotron-proton cross-section. In table 3 are given estimates of this latter cross-section on the assumption that all the incident rays are mesotron. In view of the possible presence of protons, the real mesotron-proton cross-section may be still lower than that given in the table.

We deduce that the process of scattering of mesotrons of energy $E_e \sim 10^9$ e-volts due to short-range interaction with nuclear particles takes place with a cross-section of the order, or less than, 10^{-28} cm.^{2}. No useful estimate of the variation of this cross-section with the energy transfer is possible at present.

It has been pointed out elsewhere (Wilson 1939) that the scattering of a group of low energy mesotrons (included in the general results, tables 1 and 2) was completely normal and showed no cases of large-angle scattering. This group consisted of thirty-one particles, with $E_{\text{kin}}/\mu c^2 < 4 \cdot 1$, which penetrated 2 cm. gold, corresponding to the traversal of about 100 cm. lead equivalent. The mean observed scattering for these tracks was $\bar{\theta}_{\text{obs}}/\bar{\theta}_{\text{th}} = 1 \cdot 02 \pm 0 \cdot 10$, and the group contains no example of large-angle scattering. The efficiency with which large deflexions would be observed is determined by the geometry of the counters and of the scattering bar. We estimate that for the least favourable assumption as to the distribution of large-angle scattering—an isotropic distribution—the observations exclude the possibility that as many as 10% of the particles suffer large deflexions. When predominantly forward scattering is assumed, the possible frequency of large deflexions decreases, and, for a scattering distribution corresponding to that of the Compton effect for a comparable photon energy (given by $h\nu/mc^2 \sim E$ (mesotron)$/\mu c^2$), is less than 3%.

The range in lead for scattering due to short-range forces is thus certainly of the order of 100 cm. or more for mesotrons of a mean kinetic energy less than $4\mu c^2$. This range corresponds to a cross-section $\gtrsim 10^{-27}$ cm.^{2} per proton or neutron, and hence we observe no increase of scattering at low mesotron energies as compared with that at higher energies.

6. THE MESOTRON-PROTON (NEUTRON) INTERACTION—COMPARISON WITH THEORY

The cross-section estimated in the previous section for this interaction ($\sim 10^{-28}$ cm.^{2}) is in agreement with that deduced by Bhabha (1938, 1939) in a "*classical*" *wave theory* of the mesotron. Bhabha shows that this classical treatment should describe the mesotron interaction with heavy particles up to mesotron energies of the order of the rest mass of the heavy particle, say, 10^9 e-volts. Thus our experimental energy range does not seriously exceed the valid range of the theory.

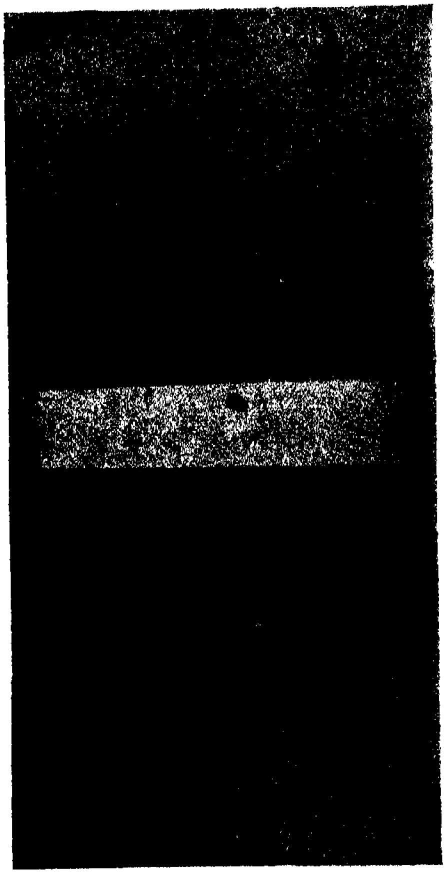

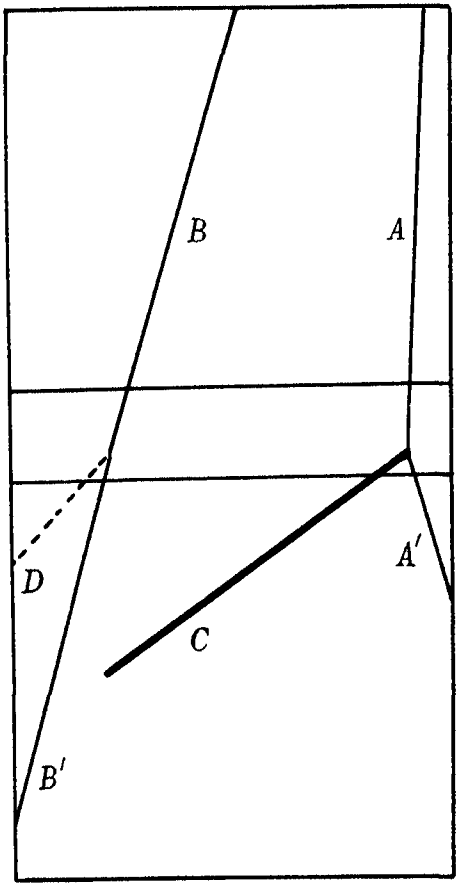
B
A
D
A′
C
B′

The well-known difficulties involved in the *quantum theory* of mesotrons allow a comparison of the observations with quantum theory only at the lowest energies ($E_{\text{kin}} \sim \mu c^2$). The calculated cross-section, which is of the order of $2\,(\hbar/\mu c)^2 \sim 10^{-25}$ cm.^{2} (Heitler 1938*a*), seems much *too* large to agree with the experimental value $\lesssim 10^{-27}$ cm.^{2} (§ 5) which is obtained for kinetic energies very little greater than the mesotron rest energy.

6.1. *Discussion of plate* 1. An example of a very close collision showing some remarkable features is given in plate 1. It is unfortunate that the photograph is technically very much poorer than the average.

The incident particle, A, which is positive with an electron energy between 10^9 and 2×10^9 e-volts, is scattered through 18° to A', and a proton, C, is ejected at an angle of 53° with the direction of A. The curvature of the proton track, C, is $1{\cdot}05 \times 10^6$ g.-cm., and hence this particle leaves the plate with an energy $0{\cdot}56 \times 10^8$ e-volts. allowing for the loss of energy traversing the plate from the point of collision, we find the initial energy of the ejected proton to be $1{\cdot}7 \times 10^8$ e-volts. The energy and momentum relations for the collision indicate very little deviation from an elastic collision.

Plate 1 also shows another more energetic penetrating particle BB' which is, as far as can be judged, copunctual and contemporary with AA' (see Wilson 1939, § 6). There is some indication that BB' produces a secondary, D, which is probably electronic. A third contemporary track appears near the top right-hand corner of the photograph, but there is no indication as to its nature. The probability that the association in time of these three tracks is the result of random coincidence is negligible. Thus we have here a definite case of associated penetrating particles in a shower. It is not clear what, if any, is the relation between such phenomena and the well-known "stars" of Blau and Wambacher (1937; Schopper and Schopper 1939) which appear to consist mainly of alpha particles and protons derived from nuclear disintegration. But the proton track C would certainly be observed as a single track in a photographic emulsion.

7. THE SCATTERING DISTRIBUTION IN THE PRESENCE OF PROTONS

For the experimental energy range, protons have a velocity appreciably less than c and therefore give rise to a rather more strongly scattered component than the predominant mesotrons. In figure 2, the modification of the tail of the curve of multiple scattering is given for proton components of 20 % and 40 % at a mean energy of $E_e = 10^9$ e-volts. The proton component, in fact, amounts probably to only about 5 % or less, and the figure shows clearly that the effect of this proportion is negligible for the number of tracks observed. The single example of large-angle scattering in the series of accurately measured photographs is also indicated in figure 2.

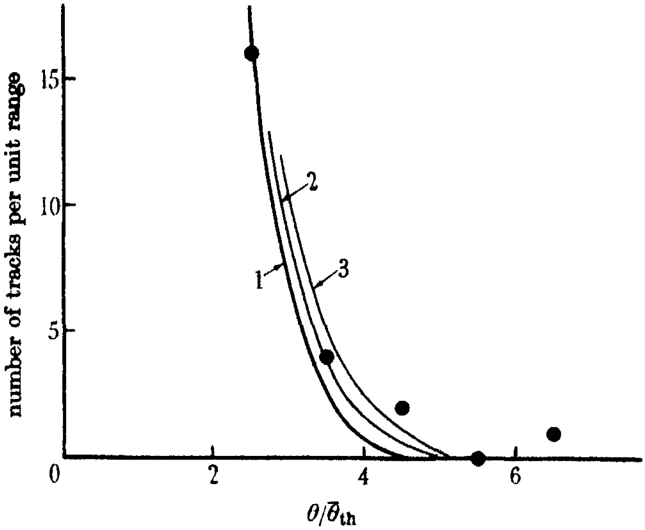

FIGURE 2. Modification of the tail of the multiple scattering curve for mesotrons in the presence of a proton component. (1) No protons, (2) 20 % protons, (3) 40 % protons. ● observed distribution of scattering—number of tracks per unit range of $\theta/\bar{\theta}_{th}$—(table 2).

8. DISCUSSION AND CONCLUSION

8.1. *Scattering in the Coulomb field.* The agreement between experiment and theory for the Coulomb scattering of mesotrons is shown in § 3 to be within the probable error of the observations and of the theory.

We have found no deviation from theory for the slowest mesotrons included in our measurements (§ 5, $E_e \sim 3 \times 10^8$ e-volts), but a considerable anomaly has been reported by Fowler and Oppenheimer (1938; Fowler 1938) for 10^7 e-volt electrons scattered in thin lead foil. These workers show that while the single large-angle scattering (which is not suppressed under the conditions of their experiment) is normal, the multiple scattering is only about 40 % of that predicted theoretically. This result suggests that the discrepancy is associated with the small deflexions arising from collisions near the upper shielding impact parameter. In our experiments, where a much thicker scattering plate is used, the relative importance of this region for multiple scattering is clearly much reduced. Hence the anomaly is probably determined by the thickness of the scattering layer rather than by the energy of the scattered particle.

8.2. *The interpretation of scattering due to short-range forces.** According to the present mesotron theory, the cross-section for the scattering of *charged* mesotrons by a proton or neutron is given, for energies of the order μc^2 (Heitler 1938*a*), by

$$\phi \simeq 4\pi\left(\frac{g^2}{\mu c^2}\right)^2 \simeq 10^{-25} - 10^{-26} \text{ cm.}^2, \tag{3}$$

where g is the characteristic "charge-constant" of the mesotron theory. The cross-section increases at higher energies, but these energies ($E_{\text{kin}} > \mu c^2$) lie outside the limits of validity of the theory.

In a classical theory for *neutral* mesotrons, Bhabha (1939) finds a much smaller cross-section:

$$\phi \simeq 8\pi/3\left(\frac{g^2}{Mc^2}\right)^2 \simeq 10^{-27} - 10^{-28} \text{ cm.}^2, \tag{4}$$

where M is the proton mass. This value, (4), is analogous to the Thomson formula for the scattering of light by electrons, and does not increase with increasing energy. The same result (4) can be derived from the quantized mesotron theory for the scattering of *neutral* mesotrons.

It should be noted that (3) is independent of the proton mass, while (4) is proportional to $1/M^2$.

The remarkable difference between (3) and (4) is due to the role which the electric charge plays in the mesotron theory, controlling to a large extent the interaction between charged mesotrons and heavy particles: a positive mesotron, for instance, can be absorbed only by a neutron and not by a proton, while no such restriction applies for neutral mesotrons. This difference of behaviour leads to the large cross-section (3).†

We have already shown (§ 6) that the experiments are not in agreement with the cross-section (3) but are consistent with (4). It might still be

---

* This section is based on a private communication for which I am indebted to Dr Heitler. The theoretical position outlined in this section is the result of discussions between Bhabha, Fröhlich, Heitler and Kemmer.

† If states of the heavy particle were possible with charges $+2e$, $+e$, the scattering cross-section (4) would apply also for *charged* mesotrons. This assumption, however, involves so many other difficulties that it would be premature to consider it seriously at the moment.

Heitler also points out that the cross-section for processes of the type

$$Y^0 + N = P + Y^-$$

does not depend on the interaction assumed, but in any case is given by (4).

possible to assume that (3) is correct for energies less than μc^2 and that the cross-section decreases very rapidly (by a factor of 100!) between μc^2 and $3\mu c^2$, but this behaviour is most unlikely. It is much more probable that (4) represents the true cross-section even for *charged* mesotrons, although this result cannot be deduced from the present mesotron theory in any form.

The small experimental cross-section for charged mesotrons at low energies has therefore an important bearing on the fundamental problems of charge exchange in the interaction of charged mesotrons with heavy particles.

I am indebted to Professor P. M. S. Blackett for his constant interest and advice during this work, and to Professor E. J. Williams and Dr W. Heitler for discussions of the theory of scattering.

SUMMARY

An extended series of accurate measurements of the scattering of mesotrons is described. These are in general agreement with our earlier measurements, and confirm within the accuracy of the experiment (about 4%) the theoretical value given by Williams (1939) for multiple Coulomb scattering.

Theory shows that the scattering by a finite nucleus should be about 10% less than that by a point nucleus. The experimental results, which have an accuracy of about 4%, definitely confirm the lower value and so can be considered as supporting the correctness of the scattering theory as applied to a finite nucleus.

The evidence for the existence of large-angle scattering due to short-range forces between mesotrons and nuclear heavy particles (protons and neutrons) is discussed. The cross-section for this type of scattering is estimated to be of the order 10^{-28} cm.^{2}, and this value is in agreement with that given by Bhabha for a "classical" mesotron theory.

There is no experimental evidence for the large increase of scattering due to short-range forces at low mesotron energies given in the quantum mechanical treatment due to Heitler. For the available mesotrons of lowest energy, the cross-section is found to be less than 10^{-27} cm.^{2}. This result is not compatible with the present development of mesotron theory, and may be interpreted as indicating a failure in the treatment of the charge-exchange which leads to the interaction between charged mesotrons and heavy particles.

REFERENCES

Bhabha 1938 *Nature, Lond.*, **141**, 117.
— 1939 *Proc. Roy. Soc.* A, **172**, 384.
Blackett and Wilson 1938 *Proc. Roy. Soc.* A, **165**, 209.
Blau and Wambacher 1937 *S.B. Akad. Wiss. Wien*, **146**, 623.
Brode and Starr 1938 *Phys. Rev.* **53**, 3.
Brunt 1931 *Combination of Observations*. Camb. Univ. Press.
Fowler 1938 *Phys. Rev.* **54**, 773.
Fowler and Oppenheimer 1938 *Phys. Rev.* **54**, 320.
Heitler 1938*a* *Proc. Roy. Soc.* A, **166**, 529.
— 1938*b* *Phys. Rev.* **54**, 873.
Schopper and Schopper 1938 *Phys. Z.* **40**, 22.
Williams 1939 *Proc. Roy. Soc.* A, **169**, 531.
Wilson 1939 *Proc. Roy. Soc.* A, **172**, 517.

The photodisintegration of the deuteron in the meson theory

By H. FRÖHLICH
H. H. Wills Physical Laboratory, University of Bristol
W. HEITLER AND B. KAHN
At present at Royal Society Mond Laboratory, Cambridge

(*Communicated by J. D. Cockcroft, F.R.S.—Received* 14 *August* 1939)

1. INTRODUCTION

Bethe and Peierls (1935) have given a theory of the photoelectric effect of the deuteron which was based on the assumption that between a neutron and a proton forces of a very short range exist. This made it possible to calculate the cross-section and the angular distribution in a way which seemed to a great extent to be independent of the nature of the nuclear forces. Massey and Mohr (1935) have extended this theory. Later on Breit and Condon (1936) have taken into account the influence of exchange forces of the Majorana type.

In recent years a theory of nuclear forces has been developed, the fundamental ideas of which are due to Yukawa (1935). In this theory, the existence of free mesons (cosmic rays) is connected with the nuclear forces in a similar way as the electromagnetic forces between electrically charged particles are correlated with the existence of light quanta (cf. Yukawa, Sakata and Taketani 1938; Bhabha 1938; Fröhlich, Heitler and Kemmer 1938).

According to this meson theory a proton (neutron) can be regarded as surrounded by a *meson field* which, owing to the exchange nature of the nuclear forces, is *electrically charged*, the charge being positive (negative) for the proton (neutron).

The charged nature of the nuclear field has the following important consequence: In treating the interaction of a nucleus with a light quantum one has to take into account not only the direct interaction of the light quantum with the protons but also its *interaction with the charged nuclear field*. The latter consists of two parts: (i) the spin independent part (g-interaction) and (ii) the spin dependent part (f-interaction). The first part gives rise to ordinary exchange forces whose influence on the photoelectric effect has in principle been considered by Breit and Condon. The second part is characteristic for the meson theory in its present form and leads, as we shall see in this paper, to results differing essentially from those of previous theories.

One can thus divide the interaction of a light quantum with a deuteron into two parts: (i) the part in which the light quantum acts directly on the proton (Bethe-Peierls), (ii) the part in which the light quantum interacts with the meson field. It will be shown in this paper that for not too high energies both are of the same order of magnitude. The dependence on the frequency ν is, however, quite different for the two parts. The contribution to the cross-section of (i) decreases, for high energies, like $1/\nu^{3/2}$, whereas the contribution of (ii) decreases only like $1/\nu^{1/2}$. For high energies the new effect is therefore preponderant. For the 17 MeV γ-rays of Li for instance the cross-section turns out to be seven times larger in the new theory than in the old one. Also the angular distribution will be seen to be very different in the new theory.

These effects are characteristic for the spin dependent exchange forces in the present form of the meson theory. We want to emphasize that the effect is mainly due to not too fast mesons and that none of the difficulties of the meson theory connected with fast mesons plays any role in these calculations. The results should have the same degree of reliability as those for the nuclear forces.

It should be possible to check the effect experimentally. We believe that such experiments on the photoelectric effect of the deuteron with hard γ-rays should be considered as a crucial test for or against the present form of the meson theory.

2. CALCULATION OF THE CROSS-SECTION

Our aim is to calculate the cross-section for the photo-disintegration of the deuteron. We shall do this, using Born's approximation. This is justified because it will turn out that the wave function of the ejected proton is not an S-wave function and therefore very little influenced by the proton-neutron interaction (this is not true for the photomagnetic effect which we shall not consider in this paper, cf. § 3).

(i) *The wave functions of the deuteron*

The wave function of a heavy particle depends on the following co-ordinates: The space co-ordinates, the spin co-ordinates and the co-ordinates describing whether the heavy particle is a proton or a neutron. The ground state of the deuteron has an angular momentum 1. It was usually assumed that it is a ^{3}S-state. From the proton-neutron interaction derived from the meson theory it follows, however, that there is a large spin-orbit coupling, and that therefore the ground state is a mixture of ^{3}S and ^{3}D$_1$ (cf. Yukawa, Sakata, Kobayasi and Taketani 1938; Fröhlich *et al.*[*] 1938). The presence of a ^{3}D$_1$ admixture to the wave function finds its expression in the existence of a quadripole moment of the deuteron, discovered recently by Kellogg, Rabi, Ramsey and Zacharias (1939).

It is, however, likely that the contribution of the ^{3}D$_1$ wave function is not very large, owing to the centrifugal forces. In this paper we are mainly interested in the effects arising from the meson character of the nuclear field. These effects are clearly shown even if we assume a ^{3}S-wave function for the ground state of the deuteron as we shall do in this paper for reasons of simplicity.

The wave function for the ground state of the deuteron can thus be written in the form

$$\Psi = \psi(1,2)\,T(1,2)\,U(1,2), \tag{1}$$

where ψ depends on the space co-ordinates $\mathbf{r}_1$, $\mathbf{r}_2$, T on the spin variables, and U on the charge variables of the two particles. For the ^{3}S-state these wave functions are

$$\left.\begin{aligned} & \qquad \alpha(1)\,\alpha(2) \\ T &= \frac{1}{\sqrt{2}}\{\alpha(1)\,\beta(2)+\alpha(2)\,\beta(1)\}, \\ & \qquad \beta(1)\,\beta(2) \\ U &= \frac{1}{\sqrt{2}}\{\xi(1)\,\eta(2)-\xi(2)\,\eta(1)\}, \end{aligned}\right\} \tag{2}$$

---

[*] In the following quoted as F.H.K.

where α, β are the two spin functions and $\xi(\eta)$ is equal to 1, (0) when the particle is a proton and equal to 0, (1) when it is a neutron. For ψ we shall assume the wave function used by Bethe and Peierls (1935):

$$\psi = \sqrt{\left(\frac{\alpha}{2\pi}\right)}\frac{e^{-\alpha r}}{r}, \quad r = |\mathbf{r}_1 - \mathbf{r}_2|, \tag{3}$$

where α is connected with the binding energy E_0 of the deuteron by

$$E_0 = \frac{\hbar^2\alpha^2}{M}. \tag{4}$$

M is the mass of the proton. The wave function (3) corresponds to a neutron-proton potential of the form of a δ-function. For the final state into which the deuteron disintegrates we assume plane waves according to the use of Born's approximation. For parallel spins this wave function is

$$\Psi' = e^{i(\mathbf{K}_1\mathbf{r}_1)+i(\mathbf{K}_2\mathbf{r}_2)}\xi(1)\,\eta(2)\left\{\begin{matrix} \alpha(1)\,\alpha(2) \\ \frac{1}{\sqrt{2}}\{\alpha(1)\,\beta(2)+\alpha(2)\,\beta(1)\} \\ \beta(1)\,\beta(2) \end{matrix}\right\}; \tag{5}$$

$\mathbf{K}_1$ is the wave number of the ejected proton, $\mathbf{K}_2$ of the neutron. Transitions into states with antiparallel spins are only due to the photomagnetic effect, which we do not consider here.

(ii) *Interaction energy*

The transition from the ground state to the final state are due to the interaction of the deuteron with the light quantum. In the theory of Bethe and Peierls (1935) the proton was considered as the only particle carrying a charge. In the meson theory we have in addition an interaction of the light quantum with the *charged* meson field.

The Hamiltonian of a meson field in the presence of both heavy particles and an electromagnetic field has been given in its complete form by Bhabha (1938). We write down the interaction part of this Hamiltonian in the notation of F.H.K. (1938), making use of the longitudinal and transverse meson wave functions $\boldsymbol{\psi}$ and $\boldsymbol{\phi}$. $\mathbf{A}$ is the electromagnetic vector potential and V the scalar potential.

The Hamiltonian consists of three parts

$$H = H' + H'' + H''', \tag{6}$$

where H' represents the interaction between the electromagnetic field and the meson field, H'' that between the meson field and each of the heavy particles, H''' is a "mixed interaction" containing the electromagnetic field, each of the heavy particles and the meson field.† The three contributions are (for one heavy particle):

$$H' = \frac{ie}{4\pi\hbar c}\left\{\operatorname{div}\boldsymbol{\psi}\left(\mathbf{A}, \boldsymbol{\psi}^* + \frac{1}{\lambda}\dot{\boldsymbol{\phi}}^*\right) + \left(\operatorname{curl}\boldsymbol{\phi}\left[\mathbf{A}, \boldsymbol{\phi}^* - \frac{1}{\lambda}\dot{\boldsymbol{\psi}}^*\right]\right)\right.$$
$$\left. + V(\dot{\boldsymbol{\phi}}\boldsymbol{\phi}^*) + V(\dot{\boldsymbol{\psi}}\boldsymbol{\psi}^*)\right\}$$
$$+ \frac{e^2}{4\pi\hbar^2c^2}\left\{|(\mathbf{A}\boldsymbol{\psi})|^2 + \frac{1}{\lambda^2}|[\mathbf{A}\dot{\boldsymbol{\psi}}]|^2 + \frac{1}{\lambda^2}|(\mathbf{A}\dot{\boldsymbol{\phi}})|^2 + |[\mathbf{A}\boldsymbol{\phi}]|^2\right.$$
$$\left. + \frac{1}{\lambda}(\mathbf{A}\boldsymbol{\psi})(\mathbf{A}\dot{\boldsymbol{\phi}}^*) + \frac{1}{\lambda}(\mathbf{A}\boldsymbol{\phi})(\mathbf{A}\dot{\boldsymbol{\psi}}^*)\right\}, \tag{7}$$

$$H'' = \frac{g}{\lambda} M \operatorname{div}\boldsymbol{\psi} + \frac{f}{\lambda}(\mathbf{S}\operatorname{curl}\boldsymbol{\phi}) + \frac{4\pi g^2}{\lambda^2}|M|^2, \tag{8}$$

$$H''' = -\frac{ieg}{\hbar c\lambda} M\left(\mathbf{A}, \boldsymbol{\psi} + \frac{1}{\lambda}\dot{\boldsymbol{\phi}}\right) - \frac{ief}{\hbar c\lambda}\left(\mathbf{S}\left[\mathbf{A}, \boldsymbol{\phi} - \frac{1}{\lambda}\dot{\boldsymbol{\psi}}\right]\right). \tag{9}$$

In these expressions it is to be understood that the complex conjugate terms have to be added to all those terms which are not automatically real. The definition of $\dot{\psi}$ is $\psi = 1/c\, \partial\psi/\partial t$. M and $\mathbf{S}$ depend on the wave functions of the heavy particles Ψ and the charge operator Π which is defined as follows:

$$\Pi\xi = \Pi^*\eta = 0, \quad \Pi\eta = \xi, \quad \Pi^*\xi = \eta, \tag{10}$$

$$M = (\Psi^*\Pi\Psi), \quad \mathbf{S} = (\Psi^*\Pi\boldsymbol{\sigma}\Psi). \tag{11}$$

$\boldsymbol{\sigma}$ is the spin vector of the heavy particle. In the Hamiltonian (7)–(9) all terms have been omitted which depend on the velocity of the heavy particles.

We expand the wave functions of the meson $\boldsymbol{\psi}$ and $\boldsymbol{\phi}$ into plane waves

$$\boldsymbol{\psi} = \sum_k Q_k \frac{\mathbf{k}}{k} e^{i(\mathbf{k}\mathbf{r})}\sqrt{(4\pi c^2)},$$

$$\boldsymbol{\phi} = \sum_k q_k \mathbf{j}\, e^{i(\mathbf{k}\mathbf{r})}\sqrt{(4\pi c^2)}.$$

q_k and Q_k are quantized according to the Pauli-Weisskopf formalism. $\mathbf{j}$ is the unit vector of polarization for transverse mesons. It has to be noticed that the wave number $\mathbf{k}$ is connected with the momentum $\mathbf{p}$ of the free meson in a different way for positive and negative mesons:

---

† We are indebted to Dr Bhabha for having drawn our attention to the existence of this term.

$$\text{for } Y^+\text{:}\quad \mathbf{p} = \hbar c\mathbf{k},$$
$$\text{for } Y^-\text{:}\quad \mathbf{p} = -\hbar c\mathbf{k}.$$

This follows immediately from the Pauli-Weisskopf formalism.

(iii) *Matrix elements*

The interaction H gives rise to a number of transitions for which we give the matrix elements. The following transitions are due to H':

(1) A longitudinal meson with wave number $\mathbf{k}$ absorbs a light quantum with wave number $\mathbf{q}$ ($\hbar\nu = \hbar cq$) and has then a wave number $\mathbf{k}'$. The law of conservation of momentum is then

$$\text{for } Y^+\text{:}\quad \mathbf{k}' = \mathbf{k}+\mathbf{q}, \qquad \text{for } Y^-\text{:}\quad -\mathbf{k}' = -\mathbf{k}+\mathbf{q}. \tag{12}$$

(2) The analogous transition for a transverse meson. The transitions in which a longitudinal meson is transformed into a transverse one through the absorption of a light quantum give no contribution to the photoelectric effect.

(3) The creation or annihilation of a pair of longitudinal mesons with absorption of a light quantum. The momentum law is for the two cases.

$$\mathbf{q} = \mathbf{k}_+ - \mathbf{k}_-, \quad \mathbf{q}+\mathbf{k}_+ - \mathbf{k}_- = 0. \tag{13}$$

(4) The same for transverse mesons. The matrix elements of H' for these four transitions are (ϵ, ϵ' are the energies corresponding to $\mathbf{k}$, $\mathbf{k}'$; $\epsilon = \hbar c\sqrt{(k^2+\lambda^2)}$; $\mathbf{e}$ is the unit vector of polarization of the light quantum):

$$\left.\begin{aligned}
H_1' &= -\frac{e\hbar^2c^2}{2}\sqrt{\left(\frac{2\pi}{\epsilon\epsilon'\hbar\nu}\right)}\left\{\frac{k}{k'}(\mathbf{k}'\mathbf{e})+\frac{k'}{k}(\mathbf{ke})\right\},\\
H_2' &= -\frac{e\hbar^2c^2}{2}\sqrt{\left(\frac{2\pi}{\epsilon\epsilon'\hbar\nu}\right)}\{([\mathbf{jk}]\,[\mathbf{j}'\mathbf{e}])+([\mathbf{j}'\mathbf{k}']\,[\mathbf{je}])\},\\
H_3' &= +\frac{e\hbar^2c^2}{2}\sqrt{\left(\frac{2\pi}{\epsilon_+\epsilon_-\hbar\nu}\right)}\left\{\frac{k_-}{k_+}(\mathbf{k}_+\mathbf{e})+\frac{k_+}{k_-}(\mathbf{k}_-\mathbf{e})\right\},\\
H_4' &= +\frac{e\hbar^2c^2}{2}\sqrt{\left(\frac{2\pi}{\epsilon_+\epsilon_-\hbar\nu}\right)}\{([\mathbf{j}_-\mathbf{k}_-]\,[\mathbf{j}_+\mathbf{e}])+([\mathbf{j}_+\mathbf{k}_+]\,[\mathbf{j}_-\mathbf{e}])\}.
\end{aligned}\right\} \tag{14}$$

H_1' and H_2' are valid both for positive and negative mesons if the momentum law (12) is taken into account. H_3' and H_4' are valid for creation and annihilation.

H'' has matrix elements for emission and absorption of mesons by a heavy particle. They are given in F.H.K. (1938), equation (32).

H''' gives rise to the following transitions:

(5) A proton emits a longitudinal Y^+ and absorbs a light quantum.
(6) A neutron emits a longitudinal Y^- and absorbs a light quantum.
(7) A proton absorbs a longitudinal Y^- and a light quantum.
(8) A neutron absorbs a longitudinal Y^+ and a light quantum.
(9)–(12) The same as (5)–(8) for transverse mesons.

These matrix elements are, for the heavy particle at the position $\mathbf{r}_0$,

$$\left.\begin{array}{l} H_5''' = \Pi^* \dfrac{2\pi eg\hbar c}{\lambda} \dfrac{1}{\sqrt{(\epsilon\hbar\nu)}} \left(\mathbf{e}\dfrac{\mathbf{k}}{k}\right) e^{-i(\mathbf{k}-\mathbf{q},\,\mathbf{r}_0)}, \\ H_6''' = -\Pi \dfrac{2\pi eg\hbar c}{\lambda} \dfrac{1}{\sqrt{(\epsilon\hbar\nu)}} \left(\mathbf{e}\dfrac{\mathbf{k}}{k}\right) e^{i(\mathbf{k}+\mathbf{q},\,\mathbf{r}_0)}, \\ H_7''' = -H_5''', \quad H_8''' = -H_6''', \\ H_9''',\ H_{10}''' \text{ are the same as } H_5''',\ H_6''' \text{ with } g\left(\mathbf{e}\dfrac{\mathbf{k}}{k}\right) \text{ replaced by } f(\boldsymbol{\sigma}[\mathbf{e}\mathbf{j}]), \\ H_{11}''' = -H_9''', \quad H_{12}''' = -H_{10}'''. \end{array}\right\} \tag{15}$$

In H_5''' we have omitted the contribution arising from the term $+\dfrac{ief}{\hbar c\lambda^2}(\mathbf{S}[\mathbf{A}\boldsymbol{\phi}])$ of H''' (and similar terms in H_6''', etc.), because these terms do not contribute to the photoelectric effect.

(iv) *Total matrix element*

Let V_{AF} be the matrix element for the transition of the deuteron from a ground state A into a final state F under the action of a light quantum. The differential cross-section of this process is then

$$d\Phi = \frac{2\pi}{\hbar c} |V_{AF}|^2 \rho d\Omega, \tag{16}$$

where $\rho d\Omega$ is the density of final energy states with the direction of the proton in the solid angle $d\Omega$. The ground state is three-fold owing to the three orientations of the spin. Disregarding the photomagnetic effect, the final state is also a triplet and transitions occur from each of the three initial states to each of the three final states. In (16) the sum has to be taken over the three final states and the average over the three initial states.

The matrix element V_{AF} consists for each of these nine transitions of three parts:

$$V_{AF} = V_a + V_b + V_c \tag{17}$$

with the following significance:

(*a*) V_a is due to a combination of the interactions H' and H'' and is a third-order matrix element. The transition takes place by means of *two* subsequent intermediate states. There exist four possible sequences of those intermediate states:

(α) (i) Emission of Y^+ by proton; (ii) absorption of light quantum by Y^+; (iii) reabsorption of Y^+ by one of the two neutrons.

(β) The same for Y^-, emitted by the neutron.

(γ) (i) Creation of a pair of mesons by the light quantum; (ii) absorption of Y^+ by neutron; (iii) absorption of Y^- by one of the protons. (ii) and (iii) can occur in the reverse order.

(δ) (i) Emission of Y^+ by proton; (ii) emission of Y^- by one of the neutrons; (iii) annihilation of the pair with absorption of the light quantum. (i) and (ii) can occur in the reverse order.

All mesons can be longitudinal or transverse. In the approximations used in our calculations (see below) all four contributions are identical and we shall only give the calculations for (α).

Let us denote by E_n and $E_{n'}$ the energies of the two successive intermediate states (i) and (ii), and E_A, E_F the energies in the initial and final states. Then V_a is given by

$$V_a = 4 \sum_{n,n'} \frac{H_{An} H_{nn'} H_{n'F}}{(E_A - E_n)(E_A - E_{n'})}, \tag{18}$$

where H_{An}, etc. are the matrix elements of $H' + H''$ for the transitions (α). For H_{An} and $H_{n'F}$ only H'' and for $H_{nn'}$ only H' gives a contribution. In the intermediate states n, n' the heavy particles are two free neutrons and have wave numbers $\mathbf{K}_1'$, $\mathbf{K}_2'$, whilst the meson has a wave number $\mathbf{k}$ in n and $\mathbf{k}'$ in n'. The conservation of momentum shows that

$$\mathbf{K}_1' + \mathbf{K}_2' + \mathbf{k} = 0, \quad \mathbf{k}' = \mathbf{k} + \mathbf{q}. \tag{19}$$

In the final state with the wave function (5) the momentum law gives

$$\mathbf{K}_1 = \mathbf{K}_1' + \mathbf{k}', \quad \mathbf{K}_2 = \mathbf{K}_2'. \tag{20}$$

In each of the intermediate states n, n' the spin functions can be either of the four functions $\alpha(1)\alpha(2)$, $\alpha(1)\beta(2)$, $\alpha(2)\beta(1)$, $\beta(1)\beta(2)$. The emitted meson can be longitudinal or transverse; in the latter case one has to take the sum over the two directions of polarization in the intermediate states.

As an example we calculate V_a for the transition $\alpha(1)\,\alpha(2)_A \rightarrow \alpha(1)\,\alpha(2)_F$ for a longitudinal meson. In this case the interaction is independent of the spin and the intermediate states have the same spin functions. According to F.H.K. (equation (32)) we have

$$\begin{aligned} H_{An} &= -\frac{g}{\lambda}\sqrt{\left(\frac{2\pi}{\epsilon}\right)}\hbar ck\iint d\tau_1\,d\tau_2\,e^{-i(\mathbf{K}_1'\mathbf{r})-i(\mathbf{K}_2'\mathbf{r})}\,\eta(1)\,\eta(2) \\ &\quad\times(\Pi_1^*\,e^{-i(\mathbf{k}\mathbf{r}_1)}+\Pi_2^*\,e^{-i(\mathbf{k}\mathbf{r}_2)})\,\frac{\xi(1)\,\eta(2)-\xi(2)\,\eta(1)}{\sqrt{2}}\,\psi(\mathbf{r}_1-\mathbf{r}_2) \\ &= \frac{2ig}{\lambda}\sqrt{\frac{\pi}{\epsilon}}\,\hbar ck\int d\tau\,e^{-\frac{1}{2}i(\mathbf{r},\,\mathbf{K}_1'-\mathbf{K}_2')}\sin\tfrac{1}{2}(\mathbf{k}\mathbf{r})\,\psi(r), \end{aligned} \tag{21}$$

where ψ is the wave function of the deuteron (3). In the second equation (21) we have separated the motion of the centre of gravity and made use of the conservation of momentum.

$H_{nn'} = H_1'$ is given by equation (14). $H_{n'F}$ is again given by F.H.K. (equation (32)):

$$H_{n'F} = -\frac{g}{\lambda}\sqrt{\left(\frac{2\pi}{\epsilon'}\right)}\hbar ck'. \tag{22}$$

The resonance denominators are

$$\left.\begin{aligned} E_A-E_n &= -E_0-\hbar c\sqrt{(k^2+\lambda^2)}-\frac{\hbar^2}{2M}(K_1'^2+K_2'^2), \\ E_A-E_{n'} &= -E_0+\hbar\nu-\hbar c\sqrt{(k'^2+\lambda^2)}-\frac{\hbar^2}{2M}(K_1'^2+K_2'^2). \end{aligned}\right\} \tag{23}$$

The double summation over n, n' in (18), viz. over $\mathbf{k}$, $\mathbf{k}'$, can be reduced to a simple integral over $\mathbf{k}$ by means of the conservation laws (19) and (20). The contribution to V_a from the transition in question is then

$$\begin{aligned} V_a &= \frac{ig^2e\hbar^2c^2}{\pi^{\frac{1}{2}}\lambda^2\sqrt{(\hbar\nu)}}\int d\tau\int d\mathbf{k}\,\frac{kk'}{\sqrt{(k^2+\lambda^2)}\sqrt{(k'^2+\lambda^2)}}\left\{\frac{k}{k'}(\mathbf{k}'\mathbf{e})+\frac{k'}{k}(\mathbf{k}\mathbf{e})\right\} \\ &\quad\times\frac{e^{\frac{1}{2}i(\mathbf{r},\,\mathbf{k}+2\mathbf{K}_2)}\sin\frac{1}{2}(\mathbf{k}\mathbf{r})\,\psi(r)}{\left(E_0+\epsilon+\frac{\hbar^2}{2M}(K_1'^2+K_2'^2)\right)\left(E_0-\hbar\nu+\epsilon'+\frac{\hbar^2}{2M}(K_1'^2+K_2'^2)\right)}. \end{aligned} \tag{24}$$

In this formula it is to be understood that all wave numbers $\mathbf{k}'$, $\mathbf{K}_1'$, $\mathbf{K}_2'$ are to be expressed by means of (19), (20), by $\mathbf{k}$, $\mathbf{q}$, $\mathbf{K}_1$, $\mathbf{K}_2$.

Before we evaluate this integral we calculate the contributions V_b and V_c to the matrix element.

(*b*) V_b is due to a combination of H'' and H''' and is a *second*-order matrix element. The transition takes place by means of *one* intermediate state. There are again four sequences of those intermediate states:

(α) (i) Emission of Y^+ by proton and absorption of light quantum; (ii) absorption of Y^+.

(β) The same for Y^-.

(γ) (i) Emission of Y^+ by proton; (ii) absorption of Y^+ with absorption of light quantum.

(δ) The same for Y^-.

Again all four sequences give the same contribution resulting in a factor 4. V_b is of the form

$$V_b = 4\sum_m \frac{H_{Am} H_{mF}}{E_A - E_m}. \tag{25}$$

For (α) H_{Am} is due to H''' and H_{mF} to H''.

We evaluate V_b for the same transition $\alpha(1)\alpha(2)_A \rightarrow \alpha(1)\alpha(2)_F$ and for a longitudinal meson. We easily find, according to (15) and F.H.K. (equation (32))

$$H_{Am} = -\frac{2\pi i c g \hbar c}{\lambda}\sqrt{\left(\frac{2}{\epsilon\hbar\nu}\right)}\left(\mathbf{e}\frac{\mathbf{k}}{k}\right)\int d\tau\, e^{-\frac{1}{2}i(\mathbf{K}_1'-\mathbf{K}_2',\mathbf{r})}\sin\tfrac{1}{2}(\mathbf{k}-\mathbf{q},\mathbf{r})\,\psi(r), \tag{26}$$

with $\mathbf{K}_1'$ and $\mathbf{K}_2'$ given by $\quad \mathbf{K}_1'+\mathbf{K}_2'+\mathbf{k} = \mathbf{q}, \qquad (27)$

$$H_{mF} = -\frac{g}{\lambda}\sqrt{\left(\frac{2\pi}{\epsilon}\right)}\hbar c k, \quad \mathbf{K}_1 = \mathbf{K}_1'+\mathbf{k}, \quad \mathbf{K}_2 = \mathbf{K}_2'. \tag{28}$$

The resonance denominator is

$$E_A - E_m = -E_0 + \hbar\nu - \epsilon - \frac{\hbar^2}{2M}(K_1'^2 + K_2'^2). \tag{29}$$

Hence V_b becomes

$$V_b = \frac{2ieg^2\hbar^2c^2}{\sqrt{(\hbar\nu)}\,\lambda^2\pi^{\frac{1}{2}}}\int d\tau\int d\mathbf{k}(\mathbf{e}\mathbf{k})\frac{e^{\frac{1}{2}i(\mathbf{k}-\mathbf{q}+2\mathbf{K}_2,\mathbf{r})}\sin\frac{1}{2}(\mathbf{k}-\mathbf{q},\mathbf{r})\,\psi(r)}{\epsilon\left(\hbar\nu - E_0 - \epsilon - \dfrac{h^2}{2M}(K_1'^2 + K_2'^2)\right)}. \tag{30}$$

Here again $\mathbf{K}_1'$, $\mathbf{K}_2'$ are expressed by $\mathbf{k}$, $\mathbf{q}$ and $\mathbf{k}_1$, $\mathbf{k}_2$.

(*c*) V_c is due to the *direct interaction* of the proton with the light quantum. There is no intermediate state.

In this transition the spin function does not change. V_c is the same for all these three transitions and is given by the well-known formula

$$V_c = \frac{e\hbar^2}{M}\sqrt{\left(\frac{\pi}{\hbar\nu}\right)}(\mathbf{K}_2\mathbf{e})\int d\tau\, e^{-i(\mathbf{K}_2\mathbf{r})}\,\psi(r). \tag{31}$$

(v) *Approximations*

We shall now confine ourselves to energies

$$\hbar\nu \ll \mu c^2 = 80 \times 10^6 \text{ e-volts}. \tag{32}$$

(μ = rest mass of meson.)

In this case we may neglect throughout the recoil of the meson due to the absorption of the light quantum and therefore replace $\mathbf{k}'$ by $\mathbf{k}$. This is justifiable because the main contributions to our integrals arise from values $k \simeq \lambda$. Furthermore, we make use of the conservation of energy in the final state

$$\frac{\hbar^2}{2M}(K_1^2 + K_2^2) = \hbar\nu - E_0 \ll \mu c^2. \tag{33}$$

The term $\frac{\hbar^2}{2M}(K_1'^2 + K_2'^2)$ in the denominators of (24) and (30) can then be neglected since $\mathbf{K}_2' = \mathbf{K}_2$ and $\mathbf{K}_1' = \mathbf{K}_1 + \mathbf{k}$ which gives the order of magnitude $\hbar^2k^2/2M \simeq \hbar^2\lambda^2/2M \simeq \mu c^2 . \mu/2M$. In the resonance denominators of (24) and (30) we can therefore neglect everything except $\epsilon \simeq \epsilon'$.

We want to mention that in making these approximations the transitions to a final *singlet* state all vanish. In these approximations we do not get therefore any photomagnetic effect. For the photoelectric effect these approximations are obviously unimportant for the energies considered.

V_a and V_b (equations (24) and (30)) are then given by

$$V_a = \frac{2ieg^2}{\pi^{\frac{1}{2}}\lambda^2\sqrt{(\hbar\nu)}}\int d\tau \int d\mathbf{k}\, \frac{k^2(\mathbf{ke})}{(k^2+\lambda^2)^2}\, e^{\frac{1}{2}i(\mathbf{k}-2\mathbf{K}_1,\mathbf{r})} \sin \tfrac{1}{2}(\mathbf{kr})\, \psi(r),$$

$$V_b = -\frac{2ieg^2}{\pi^{\frac{1}{2}}\lambda^2\sqrt{(\hbar\nu)}}\int d\tau \int d\mathbf{k}\, \frac{(\mathbf{ek})}{k^2+\lambda^2}\, e^{\frac{1}{2}i(\mathbf{k}-2\mathbf{K}_1,\mathbf{r})} \sin \tfrac{1}{2}(\mathbf{kr})\, \psi(r).$$

Inserting for $\psi(r)$ equation (3), the integration is straightforward and we obtain

$$V_a = +\frac{2^{\frac{1}{2}}g^2e\sqrt{\alpha}\,\pi(\mathbf{eK}_1)}{\lambda^2\sqrt{(\hbar\nu)}\,K_1} \times \left[\frac{\lambda^2}{K_1}\frac{\alpha+\lambda}{(\alpha+\lambda)^2+K_1^2} + \frac{\lambda-\alpha}{K_1} + \left(1+\frac{\alpha^2-2\lambda^2}{K_1^2}\right)\operatorname{arctg}\frac{K_1}{\alpha+\lambda}\right], \tag{34}$$

$$V_b = +\frac{2^{\frac{1}{2}}g^2e\sqrt{\alpha}\,\pi(\mathbf{eK}_1)}{\lambda^2\sqrt{(\hbar\nu)}\,K_1}\left[\frac{\alpha-\lambda}{K_1} - \left(1+\frac{\alpha^2-\lambda^2}{K_1^2}\right)\operatorname{arctg}\frac{K_1}{\alpha+\lambda}\right], \tag{35}$$

$$V_c = -\frac{2^{\frac{1}{2}}\pi e\hbar^2\sqrt{\alpha}\,(\mathbf{eK}_1)}{M\sqrt{(\hbar\nu)}\,(K_1^2+\alpha^2)}. \tag{36}$$

(vi) *Formulae for the cross-section*

(34) and (35) are the contributions from the $\alpha(1)\alpha(2)_A \to \alpha(1)\alpha(2)_F$ transition and from longitudinal mesons. We give the matrix elements for the other transitions and for transverse mesons without calculation. The matrix elements for transverse mesons depend on the angles between spin and light quantum. We choose the direction of $\mathbf{q}$ as the one to which the spin directions are referred. (α means spin in $+\mathbf{q}$ direction.) Let θ and ϕ be the angles

$$\theta = \sphericalangle(\mathbf{K}_1\mathbf{q}), \quad \phi = \sphericalangle(\mathbf{e};\ \mathbf{K}_1, \mathbf{q}\text{-plane}).$$

Then we have for the total matrix element $V_{AF} = V_a + V_b + V_c$:

$\alpha(1)\alpha(2) \to \alpha(1)\alpha(2)$ or $\beta(1)\beta(2) \to \beta(1)\beta(2)$:

$$V = \frac{2^{\frac{3}{2}}\pi e}{\lambda^2}\sqrt{\left(\frac{\alpha}{\hbar\nu}\right)}\cos\phi\{g^2\sin\theta(A+B)+f^2\sin\theta(C+B) +f^2\sin^3\theta(A-\tfrac{5}{4}C)-G^2\sin\theta D\};$$

$\alpha(1)\beta(2)+\alpha(2)\beta(1) \to \alpha(1)\beta(2)+\alpha(2)\beta(1)$:

$$V = \frac{2^{\frac{3}{2}}\pi e}{\lambda^2}\sqrt{\left(\frac{\alpha}{\hbar\nu}\right)}\cos\phi\{g^2\sin\theta(A+B)+\tfrac{1}{2}f^2\sin\theta C +f^2\sin\theta\cos^2\theta(2A-\tfrac{5}{2}C)-G^2\sin\theta D\};$$

$\alpha(1)\alpha(2) \to \beta(1)\beta(2)$ or $\beta(1)\beta(2) \to \alpha(1)\alpha(2)$:

$$V = -\frac{2^{\frac{3}{2}}\pi e}{\lambda^2}\sqrt{\left(\frac{\alpha}{\hbar\nu}\right)}\left\{f^2e^{i\phi}\sin\theta\left(\frac{C}{2}+B\right)+f^2\sin^3\theta\cos\phi(A-\tfrac{5}{4}C)\right\};$$

$\alpha(1)\alpha(2) \to \alpha(1)\beta(2)+\alpha(2)\beta(1)$ or $\alpha(1)\beta(2)+\beta(1)\alpha(2) \to \alpha(1)\alpha(2)$
or $\beta(1)\beta(2) \to \alpha(1)\beta(2)+\alpha(2)\beta(1)$ or $\alpha(1)\beta(2)+\alpha(2)\beta(1) \to \beta(1)\beta(2)$:

$$V = -\frac{2^{\frac{3}{2}}\pi e}{\lambda^2}\sqrt{\left(\frac{\alpha}{\hbar\nu}\right)}\left\{f^2e^{i\phi}\cos\theta\left(\frac{C}{2^{\frac{3}{2}}}+\frac{B}{\sqrt{2}}\right)+f^2\sin^2\theta\cos\theta\cos\phi\sqrt{2}(A-\tfrac{5}{4}C)\right\};$$

where

$$A = \frac{\lambda^2}{K_1}\frac{\alpha+\lambda}{(\alpha+\lambda)^2+K_1^2}+\frac{\lambda-\alpha}{K_1}+\left(1+\frac{\alpha^2-2\lambda^2}{K_1^2}\right)\operatorname{arctg}\frac{K_1}{\alpha+\lambda},$$

$$B = \frac{\alpha-\lambda}{K_1}-\left(1+\frac{\alpha^2-\lambda^2}{K_1^2}\right)\operatorname{arctg}\frac{K_1}{\alpha+\lambda},$$

$$C = \frac{\alpha+\lambda}{2K_1}+\frac{3}{2}\frac{(\alpha+\lambda)(\alpha-\lambda)^2}{K_1^3}+\left(\frac{1}{2}-\frac{\alpha^2+\lambda^2}{K_1^2}-\frac{3}{2}\frac{(\alpha^2-\lambda^2)^2}{K_1^4}\right)\operatorname{arctg}\frac{K_1}{\alpha+\lambda},$$

$$D = \frac{K_1\lambda}{K_1^2+\alpha^2},$$

$$G^2 = \frac{\mu\hbar c}{M}. \qquad (37)$$

Hence we find the differential cross-section according to (16), by taking the sum of $|V|^2$ over all the nine transitions and dividing by 3. We take the average over the directions of polarization of the light quantum and obtain

$$\begin{aligned} d\Phi = \frac{2\pi}{3}\sin\theta\, d\theta \frac{e^2\alpha K_1 M}{\hbar^3\lambda^4 c\hbar\nu}\Big\{4f^4\left(\frac{C}{2}+B\right)^2 + \sin^2\theta[3\{g^2(A+B)-G^2D\}^2 \\ -4G^2f^2D(A+B)+4g^2f^2(A+B)^2 \\ +f^4(C^2+2B^2-6BC+4A^2-4AC+8AB)]\Big\} \\ \equiv \sin\theta\, d\theta\{\Phi_{\parallel}+\sin^2\theta(\Phi_{\perp}-\Phi_{\parallel})\}. \qquad (38) \end{aligned}$$

The total cross-section is

$$\begin{aligned} \Phi = \frac{2\pi}{3}\frac{e^2\alpha K_1 M}{\hbar^3\lambda^4 c\hbar\nu}[4\{g^2(A+B)-G^2D\}^2-\tfrac{16}{3}G^2f^2D(A+B) \\ +\tfrac{16}{3}g^2f^2(A+B)^2+\tfrac{2}{3}f^4(5C^2+8A^2-8AC+16B^2+16AB)]. \qquad (39) \end{aligned}$$

In these formulae K_1 is the wave number of the ejected proton

$$\frac{\hbar^2K_1^2}{M} = \hbar\nu - E_0.$$

3. Results and discussion

We now evaluate the formulae (38) and (39) numerically. The wave function which we have used for the ground state of the deuteron corresponds to a potential with the form of a δ-function. In order to take into account the finite range of the nuclear forces, Bethe and Bacher (1936) have shown that it is sufficient to renormalize the wave function in such a way that it is normalized to

$$1+\alpha/\lambda \qquad (40)$$

instead of to unity. We therefore have to multiply the expressions (38) and (39) by this factor. For the numerical evaluation we assume the following figures:

$$E_0 = 2{\cdot}2\,\text{MeV},$$

$$\text{Meson mass} = 160\,\text{m. or } \lambda = 160\frac{mc}{\hbar} = 1{\cdot}8\alpha.$$

Hence $$1+\alpha/\lambda = 1{\cdot}56, \quad G^2/\hbar c = 0{\cdot}087.$$

For g^2 and f^2 we shall use the figures derived by Kemmer (1938) from the nuclear forces, i.e. $g^2/\hbar c = 0{\cdot}057$, $f^2/\hbar c = 0{\cdot}143$. These figures are derived from the hypothesis of charge-independent nuclear forces and may not be the true values. The order of magnitude, however, is certainly correct. The functions A, B, C, D are independent of the choice of g and f and are given in table 1. In this table we give the values of the total cross-section Φ according to equation (39) (including the factor $1+\alpha/\lambda$). $r_0 = e^2/mc^2$ is the electronic radius. For comparison, we also give the cross-section Φ_{old} according to the old theory of Bethe and Peierls (1935). For the discussion of the angular dependence we give the ratio $\Phi_{\parallel}/\Phi_{\perp}$, i.e. the ratio of the cross-sections for $\theta = 0$ and $\theta = \frac{1}{2}\pi$.

In figure 1, Φ (in units r_0^2) and the ratio $\Phi_{\parallel}/\Phi_{\perp}$ are plotted as a function of the frequency ν together with the cross-section Φ_{old} according to the Bethe-Peierls theory. In the Bethe-Peierls theory $\Phi_{\parallel} = 0$.

TABLE 1

K_1/α	$\hbar\nu$ (MeV)	A	$-B$	C	D	Φ/r_0^2	Φ_{old}/r_0^2	$\Phi_{\parallel}/\Phi_{\perp}$
0·43	2·61	0·126	0·17	0·10	0·65	0·016	0·011	0·11
0·9	3·98	0·26	0·34	0·20	0·90	0·048	0·028	0·18
1·3	5·8	0·37	0·47	0·28	0·87	0·058	0·025	0·27
2·0	11·0	0·55	0·67	0·40	0·72	0·061	0·014	0·46
2·6	17·1	0·69	0·81	0·47	0·60	0·056	0·0084	0·65
4·0	37·4	0·93	1·03	0·59	0·42	0·048	0·0030	0·86
10*	222·2	1·31	1·35	0·74	0·18	0·030	0·00022	1·0

* This value is beyond the validity of our approximations.

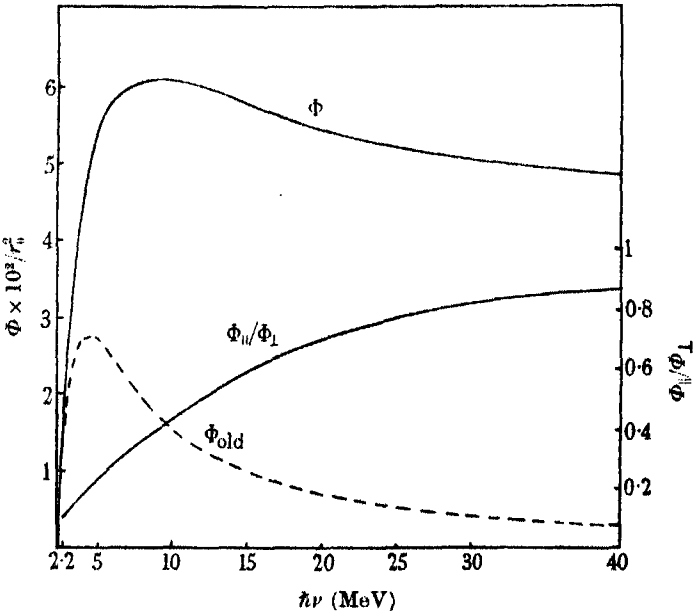

FIGURE 1

As it is seen from the figure, the total cross-section is for high frequencies very much larger than in the old theory. For the Li γ-rays (17 MeV), for instance, the cross-section is seven times larger in the new theory. The difference between the two theories is most striking in the asymptotic region for high frequencies, i.e. $\hbar\nu \gg E_0$, or $K_1 \gg \lambda, \alpha$. In this case we obtain

$$d\Phi = \frac{\pi^3}{8}\sin\theta\, d\theta \frac{1}{\lambda^2}\frac{e^2}{\hbar c}\left(\frac{f^2}{\hbar c}\right)^2 \times \frac{Mc\alpha}{\hbar\lambda^2}\sqrt{\left(\frac{Mc^2}{\hbar\nu}\right)}(3-\sin^2\theta), \tag{41}$$

$$\Phi = \frac{7\pi^3}{12}\frac{1}{\lambda^2}\frac{e^2}{\hbar c}\left(\frac{f^2}{\hbar c}\right)^2\frac{Mc\alpha}{\hbar\lambda^2}\sqrt{\left(\frac{Mc^2}{\hbar\nu}\right)}. \tag{42}$$

In the old theory, the cross-section is

$$d\Phi_{\text{old}} = 2\pi\sin\theta\, d\theta\frac{e^2}{Mc^2}\frac{\hbar}{Mc}\frac{\hbar\alpha}{Mc}\left(\frac{Mc^2}{\hbar\nu}\right)^{\frac{3}{2}}\sin^2\theta. \tag{43}$$

Hence

$$\frac{\Phi}{\Phi_{\text{old}}} = \frac{7\pi^2}{32}\left(\frac{f^2}{\hbar c}\right)^2\left(\frac{M}{\mu}\right)^3\frac{\hbar\nu}{\mu c^2}. \tag{44}$$

Thus in the new theory the cross-section decreases like $1/\sqrt{\nu}$ whereas in the old theory it decreases more rapidly, like $1/\nu^{\frac{3}{2}}$. As it is seen from equ. (42), this asymptotic behaviour is solely due to the f-type of interaction. Ordinary exchange forces also give an increase of the cross-section at smaller energies as has already been shown by Breit and Condon (1936). The angular distribution contains a constant term and a term proportional to $\sin^2\theta$. This is, however, not due as it might seem at first sight to a superposition of a S- and a P-distribution, but to a superposition of P- and F-distributions, as can be seen from the derivation in § 2. The process is a three-stage process; in each stage the angular momentum can change by one.

In the old theory the angular distribution is a pure P-distribution ($\sim\sin^2\theta$) as long as the photomagnetic effect is neglected. The latter leads to a pure S-distribution, i.e. to a term independent of θ. In the old theory (cf. Bethe and Bacher 1936), the photomagnetic effect is only appreciable for energies just above E_0 and is for high energies very small. In our theory the photomagnetic effect is zero in the approximations made in § 2. The two essential approximations which we have made were (i) $\hbar\nu \ll \mu c^2$ and (ii) $h\nu$ not too small (Born's approximation). For energies well above E_0 only the first approximation is essential, which means that the recoil of the meson due to the light quantum is neglected. If this approximation is not made we would obtain transitions to singlet terms, i.e. a photomagnetic effect, as well, but the cross-section for those transitions would be smaller by a factor of the order of at least $\hbar\nu/\mu c^2$.

The angular distribution is also influenced by the fact that the ground state of the deuteron contains a D-function. Even in the old theory one would obtain in addition to the P-, a F-distribution. The admixture of the D-wave function is probably quite small, as can be seen from the size of the quadripole moment which is about fifty times smaller than the cross-section of the deuteron (Kellogg *et al.* 1939). We, therefore, hardly expect any considerable modification of our results.

It should be possible to check this theory experimentally. At present, no experiments in the high-energy region are available. Such experiments would provide a very valuable check for the meson theory. A theory in which the nuclear forces are described by a neutral field would not lead to any such high cross-section and it is just the exchange nature of the nuclear forces which is responsible for our effect. Furthermore, as it is seen from the asymptotic formula (42) the large cross-section and the peculiar angular distribution is due to the f-type of the interaction of the meson and a heavy particle, i.e. to the spin-dependent interaction. This interaction which has no analogy in electrodynamics leads to new types of effects, such as the magnetic moment of the neutron, and to the spin-dependent proton-neutron interaction. In all these effects some kind of divergency occurs which has led to the assumption that the meson theory is only correct for small meson energies. Our effect is mainly due to mesons with kinetic energies not much higher than the rest energy, and for those energies the theory should be essentially correct.

The photoelectric effect of the deuteron provides therefore a test of some of the most interesting features of the meson theory, namely the f-type of the interaction and the charged nature of the field, in a region where it is not seriously affected by high-energy difficulties.

One of us (B. K.) would like to express his thanks to the Cavendish Professor for a grant from the Scott Fund.

SUMMARY

We have calculated the photoelectric effect of the deuteron on grounds of the meson theory of nuclear forces. In this theory the nuclear field is considered as electrically charged and, consequently, the light quantum can act on the nuclear field as well as on the proton. Because of the small mass of the meson, this effect is large. For the calculation we have assumed

for the ground state of the deuteron a ^3S-state. The result is that at high frequencies ν the cross-section is much larger than in the old theory, and decreases only like $1/\sqrt{\nu}$ as compared with the $1/\nu^{\frac{3}{2}}$ law in the Bethe-Peierls theory. Also the angular distribution is different. In addition to the $\sin^2\theta$ distribution about the direction of the γ-ray, there is a θ-independent term which becomes increasingly important for increasing energies. For the Li γ-rays (17 MeV), for instance, the cross-section is seven times larger than in the old theory and the ratio of the number of protons emitted parallel to the γ-ray to that emitted perpendicular to it is 0·7.

[*Note added in proof.*

While this paper was in press we noticed that the derivation of the matrix element (37) can be simplified if the approximations made in this paper (dipole radiation) are applied from the very beginning. The energy of the heavy particles does then not occur in the resonance denominators and the rules of ordinary matrix multiplication can therefore be applied for the summation over the intermediate states. The total matrix element then takes the following simple form:

$$V_a + V_b = ie\sqrt{\frac{2\pi}{\hbar\nu}}\int d\tau\, \psi_F^*(\mathbf{er})\, W\psi, \tag{45}$$

whilst V_c was:

$$V_c = -\frac{e\hbar}{M}\sqrt{\frac{2\pi}{\hbar\nu}}\int d\tau\, \psi_F^*(\mathbf{ep})\, \psi. \tag{46}$$

Here ψ_F is the deuteron wave function in the final state, $\mathbf{p}$ is the relative momentum of the deuteron and W the exchange potential of the deuteron (without the exchange operator) as given in F.H.K. equ. (44). Thus the meson effect finds its expression in the fact that the operator $(\mathbf{ep})/M$ which usually describes the interaction with light is replaced by

$$\frac{(\mathbf{ep})}{M} - \frac{i}{\hbar}(\mathbf{er})\, W. \tag{47}$$

This is true for dipole radiation only. Equ. (47) is in agreement with a general theorem derived by Siegert (1937) and confirmed by Lamb and Schiff (1938). These authors have also shown that the sum of the two operators (47) is equal to the operator $(\mathbf{er})$ if exact wave functions are used. We have used approximate wave functions and in this case, as shown in our paper, the consistent procedure is to take the operator (47).

The formula (45) is useful because it allows one to see more clearly in which way the frequency dependence of the cross-section is connected with the expression for the nuclear forces. The cross-section is proportional to $|V|^2\sqrt{\nu}$. From mere dimensional considerations it can easily be seen that terms of W proportional to $1/r^n$ give a contribution to the cross-section which asymptotically depends on ν like $\nu^{n-\frac{7}{2}}$. Thus our asymptotic formula (42) ($\Phi \sim 1/\sqrt{\nu}$) is due to the $1/r^3$ terms in the proton neutron interaction.]

REFERENCES

Bethe and Bacher 1936 *Rev. Mod. Phys.* **8**, 82.
Bethe and Peierls 1935 *Proc. Roy. Soc.* A, **148**, 146.
Bhabha 1938 *Proc. Roy. Soc.* A, **166**, 501.
Breit and Condon 1936 *Phys. Rev.* **49**, 904.
Fröhlich, Heitler and Kemmer 1938 *Proc. Roy. Soc.* A, **166**, 154.
Kellogg, Rabi, Ramsey and Zacharias 1939 *Phys. Rev.* **55**, 318.
Kemmer 1938 *Proc. Camb. Phil. Soc.* **34**, 354.
Lamb and Schiff 1938 *Phys. Rev.* **53**, 651.
Massey and Mohr 1935 *Proc. Roy. Soc.* A, **148**, 206.
Siegert 1937 *Phys. Rev.* **52**, 787.
Yukawa 1935 *Proc. Phys.-Math. Soc. Japan*, **17**, 48.
Yukawa, Sakata and Taketani 1938 *Proc. Phys.-Math. Soc. Japan*, **20**, 319.
Yukawa, Sakata, Kobayasi and Taketani 1938 *Proc. Phys.-Math. Soc. Japan*, **20**, 720.

Critical and co-operative phenomena
V. Specific heats of solids and liquids

BY A. F. DEVONSHIRE, PH.D.
The University Chemical Laboratory, Cambridge

(*Communicated by J. E. Lennard-Jones, F.R.S.—Received* 18 *August* 1939)

1. INTRODUCTION

In the first two papers in this series (Lennard-Jones and Devonshire 1937–8) we developed a simple method of calculating the free energy of a dense gas or a liquid in terms of interatomic forces. We used this to calculate critical temperatures and also vapour pressures and boiling-points. In later papers (Lennard-Jones and Devonshire 1939) we showed that the model used in the earlier papers was more appropriate to a solid than to a liquid, and that to obtain a satisfactory theory for a liquid we must modify it by introducing the concept of disorder. In this way we were able to account satisfactorily for the phenomenon of melting.

In this paper we propose to use the expression for the free energy obtained in the earlier papers to calculate the specific heats of solids and liquids, and also the coefficients of thermal expansion and compressibilities. As before, we confine ourselves to the case when quantum effects are negligible.

The theory of the specific heat of a solid on the assumption that it behaves like a set of harmonic oscillators has been fully discussed by Debye (1912), Born (1923), and Blackman (1934–5). But although this approximation has a wide range of validity it is probably not true for many solids at high temperatures. Damköhler (1935) has shown that c_v for the alkali halides almost certainly falls off at high temperatures, and by considering a linear chain of ions has shown that this can be accounted for by supposing that the vibrations are no longer harmonic. Our theory predicts a similar behaviour of the c_v values for solid rare gases if quantum effects can be neglected, as they can for krypton and xenon. Although no experimental values of c_v are known, the fact that our c_p values for krypton are in fair agreement with experiment indicate that the theory is approximately correct.

In a liquid the assumption that the molecules behave like simple harmonic oscillators is certainly not justified. For if this were so, the value of c_v for a monatomic liquid would tend to six calories at high temperatures whereas it is known that for argon it decreases steadily from 5·5 cal. at the melting-point down to 4·3 cal. at the critical point. The measurements show no discontinuity at this point but if continued to higher temperatures decrease steadily, reaching 3·5 cal. at 180° K. Other liquids also show a decrease. It is true that a decrease of c_v with temperature can be obtained if we assume that the frequency of vibration (ν) increases with the temperature. Magnus (1928) tried to account for the specific heat of mercury on this assumption, but found that with any reasonable law for the dependence of ν on T the rate of decrease of c_v was far too slow. The same defect would certainly hold for argon, and in any case the hypothesis seems unlikely on physical grounds. It seems much more reasonable to suppose, as we have done, that the molecules are moving in a field which is not parabolic. This has also been done by Eucken and Seekamp (1928), and Bartholomé and Eucken (1937), who both obtained a very slow decrease of c_v with temperature. They attributed the difference from the experimental results to association in the liquid, but it was certainly due in part to the fact that they assumed the potential field to be independent of the specific volume, which cannot be true. Though our value of c_v still decreases too slowly with temperature, it agrees with experiment much better than theirs. Moreover, their potential function contained adjustable constants, whereas ours is derived entirely from the law of force between molecules.

2. CALCULATIONS OF SPECIFIC HEATS

In Paper I we supposed the fields of the atoms to be spherically symmetrical and the potential to be of the form

$$\phi(r) = \phi_0\left\{\left(\frac{r_0}{r}\right)^{12} - 2\left(\frac{r_0}{r}\right)^{6}\right\}. \tag{1}$$

Now atoms obeying a law of force of this type would crystallize in the form of a face-centred cubic (Lennard-Jones and Ingham 1925) and the number of nearest neighbours of each atom would be twelve. We assume that in the liquid phase there is a tendency to this structure and that the average field in which any one moves can be represented approximately by the effect of the twelve nearest neighbours in their mean positions. Then the partition function obtained in Paper I, equation (48), can be written in the form

$$\frac{1}{N}\log F(T) = -\frac{\Phi_0}{NkT} + \tfrac{3}{2}\log(2\pi mkT/h^2) + \log(v\chi/N), \tag{2}$$

where
$$\Phi_0 = -NA\{1{\cdot}2(v_0/v)^2 - 0{\cdot}5(v_0/v)^4\}, \tag{3}$$

and is the mutual potential energy of N atoms, when arranged in a face-centred cubic lattice at their mean positions. This is easily obtained from (1) by adopting the summations given by Lennard-Jones and Ingham (1925) and by altering the notation so as to express the energy in terms of volume; thus,

$$A = c\phi_0, \quad v_0 = Nr_0^3/\sqrt{2}, \tag{4}$$

where c is the number of nearest neighbours ($= 12$), N the number of atoms in the assembly, v the total volume, and χ the fraction of the total volume which may be regarded as available to an atom; in fact

$$\chi = (1/v^*)\int \exp[-\psi(r)/kT]\,d\tau, \tag{5}$$

where the integral is taken over a unit cell of volume v^* (the specific volume) and $\psi(r)$ is the potential energy of the atom within its cell referred to that at its centre as zero. For the particular law of force defined by (1) χ is given by

$$\chi = 2\pi(2)^{\frac{1}{2}}g, \tag{6}$$

where
$$g = \int_0^{\frac{1}{4}} y^{\frac{1}{2}}\exp\left[\frac{A}{kT}\left\{-\left(\frac{v_0}{v}\right)^4 l(y) + 2\left(\frac{v_0}{v}\right)^2 m(y)\right\}\right]dy \tag{7}$$

(cf. equation (49), Paper I).

The partition function and free energy of the substance are now given by the equations

$$-\frac{A}{NkT}=\frac{1}{N}\log F=\frac{\Lambda}{kT}\left\{1\cdot2\left(\frac{v_0}{v}\right)^2-0\cdot5\left(\frac{v_0}{v}\right)^4\right\}+\tfrac{3}{2}\log\left(2\pi mkT/h^2\right)$$
$$+\log\left(2\pi\sqrt{2v^*}\right)+\log g, \qquad (8)$$

and the pressure, internal energy, entropy and specific heat by

$$\frac{pv}{NkT}=1-\frac{\Lambda}{kT}\left\{2\cdot4\left(\frac{v_0}{v}\right)^2-2\left(\frac{v_0}{v}\right)^4\right\}-\frac{4\Lambda}{kT}\left\{\left(\frac{v_0}{v}\right)^2\frac{g_m}{g}-\left(\frac{v_0}{v}\right)^4\frac{g_l}{g}\right\}, \qquad (9)$$

$$\frac{U}{NkT}=\frac{3}{2}-\frac{\Lambda}{kT}\left\{1\cdot2\left(\frac{v_0}{v}\right)^2-0\cdot5\left(\frac{v_0}{v}\right)^4\right\}-\frac{\Lambda}{kT}\left\{2\left(\frac{v_0}{v}\right)^2\frac{g_m}{g}-\left(\frac{v_0}{v}\right)^4\frac{g_l}{g}\right\}, \qquad (10)$$

$$\frac{S}{Nk}=\tfrac{3}{2}\log\left(\frac{2\pi mkT}{h^2}\right)+\tfrac{3}{2}+\log\left(2\pi\sqrt{2v^*g}\right)-\frac{\Lambda}{kT}\left\{2\left(\frac{v_0}{v}\right)^2\frac{g_m}{g}-\left(\frac{v_0}{v}\right)^4\frac{g_l}{g}\right\}, \qquad (11)$$

$$\frac{c_v}{Nk}=\frac{3}{2}+\left(\frac{\Lambda}{kT}\right)^2\left\{\left(\frac{v_0}{v}\right)^8\left(\frac{g_{ll}g-g_l^2}{g^2}\right)-4\left(\frac{v_0}{v}\right)^6\left(\frac{g_{lm}g-g_lg_m}{g^2}\right)+4\left(\frac{v_0}{v}\right)^4\left(\frac{g_{mm}g-g_m^2}{g^2}\right)\right\}, \qquad (12)$$

where $$g_l=\int_0^{\frac{1}{4}}y^{\frac{1}{2}}\,l(y)\exp\left[\frac{\Lambda}{kT}\left\{-\left(\frac{v_0}{v}\right)^4l(y)+2\left(\frac{v_0}{v}\right)^2m(y)\right\}\right]dy, \qquad (13)$$

and $$g_{ll}=\int_0^{\frac{1}{4}}y^{\frac{1}{2}}\,l^2(y)\exp\left[\frac{\Lambda}{kT}\left\{-\left(\frac{v_0}{v}\right)^4l(y)+2\left(\frac{v_0}{v}\right)^2m(y)\right\}\right]dy \qquad (14)$$

(cf. equations (50)–(55), Paper I).

To obtain c_p we use the thermodynamic relation

$$c_p=T\left(\frac{\partial S}{\partial T}\right)_p=T\left(\frac{\partial S}{\partial T}\right)_v+T\left(\frac{\partial S}{\partial v}\right)_T\left(\frac{\partial v}{\partial T}\right)_p$$
$$=c_v+T\left(\frac{\partial S}{\partial v}\right)_T\left(\frac{\partial v}{\partial T}\right)_p, \qquad (15)$$

and calculate $(\partial v/\partial T)_p$ from equation (9) and $(\partial S/\partial v)_T$ from equation (11). Equation (9) can also be used to calculate the coefficient of expansion, that is $(1/v)(\partial v/\partial T)_p$.

So far we have assumed that the atoms form an ordered array as in a crystal, but in order to account for the phenomenon of melting it is necessary to assume that in the liquid the atoms are in some way disordered. In Papers III and IV we assumed that this took place by certain atoms being transferred from their normal lattice sites to inter-lattice positions which we called β-sites. The process of melting was thus regarded as analogous to the order-disorder transformation and could be treated either by the Bethe method, as in Paper III, or by the less accurate method of Paper IV. In either case the effect is to add an extra term to the free energy of the substance. As the second method is a good deal simpler than the first, and the loss in accuracy is unimportant compared with the other approximations in the theory, we shall follow it here.

We assume that the number of β-sites is equal to the number of α-sites and that each α-site or β-site has z β-sites or α-sites surrounding it. In a configuration in which there are y pairs of neighbouring α- and β-sites we assume that the energy of the system has been increased by an amount yW, but that the available volume per atom is unaltered. Then if we use dashes to denote the additional free energy of the system and the derived functions we can show that

$$-\frac{A''}{NkT} = -\frac{zWQ(1-Q)}{kT} - 2(1-Q)\log(1-Q) - 2Q\log Q, \tag{16}$$

where Q is the fraction of occupied β-sites and is the least root of the equation

$$(2Q-1) = \tanh zW(2Q-1)/4kT. \tag{17}$$

For $zW/4kT < 1$, the only root of this equation will be $Q = \frac{1}{2}$, corresponding to a state of complete disorder, and we shall have

$$-\frac{A''}{NkT} = -\frac{zW}{4kT} + 2\log 2, \tag{18}$$

but for $zW/4kT > 1$ another root will exist. In the liquid there is complete disorder and equation (18) holds. It is easy to see that in this case $c_v'' = 0$, so that the disorder does not affect c_v. On the other hand, there is an additional pressure term given by

$$p'' = -\frac{\partial}{\partial v}A'' = -z\frac{dW}{dv}, \tag{19}$$

so that the coefficient of expansion and therefore c_p will be affected.

In Paper IV we found that $(1-Q)$ was quite appreciable in the solid state near the melting-point, so that the effect of disorder in the solid would be to increase c_v and c_p considerably. On this point, however, our theory is almost certainly in error, as we have neglected the fact that W will decrease as the disorder increases. Probably the effect of disorder on the solid is not very great, so in the calculations of the next section we have neglected it entirely.

3. NUMERICAL RESULTS

Measurements of c_v for the rare gases in the liquid state have been made on argon by Eucken and Hauck (1928), on neon by Clusius (1929), and on helium by Eucken (1914) and Keesom (1935). Our theory is certainly not applicable to helium where quantum considerations are all-important. For neon also their effect would be considerable, and in any case the neon used by Clusius is known to have been impure, so that we shall confine our comparison to the case of argon. In table 1 we give the values of c_v determined by Eucken and Hauck, with the specific volumes and temperatures at which these measurements were made, and also the values of c_v calculated by our theory. It will be seen that our values tend to vary less rapidly with temperature than they should, being too small at low temperatures and too large at high temperatures, but they agree with experiment in indicating a steady fall with temperature.

TABLE 1. SPECIFIC HEAT OF LIQUID ARGON

			c_v (cal. deg.$^{-1}$)	
T° K	v/v_0	A/kT	Obs.	Calc.
90	1·178	16·06	5·50	4·88
100	1·179	14·45	5·50	4·86
110	1·200	13·14	5·50	4·77
120	1·272	12·04	5·20	4·55
130	1·272	11·12	4·90	4·52
140	1·350	10·03	4·65	4·34
*150	1·445	9·63	4·35	4·17
160	1·445	9·03	4·00	4·16
170	1·463	8·50	3·75	4·12
180	2·029	8·03	3·50	3·65

* Critical temperature.

For the solid rare gases only the values of c_p are known, and in table 2 we give c_p calculated values (at zero pressure) as a function of A/kT together with the observed values for krypton and argon at corresponding temperatures. To determine A for krypton we assumed that A/kT was the same for argon and krypton at the melting-point. It will be noticed that the specific heat for argon is appreciably lower than that for krypton at corresponding temperatures (that is those at which A/kT is the same). This is what we should expect as for argon there must be an appreciable quantum effect, since the characteristic temperature is 80°. Hence the best test of our theory is to compare it with the observed values for krypton, and it is seen that the agreement is fairly good. The table also contains the values for c_p just above the melting-point calculated by the methods of Papers III and IV.

TABLE 2. SPECIFIC HEATS OF ARGON AND KRYPTON

				Krypton (obs.)*		Argon (obs.)†	
A/kT	c_v	$c_p - c_v$	c_p	T	c_p	T	c_p
29·0	5·60	1·16	6·76	69·0	6·51	49·9	5·90
27·0	5·57	1·28	6·85	74·1	6·66	53·5	6·10
25·0	5·53	1·45	6·98	80·0	6·83	57·8	6·29
23·0	5·48	1·61	7·09	87·0	7·06	62·8	6·55
21·0	5·43	1·86	7·29	95·2	7·35	68·8	6·90
19·20	5·38	2·11	7·49	104·2	7·70	75·3	7·34
17·82	5·33	2·45	7·78	112·2	8·28	81·1	7·80
17·24 melting-point							
16·62	‡ 5·21 § 4·89	5·46 4·41	10·67 9·30	120·3	10·67	87·1	10·06

* Clusius, 1938.

† Clusius, 1936.

‡ Calculated by the method of Paper III.

§ Calculated by the method of Paper IV.

TABLE 3. COMPRESSIBILITIES AND COEFFICIENTS OF THERMAL EXPANSION

				Nitrogen	
A/kT	v/v_0	$\alpha A/k$	$\chi A/v_0$	T	α
30·0	0·9689	2·08	0·0252	38·7	0·00179
28·0	0·9737	2·16	0·0263	41·4	0·00186
26·0	0·9796	2·24	0·0276	44·6	0·00193
24·0	0·9869	2·34	0·0291	48·3	0·00202
22·0	0·9957	2·45	0·0315	52·7	0·00211
20·0	1·0072	2·57	0·0345	58·0	0·00222
18·40	1·0191	2·71	0·0381	63·0	0·00234
17·24	1·0300	2·92	0·0415		

In table 3 we have given the calculated values of the volume at zero pressure, the cubic coefficient of thermal expansion α, and the cubic compressibility χ, as functions of A/kT. The actual values tabulated are those of v/v_0, $\alpha A/k$, and $\chi A/v_0$, since these, being pure numbers, are the same for all gases to which our theory is applicable. The only experimental result with which the values can be compared is the average thermal expansion of nitrogen between 39 and 63° K, whose value is found by Keesom and Lisman (1934) to be 0·0021. The value of A/k for nitrogen can readily be calculated from the force constants given by Lennard-Jones (1937) and is found to be 1160°. Using this value we can at once deduce the temperature corresponding to a given value of A/kT and the corresponding value of α in (degrees)$^{-1}$.

These are given in the same table, and the average value of α over the range 39–63° K is seen to be 0·0021 in agreement with experiment.

Equations (9) and (10) giving the pressure and specific heat are independent of the mass of the molecules. Our calculated values will therefore be the same for all isotopes of a given element. Differences would be found if quantum effects were allowed for, but we have considered only cases where these are small and may be neglected.

In conclusion I should like to thank Professor Lennard-Jones for suggesting this problem and for his continued interest and advice. I am also indebted to the Department of Scientific and Industrial Research for a grant.

SUMMARY

Specific heats of simple substances in the liquid or solid phase have been calculated in terms of the intermolecular forces. Comparison is made with the experimental values for krypton and argon, and fair agreement is obtained. Calculations are also made of thermal expansion and compressibility.

REFERENCES

Bartholomé, E. and Eucken, A. 1937 *Trans. Faraday Soc.* **33**, 45.
Bethe, H. 1935 *Proc. Roy. Soc.* A, **150**, 552.
Blackman, M. 1934 *Proc. Roy. Soc.* A, **148**, 365, 384.
— 1935 *Proc. Roy. Soc.* A, **149**, 117, 126.
Born, M. 1923 Atomtheorie des Festen Zustandes. *Encycl. Math. Wiss.* **5**, pt. 3, no. 25.
Bragg, W. and Williams, E. J. 1934 *Proc. Roy. Soc.* A, **145**, 699.
Clusius, K. 1929 *Z. Phys. Chem.* B, **4**, 1.
— 1936 *Z. Phys. Chem.* B, **31**, 459.
— 1938 *Ann. Phys., Lpz.*, **33**, 642.
Damköhler, G. 1935 *Ann. Phys., Lpz.*, **24**, 1.
Debye, P. 1912 *Ann. Phys., Lpz.*, **39**, 789.
Eucken, A. 1914 *S.B. preuss. Akad. Wiss.* **22**, 682.
Eucken, A. and Hauck, F. 1928 *Z. Phys. Chem.* **134**, 161.
Eucken, A. and Seekamp, H. 1928 *Z. Phys. Chem.* **134**, 178.
Keesom, W. H. and Keesom, A. 1935 *Commun. Phys. Lab. Univ. Leiden*, 235*d*.
Keesom, W. H. and Lisman, J. H. C. 1934 *Physica*, **1**, 737.
Lennard-Jones, J. E. 1937 *Physica*, **4**, 941.
Lennard-Jones, J. E. and Devonshire, A. F. 1937 *Proc. Roy. Soc.* A, **163**, 53 (Paper I).
— — 1938 *Proc. Roy. Soc.* A, **165**, 1 (Paper II).
— — 1939 *Proc. Roy. Soc.* A, **169**, 317 (Paper III); **170**, 464 (Paper IV).
Lennard-Jones, J. E. and Ingham, A. E. 1925 *Proc. Roy. Soc.* A, **107**, 636.
Magnus, A. 1928 *Z. anorg. Chem.* **171**, 73.

The emission spectrum of hydrocarbon flames

By E. C. W. Smith
*Radiation Gas Research Fellow, Imperial College
of Science and Technology, London*

(*Communicated by A. C. G. Egerton, Sec.R.S.—Received* 23 *August* 1939)

[Plates 2, 3]

INTRODUCTORY

The present investigation was commenced at the suggestion of the late Professor W. A. Bone, as a continuation of the systematic examination of flame spectra which had been carried out in his laboratories (Weston 1925 *a*, *b*; Bone and Lamont 1934; Bell 1937). It was decided to extend the work to the case of unsaturated hydrocarbons by a comprehensive study of ethylene flames, accompanied by chemical investigation of the products of reaction.

The emission spectrum of hydrocarbon flames generally, in the visible and ultra-violet regions, is characterized by the bands of the OH molecule at $\lambda\lambda$ 3428, 3122, 3064, 2875, 2811 and 2608 A, of the CH molecule at $\lambda\lambda$ 4317, 3888 and 3140 A, and of the C_2 molecule at $\lambda\lambda$ 4737, 5165, 5635 A, etc., together with an extensive diffuse band system extending through the visible and near ultra-violet, first observed by Vaidya (1934) in the ethylene flame, and ascribed by him to the molecule CHO. Other observers have suggested the molecules H.CHO (Kondratjew 1936) and CH_2 (Bell 1937) as the emitter of the system, without very satisfactory evidence of either chemical or spectroscopic nature. In addition continuous emission spectra of unknown origin are frequently observed, while an extensive diffuse banded system extending through the visible spectrum, and observed in the outer cones of many flames, has been shown by Fowler and Gaydon (1933) to be identical with the afterglow observed with CO in discharge tubes, and to be most probably emitted by excited CO_2 molecules formed in the direct combination of CO and O_2. The well-known γ bands of NO in the ultra-violet are frequently observed in intense flames when nitrogen is present. Rich, soot-forming flames of hydrocarbons exhibit a continuous spectrum having its intensity maximum in the infra-red, which is undoubtedly emitted by carbon aggregates raised to the temperature of the flame.

EXPERIMENTAL

The effect of pressure on the stationary flames of ethylene and ethylene-hydrogen mixtures burning in air

It was decided to investigate first the effect of pressure on the stationary flame of ethylene burning in air. The form of the apparatus used was precisely that described fully by Bone and Lamont (1934). It was found necessary to heat electrically the steel plugs holding the thick crystalline quartz windows by means of an external winding of nichrome wire, in order to prevent condensation of water on the windows.

The spectrum of the flame burning under these conditions at atmospheric pressure, as recorded by the Hilger E488 quartz spectrograph, figure 7, *a*, plate 2, was similar in all respects to that shown by Vaidya (1934). A minimum air supply favoured the emission of the C_2 band system, while excess air caused its almost complete disappearance, and an increase in the intensity of the OH, CH and "ethylene flame" band systems. With this apparatus exposures of the order of 1 hr. were necessary to record with adequate intensity the "ethylene flame" system and the less intense OH bands.

On allowing the pressure in the flame chamber to increase, by impeding the exit of the products of combustion, it was observed that at some pressure less than two atmospheres, dependent on the ethylene-air ratio, the flame became yellow and smoky, emitting the characteristic "carbon aggregate" continuum, and depositing carbon on the windows to such an extent that further observation was impossible.

In an attempt further to elucidate this phenomenon, the experiment was repeated with various mixtures of ethylene and hydrogen. Preliminary trials showed that at atmospheric pressure the flame of any mixture containing more than about 5–6 % of ethylene was spectroscopically identical with that of pure ethylene. On allowing the pressure to increase with such a mixture, it was first observed that the flame became almost non-luminous, the spectrum showing a very pronounced decrease in the intensity of all the bands in the visible region, only the OH bands persisting. Subsequently the flame became yellow and smoky, and carbon was deposited. The pressure range over which these changes were observed was dependent on the proportion of ethylene in the mixture, being between 1 and 11 atm. for a 6 % ethylene–94 % hydrogen mixture, and between 1 and 2 atm. for a mixture containing 26 % of ethylene. The effect is clearly shown in figure 7, *b*, *c*, *d*, *e*, *f*, plate 2.

An attempt was made to study the flame of ethylene burning in oxygen, but difficulty was experienced owing to the heating of the multitubular silica jet through which the ethylene passed, this causing its thermal decomposition, and the blocking of the tubes with carbon.

Flames at reduced pressure

An investigation of the burning of ethylene in air at pressures less than atmospheric was next made. Ethylene and air were drawn through oil-filled flowmeters, and allowed to mix at a T-piece, their rates of flow being adjusted by pinchcocks. The mixed gases passed along a tube packed with copper gauze, which served to complete the mixing and at the same time prevent the flame travelling back along it. The rate of flow of the mixed gases was controlled by another pinchcock. The gases then entered the explosion tube A shown in figure 1, of diameter 1·7 cm. and length 22·5 cm., which was provided with clear fused quartz windows, sealed on with hard red wax, thence to the aluminium electrodes B, C, between which sparks were passed from a small induction coil. The explosion flame thus ignited passed back along the tube A against the gas stream, the spectrum being observed through either of the quartz windows. The dismountable trap, D, cooled in a solid carbon dioxide-acetone mixture, served to condense any liquid products of combustion. The gaseous products passed through the tube E

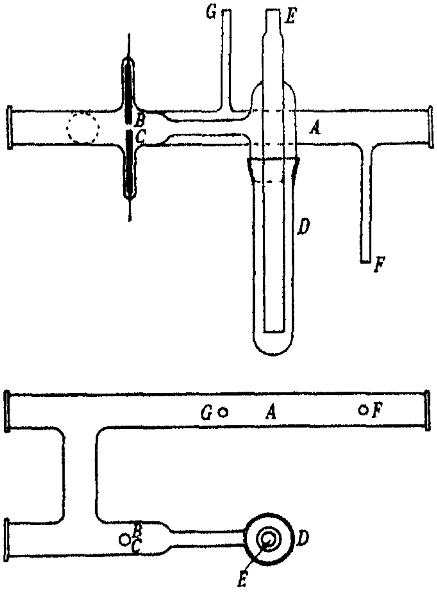

Figure 1. Apparatus.

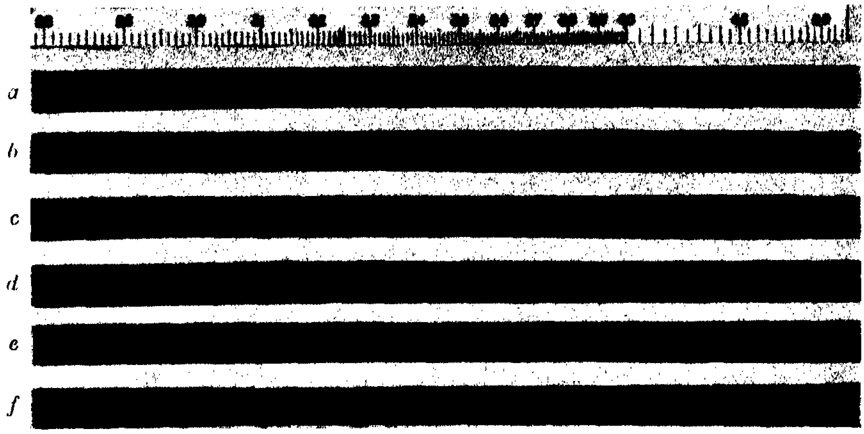

FIGURE 7. Continuous flames of ethylene and of ethylene-hydrogen mixtures burning in air at varying pressures. (*a*) Pure ethylene at atmospheric pressure. (*b*) 7·5 % C_2H_4–92·5 % H_2 at atmospheric pressure. (*c*) 7·5 % C_2H_4–92·5 % H_2 at 2 atmospheres. (*d*) 7·5 % C_2H_4–92·5 % H_2 at 5 atmospheres. (*e*) 7·5 % C_2H_4–92·5 % H_2 at 7 atmospheres. (*f*) 7·5 % C_2H_4–92·5 % H_2 at 11 atmospheres.

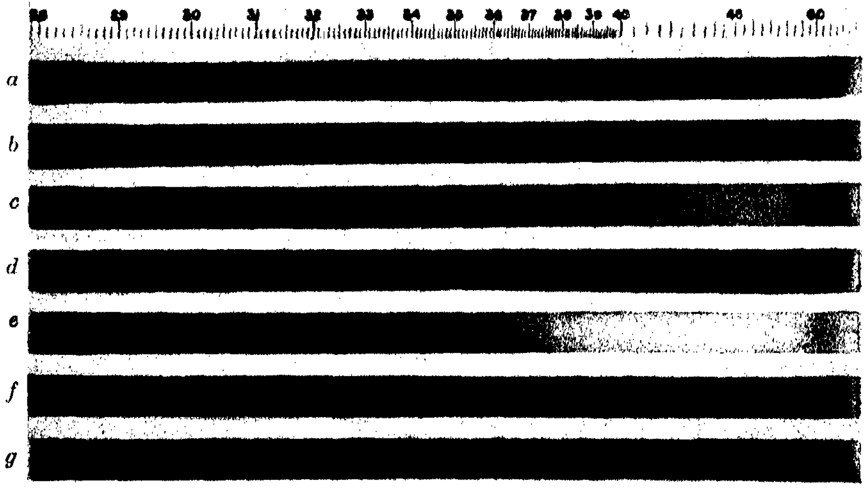

FIGURE 10. Ethylene-oxygen explosion flames at higher pressures. (*a*) 50 % C_2H_4 at 760 mm. (*b*) 46·3 % C_2H_4 at 760 mm. (*c*) 19·3 % C_2H_4 at 760 mm. (*d*) 9·4 % C_2H_4 at 760 mm. (*e*) 46·3 % C_2H_4 at 1270 mm. (*f*) 19·3 % C_2H_4 at 1400 mm. (*g*) 9·4 % C_2H_4 at 1500 mm.

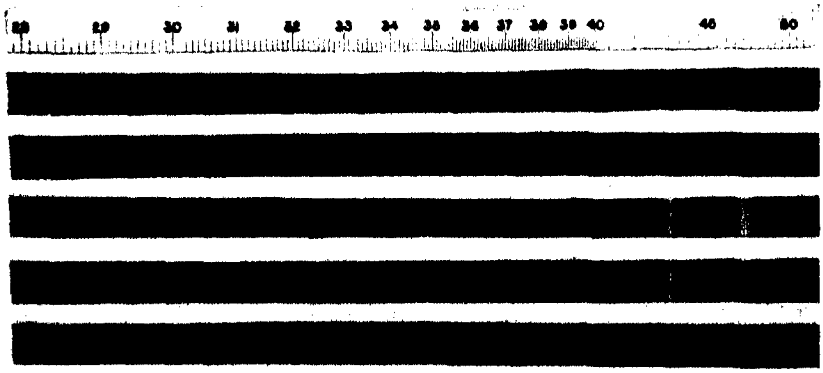

FIGURE 8. Ethylene-air explosion flames at 600 mm. pressure. (*a*) 15·0% C_2H_4. (*b*) 12·6% C_2H_4. (*c*) 10·1% C_2H_4. (*d*) 7·0% C_2H_4. (*e*) 4·0% C_2H_4.

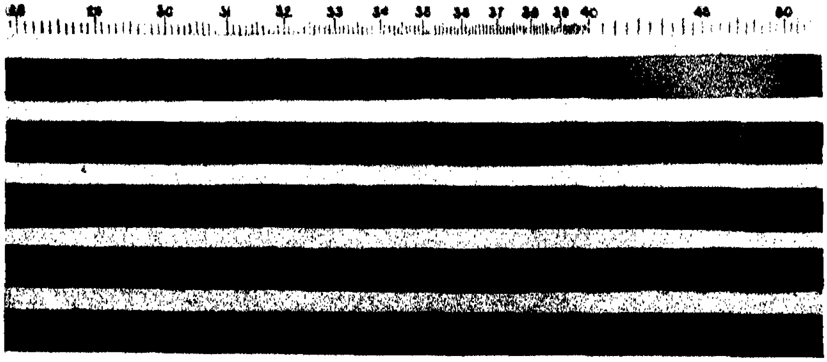

FIGURE 9. Ethylene-oxygen explosion flames at 100–150 mm. pressure. (*a*) 47·2% C_2H_4. (*b*) 38·8% C_2H_4. (*c*) 30·0% C_2H_4. (*d*) 26·9% C_2H_4. (*e*) 10·2% C_2H_4.

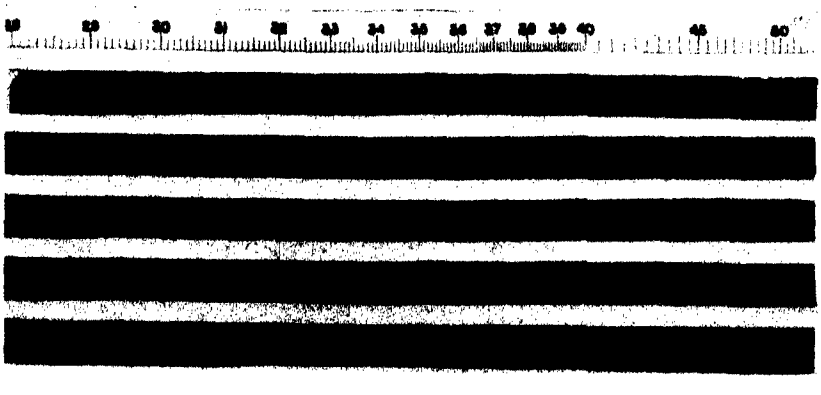

FIGURE 11. Propane-air explosion flames at 500 mm. pressure. (*a*) 9·9% C_3H_8. (*b*) 8·3% C_3H_8. (*c*) 6·5% C_3H_8. (*d*) 5·7% C_3H_8. (*e*) 4·0% C_3H_8.

and a pinchcock to the Leybold rotary oil pump. A gas burette connected at *F* served to draw off samples of the unexploded mixture; the samples of gaseous products were taken at the exit tube of the pump. A mercury manometer at *G* served to measured the pressure in the explosion tube.

Normally the process was continuous, the explosion flames passing through the tube spontaneously at intervals of a few seconds or less, but in the case of the slower flames it was possible, if desired, to hold the flames stationary in *A* by careful adjustment of the pinchcocks, so that the velocity of the flame was accurately balanced by the feed velocity of the mixture under investigation.

In connexion with the examination of the spectra of the explosion flames at reduced pressure, the apparatus provided a convenient means of determining at all pressures below atmospheric the complete inflammability ranges under the conditions of the experiment, and these have been plotted in the case of all the mixtures examined. It is important to note, however, that the limits so determined do not obey the usual criterion of ability to propagate flame throughout the whole length of the tube, but pertain to all possible forms of flame which passed into the observation tube *A*, since it was intended to make a spectrographic examination of all types of flame, including "flame caps".

By suitable adjustment of the pinchcocks it was possible to observe the changes in the nature of the flame brought about either by variation of the pressure with a given mixture, or by variation of the mixture at a constant pressure. In the latter circumstance the results were somewhat striking; figure 8, plate 3, records the emission from the flames of a series of mixtures of increasing ethylene content, exploded at 600 mm. pressure. With the very weak mixtures, containing only 3–4 % of ethylene, the flame was blue in colour, and the bands of OH and CH, and the "ethylene flame" system, were emitted strongly; no trace of the C_2 bands was observable. As the proportion of ethylene was increased to about the "theoretical" $C_2H_4:3O_2$ ratio, the flame became violet in colour, and was propagated at high speed; it was also characterized by a strong emission of the OH and CH bands, with a moderate emission of the C_2 and "ethylene flame" bands. With still greater increase in the ethylene content of the mixture, the flame became brilliantly green in colour; the OH and CH emission was recorded very strongly, but the C_2 bands had now become predominant to an extent such as to give rise to the striking green coloration of the flame. The "ethylene flame" system was relatively weak under these conditions. These flames are the characteristic "green flames" observed initially in the case of di-ethyl ether by Townend and Chamberlain (1937), and which have since been the subject of further investigation by Townend and Hsieh (1939). As the ethylene content of the mixture was increased still further, in the present case to about 12·1 %, an abrupt change was observed in the nature of the flame, which appeared with a blue head followed by a yellow smoky tail, carbon being deposited on the surface of the tube. The spectrum showed that the C_2 bands had entirely disappeared, while the "carbon aggregate" continuum was strong; this was accompanied by a weak emission of CH and OH, the "ethylene flame" system being entirely absent. With still greater ethylene concentrations, approaching the limit of inflammability, only the continuous emission was observed, OH and CH having also disappeared.

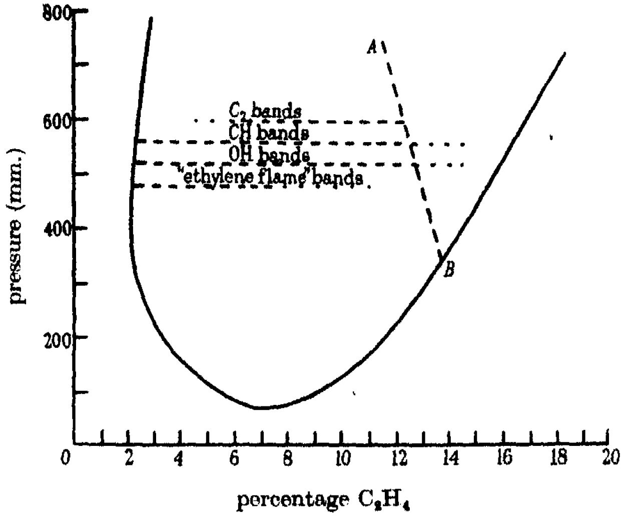

FIGURE 2. Inflammability limits for ethylene-air mixtures in glass explosion tube. The pecked lines give an indication of the intensities of the principal band systems observed in the flame, the lengths of the dashes being roughly proportional to the band intensities for the corresponding mixture.

Figure 2 shows the complete inflammability limit curve observed in this apparatus, while the line *AB* gives the approximate limits for the occurrence of carbon deposition, accompanied by the continuous emission and the disappearance of the C_2 bands. A rough indication is also given of the variation of intensity of all the band systems observed as the ethylene content of the mixture was varied. It was noted that in the case of the very rich mixtures at the higher pressure ranges, approaching the equimolecular $C_2H_4 : O_2$ mixture, explosion did not occur if the mixture was sparked continuously, but the flame was propagated right through the tube if a train of sparks was passed at intervals of several seconds. A commutator device, to provide such a train of sparks at any desired time interval, was accordingly constructed and used in the case of these mixtures.

After each run for a known time under given conditions, the trap *D* was dismounted, some 20 c.c. of distilled water added to the condensate, and the resulting solution tested for liquid products of combustion. The detailed consideration of the results obtained will be deferred to a subsequent section.

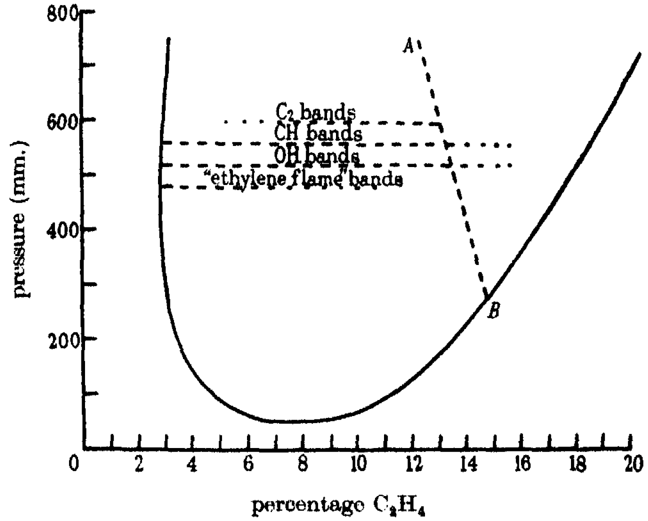

FIGURE 3. Inflammability limits for C_2H_4–O_2 : $3N_2$ in glass explosion tube.

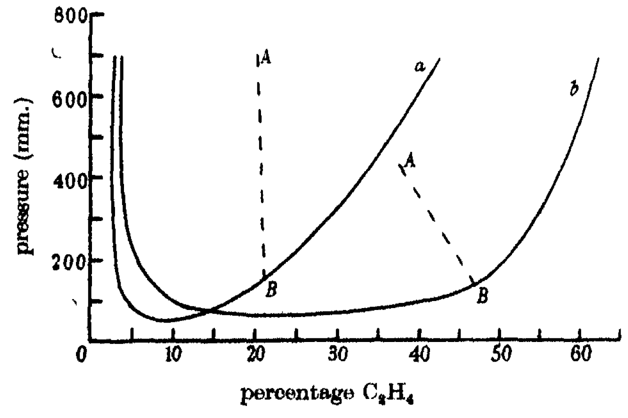

FIGURE 4. (*a*) Inflammability limits for C_2H_4–O_2 : $2N_2$ in glass explosion tube.
(*b*) Inflammability limits for C_2H_4–O_2 in steel bomb.

Similar experiments were carried out using enriched air, mixtures having the composition $O_2:3N_2$ and $O_2:2N_2$ being employed. Curves of the explosive limits observed in this apparatus are given in figures 3 and 4; they are of similar form to those observed with normal air, but the upper explosive limit is somewhat widened. Similar regions of carbon deposition were observed, and their approximate locations are indicated on the diagrams. The minimum pressure for carbon deposition is lower in the case of these enriched air mixtures, although the percentage of ethylene giving rise to deposition at pressures approaching atmospheric is not widely different.

The spectra observed with these mixtures were also very similar, showing much the same variation in the intensity of the CH, OH, C_2 and "ethylene flame" bands, as will be seen from the indications of intensity given on the diagram. With the $O_2:2N_2$ mixture the range over which the flame exhibited the characteristic green colour associated with the predominant emission of the C_2 bands was somewhat narrowed, but these bands remained at considerable intensity over a wide region of the inflammable range.

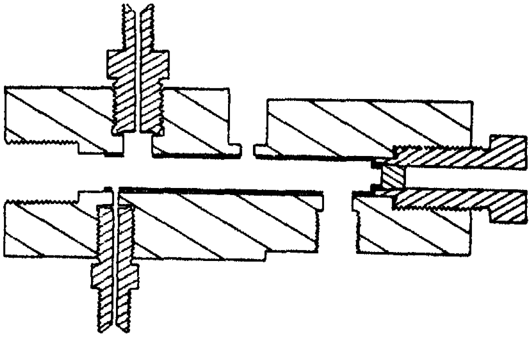

FIGURE 5. Details of construction of bomb.

Although this glass apparatus sufficed for the determination of the limiting mixtures even for the $O_2:2N_2$ mixture at the higher pressures, it was evident that the explosions in the middle of the range were much too violent to be carried out in a glass apparatus. Accordingly a small nickel steel explosion bomb was modified by the provision of plugs carrying thick crystalline quartz windows, with suitable additional plugs along its length to serve for the addition and removal of the gases, and for the determination of the pressure, and a further central aperture to admit a standard 9 mm. sparking plug. The details of the construction of this bomb are shown in figure 5. Preliminary experiments having shown that considerable corrosion of the internal surface of the bomb was caused by the reactive heated gases generated by the explosion, a "Staybrite" steel liner was fitted to the explosion chamber, together with disks of similar material on the ends of the plugs which were exposed to the gases.

The procedure adopted to provide a gas-tight seal between the quartz windows and the steel end plugs was as follows. The window having been ground with a taper of 11°, and the corresponding taper in the end plug roughly ground by means of a copper plug to be as nearly as possible similar, a silver mirror was deposited on one end and the circumferential surface of the window, and a hard layer of copper, several hundredths of an inch thick, electro-deposited on this from an ammoniacal copper cyanide solution, using a very low current density. The end surface was then cleaned, and the window lightly rubbed into the plug with a rotary motion, until it was in contact with the steel throughout its length, a little rouge being used to accelerate the process if desired. The window was then "wrung" into the plug with the exercise of some considerable pressure, causing the copper to "flow" at the surface of contact. Joints made in this way have proved very satisfactory in use over long periods.

The same arrangement of flowmeters, manometer, mixing tube and pump was used as with the glass explosion tube. Preliminary tests showed that the explosion range for a given enriched air mixture was considerably narrowed on the rich mixture side. On the other hand, for normal mixtures the emission was spectroscopically identical with that observed for the same mixture in the glass explosion tube. This fact having been established it was possible to extend the observations to pressures approaching atmospheric in the case of the $O_2 : 2N_2$ mixture.

The spectra emitted under these conditions were not markedly different from those of the less rich air mixtures. Some iron atom lines were visible on the plates, arising undoubtedly from the processes responsible for the corrosion noted previously; in some cases, also, weak band systems, apparently those of FeO, were visible on the plates. Copper lines were almost invariably present to some extent, due to contamination from the copper gauze or the copper capillary pipe used in the connexions.

The explosions of ethylene-oxygen mixtures were then examined; these were naturally very much more violent, and it was found that only those at relatively low pressures, or those of very rich or very weak mixtures at higher pressures, could safely be carried out in this apparatus. The explosion limit curve observed is given in figure 4. A region of carbon deposition, accompanied by the emission of the characteristic continuum, was observed in this case also, and is indicated on the diagram up to a pressure of some 400 mm., which was the highest pressure at which the appropriate mixture could be safely exploded in this apparatus.

The spectra of a representative set of mixtures at pressures of 100–150 mm. are given in figure 9, plate 3. It will be noted that the band systems emitted are precisely those obtained in the mixtures containing nitrogen, and that the variation of intensity of these bands is very similar to that observed previously, except that the "ethylene flame" system occurs only over a very narrow range close to the explosion limit for weak mixtures. OH and CH bands persist throughout this range, while the C_2 bands, which are not apparent with mixtures containing less than some 8 % of ethylene, increase in intensity with increasing ethylene content until, at 150 mm., they disappear abruptly at some 44 % ethylene, and the "carbon continuum" becomes prominent, accompanied only by some faint OH and CH emission. With mixtures of the order of the "theoretical" $C_2H_4:3O_2$ a somewhat different continuous spectrum, fairly uniformly distributed throughout the visible and near ultra-violet regions, is superposed on the band systems. Considerable emission of the lines of iron and copper are observed in all the plates, except those of the weakest mixtures.

Static explosions in the steel explosion bomb

In order to extend the investigation to pressures greater than atmospheric, and to ethylene-oxygen mixtures which could not be safely exploded in the flow system just described, some plates were obtained by exploding previously mixed gases confined in the same steel explosion bomb, the system being evacuated and refilled between each explosion. The arrangement of the filling system was quite conventional; the explosive mixtures were made up and stored in a separate high pressure cylinder. Pressures up to two atmospheres were measured with a mercury manometer, and higher pressures by means of a Bourdon gauge. Initial and final pressures were measured in each case, and samples of the initial mixture and gaseous explosion products taken for analysis. After filling the bomb to the requisite pressure, the filling valve was tightly closed, and the connexion between it and the rest of the system evacuated, before firing the charge.

The first set of experiments was made with ethylene-air mixtures of varying composition, in order to determine the position of the carbon deposition limit at pressures above atmospheric. In agreement with the results obtained when working with stationary flames under pressure, it was found that for any given mixture there was some pressure above which carbon deposition occurred. In the case of mixtures weak in ethylene, it was very difficult to determine the carbon deposition point, as the total luminosity of the flame was small, and moreover a certain amount of continuous emission fairly uniformly distributed throughout the spectrum was superposed on the band systems at pressures lower than that at which the deposition was observed. As far as could be ascertained, carbon deposition accompanied by the emission of the "carbon aggregate" continuum took place initially at 1500 mm. for the mixtures lowest in ethylene content within the inflammable range in the apparatus employed. No new band systems were observed, and the intensity changes in the CH, OH and C_2 systems as the composition was varied were similar to those observed at lower pressures. See figure 10, plate 2.

Experiments were also carried out with ethylene-oxygen mixtures of varying composition at initial pressures up to two atmospheres. Above this pressure the quartz windows were liable to failure due to internal cracking. The emission observed under these conditions was very different from that at lower pressures, the characteristic feature, except with mixtures of high ethylene content, being the development of an intense continuum having its intensity maximum in the violet, and stretching well into the ultra-violet region. On this was superposed some emission of the OH bands, together with lines of copper and iron. No trace of the CH, C_2 or "ethylene flame" systems was observed at pressures greater than some 300 mm. With very rich mixtures, i.e. of ethylene content more than 50 %, only the characteristic "carbon aggregate" continuum was observed. With some 40 % of ethylene in the mixture, the "violet" continuum was also developed, together with faint emission of the OH bands, and lines of copper and iron. At higher pressures, approaching two atmospheres, the copper lines at $\lambda\lambda$ 3240, 3270 A were in reversal. Weaker mixtures, containing for example about 20 % of ethylene, showed only the continuous emission, together with copper and iron lines, at pressures above 400 mm. At higher pressures, approaching two atmospheres, there was some indication that the OH bands were present in absorption, while the reversal of the copper lines at $\lambda\lambda$ 3240, 3270 A was well marked. With mixtures containing only some 10 % of ethylene, the continuum was again very strongly developed throughout the spectrum at all pressures, but the OH emission was faintly visible at pressures up to atmospheric. At pressures of the order of two atmospheres, however, the OH band was clearly in absorption.

The condensable products of the flames of ethylene in air

As previously stated, a trap cooled with a solid carbon dioxide-acetone mixture was attached to the pyrex explosion tube; the condensate in the trap was examined in an attempt to study the variation of these products with composition and pressure.

The procedure adopted was briefly as follows: the rate of flow of the ethylene was maintained as nearly as possible at 4·5 l./hr., and the air flow and exit pinchcocks adjusted to allow the required mixture to ignite at a predetermined pressure. In each case a run was continued for 1 hr., then the bottom of the trap removed, some 10 c.c. of water added, and the sample allowed to attain room temperature. The liquid was then made up to 30 c.c. and submitted to the tests described below.

The total acid in the mixture was first estimated by titration of 10 c.c. of this solution against a standard caustic soda solution, using phenolphthalein as indicator. Next the total aldehyde was determined by adding an excess of neutralized hydroxylamine hydrochloride, allowing to stand for 15 min., and titrating the hydrochloric acid released against standard caustic soda solution, using brom-phenol blue as indicator. Formaldehyde was estimated separately by comparison of the colour developed with Schiff's reagent against that of standard formaldehyde solutions, using a simple form of colorimeter. The remainder of the stock solution was tested for the presence of peroxide by addition of an acid solution of titanic sulphate. Standard solutions of hydrogen peroxide permitted a quantitative determination by comparison of the intensity of the colour produced.

Experiments were made at 300, 400, and 500 mm. with sets of representative ethylene-air mixtures. The results show some unsystematic variation probably accountable by the fact that in some cases the explosion flame travelled right down into the trap, while in others it was only propagated into the explosion tube itself. They show, quite clearly, however, that the formation of both acid and aldehyde passes through a minimum in the region of the "theoretical" $C_2H_4:3O_2$ mixture, at which the amounts of both products observed were negligibly small; in the case of the acid formation, the amounts rise regularly as the mixture is progressively weakened or enriched, to a value of some 6×10^{-5}M, i.e. about 0·03 % of the ethylene burned; the total aldehyde formation, on the other hand, increases very rapidly with the richer mixtures, to some 40×10^{-5} M, or 0·2 % of the ethylene burned for the mixtures near the upper inflammability limit. With very weak mixtures the aldehyde formation also tends to increase, but to a much less extent, some 5×10^{-5} M being obtained with mixtures containing 4 % of ethylene. The estimation of formaldehyde was probably not so accurate as that of the total aldehyde, and the results obtained show more variation, but in general about 80–90 % of the total aldehyde was formaldehyde. The peroxide tests gave erratic results, being often entirely negative, and in no case exceeding 2×10^{-5} M. Values of this order were obtained for both very rich and very weak mixtures, but those near the "theoretical" mixture were always negative. No certain indication of the effect of pressure on the formation of any of these products could be observed over the range investigated.

Systematic tests over the full range were not made in the case of the ethylene-enriched air and ethylene-oxygen mixtures, but the indications were that both qualitatively and quantitatively the formation of these products was similar in all cases.

Propane-air explosion flames at reduced pressure

For comparison with the results obtained with ethylene, an investigation was undertaken into the emission of a saturated hydrocarbon exploded in air at reduced pressures. Propane was selected for the purpose, and the flame examined in the apparatus described on p. 112 under precisely similar conditions to those used in the ethylene experiments.

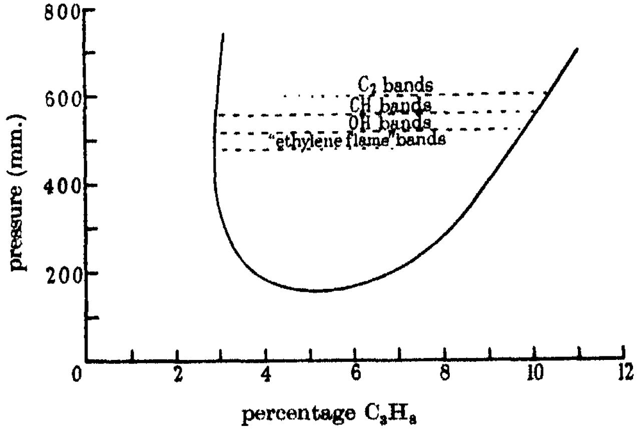

Figure 6. Inflammability limits for propane-air mixtures in glass explosion tube.

A curve of the inflammability limits was first determined, and is given in figure 6. Examination of the spectrum showed that the same band systems of OH, CH and C_2, and the "ethylene flame" were emitted, no other bands being observed (see figure 11, plate 3). The variation of intensity of these bands was also similar to that of ethylene, and is indicated on the diagram. The only outstanding difference was that there was no region in which carbon deposition occurred, within the pressure range examined. The characteristic "green flame" due to preponderance of C_2 emission stretched right up to the upper limit even at the highest pressures investigated, the range observed here being more extensive than that given by Townend and Hsieh (1939), but it is certain that this phenomenon is dependent on tube diameter, since it was noted that with certain less rich mixtures, flames which appeared blue in the main explosion tube became green when they entered the narrow tube which served to connect the manometer to the system. This fact will be discussed further in a later section.

DISCUSSION

The application of emission spectra to the elucidation of the mechanism of chemical reaction

The recognition of the possible importance of the part played by free radicals in flame and explosion reactions has given an added interest to observations of the emission spectra of such processes, since these methods allow of the identification of certain radicals present in the system, and may in some cases give information concerning the relative abundance of such species under different conditions. In attempting to apply the data obtained by this method to the determination of the nature of the chemical processes involved, a number of factors must be taken into consideration. It must first be recognized that the absence of an emission spectrum characteristic of a particular molecule or atom must not be assumed as a criterion that such a species is not present in the system. It is possible that the energy levels of the particle involved may be such as not to give rise to an emission spectrum in the region observed; or, alternatively, if such a spectrum is known to exist, the conditions of excitation in the system may not give rise to the formation of a sufficient number of excited molecules in the upper level involved in the transition. Again, the observation of an emission spectrum may be prevented by self-absorption, if the population of the appropriate lower level is sufficiently high, leading finally to the reversal of the spectrum. Further, it is most important to recognize that the species giving rise to an emission spectrum are not ipso facto those which are of importance in the main course of the chemical reaction occurring in the system; for example, we may visualize the formation by a relatively slow reaction, of a particular molecule which subsequently reacts rapidly with some other species; then, although the actual amount of this molecule formed during the course of the reaction may be very large, it is certain that the stationary concentration will never be adequate to give rise to an emission spectrum arising through normal thermal excitation, even if the other conditions necessary for the emission of such a spectrum are fulfilled.

It must also be recognized that the production of excited molecules in flame and explosion processes may take place by any of four separate methods, that is, by collision with particles of high kinetic energy derived from thermal agitation of the system owing to the heat liberated in the chemical reaction, by collisions with other excited species, by the direct formation of electronically excited molecules by chemical reaction, and by excitation consequent upon light absorption. The application of emission spectra data to the elucidation of the mechanism of chemical reaction is a complex problem, in which it is necessary to take into account all of the above-mentioned factors.

Carbon deposition and "green flames" in explosion processes

It has been suggested by Bone and Outridge (1936) that carbon deposition in explosions of equimolecular ethylene-oxygen mixtures with varying amounts of diluent gases was primarily a function of the flame temperature developed in the particular mixture. This explanation would appear to be inadequate in the light of the present investigation. The observation that the explosion flame of ethylene-air mixtures changes the nature of its emission entirely, with only a very small change of either pressure or mixture composition, from the intense "green flame" condition, characterized by the predominant emission of C_2 bands, to the yellow, smoky flame showing continuous emission in the visible region, with only faint bands of OH and CH, would appear to be of considerable interest. In this connexion it will be recalled that Klemenc, Wechsberg and Wagner (1934*a*, *b*) have postulated that the thermal decomposition of carbon suboxide, at temperatures in excess of 200° C, goes according to the reaction:

$$C_3O_2 \rightarrow C_2 + CO_2.$$

The C_2 so formed was recognized by its absorption spectrum, but rapidly polymerizes to normal solid carbon, this latter reaction having a very high temperature coefficient.

It would seem very probable that the carbon deposition observed in the present case may well be formed by an analogous reaction, if it may be assumed that the conditions of stability of the C_2 molecule under flame conditions are very critical. No information concerning such conditions of stability is to be derived from the present experiments, and the matter must await further investigation*.

---

* It has been suggested to me by Professor D. T. A. Townend that there would appear to be a correspondence between the system giving rise to carbon deposition, which apparently centres upon mixtures having about a 1:1 combustible-oxygen ratio, and discontinuities observed by Townend and Hsieh (1939) in systems giving rise to cool flames. This would suggest that this abrupt carbon deposition may be associated with a critical change in the slow combustion processes in front of the flame.

With regard to the persistence of the C_2 bands in the mixtures of greater oxygen content, it has been noted that in the present experiments with propane-air mixtures, the range over which the flame was predominantly green in colour was considerably wider than that observed by Townend and Hsieh (1939), and it has been suggested that this phenomenon is related to the diameter of the explosion tube. It is to be expected on theoretical grounds that the ${}^3\Pi C_2$ molecules will react readily with molecular oxygen in the ground state, and it would appear probable that the temperature coefficient of this reaction accounts for the observed effect.

The persistence of CH bands throughout the entire range, except for mixtures very rich in ethylene, is in accord with the theoretical expectation that these molecules, being in a ${}^2\Pi$ state, will not readily react with oxygen molecules in the lowest ${}^3\Sigma$ state.

The observation of the reversal of the OH bands in ethylene oxygen mixtures at the higher pressures is interesting, particularly as it seems generally accepted that the formation of OH radicals plays a predominant part in the combustion of hydrogen. If the range of pressures examined had not been sufficiently extensive, it might well have been assumed that the disappearance of the OH emission with increasing pressure was indicative of the suppression of the formation of OH molecules. It should be noted that Bell (1937) has explained the observed diminution with increasing pressure of the intensity of the OH systems in methane-oxygen mixtures as directly caused by the suppression of the formation of OH molecules, but it would appear possible that the phenomenon was caused by self-adsorption as in the present case.

The origin of the "ethylene flame" bands

The observations of the variation of intensity of the "ethylene flame" bands would seem to confirm the suggestion that the emitter of this system is a molecule containing oxygen. Although no direct evidence of the precise nature of this molecule can be obtained from the present experiments, the fact that the maximum intensity of this system is observed in the very weak mixtures when only CH and OH molecules are observed in emission would seem to render plausible the suggestion that the molecule concerned may well be an isomeric formaldehyde molecule of the form HC—OH. The characteristics of the observed band system are such as might be expected from a molecule of this type, while its formation would provide a possible explanation for the observed increase in the production of formaldehyde in the combustion of mixtures containing a large excess of oxygen.

I wish to express my gratitude to the Trustees of the Radiation Gas Research Fellowship, during the tenure of which the above work was carried out, and also to Professors A. C. Egerton, D. M. Newitt and D. T. A. Townend, for helpful discussions and suggestions.

SUMMARY

An examination has been made of the emission of stationary and explosion flames of ethylene in air, enriched air and oxygen, and of the explosion flames of propane in air, together with a chemical examination of the condensable products of reaction. The explosive limits of these mixtures have also been determined.

It is suggested that the carbon deposition observed at pressures in excess of some critical value with ethylene mixtures may be due to the polymerization of C_2 molecules. It would appear that the "green flame" regions observed by Townend and Chamberlain and by Townend and Hsieh for various ethers and hydrocarbons are determined solely by the stability of the same species.

It is suggested that the so-called "ethylene flame bands" which also occur in the spectra of propane and other hydrocarbon flames are possibly emitted by an isomeric formaldehyde molecule, HC.OH.

REFERENCES

Bell 1937 *Proc. Roy. Soc.* A, **158**, 429.
Bone and Lamont 1934 *Proc. Roy. Soc.* A, **144**, 250.
Bone and Outridge 1936 *Proc. Roy. Soc.* A, **157**, 234.
Fowler and Gaydon 1933 *Proc. Roy. Soc.* A, **142**, 362.
Klemenc, Wechsberg and Wagner 1934*a* *Z. Elektrochem.* **40**, 488.
— — — 1934*b* *Z. Phys. Chem.* **170**, 97.
Kondratjew 1936 *Acta phys.-chim. U.S.S.R.* **4**, 556.
Townend and Chamberlain 1937 *Proc. Roy. Soc.* A, **158**, 415.
Townend and Hsieh 1939 *J. Chem. Soc.* p. 332.
Vaidya 1934 *Proc. Roy. Soc.* A, **147**, 513.
Weston 1925*a* *Proc. Roy. Soc.* A, **109**, 177.
— 1925*b* *Proc. Roy. Soc.* A, **109**, 523.

On the production of radium E and polonium by deuteron bombardment of bismuth

By D. G. Hurst, Ph.D. (McGill), 1851 *Exhibition Scholar*,
R. Latham, B.A., *Queens' College*, and
W. B. Lewis, Ph.D., *Cavendish Laboratory, Cambridge*

(*Communicated by J. D. Cockcroft, F.R.S.—Received* 28 *August* 1939)

Introduction

Using deuterons of energies up to 4·4 MeV, Livingood (1936) observed the production of Ra E from bismuth by observing the α-particles from the polonium to which Ra E decays. The Cambridge cyclotron has been used to examine the above reaction in more detail at energies up to 9 MeV. The work of Livingood was confirmed and in addition another reaction, the direct production of Po by a (d, n) reaction, was found to occur. The variation of yield with energy has also been determined for these two nuclear reactions.

Preliminary study of the reactions

The beam was brought out through a thin platinum window into the air where the deuterons had a maximum energy of 8·8 MeV. Two specimens of bismuth were bombarded with approximately 1·5μA-min. of these particles. The α-particles from these were observed with an ionization chamber and linear amplifier and followed for about 40 days after exposure. The experiments indicate that all the α-particles observed are emitted by polonium and the reactions taking place are

(I) ${}_{83}\mathrm{Bi}^{209}(d, p)\,{}_{83}\mathrm{Ra\,E}^{210}$ followed by ${}_{83}\mathrm{Ra\,E}^{210} \rightarrow {}_{84}\mathrm{Po}^{210} + \beta$,

(II) ${}_{83}\mathrm{Bi}^{209}(d, n)\,{}_{84}\mathrm{Po}^{210}$,

with in each case the well-known radioactive transformation

$${}_{84}\mathrm{Po}^{210} \rightarrow {}_{82}\mathrm{Pb}^{206} + \alpha.$$

The specimens showed both an initial α-particle activity and in addition a rise of activity with the 5 days half-life expected from the decay of Ra E. The results are plotted in figure 1, where the points represent the observed numbers of counts per minute, and the curve the expected growth and decay of Po assuming the observed maximum number of counts and a ratio of

Ra E to Po present in the target after bombardment of 4·75 to 1. The β-particles from the two specimens were counted giving the decay curve of figure 2. The values for specimens 1 and 2 have here been adjusted to the same initial number of counts/min. It will be seen that from 24 hr. after bombardment the β-particles fall off with a 5·0 days half-life. Two other β-particle activities have since been observed with half-lives of about 3 min. and 20 min. The 3 min. period precipitates with lead from a solution of the bismuth target in nitric acid as sulphate, chloride and carbonate, and does not precipitate with bismuth, thallium or polonium.

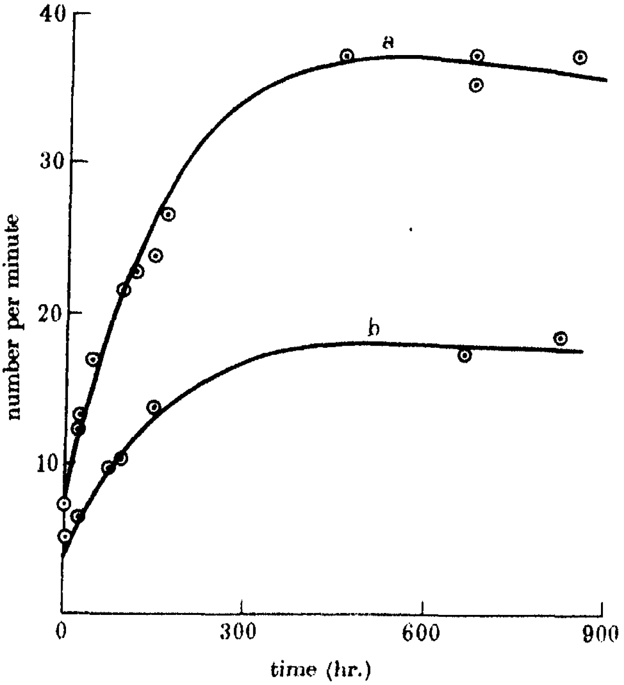

FIGURE 1. Curve a, specimen 1; Curve b, specimen 2.

The 20 min. period does not precipitate with lead, bismuth, thallium or polonium, and may therefore be a contamination.

A search for α-particles decaying or growing with periods of this order was made, with negative results.

THE EXCITATION FUNCTIONS

The two reactions $_{83}\text{Bi}^{209}$ (d, p) $_{83}\text{Ra E}^{210}$ and $_{83}\text{Bi}^{209}$ (d, n) $_{84}\text{Po}^{210}$ give an interesting opportunity of comparing the relative probabilities of the (*d*, *p*) and (*d*, *n*) processes for various energies of deuterons. Because both the above reactions lead to polonium, and the relative amounts of polonium due to the two reactions can be accurately determined, a precise determination of the relative probabilities of the (*d*, *p*) and the (*d*, *n*) reactions is possible. In general one of the products of the (*d*, *p*), (*d*, *n*) reactions is a stable isotope, and in the rare cases when both are unstable the particles emitted are of the same nature, increasing the difficulty of the experiment. In our case the fact that α-particles are emitted only by the polonium enables the growth of the Po to be followed with ease in the presence of the radiations from Ra E.

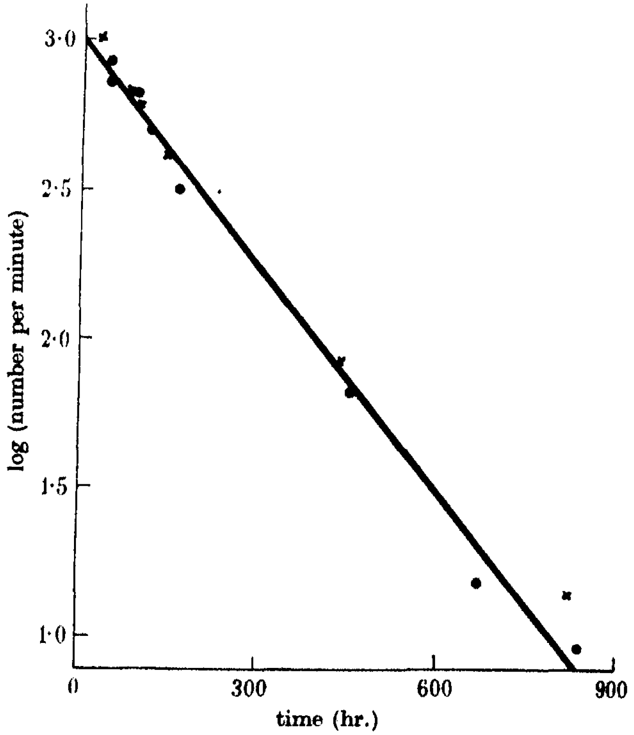

FIGURE 2. ⊙, specimen 1; ×, specimen 2.

The theoretical discussion of the (*d*, *p*) and (*d*, *n*) processes for deuterons of energies less than the potential barrier assumes two different mechanisms, and the variation of the relative yields with deuteron energy gives a numerical check of the theoretical predictions.

With this in view thin layers of bismuth were prepared by evaporating Hilger spectroscopically pure bismuth on to aluminium foils *in vacuo*. The aluminium foil was weighed before the evaporation, and after the bismuth had been deposited the foil was cut into pieces 1·2 × 2 cm. Each piece was weighed and the air equivalent was calculated from data tabulated by Livingston and Bethe (1937) on stopping powers. The air equivalent of the Bi layer was arranged to be of the order of 1 cm., i.e. about 3 mg./sq. cm.

Stacks of these foils sufficient to stop the deuterons were clamped to a water-cooled brass holder and bombarded in air with deuterons. The range in air of the deuterons was measured with a fluorescent screen from the position of the foils. A preliminary run showed that the reaction could be observed down to about 5 MeV. Below this energy the inhomogeneity of the beam due to straggling becomes large, and even though the intensities could be increased by lengthening the time of irradiation it is doubtful whether the excitation curves so obtained would have sufficient accuracy to be of value. A second run was made with thinner foils, arranged to give more points in the higher region of energy.

The counting was done with an ionization chamber, linear amplifier, and scale of ten counter, the counter being biased to record all α-particles entering the chamber. The amplifier and counter were standardized from day to day using a thin film of uranium oxide as a constant source of α-particles.

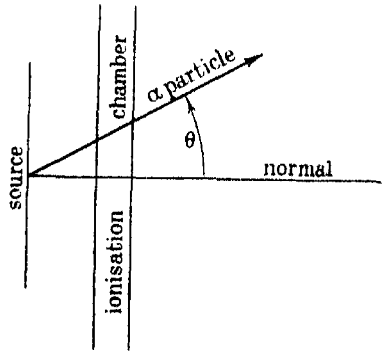

FIGURE 3

THE EFFECTS OF FOIL THICKNESS

For a plane source and a shallow ionization chamber of large area compared with the source, whether or not an α-particle from a given depth below the surface of the source is recorded, will depend on the angle θ (figure 3) which the α-particle makes with the normal to the source. For all values of θ less than a critical one there will be a sufficient length of track emerging to give a count, so that all particles within a certain solid angle are counted.

This solid angle was estimated for the conditions of the experiment. It was found that for a given yield the number of counts could be taken as proportional to the thickness of the bismuth film with, in the worst case, an error of about 3 %. This worst case corresponded to a variation of about 10 % from the mean thickness. The assumption of a plane ionization chamber of large area leads to an over-estimate of the actual error as the α-particles are partly canalized by the grid supporting the front foil of the chamber, and by the fact that the chamber is not large compared with the source.

Corrections for the varying thicknesses of the foils were therefore made by reducing them proportionally to a mean foil thickness.

Reduction of results

Similar curves to figure 1 were obtained for each foil. To reduce these to the initial amounts of RaE and Po the procedure was as follows.

If E_0 is the number of Ra E atoms formed and P_0 the number of polonium atoms formed, then the number of α-particles per second at any time t after the bombardment is proportional to:

$$P = \left(P_0 + \frac{\lambda_E}{\lambda_E - \lambda_P} E_0\right)(\tfrac{1}{2})^{n_P} - \left(\frac{\lambda_E}{\lambda_E - \lambda_P}\right) E_0 (\tfrac{1}{2})^{n_E},$$

where n_P, n_E are respectively the number of half lives of Po and Ra E since the bombardment $\left(\text{e.g. } n_P = \frac{t \text{ days}}{136}\right)$ and λ_P, λ_E are the decay constants of Po and Ra E.

In terms of x and y, where $x = (\frac{1}{2})^{n_E - n_P}$, which decreases with time, and $y = P/(\frac{1}{2})^{n_P}$, which involves directly the number of particles at any time. This becomes

$$bx + y = a, \quad a = P_0 + \frac{\lambda_E}{\lambda_E - \lambda_P} E_0,$$

$$b = \frac{\lambda_E}{\lambda_E - \lambda_P} E_0.$$

The values of a and b and hence P_0 and E_0 are readily found by plotting the number of counts and their times in terms of the variables x and y (figures 4 and 5), and drawing a straight line through the points with due recognition of the importance of the early points. This is easier and more accurate than fitting a curve of the type of figure 1.

From the values of P_0, E_0 for the different foils an excitation function showing the variation of the probability of these two reactions can be drawn. This is done in figure 6 and the actual values are given in table 1.

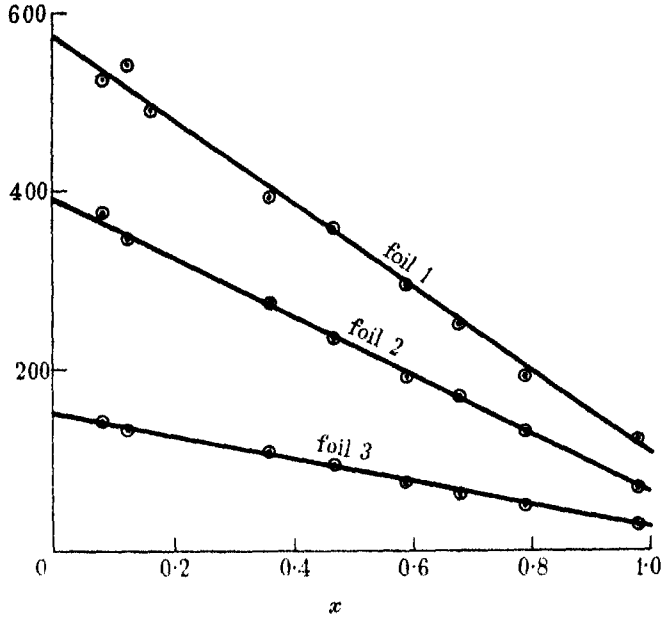

FIGURE 4

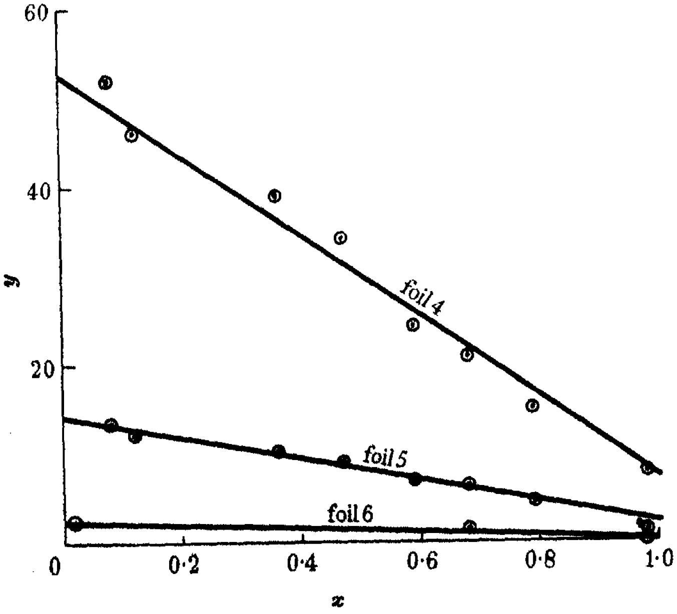

FIGURE 5

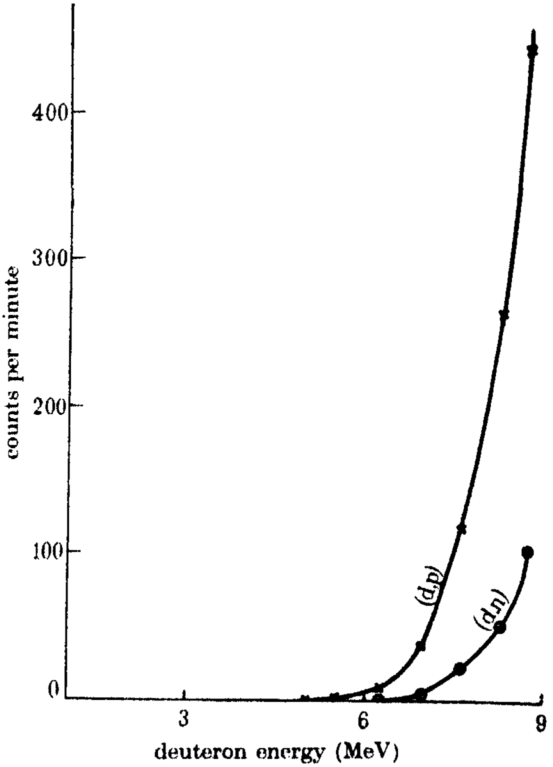

FIGURE 6

TABLE 1

Energy of deuteron MeV	Counts/min. due to Po formed from Ra E, i.e. (*d*, *p*) reaction	Counts/min. due to Po formed directly, i.e. (*d*, *n*) reaction	Ratio $\frac{(d, p)}{(d, n)}$
8·75	445	104	4·3
8·3	265	52·5	5·0
7·6	118	24	4·9
6·95	39	6·2	6·3
6·25	9·8	1·5	6·5
5·5	2·0	None observed $< 0·3$	—

ERRORS OF THE EXPERIMENT

The errors inherent in this type of experiment are large. The accuracy of the numbers of counts per min. for the (*d*, *p*) and (*d*, *n*) reactions is probably of the order of ± 5 % for the larger energies, falling off considerably as the energy is reduced. Most of the variation here is due to statistical fluctuations of the counts.

The values of the energies corresponding to a particular foil are probably correct relative to each other to about 0·2 MeV. The actual energies of the points are dependent on the initial energy of the deuterons, and this is not known to more than 0·2 or 0·3 MeV. The value of the initial energy from the magnetic field and the geometry of the cyclotron, and from the range in air using a fluorescent screen agree satisfactorily. There is no evidence from the beam in air of any appreciable inhomogeneity in ranges. The inhomogeneity due to straggling will be of the order of 0·15 MeV when the deuteron energy is reduced to 5 MeV.

DISCUSSION OF THE RESULTS

Calculations on the penetration of nuclei by charged particles by Gamow (1928, 1929) and Condon and Gurney (1928, 1929) led to results which are in agreement with experiment, for disintegrations by protons and α-particles. The deuteron however is neither a simple particle like the proton, nor a closely bound assemblage like the α-particle. It consists of a proton and neutron, with a binding energy of 2·2 MeV. This low binding energy introduces a new possibility for disintegration, namely, that the deuteron does not penetrate the barrier as a whole but that the electric field outside the nucleus disrupts the deuteron into a proton and neutron, the latter then entering the nucleus. Calculations by Oppenheimer and Phillips (1935) later extended by Bethe (1938) give a probability for this type of reaction which at low energies is higher than the probability on the Gamow theory. Owing to the high energy required for a proton to have an appreciable probability of escape from inside the nucleus and because the excitation energy is unlikely to be concentrated on one particle, it is to be expected that the actual penetration of the barrier by the deuteron will usually be followed by the emission of a neutron since this does not have to escape through the potential barrier. The excitation energy is known from the known nuclear mass defects to be in the neighbourhood of 15 MeV so that one proton is not likely to be excited to more than a small fraction of this, and the potential barrier is about 9·7 MeV.

We are thus led to expect that the (d, n) reaction will follow if the deuteron goes into the nucleus, while the (d, p) reaction will be mainly due to an Oppenheimer-Phillips process. The latter assumption is necessary to explain the large ratio, 4 to 6, between the (d, p) and (d, n) reactions in favour of the (d, p) reaction.

In the calculations certain factors such as the "sticking probability" enter which are not known to a factor of 100 or more. However, it is to be expected that in the region of deuteron energies with which we are concerned these factors will not vary appreciably compared with the variation of a factor of the form $e^{-\gamma}$ occurring in both theories. This on the Gamow theory is proportional to the chance of the deuteron penetrating the potential barrier.

We have calculated the values of γ as follows:

(1) Gamow: $$\gamma = \left\{\frac{4M^{\frac{1}{2}}Ze^2}{\hbar I^{\frac{1}{2}}}\epsilon^{-\frac{1}{2}}f(\epsilon\rho)\right\},$$

where $$\epsilon = \frac{\text{Energy } E \text{ of incident deuteron}}{\text{Binding energy } I \text{ of deuteron}},$$

$$f(x) = \text{arc}\cos x^{\frac{1}{2}} - x^{\frac{1}{2}}(1-x)^{\frac{1}{2}},$$

$$\rho = (I/Ze^2)\,R, \quad R = \text{radius of nucleus.}$$

ρ is the ratio of the deuteron binding energy to height of the potential barrier and is assumed for the calculations to be 0·22.

(2) Oppenheimer-Phillips. Bethe (1938):

$$\gamma = \left\{\frac{4M^{\frac{1}{2}}Ze^2}{\hbar I^{\frac{1}{2}}}F(\epsilon\eta_0\rho)\right\},$$

where $$F(\epsilon\eta_0\rho) = \epsilon^{-\frac{1}{2}}f(\epsilon\eta_0) + \phi(\eta_0\rho),$$

$$\eta_0 = (I/Ze^2)\,r_0,$$

r_0 = the distance of the deuteron from the centre of the nucleus when it breaks up.

For $\eta_0 = \rho$, $r_0 = R$ and the deuteron reaches the nucleus before breaking up, $\phi(\eta_0\rho)$ becomes zero and the Oppenheimer-Phillips formula becomes identical with the Gamow formula.

$\eta_0 = \rho$ occurs at a value of the deuteron energy:

$$E = Ze^2/R - I = 7{\cdot}6\,\text{MeV}.$$

Figure 7 shows curves of the values of γ calculated from the above compared with curves of the logarithms of the yields for the (d, p) and (d, n) reactions. Agreement with theory occurs if the theoretical and experimental curves are parallel.

It will be seen that for lower energies the (d, n) reaction agrees closely with the Gamow curve.

The observed ((d, p)) curve will consist of two parts, the yield due to the Oppenheimer-Phillips process, and the yield due to actual penetration of the nucleus, so it might be expected to have an intermediate slope. The slope is in fact slightly less than the Gamow curve, lending some support to the view that the Oppenheimer-Phillips process is taking place. An upper limit can be set to the contribution due to penetration of the nucleus by assuming that it is equal to the (d, n) yield, because, as mentioned previously, once the compound nucleus is formed the emission of a neutron is much more likely. A plot of $\log_e\{(d, p)$ yield $- (d, n)$ yield$\}$ certainly does show better agreement with the Oppenheimer-Phillips process, but the improvement is not marked.

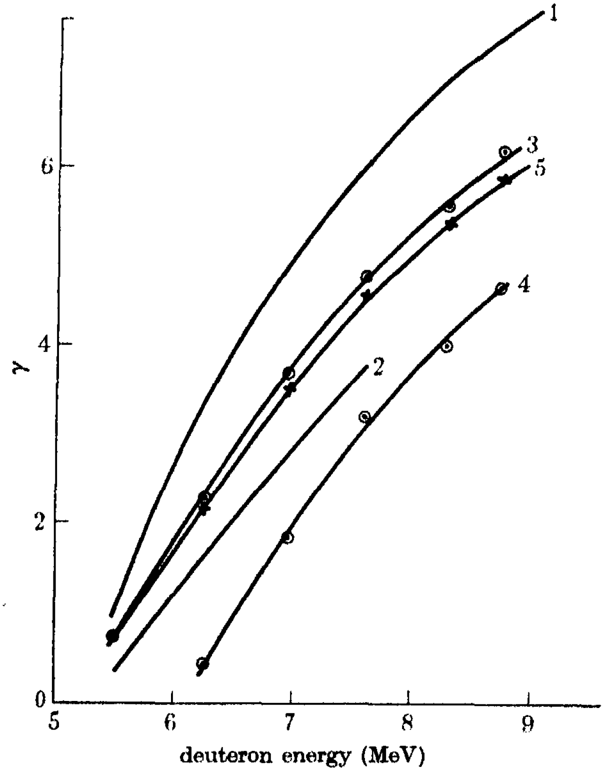

FIGURE 7. The calculated and experimental values of γ.
Curve 1. γ on the Gamow Theory.
Curve 2. γ on the Oppenheimer-Phillips Theory.
Curve 3. $\log_e\{(d, p)$ yield$\}$.
Curve 4. $\log_e\{(d, n)$ yield$\}$.
Curve 5. $\log_e\{(d, p)$ yield $- (d, n)$ yield$\}$.

We find that even at energies higher than 7·6 mV the (d, p) process remains more probable than the (d, n) by a factor of 4 to 5. This may possibly be due to contributions to the Oppenheimer-Phillips process by higher states of angular momentum of the incident particle.

The experimental evidence cannot be used to decide whether there is any definite threshold for the (d, n) reaction at an energy where the (d, p) reaction is still probable. The yield at low energies is very small and consequent errors prevent any decision for or against an initial activity in Livingood's samples. Owing to the spread of energies when the beam energy is reduced by foils, it would be difficult to detect a threshold at the low energies involved.

It is noteworthy that the formation of Po from bismuth is one of the few observed (d, n) reactions in the heavy elements.

We wish to express our thanks to Dr Heitler and Dr Kahn for discussions of the theoretical points involved. We wish to thank Dr J. D. Cockcroft, and also A. K. Solomon, A. E. Kempton, D. H. T. Gant, R. Emrich, R. S. Krishnan, C. G. Tilley, who have assisted in the construction of the cyclotron.

SUMMARY

The Cambridge cyclotron has been used to examine the reactions occurring when bismuth is bombarded with deuterons of energies up to 8·7 MeV.

The reactions found to take place are the formation of Ra E by a (d, p) process, and of Po by a (d, n) process. The Ra E subsequently decays into Po by the emission of an electron; with a 5 days' half-life.

By determining the amounts of Po formed directly, and indirectly following the decay of Ra E, it has been possible to measure the relative yields of the (d, p) and (d, n) reactions at various energies of the deuteron.

The excitation functions for the two reactions have been compared with the values to be expected on theoretical grounds.

REFERENCES

Bethe, H. A. 1938 *Phys. Rev.* **53**, 39.
Condon, E. U. and Gurney, R. W. 1928 *Nature, Lond.*. **122**, 439.
— — 1929 *Phys. Rev.* **33**, 127.
Gamow, G. 1928 *Z. Phys.* **51**, 204.
Gamow, G. and Houtermans, F. 1929 *Z. Phys.* **52**, 496.
Livingood, J. J. 1936 *Phys. Rev.* **49**, 876; **50**, 425.
Livingston, M. S. and Bethe, H. A. 1937 *Rev. Mod. Phys.* **9**, 272.
Oppenheimer, R. and Phillips, M. 1935 *Phys. Rev.* **48**, 500.

The torsional flexibility of aliphatic chain molecules

By Alex Müller

(*Communicated by Sir William Bragg, F.R.S.—Received 26 October* 1939)

The rotation of the CH_3 groups round the single C—C bond in ethane is associated with a threshold energy of about 3000 gcal./gmol. or 2×10^{-13} erg/mol. (Schäfer 1938; Kistiakowsky, Lacher and Strutt 1939). In an aliphatic CH_2 chain where the carbon atoms are linked together by single bonds the corresponding energy must be of the same order and is most likely rather smaller. Supposing we consider any particular C—C bond in the chain and treat the two parts at each side of this bond as rigid rotators, then their kinetic energy would be $2 \times \frac{1}{2}\kappa T$ which at room temperature amounts to about one-fifth of the threshold energy. It seems very likely under these circumstances that a chain molecule of say ten to twenty carbon atoms should already at room temperature show signs of distortion due to internal rotation. If this is true, then the previously observed increase of the crystal symmetry at the melting-point of paraffins (Müller 1930, 1932) and the corresponding changes of the polarization of long-chain ketones (Müller 1937, 1938) can no longer be ascribed entirely to a rotation of the molecule in the field of the surrounding molecules but must at least partly be due to this internal distortion. It is clear that a distortion of this type tends to destroy the anisotropy of the molecule and to give an apparent isotropy to the crystal.

The present experiments were made in order to obtain an estimate of the magnitude of the distortion effect. It is found to be surprisingly large.

The principle of the experiment is the following: The polarization/temperature curves are investigated experimentally for two normal chain ketones. The two substances are shown in figure 1. They have two ketone dipoles each and since they differ only by one CH_2 group are chemically very similar to each other. The essential difference between the two lies in the orientation of the two dipoles in relation to each other. The ketone with ten carbon atoms has according to the diagram its two oxygen atoms on opposite sides of the carbon chain. Since the dipole is associated with the ketone group, the two identical dipoles point in opposite direction and are therefore compensated. If the chain between the two dipoles were absolutely rigid, this substance would be electrically neutral at any temperature and the bulk of the material would essentially behave like a paraffin. In other words, there would be no increase of the polarization at the melting-point. The substance with eleven carbon atoms should under those circumstances behave in a totally different way. In this substance the two dipoles lie parallel and point in the same direction. The substance should therefore show very strong dipole effects. If, on the other hand, the chain between the dipoles is not rigid, then the two dipoles would be under no constraint and the two substances would both show an increase of the polarization at the melting-point.

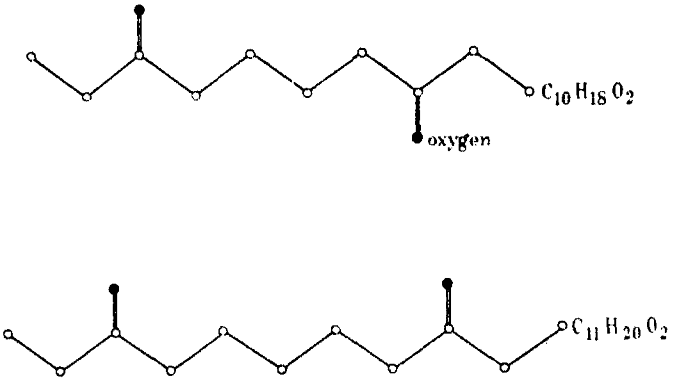

FIGURE 1

MATERIAL

The writer is much indebted to Dr J. W. Oldham in this laboratory for the synthesis of the two double ketones. The $C_{10}H_{18}O_2$ melts at 63·5° C, the $C_{11}H_{20}O_2$ at 67·5° C. Both substances crystallize in white flakes. It is not difficult to separate small single crystals suitable for X-ray analysis. The two substances give very similar pictures. The long spacings differ in length as is to be expected from the chemical formula. The increase is the same as is found in the normal form of the hydrocarbon series. The crystals have very nearly trigonal symmetry with regard to the chain axes. This is confirmed by optical examination which shows that the two substances are nearly uniaxial. The positions of the two oxygen atoms in the chain is easily checked by measuring the intensities of several orders of the long spacing. The calculation agrees with the observed intensities.

There remains only one uncertainty with regard to the position of the dipoles in the crystals. It is assumed in the previous section that the dipoles are either parallel or antiparallel in the undistorted molecules. A direct test which would require a detailed X-ray analysis has not been made yet, but there are indirect arguments which seem to speak in favour of the assumption. First, it is difficult to see why the divalent ketone oxygen on substituting it for two symmetrically placed hydrogens in the hydrocarbon chain should destroy the symmetry. Secondly, if the C—O bond were not symmetrically placed in relation to the carbon chain isomers should result on substituting one of the ketone oxygens by two dissimilar monovalent atoms or radicals. No such isomers seem to exist.

There is a further point to be considered. In C_{10} where the dipoles are assumed to be antiparallel the corresponding dipole energy is a minimum. In C_{11} this energy is a maximum and consequently the two dipoles tend to twist the chain which lies between the two ketone groups. The dipole energy is μ^2/R^3, where $\mu = 2{\cdot}8 \times 10^{-18}$ and $R = 7{\cdot}8$ A, the distance between the dipoles. The energy is therefore $1{\cdot}6 \times 10^{-14}$ erg, whereas the threshold is about 2×10^{-13} erg. In other words, the dipole energy is not large enough to produce an appreciable deformation of the molecule.

EXPERIMENTAL

The apparatus for measuring the dielectric constants is identical with that used in previous research. The wave-length is about 20 m. A slight change is made in the thermostatic control of the temperature. The oil circulating pump is completely immersed in the Dewar flask. The substance condenser is reduced in size and contains only about 1 c.c. of substance. The accuracy of the measurements is slightly decreased but this disadvantage is out-weighed by the better temperature control and the fact that experiments are feasible with small quantities of material. The design of the condenser is shown in figure 2. A word may be said about the absolute value of the dielectric constants. There is the well-known difficulty which arises from the incomplete filling of the condenser with the solid material. This effect is particularly marked with substances of the kind used in this work on account of their large contraction at the setting point. It is found that this difficulty can at least partly be overcome by the following procedure. The condenser after being dried and exhausted is gradually filled up with the

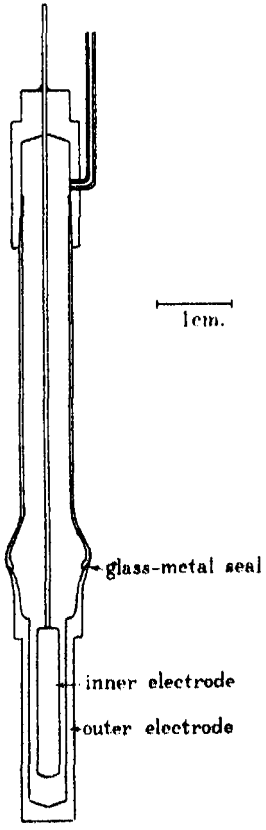

FIGURE 2

substance and the occluded gas is pumped off. The substance is solidified from the bottom and reheated if any signs of gas bubbles are visible. A condenser filled in this way will give reproducible results. If this precaution is not taken, lower values for the dielectric constants result but subsequent series of experiments still reproduce with these lower values. In the present work the absolute values are of minor importance.

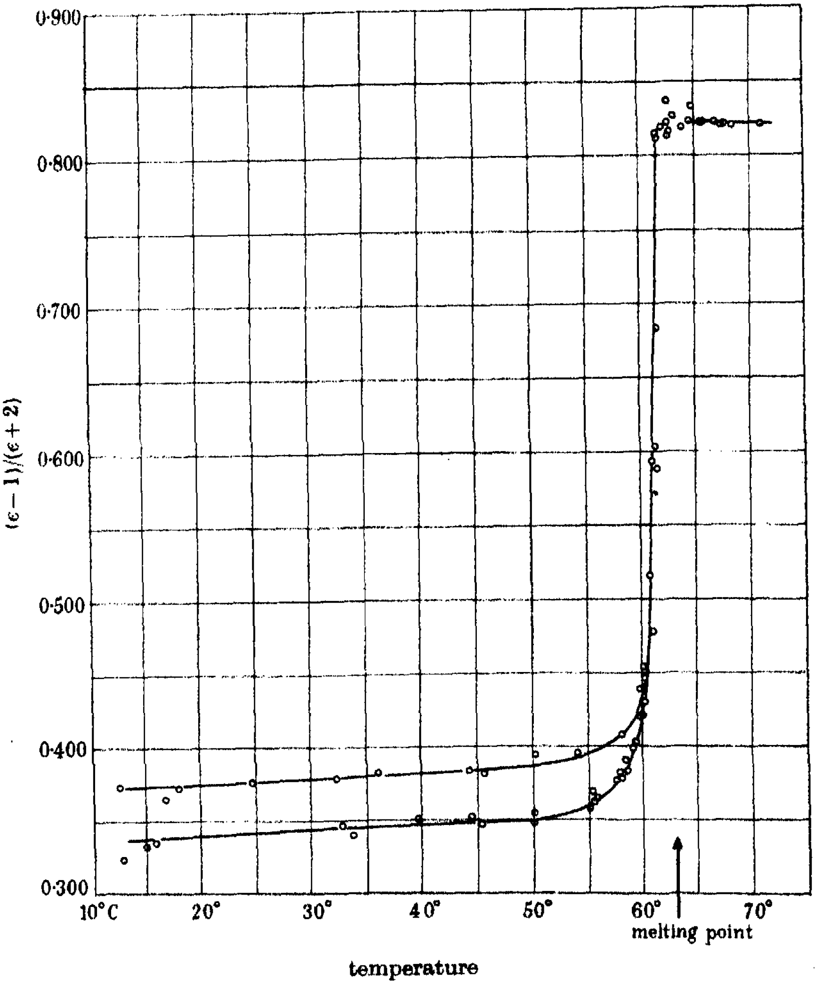

FIGURE 3. Observed $(\epsilon-1)/(\epsilon+2)$ of ketone $C_{10}H_{18}O_2$.
Upper curve, experiments after vacuum treatment;
lower curve, subsequent observations.

DISCUSSION OF THE RESULTS

The result of the experiments are given in two sets of curves (figures 3, 4), each referring to one of the two substances. One curve represents all the observations obtained during the first heating of the condenser and its contents, these being previously filled in under vacuum. The other curve gives the observations obtained during the subsequent heating. Owing to the absence of interstices in the dielectric, the first curve shows higher values

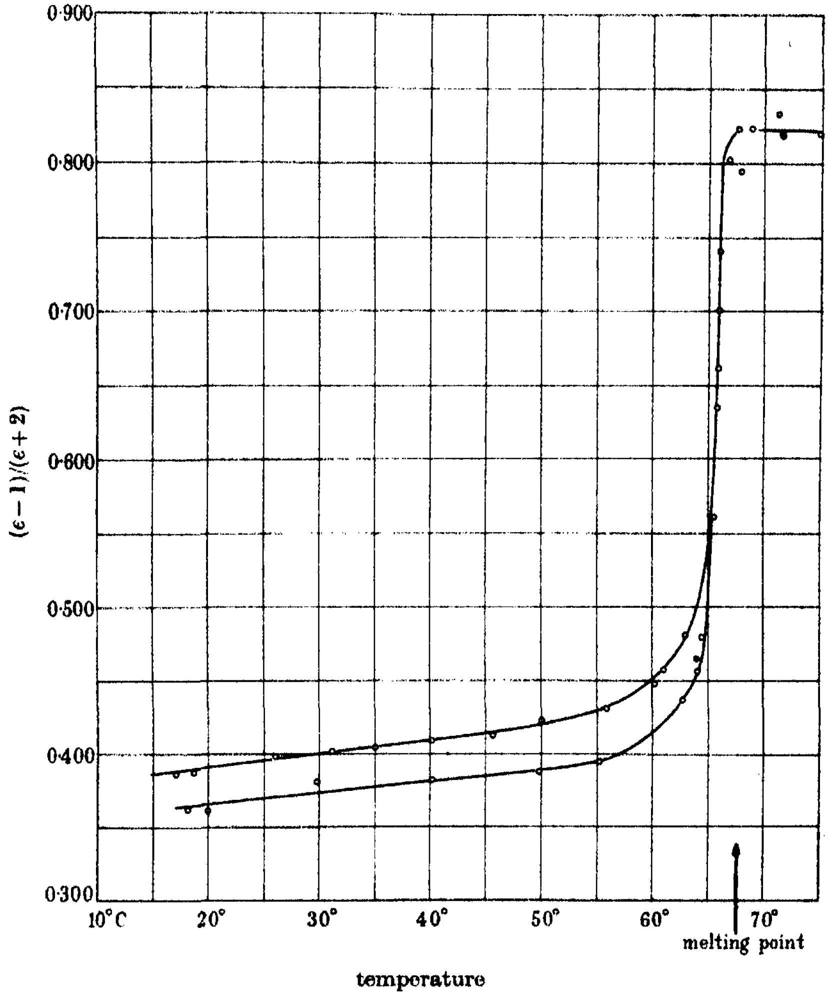

FIGURE 4. Observed $(\epsilon-1)/(\epsilon+2)$ of ketone $C_{11}H_{20}O_2$.
Upper curve, experiments after vacuum treatment;
lower curve, subsequent observations.

for $(\epsilon - 1)/(\epsilon + 2)$ than the second curve. This holds essentially for observations of the solid state. As the temperature gets higher the two sets of observations become identical.

Comparing now the corresponding observations of the two ketones, the following facts appear. The substance with the compensated dipoles has a slightly lower polarization than that with the non-compensated dipoles. This difference would be enhanced if the observed values were reduced to equal dipole concentration, since the substance with the compensated dipole has one CH_2 group less than the other substance. On heating the two substances it is found that the $(\epsilon - 1)/(\epsilon + 2)$ of the compensated ketone rises at first more slowly than the corresponding values of the non-compensated ketone. Near the melting-point the reverse takes place. The curve representing the polarization of the compensated ketone begins to rise more rapidly and at the melting-point itself the two curves reach approximately the same maximum value. The two sets of curves have essentially the same shape, the incomplete filling of the condenser does therefore not alter the phenomenon.

The conclusions drawn from these observations are the following. Consider first the substance with the non-compensated dipole. The individual molecule of this substance has a strong dipole moment, but since the molecules are fixed in a random position the dipole effect of the solid material is small. An increase of the temperature sets the molecules free and thus produces the observed rise of $(\epsilon - 1)/(\epsilon + 2)$.

For the ketone with the compensated dipoles the conditions are different. The rise of the temperature has a double effect. It produces again an increase of the motion of the molecules but this alone would not produce an external effect if the dipole moments of the individual molecule remained compensated. If, as the experiments show, there is an increase of the polarization, there must exist a distortion of the molecule due to the thermal agitation. The main result of the present investigation is the fact that this distortion is so large that the two substances have practically the same polarization at their melting-points.

We are therefore led to the conclusion that when dealing with the structure of a solid long-chain substance we have to take into account the torsional flexibility of the constituent chain molecules.

The two preponderant types of motion in the solid are the rotation of the molecule as a whole and the internal torsional vibration of the molecule. It is interesting to obtain an estimate of the potential energies involved in these two types of motion. The threshold energy of the internal rotation as already given in the introduction is of the order of 2×10^{-13} erg. The threshold energy of the rotation of the whole molecule depends obviously upon the temperature and becomes very small when the substance is near its melting-point. It changes very rapidly near the melting-point and reaches a nearly temperature-independent level later. This has been calculated in a previous paper (Müller 1936) and amounts to about 5×10^{-14} erg per CH_2 group. We take, for example, a chain molecule of four carbon atoms which has the length equal to the distance between the two dipoles in one of the ketones treated in this paper. The threshold energy of rotation of this molecule is $4 \times 5 \times 10^{-14}$ erg, i.e. it is of the same magnitude as the threshold energy of the internal rotation. The probabilities of rotation in bulk and of internal rotation are therefore of the same order in this particular case. These estimates agree with the present observations and suggest that internal distortion of the molecule in the solid is appreciable even when dealing with comparatively short chains. This is the main result of the present work. It suggests a modification of the view that the increase of the apparent symmetry of chain substances near their melting-points is due to rotation of the molecule as a whole. This increase may just as likely be due to internal distortion of the chains. More experiments will have to be done before this problem can be settled in a satisfactory manner.

In connexion with this, two papers (Sillars 1938; Pelmore 1939) are quoted. Both deal with the relaxation time of dipole chain molecules dissolved in paraffins. From the figures given by the authors it follows that the relaxation times depend upon the chain lengths of the dipole substances, but it is obvious that there is no simple linear relation between the two. No definite conclusion is given in these papers as regards the mechanism of the relaxation phenomenon. If the present view is accepted, it becomes clear that no linear relation is to be expected.

The writer wishes to express his thanks to the Director and the Managers of the Royal Institution for their interest in this work.

SUMMARY

A series of measurements is made of the dielectric polarization of two diketones. The two substances consist of aliphatic chain molecules each carrying two C—O dipoles. These two dipoles are differently situated in the two substances. In one substance, $C_{10}H_{16}O_2$, the two dipoles are antiparallel and tend to neutralize each other; in the other, $C_{11}H_{20}O_2$, they are on the same side of the chain axis and therefore reinforce each other. From the behaviour of the two substances in the neighbourhood of their melting-

points it is concluded that even comparatively short chains suffer considerable distortion under the influence of temperature. Estimates from other observations support this conclusion.

REFERENCES

Kistiakowsky, G. B., Lacher, J. R. and Strutt, F. 1939 *Chem. Phys.* **7**, 281, 290.
Müller, A. 1930 *Proc. Roy. Soc.* A, **127**, 417.
— 1932 *Proc. Roy. Soc.* A, **138**, 514.
— 1936 *Helv. Phys. Acta,* **9**, 626.
— 1937 *Proc. Roy. Soc.* A, **158**, 403.
— 1938 *Proc. Roy. Soc.* A, **166**, 316.
Pelmore, D. R. 1939 *Proc. Roy. Soc.* A, **172**, 502.
Schäfer, K. 1938 *Phys. Chem.* B, **40**, 357.
Sillars, R. W. 1938 *Proc. Roy. Soc.* A, **169**, 66.

Wave form, energy and reflexion by the ionosphere of atmospherics

By T. H. Laby, F.R.S., J. J. McNeill,
F. G. Nicholls and A. F. B. Nickson
Natural Philosophy Laboratory, University of Melbourne

(*Received* 6 *June* 1939)

[Plates 4, 5]

Introduction

The Society has published a number of papers on various aspects of lightning, including those of C. T. R. Wilson on changes in the earth's electric field; Appleton, Watt and Herd's observations of a similar kind but at a greater distance from the discharge, and Schonland and others' interpretation of photographs of lightning. References to these and other investigations are given by Appleton and Chapman (1937) and Schonland (1938). The evidence that lightning is the source of atmospherics has been considered by one of the authors (Laby 1936), and Goodlet (1937) has reviewed the conclusions reached in the study of the effect of lightning on power transmission lines.

Observations on the wave form of atmospherics by physicists of the Radio Research Board of Australia and others were begun in this laboratory at the end of 1935, and evidence that atmospherics are reflected at the ionosphere was later obtained (Laby, Nicholls, Nickson and Webster 1937).

Principles of the method

If a lightning discharge may be idealized as equivalent to a vertical hertzian (dipole) oscillator, then its electric field at any instant at a point P, distant r from the axis of the oscillator, may be described as being the vector sum of:

(1) the "electrostatic" field of the dipole, which is proportional to $1/r^3$;
(2) the induction field, proportional to $1/r^2$;
(3) the radiation field, proportional to $1/r$.

The phase relations of these fields change with r.

The design of an instrument to record without distortion the wave form of this field for an atmospheric is very exacting. It must record changes in the electric field which occur in a few microseconds, but which may last for a number of milliseconds. The lightning flash which produces the atmospheric may be at any distance, and in what follows it was from 1 to 1200 km., and thus the electric field had a wide range of values. The instrument used consists of an aerial and an aperiodic amplifier connected to a cathode-ray tube, the spot of this tube being photographed on a rapidly moving film. The measures taken to give the instrument the required characteristics are stated in a later section. An examination of the oscillograms obtained with it shows the extent to which the instrument meets the requirements, which have been stated, and it is evident that it meets most of them.

A linear aerial is connected in series with a non-inductive resistance and a variable condenser to earth, as shown in figure 1. The amplifier may be connected in parallel with the condenser or the resistance. The values of this resistance and the total capacity to earth of the aerial determine its time constant, which should be small compared with the period of the oscillations to be recorded.

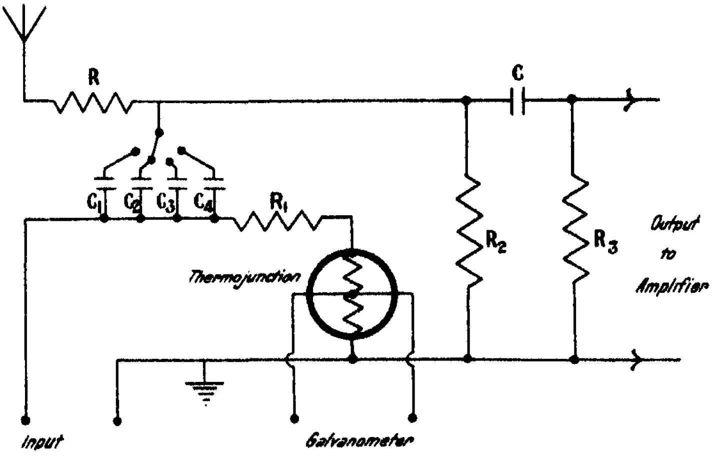

FIGURE 1

In our experiments the amplifier is connected across the condenser so that the former amplifies the potential across the latter, and a record of the variation in the electric field near the aerial, E V/m., is obtained. If the potential across the variable capacity in the aerial circuit is v V, the field strength at that instant is given by the expression

$$Eh_0 = v(C_0 + C)/C_0,$$

where h_0 metre is the "effective height" of the aerial,

C_0 farad is the capacity to earth of the aerial,

and C farad is the capacity of the condenser across which v is recorded.

Observations given later, those of other workers in this field, and photographs of lightning discharges, show that the oscillations in an atmospheric are rarely of so short duration as 10 μsec., but a succession of pulses may last some msec. The aerial, aperiodic amplifier and oscillograph, if the correct wave form is not to be distorted by the recording system, must be designed for this range of periods.

DESCRIPTION OF APPARATUS

The units comprising the oscillograph are shown in figure 2.

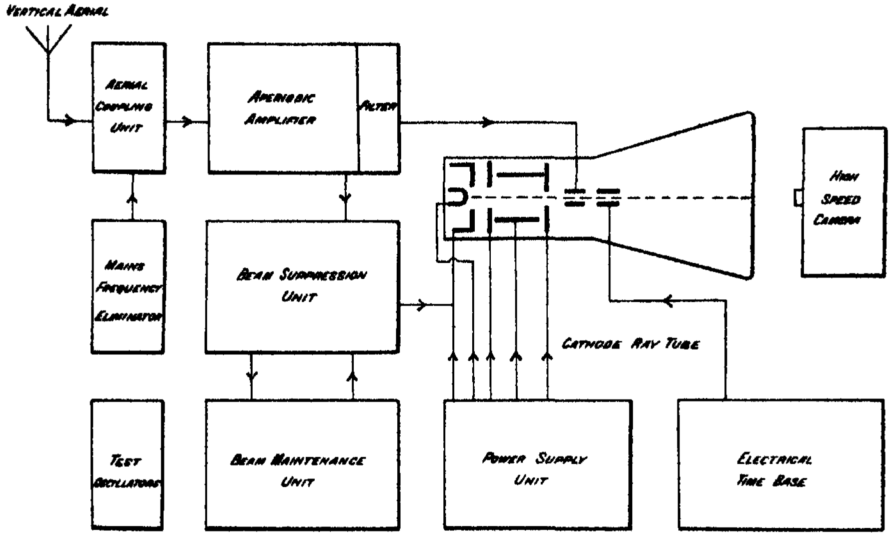

FIGURE 2

Aerial. The aerial used is an open L type 60 m. long. The values found by measurement for its equivalent height and capacity were $h_0 = 15$ m. and $C_0 = 470\,\mu\mu$F. The aerial coupling circuit is shown in figure 1. The condensers C_1, C_2, C_3, C_4 have the values 114, 370, 2000, 4750 μμF respectively, and by selection of the condenser in circuit the ratio V/Eh can be varied. A resistance of 1000 Ω in series with the aerial is sufficient to render it aperiodic, but 10,000 Ω was inserted to reduce the interference of broadcasting signals with the reception of atmospherics. The time constant of the aerial alone is 4·7 μsec. and for the maximum value of C

$$(C_0 + C_4)\,R = 52{\cdot}2\,\mu\text{sec.}$$

In order to reduce the effect of electrically charged rain, and of the slowly varying electric field of thunder clouds near the aerial, a condenser was inserted in series with the aerial, and it was earthed through a high resistance.

Filter. In order to reduce the interference from broadcasting stations, a filter which attenuated currents above a frequency of 500,000 c./sec. was inserted between the amplifier and the plates of the cathode-ray tube. It required to be specially designed for this position, where it has to work into a very large resistance. Later, a filter was designed which enabled the time constant of the aerial circuit to be materially reduced, namely to a maximum value of 15μsec., but it was not used in these observations.

Compensation of 50 *c./sec. interference.* The inductive action of the power mains on the aerial was undesirably large. It was compensated by means of a 50 c./sec. e.m.f. variable in phase and in amplitude obtained from a circuit constructed according to one developed by O. O. Pulley (1936).

Aperiodic amplifier. The function of this amplifier is to give linear amplification over a wide range of frequency and amplitudes. The details of the design have been described by H. C. Webster (1937).

The instrument applies principles developed by von Ardenne and applied in television receivers. The circuit is a resistance-capacity coupled, push-pull one. When tested the amplification proved to be approximately linear over the range of frequencies 50–400,000 c./sec. (600,000–750 m.) and for a voltage amplification of 120 with an output up to 200 V. The amplifier is insensitive to variations in the supply voltage.

Calibration of oscillograph. The overall amplification of the oscillograph was regularly measured by connecting to it the terminals of a non-inductive resistance, through which passed a known current, of frequency 1000 c./sec., measured by means of a vacuum thermojunction. The p.d. so injected into the amplifier was about 2 V, and the resulting deflection of the cathode spot was photographed. In this way the gain of the amplifier and the speed of the film were recorded on the film.

Cathode-ray beam suppression unit. If the cathode-ray beam impinged on the screen continuously, the latter would be damaged and the photographic film would be fogged. A unit was constructed to suppress the beam until an atmospheric was received, when the beam was restored to its full intensity. This operation required 10^{-5} sec. with the unit to be described.

Portion of the amplifier output voltage is applied to the input of the beam suppression unit. This causes the modulation electrode (normally held at a high negative potential) to become positive whenever the amplifier output exceeds a finite value in either direction, thus allowing the cathode spot to reach full brilliance. The circuit diagram of this unit is shown in figure 3. The output circuit has been modified from that described elsewhere.

Cathode beam maintenance unit. Maintains the spot at full brilliance for a specified time after the reception of an atmospheric greater than a predetermined intensity.

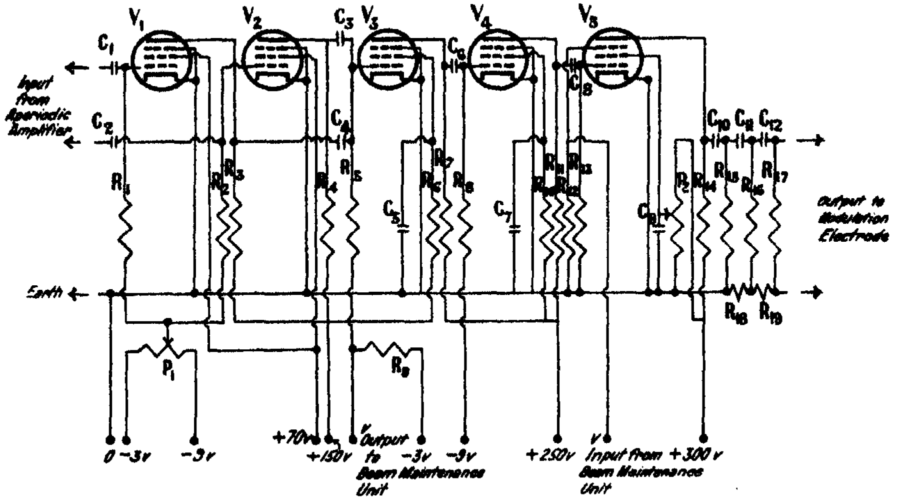

FIGURE 3

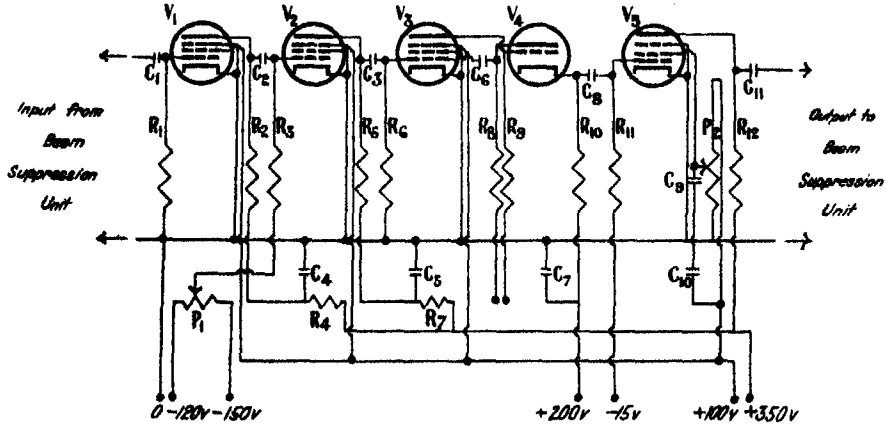

FIGURE 4

A pair of hard valves are arranged in an asymmetric multivibrator circuit to discharge a condenser whenever the input voltage exceeds a specified limit. This limit is altered by varying the negative bias potential applied to the grid of V_2, figure 4. The output of this unit is injected at the suppressor grid of the output valve of the beam suppression unit, causing a positive potential to be applied to the modulation electrode of the cathode-ray tube for a period determined by the time constant CR, which is 5 msec.

Cathode-ray tube and power supply. A high vacuum photographic cathode-ray tube, Cossor 3271 J, is used. The power supply provides a maximum potential of 3000 V for the third anode and variable voltages for the other electrodes to enable intensity and focusing to be controlled.

Testing equipment. The apparatus also includes a linear time base and a frequency range 50–1,000,000 c./sec. for visual observations, and oscillators 1000, 10,000, 100,000 and 10^6 c./sec. for the purposes of testing and alignment.

Camera. The camera enables the trace on the fluorescent screen of the cathode-ray tube to be recorded with adequate resolution and minimum wastage of film.

The film is carried on the periphery of a drum, belt driven from an a.c. induction motor on the film. The camera lens ($f = 5$ cm. of aperture $F/2$) focuses the fluorescent screen. A length of film is exposed by removing the lens cap. The camera is loaded with 10 m. of film, and fresh portions of film can be drawn for exposure from a magazine inside the drum. The induction motor, having a small and constant load, has a constant speed. The use of cylindrical pulleys running on ball-bearings and a very thin endless belt under constant tension prevent belt slip.

The film speed can be varied from 3–12 m./sec. by changing the pulleys.

Photographic technique. Experiments using a number of different films and various developers were made to determine the most suitable photographic method for use in recording the trace of the spot of the cathode-ray tube.

The final choice was Kodak Super X 35 mm. ciné film developed in a Mees developer for 20 min. at 20° C. Tests showed that spot writing speeds up to 3 km./sec. could be recorded. The accompanying plates, to be described later, clearly indicate the present state of the photographic technique.

RAY THEORY OF REFLEXION AT AN IONOSPHERE

An examination of some of the oscillograms obtained made it evident that, in addition to the ground wave, there were waves which had been reflected at an ionosphere. The simplest assumptions may be made in the first instance to explain this type of oscillograph.

The simple assumptions that the ground and sky waves have the velocity of light and that the sky waves are rays, which are optically reflected at the surfaces of the ionosphere and the earth, are found to be in close agreement with observation. The surfaces of the earth and of the ionosphere are first assumed plane and parallel, the height of the ionosphere being h km. It is then shown that a simple correction allows for these surfaces being spheres.

In figure 5, S is the source of the atmospheric which is received at O. Its distance, SO, is d km. SCO is the ground ray, and SAO is the sky ray once reflected at the ionosphere at A, and $SBCDO$ is the ray twice reflected at the ionosphere. I_1 and I_2 are the corresponding images of S. θ_1 and θ_2 are the angles of incidence at O of these rays.

$$SI_1 = 2h. \qquad SI_2 = 4h.$$

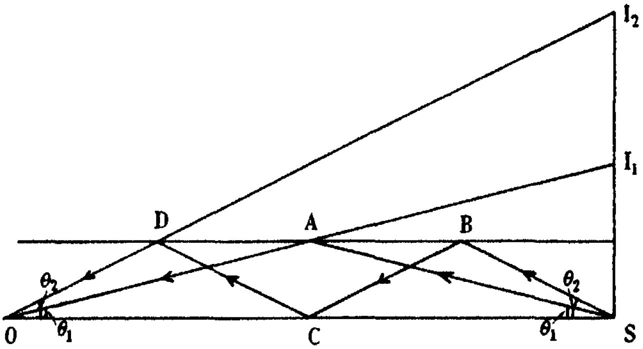

FIGURE 5

Let t_g sec. be the time taken by the ground wave and t_n sec. be that taken by the sky wave (reflected n times at the ionosphere and $(n-1)$ times at the ground) to reach O; then

$$t_g . c = d,$$

and $$t_n . c = 2hn \operatorname{cosec} \theta_n,$$

where $$c = 3 \times 10^5 \text{ km./sec.}$$

The intervals of time between the arrival of the ground wave, and the once reflected sky wave, etc., are

$$\Delta t_1 = t_1 - t_g = 2h \operatorname{cosec} \theta_1 / c - d/c,$$

$$\Delta t_2 = t_2 - t_1 = 2h(2 \operatorname{cosec} \theta_2 - \operatorname{cosec} \theta_1)/c,$$

$$\Delta t_n = t_n - t_{n-1} = 2h(n \operatorname{cosec} \theta_n - \overline{n-1} \operatorname{cosec} \theta_{n-1})/c,$$

$$\tan \theta_n = 2nh/d.$$

CORRECTION FOR CURVATURE OF THE EARTH

For a plane earth, the expression for $t_n . c$ reduces to

$$t_n . c = \surd(4n^2h^2 + d^2).$$

If R km. is the radius of the earth and θ is the angle subtended at the centre of the earth by an arc of length $d/2n$, then, in fig. 6,

$$QS = d/2n = R\theta,$$

$$l^2 = h^2 + R(h+R)\,\theta^2$$

$$= h^2 + d^2/4n^2(1 + h/R),$$

putting $1 - \theta^2/2$ for $\cos\theta$.

Now $c . t_n = 2nl$,

therefore

$$c . t_n = \surd\{4n^2h^2 + d^2(1 + h/R)\}.$$

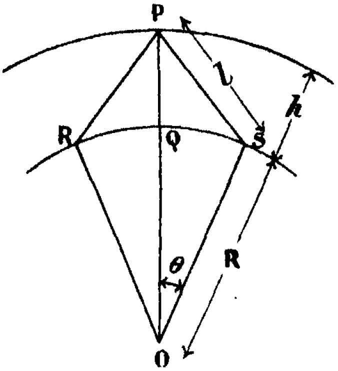

FIGURE 6

If the corresponding values of the distance to fit the observed time intervals are d for a plane earth, and d' for the spherical earth, then

$$d' = d\surd(1 + h/R).$$

The factor $\surd(1 + h/R)$ is nearly unity, for values of h of the order of 80 km.; the correction to d amounts to 0·6 %, of the same order as the experimental error, and hence the first relation has been used in all the calculations.

NUMERICAL REDUCTION OF OSCILLOGRAMS

If an oscillogram shows the arrival of the ground wave, and the arrival of the sky waves can be identified, the distance along the oscillograph film from the first peak produced by the ground pulse to the peak of the sky pulses reflected 1, 2, 3, ... times can be measured. Multiplying these distances by the known speed of the film, the times t_1, t_2, ... are obtained. n is 6 or 7 for a number of films, and the problem is to find the values of h and d which give the best fit for the observed values of $t_1, t_2, \ldots t_n$.

It is evident that if the source is close to the oscillograph, that is, d is small compared with h, the intervals $\Delta t_1, \Delta t_2, \ldots$ will be the same and equal to $2h/c$. If d is large compared with h, then the intervals are small, but become larger as n increases.

Two methods have been used to find h and d. One is finding the values of h and d which give the best fit (determined by the "least square" condition) to the equation

$$ct_n = 2n(h^2+d^2/4n^2)^{\frac{1}{2}}-d.$$

The other is to calculate $\Delta t_n . c/2h$ in terms of $d/2h$. From the previous section

$$\Delta t_n = t_n - t_{n-1} = 2h(n \operatorname{cosec} \theta_n - \overline{n-1} \operatorname{cosec} \theta_{n-1})/c,$$

$$\Delta t_n c/2h = n \operatorname{cosec} \theta_n - \overline{n-1} \operatorname{cosec} \theta_{n-1}$$

and $$d/2h = n \cot \theta_n.$$

In figure 7, for fixed values of $d/2h$, the intervals $\Delta t_n . c/2h$ have been evaluated for each value of n, and are plotted in such a way as to show the ratio of each interval to the one before, and the one following.

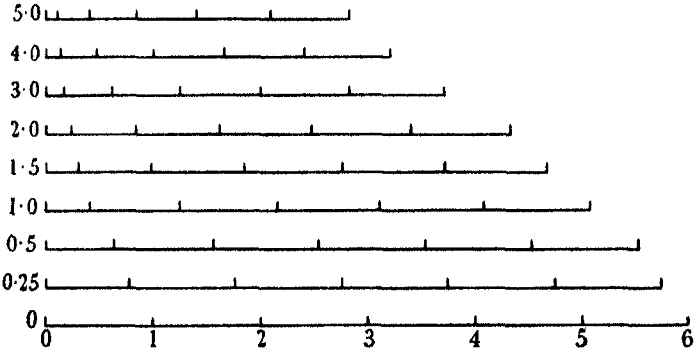

FIGURE 7

As an example for calculation, one record gives the following measurements. The unit for t is the msec. and for d and h the kilometre.

n	1	2	3	4	5	6	7
t_n (measured)	0·21	0·60	1·08	1·62	2·14	2·69	3·23

From these measurements, $\Delta t_n = t_n - t_{n-1}$ is found.

Δt_n	0·21	0·39	0·48	0·54	0·52	0·55	0·54

These ratios can be referred to unity.

Δt_n	1·0	1·85	2·28	2·57	2·48	2·62	2·57

The problem now is to find what value of $d/2h$ will give ratios $t_n - t_{n-1}$ nearest in value to those above.

Try $d/2h = 1$. Then from the figure, the ratios are

$\Delta t_n . c/2h$ 1·0 1·98 2·24 2·32 2·36 2·38

$d/2h = 1{\cdot}5$ will cause the ratios to increase.

$\Delta t_n . c/2h$ 1·0 2·30 2·83 3·03 3·13 3·18

The correct value for $d/2h$ is thus between 1·0 and 1·5. The ratios for any value of $d/2h$ not given in figure 7 can be obtained by interpolation. As an example, take $d/2h = 1{\cdot}1$. This gives the set of values below.

1·0 2·05 2·36 2·46 2·51 2·55

This set is obviously the closest of the three to the observed figures. A value of $d/2h$ that would bring the calculated values closer to the observed values could be found in the same manner.

Suppose the value $d/2h = 1{\cdot}1$ is the best solution, then for the first reflected pulse, from the ray theory of reflexion,

$$\Delta t_1 = t_1 - t_g = 2h/c \operatorname{cosec} \theta_1 - d/c,$$

and
$$\tan \theta_1 = 2h/d = 1/1{\cdot}1 = 0{\cdot}91,$$

so
$$\Delta t_1 . c/2h = \operatorname{cosec} \theta_1 - \cot \theta_1 = 0{\cdot}39.$$

From the observed values on the oscillogram, $\Delta t_1 = 0{\cdot}21$; therefore

$$\frac{c}{2h} = \frac{0{\cdot}39}{0{\cdot}21},$$

giving
$$h = 81\,\text{km}.$$

As
$$\frac{d}{2h} = 1{\cdot}1, \quad d = 179\,\text{km}.$$

In the same way, using figure 7, it is possible to reduce any set of observations, enabling h, the height of the reflecting layer, and d, the distance of the source, to be determined.

The solution of the equation

$$ct_n = 2n(h^2 + d^2/4n^2)^{\frac{1}{2}} - d$$

for h and d, with the different values for n, is an alternative manner for the reduction of this set of observations.

In the following table are given the observed values of t_n and the values of t_n calculated by the above expression if $h = 83$ and $d = 215$.

n	1	2	3	4	5	6	7
t_n obs.	0·21	0·60	1·08	1·62	2·14	2·69	3·23
t_n calc.	0·19	0·60	1·09	1·61	2·14	2·68	3·22
$\Delta t = t_{\text{obs}} - t_{\text{calc}}$	+0·02	0	−0·01	+0·01	0	+0·01	+0·01
$\Delta^2 t$	4	0	1	1	0	1	1
							$\Sigma(\Delta^2 t) = 8$

It can be shown that this is the best fit by drawing a figure in which the value of $\Sigma\Delta^2 t$ is plotted against d for values of $h = 80$, 81, 82, 83 and 84, when it becomes evident that if a minimum value for the sum of the squares of the residuals, $\Sigma\Delta^2 t$, is taken as a criterion of what is the best fit, then $h = 83$ and $d = 215$ satisfies that condition. Further, it is evident that a change in h of 1 km. and in d of 10 km. affects the value of $\Sigma\Delta^2 t$ in a detectable manner.

The slight difference in the result obtained by the two methods is due to the use of the approximate value of $\frac{d}{2h} = 1{\cdot}1$ in the first solution, and that only one value of Δt_n is used in finding d and h, whereas the method of least squares uses all the values obtainable.

In the following table are given all the heights and distances which have been obtained from oscillograms showing a number of reflections of an atmospheric at an ionosphere. While a large proportion of oscillograms show the presence of reflected waves, the wave form is of such a complicated nature that it is very difficult to fix the positions of the reflected waves with any certainty, and to determine the exact time-intervals between each wave. The oscillograms, upon which the table was based, were sufficiently definite for satisfactory measurements to be made.

TABLE 1

Time	Date	n	h	d	$\Sigma\Delta^2 t$
0115	20. ii. 37	7	83	215	8
0130	20. ii. 37	7	81	310	24
0145	20. ii. 37	6	80·5	320	0
0152	20. ii. 37	7	75	200	85
1059	27. ii. 37	6	54	180	18
1109	27. ii. 37	6	70	460	14
1525	4. ii. 37	7	60	360	19
1540	1. ii. 37	6	68	440	14
1545	1. ii. 37	5	66	310	32
1556	1. ii. 37	6	80	1050	14
1700	6. xi. 36	7	79	430	17
1715	6. xi. 36	7	78	440	49
1715	6. xi. 36	8	78	440	31
2100	2. xi. 37	7	56	430	92

INTERPRETATION OF TYPICAL OBSERVATIONS

Appleton and Chapman and Schonland and co-workers have suggested that the electric field changes due to a close lightning discharge include three characteristics:

(1) A comparatively slow field change caused by the leader stroke of the lightning discharge, with a duration between 100 and 200 msec.

(2) A very rapid change in the field due to the return stroke of the same order of magnitude as that due to the leader stroke but of much shorter duration.

(3) A final slow non-oscillatory field change of about 300 msec. duration.

The second and third parts of the discharge may be repeated in subsequent discharges along the same channel.

Our results confirm the above conclusions, and oscillogram (i) figure 8, plate 4, is a typical example which we interpret as follows:

(*a*) From 0 to 8 msec. a slow initial change of field is shown.

(*b*) At 8 msec. a very rapid change of field of equal magnitude to the first change occurred, followed by a slow field change.

(*c*) At 14 msec. a second return stroke change has occurred, followed by a second slow change.

(*d*) At 23 msec. from the commencement, a third return stroke has occurred, and is followed by a third slow field change.

In figure 8, plate 4, (ii) the leader process lasts only 2 msec. but the fine structure is more apparent than the slow field change of (i). At 2 msec. a very rapid return stroke causing a field change of 4 V/m. occurs, and is followed by a gradually decreasing field and a second return stroke occurring 36 msec. from the beginning.

A leader of ½ msec. duration is recorded in figure 8, plate 4, (iii) and one of 6 msec. in (iv). In both the fine structure of the process is apparent.

In the two discharges shown in (v) and (vi), the fine structure is shown in greater detail by the use of a high film speed. These two records show striking similarity to the fine structure reported by Appleton and Chapman.

The marked similarity between wave form oscillograms occurring within a small time interval, such as 100 msec. as shown in (vii), (ix), (xi), (xviii) and (xxiii), we attribute to successive discharges of naturally decreasing intensity along the same discharge channel.

These records together with (x), (xii), (xiii), (xiv) and (xv) show that the use of the beam suppression unit results in the loss of very little of the initial part of the oscillogram, as these were received while the normally suppressed cathode ray spot was at full intensity. Individual notes on these records show a symmetrical wave form (x) showing the presence of a small reflected wave; a damped periodic wave followed by a similar smaller wave 22 msec. later (xi), the latter having a small high-frequency oscillation preceding it; a very simple pulse of three half waves (xiii); and two oscillograms (xiv) and (xv), showing maximum amplitude some half waves from the beginning of the record.

A type of wave form occurring less frequently than the damped periodic type is shown in records (xvi) and (xvii). It consists of an aperiodic field change with a superimposed high frequency oscillation. We find this type to be less frequent in occurrence than the reports of Appleton and Chapman and Norinder would indicate.

The records from (xviii) to (xxii) show the alteration by reflexion of the original wave form, and that reflected waves continue to arrive after the ground wave has ceased. A typical example is shown in (xviii). This oscillogram, of duration 76 msec., shows three discharges, the second being 48·8 msec. after the first, and the third 25·3 msec. after the second. The wave forms are similar, and this is interpreted as three discharges along the same path, giving a ground wave, followed in each case by reflected waves. Record (xxii) shows how the first reflected wave has interfered with the ground wave, and apparently has resulted in cancellation of the later part of the original wave form.

Similarity between oscillograms recorded over large time intervals (more than a minute) are illustrated in figures (xxiv)–(xxix). These oscillograms are discussed fully in the following section.

Records taken at slow camera speed show a small high-frequency component occurring after the initial wave (figure 9, xxx–xxxiii); and the characteristic "slow tail" similar to that described by Appleton, Watt and Herd (1926) (figure 9, plate 5, xxxiv–xxxvi).

AN INTERPRETATION OF THE SIMILARITY OF ATMOSPHERIC WAVE FORM

At first we interpreted the half waves of small amplitude which follow the first half wave to be reflected pulses. The first was assumed to be the main pulse. This theory raised the difficulty that only a small percentage of the main pulses showed these subsidiary pulses. The values of the height of the reflecting layer, calculated from this interpretation of the oscillograms, were not inconsistent with the accepted value for the height of the ionized *E* layer.

Two hypotheses then required investigation. The first is that an atmospheric consists of an aperiodic pulse propagated along the ground, followed by pulses reflected 1, 2, 3, ... n times at the ionosphere. Each oscillogram would consist of the ground pulse followed by reflected ones at such time intervals as to produce a continuous wave form. The times of arrival of the reflected waves and therefore the wave form of the oscillogram is determined by the distance, d, of the source of the atmospheric, and the height, h, of the reflecting layer. The explanation of the observed occurrence of pulses of alternative positive and negative sign is not evident on the assumptions that have been made above.

The other hypothesis is that the electrical discharge which radiates an atmospheric is a damped oscillation with a period determined by the instantaneous resistance, inductance and capacity.

The theories will be considered with special reference to oscillograms (xxiv–xxvi) in figure 9, plate 5. The most obvious characteristic of these pulses, which extend over a period of 12 minutes, is their striking similarity; measurements of the oscillograms show them to be similar to the smallest detail. This is attributed on the first hypothesis not to a repetition of successive discharges of exactly similar electrical oscillations, but to the fact that d and h remained unchanged during the time in which the oscillograms were observed. On this view, the approximately constant value of d and h mainly determine the form of the oscillogram, and d and h probably change more slowly than the conditions which determine the period of oscillation of an electrical discharge in a thunderstorm.

It is unlikely, however, that a series of reflected pulses could produce a continuous varying sine wave such as are recorded in the oscillograms under discussion. The values of h and d calculated for these oscillograms on the first interpretation give $d = 280$ km. and $h = 80$ km.

There are three grounds for not accepting this interpretation:

(1) The observed field strength requires d to be much closer than 280 km.

(2) Meteorological observations recorded a storm at $d = 60$ to 80 km.

(3) The amplitude of successive sky waves at first increases, then rapidly decreases, which is difficult to explain.

Our interpretation of the oscillograms is that the first five half periods are those of a damped oscillation, the slight discontinuity seen in the oscillogram after these five pulses being caused by the arrival of the once reflected wave. The small amplitude of this wave is attributed to the low intensity of the electromagnetic wave which is emitted by a vertical oscillator in a direction making an angle of 20° with the vertical. This assumes that the electrical discharge (lightning) was approximately vertical. The once reflected wave shows the phase reversal expected after a single reflexion. As only one reflected wave can be identified, d and h cannot be calculated from the oscillogram. d is assumed to be 70 km. as given by meteorological observation, and the value of h is found to be 95 km. The measured average field strength is 3 V/m., which gives a value $Ed = 210$ V. The mean observed value of a large number of observations is 212 V. (See following section.)

RELATION BETWEEN FIELD STRENGTH AND DISTANCE OF ATMOSPHERIC SOURCES

The oscillograms as recorded enable the peak field strength and the wave-length of the head of the atmospheric pulse to be determined directly. In measuring the wave-length only the initial two half waves were used, as the wave-length increases from the head to the tail of the pulse. The mean wave-lengths and peak field strengths of a number of atmospherics from sources at varying distances are entered in table 2.

TABLE 2. DISTANCE, WAVE-LENGTH AND FIELD STRENGTH OF ATMOSPHERIC SOURCES

No. of observations	Period	d km.	λ km.	E V/m.	Ed V	hI kmA
7	1518–1600	1000	27	0·10	100	9,600
4	1515–1540	800	24	0·15	120	9,670
6	1723–1726	800	20	0·34	272	18,900
5	1611–1618	350	22	0·66	231	15,100
4	1059–1149	300	35	1·07	321	32,000
4	1634–1647	200	38	1·16	232	24,500
5	1340–1351	70	41	2·98	209	23,100
35						18,000

From the table it can be seen that the field strength decreases as the distance of the source increases. The product of the field strength and distance is more nearly constant and lies within a range of ratio three-to-one for 80 % of the cases.

As we are concerned only with that part of the wave propagated along the ground, we use the exponential term in the Austen Cohen formula, $e^{-\cdot 0015d/\sqrt{\lambda}}$, to correct for decrease of field strength due to diffraction of the wave over the earth's surface, for Love has shown that this term is $e^{-9\cdot 6dR/\sqrt{\lambda}}$, where R is the earth's radius, 6370 km. and $9\cdot 6/R = 0\cdot 0015$. Thus the field intensity is given by

$$E = 0\cdot 377 \frac{hI}{\lambda d} e^{-\cdot 0015d/\sqrt{\lambda}},$$

where E V/m. = field strength, λ km. = wave-length,
d km. = distance, I A = current,
and h km. = effective height of radiator.

This expression enables the factor hI to be evaluated for each oscillogram as the peak field strength and the wave-length can be measured, while the distance is found by the method described on page 155.

In table 2 the following quantities are entered: the period during which the number of oscillograms, summarized in each line, were observed, the value of d for each group of observations, and the mean values of λ, E, Ed and hI. It will be noted that the period ranges from 3 to 50 min.: d is taken as constant for these periods.

When the product hI is obtained for each of the thirty-five observations summarized in the above table, 90 % of the values are found to lie within a range of ratio four-to-one. This confirms the conclusions made by C. T. R. Wilson, that the electric moment of lightning discharges is sensibly constant, and by Munro and Huxley, and Boswell and Wark, that the radiated peak power from atmospherics has a small range of values. The original observations show that the values of hI for any single source of atmospherics lie well within a ratio range of two-to-one.

Accepting Goodlet's average value of 30,000 A for the current in a lightning flash, it is possible to find a value of h. When a mean is taken of the thirty-five values of hI summarized in the table, the effective height of the discharge column of the lightning flash is 0·6 km.

PEAK POWER AND TOTAL RADIATED ENERGY OF ATMOSPHERIC SOURCES

By analogy with the power required in a radio transmitter situated on the ground to produce a field strength E mV/m., the power radiated by the lightning flash can be expressed as

$$P = d^2E^2/300^2\Phi^2,$$

where P kW = radiated power, E mV/m. = field strength,

d km. = distance, and Φ = Sommerfeld factor.

The factor Φ allows for the effect of the earth's curvature and finite ground conductivity, and is unity for distances of a few hundred kilometres and the long wave-length which may be regarded as characteristic of an atmospheric.

This relation will be valid only when the induction field of the flash is small in relation to the radiated fields. For sources distant more than one-half wave-length the error will be less than 30 %. In the evaluation of the power of a lightning flash, this error will be much smaller if the radiation field of a lightning flash is observed at more than 100 km. The limitations to the

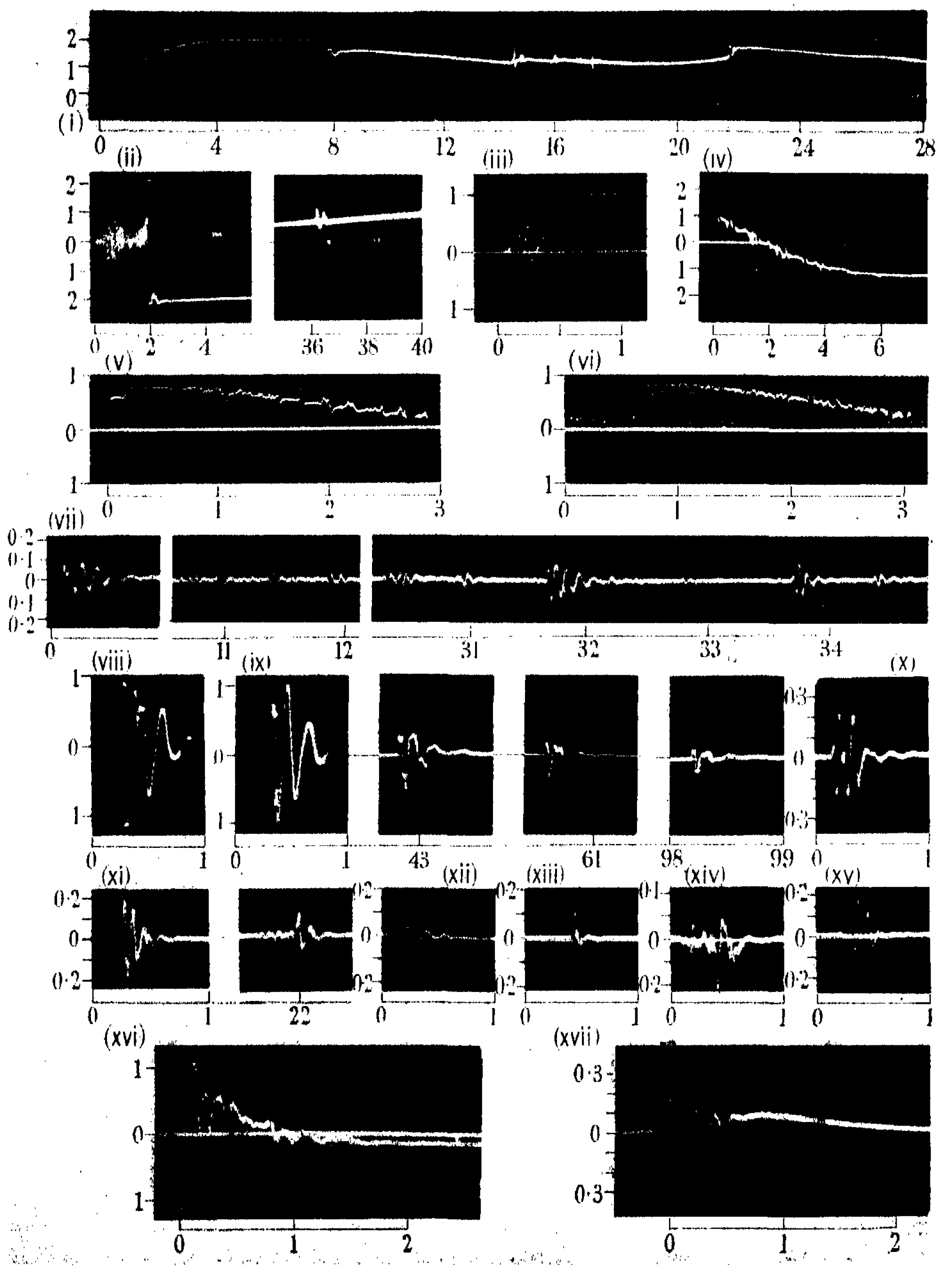

FIGURE 8. (i) leader stroke: three discharges, 8, 15, 23 msec. later; (ii) leader stroke: two discharges, 2, 36 msec. later; (iii) leader stroke: one discharge, ½ msec. later; (iv), (v), (vi) fine structure of leader stroke; (vii), (ix) initial wave form and series of similar wave forms; (ix), (viii) closely similar wave forms; (x) initial portion of wave recorded, with reflected wave; (xi), (xii), (xiii), (xiv), (xv) little wave form is lost by use of beam suppression unit; (xvi), (xvii) aperiodic wave form with superimposed high frequency oscillation.

Horizontal scale: Time in msec. Vertical scale: Field strength in V/m.

(*Facing p.* 160)

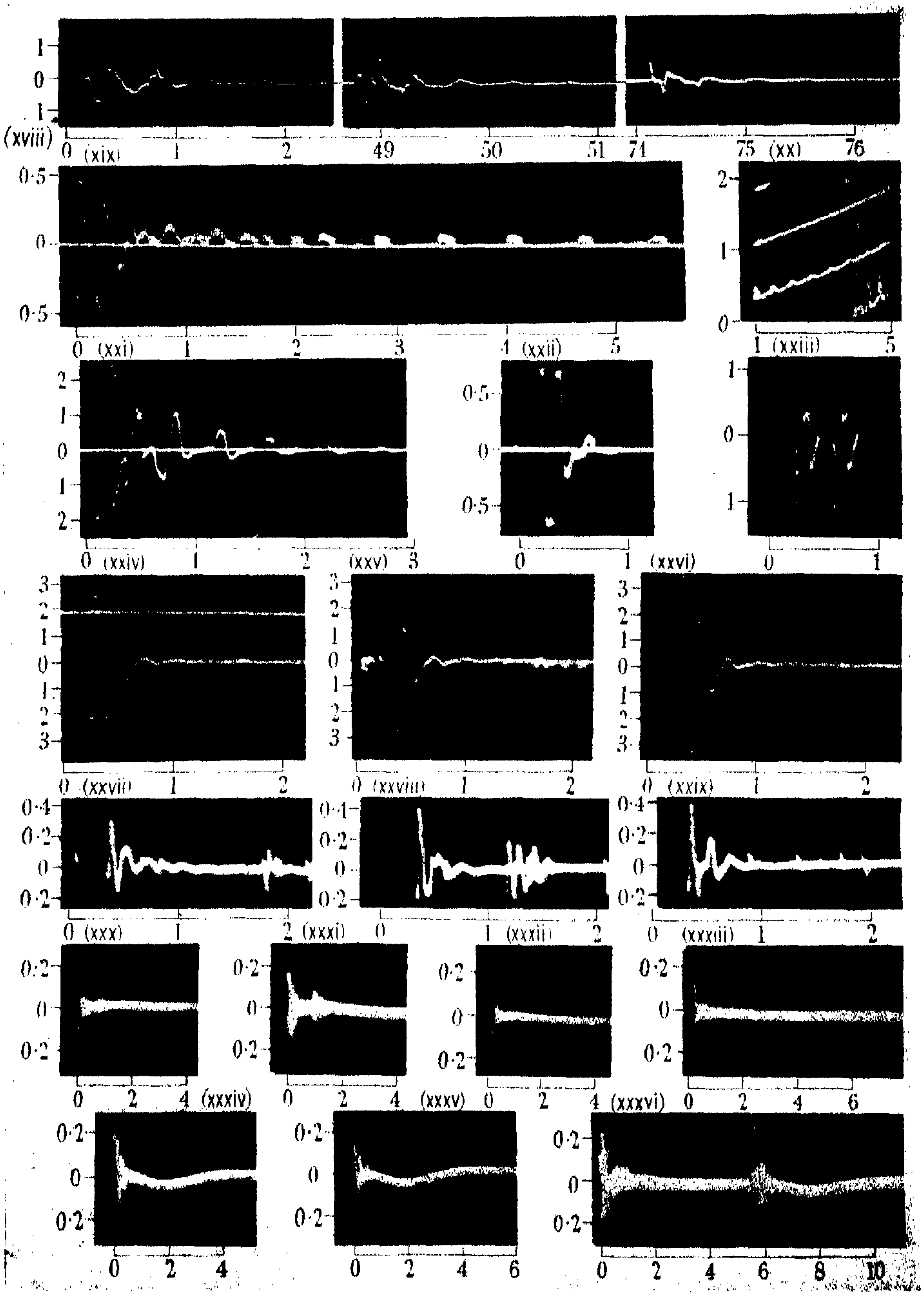

FIGURE 9. (xviii) Three similar discharges each showing clear reflexion; (xix) large number of reflexions; (xx) unidirectional pulse with many reflexions; (xxi) wave form modified by reflexion; (xxii) highly damped wave form; (xxiii) closely similar wave forms; (xxiv), (xxv), (xxvi) three similar wave forms, over period of 12 min.; (xxvii), (xxviii), (xxix) similar wave forms, over 3 min. period; (xxx), (xxxi), (xxxii), (xxxiii) main discharge together with high frequency ripple; (xxxiv), (xxxv), (xxxvi) oscillograms showing low frequency "tail".

Horizontal scale: Time in msec. Vertical scale: Field strength in V/m.

validity of the expression for the radiated power are not severe. We find that the wave form of an atmospheric at a great distance is different from that near a lightning flash. A good proportion of the oscillograms to be discussed have been taken from sources between 100 and 400 km., and the relation given above is valid for these observations.

The peak power is proportional to the square of the product Ed which is given in table 2 for a number of atmospherics. When calculated for each of the series of observations summarized in that table, the peak power is found to be

$$1{\cdot}11 \quad 1{\cdot}60 \quad 8{\cdot}21 \quad 5{\cdot}92 \quad 11{\cdot}43 \quad 5{\cdot}98 \quad 4{\cdot}85 \quad \times 10^5\,\text{kW}$$

with a mean value of $5{\cdot}6 \times 10^5$ kW.

The total radiated energy can be found from the relation

$$\begin{aligned}\text{Energy} &= \int P\,dt \\ &= d^2/300^2\Phi^2\int E^2\,dt,\end{aligned}$$

where the integration is taken over a period long enough to include the complete atmospheric. The expression inside the integral is determined by graphical means from the recorded oscillograms which give the variation of the electric field with time. In determining the energy, care has to be taken to include that part of an oscillogram which is due to the ground wave, and to exclude wave forms which are the resultant of ground waves and waves reflected from the ionosphere.

A study of the atmospheric wave forms shows that most of the energy is associated with the first few half waves, and only occasionally does the tail contribute an appreciable amount. This is so because the energy is proportional to the square of the field strength. A mean value for the total energy of an atmospheric is found to be 200 kW sec., and the values obtained for individual atmospherics are found to lie within a definite range of values.

These figures for the total energy and maximum power of the electromagnetic energy radiated by a lightning flash show that while the peak power is extremely large, the total energy is not, and must be very small compared with other forms of energy of a thunder cloud.

VELOCITY OF GROUND WAVE AND SKY WAVE

It appears that the elementary theory of reflexion, which has been given earlier, fits the observations to the accuracy possible from measurements on the recorded oscillograms. This might not have been expected as the very long damped wave, to which the atmospheric pulse approximates, must, according to the well-verified existing theory of the propagation of such waves through an ionized medium, be gradually deflected at the ionosphere before returning to the earth. However, investigation of the theory shows that such an effect would be comparatively small for these waves, and thus little error is introduced in assuming plane reflexion to take place at the ionosphere.

The suggestion has been made by some recent writers that the ground wave has a velocity less than that of light, but the values observed for the various time-intervals between the arrival of the ground wave and the various sky waves seem incapable of explanation if the velocity of the ground wave is not the same as that of the sky wave. A consideration of the five oscillograms in table 1 for which the distance of the source, d, is largest shows that if the velocity of the once reflected sky wave is that of light, then the ground wave has that velocity to 0·7 %.

The work described in this paper has been carried out in Melbourne as part of the atmospherics research programme of the Radio Research Board of the Council for Scientific and Industrial Research of the Commonwealth of Australia.

The authors wish to thank Dr H. C. Webster, who was largely responsible for the design and construction of the apparatus used in the research.

SUMMARY

The wave form of the electromagnetic pulse radiated from a lightning flash, known as an atmospheric, has been studied.

The atmospherics are received on a vertical aerial which is connected through an aperiodic amplifier to a cathode ray tube. The spot on the screen of the tube is photographed on a film fixed to the external surface of a cylindrical drum which rotates at a uniform peripheral speed.

Many hundreds of wave forms have been recorded from atmospheric sources 70–1500 km. distant, and incidental to the observations we have made, evidence has been obtained of the reflexion of atmospherics at an ionized layer. Such records show the intervals of time elapsing between the arrival of the first pulse along the ground and the various reflected pulses.

From the simple theory and methods of reduction given in the paper, it is possible to determine the height of the reflecting ionized layer and the distance of the flash. When this is done, the height of the layer is found to be

between 53 and 82 km., values in reasonable agreement with the lower limits of the *E* layer.

The observations are consistent with the sky wave and the ground wave, having the same velocity to 0·7 %.

Oscillograms of typical atmospheric wave forms are shown, together with a possible interpretation of many of them. The assumption is made that the electrical discharge which radiates an atmospheric is a damped oscillation with a period determined by the instantaneous resistance, inductance and capacity.

The relation between the distance of an atmospheric source and its field strength is found to be linear and figures are given for the peak power and the total energy radiated as found from representative examples.

REFERENCES

Appleton, E. V. and Chapman, F. W. 1937 *Proc. Roy. Soc.* A, **158**, 1.

Appleton, E. V., Watson Watt, R. A. and Herd, J. F. 1926 *Proc. Roy. Soc.* A. **111**, 615.

Boswell, R. W. and Wark, W. J. 1936 *Quart. J. R. Met. Soc.* **62**, 499.

Goodlet, B. L. 1937 *J. Instn Elect. Engrs*, **81**, 1.

Laby, T. H. 1936 *Quart. J. R. Met. Soc.* **62**, 507.

Laby, T. H., Nicholls, F. G., Nickson, A. F. B. and Webster, H. C. 1937 *Nature, Lond.*, **139**, 837.

Love, A. E. H. 1915 *Phil. Trans.* A, **215**, 105.

Munro, G. H. and Huxley, L. G. H. 1932 *Rep. Aust. Radio Res. Bd.* no. 5.

Pulley, O. O. 1936 *Wireless Engr.* **13**, 593.

Schonland, B. F. J. 1938 *Proc. Roy. Soc.* A, **164**, 132.

Webster, H. C. 1937 *Proc. Phys. Soc.* **49**, 654.

Wilson, C. T. R. 1920 *Phil. Trans.* A, **221**, 73.

Determinations of the Rydberg constants, e/m, and the fine structures of H_α and D_α by means of a reflexion echelon

By J. W. Drinkwater, Sir Owen Richardson, F.R.S. and W. Ewart Williams, *King's College, London*

(*Received* 23 *August* 1939)

[Plates 6, 7]

1. Introduction

During the last few years many investigations have been carried out with the object of determining the fine structure of the red Balmer line of Hydrogen, H_α, and its corresponding analogue, D_α, in the heavier isotope Deuterium. It is only in these cases that the positions and relative intensities of the components can be accurately calculated in terms of the fundamental constants e, h, c, etc. The results are thus of considerable importance as affording a direct check on the fundamental basis of the quantum theory.

When account is taken of the effects of electron spin and the relativity variation of mass with velocity, the wave mechanical equations of Dirac give a result for the structure and intensity ratios identical with that given by the "Sommerfeld formula" which was an earlier attempt to make allowance for the relativity effect.

The term scheme and the distribution of the components of H_α (and D_α) are shown in figure 1. The numbers in brackets are the calculated intensities and the component separations are given in units of 0·001 cm.$^{-1}$. Following R. C. Williams (1938), the components have been assigned numbers 1, 2, 3, etc. in order of their relative intensities. Because of their Doppler widths, components 1 and 4 are not resolved but appear as a single line, often termed the main line, and this is designated by us as $\hat{14}$. Similarly 3 is not clearly separated from 2 which together form the second line of the apparent doublet. Component 2 is supposed to consist of two lines ending on the $2\,{}^2S_{\frac{1}{2}}$ and $2\,{}^2P_{\frac{1}{2}}$ levels with relative intensities 1 : 2·4, while the constituents of 3, ending on the same levels, have a ratio 1 : 10·4 as shown in the figure. A necessary consequence of the wave mechanical solution of this problem is that the double levels shown in the diagram should be coincident.

Unfortunately, the measure of agreement between the results of different experimenters has been by no means good, the discrepancies being more pronounced in the more recent investigations. According to several American observers, the separation of the main doublet is appreciably less than that expected on theoretical grounds, while the separation of the third component from the second is very considerably more. In addition, the intensity ratios between the lines bear little relationship to the theoretical values, the second line instead of being less is equal to or even greater than the so-called main component.

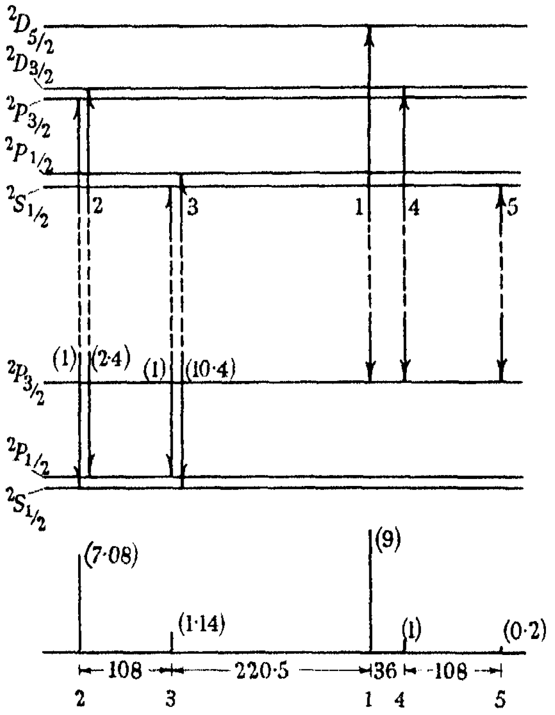

Figure 1

Heyden (1937) in an exhaustive investigation of D_α has concluded that the separations of the components are in close agreement with the theoretical values and for the first time obtains intensity ratios in accordance with theory. She further concludes from the extra width and lack of symmetry of the main line that it is a blend of two components but that the experimental accuracy does not warrant any attempt to fix the separation position or intensity of the fourth component.

More recently R. C. Williams (1938), in a further study of the fine structures of H_α and D_α, is critical of the results of Heyden on account of the very large grain of her plates. This criticism seems to some extent to be justified since the actual oscillations in the microphotometer record, presumably due to grain effect or dust, have an amplitude equal to a large fraction of the intensity of the third component. He confirms the earlier results of R. C. Williams and Gibbs (1934) and of Spedding, Shane and Grace (1935), that the separation of the main components is considerably less than the theoretical value, while he finds the separation of the second and third components to be very much greater. Pasternack (1938), in an attempt at explaining the discrepancy, refers to as yet unpublished results by Houston and Robinson which support the conclusions of R. C. Williams.

This uncertainty with regard to the structure of H_α and D_α has caused Bearden (1938) to question the validity of spectroscopic methods of determining the ratio e/m. Dunnington (1937) pointed out that a discrepancy still existed between the weighted mean of the spectroscopic determinations and the results obtained by free electron methods. By including the high value determination of Bearden which employs refraction of X-rays among the spectroscopic methods and a new low valued result by the crossed fields method (Shaw 1938), Birge (1938) concludes that the difference has shrunk to an amount equal to the average deviation to be expected from the assigned probable errors. Bearden (1939), however, objects to the classification of his work into the spectroscopic class and maintains that "the situation is found to be just as serious as that which led Birge in 1929 to retain two values of e/m".

The accepted value of the Rydberg constant for hydrogen rests solely on the work of Houston (1927). He measured the air wave-lengths of H_α and H_β, using as his standard the value 5015·675 A as the air wave-length of the helium line. His vacuum wave numbers, calculated on the basis of the Meggers and Peters (1918) formula, for the refractive index of "normal" air are $0{\cdot}009_8$ cm.$^{-1}$ and $0{\cdot}063_8$ cm.$^{-1}$ higher than the values obtained from the much more accurate formula of Kösters and Lampe (1934). (Due to an arithmetical error, the wave number quoted for H_β is 0·0423 cm.$^{-1}$ higher than that given by the Meggers and Peters formula. Actually the difference in the wave numbers obtained with the two formulae is $0{\cdot}009_1$ near H_α and $0{\cdot}018_4$ near H_β.)

The value of R_H deduced from the measurement of H_α has to be reduced by $0{\cdot}070_6$ cm.$^{-1}$, which is nearly five times as great as the $\pm 0{\cdot}015$ cm.$^{-1}$ limit given for this line. As pointed out by Houston, a further uncertainty exists since the standard of comparison is a helium wave-length in air and not the red cadmium spectroscopic standard.

Hitherto, all the precision measurements of these quantities have been made by means of the Fabry-Perot interferometer which was the only method available that would yield the desired accuracy. It is highly desirable that other methods should also be used wherever possible. During the last few years, one of us (W. E. W. 1933) found a method of constructing reflexion echelons and by adding reference mirrors devised a new way of measuring wave-numbers. Since the echelon could be placed in vacuum, all difficulties in connexion with the refractive index and dispersion of air are eliminated. Furthermore, it will be seen that since the echelon plates are individually made, any small errors in the construction of the plates will have a random distribution while with the Fabry-Perot interferometer, owing to the multiple reflexion principle involved, the effect of any small error in a plate is strictly cumulative.

If the various components of H_α and D_α were actually clearly separated, it would only be necessary to have an instrument of sufficiently high resolving power to get accurate values of the wave-length and separation. Any increase in the resolving power of the instrument beyond this point would not materially contribute to any higher accuracy. Since in practice the components are often blended together due to their Doppler widths, the resultant composite curve has to be obtained with the greatest accuracy possible in order that the subsequent analysis of this curve can be correctly made. The maximum plate thickness (in the case of the echelon) or plate separation (for the Fabry-Perot) that may be used is about 7 mm.; any larger values would lead to complications due to the overlapping of orders. In the region of H_α a heavily silvered Fabry-Perot interferometer should have theoretically the same resolving power as a 35 plate reflexion echelon of the same thickness. In practice, owing to the cumulative effect referred to, the resolving power is appreciably less. The 40 plate reflexion echelon used in this investigation is therefore considerably better than the interferometer of similar gap and this is the reason why it has been possible to obtain data on the position and intensity of the fourth component for the first time.

2. LIGHT SOURCES

(*a*) *Atomic beam experiments*

The ideal method of reducing the Doppler width of the lines would be to excite an atomic beam of the gas, placing the collimator of the spectrograph perpendicular to the direction of the beam. The method has been successfully used for examining the resonance lines and to a less extent for other lines of elements that can be easily condensed.

A preliminary trial showed that a tube containing hydrogen at a pressure of 10^{-3}–10^{-4} mm. could be successfully excited by a powerful 3 m. short wave oscillator, and calculations indicated that it should be possible to obtain an atomic beam at this order of pressure if the fastest available mercury diffusion pumps were employed. We were, however, unable to excite such a beam, either with the oscillator or by heavy electronic bombardment. A visible beam could only be obtained at a much higher pressure using multiple slits in place of the single ones normally employed. Under these conditions, the beam was only slightly brighter than the remainder of the chamber so that the background intensity had too high a proportion for the method to be practical in our case. It is possible that diffusion pumps using a type of oil not attacked by nascent hydrogen would reduce the background to the necessary low level.

(*b*) *Discharge tube experiments*

Using a Wood type long discharge tube of thin Pyrex wall 1 cm. internal diameter, the intensities of the two main components were approximately equal, irrespective of the rate of flow of damp hydrogen through the tube and apparently independent of the pressure in the tube. The same results were obtained when the inside wall was coated with metaphosphoric acid, the only difference being that the "black stage", showing practically no molecular spectrum, was much more quickly arrived at. In both cases considerable trouble was caused by the accumulation of ice on the inner wall of the portion submerged in liquid air.

Following the observations of Heyden (1937), who obtained the theoretical intensity ratio of 0·8 for these components by using a small proportion of hydrogen in helium, we investigated the conditions necessary for this result. As all the helium obtainable in this country already contains too high a proportion, it was necessary to eliminate this hydrogen so that definite known proportions could be added. This was done by adding to the discharge tube a palladium tube, which, when electrically heated for 2 or 3 hours, effectively cleared all traces of hydrogen from the helium and known amounts of pure hydrogen could be added as desired. In experiments with deuterium, a second discharge tube was prepared; after removing the hydrogen from the helium, pure deuterium was obtained by electrolysis of practically pure deuterium oxide, to which a small amount of NaOD had been added. The gas was freed from oxygen and water vapour by passing it through an electrically heated palladium tube fitted as an internal seal in the pyrex tubing. After repeated flushing with deuterium and cleaning out by means of the first palladium tube, while a heavy current was maintained in the discharge tube, no trace of the lighter isotope could be detected in the discharge. After about 6–10 hours with the discharge running, photometric tests showed hydrogen amounting to 2 or 2·5 % of the deuterium (the latter in turn being only 2–4 % of the gas in the discharge tube). As it was found impossible to eliminate this impurity which seemed to be gradually liberated by the electrodes or the glass (or both), the tube was frequently cleaned out and only those exposures were used which the photometric test taken subsequently showed that the hydrogen did not exceed 2 % of the deuterium.

The tubes were excited by direct current through a ballast resistance from a 1500 or a 1750 V source with a current of between 5 and 7 mA and with an average potential fall of the order of 10 V/cm. In order to avoid the concentration of hydrogen (or deuterium) at one electrode, it was necessary to reverse the direction of the current several times during the exposure. The exposure times varied between 30 and 60 min. for the Ilford hypersensitive (backed) panchromatic plates, used in conjunction with a fine grain developer.

3. SPECTROSCOPIC EQUIPMENT AND METHODS

The interferometer used was a 40 plate reflexion echelon which has been described by one of us (W. E. W. 1933). The thickness of each plate is 6·88 mm., so that according to Rayleigh's criterion it should be capable of resolving two monochromatic lines (of equal intensity) whose wave numbers differ by 0·018 cm.$^{-1}$. In practice, we find that two violet components from a water-cooled mercury arc with a separation of 0·023 cm.$^{-1}$ are clearly separated; hence we can conclude that at least for the visible region the resolving power of the instrument cannot be far short of its theoretical value. The wave-number range between successive orders of interference is 0·727 cm.$^{-1}$, which is a convenient value for observing the hydrogen "doublet" with a separation according to the Sommerfeld formula of 0·332 cm.$^{-1}$. A Hilger E 1 spectrograph with a glass train served as the auxiliary instrument, its dispersion being perpendicular to that of the echelon. With a fairly narrow E 1 slit, the hydrogen and deuterium lines could be separated and the photometric comparison to find the amount of H mixed with D was carried out in this way. A wide E 1 slit (about ½ mm.) had to be used with the echelon to minimize grain effect when the plates were microphotometered.

The echelon is equipped with two plane mirrors; the images of the collimator slit in these mirrors serve to provide fiduciary marks for wavelength measurement and to determine the change in magnification of the optical system with wave-length since the achromatism is only partial. Figure 3, plate 6 gives a complete trace of D_α showing the reference mirror images. As the instrument is used in an evacuated case, the wave numbers are found directly without the necessity of correcting for the refractive index of air. No correction need be applied for the variation of the phase change at reflexion with wave-length, since the phase change, whatever its value, will be the same at each step. Contrary to the case of the Fabry-Perot interferometer, the dispersion of the echelon is uniform over its range to well within the accuracy of measurement and the calculation of wave-length or interval is merely a matter of simple proportion.

On the other hand, the precise form of each element of the echelon, each step being 1 mm. wide, causes the intensities and possibly the forms of the components to be seriously altered. This distortion can be expressed in terms of the intensity envelope defined by:

$$M = \frac{\sin^2 X}{X^2}, \quad \text{where} \quad X = \frac{\pi s(\alpha+\beta)}{\lambda},$$

s being the echelon step width, λ the wave-length and α and β the angles of incidence and reflexion for the reflecting surface of the echelon step. It is because of this diffraction effect at each step that the whole of the available light is concentrated into one or two orders of interference. As a result, the centres of gravity of broad spectral lines are displaced towards the centre of the envelope.

In order to obtain true values of the intensities a correction was applied in the following way. On each plate, in addition to the simultaneous exposures of the red cadmium and H_α (or D_α), an exposure with a white light source was given together with the "plate characteristic". When a photometer trace of this white light pattern was taken at a position corresponding to the wave-length of H_α, the position of the maximum could be accurately located with respect to the fiduciary lines from the echelon mirrors. From a knowledge of the "order distance" for the red cadmium line and the variation in the magnification of the auxiliary spectrograph (given by the ratio of the mirror image distances for Cd and H_α) the order distance for H_α could be calculated, since the angle between successive orders is proportional to the wave-length. Hence, for a point at any given distance d from the centre of intensity, the appropriate X_d value is $X_d = \pi d/(\text{interorder distance})$, and the true intensity corresponding to that point is the observed intensity multiplied by $X_d^2/\sin^2 X_d$. A test with the white light curve showed that the shape of the intensity envelope corresponded with the value to within the limits of accuracy of the photometric measurements.

The magnitude of this effect can be seen from figure 2 which is derived from the results of an actual plate of H_α (F 73 B shown as figure 4 on plate 6).

The lower curves *A*, *B* are the actual intensity readings observed, plotted against distance along the plate. Using the notation of figure 1, *A′* and *B′* correspond to the main line of the doublet (a blend of components 1 and 4) while component 2 is in single order position almost central with respect to *C* the centre of the intensity envelope. The correction required for 2 is very small but becomes large for *B′* and especially so for *A′*, where the displacement of the centre of gravity of the curve *AA′* is very considerable. We should have some doubts regarding the accuracy of the corrected curve for points well away from *C* were it not for the fact that the wave number of $\hat{1}4$ determined from *A* agrees with that from *B* within 0·001–0·002 cm.$^{-1}$.

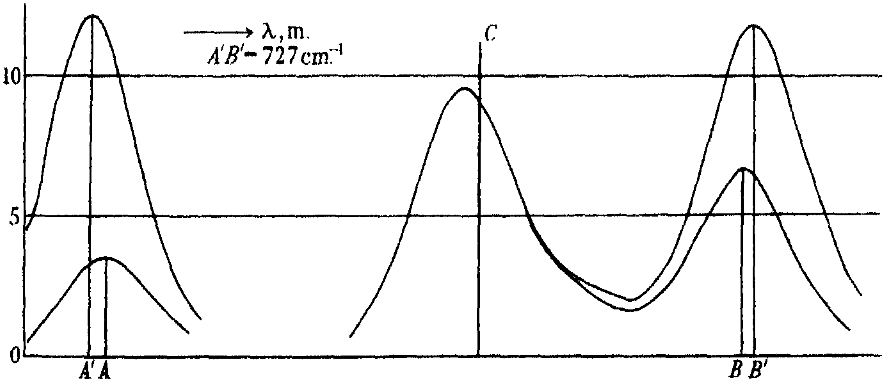

FIGURE 2

Actually the small difference in intensity between *A* and *B* (which should be equal) enables us to obtain the magnitude of the fraction of the light scattered at the various optical surfaces (of the order of 5 %) and which is not subject to the intensity envelope law. This information will be seen to be very valuable when we come to consider the intensity measurements.

As a final check on the accuracy of the corrections curve a series of wave-length measurements of the main $\hat{1}4$ line was made, in which the position of this line was moved across the intensity envelope, by admitting successive small amounts of dry air into the echelon chamber. Since the refractive index of normal air for $\lambda 6438$ A is approximately 1·000276, a pressure of 131 mm. changes the order of interference (approximately 21000) by unity. From the formula of Kösters and Lampe (1934) $\mu_{H\alpha} - \mu_{6438} = 0{\cdot}144 \times 10^{-6}$, hence the differential change of order between the two wave-lengths due to dispersion is 0·0005 for an order change of unity (or a pressure change of 131 mm.). This change is too small to be detected. Table 1 given below shows the variations in the measured wave number of $\hat{14}$ for H_α as its position is changed from double to single order position.

TABLE 1

	Order of interference		Wave number
Exposure no.	Cadmium	Hydrogen	of $\hat{14}$ cm.$^{-1}$
F 73 (B)	21361·456	20956·606	15233·065
(C)	·537	·682	·065
(D)	·644	·790	·067
(E)	·741	·879	·063
(F)	·825	·962	·063

No systematic variation of the wave number value with position in the intensity envelope is found.

The envelope effect is, however, extremely valuable in another respect. The third component, blended with the second in H_α and only just resolvable in D_α, can be so placed with reference to the centre of intensity that it can in effect be magnified by causing a reduction of intensity of neighbouring strong components. An example of this exaggeration is seen in figure 6, plate 7, where the third component in D_α can be clearly observed.

4. PHOTOMETRY AND REDUCTION OF THE PLATES

The plate characteristic was obtained from an Ilford optical wedge placed in contact with the E 1 slit. The wedge was independently calibrated on three occasions, its graduation determined and its linearity checked except for high and low densities where the measurements were difficult. All exposures were made on Ilford hypersensitive (backed) plates and a fine grain developer was used. During development, the plate was continuously agitated in order to minimize the Eberhard effect. The exposure times were between 30 and 60 min., depending on the concentration of H or D and on the position of the components in the intensity envelope.

The microphotometer used was an adaptation of one built in the Wheatstone Laboratory to the designs of Dr W. H. J. Childs. A common shaft drives the bromide paper carriage and also moves the photographic plate. In order to vary the magnification, the plate is not moved directly by its micrometer screw; the nut displaces a geometrically supported carriage on which is mounted a variable angle wedge. The plate holder bears perpendicularly against this wedge and moves a small amount as the wedge is displaced. In order to obtain sufficient magnification for these experiments, the adjustable wedge was replaced by a solid steel wedge which was optically ground and polished flat to two wave-lengths of green light by Messrs Hilger.

Tests of the linearity of the movement of the paper carriage and the wedge carriage against the rotation of the common shaft along the whole range showed no measurable deviation.

A further test was the determination of the fractional part of the order of interference for the red cadmium line for three plates, both by the usual photomeasuring micrometer and by means of the photometer trace. Typical results are given in table 2 below.

TABLE 2

	Fractional order of interference $\lambda 6438$ A	
Plate no.	Micrometer	Photometer trace
F 73 (B)	0·456	0·456
(C)	0·537	0·537
(D)	0·644	0·643

Clearly the error in determining the fractional part for the standard line is within one-thousandth part of one order. The reproducibility of the microphotometer was checked by making a number of traces of a graticule in both directions. The two traces on each sheet of bromide paper were identical but displaced relative to each other by about 1 mm. due to backlash.

The size of the order distance as imaged on the thermopile slit was 15 mm. The slit width was 0·17 mm. (1/88 of the interorder distance) so that very little detail was lost on this account, since the echelon at best could not "resolve" less than 1/40th of the order distance.

The method used for obtaining the corrected intensity curve depended on whether wave-length or fine structure was to be determined. In wave-length measurements, the position of the "centre of gravity" of the upper portion of the main 14 line had to be found, with reference to the midpoint of the reference mirror images which was our (virtual) fiduciary line. (The reasons for neglecting the lower portion of the intensity curve are discussed in § 5 (*b*), p. 179.) Since the reference images on the trace were approximately 25 cm. apart while the interorder distance was 11·65 cm., any unequal shrinkage of the bromide paper might cause an appreciable error in the determination of the fractional part. To avoid this, a photometer curve of a previously calibrated graticule was added to each trace and the position of a point determined in terms of its distances to the centre lines of the neighbouring graticule marks. Examples of these graticule mark curves can be seen in plates 6, 7, figures 4–7. The points of intersection of the H_α (or D_α) curve and various intensity levels obtained from the characteristic curve were transferred with a drawing-board and set-square on to smooth drawing paper. The distance from any such point to the centre of the intensity envelope (only approximately at the midpoint of the reference images) was measured and expressed in terms of the order distance. The appropriate factor by which the observed intensity had to be multiplied was then found from a large scale graph of the function $X^2/\sin^2 X$ against fractional order and the ordinate at this point given this corrected value. With a sufficient number of such points the actual intensity curve is established; the central line, given by bisecting different levels of the portion between 0·4 and 0·9 of the maximum, was taken as the "centre of gravity" of the line. The extreme peak portion was neglected as neither position nor intensity could be accurately determined in this case. No allowance need be made for the displacement of the point of maximum intensity from the centre of gravity of the unresolved blend in a case of this kind. This central line was then measured with respect to the centre lines of the neighbouring graticule marks.

A test of the reproducibility of the results was made by determining the fractional parts from four separate microphotometer traces of the same exposure of H_α. The values were $0{\cdot}281_4$, $0{\cdot}285_4$, $0{\cdot}284_8$, $0{\cdot}281_4$, giving a root mean square error value of $0{\cdot}001_8$.

In the measurement of fine structures, the largest peak separation involved is only about a quarter of the distance between the mirror images; over this distance it could be safely assumed that the shrinkage of the bromide paper would be sufficiently uniform. The distances of the points of intersection of the observed curve and the various intensity levels given by the characteristic curve were measured from the centre of the intensity envelope. By using a transparent scale and a magnifying glass, the values could generally be obtained to within 0·1 mm. These were then transferred (after correction for envelope effect) to large sheets of graph paper on a ten times larger scale so that 1 cm. on the graph corresponded to $6{\cdot}24 \times 10^{-3}$ cm.$^{-1}$, the interorder distance being 116·5 cm. on these graphs. The ordinates were chosen (approximately 20–25 cm. for the strongest component) so that the maximum slope of the curve should be about 45°. Further details are given in § 5(*b*) where the fine structure results are discussed.

5. RESULTS

(*a*) *Wave-length measurements, Rydberg constant and the ratio e/m*

The standard used for comparison was the value* 6440·2498 A as the vacuum wave-length corresponding to the accepted value of 6438·4696 A for the wave-length of the red cadmium line in "normal" air. Sears and Barrell's (1934) value for the index of "normal" air for this wave-length has been used for the conversion; the results would be substantially the same if the formulae of Perard (1934) or Kösters and Lampe (1934) were used. If another value* of the vacuum wave-length of red cadmium should be standardized, the wave number values given in this paper will all have to be scaled accordingly. The actual source employed, a G.E.C. Cadmium "Osira" lamp, had been compared with a hollow cathode discharge by Williams and Gogate (1938) to a high degree of precision, using a Fabry-Perot interferometer with a path difference of 20 cm. No detectable difference in wave-length was observed.

---

* Since the data in this paper were worked out, the results of Barrell and Sears (1939) have become available. These change this value from 6440·2498 to 6440·2491 A and values of the important final quantities adjusted to this have been inserted in this paper.

Table 3 shows the effect of varying the total pressure in the discharge tube containing 3–4 % hydrogen in helium and a current of 7 mA, liquid air cooling.

TABLE 3

Plate no.	Pressure mm.Hg	Intensity ratio	Wave number of $\widehat{14}$ line cm.$^{-1}$	Approximate half-width in cm.$^{-1}$
F 75 (A)	3·2	0·77	15233·067	0·15
(B)	2·0	0·79	·067	$0{\cdot}15_5$
(C)	1·0	0·83	·066	0·15
(D)	0·5	0·92	·069	0·15
(E)	0·2	1·02	·076	$0{\cdot}16_5$

The third column gives the ratio between the two components of the "apparent doublet". When the total pressure is below 1 mm., the relative increase in the intensity of the higher frequency line (a blend of components 2 and 3) is accompanied by an increase of the frequency and the half width of the main line.

A further experiment was carried out in which the total pressure was kept sensibly constant while the partial pressure of hydrogen was varied by means of the palladium tube; with a total pressure of 1·3 mm., a current of 7 mA and liquid air cooling, the results are given in table 4 below.

TABLE 4

Exposure no.	Percentage of hydrogen	Intensity ratio	Wave number of $\widehat{14}$ line cm.$^{-1}$	Approximate half-width in cm.$^{-1}$
F 77 (A)	9	$0{\cdot}86_3$	15233·060	$0{\cdot}17_8$
(D)	3–4	$0{\cdot}82_8$	·066	$0{\cdot}14_1$
(F)	0·2	$0{\cdot}74_7$	·065	$0{\cdot}18_6$

The lower hydrogen percentages were obtained indirectly from the relative intensities of the red lines of helium and hydrogen and are only approximate. At too high a partial pressure of hydrogen, the "centre of gravity" of the main line moves to the red. It will be noticed that its displacement is in the same direction as that in table 3 whereas the change in the intensity ratio in table 4 is in the opposite direction to that given by table 3.

Taken together, these tables show that even the hydrogen-in-helium type of discharge gives the theoretical intensity ratio over a limited range of operating conditions only. The shifts of the main line, especially when due to low pressure, seem large enough to account in some measure for the differences between the results of various observers.

Table 5 gives the collected results for wave number of the "centre of gravity" of the upper portion of the main $\hat{1}4$ line of H_α. Apart from the results already quoted in tables 3 and 4, which have been included because the intensity ratios are substantially the theoretical values, the remainder of the table refers to a total pressure of between 1 and 2 mm., a hydrogen content of 2–4 %, liquid air cooling and a current of 5–7 mA. The reason for this selection is that it is only within or close to this range of operating conditions that the half width of the $\hat{1}4$ line is a minimum; at the same time the ratio of the intensities of the $\hat{1}4$ and 2 lines is close to the theoretical value.

TABLE 5

Exposure no.	Wave number of $\hat{1}4$ line of H_α in cm.$^{-1}$
F 73 (B)	15233·065
(C)	·065
(D)	·067
(E)	·063
(F)	·063
F 75 (A)	·067
(B)	·067
(C)	·066
F 77 (D)	·066
(F)	·065

Average value $15233{\cdot}065_4$ cm.$^{-1}$ (R.M.S. error $0{\cdot}001_4$ cm.$^{-1}$). Corrected to Barrell and Sears (1939) this becomes $15233{\cdot}067_0$ cm.$^{-1}$.

Approximately half of the above results are determinations on two orders. The fractional part for the cadmium line for each exposure was determined independently by two observers and involved 48 readings.

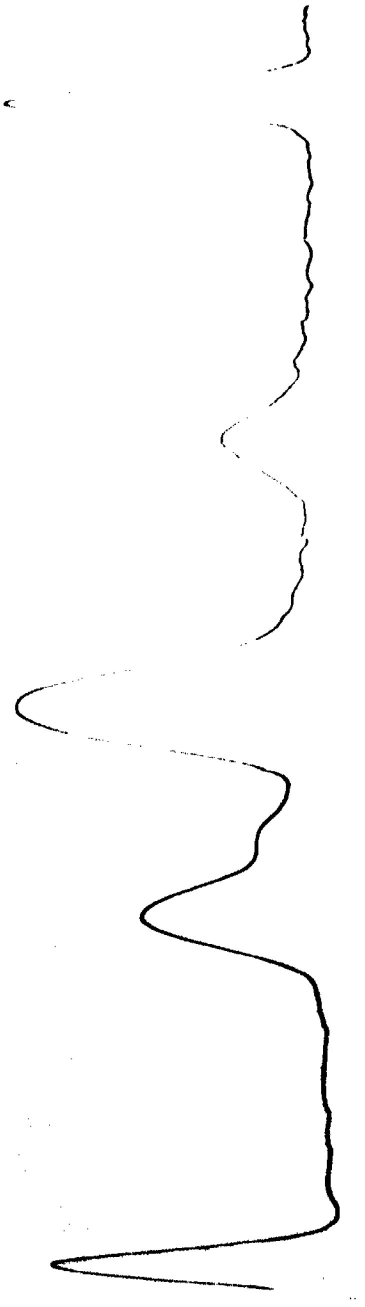

FIGURE 3. Complete trace of D_x showing the reference mirrors.

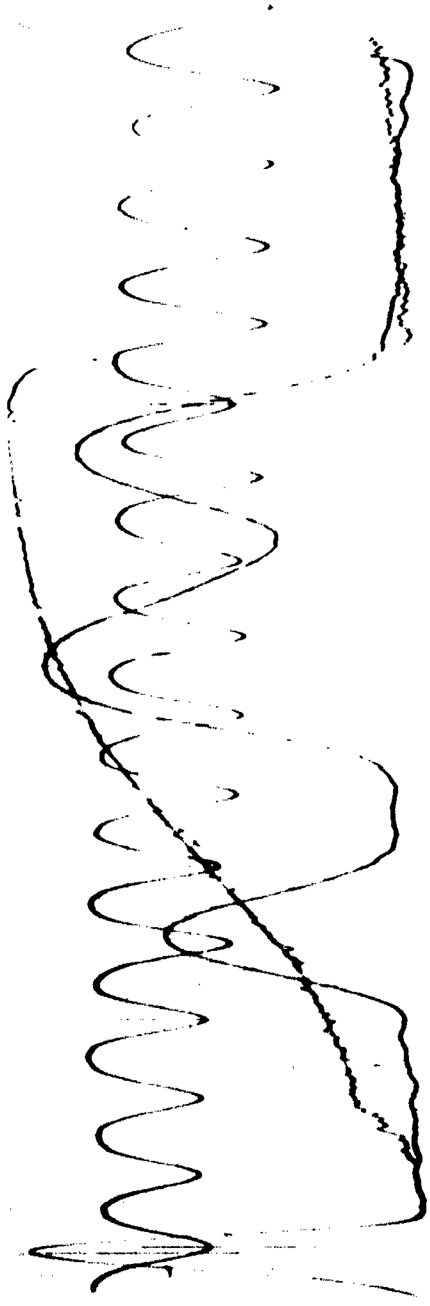

FIGURE 4. Trace of H_x from which the corrected curve in figure 2 has been obtained. F73B.

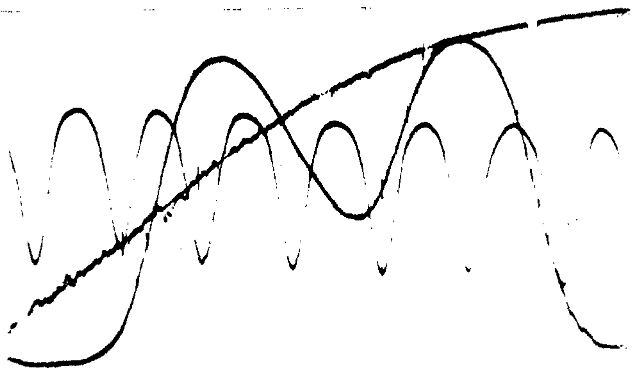

FIGURE 5. Small portion of H_α trace. F 77 D.

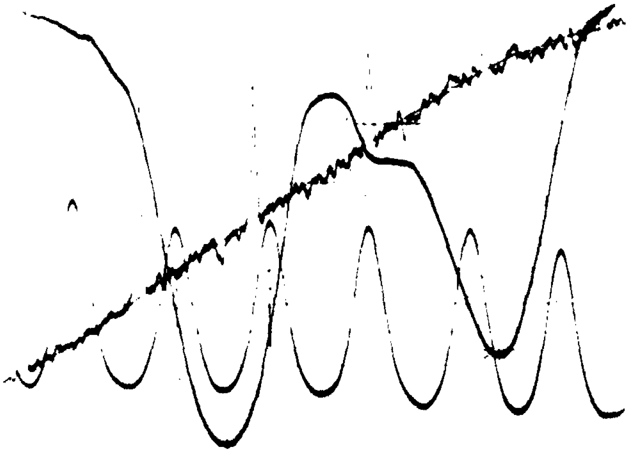

FIGURE 6. The effect of the third component in D_α has been apparently increased by altering the pressure in the echelon chamber. This curve when corrected for the envelope effect gives an almost identical curve with the corrected curve for figure 7.

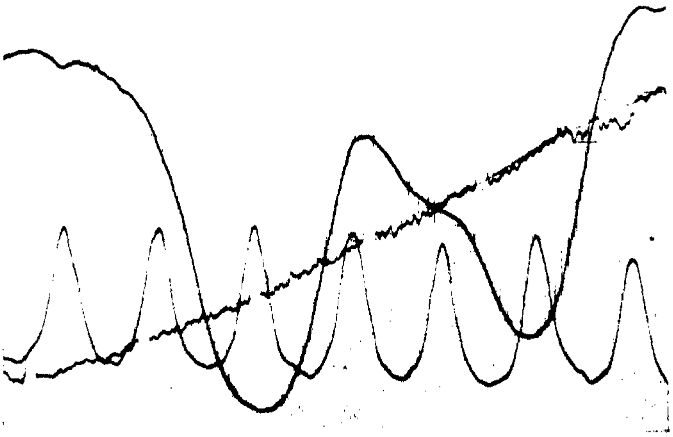

FIGURE 7. F 103 A. D_α $\hat{14}$ in single order position.

Rydberg constant for hydrogen, R_H. If the fine structure of H_α is in accordance with theory, the frequency R_H $(1/2^2-1/3^2)$ lies (0·072–0·0036)* cm.$^{-1}$ lower in frequency than the observed centre of the $\hat{14}$ line.

Thus $R_H = 36/5\ (15{,}233{\cdot}0654-0{\cdot}0694)$

$= 109{,}677{\cdot}571$ cm.$^{-1}$ (R.M.S. error 0·010 cm.$^{-1}$),

or, when adjusted to Barrell and Sears (1939), $109{,}677{\cdot}58_3$ cm.$^{-1}$.

The corresponding value of R_H given by Houston (1927) is:

$109{,}677{\cdot}759 \pm 0{\cdot}008$ cm.$^{-1}$.

The corresponding results for D_α are given in table 6. It was a matter of some difficulty to arrange that both D_α and the cadmium standard (which were simultaneously exposed) received the optimum exposure. The exposures in which the cadmium standard was in single order position were somewhat over-exposed, and to avoid any risk of error due to this cause these were not used for wave number determinations.

TABLE 6

Exposure no.	Wave number of $\hat{14}$ line of D_α in cm.$^{-1}$
F 101 (B)	15237·211
(C)	·209
(D)	·210
(E)	·208
F 103 (B)	·210
(C)	·211
(D)	·208

Average value $15{,}237{\cdot}209_6$ cm.$^{-1}$ (R.M.S. error $0{\cdot}001_3$ cm.$^{-1}$). Corrected to Barrell and Sears (1939) this becomes $15{,}237{\cdot}211_2$ cm.$^{-1}$.

The Rydberg constant R_D for deuterium is therefore:

$R_D = 109{,}707{\cdot}40_9$ cm.$^{-1}$ (R.M.S. error $0{\cdot}009_2$ cm.$^{-1}$),

or adjusted to Barrell and Sears (1939) $109{,}707{\cdot}42_1$ cm.$^{-1}$.

---

* Houston made a correction of 0·0056 for the displacement of the observed line from component 1. R. C. Williams and Gibbs (1934) point out that it should be 0·0063 cm.$^{-1}$; this is the displacement of the centre of gravity of the three components no. 1, 4 and 5 from the position of no. 1. If one determines the "centre of gravity" from observation of the upper part of the curve, the fifth component will have a negligible effect. If Doppler curves of half-width 0·135 cm.$^{-1}$ and intensities 0·2, 1 and 9, with respective separations of 0·108 and 0·036 cm.$^{-1}$, are graphed on a sufficiently large scale, it is easy to verify that the central line of the upper part of the resultant complex is very closely 0·0036 cm.$^{-1}$ from the centre of the strongest component.

Combining these results with the values of Bainbridge given by Livingstone and Bethe (1937) for the masses of the hydrogen and deuterium atoms, we obtain the mass of the electron from the formula given by R. C. Williams,

$$m = \frac{\mathrm{H}^+\mathrm{D}^+(\nu_\mathrm{D} - \nu_\mathrm{H})}{\mathrm{D}^+\nu_\mathrm{H} - \mathrm{H}^+\nu_\mathrm{D}}$$

$$= (5{\cdot}48646 \pm 0{\cdot}0005) \times 10^{-4} \text{ mass units.}$$

Taking the value of the Faraday as $9651{\cdot}31 \pm 0{\cdot}80$* abs. e.m.u. g.-equiv.$^{-1}$ (Birge), $e/m = F/m = (1{\cdot}7591 \pm 0{\cdot}0004) \times 10^7$ e.m.u./g.* From the relation

$$M_\mathrm{H}/m = e/m/e/M_\mathrm{H} = e/m/9573{\cdot}48,$$

$$M_\mathrm{H}/m = 1837{\cdot}4_6{}^*.$$

Since

$$R_\infty = R_\mathrm{H}(1 + m/M_\mathrm{H}),$$

$$R_\infty = 109{,}737{\cdot}26 \text{ cm.}^{-1*} \text{ (R.M.S. error} \pm 0{\cdot}020 \text{ cm.}^{-1})$$

or $109{,}737{\cdot}27_2$* corrected to Barrell and Sears (1939).

The value of the Rydberg constant for hydrogen just given is $0{\cdot}17_5$ cm.$^{-1}$ lower than the value quoted by Birge (1929) which is based on Houston's results. The difference is partly accounted for by the complications of air refractive indices, already discussed, and to a very small extent to the correction of 0·0053 cm.$^{-1}$ (in place of our 0·0036 cm.$^{-1}$) as the displacement of the observed centre of the 14 line from that of the strongest component. The difference, in the main, must be due to the value taken for the wavelength of the 5015 helium line which was used as the standard. The discrepancy between the value of R_∞ given above and Houston's value ($109{,}737{\cdot}424 \pm 0{\cdot}020$ cm.$^{-1}$) is slightly greater because of changes in the accepted values of the Faraday and atomic masses.

It seems to be a pure coincidence that the value of the ratio e/m ($1{\cdot}7591 \pm 0{\cdot}0004 \times 10^{-7}$) given above happens to be exactly equal to the most probable value recommended by Birge (1938) and also by Bearden (1939). The spread of the values in the spectroscopic results (especially when the Zeeman effect method is included) is much too wide for the average, even when weighted, to have such a definite meaning. Some of the results usually included are open to serious criticisms on what might be termed purely instrumental grounds. It is interesting to note that the simple mean of the four most recent determinations of e/m by the four different methods of direct velocity measurement, magnetic deflexion, crossed fields and X-ray refraction, is $1{\cdot}7591_7$, in close agreement with the results of this investigation. This seems to show that no real difference of measurable amount can exist between the value of the ratio, whether it is determined by a free or a bound electron method.

---

* See note at end of paper.

(*b*) *The fine structure of* H_α *and* D_α

After making allowance for the scattered light as shown on p. 170, large-sized graphs, drawn to a frequency scale of 1 cm. $= 6{\cdot}24 \times 10^{-3}$ cm.$^{-1}$, were obtained as follows. The point of greatest intensity on the trace was given the arbitrary value 10, so that after correction for the envelope effect the maximum value would lie between 10 and 15 units. With 2 cm. as the unit, so that the maximum ordinate of the $\hat{14}$ line varied between 20 and 30 cm., the greatest slope of the curve was approximately 45°. The fluctuations of the individual readings from a smooth curve depended on the magnitude of the envelope factor that had to be applied; for a line or component in single order position, the deviation rarely amounted to more than 1–2 mm., increasing to 4–7 mm. for the outer wings of a line in double order position. Between 50 and 80 individual readings completed a curve. With graphs on this scale, all errors in plotting are eliminated and the magnitude of any departure from a Doppler curve being fitted to it can be seen with ease. Tables were drawn of the co-ordinates of probability curves of various ordinates and half widths and the plotted curves cut out from similar graph paper. The case of D_α, as the easier problem, was first examined.

Table 7 gives a summary of the analysis of six plates of D_α. The second column shows the component that is nearest to the centre of intensity of the envelope; when two are indicated, the centre is nearer the component with the number in italics. The double values for the $\hat{14}$–2 separation for F 101 D, F 103 D and F 103 E in the third column indicate two separate measurements, $\hat{14}$ to 2 in one order and 2 to $\hat{14}$ in the next order. Errors due to incorrect determination of the envelope effect would cause differences in opposite directions between these results so that the discrepancy would be doubled. The actual intensities are given in the fifth column and are expressed as ratios in the sixth, in terms of the component 2 which is taken at its theoretical value of 7·08. The next column gives the observed half-widths of the second and third components; the contribution of the instrumental half-width of about 0·036 cm.$^{-1}$ and the microphotometer half-width (0·020 cm.$^{-1}$) are included in these values.

The separation 2–3 for F 103 A is omitted because of the large envelope factor to the readings for component 2 in this case. This makes the value uncertain, in comparison with the results of other plates. Similarly for most of the other plates, $\hat{14}$ is in double order involving large factors for the outer

TABLE 7. D_α

Plate no.	Component nearest single order	Separation $\hat{14}$–2 cm.$^{-1}$	Separation 2–3 cm.$^{-1}$	Intensities			Ratios		Half-widths cm.$^{-1}$		Notes
				$\hat{14}$	2	3	$\hat{14}$	3	2	3	
F101D	2	$0{\cdot}321_3$ $0{\cdot}321_6$	$0{\cdot}112_9$ $0{\cdot}114_8$	10	6·6	1·56	10·7	1·67	0·097	0·120	Scattered 0·25. Coherent 0·5. 3 not symmetrical
F101E	*2–3*	$0{\cdot}318_2$	$0{\cdot}115_4$	12·3	8·5	1·7	$10{\cdot}2_5$	1·42	0·092	0·094	Scattered 0·25. Coherent 1·0
		$0{\cdot}318_2$	$0{\cdot}121_7$	13·8	9·6	2	10·2	1·48	0·094	0·095	Scattered 1. Coherent 0·3
F101F	*3*–$\hat{14}$	$0{\cdot}320_7$	$0{\cdot}119_2$	9·8	5·95	1·2	11·7	1·43	0·091	0·121	Scattered 0·25. Coherent 0·45
F103A	$\hat{14}$	$0{\cdot}320_4$	—	9·4	7	—	9·5	—	—	—	Scattered 0·2. Coherent 0·5
F103D	*2*–$\hat{14}$	$0{\cdot}318_8$ $0{\cdot}320_1$	$0{\cdot}120_7$	12	9·5	2	8·9	1·49	0·095	0·110	Scattered 0·4. Coherent 0·65
F103E	2	$0{\cdot}322_9$ $0{\cdot}322_0$	$0{\cdot}123_2$	13·8	9·25	1·85	10·6	0·142	0·095	0·120	Scattered 0·5. Coherent 0·5. 3 not symmetrical
Weighted averages:		$0{\cdot}320_5$	$0{\cdot}119_0$				10·2	1·45	0·094	0·108	

wings so that the half-width of this line is also omitted. The differences in the results from plate to plate are real in the sense that they do not arise either from errors in measuring the traces or in fitting the Doppler curves. Several of the traces have been re-measured at different times and new curves fitted to the graphs. The differences, except for the separation of 2–3 in F 101 D (the extreme values are given in the table), have been negligibly small. In general, the resultant of the Doppler curves fitted would coincide with the graph, between intensity values 1 and 9, to within about 2 mm. Two exceptions to this occurred; in F 101 E a peculiar indentation on the upper part of the high frequency side of $\widehat{14}$ left a gap of about 5 mm. from the Doppler curve that fitted it at lower levels. This must either be due to a defect in the plate or to a local disturbance of the galvanometer when the recording was made. In F 101 D the low intensity portion (below 1) of the high frequency side of 2 could not be fitted to a Doppler curve; two alternatives are possible, the third component could be found by simply reversing the high frequency side of 2 or by using the Doppler curve that best fitted the greater part of the curve. The choice made no difference in the value of the $\widehat{14}$–2 separation, but the value of the 2–3 separation is affected as shown in the table. In neither case was the third component symmetrical.

It is sometimes difficult to get an accurate value for the fraction scattered when the double order components differ widely in intensity on the trace and also when the intensities are nearly equal. The straightforward analysis of F 101 E led to a scattered intensity of 0·25 and a "coherent" background of 1. A total background of 1·25 could not be avoided in this fairly heavily exposed plate, but the relative proportion of the "coherent" light seemed high. An analysis was made, based on the other extreme that the scattered intensity was 1, in which case the "coherent" fraction becomes approximately 0·3. The only material difference is that the 2–3 separation is increased by 0·006 cm.$^{-1}$ in the second case.

F 103 A, plate 7, figure 7 is probably the most interesting; the main line $\widehat{14}$ is practically in exact single order position and the intensity readings for the contour should have the maximum accuracy. A decidedly better fit is obtained by using two Doppler curves (each of half-width 0·094 cm.$^{-1}$ and intensity ratio 9 : 1) than when a slightly wider single Doppler curve is chosen. The separation of the components 1 and 4 is 0·044 cm.$^{-1}$ as compared with the theoretical value of 0·036 cm.$^{-1}$. Considering the closeness of the components and the disparity in their intensities, the agreement is as good as could be expected. The half-width value for 2 was found to be 0·090 cm.$^{-1}$, but as it is only approximate (due to the large factor for 2) it has been omitted from the table.

In obtaining the average values, both results for the 2–$\widehat{14}$ separation in F 101 E have been included; since the third component is not symmetrical in F 101 D and F 103 E, the 2–3 separations (average value for F 101 D) have only been given half the weight of the other values.

Table 8 gives the corresponding results of the analysis of four plates of H_α. Owing to the greater half-width of the components, with a substantial overlap of both 2 and $\widehat{14}$ in the region of the third component, the analysis is much more laborious and necessarily less accurate.

DISCUSSION OF THE FINE STRUCTURE RESULTS

The first point of interest is that in addition to the scattered light, which in some degree is inevitable with all optical instruments, there is also an appreciable proportion of coherent light. Since it is greater with hydrogen than deuterium, the probability is that it is due to molecular lines which lie in the spectrum region corresponding to the width of the E 1 slit. It may be that in a dry hydrogen-helium mixture the molecular spectrum has a greater relative intensity than in a damp hydrogen discharge. Since the theoretical intensity ratio between the main components cannot be obtained with the latter type of discharge, it is manifestly incorrect and unfair to use it to test the theory, especially since the components of greatest interest are incompletely resolved.

The $\widehat{14}$–2 separation for D_α of $0{\cdot}320_5$ cm.$^{-1}$ implies a value of $0{\cdot}316_9$ cm.$^{-1}$ for the separation between the main components 1–2. This is approximately 0·003 cm.$^{-1}$ smaller than the value given by R. C. Williams and $0{\cdot}011_6$ cm.$^{-1}$ less than the theoretical value. The corresponding separation for H_α, $0{\cdot}319_8$, gives a separation of $0{\cdot}316_2$ cm.$^{-1}$ between the main components 1 and 2 (the effect of the third component on both 2 and $\widehat{14}$ had already been taken into account in determining the positions of 2 and $\widehat{14}$). This value is almost identical with the average value given by R. C. Williams ($0{\cdot}316_8$ cm.$^{-1}$).

The greatest discrepancies occur in the measurement of the 2–3 separation. For D_α, in place of the theoretical value of 0·108 cm.$^{-1}$ we obtain a fairly constant value of 0·119 cm.$^{-1}$ which compares with 0·130 cm.$^{-1}$ found by R. C. Williams.

Pasternack (1938) has pointed out that the assumption of a perturbation of 0·030 cm.$^{-1}$ of the $2\,{}^2S_{\frac{1}{2}}$ level would account for both results of R. C. Williams. Since component 2 is the sum of two lines of relative intensity 1 and 2·4 ending on the $2\,{}^2S_{\frac{1}{2}}$ and $2\,{}^2P_{\frac{1}{2}}$ respectively (see figure 1), the centre of gravity of the composite line should be displaced by about 0·010 cm.$^{-1}$

TABLE 8. H_α

Plate no.	Component nearest single order	Separation $\widehat{14}$–2 cm.$^{-1}$	Separation 2–3 cm.$^{-1}$	Intensities			Ratios		Half-widths cm.$^{-1}$		Notes
				$\widehat{14}$	2	3	$\widehat{14}$	3	2	3	
F73B	2	0·318$_9$ 0·321$_7$	0·129$_2$	11·1	8·9	2	8·9	1·59	0·125	0·146	Background 0·26. Coherent 0·8
F73D	3	0·321$_4$	—	10·5	8·5	—	8·75	—	—	—	Background 0·3. Coherent 1·2
F75A	2–3	0·318$_2$	0·134$_2$	11·25	8·0	1·6	9·9$_5$	1·42	0·141	0·127	Scattered 0·25. Coherent 1·1. 3 unsymmetrical
F77D	3	0·318$_9$	0·131$_7$	10·5	8·4	1·8	8·8$_5$	1·52	0·124	0·135	Total scattered plus coherent = 1·25
Average values:		0·319$_8$	0·131$_7$				9·1	1·51	0·130	0·136	

to the red, so that the 2–14 separation is reduced by this amount. Component 3, consisting of a doublet of lines ending on the same levels with an intensity ratio of 10·4 to 1, will have its centre displaced approximately three times as much in the same direction, so that the 2–3 separation is increased.

Fröhlich, Heitler and Kahn (1939) have recently calculated the deviation from a Coulomb law of force for the proton according to the mesotron theory of nuclear particles, and predict a displacement of the hydrogen 1 S level of the order of 3 cm. and about one-eighth of this for the 2 S level.

Although the results for hydrogen given in Table 8 apparently support this hypothesis, there are certain other factors that appear to rule out the possibility of this explanation. The first is that the unsymmetrical third component should have a definitely lower half-width than the second owing to the disparity in intensities of the constituents of the third component. In practice, both for D_α and H_α, with one exception, the half-width of the third component is always greater than that of the second. In addition, the intensity of the third component is much too high. The ratio of intensities of the main components 1 and 2 is substantially the theoretical value, hence one would expect the third component in a multiplet to have its theoretical intensity. On the average, our results for the third component in D_α show it to have an intensity 1·3 times its theoretical value, while in the experiments of R. C. Williams the factor is 2·2.

A probable explanation of a part of the difference, at least in our case, is the difficulty of obtaining a deuterium discharge free from hydrogen. Although a fresh tube was used and the D_2O and NaOD were over 99 % pure, the glass walls and electrodes of the discharge tube appeared to be giving off hydrogen continuously. Even after repeated flushing with deuterium over several weeks, it was found impossible to obtain a discharge, which, after running for a few hours, gave a ratio H_α/D_α less than 2 % and the ratio steadily increased as the discharge was continued. The tube was therefore regularly cleaned out and refilled with fresh deuterium, the hydrogen impurity being determined after each echelon exposure plate.

With a wave number difference of 4·1442 cm.$^{-1}$ between corresponding components, the interference patterns of the two isotopes will coincide when the path difference $2t = n/4{\cdot}1442$ cm. where n is an integer. The value of $2t$ for $n = 4$ is 0·9652 cm. and it increases by 0·2413 cm. for each successive coincidence. In our case $2t = 1{\cdot}3757$ cm. which is 0·1692 cm. higher than $n = 5$. Hence the H_α pattern, if present, should be displaced 0·1692/0·2413 or 0·7012 of an order to the long wave side of that of D_α. Since an order here is 0·727 cm.$^{-1}$, the displacement is $0{\cdot}509_7$ cm.$^{-1}$. This displacement to the red is equivalent to a shift of $0{\cdot}217_3$ cm.$^{-1}$ to the blue for the next order. Their relative positions for an equal mixture are approximately drawn to scale in figure 8*a*. The 5 mm. etalon used by R. C. Williams would give a displacement of $(1 - 0{\cdot}9652)/0{\cdot}2143$ or $0{\cdot}144$ of an order, and since the inter-order distance for a 5 mm. etalon is 1 cm.$^{-1}$ the shift of the H_α pattern would be approximately $0{\cdot}144$ cm.$^{-1}$ to the red as shown in figure 8*b*. (No allowance has been made for air index as the etalon thickness is only approximate.)

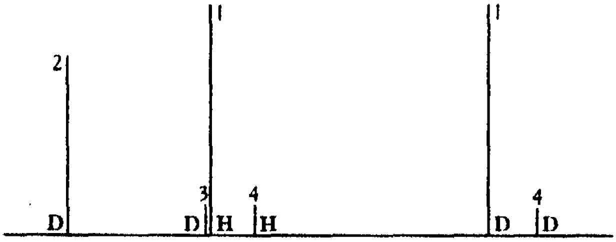

FIGURE 8*a*

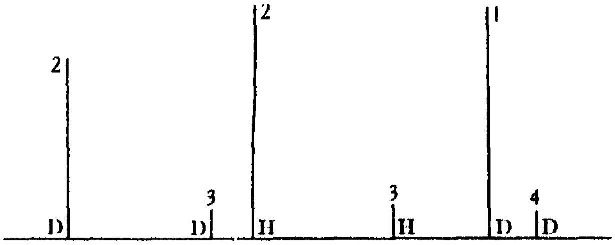

FIGURE 8*b*

In our case, the main component of hydrogen 1H would almost exactly coincide with the third component of deuterium and cause no error in the 2–3 separation. Plate F 104 taken immediately after F 103 E showed $H_\alpha/D_\alpha = 2\,\%$. Hence component 3 should have an increased intensity of 1·34. The average value is 1·45. In the experiments of R. C. Williams, the component 2H will tend to increase the 2–3 separation. If the increased intensity of the third component is entirely due to hydrogen impurity, the 2–3 separation for D_α will be approximately $0{\cdot}125$ cm.$^{-1}$ as compared with the observed value of $0{\cdot}130$ cm.$^{-1}$.

The objections to Pasternack's hypothesis concerning line width and intensity of the third component are even stronger in the case of H_α. We observe that in hydrogen, the sum of the coherent and scattered light is always relatively higher than with deuterium. In H_α the sum varies from 1·06 to about 1·5, the 2–3 separation being lowest when the total sum is lowest. As previously explained, the amount of scattering cannot always be exactly determined although the sum of the scattered plus the coherent can be fairly accurately assessed. If as a rough approximation we assume the scattered light to be constant, the variations must be due to differences in the relative intensity of the secondary spectrum lines in the region covered by the E 1 slit. The third component has only 1/18th of the total intensity of H_α, and the group of secondary lines in this band may well have an intensity of this order since the interference patterns of many lines will overlap more or less completely.

Unless a method of eliminating the secondary spectrum can be found, it will only be possible to obtain more accurate data on the structure of H_α by analysing the patterns obtained from a number of etalons (or echelons) of increasing plate thickness. This will not be possible for deuterium unless the hydrogen contamination can be maintained below about 0·5 % and for this purpose the tap grease in the apparatus should be free from the lighter isotope.

We have therefore come to the conclusion that no real evidence has yet been found to show that the fine structure patterns of H_α and D_α depart substantially from the values calculated on the basis of Dirac's theory.

We wish to express our thanks to the Leverhulme trustees for the grant of a fellowship to one of us (W. E. W.) during the tenure of which a part of this work was done. We are further indebted to the Department of Scientific and Industrial Research for an Assistantship granted to one of us (J. W. D.). We are also much indebted to the Royal Society for providing most of the expensive optical equipment.

SUMMARY

The wave numbers of the main lines of H_α and D_α have been directly determined in vacuo by means of a 40 plate reflexion echelon. The liquid air cooled discharge tube containing helium with a small percentage of hydrogen (or deuterium) gave approximately the theoretical ratio between the intensities of the "apparent doublets" over the optimum range of operating conditions, which was investigated. With 6440·2491 A as the vacuum wavelength of the red cadmium line, the wave number of the "centre of intensity" of the main line of H_α is $15{,}233{\cdot}067_0$ cm.$^{-1}$ (R.M.S. error $0{\cdot}001_4$ cm.$^{-1}$) and the Rydberg constant $R_H = 109{,}677{\cdot}58_3$ cm.$^{-1}$ (R.M.S. error $0{\cdot}01_0$ cm.$^{-1}$). For the heavier isotope the corresponding values are $15{,}237{\cdot}211_2$ cm.$^{-1}$ (R.M.S. error $0{\cdot}001_3$ cm.$^{-1}$) and $R_D = 109{,}707{\cdot}42_1$ cm.$^{-1}$.

The mass of the electron, using the atomic values of Bainbridge, is

$$m = (5{\cdot}48646 \pm 0{\cdot}0005) \times 10^{-4} \text{ atomic unit.}$$

Taking the Faraday constant as 9651·31 ± 0·80 coulombs, we get

$$e/m = (1{\cdot}7591 \pm 0{\cdot}0004) \times 10^{7} \text{ e.m.u./g.}$$

With $e/M_{\mathrm{H}} = 9573{\cdot}48$, we obtain $M_{\mathrm{H}}/m = 1837{\cdot}4_6$ and $R_\infty = 109{,}737{\cdot}27_2$ cm.$^{-1}$.

Seven microphotometer records of D_α and four of H_α have been analysed; denoting the components in order of their relative intensities and $\widehat{14}$ to indicate the centre line of the unresolved doublet of the first and fourth component (termed the main line), we find $\widehat{14}$–2 for $\mathrm{D}_\alpha = 0{\cdot}320_5$ cm.$^{-1}$ with a spread of 0·004 cm.$^{-1}$ and 2–3 = 0·119 cm.$^{-1}$ with a spread of about twice the amount. The observed half-width values for the second and third components are 0·094 cm.$^{-1}$ and 0·108 cm.$^{-1}$, the latter being frequently obviously unsymmetrical. An analysis of the $\widehat{14}$ doublet places component 4 at $0{\cdot}04_4$ cm.$^{-1}$ from component 1. The corresponding values for H_α are $0{\cdot}319_8$ cm.$^{-1}$ and $0{\cdot}131_7$ cm.$^{-1}$ with half-widths of 0·130 cm.$^{-1}$ and 0·136 cm.$^{-1}$

Although these values appear to support Pasternack's suggestion of a perturbation of the $2\,{}^2\mathrm{S}_{\frac{1}{2}}$ level, the increased intensity of the third component coupled with an increased half-width, in addition to other evidence, gives us ground for supposing that the discrepancies are caused by molecular lines in this region. We conclude that no real evidence has yet been obtained to show that the fine structures depart substantially from the values calculated from Dirac's equations.

[*Note added in proof.* Since this paper was set up in type, R. T. Birge in a private communication to one of us (W. E. W.) states that he now considers that the most probable value of the quantity q defined by the equation

$$\text{International ampere} = q \text{ absolute ampere}$$

should be changed from 0·99993 to 0·99986 ± 0·00002. This value is derived from some recent work at the Bureau of Standards and ends a conflict of some years between them and the National Physical Laboratory. If this value of q is adopted, the value of the Faraday constant F (physical scale) is changed from 9651·31 ± 0·80 to 9650·6 ± 1·0 abs. e.m.u. g.-equiv.$^{-1}$. This would change the value of several of the constants which are determined in this paper, including e/m from 1·7591 ± 0·0004 to 1·7590 ± 0·0004 e.m.u. g.$^{-1}$. Furthermore, Birge considers that the value 9573·48 of e/M_{H} we have used should be lowered to $9591{\cdot}4_1 \pm 1{\cdot}0_2$. If this value is accepted as well as the new value of F our value of M_{H}/m will be raised from $1837{\cdot}4_6$ to $1837{\cdot}7_2$. This change in M_{H}/m makes a small change of 0·0084 cm.$^{-1}$ in the value of R_∞ from $109737{\cdot}27_2$ to $109737{\cdot}26_{36} \pm 0{\cdot}020$ cm.$^{-1}$ R.M.S. error which is what it was before applying the Barrell and Sears (1939) correction.]

REFERENCES

Barrell, H. and Sears, J. E. 1939 *Phil. Trans.* A, **238**, 1.
Bearden, J. A. 1938 *Phys. Rev.* **54**, 698.
— 1939 *Phys. Rev.* **55**, 584.
Birge, R. T. 1929 *Rev. Mod. Phys.* **1**, 1.
— 1938 *Phys. Rev.* **54**, 972.
Dunnington, F. G. 1937 *Phys. Rev.* **52**, 475.
Fröhlich, H., Heitler, W. and Kahn, B. 1939 *Proc. Roy. Soc.* A, **171**, 269.
Heyden, M. 1937 *Z. Phys.* **106**, 499.
Houston, R. A. 1927 *Phys. Rev.* **30**, 608.
Kösters, M. W. and Lampe, W. 1934 *Phys. Z.* **35**, 223.
Livingstone, M. S. and Bethe, H. A. 1937 *Rev. Mod. Phys.* **9**, 373.
Meggers, W. F. and Peters, C. G. 1918 *Bull. U.S. Bur. Stand.* **14**, 697.
Pasternack, S. 1938 *Phys. Rev.* **54**, 1113.
Perard, A. 1934 *Trav. Bur. int. Poids Mes.* **19**, 1.
Sears, J. E. and Barrell, H. 1934 *Phil. Trans.* A, **233**, 143.
Shaw, A. E. 1938 *Phys. Rev.* **54**, 193.
Spedding, F. H., Shane, C. D. and Grace, N. S. 1935 *Phys. Rev.* **47**, 38.
Williams, R. C. 1938 *Phys. Rev.* **54**, 558 and 568.
Williams, R. C. and Gibbs, R. C. 1934 *Phys. Rev.* **45**, 491.
Williams, W. E. 1933 *Proc. Phys. Soc.* **45**, 699.
Williams, W. E. and Gogate, D. V. 1938 *Proc. Roy. Soc.* A, **167**, 509.

Statistical thermodynamics of super-lattices*

BY R. H. FOWLER, F.R.S., *Cambridge* AND
E. A. GUGGENHEIM, SC.D., *Imperial College of Science*

(*Received* 19 *October* 1939)

1. INTRODUCTION

There is no need to define super-lattices, since they have been so freely discussed in recent years. An excellent summary of the subject, with complete references to the literature, has been given by Nix and Shockley (1938). The application of statistical mechanics to the theoretical development is due to Gorsky (1928) and to Bragg and Williams (1934). Improved approximations have since then been introduced by Bethe (1935), Peierls (1936) and Kirkwood (1938), all of which are fully reviewed by Nix and Shockley (1938). We shall therefore be able to confine ourselves to a comparison, at a later stage, of their formulae with those which we shall derive here.

We introduce in this paper a new method of approach which we shall call *the quasi-chemical method*. The method was first devised and used by Guggenheim (1935) in a treatment of regular solutions. An error in this treatment was corrected by Rushbrooke (1938), who showed that the correct treatment by the quasi-chemical method is equivalent to the use of Bethe's method in its first approximation. It has recently been shown (Guggenheim 1938) that the quasi-chemical method is equivalent to the method of Bethe, and in certain respects more convenient to use, not only for regular solutions but for a whole class of assemblies which may be called *regular assemblies*. The class includes regular solutions, monolayers on solids, solutions of hydrogen in palladium, and mixed crystals, provided there is no long-range order. We shall here show that the last proviso may be removed; the quasi-chemical method may be applied with equal rigour and convenience to an assembly in which long-range order is present. In the first part of this paper we shall confine ourselves to alloys such as β-brass, in which in the ordered state there are equal numbers of lattice points of each of two types a and b, all the nearest neighbours of a's being b's and vice versa, and equal numbers of atoms of each of two types A and B. This is the ideal case and the simplest example of an assembly showing long-range order. We discuss the new method and compare it with the older methods in full detail for this case, showing that it is equivalent to Bethe's method in its first approximation. In this comparison the precise statistical significance of Bethe's method becomes fully apparent, for perhaps the first time. We then proceed to apply the new method to the more general case, by removing the restriction to equal numbers of atoms A and B. The superior power of the quasi-chemical method becomes evident at this stage. It should also be applicable more widely to other types of lattice.

---

* This paper was written for the Physics Conference at the International Exhibition at Zurich and communicated to the organizers at the end of June. Owing to the war it has become necessary to withdraw it and make other arrangements for publication. In the meantime a paper by Bethe and Kirkwood (1939) has appeared giving some of our more important results without proof.

2. THE ENERGY OF A CRYSTAL COMPOSED OF EQUAL NUMBERS OF ATOMS A AND B

We start by considering a crystal composed of $2N$ atoms, of which N are A's and N are B's (e.g. β-brass; $A \equiv \text{Cu}$, $B \equiv \text{Zn}$). The presence of long-range order means that one can distinguish two types of lattice points a and b; each a is assumed to have z sites b as neighbours, and each b to have z sites a (in β-brass, $z = 8$).

Let us denote by Nr the number of a sites occupied by A atoms; here Nr will also be equal to the number of b sites occupied by B atoms. The number of a sites occupied by B's, and the number of b sites occupied by A's will both be $N(1-r)$. There are in the crystal zN pairs of neighbouring sites ab, whose arrangements must now be specified. We use the symbols A/a, etc. to mean an atom A on a site a, etc.; and A/a, B/b, etc. to mean a pair of neighbours AB of which the A is on an a site and the B on a b site, etc. In any configuration of given r we have the following relations:

$$[A/a, B/b] + [A/a, A/b] = [A/a, B/b] + [B/a, B/b] = zNr, \tag{2·1}$$

$$[A/a, A/b] + [B/a, A/b] = zN(1-r), \tag{2·2}$$

in which the [ ] denote the numbers of pairs of the type specified by the enclosed symbols. It follows that one more parameter is sufficient to specify the most general possible arrangements of pairs for given r. We use a parameter x, so defined that zNx is the number of pairs of type A/a, A/b. In the perfectly ordered state $x = 0$. The number of pairs of each type for given r and x is shown in table 1.

The current theories of super-lattices all assume that the configurational energy is equal to the sum of independent contributions due to each pair of neighbours. Denoting the contribution of an AA pair by χ_{AA}, etc. and using table 1, the energy of a configuration of given r and x is found to be

$$zN\chi_{AB} + zNx(\chi_{AA} + \chi_{BB} - 2\chi_{AB}),$$

independent of r. Writing

$$2\chi = \chi_{AA} + \chi_{BB} - 2\chi_{AB}, \tag{2·3}$$

we see that the configurational energy is

$$zN(\chi_{AB} + 2x\chi). \tag{2·4}$$

Thus 2χ is the work required to replace two AB pairs by an AA pair and a BB pair.

TABLE 1. NUMBERS OF PAIRS FOR A SIMPLE *ab* LATTICE OCCUPIED BY EQUAL NUMBERS OF *A*'S AND *B*'S

$[A/a, B/b]$	$[A/a, A/b]$	$[B/a, B/b]$	$[B/a, A/b]$
$zN(r-x)$	zNx	zNx	$zN(1-r-x)$

To determine the equilibrium properties of the alloy the essential problem is to determine the average or equilibrium value $\bar{x}$ of x. The quasi-chemical method consists in making the assumption that, in the equilibrium state,

$$\frac{[A/a, B/b]\,[B/a, A/b]}{[A/a, A/b]\,[B/a, B/b]} = e^{2\chi/kT}. \tag{2·5}$$

If we replaced the right-hand side of the equation by unity, we should obtain a random distribution of pairs (consistent with a given value of r), and this approximation leads to the formulae of Gorsky and of Bragg and Williams. The exponential factor favours the configurations with pairs of lower energy at the expense of those of higher energy in the manner characteristic of a chemical dissociative equilibrium, since -2χ is the amount by which the energy of the two AB pairs in the numerator on the left-hand side of (2·5) exceeds that of the AA and BB pairs in the denominator. We shall not at this stage attempt any more rigorous justification of (2·5). The analogous formula in the absence of long-range order has been discussed at length (Rushbrooke 1938; Guggenheim 1938) and leads to acceptable results. For the present we treat (2·5) as a reasonable guess and examine the conclusions to which it leads.

Using the values of table 1, we obtain for equilibrium $x = \bar{x}$,

$$(r-\bar{x})(1-r-\bar{x}) = \bar{x}^2 e^{2\chi/kT}, \tag{2·6}$$

with the relevant root

$$\bar{x} = \frac{\{1+4r(1-r)(e^{2\chi/kT}-1)\}^{\frac{1}{2}}-1}{2(e^{2\chi/kT}-1)}, \tag{2·7}$$

giving the equilibrium value of $\bar{x}$ for given r according to the quasi-chemical method. If we introduce the usual long-range order s defined by

$$r = \tfrac{1}{2}(1+s), \quad (1-r) = \tfrac{1}{2}(1-s), \tag{2·8}$$

formula (2·7) becomes

$$\bar{x} = \frac{\{1+(1-s^2)(e^{2\chi/kT}-1)\}^{\frac{1}{2}}-1}{2(e^{2\chi/kT}-1)}. \tag{2·9}$$

Substituting this value of $\bar{x}$ for x in (2·4), we obtain for the equilibrium energy $E(s)$ of the crystal, averaged over all states of given long-range order s,

$$\frac{E(s)}{Nz\chi} - \frac{\chi_{AB}}{\chi} = \frac{\{1+(1-s^2)(e^{2\chi/kT}-1)\}^{\frac{1}{2}}-1}{e^{2\chi/kT}-1}, \tag{2·10}$$

which can be written in the alternative form

$$\frac{E(s)}{Nz\chi} - \frac{\chi_{AB}}{\chi} = \frac{1-s^2}{\{1+(1-s^2)(e^{2\chi/kT}-1)\}^{\frac{1}{2}}+1}. \tag{2·11}$$

If we replace the exponential in (2·11) by unity, we see at once that we recover the approximation of Bragg and Williams,

$$\frac{E(s)}{Nz\chi} - \frac{\chi_{AB}}{\chi} = \tfrac{1}{2}(1-s^2). \tag{2·12}$$

3. THE FREE ENERGY FOR GIVEN LONG-RANGE ORDER

From formula (2·11) for the equilibrium energy $E(s)$ we can derive the free energy $F(s)$ for given s by integrating the thermodynamic relation

$$\frac{\partial\{F(s)/T\}}{\partial(1/T)} = E(s). \tag{3·1}$$

If the fixed limit of integration is taken at $1/T = 0$, $T = \infty$, the integration constant in $F(s)/T$ is $-k\log g(s)$, where $g(s)$ denotes the number of distinguishable configurations of given s, and is given by

$$g(s) = \left[\frac{N!}{(Nr)!\,(N-Nr)!}\right]^2, \tag{3·2}$$

$$\log g(s) = N\{2\log 2-(1+s)\log(1+s)-(1-s)\log(1-s)\}. \tag{3·3}$$

A detailed derivation of this formula is given, for example, by Kirkwood (1938), as well as in several others of the papers referred to.

Using (2·11) and (3·3) in the integrated form of (3·1), we obtain

$$\frac{F(s)-Nz\chi_{AB}}{NkT} = (1+s)\log(1+s)+(1-s)\log(1-s)-2\log 2+ \\ +\tfrac{1}{2}z\int_0^{2\chi/kT}\frac{1-s^2}{\{1+(1-s^2)(e^{2\chi/kT}-1)\}^{\frac{1}{2}}+1}\,d\left(\frac{2\chi}{kT}\right). \quad (3·4)$$

To evaluate this integral we may conveniently use the substitution

$$\{1+(1-s^2)(e^{2\chi/kT}-1)\}^{\frac{1}{2}} = \alpha, \quad (3·5)$$

when the integral rationalizes and we find

$$\frac{F(s)-Nz\chi_{AB}}{NkT} = (1+s)\log(1+s)+(1-s)\log(1-s)-2\log 2+ \\ +\tfrac{1}{2}z\left\{(1+s)\log\frac{\alpha+s}{1+s}+(1-s)\log\frac{\alpha-s}{1-s}-2\log\frac{\alpha+1}{2}\right\}. \quad (3·6)$$

We observe incidentally that, if we choose to take as energy zero the completely ordered crystal, $\chi_{AB}=0$, and all terms in χ_{AB} may be omitted throughout. We prefer, however, to keep our formulae independent of any arbitrary choice of energy zero, especially since there has been occasional confusion on this point.

4. EQUILIBRIUM STATE AT A GIVEN TEMPERATURE

Having obtained an explicit formula for the configurational free energy $F(s)$ as a function of T for any given s, we have now merely to minimize $F(s)$ at each temperature. The value of s so determined is then the equilibrium value of s at that temperature, and the remaining equilibrium properties follow at once by using this value of s in $F(s)$ and $E(s)$. For high values of χ/kT the minimizing value of s has a value greater than zero, which decreases as χ/kT decreases. At a certain value of χ/kT ($\simeq 0·288$) the minimizing value of s becomes zero, and remains zero for all lower values of χ/kT. All this is well known, and it is only the exact quantitative deductions obtained by the quasi-chemical method that call for comparison with those obtained by other methods. Using formula (3·6) for $F(s)$, we find with the help of (3·5) that

$$\frac{1}{NkT}\frac{\partial F(s)}{\partial s} = -(\tfrac{1}{2}z-1)\log\frac{1+s}{1-s}+\tfrac{1}{2}z\log\frac{\alpha+s}{\alpha-s}, \quad (4·1)$$

$$\frac{1}{NkT}\frac{\partial^2 F(s)}{\partial s^2} = -\frac{z-2}{1-s^2}+\frac{z}{\alpha(1-s^2)}. \quad (4·2)$$

All stationary values of $F(s)$ are given by the root of

$$\log\frac{\alpha+s}{\alpha-s}=\left(1-\frac{2}{z}\right)\log\frac{1+s}{1-s}. \tag{4·3}$$

Equation (4·3) is always satisfied by $s=0$. At temperatures less than a Curie temperature T_c it is also satisfied by another value s^* of s. It can be verified algebraically that, when $T<T_c$, $s=s^*$ gives the minimum and $s=0$ a maximum of $F(s)$. The equilibrium state is therefore given for $T<T_c$ by $s=s^*>0$. When $T>T_c$ the only stationary value is $s=0$ and this gives the minimum of $F(s)$. When $T<T_c$ there must be some point of inflexion between s^* and 0 at which $\partial^2F(s)/\partial s^2=0$. As $T\to T_c$, $s^*\to 0$ and so therefore must the inflexion. It follows that T_c is determined by the simultaneous satisfaction of the equations

$$\frac{\partial^2F(s)}{\partial s^2}=0,\quad \frac{\partial F(s)}{\partial s}=0,\quad s=0. \tag{4·4}$$

Using (4·1) and (4·2), these conditions reduce to $\alpha=z/(z-2)$, or

$$e^{\chi/kT_c}=z/(z-2). \tag{4·5}$$

$$\frac{\chi}{kT_c}=\log\frac{z}{z-2}. \tag{4·6}$$

This is exactly the Curie temperature given by Bethe's method. Equations (4·3) and (2·9), which may be taken in the form

$$\frac{1+s}{1-s}=\left(\frac{\alpha+s}{\alpha-s}\right)^{z/(z-2)}, \tag{4·7}$$

$$\frac{E(s)}{Nz\chi}-\frac{\chi_{AB}}{\chi}=\frac{1-s^2}{\alpha+1}, \tag{4·8}$$

with

$$\{1+(1-s^2)(e^{2\chi/kT}-1)\}^{\frac{1}{2}}=\alpha, \tag{4·9}$$

supplemented of course by $F(s)$ if required, give the equilibrium state according to the quasi-chemical method.

5. EQUIVALENCE OF THE QUASI-CHEMICAL AND BETHE'S METHODS

The identity of (4·6) for T_c with the corresponding equation given by Bethe suggests the possibility that the results of the two methods, in this case at least, are identical. The set of equations containing the results of Bethe's method for this case may be put in the form (Bethe 1935, § 6)

$$\frac{1+s}{1-s} = \epsilon^{z/(z-1)}, \tag{5·1}$$

$$E(s) = \text{const.} + Nz\chi\left\{\frac{\epsilon}{\epsilon + e^{\chi/kT}} \frac{2}{1+\epsilon^{z/(z-1)}}\right\}, \tag{5·2}$$

where ϵ is a parameter given by the correct root of the equation

$$\epsilon = \left[\frac{\epsilon e^{\chi/kT}+1}{\epsilon + e^{\chi/kT}}\right]^{z-1}. \tag{5·3}$$

Somewhat surprisingly equations (4·7–4·9) and (5·1–5·3) are fully equivalent. We can combine equations (5·1, 5·2) to give an expression for $E(s)$ of the form

$$\text{const.} + Nz\chi\epsilon(1-s)/(\epsilon + e^{\chi/kT}).$$

If we define ϵ', not yet necessarily Bethe's ϵ, by the equation

$$\frac{\epsilon'}{\epsilon' + e^{\chi/kT}} = \frac{1+s}{\alpha+1}, \tag{5·4}$$

so as to make the energy expressions (4·8) and (5·2) agree formally, and use equations (4·7) and (4·9), we can show that ϵ' also satisfies (5·1) and (5·3) and is therefore identical with Bethe's ϵ.

These elegant tricks are, however, far from satisfactory as a complete account of the relationship. By returning to the foundations of Bethe's method one can establish its complete equivalence to the quasi-chemical method for lattices of this type for any values of the atomic ratios, not merely for equality.

The essence of Bethe's method is the construction of a grand partition function for a sample group of sites; in Bethe's own exposition for an a site and its z neighbours b, and for a b site and its z neighbours a. When the central site is an a site, the configurational factor in the grand partition function for the sample is of the form

$$\Xi^a = \lambda_A(\lambda_A\eta_{AA}\epsilon_A^a + \lambda_B\eta_{AB}\epsilon_B^a)^z + \lambda_B(\lambda_A\eta_{AB}\epsilon_A^a + \lambda_B\eta_{BB}\epsilon_B^a)^z. \tag{5·5}$$

In this expression the λ's are the distribution parameters or absolute activities of the atoms A and B; η_{AA}, etc. are a shortened notation for $e^{-\chi_{AA}/kT}$, etc.; and the ϵ_A^a, ϵ_B^a are Bethe's correcting factors for the average effect of the rest of the assembly for an A and a B atom on a site b as neighbour to a central site a. There is a corresponding expression for a group with a central site b which we need not trouble to write down. The fundamental *assumption of Bethe's method is that the other interactions can be allowed for in the mean by correcting factors of this form whose values are to be* obtained by an equation of consistency. Now it is an essential property of any type of partition function that its terms are proportional to the fraction of time that the assembly occupies the corresponding states or configurations. If therefore we select a pair of sites consisting of the central a and a particular neighbour b, the corresponding terms in the partition function (5·5) for a pair A/a, A/b are

$$\lambda_A . \lambda_A \eta_{AA} \epsilon_A^a (\lambda_A \eta_{AA} \epsilon_A^a + \lambda_B \eta_{AB} \epsilon_B^a)^{z-1};$$

there are similar expressions for the frequency of occurrence of other types of pairs. We have therefore

$$\left.\begin{aligned}
[A/a, A/b] &\propto \lambda_A . \lambda_A \eta_{AA} \; \epsilon_A^a (\lambda_A \eta_{AA} \epsilon_A^a + \lambda_B \eta_{AB} \epsilon_B^a)^{z-1}, \\
[A/a, B/b] &\propto \lambda_A . \lambda_B \eta_{AB} \; \epsilon_B^a (\lambda_A \eta_{AA} \epsilon_A^a + \lambda_B \eta_{AB} \epsilon_B^a)^{z-1}, \\
[B/a, A/b] &\propto \lambda_B . \lambda_A \eta_{AB} \; \epsilon_A^a (\lambda_A \eta_{AB} \epsilon_A^a + \lambda_B \eta_{BB} \epsilon_B^a)^{z-1}, \\
[B/a, B/b] &\propto \lambda_B . \lambda_B \eta_{BB} \epsilon_B^a (\lambda_A \eta_{AB} \epsilon_A^a + \lambda_B \eta_{BB} \epsilon_B^a)^{z-1}.
\end{aligned}\right\} \qquad (5{\cdot}6)$$

On forming the ratio $[A/a, B/b]\,[B/a, A/b]/[A/a, A/b]\,[B/a, B/b]$ we find from these equations

$$\frac{[A/a, B/b]\,[B/a, A/b]}{[A/a, A/b]\,[B/a, B/b]} = \frac{\eta_{AB}^2}{\eta_{AA}\eta_{BB}} = e^{2\chi/kT}, \qquad (5{\cdot}7)$$

which is precisely the fundamental equation (2·5) of the quasi-chemical method. Since all the equilibrium properties of the alloy follow thermodynamically from (2·5), we may infer from the identity of (5·7) and (2·5), together with the self-consistency of Bethe's equations, that the two methods are completely equivalent. This inference holds here for all atomic ratios, not merely for the special case of equality, for which we have already verified it in detail in the earlier part of this section.

From the way in which the extra factors $(\;)^{z-1}$ eliminate themselves from (5·7), it is clear that it is unnecessary to consider in Bethe's manner a group of $z+1$ sites. A group of a pair of neighbouring sites is sufficient and fully equivalent, since in this type of lattice the neighbours of a site are not nearest neighbours of each other. If we construct Ξ^{ab} for a pair of neighbouring sites, we find

$$\Xi^{ab} = \lambda_A(\lambda_A \eta_{AA} \zeta_A^a + \lambda_B \eta_{AB} \zeta_B^a) + \lambda_B(\lambda_A \eta_{AB} \zeta_A^a + \lambda_B \eta_{BB} \zeta_B^a), \qquad (5{\cdot}8)$$

in which the ζ's are appropriate correcting factors for the interaction of one atom of the pair with all other atoms except the other atom of the pair.

It is possible, but not necessary, to correlate these ζ's with the ϵ's in (5·5). We then find

$$[A/a, A/b] \propto \lambda_A . \lambda_A \eta_{AA} \zeta_A^a,$$

and three similar formulae, which lead as before to (5·7).

It is of some importance to observe that z does not enter the fundamental equation (2·5) or (5·7) at all, and only enters the final formula for $E(s)$ or $F(s)$ as the ratio ($\frac{1}{2}z$) of the number of pairs to the number of sites, because the two parts of $F(s)$ depend, one on the number of pairs, and the other on the number of sites.

The results of Bethe's method for a simple *ab* lattice with equal numbers of atoms A and B have been thoroughly discussed elsewhere. Since the results of the quasi-chemical method are the same, we need not discuss them further in this case.

6. COMPARISON WITH KIRKWOOD'S RESULTS

Kirkwood (1938) has given an expansion for $F(s)/NkT$ in powers of χ/kT, up to and including the term in $(\chi/kT)^3$, which is exact for the assumed model, in which the only interactions are those between pairs of nearest neighbours. It is easy to study rigorously the accuracy of Bethe's or the quasi-chemical method by expanding $F(s)/NkT$ as given by (3·6) in powers of χ/kT. We find by expansion that

$$\frac{F(s)-F(1)}{NkT} = (1+s)\log(1+s)+(1-s)\log(1-s)-2\log 2 +$$
$$+z\left\{\tfrac{1}{2}(1-s^2)\frac{\chi}{kT}-\tfrac{1}{8}(1-s^2)^2\left(\frac{\chi}{kT}\right)^2-\tfrac{1}{12}s^2(1-s^2)^2\left(\frac{\chi}{kT}\right)^3+\dots\right\}. \tag{6·1}$$

Equation (6·1) agrees exactly with Kirkwood's result (1938), when allowance is made for the different notation and an error of sign in Kirkwood's last term is corrected, the necessity for which was pointed out by Chang (1939*a*).

The accuracy of the quasi-chemical method for higher powers of χ/kT cannot be estimated in the absence of exact formulae of Kirkwood's type for these higher terms.

In case comparisons between the result of the quasi-chemical method and accurate expansions in powers of $1/T$ beyond $1/T^3$ may some day be possible, we include the result of expanding (3·6) in powers of χ/kT up to and including $(\chi/kT)^6$. It is

$$\begin{aligned}\frac{F(s)-Nz\chi_{AB}}{NkT} &= (1+s)\log(1+s)+(1-s)\log(1-s)-2\log 2+\\ &+z\left[\tfrac{1}{2}(1-s^2)\frac{\chi}{kT}-\tfrac{1}{4}(1-s^2)^2\frac{1}{2!}\left(\frac{\chi}{kT}\right)^2-\tfrac{1}{2}s^2(1-s^2)^2\frac{1}{3!}\left(\frac{\chi}{kT}\right)^3+\right.\\ &+(\tfrac{1}{8}+\tfrac{3}{4}s^2+\tfrac{15}{8}s^4)(1-s^2)^2\frac{1}{4!}\left(\frac{\chi}{kT}\right)^4-(\tfrac{1}{2}-9s^2+\tfrac{21}{2}s^4)s^2(1-s^2)^2\frac{1}{5!}\left(\frac{\chi}{kT}\right)^5-\\ &\left.-(\tfrac{1}{4}+30s^4-105s^6+\tfrac{315}{4}s^8)(1-s^2)^2\frac{1}{6!}\left(\frac{\chi}{kT}\right)^6+\dots\right].\end{aligned} \tag{6·2}$$

7. UNEQUAL NUMBERS OF ATOMS A AND B

Even the formulae for a simple ab lattice become very complicated when worked out in Bethe's manner for unequal numbers of atoms A and B (Easthope 1937). The work is greatly simplified by use of the quasi-chemical method, and the results are naturally the same.

Of the N sites a let Nr (r for right) be occupied by atoms A, and $N(1-r)$ by atoms B. Of the N sites b let Nq (q for queer) be occupied by atoms A, and $N(1-q)$ by atoms B. We may without loss of generality assume that $r+q \leqslant 1$, i.e. fewer A's than B's. Let us define x as before so that zNx is the number of pairs $(A/a, A/b)$. Then the zN pairs of neighbouring sites must be occupied as in table 2.

TABLE 2

$[A/a, B/b]$	$[A/a, A/b]$	$[B/a, B/b]$	$[B/a, A/b]$
$zN(r-x)$	zNx	$zN(1-r-q+x)$	$zN(q-x)$

The formulae establishing table 2 are simple extensions of (2·1) and (2·2). The configurational energy is now

$$zN(r+q)\chi_{AB}+zN(1-r-q)\chi_{BB}+zNx(\chi_{AA}+\chi_{BB}-2\chi_{AB}),$$

or, for shortness,

$$E^0+zNx2\chi. \tag{7·1}$$

E^0 is then the configurational energy for the greatest possible order, and χ is still defined by (2·3).

The equation of quasi-chemical equilibrium is

$$(r-\bar{x})(q-\bar{x}) = \bar{x}(1-r-q+\bar{x})e^{2\chi/kT}. \tag{7·2}$$

The relevant solution is

$$\bar{x} = \frac{\{1+[2(1-r-q)+4rq]\,y+(1-r-q)^2\,y^2\}^{\frac{1}{2}}-1-(1-r-q)\,y}{2y}, \tag{7·3}$$

where we have written, for shortness' sake,

$$y = e^{2\chi/kT}-1. \tag{7·4}$$

The equilibrium configurational energy is given by substituting $\bar{x}$ from (7·3) for x in (7·1), being then given as a function of r and q; these variables are equivalent to the long-range order and the atomic ratio. If $\theta_A 2N$ is the number of A atoms, $r+q \leqslant 1$ is equivalent to $\theta_A \leqslant \frac{1}{2}$. We may define the long-range order s, in accordance with the usual convention, so that the number of A atoms on a sites is $N\theta_A(1+s)$. We then have

$$\left.\begin{aligned} r &= \theta_A+\theta_A s, & 1-r &= \theta_B-\theta_A s \\ q &= \theta_A-\theta_A s, & 1-q &= \theta_B+\theta_A s \end{aligned}\right\} \quad (\theta_A+\theta_B=1, \quad \theta_A \leqslant \tfrac{1}{2}). \tag{7·5}$$

In terms of θ_A, θ_B and s

$$\bar{x} = \frac{\{1+[2(\theta_B-\theta_A)+4\theta_A^2(1-s^2)]\,y+(\theta_B-\theta_A)^2\,y^2\}^{\frac{1}{2}}-1-(\theta_B-\theta_A)\,y}{2y}, \tag{7·6}$$

$$\frac{E(s)-E^0}{Nz\chi} = \frac{\{1+[2(\theta_B-\theta_A)+4\theta_A^2(1-s^2)]\,y+(\theta_B-\theta_A)^2\,y^2\}^{\frac{1}{2}}-1-(\theta_B-\theta_A)\,y}{y}, \tag{7·7}$$

$$F(s)-E^0 = -kT\log g(N,\theta_A,s)+T\int_0^{1/T}\{E(s)-E^0\}\,d\left(\frac{1}{T}\right). \tag{7·8}$$

The number of distinct configurations $g(N,r,q)$ or $g(N,\theta_A,s)$ is now given by

$$g(N,r,q) = \frac{N!}{(Nr)!\,(N-Nr)!}\,\frac{N!}{(Nq)!\,(N-Nq)!}. \tag{7·9}$$

On converting to θ_A and s we find that

$$\begin{aligned} \log g(N,\theta_A,s) = -N[&(\theta_A+\theta_A s)\log(\theta_A+\theta_A s)+(\theta_B-\theta_A s)\log(\theta_B-\theta_A s)+ \\ &+(\theta_A-\theta_A s)\log(\theta_A-\theta_A s)+(\theta_B+\theta_A s)\log(\theta_B+\theta_A s)]. \end{aligned} \tag{7·10}$$

On changing the variable of integration to y by (7·4), so that

$$\frac{2\chi}{k}\,d\left(\frac{1}{T}\right) = \frac{dy}{y+1}, \tag{7·11}$$

we can reduce $F(s)$ to

$$\frac{F(s)-E^0}{NkT} = (\theta_A+\theta_A s)\log(\theta_A+\theta_A s)+(\theta_B-\theta_A s)\log(\theta_B-\theta_A s)+$$
$$+(\theta_A-\theta_A s)\log(\theta_A-\theta_A s)+(\theta_B+\theta_A s)\log(\theta_B+\theta_A s)+$$
$$+\tfrac{1}{2}z\int_0^v \frac{\{1+[2(\theta_B-\theta_A)+4\theta_A^2(1-s^2)]y+(\theta_B-\theta_A)^2y^2\}^{\frac{1}{2}}-1-(\theta_B-\theta_A)y}{y(y+1)}\,dy. \tag{7·12}$$

The second (integral) term can also be written in the form

$$\tfrac{1}{2}z4\theta_A^2(1-s^2)\int_0^v\frac{dy}{y+1}\times$$
$$\times\frac{1}{\{1+[2(\theta_B-\theta_A)+4\theta_A^2(1-s^2)]y+(\theta_B-\theta_A)^2y^2\}^{\frac{1}{2}}+1+(\theta_B-\theta_A)y}. \tag{7·13}$$

This second form can be evaluated by the usual procedure of factorizing the radical in the form

$$1+[2(\theta_B-\theta_A)+4\theta_A^2(1-s^2)]y+(\theta_B-\theta_A)^2y^2=\{(\theta_B-\theta_A)y+p\}\{(\theta_B-\theta_A)y+p'\}, \tag{7·14}$$

and making the substitution

$$\left[\frac{(\theta_B-\theta_A)y+p}{(\theta_B-\theta_A)y+p'}\right]^{\frac{1}{2}}=\beta. \tag{7·15}$$

The integral reduces to

$$\tfrac{1}{2}z4\theta_A^2(1-s^2)\,2(p'-p)\times$$
$$\times\int_{(p/p')^{\frac{1}{2}}}^{\beta}\frac{\beta\,d\beta}{(\beta+1)[\beta(p'-1)+(1-p)][\beta^2(p'-\theta_B+\theta_A)-(p-\theta_B+\theta_A)]}, \tag{7·16}$$

which gives an expression involving logarithms of functions of p, p' and β. We shall not trouble to write this down explicitly here, since the explicit value of $F(s)$ can be derived in a complete form even more simply by the method expounded in § 8. The determination of s requires the evaluation of $\partial F(s)/\partial s$, and this is so much simpler than $F(s)$ that we shall give the complete expression. On differentiating the form (7·12), we find

$$\frac{1}{NkT}\frac{\partial F(s)}{\partial s}=\theta_A\log\frac{(1+s)(\theta_B+\theta_A s)}{(1-s)(\theta_B-\theta_A s)}-$$
$$-\tfrac{1}{2}z4\theta_A^2 s\int_0^v\frac{dy}{(1+y)\{1+[2(\theta_B-\theta_A)+4\theta_A^2(1-s^2)]y+(\theta_B-\theta_A)^2y^2\}^{\frac{1}{2}}}. \tag{7·17}$$

On making the substitution (7·15), we find that

$$\int_0^y \frac{dy}{(1+y)\{\ldots\}^{\frac{1}{2}}} = 2\int_{(p/p')^{\frac{1}{2}}}^{\beta} \frac{d\beta}{\beta^2(p'-\theta_B+\theta_A)-(p-\theta_B+\theta_A)}. \tag{7·18}$$

On evaluating the integral and reducing to the original variables, we find that

$$\frac{1}{NkT}\frac{\partial F(s)}{\partial s} = \theta_A \log\frac{(1+s)(\theta_B+\theta_A s)}{(1-s)(\theta_B-\theta_A s)} - $$
$$-\tfrac{1}{2}z(2\theta_A)\log\frac{\theta_B+\theta_A s^2+(\theta_B-\theta_A s^2)\,y-s\{\ldots\}^{\frac{1}{2}}}{(1+y)(1-s)(\theta_B-\theta_A s)}. \tag{7·19}$$

Alternative forms of the second logarithm are

$$-\tfrac{1}{2}z(2\theta_A)\log\frac{(1+y)(1+s)(\theta_B+\theta_A s)}{\theta_B+\theta_A s^2+(\theta_B-\theta_A s^2)\,y+s\{\ldots\}^{\frac{1}{2}}}, \tag{7·20}$$

$$-\tfrac{1}{2}z\theta_A\log\frac{(1+s)(\theta_B+\theta_A s)}{(1-s)(\theta_B-\theta_A s)}\left[\frac{\theta_B+\theta_A s^2+(\theta_B-\theta_A s^2)\,y-s\{\ldots\}^{\frac{1}{2}}}{\theta_B+\theta_A s^2+(\theta_B-\theta_A s^2)\,y+s\{\ldots\}^{\frac{1}{2}}}\right]. \tag{7·21}$$

By using the form (7·21) it may be readily verified that this $\partial F(s)/\partial s$ reduces to the form (4·1) when $\theta_B = \theta_A = \frac{1}{2}$.

The evaluation of $\partial^2 F(s)/\partial s^2$, and its use to determine the Curie temperature as a function of concentration, is also a simple matter, using any one of the forms for $\partial F(s)/\partial s$. It is hardly worth while writing down the complete expression. It is found that $\partial^2 F(s)/\partial s^2 = 0$ for $s = 0$ when

$$\frac{z-2}{z} = \frac{\{[1+(\theta_B-\theta_A)\,y]^2+4\theta_A^2 y\}^{\frac{1}{2}}}{1+y}, \tag{7·22}$$

while $\partial F(s)/\partial s$ always vanishes for $s = 0$. It may be shown further that a non-zero root of $\partial F(s)/\partial s = 0$ always enters at $s = 0$, so that equation (7·22) determines a Curie temperature, as in the simple case $\theta_B = \theta_A = \frac{1}{2}$. Solving (7·22) for y, we find

$$y_c+1 = e^{2\chi/kT_c} = 4\left(\frac{z}{z-2}\right)^2\theta_A\theta_B\bigg/\left\{1-\left(\frac{z}{z-2}\right)^2(\theta_B-\theta_A)^2\right\}. \tag{7·23}$$

This equation, previously obtained by Easthope (1937) using Bethe's method, gives the complete variation of T_c as a function of concentration to this approximation for the simple *ab* lattice. The maximum value of T_c occurs for $\theta_A = \theta_B = \frac{1}{2}$.

We shall not pursue the analysis further, since we already know that the results we shall obtain are equivalent to those of Bethe's method in a form which has already been given by Chang (1938, 1939*a*).

8. AN APPROXIMATE COMBINATORY FORMULA AS A BASIS FOR THE QUASI-CHEMICAL METHOD

We have so far treated formulae (2·4) or (7·2) as fundamental hypotheses of the quasi-chemical method, which we have introduced without further support than their own inherent reasonableness, by analogy with the law of mass action in gaseous chemical equilibria. We shall now show that these formulae, more particularly (7·2) which included (2·6) as a special case, are equivalent to an approximate combinatory formula for the number of configurations of the assembly with given values of r and q and a given value zNx, of the number of pairs, $[A/a, A/b]$. If we could assume that the number of such configurations may be calculated as if the various types of pairs do not interfere with one another, then, since there are zN pairs grouped as in table 2, the number of configurations would be

$$\frac{(zN)!}{\{zN(r-x)\}!\,\{zNx\}!\,\{zN(1-r-q+x)\}!\,\{zN(q-x)\}!}. \tag{8·1}$$

This is of course incorrect, firstly because the different pairs do in fact necessarily interfere with one another at least to some extent, and secondly because (8·1) would not give, when summed over all values of x, the correct total number of configurations. We can remove the second defect by inserting a normalizing factor independent of x, and writing for the number of configurations $g(N,r,q,x)$

$$g(N,r,q,x) = h(N,r,q)\frac{(zN)!}{\{zN(r-x)\}!\,\{zNx\}!\,\{zN(1-r-q+x)\}!\,\{zN(q-x)\}!}. \tag{8·2}$$

We can moreover evaluate $h(N,r,q)$ in (8·2), at least approximately, without much trouble. For

$$\Sigma_x g(N,r,q,x) = g(N,r,q),$$

and on using (7·9) we find

$$h(N,r,q)\,\Sigma_x \frac{(zN)!}{\{zN(r-x)\}!\,\{zNx\}!\,\{zN(1-r-q+x)\}!\,\{zN(q-x)\}!} =$$

$$= \frac{N!}{(Nr)!\,(N-Nr)!}\,\frac{N!}{(Nq)!\,(N-Nq)!}. \tag{8·3}$$

Now we can sum the Σ_x in (8·3) with sufficient accuracy by identifying Σ_x with its maximum term. The maximum term is determined by the condition

$$(r-x)(q-x) = x(1-r-q+x), \tag{8·4}$$

which gives

$$x = rq, \tag{8·5}$$

the value of x which corresponds to purely random arrangements of pairs of neighbours. It follows that, with sufficient accuracy,

$$h(N,r,q) = \frac{(N!)^2}{(Nr)!\,(N-Nr)!\,(Nq)!\,(N-Nq)!} \times \frac{\{zN(r-rq)\}!\,\{zNrq\}!\,\{zN(1-r-q+rq)\}!\,\{zN(q-rq)\}!}{(zN)!}. \tag{8·6}$$

The corresponding explicit expression for $g(N,r,q,x)$ is

$$g(N,r,q,x) = \frac{(N!)^2}{(Nr)!\,(N-Nr)!\,(Nq)!\,(N-Nq)!} \times \frac{\{zN(r-rq)\}!\,\{zNrq\}!\,\{zN(1-r-q+rq)\}!\,\{zN(q-rq)\}!}{\{zN(r-x)\}!\,\{zNx\}!\,\{zN(1-r-q+x)\}!\,\{zN(q-x)\}!}. \tag{8·7}$$

So far we have merely been investigating the form of $g(N,r,q,x)$ to which our suggested approximation for the number of configurations of given x leads us. We have now to apply the result to the thermodynamic problem. Since by (7·1) the configurational energy for given x is $E^0+zNx2\chi$, the configurational partition function for given r, q, in this approximation, is

$$\Sigma_x\, g(N,r,q,x)\, e^{-(E^0+zNx2\chi)/kT}. \tag{8·8}$$

It follows that $F(r,q)$ and $E(r,q)$ may be derived at once from (8·8) by searching for the maximum term in (8·8) and so evaluating this part of the partition function. The condition for the maximum term, $x=\bar{x}$, gives

$$(r-\bar{x})(q-\bar{x}) = \bar{x}(1-r-q+\bar{x})\,e^{2\chi/kT}, \tag{8·9}$$

which is precisely the condition (7·2) for quasi-chemical equilibrium. It follows at once that the hypothesis of the non-interference of pairs, and the approximate combinatory formula for numbers of configurations to which it leads, also lead to all the equilibrium results which we have deduced by the quasi-chemical method. The two assumptions are in fact exactly equivalent to each other; what we have just proved may be described by saying that the hypothesis of the non-interference of pairs, (8·7), implies all the results of the quasi-chemical method. The converse implication, which completes the proof of equivalence, has been proved recently in a paper by Chang (1939*b*). He has shown that the equations of Bethe's method for this case, which we have seen in § 5 to be equivalent to a quasi-chemical equilibrium, imply a combinatory formula which is equivalent to (8·7). We refer the reader for a proof to Chang's paper.

It will be observed that, if we evaluate the logarithm of the partition function (8·8), we evaluate $F(r,q)$ or $F(\theta_A, s)$. This is much the most direct and simple method of writing down $F(r,q)$ or $F(\theta_A, s)$ explicitly, and we give the result, since it is not unlikely to prove of general utility in the future. By the general formula relating free energies and partition functions, using (8·8),

$$F(r,q) = -kT\log g(N,r,\bar{x}) + E^0 + zN\bar{x}2\chi, \tag{8·10}$$

where $\bar{x}$ is the relevant root of (8·9), that is, by (7·3),

$$\bar{x} = \frac{\{1+[2(1-r-q)+4rq]\,y+(1-r-q)^2y^2\}^{\frac{1}{2}}-1-(1-r-q)\,y}{2y}, \tag{8·11}$$

y being short for $e^{2\chi/kT}-1$. The values of θ_A, and s in terms of r and q, according to (7·5) are given by

$$s = \frac{r-q}{r+q}, \quad \theta_A = \tfrac{1}{2}(r+q). \tag{8·12}$$

Then

$$\begin{aligned}\frac{F(r,q)-E^0}{NkT} = {} & [r\log r+(1-r)\log(1-r)+q\log q+(1-q)\log(1-q)]+ \\ & +z[(r-\bar{x})\log(r-\bar{x})+\bar{x}\log\bar{x}+(1-r-q+\bar{x})\log(1-r-q+\bar{x})+(q-\bar{x})\log(q-\bar{x})]- \\ & -z[(r-rq)\log(r-rq)+rq\log rq+(1-r-q+rq)\log(1-r-q+rq)+(q-rq)\log(q-rq)]+ \\ & +z\frac{2\chi}{kT}\bar{x},\end{aligned} \tag{8·13}$$

where $\bar{x}$ maximizes $F(r,q)$ as a function of $\bar{x}$, and is given by (8·11). It may be shown that in the simple case when $\theta_A = \theta_B = \frac{1}{2}$ or $r+q=1$, $F(r,q)$ given by (8·13) reduces to $F(s)$ given by (3·6), and further that $\partial F(s)/\partial s$ calculated from (8·13) agrees with (7·21). In computing $\partial F(s)/\partial s$ we need not vary $\bar{x}$.

Equation (8·13) contains the whole of Bethe's first approximation, or the quasi-chemical method in its simplest and at the same time its most powerful and complete form.

9. FURTHER APPLICATIONS OF THE QUASI-CHEMICAL METHOD

In this paper we have merely examined by the proposed new method the details of the formation of a super-lattice in a lattice of the simplest *ab* type. The new method, however, is so much more direct than Bethe's method as usually applied, that one is encouraged to formulate its application to more complicated types of lattice, in which super-lattice formation can be treated by Bethe's technique only with considerable difficulty.

Peierls (1936) has already discussed an ab_3 lattice of the type found in Cu_3Au by an extension of Bethe's method. He uses an approximation in which all the interactions between nearest neighbours in a group consisting of a central atom and its twelve neighbours are included explicitly, and other interactions taken into account by means of the ϵ factors. This is an approximation in which the group contains rings of three nearest neighbours, and is more elaborate than any case which can be treated directly by the quasi-chemical method. Peierls dismisses as insufficiently accurate in this case an approximation which could be treated quasi-chemically, and no results have been given for such an approximation, in which one proceeds on the basis of the effective non-interference of pairs. In view, however, of (1) the intractable nature of the equations resulting from Peierls' approximation, (2) the certainty that the results of the quasi-chemical method will be at any rate more accurate than those of Bragg and Williams, and (3) the comparative simplicity of the equations, it seems well worth while to derive the results of the quasi-chemical method for ab_3 lattices (Cu_3Au type) and for other simple close-packed lattices. Their study seems likely to prove extremely helpful to a better understanding of the process of ordering in such lattices. Beside the ab_3 type one can study in a similar way an ab close-packed lattice of CuAu type in which order means alternate planes of unlike atoms (Wilson 1938). It is more than likely that the method is of still wider application, since it provides in all cases an approximation at least one stage better than that provided by the approximation of Bragg and Williams. The results of course are no longer identical with those of an approximation as elaborate as that used by Peierls. Results, however, obtained by the systematic exploration of the hypothesis of the non-interference of pairs (the quasi-chemical method) may nevertheless prove of considerable value.

SUMMARY

This paper establishes the precise statistical basis of Bethe's method of discussing order-disorder phenomena in super-lattices in Bethe's first approximation. It shows that for cubic lattices of the type here considered, in which all points of one super-lattice have as nearest neighbours points of the other super-lattice only, Bethe's first approximation is equivalent to the use of a method which we call the quasi-chemical method. The quasi-chemical method is an approximation which proceeds by assuming that

the bond between any pair of nearest neighbours may be treated as if it were a chemical molecule, and the number of arrangements with given numbers of bonds as if the bonds did not interfere with each other. This method had previously been devised by one of us for the class of assemblies called *regular*, but it has not previously been applied to assemblies with long range order.

In the simple case considered, all the details of Bethe's method and the quasi-chemical method and the approximation on which they are based, and the relationship between them, can be made perfectly explicit. There seems reason to hope that the greater power of these explicit methods may enable them to be applied successfully for more complicated lattices, for which at present only the much rougher approximation of Bragg and Williams can be carried through.

REFERENCES

Bethe, H. A. 1935 *Proc. Roy. Soc.* A, **150**, 552.
Bethe, H. A. and Kirkwood, J. G. 1939 *J. Chem. Physics*, **7**, 578.
Bragg, W. L. and Williams, E. J. 1934 *Proc. Roy. Soc.* A, **145**, 699.
Chang, T. S. 1938 *Proc. Camb. Phil. Soc.* **34**, 224.
— 1939*a* *Proc. Camb. Phil. Soc.* **35**, 265.
— 1939*b* *Proc. Roy. Soc.* A, **173**, 48.
Easthope, C. E. 1937 *Proc. Camb. Phil. Soc.* **33**, 502.
Gorsky, W. 1928 *Z. Phys.* **50**, 64.
Guggenheim, E. A. 1935 *Proc. Roy. Soc.* A, **148**, 304.
— 1938 *Proc. Roy. Soc.* A, **169**, 134.
Kirkwood, J. G. 1938 *J. Chem. Physics*, **6**, 70.
Nix, F. C. and Shockley, W. 1938 *Rev. Mod. Phys.* **10**, 1.
Peierls, R. 1936 *Proc. Roy. Soc.* A, **154**, 207.
Rushbrooke, G. S. 1938 *Proc. Roy. Soc.* A, **166**, 296.
Wilson, A. H. 1938 *Proc. Camb. Phil. Soc.* **34**, 81.

The absorption spectra of ethylene, deutero-ethylene and some alkyl-substituted ethylenes in the vacuum ultra-violet

By W. C. Price and W. T. Tutte
Physical Chemistry Laboratory, Cambridge

[Plates 8, 9]

(*Communicated by R. G. W. Norrish, F.R.S.—Received* 14 *August* 1939)

Because of the great importance to organic chemistry of the double C=C bond and the resonance effects which arise from the conjugation of double bonds, the electronic spectra of the molecules ethylene and butadiene (see following paper) are of very considerable interest. Unfortunately it is not possible to obtain these spectra in emission since an electrical discharge tends to disrupt polyatomic molecules into diatomic fragments. However, the spectra can be obtained in absorption. It is found that the first strong bands appear in the neighbourhood of 2000 A and that they extend towards shorter wave-lengths far into the vacuum ultra-violet. The instruments which have been employed in this present investigation are two vacuum grating spectrographs. These were used in conjunction with a source of the Lyman continuum which enabled the absorption to be followed down to about 1000 A (Rathenau 1933; Collins and Price 1934: details of the experimental technique are given in these articles). A certain amount of earlier work has been done on ethylene and butadiene by Scheibe and Grieneisen (1934). As these authors employed the molecular hydrogen continuum in conjunction with fluorite spectrographs in their investigations, their measurements were limited to the region above 1650 A and under the circumstances no attempts at analysis were made. The extension of the investigations to shorter wave-lengths by the present methods has given a more complete picture of the absorption. From this and with the help of more recent ideas on the structure of these molecules it has been possible to arrive at a satisfactory analysis of the bands. A preliminary account of the spectrum of ethylene together with a tentative analysis has been given by Price (1935). By obtaining the spectrum of tetra-deutero-ethylene (and also C_2H_3D) to compare with that of C_2H_4 we have been able to put this analysis on a firm basis, to correct minor defects and also to correlate a great deal of additional data.

The spectrum of ethylene is shown in figure 1, plate 8; the upper picture is of heavy ethylene (C_2D_4), the lower one of light ethylene. At pressures of about 0·01 mm. in a path length of 2 m., the absorption starts abruptly around 1745 A. It appears as a well-defined pattern of bands which extend down to about 1600 A. Below this wave-length there is a region of relative transparency, the next strong set of bands starting around 1390 A. It is clear that the pattern which appears in the neighbourhood of 1700 A is repeating itself here with some modifications and with smaller intensities. At shorter wave-lengths there is another region of transparency followed at about 1290 A by another set of absorption bands weaker than the previous ones. Comparison with the analogous systems in C_2D_4 and C_2H_3D and many other reasons indicate that the sets correspond to separate electronic transitions. In fact the spectrum is typical of a system of electronic bands converging to an ionization potential similar for example to that observed for acetylene (Price 1935). If the ν_0's of such a system are taken, then it is to be expected that they will fit approximately into a Rydberg formula, the limit of which will correspond to the ionization potential of the molecule. The lower members of such a series might be expected to deviate appreciably from the formula, though when the excited orbits are very large in comparison with the dimensions of the molecule the agreement should be better. The following Rydberg series were thus constructed for (*a*) C_2H_4 and (*b*) C_2D_4.

$$\nu_0^n = 84{,}750 - R/(n+0{\cdot}91)^2 \quad n=2,3,4, \text{etc.} \tag{1a}$$

$$\nu_0^n = 84{,}850 - R/(n+0{\cdot}92)^2 \quad n=2,3,4, \text{etc.} \tag{1b}$$

TABLE 1. OBSERVED AND CALCULATED FREQUENCIES OF C_2H_4 IN SERIES (1*a*) and C_2D_4 IN SERIES (1*b*)

C_2H_4 series (1*a*)		C_2D_4 series (1*b*)	
Obs.	Calc.	Obs.	Calc.
57,340	54,660	57,620	55,068
71,790	71,790	72,020	71,978
77,600	77,572	77,710	77,708
80,215	80,198	80,360	80,316
81,625	81,608	—	—

The bands used to form the series were of course those which were indicated as being ν_0 in type from the fact that they suffered a small shift to short wave-lengths in going from C_2H_4 to C_2D_4. It was found most desirable to choose the constants in the formula so that the third, fourth and fifth members fitted well. This is done because there are many good reasons for expecting the first member to deviate somewhat from such a series while

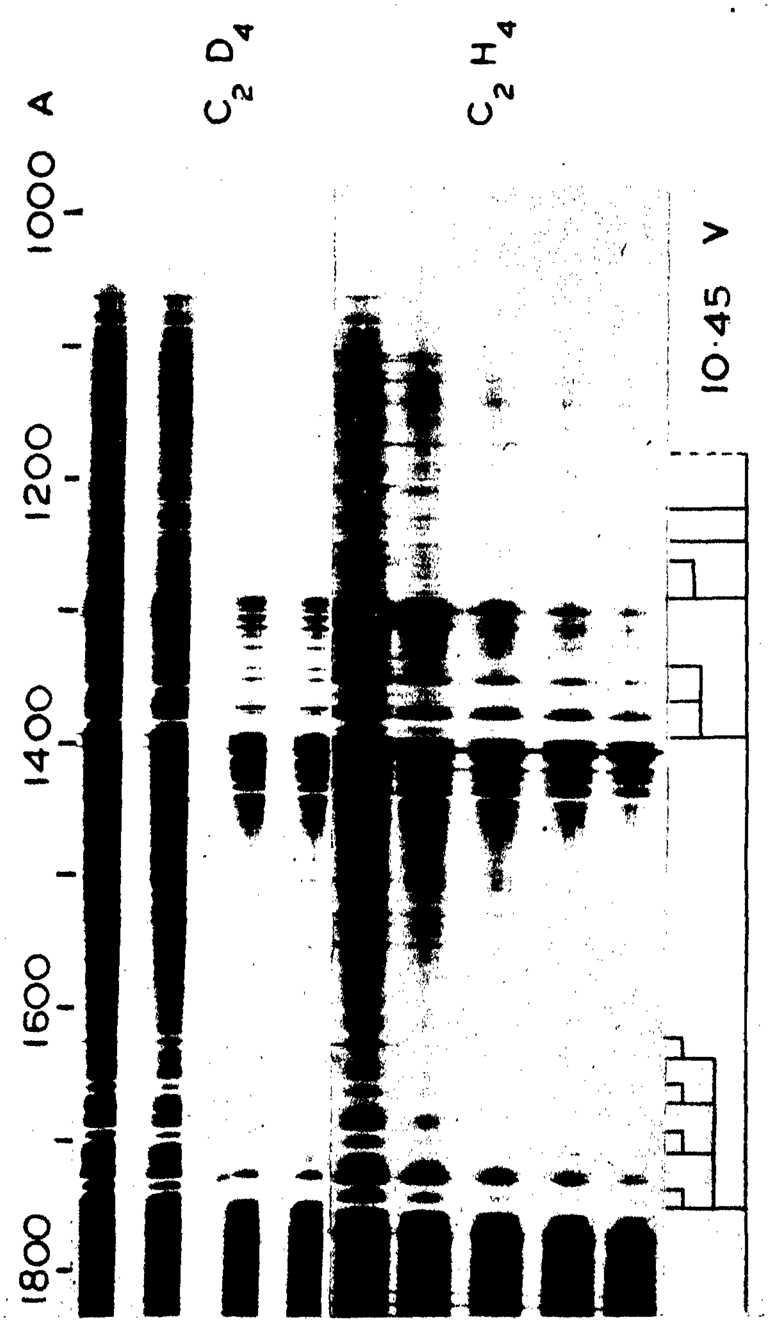

FIGURE 1. The absorption spectra of tetra-deutero-ethylene and light ethylene.

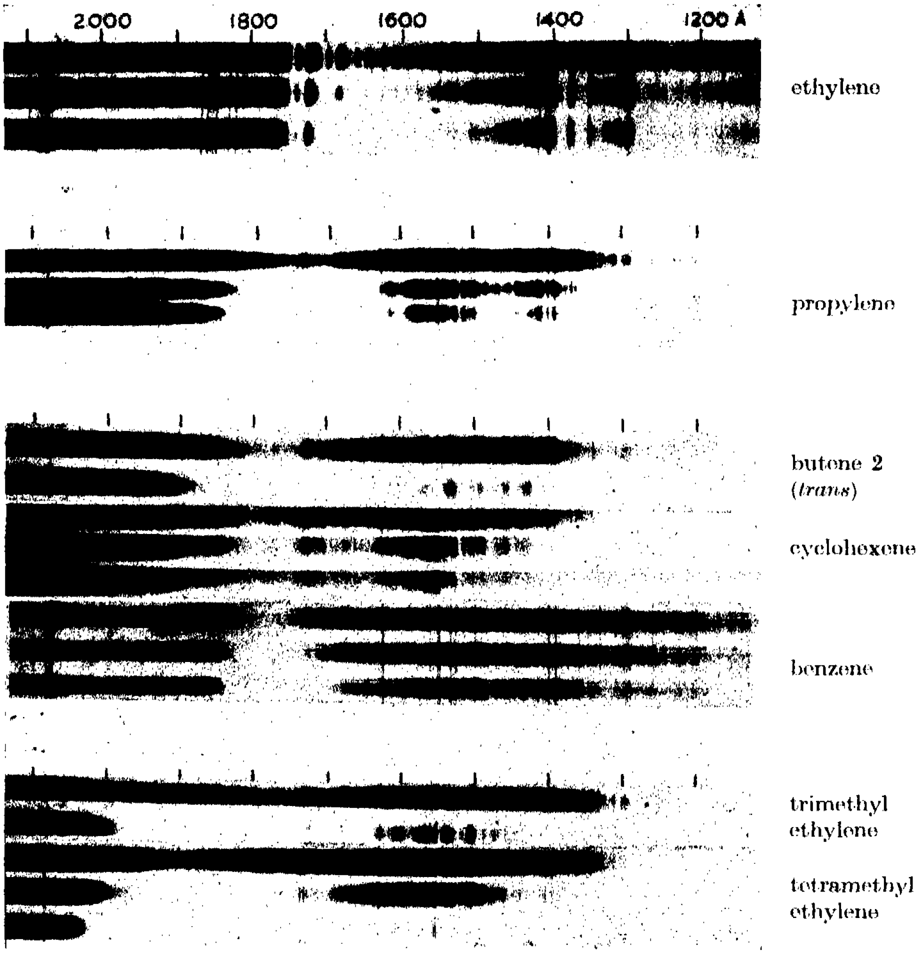

FIGURE 2. The absorption spectra of ethylene, propylene, butene 2 (*trans*), cyclohexene, benzene, trimethyl ethylene and tetramethyl ethylene.

the diffuseness and weakness of some of the higher members make their identification a little uncertain. Table 1 shows the agreement of the calculated with the observed values. The values given are considered accurate within 10–15 cm.$^{-1}$.

The ionization potential of ethylene deduced from the limit is 10·45 V, that of heavy ethylene being only about 0·01 V higher. This difference is of the same order as the difference between corresponding ionization potentials of C_6H_6 and C_6D_6. The possible error in the ionization potential introduced by the extrapolation involved in the formula is considered to be less than three or four hundredths of an electron volt. The electron impact value given by Kusch, Hustrulid and Tate (1937) is $10·80 \pm 0·05$ V The order of the agreement is that usually obtained between the electron impact and spectroscopic values. It is clear that the absorption bands and the ionization potential associated with them refer respectively to the excitation and removal of a "π" electron from the double bond The electrons in the basic $[\sigma]^2$ single C—C and C—H bonds do not give rise to strong absorption until shorter wave-lengths (cf. ethane and methane starting around 1350 and 1250 A respectively) and moreover they are expected to have considerably higher ionization potentials, about 12–13 V for C—C and ~14·5 V for C—H (Mulliken 1935).

Evidence of two other much weaker Rydberg series going to the same ionization potential was found in ethylene. They were established definitely as different electronic systems by the fact that their ν_0 bands were shifted to short wave-lengths by the isotope substitution. The first members of these two series start around 1518 and 1436 A respectively and subsequent members are given approximately by changing the denominators in (1a) to $(n+0·4)^2$ and $(n+0·7)^2$.

It is significant that the term values of the series (1a) in ethylene are very close to those of series II in acetylene where a π electron is also being removed. Moreover, there is some indication that the ethylene bands are double headed and they are certainly shaded towards the red like these particular acetylene bands. (Also, as will be shown later, the reduction in CC valence frequency is of the same order in both cases ($1974 \rightarrow 1785$ in C_2H_2, $1623 \rightarrow 1370$ in C_2H_4).) Since the acetylene series has been interpreted as ${}^1\Sigma_g \rightarrow (\pi_u)^{-1} nx\sigma_g, {}^1\Pi_u$, the ethylene series probably has the analogous interpretation ${}^1A_{1g} \rightarrow [x+x]^{-1} nsa_{1g}, {}^1B_{3u}$ (for the explanation of the group theory notation see Mulliken 1935, 1937).

VIBRATIONAL STRUCTURE

It is clear that in ethylene, as also in acetylene, the main spacing of the vibrational pattern is due to a modified CC valence vibration. The separation between consecutive pairs of the 1700 A pattern is about 1370 cm.$^{-1}$ in C_2H_4 and 1290 cm.$^{-1}$ C_2D_4. This is undoubtedly the totally symmetrical valence frequency of the double bond, i.e. $\nu_t^{(1)}\|$, which has a value of 1623 cm.$^{-1}$ in the ground state (1515 cm.$^{-1}$ in C_2D_4). Although there are fifteen different vibration frequencies in ethylene, this frequency separation may be assigned to $\nu_t^{(1)}\|$ with considerable certainty for the following reasons: (*a*) the change in the frequency resulting from the isotopic substitution is about what would be expected from the mass factors, i.e. $\frac{1370}{1290} = 1{\cdot}062$, $\sqrt{\frac{16(CD_2)}{14(CH_2)}} = 1{\cdot}069$; (*b*) the relatively small number of bands that appear, the intensity distribution in the progression and the fact that the bands are shaded towards the red, all indicate that there has been a small diminution in the frequency as a result of the excitation, thus agreeing with the change in frequency 1623 → 1350 cm.$^{-1}$; (*c*) the assignment is in agreement with the selection rules of Herzberg and Teller (1933) which state that in absorption from a non-vibrating ground state only totally symmetrical vibrations can appear strongly if the electronic transition is an allowed one; (*d*) as the electron being excited is one of the "π" valence electrons of the double bond, it is clear that its excitation will set up vibration in this bond. If the excitation were of an electron from a CH bond, a CH valence vibration would be expected to appear which would be reduced as a result of the isotopic substitution by the rather large mass factor $\approx 1/\sqrt{2}$ and further the large diminution in vibration frequency from ~ 3000 to 1370 cm.$^{-1}$ would give rise to much larger zero point energy changes than those actually observed. Some difficulty is encountered in getting a good value of this $\nu_t^{(1)}\|$ frequency for the second Rydberg system of C_2H_4 at 1390 A because the second members of the pattern seem to suffer an abnormal splitting. The mean value found was 1450 cm.$^{-1}$. This is somewhat higher than the value 1370 cm.$^{-1}$ obtained for the first (1740 A) system. This increase in $\nu_t^{(1)}\|$ might have been regarded as spurious if it were not for the fact that the 1390 A pattern is much clearer in the heavy ethylene and the $\nu_t^{(1)}\|$ separation there could be definitely established as 1360 cm.$^{-1}$ compared with 1290 cm.$^{-1}$ in the first Rydberg pattern. The value in the third Rydberg pattern of C_2D_4 which also appeared more clearly than in C_2H_4 was 1330 cm.$^{-1}$. Thus it seems that the first Rydberg orbital is a little antibonding compared with the subsequent ones. This is in agreement with its being found at slightly shorter wave-lengths than is predicted from the Rydberg formulae (1) (see table 1), and also with the greater zero point energy shifts found for this transition as compared with the higher Rydberg bands. Although for various reasons, no vibration frequencies could be established for Rydberg states higher than the third, there can be little doubt that the values of $\nu_f^{(1)}\|$ in these states and also in the ion is not far from 1450 cm.$^{-1}$ for C_2H_4 and 1350 for C_2D_4. The earlier tentative conclusion that it diminished to a low value is no longer tenable. Other good reasons for abandoning it are that as a single π electron only contributes less than one-quarter of the bond strength of the double bond its complete removal would not be expected to have a very large effect on the bond and secondly, if the frequency were actually reduced to a small value it would be almost certain that a great increase in the internuclear distance would accompany the change. Thus on the Franck-Condon principle, long vibrational progressions would be expected to take the place of the short ones observed. This is not the case and in fact the shorter wave-length patterns contain fewer, not more, bands than the longer wave-length ones.

The bands in the region around 1700 A appear in pairs. In the case of C_2H_4 their separation is 470 cm.$^{-1}$; for C_2D_4 it is 300 cm.$^{-1}$. The first band of the C_2D_4 system is shifted to shorter wave-lengths by 280 cm.$^{-1}$ relative to that of C_2H_4, in accordance with its ν_0 character. The second is also shifted to shorter λ but only by 95 cm.$^{-1}$ and it must clearly be regarded as a vibrational transition accompanying the main electronic transition. Some indication of the nature of this vibration is obtained from the ratio of its magnitudes in the light and heavy molecules, i.e. $470/300 = 1{\cdot}57$. This mass factor is closer to $\sqrt{D/H} = 1{\cdot}41$ than $\sqrt{CD_2/CH_2} = 1{\cdot}069$. The most likely vibration having this mass factor which can be assigned to such a frequency difference is that involving the twisting of the two CH_2 groups about the $C{=}C$ bond. Its value in the ground state is not known exactly but is generally assumed to be 750–800 cm.$^{-1}$. The separation in the excited states appears to have a constant value of 470 cm.$^{-1}$ for C_2H_4 and 300 cm.$^{-1}$ for C_2D_4 in the first, second and third members of the Rydberg series (1). An important intensity change occurs in the bands of this small "doublet" separation in going to the second, third, etc. Rydberg systems. While in the 1740 A system both components of the doublet are equally strong, in the 1390 A and subsequent systems the long wave-length component is very much weaker than the short wave-length one. There seems to be no obvious explanation of this peculiarity. The weakening of the ν_0 bands increases the difficulty of getting high members of the Rydberg series and also of following the δ vibration to higher electronic states. It is also rather strange that only one quantum of this vibration is allowed to appear at a time. This is perhaps not so very unusual as a similar instance occurs in the B and C systems of CH_3I (Price 1936). It does appear, however, that C_2H_4 which is plane in the ground state remains so in the excited and ionic states considered here, since any appreciable departure from the plane ought to cause the appearance of many quanta of the twisting vibration. In contrast to these states is the somewhat weaker system appearing at longer wave-lengths (Snow and Allsopp 1934; Scheibe and Grieneisen 1934). This consists of a long diffuse progression with a frequency separation which has a mean value of about 750 cm.$^{-1}$ though it varies over a range of 100 cm.$^{-1}$ (possibly as a result of the difficulty in measuring these diffuse bands or because of the superposition of other frequency separations on the main pattern). This progression increases regularly in intensity from about 2000 A up to 1750 A after which there is difficulty in following it because of the predominating intensity of the Rydberg bands. There is no doubt, however, that it has its maximum at still shorter wave-lengths, and it seems in fact that it might identify itself with the continuous absorption having a maximum at 1630 A which appears as a background to the discrete Rydberg absorption in this region. The electronic transition associated with the progression has been interpreted as $(\pi+\pi)\rightarrow(\pi-\pi)$ or in Mulliken's more detailed notation as ${}^1A_{1g}\rightarrow[x+x, b_{3u}]^{-1}[x-x, b_{2g}], {}^1B_{1u}$ or $N\rightarrow V$. Now it can be shown theoretically (Mulliken 1932) that the equilibrium position of this upper state is one in which the two CH_2 planes are mutually perpendicular*, thus a large number of quanta of the twisting vibration must be expected to be present in the transition. It is therefore possible that the 750 cm.$^{-1}$ difference corresponds to the twisting vibrations though it may be a reduced C=C valence vibration.

An interesting feature of the C_2D_4 spectrum around 1700 A is that an additional weak member appears in the pattern. It is situated about 730 cm.$^{-1}$ from the main bands. It combines with the C=C valence vibration but not with the "δ" vibration. It may possibly arise from a small amount of C_2D_3H present as impurity, being most probably some unsymmetrical vibration which becomes permitted because of the lack of symmetry of C_2D_3H. As no C_2D_3H was available at the time, it was not possible to test this hypothesis. However, the spectrum of C_2H_2D was obtained, but was not found to exhibit any similar bands. It was nevertheless interesting in that all its shifts relative to C_2H_4 were found to be about a quarter of those of

---

* Incidentally this is the explanation of *cis-trans* photoisomerism by absorption of light in $N\rightarrow V$ type transitions.

C_2D_4 relative to C_2H_4. Thus the small pattern spacing attributed to C=C twisting was found to be about 415 cm.$^{-1}$ as compared with 470 cm.$^{-1}$ for C_2H_4 and 300 for C_2D_4, and the large pattern spacing (C=C valence) was found to be 1350 compared with 1390 and 1290 respectively. The ionization potential had of course an intermediate value.

Table 2 gives a list of frequencies of bands in the first Rydberg states of the molecules together with the vibration frequencies occurring in the pattern. The values in the $\nu_i^{(1)}\|$ column are obtained by subtracting one frequency from another two places above it; those of δ by subtracting it from the frequency directly above. In addition to the frequencies given in the table for C_2D_4 four others corresponding to a new type of vibration of ~730 cm.$^{-1}$ were observed. They are 58,340, 59,650, 60,930 and 62,195 cm.$^{-1}$. Their differences which are 1310, 1280 and 1265 respectively show the main C=C valence vibration while the separations from the main bands are 720, 740, 740 and 735 respectively.

TABLE 2. FREQUENCIES OF BANDS IN 1700 A PATTERN OF C_2H_4, C_2D_4 AND C_2H_3D TOGETHER WITH THE VIBRATION FREQUENCIES CHARACTERISTIC OF THE PATTERN

$\nu\,(C_2H_4)$	$\nu_i^{(1)}\|$	δ	$\nu\,(C_2D_4)$	$\nu_i^{(1)}\|$	δ	$\nu\,(C_2H_3D)$	$\nu_i^{(1)}\|$	δ
57,340			57,620			57,415		
57,815		475	57,910		290	57,825		410
58,715	1375		58,910	1290		58,765	1350	
59,185	1370	470	59,200	1290	290	59,180	1355	415
60,070	1355		60,190	1270		60,100	1335	
60,530	1345	460	60,480	1280	290	60,505	1325	405
Very diffuse			61,460	1270		61,400	1300	
,,			61,750	1270	290	61,820	1315	420

The shift to short wave-lengths of the ν_0 band of the 1750 A system[*] arising from the isotope substitution is 280 cm.$^{-1}$. This is quite large compared for example with the shifts of about 40 cm.$^{-1}$ found in $C_2H_2 \rightarrow C_2D_2$ (Price 1935) and of between 30 and 40 cm.$^{-1}$ for $C_6H_6 \rightarrow C_6D_6$ (Price and Wood 1935). It is even larger than the shift of 203 cm.$^{-1}$ found for the 2500 A band of benzene [38,292 (C_6D_6)–38,089 (C_6H_6)], the excited orbital of which is known to be strongly antibonding[†] (Sponer, Nordheim, Sklar and Teller

[*] $$\delta\nu_0 = \tfrac{1}{2}[\Sigma(\omega'' - \omega^{*''}) - \Sigma(\omega' - \omega^{*'})].$$

ω and ω^* refer to the light and heavy molecules respectively, $''$ refers to the ground and $'$ to the excited state. If the vibration frequencies are diminished by the excitation, then this shift is positive.

[†] It is worth noting that this fairly low value of 203 cm.$^{-1}$ makes it highly improbable that the CH valence frequencies and most of the CH distortion frequencies are much affected by the excitation.

1939). There are two main factors which can account for such a large zero point energy shift and possibly both of them are contributing in this case. First, the upper state may be so strongly antibonding that even those vibrations which depend mainly on a mass factor of $\surd CH/CD$ are reduced to such an extent by the vibration that the zero point energy difference between the upper and lower states is changed considerably. Secondly, it is possible that those vibrations which are hydrogen-dependent are being considerably reduced by the excitation. It is clear from the spectrum that neither the hydrogen valence nor the "in plane" distortion frequencies are much affected by the excitation since neither of the modes $\nu_l^{(2)}\|$ or $\delta_l\|$ can reasonably be interpreted as being present in the accompanying vibrational pattern. Further, the reduction in the C=C valence frequency is too small to account on its own for the shift. There remains the $\delta_\perp$ and the δ (twisting) vibrations both of which are hydrogen dependent. It appears from theoretical considerations that changes in the frequency of the latter probably make the greatest contribution to the zero point energy shift. This can be supported by the fact that such a vibration seems to be present in the vibrational pattern where it is considerably reduced (by about 40 %) from its value in the ground state. According to the analysis given by Sponer *et al.* (1939) for the 2500 A system of benzene, there appears one vibration, the so-called E_u^+ vibration or the ν_{16} of Wilson (1934), which is reduced by about this amount (400 → 240 cm.$^{-1}$) as a result of the excitation of the π electron. This vibration is of a somewhat similar type to the twisting vibration in ethylene being actually a twisting of the benzene hexagon. It differs from the ethylene vibration in not being hydrogen-dependent. Thus it appears that the large zero point energy shift of benzene is probably due to the great antibonding and to the great number of vibrations affected, while that in ethylene is principally due to the fact that a vibration which is hydrogen dependent is strongly affected.

SPECTRA OF THE ALKYL-SUBSTITUTED ETHYLENES

The spectra of the various alkyl-substituted ethylenes are of interest because it is known from the work of Kistiakowsky and his collaborators (1936) that the heats of hydrogenation of double bonds are considerably affected by the nature of the groups attached to them. As the π electrons are the ones which are involved in the hydrogenation process, it follows that their energy states are changed by such substitutions. These changes will reflect themselves in the spectra of these electrons. In fact the work of Carr and Stücklen (1936, 1938) shows that the bands in the Schumann region are shifted progressively to longer wave-lengths for each hydrogen which is substituted. The long wave-length shift of the spectra and the diminution in the heat of hydrogenation show parallel effects with alkyl substitution as indicated in figure 3. We have used in this graph the shifts indicated in figure 3 of Carr and Stücklen (1936). It will be noticed that the greatest shift for a single hydrogen substitution occurs in going from ethylene to propylene (~ 3500 cm.$^{-1}$), a change which also corresponds to the largest diminution in heat of hydrogenation (2·7 kcal.). The smallest is in going from trimethyl ethylene to tetramethyl ethylene (2000 cm.$^{-1}$) and it corresponds to the smallest diminution (0·3 kcal.) in the heat of hydrogenation.

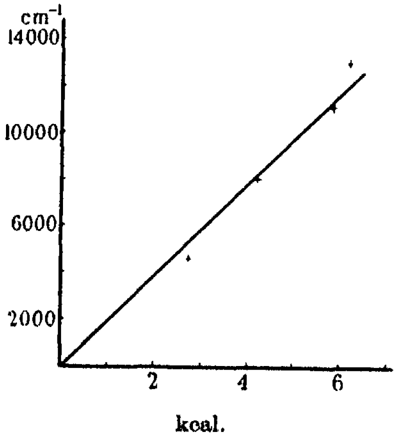

FIGURE 3. Long wave-length shifts plotted against diminution in heat of hydrogenation with increasing alkyl substitution.

The spectrum of propylene is shown in figure 2. It is clear that the first strong absorption is shifted to long wave-lengths relative to that of ethylene. Most of the discrete structure which forms such a striking part of the absorption pattern of ethylene has been obliterated and the whole system has been fused into a region of diffuse absorption with a maximum around 1730 A. After this there is a short region of transparency followed by another set of fairly diffuse bands occurring just below 1500 A and then another still weaker set just below 1400 A. If these last two sets are consecutive Rydberg series members as seems most probable from their appearance, then extrapolation in a Rydberg formula suggests an ionization potential of about 9·6 V. Support for this value comes from a recent electron impact value of 10·0 V obtained by Delfosse and Bleakney (1939). Although it is 0·4 V higher than the one suggested here, this is in accord with the fact that electron impact ionization potentials are usually a few tenths of a volt higher than minimum ionization potentials because they correspond to vertical ionization processes (cf. the spectroscopic ionization potentials of C_2H_4, C_6H_6 are 10·45 and 9·19 V; the impact values are 10·8 and 9·6 V respectively). Further confirmation is supplied by the fact that the regions of absorption of propylene lie very close to corresponding regions in *cis*-dichloro-ethylene for which Mahncke and Noyes (1935) have found a fairly well-developed Rydberg series of bands converging to an ionization potential of ~ 9·6 V. They also obtain by electron impact methods a value of 9·7 ± 0·3, thus confirming the conclusion based on their spectroscopic interpretation. We consider the rather large drop in the ionization potential of the π electron in going from ethylene to propylene ($10{\cdot}45 - 9{\cdot}6 = 0{\cdot}85$ V) to be due to the transfer of negative charge from the methyl group into the neighbourhood of the double bond. The ionization potential of propylene is of importance for comparison with that of butadiene. The discussion of this will be given in the following paper.

BUTENE AND CYCLOHEXENE

Butene 2 (*trans*) is shifted to long wave-lengths relative to propylene. In fact the spectra of the alkyl substituted ethylenes can be classified into groups according to the number of C—C bonds adjacent to the double bond (Carr and Stücklen 1936). The molecules in each group have their absorption regions at closely the same wave-lengths and as the relative number of adjacent CC bonds is increased the groups are progressively displaced towards the red. Cyclohexene and even benzene fall into the butene group containing two adjacent CH and two adjacent CC bonds. The case of benzene is really a coincidence since its electronic structure is quite different from the other molecules. It just happens that the four mobile electrons in the outer doubly degenerate orbital have binding energy "β" per electron, which is the same as that for electrons in the unconjugated double bond. As these electrons are surrounded by the same relative numbers of C—H and C—C bonds, it is therefore not surprising that the transitions should occur at approximately the same wave-length. This is really very fortunate since, while the more highly excited bands of butene and cyclohexene are too diffuse for them to be extrapolated with accuracy to the photoionization limit, this procedure can be performed for benzene (Price and Wood 1935). Thus the ionization potentials of these molecules may be taken as about the same as that of benzene, i.e. 9·2 V, the estimate being probably correct to within 0·05 V. In the same way it was found that the spectrum of trimethyl ethylene fell very close to that of toluene ionization potentials ~ 8·75 V and that of tetramethyl ethylene close to that of ortho-xylene, the ionization potential of which is not known exactly but is probably ~ 8·3 V.

Some general features of the first strong resonance bands of these substituted ethylenes are worthy of comment. First, it seems that these bands tend to collect more and more of the intensity from the more highly excited bands as more alkyl groups are substituted for hydrogen atoms. This is true in the aromatics as well as in the simple derivatives. In tetramethyl ethylene and xylene almost the whole of the intensity is concentrated in the first band. Secondly, although this band shifts to long wave-lengths with alkyl substitution, the shift is considerably less than the diminution in ionization potential. This indicates that the upper state is becoming increasingly antibonding with the alkyl substitution. Possibly some explanation of this may be forthcoming in terms of Mulliken's ideas on hyperconjugation.

It should also be mentioned that for all these molecules diffuse absorption from C—C and C—H bonds were observed at shorter wave-lengths. This increased in intensity and spread up towards 1450 A with increase in the alkyl part of the molecule.

COMPARISON WITH THE SPECTRA OF THE DICHLORO-ETHYLENES

Some instructive comparisons can be made with the spectra of the dichloro-ethylenes (Mahncke and Noyes 1935) which have already been referred to in connexion with the spectrum of propylene. For *cis*-dichloroethylene it was found that the first strong bands appear around 1850 A. These correspond to the C_2H_4 bands around 1700 A. They are followed to shorter wave-lengths 1570–1350 A by bands which are certainly analogous to the ethylene bands from 1450–1200 A, the bands of the halogen substituted molecule being shifted to long wave-lengths by some 7000 cm.$^{-1}$ (e.g. 72,170–65,164). This shift persists right up to the ionization potentials which are 84,800 cm.$^{-1}$ (10·45 V) and 77,800 cm.$^{-1}$ (9·6 V) for C_2H_4 and $C_2H_2Cl_2$ respectively and it is clear that here also a corresponding C=C electron is being excited and photoionized. The various electronic states appear as vibrational patterns with separations of 1430 cm.$^{-1}$. This separation can be interpreted as the excited C=C valence vibration (1587 cm.$^{-1}$ in the ground state) and its appearance lends some support to the idea that a π electron is being removed from the double bond.

The diminution in the ionization potential seems at first rather strange since on a purely inductive (charge transfer) effect it might be expected that the chlorine atoms which are more electronegative than the carbon atoms would remove negative charge from the double bond and so increase its ionization potential. A similar case occurs in the spectra of the phenyl halides where the ionization potential of the mobile electrons is diminished rather than increased by the halogen substitution and all bands undergo a shift to long instead of to short wave-lengths. It will be seen in a later paper dealing with these molecules that the effect is caused by resonance to those ionic structures which are postulated to explain the ortho-para directing effect of substituents possessing unshared electron pairs. Resonance to similar ionic states

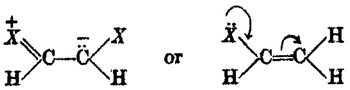

is probably effective in reducing the ionization potentials of the double bond electrons of the halogen substituted ethylenes below the values which might otherwise be expected. The effect is also observed in chloroprene (see following paper) and the evidence indicates that it is accompanied by a corresponding increase in the ionization potential of the non-bonding $p\pi$ electrons of the chlorine atom. This evidence is based on the appearance of the D bands at 1427 A, whereas in ethyl and *n*-propyl chloride they are located at the longer wave-lengths 1465 and 1475 A respectively.

Another interesting point in connexion with these halogen substituted ethylenes which supports the foregoing explanation is the following. Duchesne (1937) and Linnett and Thompson (1937) find that for tetrachloroethylene abnormally low values are obtained for the force constant of the C=C bond when the frequencies are fitted into very plausible potential functions of the valence force field type. This they explain is probably due to resonance to structures similar to those which we suggest are responsible for lowering the ionization potential of the "π" electrons of dichloro-ethylene.

Mahncke and Noyes (1935) find the much higher ionization potential of ~ 11·3 V for *trans*-dichloro-ethylene, although its absorption bands occur at closely the same wave-lengths as those of the *cis*-molecule. Comparison with the spectroscopic ionization potential of ~ 11·2 V for methyl chloride (Price 1936) indicates clearly that this corresponds to the ionization of a "$p\pi$" Cl electron. The fact that Mahncke and Noyes did not find an electron impact value of ~ 9·6 V for *trans*-dichloro-ethylene is probably due to shielding of the electrons in the C=C bond by the Cl atoms in the *trans* position.

In conclusion we should like to thank the Department of Scientific and Industrial Research for a maintenance grant made to one of us; the Imperial Chemical Industries for a grant for apparatus; Dr G. H. Twigg of the Colloid Chemistry Department for making the heavy ethylene available, and Professor E. H. Farmer of Imperial College for supplying us with some of the alkyl substituted ethylenes.

SUMMARY

The absorption spectra of C_2H_4, C_2D_4 and C_2H_3D have been investigated in the region 2000–1000 A. The spectra are interpreted as arising from the excitation and photoionization of the "π" electrons of the double bond. The ionization potential obtained by the extrapolation of successive excited states in Rydberg series is 10·45 V probably accurate to 0·03 V. The spectra of (*a*) propylene, (*b*) butene 2 (*trans*) and cyclohexene, (*c*) trimethyl ethylene, (*d*) tetramethyl ethylene, are shifted progressively to long wave-lengths corresponding to reductions of their ionization potentials to (*a*) 9·6 V, (*b*) 9·2 V, (*c*) 8·75 V and (*d*) 8·3 V. This is probably a charge transfer or inductive effect brought about by the additional alkyl groups.

The spectrum of *cis*-dichloro-ethylene is discussed and its low ionization potential of 9·6 V is attributed to resonance to ionic states similar to those postulated to explain the ortho-para substituting properties in the phenyl halides. The value 11·3 V obtained for *trans*-dichloro-ethylene by Mahncke and Noyes is attributed to a non-bonding "$p\pi$" Cl electron.

REFERENCES

Carr and Stücklen 1936 *J. Chem. Phys.* **4**, 760–768.
— — 1938 *J. Chem. Phys.* **6**, 55–61.
Collins and Price 1934 *Rev. Sci. Instrum.* **5**, 423–425.
Delfosse and Bleakney 1939 *Phys. Rev.* **56**, 208 (A).
Duchesne 1937 *Nature, Lond.*, **139**, 288.
Herzberg and Teller 1933 *Z. Phys. Chem.* **18B**, 88–102.
Kistiakowsky, *et al.* 1936 *J. Amer. Chem. Soc.* **59**, 137–153.
Kusch, Hustrulid and Tate 1937 *Phys. Rev.* **52**, 843–854.
Linnett and Thompson 1937 *J. Chem. Soc.* pp. 1393–1396.
Mahncke and Noyes 1935 *J. Chem. Phys.* **3**, 536–540.
Mulliken 1932 *Phys. Rev.* **41**, 751–758.
— 1935 *J. Chem. Phys.* **4**, 517–528.
— 1937 *J. Chem. Phys.* **5**, 159–173.

Price 1935 *Phys. Rev.* **47**, 444–452.
— 1936 *J. Chem. Phys.* **4**, 539–551.
Price and Wood 1935 *J. Chem. Phys.* **3**, 439–444.
Rathenau 1933 *Z. Phys.* **87**, 32–56.
Scheibe and Grieneisen 1934 *Z. Phys. Chem.* **25B**, 52–56.
Snow and Allsopp 1934 *Trans. Faraday Soc.* **30**, 93–99.
Sponer, Nordheim, Sklar and Teller 1939 *J. Chem. Phys.* **7**, 207–230.
Wilson 1934 *Phys. Rev.* **45**, 706–714.

The absorption spectra of conjugated dienes in the vacuum ultra-violet (1)

BY W. C. PRICE AND A. D. WALSH
Physical Chemistry Laboratory, Cambridge

(*Communicated by R. G. W. Norrish, F.R.S.—Received* 14 *August* 1939)

[Plates 10, 11]

Butadiene is important as the simplest example of resonance between two conjugated double bonds. The comparison of its ultra-violet absorption spectrum with that of ethylene might be expected to give some indication of the way the π electrons of the molecule are affected by the resonance. The electronic structures of a number of molecules for which resonance is important have been worked out theoretically by Hückel (1935), Lennard-Jones (1937), Sklar (1937) and Mulliken (1939*a* and *b*). The purpose of the present work is to obtain spectroscopic data with which the theoretical expectations can be compared. As most of the strong absorption bands of these molecules occur at wave-lengths less than 2000 A, the investigation falls naturally into the region of vacuum spectroscopy.

The first strong absorption of 1, 3 butadiene (presumably *trans*) occurs in the neighbourhood of 2170 A (see figure 1, plate 10) where there begins a well-marked progression of four diffuse bands having an average frequency separation of 1440 cm.$^{-1}$ (table 5). This vibration is doubtless the symmetrical C=C valence vibration somewhat reduced by the excitation from its value of about 1634 cm.$^{-1}$ in the ground state (Dadieu and Kohlrausch 1930). It is to be compared with the analogous separation of 1370 cm.$^{-1}$ appearing in the first Rydberg band in ethylene where the assignment to the C=C valence vibration (1623 cm.$^{-1}$ in the ground state) can be made with certainty. It will be convenient to call the above transition the $N \rightarrow V_1$ transition. The explanation of this notation will be given in the discussion. Towards shorter wave-lengths some fairly strong individual bands appear which because of their isolation must be regarded as different electronic states. There are also a number of pairs of bands with separations of about 350 cm.$^{-1}$ between each component. These, by analogy with the spectrum of ethylene, probably represent a twisting vibration about the C=C bond. At 1760 A a diffuse set of bands appears which spreads at high pressures both to long and to short wave-lengths. A separation of about 1500 cm.$^{-1}$ is evident, but the diffuseness of the bands and a background of continuous absorption prevents any very accurate measurements being obtained. This system is thought by Mulliken (1939*b*) to be $N \rightarrow V_{2,3}$ in type. (In order that the variation in absorption may be more easily observed a line has been drawn along the base of the second exposure. It can be seen that above it an absorption curve is drawn with respect to this base line. The explanation of this effect is that the intensity of the continuum varies across its width, being a maximum at the centre as a result of certain peculiarities of the experimental set-up.)

Below 1520 A the bands are somewhat different in character. Although they are sufficiently close together so that at first glance it might be expected that at least some of them would fit into a vibrational pattern, none were found to do so. Thus they all appear to be different vibrationless electronic transitions. The absence of any pronounced shading either to short or to long wave-lengths supports this to some extent, since it is necessary that changes in the moments of inertia should be small if no vibrations are to appear. An inspection shows that they exhibit the general characteristics of bands approaching an ionization potential, i.e. they get weaker and crowd closer together towards shorter wave-lengths eventually fusing into a photoionization continuum. It was found that most of the strong bands fitted into the following Rydberg series:

$$\nu_0^n = 73{,}115 - R/(n+0{\cdot}90)^2 \quad n = 2, 3, 4 \text{ etc.} \tag{1a}$$

$$\nu_0^n = 73{,}066 - R/(n+0{\cdot}50)^2 \quad n = 3, 4, 5 \text{ etc.} \tag{1b}$$

The series are marked in the photograph. The order of the agreement between the observed and calculated frequencies is shown in table 1. It is very good, especially for the higher members which show up with line-like sharpness on the plate.

The first member of each series appears as a multiplet. The multiplet separations, however, quickly diminish to zero in going to higher members.

This multiplicity is rather similar to that observed in the analogous bands of benzene (Price and Wood 1935), where it was shown to be electronic (not vibrational) in origin. The mean limit of series (1*a*) and (1*b*) corresponds to an ionization potential of 9·022 V, the probable error being about 0·01 V. Though there is no electron impact value for the ionization potential of butadiene at present available with which to compare it, the above value can be accepted with considerable confidence as there are theoretical reasons which will be explained later for expecting the ionization potential of butadiene to be slightly less than that of benzene (9·19 V, Price and Wood 1935). Certain other bands were observed below 1370 A. As this corresponds to an energy greater than the first ionization potential, these bands must be due to the excitation of an electron from a more strongly bound molecular orbital. They are the only bands which can reasonably correspond to Mulliken's $N \rightarrow V_4$ transition and show a maximum about 1280 A. The nature of the electron removed at the first ionization potential of 9·02 V will be discussed in a later paragraph.

TABLE 1. TABLE SHOWING THE OBSERVED AND CALCULATED FREQUENCIES OF THE BUTADIENE BANDS OF SERIES (1*a*) AND (1*b*)

	Series (1*a*)		Series (1*b*)	
n	Obs. cm.$^{-1}$	Calc. cm.$^{-1}$	Obs. cm.$^{-1}$	Calc. cm.$^{-1}$
2	60,112	60,067	—	—
3	65,900	65,900	64,500	64,108
4	68,570	68,545	67,617	67,647
5	69,987	69,963	69,436	69,438
6	70,829	70,810	70,446	70,469
7	71,369	71,357	71,095	71,115

The spectrum of isoprene. The absorption of isoprene (figure 1, plate 10) parallels in almost every feature that of butadiene except that the analogous bands of isoprene are shifted by between 1300 and 1800 cm.$^{-1}$ towards long wave-lengths relative to those of butadiene. Starting at 2210 A a progression of three diffuse bands with a separation of about 1450 cm.$^{-1}$ appear. These bands though somewhat more diffuse are very similar to the first ($N \rightarrow V_1$) set of bands in butadiene and they also appear at very nearly the same pressures. It is probable that as before the valence frequency of the C=C bond is being excited. The next absorption bands following this system are a pair of bands at 1909 and 1892 A which clearly belong to a different electronic transition and as far as can be ascertained are unaccompanied by vibrational structure. In this respect they resemble the band in butadiene at 1863 A. To shorter wave-lengths at 1800 A a second diffuse progression appears. This is somewhat similar to the first (2200 A) progression, only it is considerably weaker. It resembles the second diffuse region occurring around 1750 A in butadiene. The first member of the progression is by far the strongest. The frequency separation between the members is ~ 1640 cm.$^{-1}$. At shorter wave-lengths particularly below 1600 A the bands are weaker and get close together, suggesting that as in butadiene they are approaching the ionization limit. This indeed was found to be the case and several Rydberg series converging to a limit of ~ 71,350 cm.$^{-1}$ or 8·805 V were established among the bands

$$\nu_0^n = 71{,}353 - R/(n+0{\cdot}90)^2 \quad n = 3, 4, 5, \text{ etc.} \qquad (2a)$$

$$\nu_0^n = 71{,}321 - R/(n+0{\cdot}50)^2 \quad n = 2, 3, 4, \text{ etc.} \qquad (2b)$$

As can be seen from table 2 very many members were obtained for the strongest series and the agreement of the higher members with the formula is particularly good. The error in extrapolating to the limit is probably not more than 100 cm.$^{-1}$ or 0·01 V. No vibrational structure was found to accompany the bands which occur below 1600 A and they were clearly of a vibrationless electronic type. Some difficulty was experienced due to diffuse absorption from C—H and C—C bonds which with increase in pressure tended to spread up from below 1400 A to long wave-lengths. However, this did not seriously interfere with the determination of the convergence limit. As in butadiene $N \rightarrow V_4$ transitions were found to occur just below the first photoionization limit.

TABLE 2. TABLE SHOWING THE OBSERVED AND CALCULATED FREQUENCIES OF THE ISOPRENE BANDS OF SERIES (2*a*) AND (2*b*)

	Series (2*a*)		Series (2*b*)	
n	Obs. cm.$^{-1}$	Calc. cm.$^{-1}$	Obs. cm.$^{-1}$	Calc. cm.$^{-1}$
2	—	—	54,419	53,763
3	63,967	64,138	62,475	62,363
4	66,821	66,783	65,841	65,902
5	68,220	68,201	67,661	67,693
6	69,068	69,048	?	—
7	69,580	69,595	?	—
8	69,970	69,968	69,804	69,802
9	70,233	70,233	—	—

The spectrum of βγ dimethyl butadiene. As might be expected the spectrum of this substance (figure 2, plate 11) is very similar to that of butadiene and isoprene except that it is shifted still farther to long wave-lengths on account of its additional methyl groups. Again the spectrum starts with a progression of three strong diffuse bands ($N \rightarrow V_1$) separated by the C=C frequency. Its value seems to be somewhat diminished in $\beta\gamma$ dimethyl butadiene and chloroprene relative to that in butadiene and isoprene (see table 5). At 1920 A these are followed by a pair of bands analogous to those which occur around 1900 A in isoprene and 1880 A in butadiene. Although at first sight there is one continuous progression of bands between 1920 and 1700 A, it is clear by a comparison with the spectra of the other molecules that the $N \rightarrow V_{2,3}$ system starts at 1810 A and is not connected with the bands at 1920 and 1860 A. The separation (C=C vibration) is ~ 1650 cm.$^{-1}$. Below 1600 A it was again possible to establish Rydberg series, the bands showing strong analogies with those of the previous molecules. The main series found are

$$\nu_0^n = 70{,}240 - R/(n+0\cdot 90)^2 \quad n=3, 4, 5, \text{ etc.} \qquad (3a)$$

$$\nu_0^n = 70{,}249 - R/(n+0\cdot 50)^2 \quad n=3, 4, 5, \text{ etc.} \qquad (3b)$$

TABLE 3. TABLE SHOWING THE OBSERVED AND CALCULATED FREQUENCIES OF THE DIMETHYL BUTADIENE BANDS OF SERIES (3*a*) AND (3*b*)

	Series (3*a*)		Series (3*b*)	
n	Obs. cm.$^{-1}$	Calc. cm.$^{-1}$	Obs. cm.$^{-1}$	Calc. cm.$^{-1}$
3	63,053	63,026	61,528	61,291
4	65,696	65,670	64,912	64,830
5	67,078	67,088	66,703	66,621
6	67,927	67,935	67,657	67,652
7	68,478	68,481	68,298	68,296
8	—	—	68,746	68,731

The ionization potential corresponding to the limit is 8·668 V, a drop of 0·14 V relative to isoprene which itself is lower by 0·21 V than butadiene. This gradual diminution in the ionization potential we attribute to transfer of negative charge from the methyl group into the neighbourhood of the double bond (i.e., inductive effect). It may be compared for example with the diminution of ionization potential of 0·2 V in going from methyl to ethyl iodide (Price 1936). The fact that the addition of the second methyl group produces less lowering than the first is evidence of a tendency towards saturation.

The spectrum of chloroprene. The three molecules already dealt with indicate by the successive lowering of the ionization potentials, that the effect of alkyl groups on the mobile electrons of butadiene is purely an inductive one. The effect of halogen substituents (also OH, NH_2, etc.) in benzene is known to involve another effect known as the mesomeric or resonance effect. As a result of this effect additional resonance structures involving changes in the non-bonding electrons of the substituent atom or group become important. The previous paper shows how the effect reveals itself in the spectra of the chloro-ethylenes as an abnormal reduction in their ionization potentials; the bands are shifted to long wave-lengths where on a purely inductive effect alone the opposite might have been expected. This is indeed found to occur for chloroprene also. Its spectrum which is very similar to the spectrum of the previous three molecules is shifted to long wave-lengths relative to that of butadiene by about the same amount as isoprene. In the photograph lines have been drawn along spectra 1 and 5. The automatically drawn absorption curves lying above these lines are interesting. The first shows clearly the four humps of the C=C vibrational progression. The second shows the diffuse absorption in the region 1750 A which may be interpreted either as $N \rightarrow V_{2,3}$ or alternatively as the second Rydberg member of the diffuse absorption around 2000 A. Below 1600 A it was again found that the bands were of a vibrationless electronic type and could be fitted into many membered Rydberg series converging to a common photoionization limit. The following formulae were found to represent the strongest series:

$$\nu_0^n = 71{,}215 - R/(n+1\cdot10)^2 \quad n = 3, 4, 5, \text{etc.} \qquad (4a)$$

$$\nu_0^n = 71{,}190 - R/(n+0\cdot50)^2 \quad n = 3, 4, 5, \text{etc.} \qquad (4b)$$

TABLE 4. TABLE SHOWING THE OBSERVED AND CALCULATED FREQUENCIES OF THE CHLOROPRENE BANDS OF SERIES (4*a*) and (4*b*)

	Series (4*a*)		Series (4*b*)	
n	Obs. cm.$^{-1}$	Calc. cm.$^{-1}$	Obs. cm.$^{-1}$	Calc. cm.$^{-1}$
3	64,740	64,687	62,485	62,232
4	67,012	66,996	65,822	65,771
5	68,275	68,266	67,574	67,562
6	—	—	68,574	68,593

The limit corresponds to an ionization potential of 8·787 V probably accurate to 0·01 V. It is only 0·02 V less than that of isoprene and there is in fact a fascinating "one to one" correspondence amongst the bands, those of chloroprene being shifted by a few A.U. to long wave-lengths relative to those of isoprene. Such a correspondence could hardly occur if the interpretation of the bands as isolated vibrationless electronic transitions were not correct. A similar correspondence of course extends to butadiene and $\beta\gamma$ dimethyl butadiene and it is made evident by the approximate equality of the Rydberg denominators of corresponding series. It means that while the term values of the excited states remain approximately constant those of the ground states are being affected by the substitution.

At about 1430 A there occurs a group of fairly strong bands which has no analogue in the spectra of the alkyl substituted butadienes. Comparison with the spectra of the alkyl chlorides (Price 1936) indicates that these bands arise from the excitation of a non-bonding $p\pi$ electron from the chlorine atom. They are in fact analogous to the so-called "D" bands of methyl chloride. They are also observed in dichloro-ethylene, phenyl chloride, etc. Judging from the wave-length at which the "Cl" absorption occurs, the ionization potential of the "$p\pi$" electrons in this molecule may be estimated as $\sim 10{\cdot}9$ V.

It might be expected superficially that the ionization potential of the "π" electrons of the double bond in chloroprene would be greater than that in butadiene, since on account of the high electron affinity of chlorine, it would tend to draw away negative charge from the neighbourhood of the double bond and so increase the effective positive charge from which the electron is escaping. The fact that the contrary is the case can be explained by the effect of resonance to the structure

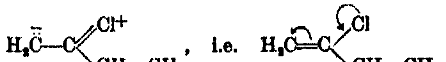

Such a structure while it explains reduction in ionization potential of the double bond by transfer of negative charge towards it and reduction in bonding of the π electrons also implies increase in the ionization potential of the "Cl" electrons. Evidence for this is that the "D" band occurs at shorter wave-lengths (~ 1438 A) in chloroprene than in ethyl or propyl chloride (1465 and 1475 A respectively). Comparison with the position of the "D" bands in methyl chloride (1406 A) would not be a fair one because to avoid differences in charge transfer effects the carbon atom bound to the chlorine should have the same number of C—H and C—C bonds attached to it as the alkyl chloride with which it is being compared. It might also be mentioned that the D bands in dichloro-ethylene and phenyl chloride occur at closely the same wave-length as in chloroprene and thus a corresponding increase in the ionization potential of the Cl electrons is also indicated for these molecules.

Discussion. It may at first sight appear rather curious that the removal to high Rydberg orbits of a π electron which has considerable bonding power causes hardly any vibrational bands to appear. The spectrum at short wavelengths (< 1600 A) is composed almost entirely of vibrationless electronic transitions and resembles closely that of a non-bonding electron. The same phenomenon was found for benzene (Price and Wood 1935) where the analysis was confirmed by the use of heavy benzene (C_6D_6). The following seems to be a satisfactory explanation of this curious anomaly: As a result of the process of resonance all the "π" electrons are shared between the two double bonds and the removal of one such electron from butadiene for example can be regarded as the removal of only one half an electron from each double bond. Thus the internuclear distances and vibration frequencies will only be diminished by a half of what they would be in relatively isolated double bonds where the whole effect is localized in one and not spread out over many bonds as in conjugated systems. As a matter of fact because of the splitting up of the four electrons into two groups, which will be discussed later, the removal of one π electron in butadiene only has ~ 0·36 the effect which might be expected for example in ethylene. In benzene it is a third. Thus each bond is altered only very slightly and the molecule can accommodate itself easily to the excitation without much vibration being invoked by the Franck-Condon Principle. Even when a "π" electron is removed to a fairly strong antibonding orbital, the fact that it is shared among all the double bonds of the molecule reduces its effect on each individual bond. Thus in the 2500 A band of benzene, which undoubtedly corresponds to a fairly strong antibonding orbital (Sklar 1937), the main frequency is only reduced from 991 to 920 cm.$^{-1}$. Wherever there is evidence of the existence of vibrational structure in the absorption spectra of conjugated molecules it may be expected that the upper state is to some extent antibonding in

TABLE 5. TABLE SHOWING THE SEPARATION OF THE FIRST DIFFUSE BANDS OF BUTADIENE, ISOPRENE, $\beta\gamma$ DIMETHYL BUTADIENE AND CHLOROPRENE

Butadiene		Isoprene		Dimethyl butadiene		Chloroprene	
Frequency cm.$^{-1}$	Separation cm.$^{-1}$	Frequency cm.$^{-1}$	Separation cm.$^{-1}$	Frequency cm.$^{-1}$	Separation cm.$^{-1}$	Frequency cm.$^{-1}$	Separation cm.$^{-1}$
46,240		44,820		43,800		45,120	
	1420 ± 50		1500 ± 100		1400 ± 100		1250 ± 100
47,660		46,320		45,200		46,370	
	1450 ± 50		1450 ± 100		1350 ± 100		1180 ± 100
49,110		47,770		46,550		47,550	
	1440 ± 50						
50,550							

character. This is what happens in the band system which is observed in the neighbourhood of 2100 A in butadiene (also in isoprene, etc.). It was at first thought that this transition was completely analogous to the first Rydberg series band of ethylene at 1750 A because the two systems have closely equal term values ($\sim 27,000$ cm.$^{-1}$) and are the first strong absorption bands of both molecules and also are of comparable strength. However, the 2100 A band in butadiene does not fit on very well as a Rydberg series member of the bands at shorter wave-length. It is obviously different in character from them being represented by a vibrational progression rather than a single atom-like vibrationless transition. Further, if this band were quite analogous to the 1750 A band we should only expect half the reduction of the C=C frequency which occurs in that molecule, i.e. $\frac{1}{2}(1623 - 1370) = 127$ cm.$^{-1}$. Actually the reduction is ~ 190 cm.$^{-1}$ $(1640 - 1450)$, i.e. slightly more than might be expected, and this may be taken as evidence of the slightly antibonding character of this transition with respect to the first Rydberg band of ethylene. The degree of antibonding is not very large—a fact which is supported by the close equality of the term values of the two states (i.e. if the first Rydberg band in ethylene acquires antibonding power in butadiene, then this should be accompanied by a reduction in its term value). Mulliken (1939*a*) interprets the transition as one of the charge transfer type and attributes its great predominating intensity to this fact. The configuration of the normal state N of butadiene can be written as $\chi_1^2\chi_2^2$ as far as the π electrons are concerned. Two electrons occupy the χ_1 orbital which gives bonding in all the bonds between the carbon atoms and two fill χ_2 which is only bonding in the C=C bonds. It corresponds to the $(-1{\cdot}62\beta)^2(-0{\cdot}62\beta)^2$ configuration of Hückel (1937), β being the resonance integral between "π" electrons on adjacent atoms. Lennard-Jones (1937) points out that Hückel's simplifying assumption that all the CC distances are equal is not true in practice. He derives the energies for the orbitals for bond distances C—C = 1·44 A and C=C = 1·35 A. These are $\pm 50{\cdot}7$ kcal. (χ_1 and χ_4) and $\pm 24{\cdot}4$ kcal. (χ_2 and χ_3) with $\beta_d = 35$ kcal. Mulliken (1939*a*) using Lennard-Jones's results with slightly modified bond distances gives $\pm 1{\cdot}422\beta$ and $\pm 0{\cdot}674\beta$ for the energies. There are four possible non-Rydberg transitions corresponding to the jump of an electron from either $\chi_1(-1{\cdot}674\beta)$ or $\chi_2(-1{\cdot}422\beta)$ to either of the antibonding orbitals $\chi_3(0{\cdot}674\beta)$ or $\chi_4(1{\cdot}422\beta)$. These transitions Mulliken calls $N \rightarrow V_1, V_2, V_3, V_4$, the four excited states being $\chi_1^2\chi_2\chi_3$, $\chi_1^2\chi_2\chi_4$, $\chi_1\chi_2^2\chi_3$, $\chi_1\chi_2^2\chi_4$. It can be seen that $N \rightarrow V_1$ is the longest wave-length transition, $N \rightarrow V_2$ and $N \rightarrow V_3$ coming next, both corresponding to the same energy change, and finally $N \rightarrow V_4$ is the shortest wave-length transition of this type. Mulliken finds the total theoretical dipole strengths of these transitions to be very large but their relative strengths depend on the symmetry of the molecule. Thus $N \rightarrow V_{2,3}$ are suppressed when the double bonds are in the "*trans*" position. They are allowed in the "*cis*" position but $N \rightarrow V_1$ is diminished in intensity and $N \rightarrow V_4$ forbidden (Mulliken 1939*a*, table 5). The frequencies of the transitions cannot be calculated by just taking the difference of the binding energies, since it is necessary to add to the energy of the excited orbitals a term to allow for changes in the electronic interaction energy resulting from the excitation. This term is apparently very large, being about 27,000 cm.$^{-1}$ ($\sim$80 kcal.) in C_2H_4 and butadiene if Mulliken's interpretation of the spectra is correct [Goeppert-Mayer and Sklar (1938) by theoretical calculations find interaction energies of this magnitude for C_6H_6]. The question we should like to be able to answer is whether the butadiene bands in the neighbourhood of 2100 A can be interpreted as Mulliken's $N \rightarrow V_1$ transition or whether they are first Rydberg bands of a type $(\pi)^{-1}\,3s$. If the latter suggestion is correct, then there are certainly no other bands of the required intensity which could be interpreted as $N \rightarrow V_1$. If the former suggestion is correct, then one might ask what has become of the first Rydberg state. For a large molecule like butadiene the orbital of the first Rydberg state is expected to lie to a considerable extent within the dimensions of the molecule. The resulting interaction might transform it into an orbital of the V_1 type. With larger molecules and especially those corresponding to conjugated systems it appears that the earlier Rydberg states might be made to take upon themselves the character of V states, that they may be simply replaced by these states or that there may be a certain amount of mixing of the two R and V types. Evidence for this comes from the tendency of the first Rydberg orbital in the substituted ethylenes to acquire V characteristics with increase in the amount of alkyl substitution. These characteristics are briefly a tendency to acquire intensity at the expense of higher Rydberg bands, a departure from the Rydberg formula and a more complicated vibrational structure differing consider-

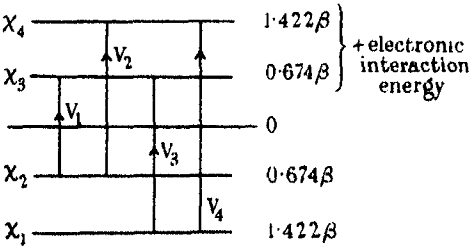

FIGURE 3. Energy levels and $N \rightarrow V$ transitions in butadiene.

ably from the higher Rydberg states where these are still observable. Thus in ethylene the resemblance between the band at 1740 A and that at 1390 A is very marked, while in propylene this resemblance is already lost. More striking evidence that these long wave-length bands really have some $N \rightarrow V_1$ character comes from the spectra of the dienes. Here the theory predicts that the transitions should be relatively weaker for the *cis* (cyclic) dienes than for *trans* dienes, the probability of the transition depending upon the symmetry of the molecule. These expectations are borne out experimentally (Mulliken 1939*a*).

In justifying his theory Mulliken works out a value for β (the resonance integral for the double bond; ϵ in his notation) from the difference of the first strong $N \rightarrow V_1$ bands in butadiene $(2 \times 0{\cdot}674\beta + C)$ and $N \rightarrow V_1$ for C_2H_4 $(2 \times \beta + C)$; C is the electronic interaction constant. We consider that he should have used the value for propylene in order to make both the electronic interactions the same and to allow for charge transfer effects by surrounding both double bonds by 3CH and one C—C bond*. It happens that the value for ethylene used by Mulliken (i.e. 58,000 cm.$^{-1}$ or 1724 A) just accidentally corresponds to $\nu_{\max}$ in propylene. From our plates (see previous article) it does not correspond to $\nu_{\max}$ in ethylene which is around 1630 A. Thus the derivation of β from $\nu_{\max}$ (propylene) $-$ $\nu_{\max}$ (butadiene) $= 58{,}000 - 48{,}300 = 2 - 2 \times 0{\cdot}674\beta$ giving $\beta = 15{,}200$ cm. or 1·87 V or 43 kcal. works out to the same value as Mulliken obtained. Another method of getting β is to make the very reasonable assumption that the difference between the ionization potentials of propylene and butadiene is equal to the difference in binding energy of the π electrons in the two molecules. This gives $9{\cdot}6 - 9{\cdot}02$ V $= \beta - 0{\cdot}674\beta$ or $\beta = 1{\cdot}8$ V in agreement with the previous value. A similar comparison can be made between isobutene and $\beta\gamma$ dimethyl butadiene for which the ionization potentials are $\sim 9{\cdot}20$ V and 8·67 V. This gives a value for β of 1·6 V. One cannot get a value of β from cyclohexene and benzene because the electrons in the comparable groups both have the binding energy β and therefore may be expected to have the same ionization potentials. That this is so is indicated by the close identity of the bands of these molecules at wave-lengths less than 1850 A. In fact this identity may be used to show that the strong absorption in benzene $\lambda 1790$ is probably $\chi_1^2 \chi_{2,3}^4 \rightarrow \chi_1^2 \chi_{2,3}^3 \chi_{4,5}$ in character.

---

* In any case it is sure that the *strong* bands of butadiene should be compared with the *strong* bands of the unconjugated molecule. The relatively weak "step out" occurring in ethylene from 2000–1750 A, which Mulliken used, has its analogy in a similar "step out" in butadiene from 2300–2170 A (Scheibe and Grieneisen 1934) and is not comparable with the strong bands of butadiene.

All the ionization potentials given here for the dienes clearly belong to the ionic state $\chi_1^2\chi_2$, the least bonding orbital χ_2 corresponding to the minimum ionization potential. It is not possible to observe the photoionization of electrons in χ_1 because they are expected to have an ionization potential a few volts higher than χ_2 and their resonance bands fall in a region where there is very strong continuous absorption from electrons in single C—C and C—H bonds. The first strong absorption bands of the χ_1 electron can usually be observed superimposed upon the photoionization continuum of the χ_2 electrons. This also occurs in benzene (the ionization potential at 9·19 V being to $\chi_1^2\chi_{2,3}^3$, Price and Wood 1935). As it seems possible that these first strong bands correspond to $N \rightarrow V_4$ type transitions in the same way as the first strong bands of the χ_2 electrons probably correspond at least partly to $N \rightarrow V_1$ transitions, they will be treated in the following paragraph as though this were actually the case.

If the electronic interaction energy is the same for the transitions $N \rightarrow V_1$, V_2, V_3, V_4, then $V_{2,3} - V_1 = V_4 - V_{2,3} = 0{\cdot}748\beta$ and $V_4 - V_1 = 1{\cdot}496\beta$ (Mulliken 1939*a*, table 4). In the following table the values of $\nu_{\max}$ for the V_1, $V_{2,3}$, and V_4 states are given together with the values of β calculated from the above relations.

TABLE 6. TABLE SHOWING THE FREQUENCIES OF THE $N \rightarrow V$ BANDS OF BUTADIENE, ISOPRENE, DIMETHYL BUTADIENE AND CHLOROPRENE

Molecule	V_1	$V_{2,3}$	V_4	β in kcal. from $V_{2,3}-V_1$	β in kcal. from V_4-V_1
Butadiene	48,300	57,800	77,000	36	55
Isoprene	46,300	56,300	74,000	38	53
$\beta\gamma$ dimethyl butadiene	45,500	56,000	—	40	—
Chloroprene	46,500	56,800	—	39	—

It appears that while the β's calculated from $V_{2,3} - V_1$ separations are fairly reasonable those from $V_4 - V_1$ (also $V_4 - V_{2,3}$) are much too large. This is probably due to variation in the electronic interaction energy and is to be expected from the fact that while in the $V_2 - V_1$ difference the same electron is involved, for the $V_1 - V_4$ difference the bands used correspond to the excitation of a different electron.

Before accepting the values of β derived in the above table attention should be called to certain difficulties with respect to the interpretation of the bands as $N \rightarrow V$ transitions. The V states which give rise to bands at shorter wavelengths are theoretically more strongly anti-bonding than those giving rise to longer wave-length band systems. This would lead us to expect lower vibrational frequencies for the shorter wave-length systems. Actually in practice the reverse is nearly always the case. For instance the C=C frequency in the $N \rightarrow V_1$ states of the dienes is around 1450 cm.$^{-1}$ and is less than that in the $N \rightarrow V_{2,3}$ states ($\sim$1500–1600 cm.$^{-1}$) which according to $N \rightarrow V$ interpretation are more strongly antibonding. Also in benzene the 2000 A system has been interpreted by Sklar (1937) as more antibonding than the 2500 A system, yet the breathing frequency in the former is 960 cm.$^{-1}$ (Carr and Stücklen 1938) as compared with only 920 cm.$^{-1}$ in the latter. Similar differences are shown by the 3000 and 2000 A systems of SO_2 and CS_2 (Price and Simpson 1938). The change in bonding due to the excitation of an electron is equal to the bonding of this electron in the ground state plus its antibonding power in the excited state. Evidence from vibrational frequencies indicate that this second factor is smaller the shorter the wave-length of the band concerned, instead of being larger as the $N \rightarrow V$ explanation would lead us to expect. It might possibly be that the attenuation of the excited orbital is such that the antibonding is in fact less, but that the electronic interaction increases to prevent the shift to long wave-lengths which would automatically follow. Thus the transition could retain the qualities of an $N \rightarrow V$ transition though the quantitative contributions to the total energy involved would be considerably different. A theoretical explanation of this anomaly is certainly desirable. If the much weaker system in ethylene between 2000 A and 1750 A, which shows far greater frequency reduction (the C=C vibration being probably reduced to $\sim$800 cm.$^{-1}$: Scheibe and Grieneisen 1934), is really the pure $N \rightarrow V_1$ transition in ethylene, then by analogy it is the weak "step out" between 2300 and 2170 A in butadiene which really corresponds to the pure $N \rightarrow V_1$ transition in this molecule. If this is correct, then Mulliken's intensity predictions for $N \rightarrow V$ transitions must be in error.

The existence of $N \rightarrow V_{2,3}$ absorption indicates according to Mulliken (1939*b*), the presence of a certain amount of *cis* butadiene (he estimates 20 %). If there is a difference in the stability of the two forms arising for instance from the greater repulsion between the two double bonds in the *cis* as compared with the *trans* positions, then it might be expected that the *cis* form would have a lower ionization potential than the *trans*. Certainly the cyclic dienes seem to have considerably lower ionization potentials of the *trans* dienes judging from their absorption spectra In butadiene we were unable to find any evidence of a lower ionization potential corresponding to the *cis* form. Thus it seems that butadiene is mainly *trans* and that the $N \rightarrow V_{2,3}$ transition occurs in violation of Mulliken's selection rule or that it has some other interpretation, e.g. as a Rydberg transition.

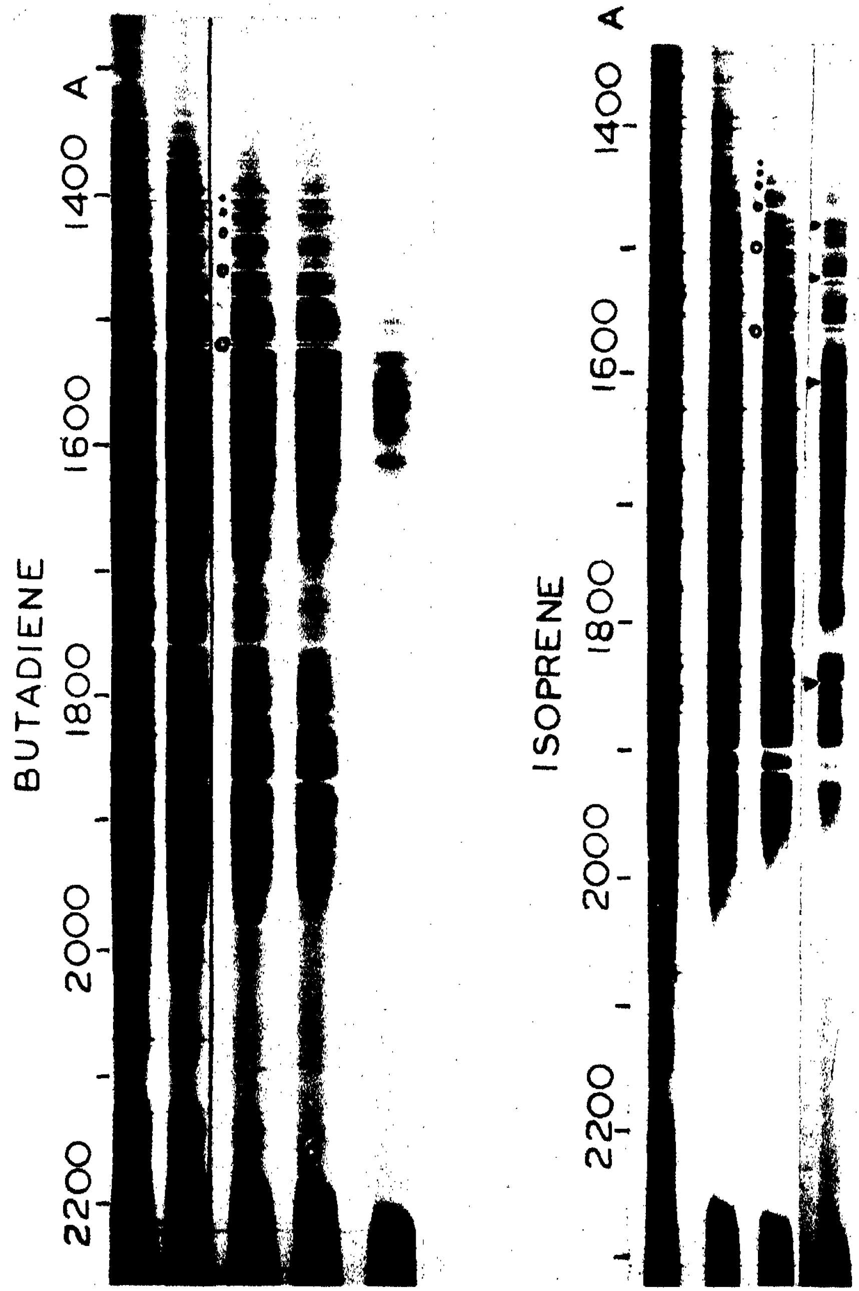

FIGURE 1. The absorption spectra of butadiene and isoprene.

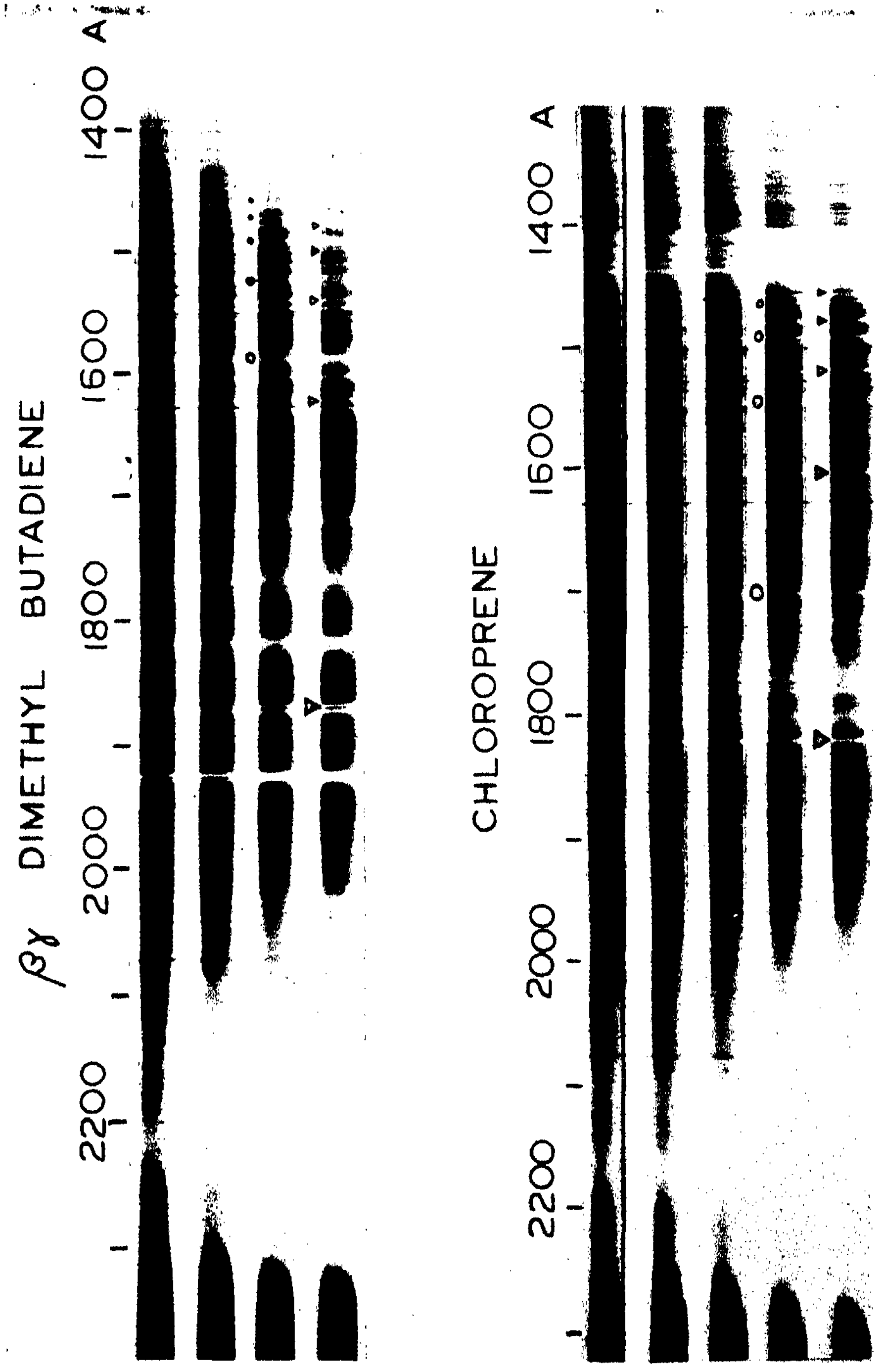

Figure 2. The absorption spectra of βγ dimethyl butadiene and chloroprene.

It appears from the spectra that some of the earlier Rydberg series members are weaker than they might be expected to be relative to the higher members by comparison with Rydberg series in atoms. There are several reasons for this. Firstly, the wave functions of the earlier Rydberg series members may be modified by the extensive structure of the molecule; secondly, the continuum may be stronger at long than at short wave-lengths particularly if the absorption falls in the neighbourhood of an emission line and finally the shorter wave-length bands may be enhanced by a weakening of the continuum due to a background of continuous absorption.

The samples of butadiene, isoprene and chloroprene were I.C.I. products made available to us by the kindness of Dr H. W. Melville of the Colloid Chemistry Department. The $\beta\gamma$ dimethyl butadiene was prepared in a very pure state by the method suggested by Kyriakides (1914). In conclusion we should like to thank the Department of Scientific and Industrial Research and the Imperial Chemical Industries for financial assistance. We are also indebted to Professor J. E. Lennard-Jones for several interesting and fruitful discussions.

SUMMARY

The absorption spectra of butadiene, isoprene, $\beta\gamma$ dimethyl butadiene and chloroprene have been investigated in the region 2500–1000 A. They are all very similar. The first strong bands appear as short diffuse progressions involving the C=C vibrational frequency but no vibrational structure is observed in the bands below 1600 A. The latter are interpreted as vibrationless electronic transitions converging to the first photoionization limit $\chi_1^2\chi_2$ of the "mobile" electrons. The extrapolation of successively excited states in Rydberg series gives the following very accurate values of the molecular ionization potentials: butadiene 9·02 V; isoprene 8·81 V; $\beta\gamma$ dimethyl butadiene 8·67 V; chloroprene 8·79 V.

The diminution in the ionization potential with alkyl substitution is interpreted as a simple inductive effect. The diminution in chloroprene involves the mesomeric as well as the inductive effect. The non-appearance of vibration bands accompanying the Rydberg transitions is a direct result of the resonance. As the electron is shared between two bonds, its removal has only one half the effect on each and this is apparently inadequate to cause the appearance of vibrational bands. Attempts are made to evaluate the resonance integral from various features of the spectra and from the ionization potentials. It is pointed out that the main difficulty with Mulliken's $N \rightarrow V$ interpretation of the strong bands of the dienes (also that of

Sklar's for benzene, etc.) is that the shorter wave-length transitions are interpreted as being the more strongly antibonding. The reverse is observed to be the case as judged from the vibration frequencies appearing in the spectra.

REFERENCES

Carr and Stücklen 1938 *J. Chem. Phys.* **6**, 55–61.
Dadieu and Kohlrausch 1930 *Ber. Dtsch. Chem. Ges.* B, **63**, 1657–1666.
Goeppert-Mayer and Sklar 1938 *J. Chem. Phys.* **6**, 645–652.
Hückel 1935 *Physical Society Int. Conf. Phys.*, London.
— 1937 *Z. Electrochem.* **43**, 752–788.
Kyriakides 1914 *J. Amer. Chem. Soc.* **36**, 987–993.
Lennard-Jones 1937 *Proc. Roy. Soc.* A, **158**, 285–296.
Mulliken 1939*a* *J. Chem. Phys.* **7**, 121–135.
— 1939*b* *J. Chem. Phys.* **7**, 373.
Price 1936 *J. Chem. Phys.* **4**, 539–551.
Price and Simpson 1938 *Proc. Roy. Soc.* A, **165**, 272–291.
Price and Wood 1935 *J. Chem. Phys.* **3**, 439–444.
Scheibe and Grieneisen 1934 *Z. Phys. Chem.* **25** B, 52–56.
Sklar 1937 *J. Chem. Phys.* **5**, 669–681.

Investigations of infra-red spectra (2·5—7·5μ). Absorption of water

BY J. J. FOX AND A. E. MARTIN

(*Communicated by Sir Robert Robertson, F.R.S.—Received* 15 *August* 1939)

INTRODUCTION

During recent years much information has been obtained concerning the infra-red absorption of hydroxy bodies in the region about 3μ. A number of investigators (Errera and Mollet 1936; Errera 1937*a*; Buswell, Deitz and Rodebush 1937; Buswell, Rodebush and Roy 1938; Davies and Sutherland 1938*a*, *b*; Fox and Martin 1937) have shown that at low concentrations in carbon tetrachloride a hydroxy body, whether an alcohol, phenol or carboxylic acid, has a sharp OH band at 2·75–2·83μ, and as the concentration increases this band diminishes rapidly and is replaced by a wide intense band at longer wave-lengths, 3μ and higher. The sharp band is due to the valency O-H vibration in the monomer, while at higher concentrations the molecules interfere with one another and modify the nature of the O-H vibrations in a manner which depends somewhat on the nature of the compound concerned.

Water, as a simple hydroxy body of special interest, has been investigated by many workers. The vapour spectrum consists of vibration-rotation bands in the photographic (Mecke 1933; Baumann and Mecke 1933; Freudenberg and Mecke 1933) and near infra-red (Plyler 1932; Plyler and Sleator 1931; Sleator 1918; Sleator and Phelps 1925), and pure rotation bands in the far infra-red to 75μ (Randall, Dennison, Ginsburg and Weber 1937); it has been thoroughly explored but is very complex, and its interpretation is still by no means complete in all regions. Two modes of vibration of the isolated water molecule can be identified from the infra-red data, one a little less than 2·7μ, corresponding to a valency O-H vibration, as in alcohols and other hydroxy bodies, and the other near 6μ attributable to the angular deformation frequency of the H-O-H molecule.

In the liquid state water has received considerable attention, and bands at 3, 4·7 and 6μ have been studied together with combination bands at lower wave-lengths. The band at 4·7μ has no counterpart in the vapour spectrum and on this account has been attributed to associated water molecules; Bode (1909) showed that this band moved to 4·5μ in ice. Collins (1925) examined some of the combination bands up to 2μ at different temperatures, while Plyler (1924) measured the absorption of ice at some of these wave-lengths. Combining the vapour measurements with those of Collins and Plyler, it is found that the frequency increases in the order, ice—water at 0° C—water at 100° C—water vapour, for these combination bands. Ganz (1937) using a prism spectrometer measured the temperature dependence of the water bands at 3, 4·7 and 6μ. He found that as with the combination bands, that at 3μ increased in frequency with rise of temperature, but the other two bands showed the reverse phenomena, the 4·7μ band being greatly affected by change of temperature. These observations on the variation with temperature of the water bands have not so far been explained. In collaboration with Sir R. Robertson and using a prism apparatus, the writers had already made observations in 1935 similar to those of Ganz, but it was considered that to obtain results of the desired precision the resolution of a grating spectrometer was essential, and the present communication deals, among other matters, with measurements made by us with such an apparatus. It is now generally understood that there are important differences between the spectrum of a liquid hydroxy body and the spectrum of a solution in a non-polar solvent such as carbon tetrachloride, in which the substance is present in the monomeric form when sufficiently dilute. A comparison of the spectra of the liquid at different temperatures, and of the monomeric substance (in vapour and in solution) is valuable in deciding problems connected with the structure of the liquid. In the case of water considerable progress along these lines has been made by Cross, Burnham and Leighton (1937) from a consideration of Raman data. It is our aim in the present communication to continue this study of the structure of water, using our newer infra-red data.

Attempts have been made to investigate the infra-red absorption of water dissolved in non-polar solvents, but owing to the low solubility of water in such solvents the earlier results obtained were only partially successful (cf. Bosschieter and Errera 1937; Kinsey and Ellis 1937). Recently, however, Borst, Buswell and Rodebush (1938), using a 12·5 cm. cell of carbon tetrachloride (or carbon disulphide) saturated with water at room temperature, were able to observe the essential details of the absorption bands in the region of 3μ. Two distinct bands were found corresponding to the vibrations ν_1 and ν_2 (figure 1) in the isolated water molecule, and as is to be expected the symmetrical vibration (strong in the Raman spectrum) was much weaker in intensity than the other. These observations, together with the absence of absorption in the position where the OH frequency is found in associated compounds, show that water in carbon tetrachloride is monomeric.

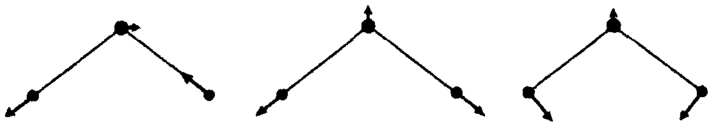

ν_1 3756 cm.$^{-1}$

ν_2 3654 cm.$^{-1}$

ν_3 1595 cm.$^{-1}$

FIGURE 1. Modes of vibration of the isolated water molecule.

Some interesting observations have also been made by Errera (1937*b*) for water in dioxan over a wide concentration range. In this solvent, at a concentration of 0·1–1 %, water has two bands at 3515 and 3575 cm.$^{-1}$ (2·85 and 2·80μ), but here the frequency changes from ν_1 and ν_2 of monomeric water are greater and the intensity of absorption is increased in comparison with water in carbon tetrachloride, so that the spectrum cannot be regarded as that of monomeric water but rather of the complex formed between water and dioxan. Errera and Sack (1938) have pointed out the extreme sensitivity of the infra-red absorption spectrum as a means of detecting traces of water.

In the present communication we shall describe our own measurements of the absorption of water dissolved in carbon tetrachloride, paying special attention to the quantitative aspect. On the whole our results in the 3μ region agree with those of Rodebush *et al.* (1938).

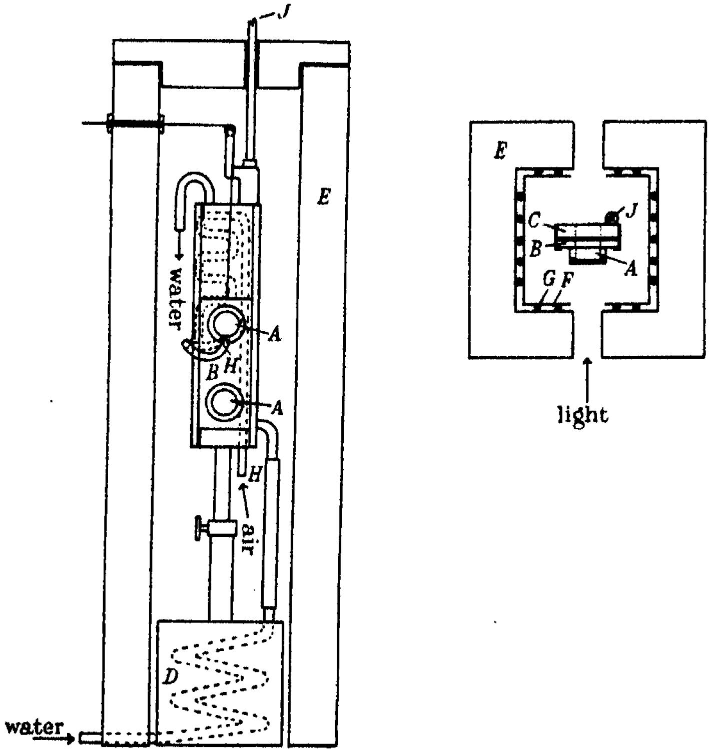

FIGURE 2. Apparatus for measuring the absorption of ice and of water at different temperatures.

EXPERIMENTAL

Absorption of ice and of liquid water at different temperatures

A brief description of the grating spectrometer used in this work and of general technique has already been given (1937, 1938). Great care was taken to eliminate water vapour and carbon dioxide from the whole of the spectrometer by the lavish use of P_2O_5 and caustic potash, and by using only metal or glass in the construction of the outer case of the instrument and for internal fittings. Absorption cells were made up from fluorite plates, 1 in. in diameter, separated by washers, usually of metal foil, of the desired thickness. The cell with the water enclosed was placed in a brass mount *A* (figure 2) into which screwed a cap for holding the fluorite plates firmly together. A second pair of plates, suitably spaced, was similarly mounted and served as a blank. Freshly boiled distilled water was used in these experiments. Extremely thin water layers are required, e.g., at the maximum of the 3μ band in ice a thickness of 0·001 mm. absorbs about 75 % of the radiation. Most of the earlier workers used such thick films that the light apparently transmitted was largely stray radiation in the appartus, and for this reason the absorption bands obtained were very broad and appeared to shift as the thickness of the film was varied. Plyler and Craven (1934) used films as thin as 0·001 mm., but Ganz (1937) did not use layers thinner than 0·005 mm. For spacing the fluorite plates we generally used washers of metal foil, but for layers as small as 0·003 mm., metal washers were troublesome to handle and those of celluloid were preferred. The celluloid film was made by floating a solution of celluloid in amyl acetate on a level piece of plate glass and when dry stripping off the film in water. All the washers were cut with sharp steel punches. For thicknesses of 0·003–0·001 mm., no washer was used; a drop of water was pressed between the fluorite plates and these were held together in the screw mount. After absorption measurements had been made, an estimate of the mean thickness of the water film was obtained by weighing the fluorite plates, with and without the water film (0·001 mm. $\approx$ 0·5 mg.).

The apparatus with which the temperature of the water film was varied is shown in figure 2. Each cell in its mount, A, screws into a thick brass plate B which slides smoothly in grooves on the outside of a hollow brass box C, through which water from a vessel fitted with a toluene/mercury gas regulator is pumped. This part of the apparatus is mounted in a heavy lead block D containing a spiral tube through which water from the thermostat also flows. Surrounding the whole apparatus is a heat insulating box E, made of expanded rubber and provided with holes for the light beam. The inside of this box towards the top is lined with copper sheet F which can also be brought to the same temperature as the rest of the apparatus by circulating the water from the thermostat through metal tubing G in close contact with the copper. Temperatures approaching 100° C are readily obtainable, although with the thinner water films examined, evaporation of the water limited the maximum temperature to 60–70° C. Ice films were obtained by pumping the liquid from a salt and ice freezing mixture through the apparatus, and when a temperature of about -15° C had been attained the water film was solidified by jolting the cell. At the lower temperatures there was a tendency for the fluorite plates to become cloudy owing to deposition of moisture from the surrounding air. This trouble was obviated by directing a current of dry air against each fluorite plate of whichever pair was in the light beam. This current of air was cooled by passing through a metal tube *H*, inside the body of the apparatus *C*, in contact with the cold circulating brine. A thermometer *J* projecting through the insulating box enabled the temperature to be determined at any time, while a change over from cell to blank and also complete cut-off of the radiation were arranged by sliding the brass plate *B* up and down in the grooves by means of a cord worked from outside. Stops were provided for limiting the movement so that either cell came exactly into the beam as desired.

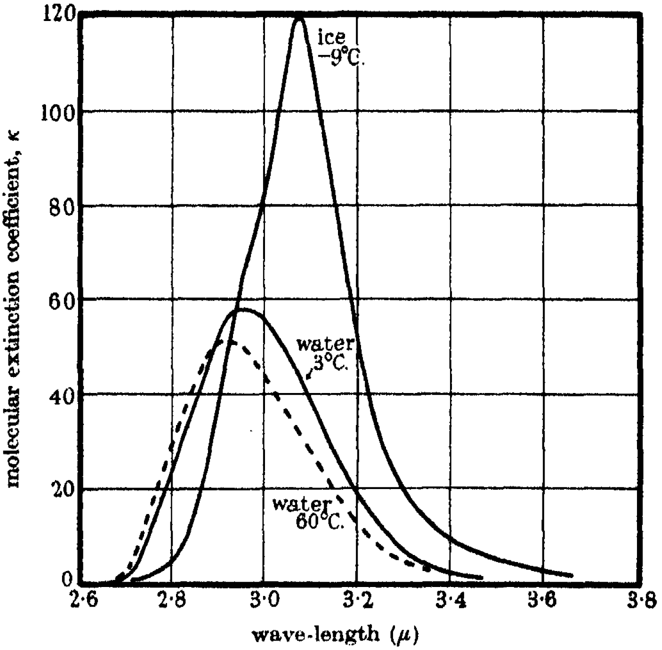

FIGURE 3. Absorption of ice and of water.

Figures 3–5 and table 1 show the results obtained for the absorption bands at 3, 4·7 and 6μ, both for water at a high and a low temperature, and also for ice at a few degrees below zero. The molecular extinction coefficient κ is defined as $1/cl \log_{10} I_0/I$, where I_0 is the radiation transmitted by the empty cell and I the amount transmitted by the cell containing the water. l is the length of the cell in cm. and c the "concentration" of water in moles per litre, i.e. $\frac{1000}{18}\rho$, where ρ is the density of water at the temperature of the experiment. The blank cell compensates for some of the reflexion losses and for any absorption in the fluorite plates, but there remains a small difference in the reflexion losses at the inner fluorite/air and fluorite/water surfaces of the two absorption cells. This small difference was estimated and found to be almost constant over the wave-length range studied. When calculating κ for ice it was assumed that cl remained unchanged on passing from water to ice. This is reasonable, since it was found that the original water value was obtained when the ice melted. Other workers have sometimes recorded their results in terms of the mass absorption coefficient $(1/l\rho \log I_0/I)$, but we use κ so that the results for liquid water and ice can be readily compared with those for other hydroxy bodies as well as water vapour and water dissolved in carbon tetrachloride.

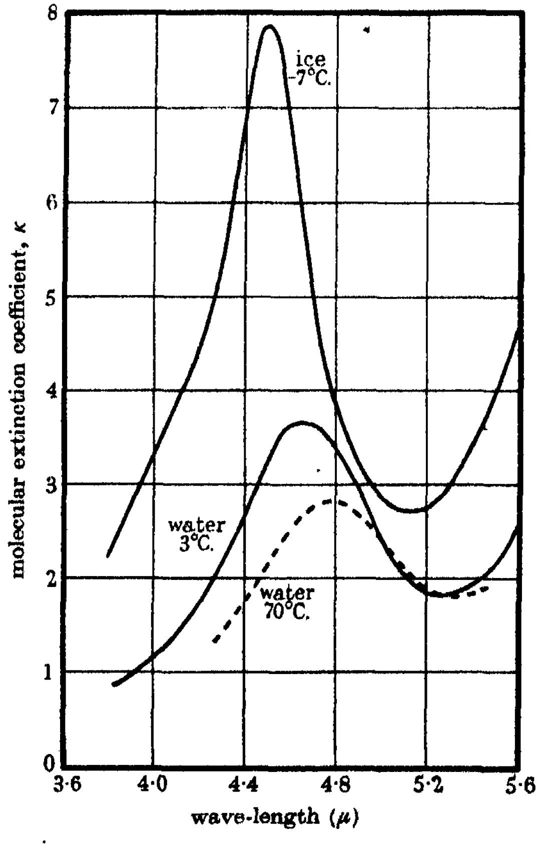

FIGURE 4. Absorption of ice and of water.

With regard to ice we may recall that Plyler (1924) found absorption bands at 0·79–0·81, 0·89–0·92, 1·02–1·06, and 1·26–1·29μ. A thickness of 5 mm. was used, and the absorption maximum and intensity of each band varied a little according to the manner in which the ice crystal was cut with respect to the optic axis. In our experiments no control of the direction of the optic axis was possible, and our ice specimens must be regarded as a mixture of crystals with all possible orientations. We found that successive freezings of the water gave the same absorption within experimental error.

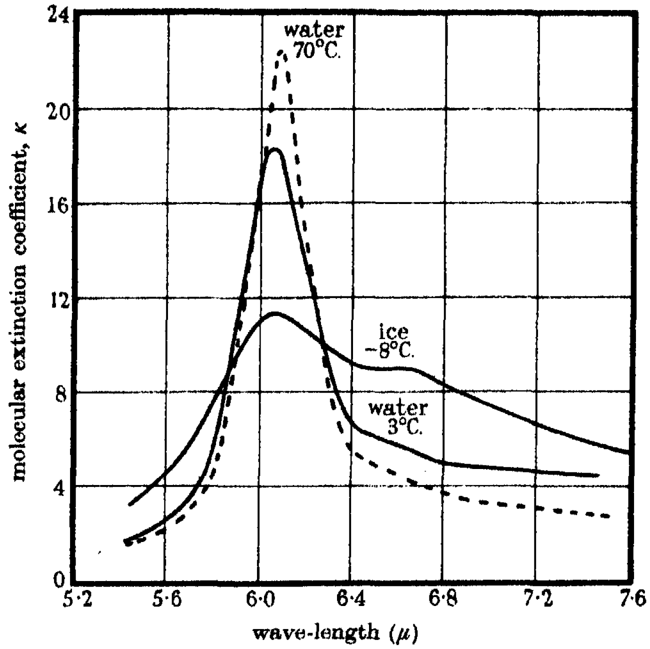

FIGURE 5. Absorption of ice and of water.

TABLE 1. TEMPERATURE DEPENDENCE OF THE ABSORPTION BANDS OF WATER AT 3, 4·7 AND 6μ, AND THEIR POSITIONS IN ICE

	3μ band—frequencies in cm.$^{-1}$		
Water at 60° C	Water at 19° C	Water at 3° C	Ice at −9° C
3426	3395	3382	3256
	4·7μ band—frequencies in cm.$^{-1}$		
Water at 70° C	Water at 21° C	Water at 3° C	Ice at −7° C
2092	2128	2146	2222
	6μ band—frequencies in cm.$^{-1}$		
Water at 70° C	Water at 20° C	Water at 3° C	Ice at −8° C
1642	1646	1649	1644

All these frequencies are probably accurate to ± 2 cm.$^{-1}$, with the exception of ice at 6μ.

When it is remembered that rarely if ever has liquid water been examined in the region 2·5–7·5μ with the high dispersion here available, our results are in reasonable agreement with those of previous workers. The composite structure of the 3μ band of water reported by Plyler and Craven (1934), and also the new bands found by these workers at $5{\cdot}56$ and $5{\cdot}83\mu$, have not been substantiated by us. Recently, Collins (1939) has reported a band in liquid water at $2{\cdot}52\mu$ (κ max. $= 0{\cdot}61$), and this we have confirmed. We find the wave-length of the maximum of the band to be $2{\cdot}515\mu$ at 21° C, while κ max. $= 0{\cdot}46$. This band is too small to be shown on the scale used for figure 3.

Infra-red absorption of water dissolved in carbon tetrachloride-quantitative aspect

The solubility of water in carbon tetrachloride has been measured by Clifford (1921), and by Rosenbaum and Walton (1930). Clifford's method was to bubble air dried with calcium chloride into the saturated carbon tetrachloride, and to absorb the moisture carried off by the air in calcium chloride tubes.

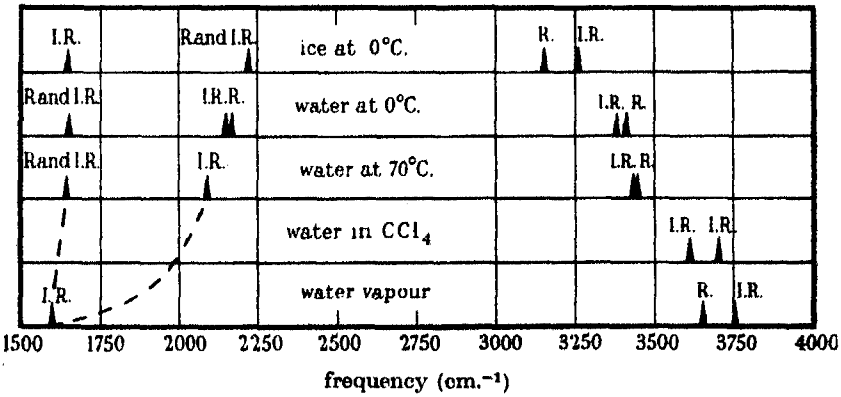

FIGURE 6. Raman and infra-red vibrational frequencies of water as vapour, liquid, solid, and in solution in CCl_4. Data taken from table 5.

Instead of calcium chloride as a drying agent we have substituted P_2O_5, and by using a bubbler incorporating a sintered glass filter we have speeded up the drying process considerably so that it is possible to dry a solution in 10–15 min. As the supply of air required is quite small, a blow-ball fitted with a screw clip for regulation is convenient. The absorption tube containing P_2O_5 is attached directly to the bubbler by means of a ground joint. After the desired period of drying, the bubbler is removed and a current of dry air passed through the absorption tube for 5 min. to remove CCl_4 vapour. The increase in weight of the absorption tube gives the amount of water removed from the carbon tetrachloride. Experiments were carried out in which carbon tetrachloride saturated with water was dried in this manner for different periods of time, at the end of which each sample was examined with the grating spectrometer. The absorption cell was filled directly from the bubbler through a tube which was attached by an interchangeable ground joint. The gradual removal of water was shown by the

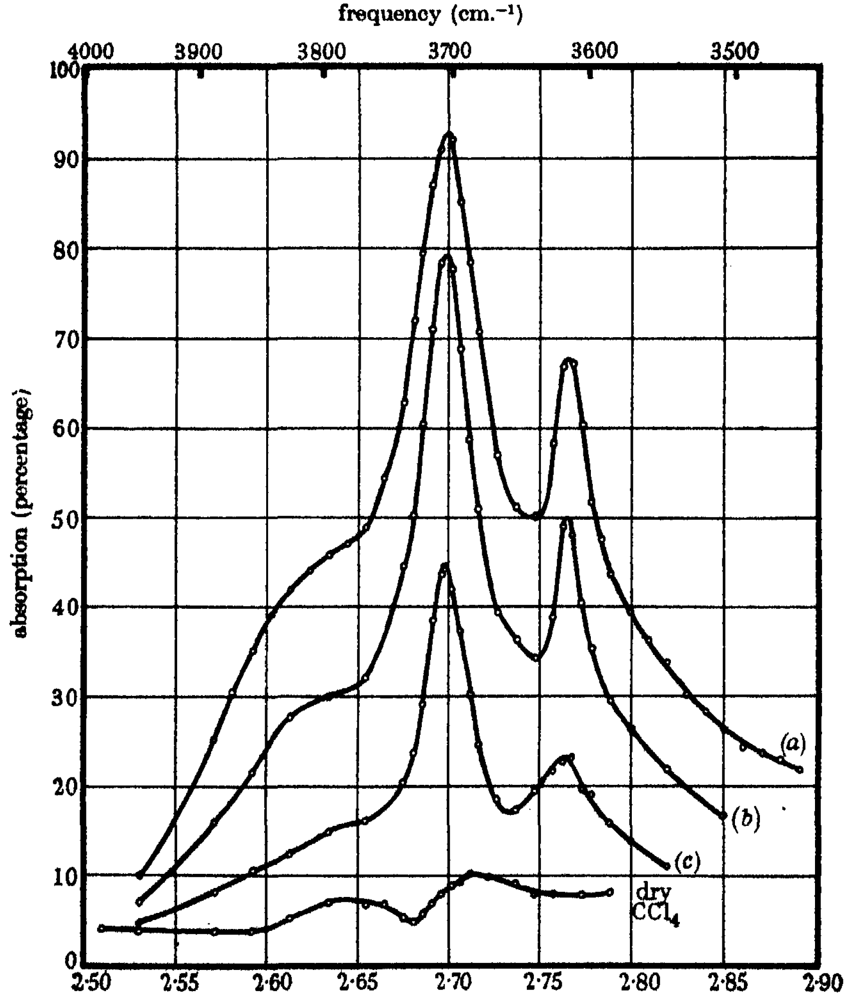

FIGURE 7. Absorption of carbon tetrachloride with water in solution: (*a*) 100 %, (*b*) 54·7 %, (*c*) 18·2 % saturated at 18·3° C. The break in the curve for dry carbon tetrachloride at 2·68μ is due to absorption of water vapour in the air in the blank cell.

diminution of the infra-red absorption, and a comparison was made with the weight of water collected. Typical absorption curves are shown in figure 7. The absorption cell was 5 cm. long, 2 cm. in diameter internally, and was made of brass. The end-plates were of fused silica, $\frac{1}{2}$ mm. thick: we may remark that this substance is excellent for the purpose, absorption being negligible up to about 4μ. The end-plates were attached to the tube with a trace of fish-glue, reinforced on the outside with shellac. The fish-glue was allowed to dry and the cell containing dry carbon tetrachloride left for several days. After this there was no noticeable tendency for perfectly dry carbon tetrachloride to pick up moisture from the cell. As a comparison cell a piece of brass tube with one silica window, equal in thickness to the two plates in the absorption cell, was used. In this way the reflexion losses and any absorption of the silica were practically allowed for, the measured absorption of the solution of water in the absorption cell being the combined absorption of carbon tetrachloride and water. A small correction to our results (figure 7) is necessary, since the optical path when using the comparison cell contains 5 cm. of air, with some water vapour, in place of 5 cm. of carbon tetrachloride in the absorption cell. Owing to the difference in optical path when the 5 cm. layer of carbon tetrachloride was substituted for the comparison cell, the cells were used with parallel radiation, obtained from a Nernst filament and rock-salt lens. A second lens collected the light passing through the cell and focused it on to the slit of the spectrometer.

TABLE 2. ABSORPTION OF CARBON TETRACHLORIDE CONTAINING VARYING AMOUNTS OF WATER (5 CM. CELL) IN RELATION TO THE CONCENTRATION OF WATER

Wave-length (μ)	d (dry CCl_4)	d_1 (*a*, figure 7; completely saturated)	d_1 (*b*, figure 7)	d_1 (*c*, figure 7)	Ratio d_1-d for partly dry CCl_4 to d_1-d for saturated CCl_4	
					(*b*)	(*c*)
2·592	0·018	0·188	0·105	0·051	0·512	0·194
2·613	0·024	0·236	0·140	0·058	0·547	0·161
2·634	0·032	0·267	0·155	0·070	0·524	0·162
2·654	0·031	0·290	0·168	0·076	0·529	0·174
2·675	0·024	0·428	0·254	0·099	0·570	0·186
2·696	0·036	1·181*	0·663	0·249	0·548	0·186
2·716	0·037	0·530	0·308	0·123	0·550	0·174
2·737	0·042	0·310	0·197	0·082	0·578	0·149
2·758	0·036	0·378	0·214	0·105	0·520	0·202
2·778	0·041	0·315	0·189	0·091	0·540	0·183
		Mean of all measurements			0·547	0·182
		By absorption of water with P_2O_5			0·565†	0·218‡

* Obtained from measurements with a 1 cm. cell.

† 3·0 mg. of water absorbed per 100 g. of saturated solution.

‡ 5·4 mg. of water absorbed per 100 g. of saturated solution.

With this arrangement there was no change of focus of the image on the slit when the absorption cell was replaced by the comparison cell.

In table 2 are given values for the optical density d at a few different wave-lengths for carbon tetrachloride with varying amounts of water in solution. d is defined as $\log I_0/I$, where I_0 is the radiation transmitted by the comparison cell and I the amount transmitted by the absorption cell. If d is the density at a given wave-length for thoroughly dry carbon tetrachloride and d_1 is the value for a solution of water in carbon tetrachloride, then $d_1 - d$ depends only on the absorption of the water and is corrected for the absorption of carbon tetrachloride and water vapour in the 5 cm. air path. The molecular extinction coefficient κ is $(d_1 - d)/cl$, where c is the concentration of water in moles per litre, and l is the cell length in cm. According to Beer's law $d_1 - d$ is proportional to the water content, and in figure 8 and table 2 it will be seen that within the limits of accuracy of the method this is the case. Our results correspond with a value 0·0069 g. of water per 100 g. of carbon tetrachloride saturated at 18·3° C. This value is in accord with the

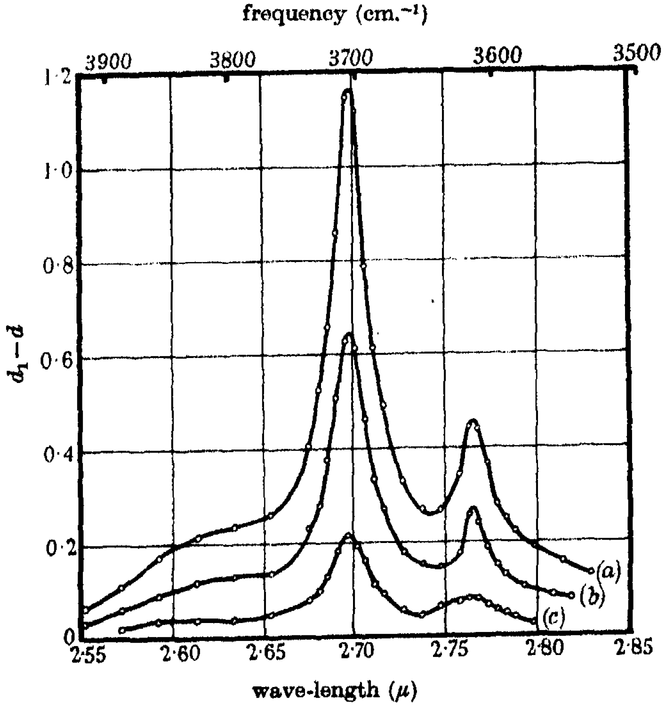

FIGURE 8. Absorption of water dissolved in carbon tetrachloride after correcting for the absorption of the latter: (*a*) 100 %, (*b*) 54·7 %, (*c*) 18·2 % saturated at 18·3° C.

determinations of Clifford (1921; 0·010 % at 24° C and 0·013 % at 28·5° C), and of Rosenbaum and Walton (1930; 0·0071 % at 10° C, 0·0084 % at 20° C, and 0·0109 % at 30° C, with an accuracy claimed to be better than 0·001 %).

Reference to figure 7 shows that a 50 mm. layer of carbon tetrachloride absorbs 10 % or less of the radiation between 2·5 and 2·8μ. A small negative peak of about 4 % at 2·68μ is due to the absorption of 5 cm. of moist air when the comparison cell was in use as already mentioned. Davies and Sutherland (1938*b*), however, found an absorption band in a 6·02 mm. layer of dry carbon tetrachloride with a maximum of 25 % absorption near 2·70μ. This absorption was attributed to carbon tetrachloride itself, but in view of the fact that their maximum occurs just where we find the main absorption peak of water dissolved in carbon tetrachloride, it seems likely that their carbon tetrachloride still contained a little water.

In figure 9 we have attempted to split up the absorption curve of water in carbon tetrachloride into its component parts. The area of each band is approximately 1·4$f\kappa$ max. (Fox and Martin 1938), where f is the band half-width in cm.$^{-1}$ and κ max. is the maximum value of the molecular extinction coefficient κ. On this basis ν_1 is 2·1 times as intense as ν_3, while we find the frequencies 3705 and 3614 cm.$^{-1}$, respectively, as compared with 3702 and 3611 cm.$^{-1}$ by Borst *et al.* (1938). Our frequencies are corrected to vacuum and are believed to be accurate to within 1 cm.$^{-1}$. The absorption curves shown in figure 8 are similar to those obtained by Borst *et al.*, but the fine structure on the bands found by these workers could not be repeated by us, although a very careful search was made. In our apparatus the whole of the optical path, with the exception of 1 ft. in the air of the room, was thoroughly dried and freed from CO_2 with P_2O_5 and stick potash. The infra-red absorption of water vapour in these conditions was small, so that the energy incident on the cell containing the carbon tetrachloride solution of water did not vary much over the region of absorption of water vapour about 3700 cm.$^{-1}$. Unless the precaution of removing water vapour was taken, the energy curve fluctuated violently due to the vibration-rotation bands of water vapour as the wave-length was varied. With such an uneven energy curve, if there were the slightest difference in alignment between the absorption cell and the comparison cell (which in this experiment was similar to the absorption cell and contained *thoroughly* dry carbon tetrachloride) a spurious structure was superimposed on the measured absorption curve (cf. Robertson and Fox 1928). By deliberately increasing the water-vapour content of our optical path we were able, in one experiment, to obtain a slight apparent structure on our water bands, something like that shown by

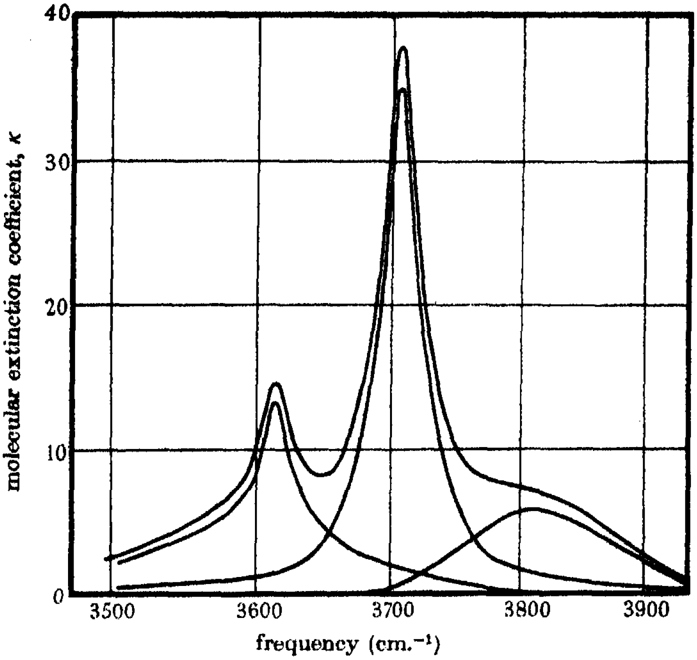

FIGURE 9. Graphical separation of the absorption bands of water in carbon tetrachloride.

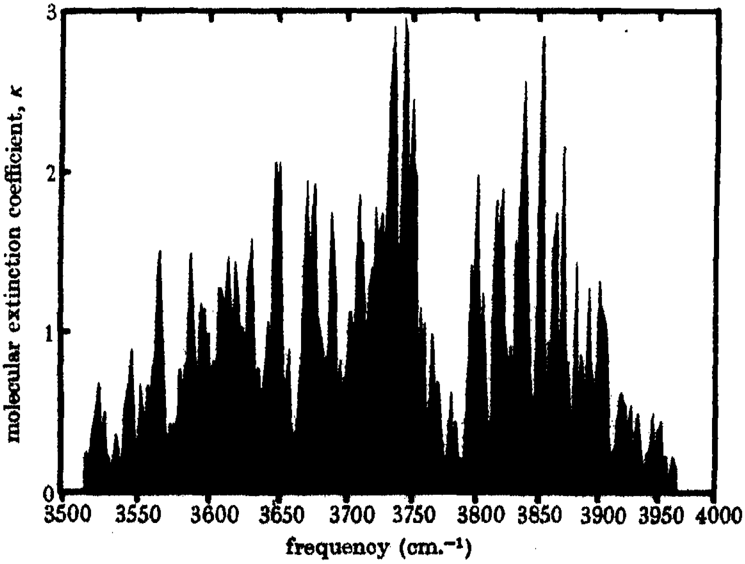

FIGURE 10. Absorption of water vapour in the region 2·5–2·85μ.

Rodebush *et al.* In our search for this fine structure we used smaller slits than we normally employ in order to have the best possible chance of resolving any fine structure.

Absorption of water vapour in the region 2·5–2·85μ

We have in our apparatus ample reserve of resolving power to find any significant structure of the order of 1–2 cm.$^{-1}$, and in order to compare the absorption of water in carbon tetrachloride with water as vapour we have explored the spectrum of the vapour in the region about 3700 cm.$^{-1}$. In figure 10 a general idea of the band system is given; the absorption for most of the band was less than 60 %. The individual peaks check well with the measurements of Plyler and Sleator (1931); a general picture of the band system obtained by these workers is not easily derived from their data. Figures 9 and 10 show the essential differences between the spectrum of water as vapour and in carbon tetrachloride solution. Allowing for the difficulty involved in comparing two such different spectra, the intensity of absorption of monomeric water would appear to be much smaller in the vapour state than when dissolved in carbon tetrachloride. We would here stress the fact that the individual rotational lines are suppressed in solution. We have found this to hold also for methane, ethane, ethylene and methyl bromide dissolved in carbon tetrachloride, and in these cases the absorption curve in solution is approximately the envelope of the vibration-rotation bands. As a further example of this, figure 11 shows the absorption curve for ethylene in solution in carbon tetrachloride as compared with the results of Levin and Meyer (1928) for the gas.

DISCUSSION

Infra-red absorption of monomeric water (water vapour and water in carbon tetrachloride)

The isolated water molecule has three modes of vibration, ν_1, ν_2 and ν_3, depicted approximately in figure 1. ν_1 and ν_2 are essentially O-H valency vibrations and are to be expected near 3700 cm.$^{-1}$, where such vibrations are generally found for hydroxy bodies. ν_3 is an angular deformation frequency and occurs at a much lower frequency; it is therefore easily distinguished from the others. The infra-red vibration frequencies for water vapour have been discussed by Mecke (1933), Baumann and Mecke (1933), Freudenberg and Mecke (1933) and by Bonner (1934), and the three fundamental frequencies from which the other bands can be derived have been given as follows:

$$\nu_1 = 3756{\cdot}5 \text{ cm.}^{-1}, \quad \nu_2 = 3604{\cdot}6 \text{ cm.}^{-1}, \quad \nu_3 = 1595{\cdot}5 \text{ cm.}^{-1}.$$

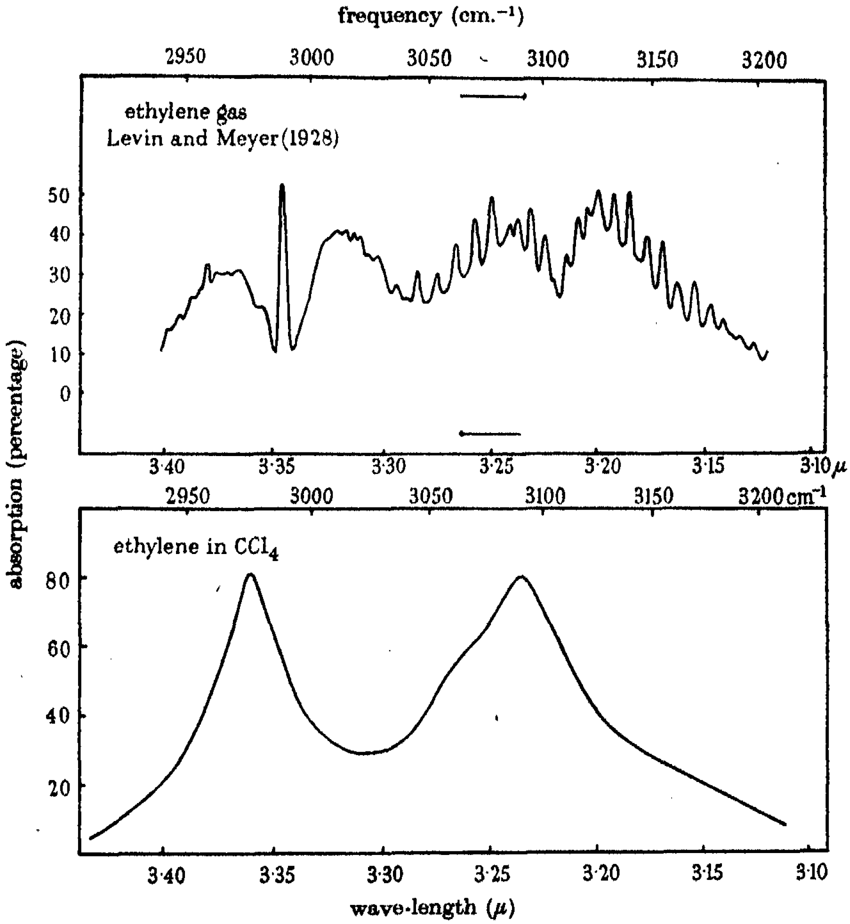

FIGURE 11. Suppression of the rotational structure of absorption bands of ethylene dissolved in carbon tetrachloride.

It should be noted that ν_2 is a calculated value and has not been directly observed in the infra-red spectrum of water vapour. Since it is a symmetrical vibration it is found in the Raman spectrum, but at 3654 cm.$^{-1}$ (Johnston and Walker 1932; Bender 1935) and not 3605 cm.$^{-1}$. Sutherland (1933) has suggested that a difference between a frequency observed in the infra-red and in the Raman spectrum might be due to the fact that the Raman frequency was obtained from measurements on the vapour at more than 760 mm. pressure, whereas the infra-red measurements were made on water vapour in the air at a pressure of a few mm. This is not borne out by experiments at different pressures in the infra-red, and further the Raman frequency at 3654 cm.$^{-1}$ in the vapour is only reduced to 3600 cm.$^{-1}$ in the liquid at 374° C (Cross *et al.* 1937), a frequency shift comparable with that which occurs with ν_1 (vapour) when water is dissolved in carbon tetrachloride. We believe that the discrepancy between the Raman and infra-red values for ν_2 lies in the limitations of the theoretical treatment (Bonner 1934). According to this worker if n_1, n_2 and n_3 are the quantum numbers associated with the three different fundamental modes of vibration, then the vibration frequency ν is given by

$$\nu = n_1x_1 + n_2x_2 + n_3x_3 + n_1^2x_{11} + n_2^2x_{22} + n_3^2x_{33} + n_1n_2x_{12} + n_1n_3x_{13} + n_2n_3x_{23}, \tag{1}$$

where x_1 to x_{23} are constants. The three fundamental frequencies are

$$\nu_1 = x_1 + x_{11}, \quad \nu_2 = x_2 + x_{22} \quad \text{and} \quad \nu_3 = x_3 + x_{33}.$$

Bonner studied seventeen well-known frequencies for water vapour and having used nine frequencies to evaluate x_1 to x_{23} was able to calculate the remaining eight. The agreement with observed values was very good except for ν_2. The reason for this discrepancy appears to be due to the fact that x_1 to x_{23} actually vary slightly from band to band, and this can be demonstrated simply as follows. Possible variations in x_3, x_{33}, x_{13} and x_{23} are avoided by considering only vibrations for which $n_3 = 0$. They are listed in table 3, and putting in the appropriate values in equation (1) we have

$$a = x_1 + x_{11} = \nu_1, \tag{2}$$

$$b = x_1 + x_{11} + x_2 + x_{22} + x_{12} = \nu_1 + \alpha + x_{22}, \tag{3}$$

$$c = x_1 + x_{11} + 2x_2 + 4x_{22} + 2x_{12} = \nu_1 + 2\alpha + 4x_{22}, \tag{4}$$

$$d = x_1 + x_{11} + 3x_2 + 9x_{22} + 3x_{12} = \nu_1 + 3\alpha + 9x_{22}, \tag{5}$$

$$e = x_1 + x_{11} + 4x_2 + 16x_{22} + 4x_{12} = \nu_1 + 4\alpha + 16x_{22}, \tag{6}$$

$$f = 3x_1 + 9x_{11} = \beta, \tag{7}$$

$$g = 3x_1 + 9x_{11} + x_2 + x_{22} + 3x_{12} = \beta + \gamma + x_{22}, \tag{8}$$

$$h = 3x_1 + 9x_{11} + 2x_2 + 4x_{22} + 6x_{12} = \beta + 2\gamma + 4x_{22}, \tag{9}$$

where $x_2 + x_{12} = \alpha, \quad 3x_1 + 9x_{11} = \beta \quad \text{and} \quad x_2 + 3x_{12} = \gamma.$

ν_1 and x_{22} can be calculated from equations (3), (4) and (5), and from (4), (5) and (6). The values are respectively 3750·6 and 3728·3 cm.$^{-1}$ for ν_1, and

$-71{\cdot}2$ and $-74{\cdot}9$ cm.$^{-1}$ for x_{22}. A third value for x_{22} can be obtained from equations (7), (8) and (9) and is $-54{\cdot}9$ cm.$^{-1}$. It is clear from this that x_{22} is not constant for the different sets of frequencies, and therefore the calculated value of ν_2, (x_2+x_{22}), will also be liable to some error. The calculations show that the tendency in equations (2)–(6) is for ν_1 to diminish as n_2 increases, and presumably ν_2 will similarly diminish as n_1 increases. Thus the calculated value of ν_2 is likely to be lower than the fundamental, for which $n_1 = 0$, and this is just what is found.

TABLE 3. VIBRATION FREQUENCIES OF WATER VAPOUR FOR WHICH $n_3 = 0$

Assignment			Observed frequency in water vapour (cm.$^{-1}$)	Assignment			Observed frequency in water vapour (cm.$^{-1}$)
n_1	n_2	n_3		n_1	n_2	n_3	
1	0	0	3756·5 $= a$	3	0	0	11032·36 $= f$
1	1	0	7253·0 $= b$	3	1	0	14318·77 $= g$
1	2	0	10613·12 $= c$	3	2	0	17495·48 $= h$
1	3	0	13830·92 $= d$				
1	4	0	16899·01 $= e$				

When water is dissolved in carbon tetrachloride two absorption bands are found near 3700 cm.$^{-1}$, and these have been identified as ν_1 and ν_2 by Rodebush *et al.* From our results (figure 9 and table 5) we find that ν_1 shifts from 3756 in the vapour to 3705 cm.$^{-1}$ in carbon tetrachloride, and that if we assume the second frequency to be ν_2 the shift is from 3654 in the vapour (Raman) to 3614 cm.$^{-1}$. The percentage frequency shifts are almost the same, as indeed is to be expected, since any alteration in the force constant of the O-H bond by surrounding molecules will affect the frequencies equally to a first approximation. The frequency shift of an OH or other group in a solvent or in the pure liquid is a measure of the interaction between the molecules of the solute and solvent, or between the solute molecules themselves. The frequency shift 40–50 cm.$^{-1}$ in carbon tetrachloride found for OH is much greater than the shift observed for CH groups (~ 6 cm.$^{-1}$ in carbon tetrachloride; Fox and Martin 1938), and this can be attributed to the fact that the dipole moment of OH is much greater than that of CH ($\sim 1{\cdot}7:0{\cdot}3$). The small band of water in carbon tetrachloride (figure 9) at about 3810 cm.$^{-1}$ is visible also in the curves of Rodebush *et al.*, and appears to follow the envelope of the rotation lines at about 3850 cm.$^{-1}$ in the vapour spectrum (figure 10). The band which occurs in carbon tetrachloride at 3614 cm.$^{-1}$ and which has been assumed to be ν_2 might likewise be regarded as the envelope of the rotation lines in that region, but in view of its sharpness and intensity compared with the band at 3810 cm.$^{-1}$, we believe that essentially it does represent the ν_2 frequency of the water molecule. In the vapour spectrum the ν_2 band system is doubtless masked by the intense ν_1 band, and the difficulty of locating the ν_2 band system has been discussed by Mecke (1933) in the light of Dennison's theory of the plane asymmetrical rotator (1931).

Infra-red absorption of ice and of liquid water at different temperatures

Curves showing the absorption of ice and of liquid water near 0° C and at a higher temperature are given in figures 3–5, and the frequencies of these bands will be found in table 1. There is a significant change in each band, both when ice melts and when water is heated to about 70° C, but the former change is much the greater. By far the most intense band is that at 3μ, and at room temperature κ max. is 55 as compared with 91 for phenol in carbon tetrachloride (Fox and Martin 1937); the band is, however, rather wider in the case of water. We have shown that many alcohols have a value of κ max. of about this magnitude, except in cases where association is exceptionally difficult, e.g. triphenylcarbinol. In carbon tetrachloride κ max. for water drops from 55 to 38 (figure 9), and in the vapour state to a much lower value (cf. figure 10 and p. 248). The high value for water in carbon tetrachloride shows that while the general shape of the absorption curve and position of the bands is not greatly altered in that solvent (cf. Buswell *et al.* 1938), the carbon tetrachloride molecules play quite an important part in the absorption phenomena. The foregoing measurements show that the intensity of absorption is very much increased on association, and since we know on general grounds that this is greatest in ice and diminishes as the temperature of water is raised, we should expect the absorption to vary accordingly. Figure 3 shows that this is the case. We see that when ice melts, the spectrum, both as regards intensity and position of the maximum, changes greatly, but that the change on raising the temperature of the water from 3 to 60° C is comparatively small, although in the right direction. It should be remembered that 3–60° is but a small part of the range of existence of liquid water: 0° to the critical temperature (374° C). Raman measurements (Cross *et al.* 1937) indicate that the association of water is almost broken down at 374° C, and at the rate at which the maximum shifts over the range studied by us, it appears probable that when a temperature of 374° C has been attained, the maximum will reach $2{\cdot}7\mu$ ($\sim$3700 cm.$^{-1}$), the position of the main peak in CCl_4. It is significant that the 3μ band of water rises sharply from $2{\cdot}7\mu$, which is the limiting wave-length for the O-H vibration. It is interesting to note that the ice band contains a small hump on the side in the position of the water band and presumably indicates a slight tendency towards the water structure in ice a little below the melting point.

The $4{\cdot}7\mu$ band (~ 2130 cm.$^{-1}$) which is absent in the vapour spectrum has been interpreted as a combination of the frequency ν_3 (figure 1), which is found at 1595 cm.$^{-1}$ in the vapour (~ 1650 in ice and water), and a frequency of hindered rotation ν_R of 601 cm.$^{-1}$ in ice and ~ 500 cm.$^{-1}$ in water (*vide infra*). This interpretation was first put forward by Ellis (1931), although at that time the evidence for a frequency ~ 500 cm.$^{-1}$ was meagre. The frequency ~ 2170 cm.$^{-1}$ which occurs in the Raman spectrum of liquid water has been explained in a similar manner (cf. Cross *et al.* 1937). Accordingly, to a first approximation we have

$$\nu_3' + \nu_R = 1644 + 601 = 2245 \text{ for ice (observed by us, 2222)}$$
$$\text{and } 1646 + 500 = 2146 \text{ for water (observed by us, 2128 at 21° C).}$$

The determinations of ν_R for water are not definite enough for us to check our measurements of the movement of the $4{\cdot}7\mu$ band in water at different temperatures. However, the frequency ν_R must diminish with rise of temperature until it finally vanishes in the vapour state, so that the $4{\cdot}7\mu$ band should tend to approach ν_3 (1595 cm.$^{-1}$). Figures 4 and 6 show that this is the case, and it is noteworthy that the observed rate of shift of the $4{\cdot}7\mu$ band is about that required. The intensity of this band is very much greater in ice, and in water diminishes fairly rapidly as the temperature is raised.

Our results for the 6μ band are somewhat less definite than for the other bands. Figure 5 shows that the intensity is less in ice than in water, and in the latter increases with rise of temperature. The shift as the temperature rises is towards longer wave-lengths as for the $4{\cdot}7\mu$ band, but the shift on changing to ice is small and probably not significant owing to the fact that the band in ice is broad and contains at least one other component at longer wave-lengths, of which there is a suggestion even in the water curves.

Both for the hindered rotation ν_R and for the hindered deformation vibration ν_3' in water and ice (figure 12), the hydrogen atoms may to a first approximation be considered as moving at right angles to the OH bonds, while the oxygen atom is almost stationary. Now $\nu_R = \frac{1}{2\pi}\sqrt{\frac{k_1}{m}}$, where m is the mass of a hydrogen atom and k_1 is the appropriate force constant, while for an isolated water molecule $\nu_3 = \frac{1}{2\pi}\sqrt{\frac{k_3}{m}}$, where k_3 is the force constant appropriate to this case. For the vibration ν_3' in water and ice both force constants come into play owing to the constraints imposed by surrounding molecules so that we may take $\nu_3' = \frac{1}{2\pi}\sqrt{\frac{k_1+k_2}{m}}$. Thus $\nu_3' = \sqrt{(\nu_3^2+\nu_R^2)}$, and since $\nu_3 = 1595$ cm.$^{-1}$ and $\nu_R = 601$ cm.$^{-1}$, $\nu_3' = 1704$ cm.$^{-1}$ in ice as compared with the observed value 1644 cm.$^{-1}$. In water $\nu_R \approx 500$ cm.$^{-1}$ and $\nu_3' = 1671$ cm.$^{-1}$ as compared with 1646 cm.$^{-1}$ (observed). The values calculated for ν_3' in ice and water may well be too high since the deformation force constant k_2 is likely to be lower in a 4 co-ordinated structure for which the HOH angle approaches 109° 28′ than in the isolated molecule where the angle is 104° 36′. Allowing for this effect, the qualitative agreement with experiment is satisfactory in that an increase of frequency is predicted on going from vapour to liquid or solid.

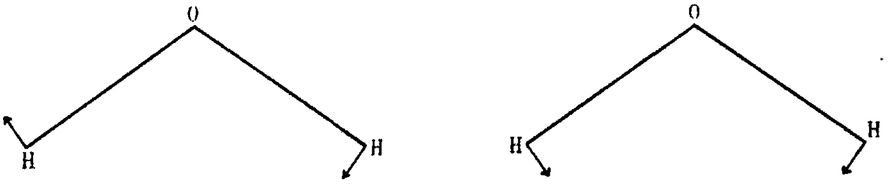

ν_R (water and ice) ν_3' (water and ice)

FIGURE 12

It is of interest to note that while in the water spectrum the 3μ band is much more intense than that at 6μ, in the vapour the opposite behaviour is found. Our observations show that in water with rise of temperature the 3μ band diminishes, while the 6μ band increases, so that there is now no difficulty in reconciling these facts.

For a long period it was thought that a number of the infra-red absorption bands of liquid water were to be attributed to a fundamental frequency near 6μ and harmonics of this, but it now becomes clear that the harmonics of ν_1, ν_2 and ν_3 are vanishingly small in liquid water. Among the seventeen frequencies of water vapour considered by Bonner there are only two harmonics ($\sim 3\nu_1$ and $\sim 2\nu_3$), and even these cannot be found in liquid water. We may make tentative assignments for the more important liquid water bands, assuming that a relation of the type used by Bonner (1) can be applied to the liquid. Since the water bands as determined by Collins (1925) are generally much sharper at his highest temperature (95° C), we have taken the data at this temperature and compared the values with those for the vapour. To calculate the eight observed frequencies, six constants in equation (1) have to be evaluated. The first three frequencies (denoted by †) were used and the remaining three constants were chosen to fit the other five frequencies as well as possible. The constants (notation of Bonner) are $x_1+x_{11} = 3453$, $x_2+x_{12} = 3594$, $x_3+x_{33} = 1640$, $x_{22} = -79$, $x_{23} = -110$, and $x_{13} = 62$ cm.$^{-1}$.

TABLE 4. ASSIGNMENT OF COMBINATION BANDS OF LIQUID WATER

Assignment			Frequency observed in vapour, cm.$^{-1}$	Frequency observed in liquid, at 95° C, cm.$^{-1}$	Frequency calculated in liquid, at 95° C, cm.$^{-1}$
n_1	n_2	n_3			
1	0	0	3756·5	3453*	3453†
0	0	1	1595·5	1640*	1640†
1	0	1	5332	5155	5155†
1	1	0	7253	6993	6968
1	1	1	8807	8547	8560
1	2	0	10613	10309	10325
1	2	1	12151	11834	11807
1	3	0	13831	13514	13524

* These are obtained from our measurements.

Since both ν_1 and ν_2 have considerably lower frequencies in the liquid than in the vapour, and increase with rise of temperature, it is to be expected that the combination frequencies of liquid water (table 4) which mainly involve n_1 and n_2 will behave similarly. ν_3 does of course show opposite behaviour to a slight degree but is quite swamped by the other two. It is satisfactory that the combination frequencies as assigned in the table are all lower than in the vapour. Further, Collins (1925) showed that for all these bands the frequency increased with rise of temperature, although less rapidly (expressed as a percentage) than ν_1 and ν_2. The assignments of table 4 are compatible with this decline of temperature dependence for higher combinations, and a reasonable explanation is that as the vibrational energy of the water molecule increases it becomes less and less affected by surrounding molecules.

To complete this discussion we may observe that liquid water has not been examined in any great detail in the far infra-red, but Cartwright (1935) has reported a band at 60μ (167 cm.$^{-1}$) in light and heavy water, and in ice. This frequency is also observed in the Raman spectrum and is regarded as a hindered translation frequency of a single water molecule in the water "lattice". Another low frequency at 500 cm.$^{-1}$ was found by Rubens and Ladenburg (1909) in the reflexion spectrum of water, and in the absorption spectrum by Cartwright (1936). This again has its counterpart in the Raman spectrum and is regarded as a frequency of hindered rotation of a water molecule in the water "lattice".

Raman data for water and ice

Many investigations of the Raman spectrum of water have been made, and although there are discrepancies in the results, the essential details are fairly clear and the data are summarized in table 5 and figure 6, together with infra-red frequencies for comparison. A very complete bibliography of the Raman investigations has been given by Hibben (1937), and still more recent measurements are due to Cross *et al.* (1937). The band ~ 3000 cm.$^{-1}$ has a complex structure which varies with temperature, both in ice and water, and its interpretation has been given in some detail by Cross *et al.*

The frequency ν_3 appears to be very weak or absent in the Raman spectrum of water vapour, weak but distinct in liquid water, and practically absent in ice. Under these conditions one can say little about the variation of this frequency with change of state, but it may be noted that Cross *et al.*, and Bauer and Magat (1938) have calculated the frequency increase to be expected on passing from vapour to ice and agree that it should be 70–80 cm.$^{-1}$. In checking this frequency shift these investigators compared the infra-red frequency 1595 cm.$^{-1}$ for the vapour with the Raman frequency 1630–1660 cm.$^{-1}$ in liquid water. This is open to the objection that the Raman frequency in water vapour *might* be different from 1595 (cf. the case of ν_2), and indeed Johnston and Walker (1932) claimed to find 1648 cm.$^{-1}$, a value which however has never been confirmed.

TABLE 5. RAMAN AND INFRA-RED FREQUENCIES OF WATER IN VARIOUS STATES

Monomeric water			Liquid water at 70° C		Liquid water at 0° C		Ice at 0° C	
(Gas) Raman	(Gas) I.R.	(CCl_4) I.R.	Raman	I.R.	Raman	I.R.	Raman	I.R.
	3756 (ν_1)	3705		3434		3379		3259
3654 (ν_2)		3614	3448*		3413*		3156†	
	1595 (ν_3)		1630–1660	1642	1630–1660	1650		1644
				2092	~2170	2149	2225‡	2222

* Maximum intensity of main band, Cross *et al.* (1937).
† Cross *et al.*
‡ Hibben (1937).

Besides the Raman frequencies shown in table 5 several workers have found frequencies less than 1000 cm.$^{-1}$. Magat (1934) gave 175, 500 and 740 cm.$^{-1}$ for water; Hibben, 144 and 440 cm.$^{-1}$ at 28° C, and 149 and 450 cm.$^{-1}$ at 88° C, in water, while in ice these shifts became 205 and 601 cm.$^{-1}$, and were much more distinct. Cross *et al.* found $\sim$ 200 and 320–1020 cm.$^{-1}$ for water at 40° C, and 210 cm.$^{-1}$ in ice. Considering these data together we have two well-defined shifts for ice, 205–210 and 601 cm.$^{-1}$, and less accurately $\sim$ 175 and $\sim$ 500 cm.$^{-1}$ for water. The lower frequency is described as a hindered translation ν_T and the higher as a hindered rotation or libration ν_R. Bernal and Tamm (1935) estimated these frequencies to be about 170 and 480 cm.$^{-1}$ in ice and used them to calculate the specific heat of ice at the melting point. Cross *et al.* have also calculated these frequencies approximately from the four co-ordinated structure to be discussed in the following section.

The structure of ice and liquid water

The arrangement of oxygen atoms in ice is known from X-ray studies (cf. Barnes 1929), and it is known that each oxygen atom is tetrahedrally surrounded by four others. The number of water molecules per c.c. is $\frac{3\sqrt{3}}{8r^3}$, where r is the O-O distance, and taking the density of ice at 0° C to be 0·9168 and Avogadro's number $6{\cdot}025 \times 10^{23}$, the O-O distance is found to be 2·77 A at 0° C and 2·73 A at 0° K, after allowance for the contraction of ice on cooling. There is less certainty about the positions of the hydrogen atoms, but the work of Pauling (1935) and Cross *et al.* makes it reasonable to place the hydrogen atoms on the O-O lines at a distance of about 1 A from the parent oxygen atom and 1·77 A from the oxygen atom which forms the hydrogen bond, so that each oxygen atom is tightly bound to two hydrogen atoms and loosely bound to two others. According to Bernal and Fowler (1933) this tetrahedral unit is built up to form a semi-crystalline lattice in liquid water. When a hydrogen bond forms, the frequency of the OH valency vibration is reduced considerably, as when water vapour becomes liquid and again when water changes to ice (table 5). Since both valency vibration frequencies are mainly determined by the OH force constant, any alteration of this by the fields of force of the surrounding molecules should affect both frequencies equally to a first approximation. The data for water vapour and ice are quite accurate and may be used to show that this is the case as follows:

$$\frac{\text{Infra-red frequency in water vapour}}{\text{Infra-red frequency in ice at } 0^\circ\text{ C}} = \frac{3756{\cdot}5}{3259} = 1{\cdot}153,$$

while $$\frac{\text{Raman frequency in water vapour}}{\text{Raman frequency in ice at } 0^\circ\text{ C}} = \frac{3654}{3156} = 1{\cdot}158.$$

The structure of liquid water proposed by Bernal and Fowler (1933) accounts satisfactorily for many of the physical properties of water, and it should be possible to adapt their ideas to our particular problem of explaining the infra-red data. The change which occurs when ice melts modifies profoundly the infra-red spectrum (figures 3–5) and yet the energy change (1·43 kcal./mole) is small compared with the total energy necessary to break completely all the hydrogen bonds, 11·6 ± 0·4 kcal./mole. Two possibilities arise: either the 1·43 kcal. is used in a general weakening of *all* the hydrogen bonds to the extent of about 12 %, or only a proportion of the hydrogen bonds is affected, but to a correspondingly greater degree. Actually the change in the hydrogen bonds must follow some form of probability curve; the number of bonds which are completely broken is small, but appreciable, since figure 3 shows that some water molecules absorb at a wave-length close to that of the isolated water molecule ($\sim 2 \cdot 7\mu$). Another small proportion of the bonds may be regarded as practically unchanged, but the majority are weakened by about 12 %, corresponding to the observed frequency changes 3259 to 3379 (infra-red) and 3156 to ~ 3400 (Raman).

We may consider at this point a more normal liquid than water, which we will suppose is made up of spherical molecules having no tendency to orient themselves in any particular manner with respect to each other. In this ideal liquid it is easy to show that one molecule can be surrounded by twelve others all touching it and each other, and if this form of packing is continued throughout the body of the liquid then the volume per molecule is $d^3/\sqrt{2}$, where d is the diameter of the molecule, i.e. the distance of closest approach of two molecules. If this ideal liquid has a density equal to that of water at the critical point, 0·4 g./cm.^{3}, then d turns out to be 4·7 A, and the distance apart of any two oxygen atoms of adjacent molecules in water at the critical point will also be about this value as compared with a distance of 2·77 A in ice at 0° C. At a distance of $\sim 4 \cdot 7$ A the intermolecular forces are known to be small, in agreement with the observation of Cross *et al.* that the Raman frequency only drops from 3654 in the vapour to 3600 cm.$^{-1}$ in water at the critical temperature. As water is cooled from the critical temperature, instead of one molecule being surrounded by some twelve others at a distance of $\sim 4 \cdot 7$ A, the molecules orient themselves with respect to each other more and more definitely as the temperature falls until finally the structure "locks" in the form of ice in which each molecule is surrounded by only four others, but at the much smaller distance of 2·77 A. If we assume that the part of the water absorption band at 3μ, for which λ is greater than λ max. of ice, is attributable to ice-like molecules, then only about one in three of the molecules in liquid water near 0° C can be in the same state as in ice (e.g., κ max. in ice is 120 while κ for water at the same wave-length is 46, figure 3), and probably the proportion is more like one in four or five when an allowance is made for a certain amount of "water structure" in ice. This suggests that a common unit in liquid water at the lower temperatures is one molecule surrounded by four others, each of these having one or both hydrogen atoms more or less free. This would allow one molecule in five to give the ice-like spectrum while the other four give OH valency frequencies, both in Raman and infra-red, intermediate between the values found for ice and water vapour, as experiment shows. If each group of five molecules is regarded as a spherical "molecule" around which twelve similar ones can be packed, then the diameter d can be found as indicated above and is 5·9 A, while in ice the average distance of closest approach of two such tetrahedral "molecules" is ~5·5 A (approximately twice the O-O distance). By packing twelve "molecules" round one we shall have on an average three for each of the four external oxygen atoms of the central "molecule", so that when water freezes only a comparatively slight rearrangement of the molecules is required.

[*Paragraph added* 8 *November* 1939.] It is of interest to examine these conclusions in the light of recent X-ray diffraction measurements on water, such as those of Morgan and Warren (1938). At 1·5° C the radial distribution curve shows a fairly sharp peak near 2·85 A corresponding to the average separation of the nearest oxygen atoms (cf. 2·77 A in ice), while a second rather diffuse peak at about 4·5 A is attributed to the second nearest neighbours O_1O_3 $(O_1\overset{O_2}{\diagup\,\diagdown}O_3)$. These values for O_1O_2 and O_1O_3 are consistent with the angle $O_1O_2O_3$ being close to the tetrahedral value for which $O_1O_3 = \sqrt{8/3}\,O_1O_2$. The half-area of the first peak indicates that each molecule has on the average ~2 nearest neighbours at a distance not more than 2·85 A, and this is in fair agreement with the idea of tetrahedral units mentioned above, since in any such group of five molecules the central one has four neighbours at a distance of ~2·77 A, while the other four have at least one neighbour each at this distance and others at greater distances ~3·5 A (for which considerable evidence is found in the radial distribution curve). The average number of neighbours at a distance ~2·77 A is at least $\frac{1\times4+4\times1}{5} = 1{\cdot}6$, as compared with ~2 up to 2·85 A (see above).

We desire to thank Mr R. Phipps for his aid in constructing some of the apparatus described and Mr F. S. Benge for assistance in many directions, especially in taking observations.

SUMMARY

1. The absorption spectrum of water in the form of gas, liquid, solid, and in solution in carbon tetrachloride has been investigated in the region 2·5–7·5μ.

2. In the liquid and solid the bands at 3, 4·7 and 6μ have been studied, and their variation with temperature in the liquid determined. The 3μ band moves to higher frequencies as the temperature increases, while the 4·7 and 6μ bands move in the opposite direction. This behaviour is attributed to hydrogen bonds between water molecules reducing the OH valency frequencies but increasing the angular deformation frequency by reason of the constraints imposed by the surrounding molecules. Since the hydrogen bonds are at their strongest in ice and become progressively weaker when ice melts and the temperature of the water is raised, we expect to find the frequencies in the order, ice—water at 0° C—water at 100° C—vapour, in accordance with the observations. The 4·7μ band is a combination of the deformation frequency and the frequency of hindered rotation ν_R, about 500 cm.$^{-1}$, which has previously been observed both in the Raman and infra-red spectra; its large temperature variation is due to the rapid diminution of ν_R with rise of temperature until finally it vanishes in the vapour state.

3. The absorption of water in carbon tetrachloride about 2·7μ has been studied and the results of Rodebush *et al.* confirmed, except that the suggestion of rotational structure reported by these workers could not be substantiated. Our values for the valency vibration frequencies are 3705 and 3614 cm.$^{-1}$, and are 40–50 cm.$^{-1}$ less than the corresponding vapour values. A rapid method of eliminating water from carbon tetrachloride (and some other solvents and solutions) is described, and a value obtained for the solubility of water in carbon tetrachloride.

4. Water vapour was examined in the region of 2·7μ and it was found that the apparent maximum value of the molecular extinction coefficient is only about 3, as compared with 38 for a solution in carbon tetrachloride, 55 for liquid water, and 120 for ice. The increase of intensity of absorption on association is thus very marked.

5. It is well known that there is a discrepancy between the Raman frequency 3654 (ν_2) and the value of 3605 deduced from infra-red data; it is shown to be due to the fact that while Bonner's relationship between the

fundamental and combination frequencies is a good approximation, it is not exact enough to give a reliable value for ν_2.

6. Some of the more important combination bands of liquid water are considered in relation to the vapour frequencies, and a law similar to that used by Bonner for the vapour frequencies appears to hold for the liquid. In each case the frequency in the liquid is lower than in the vapour, and so the observed shift to higher frequencies with rise of temperature naturally follows.

7. The structure of liquid water is briefly discussed, mainly from the point of view of its infra-red spectrum.

REFERENCES

Barnes, W. H. 1929 *Proc. Roy. Soc.* A, **125**, 670.
Bauer, E. and Magat, M. 1938 *J. Phys. Radium*, **9**, 319.
Baumann, W. and Mecke, R. 1933 *Z. Phys.* **81**, 445.
Bender, D. 1935 *Phys. Rev.* **47**, 252.
Bernal, J. D. and Fowler, R. H. 1933 *J. Chem. Phys.* **1**, 515.
Bernal, J. D. and Tamm, Ig. 1935 *Nature, Lond.*, **135**, 229.
Bode, G. 1909 *Ann. Phys., Lpz.*, (4), **30**, 326.
Bonner, L. G. 1934 *Phys. Rev.* **46**, 458.
Borst, L. B., Buswell, A. M. and Rodebush, W. H. 1938 *J. Chem. Phys.* **6**, 61.
Bosschieter, G. and Errera, J. 1937 *C.R. Acad. Sci., Paris*, **204**, 1719.
Buswell, A. M., Deitz, V. and Rodebush, W. H. 1937 *J. Chem. Phys.* **5**, 84.
Buswell, A. M., Rodebush, W. H. and Roy, M. F. 1938 *J. Amer. Chem. Soc.* **60**, 2239.
Cartwright, C. H. 1935 *Nature, Lond.*, **136**, 181.
— 1936 *Phys. Rev.* **49**, 470.
Clifford, C. W. 1921 *Industr. Engng Chem.* **13**, 628, 631.
Collins, J. R. 1925 *Phys. Rev.* **26**, 771.
— 1939 *Phys. Rev.* **55**, 470.
Cross, P. C., Burnham, J. and Leighton, P. A. 1937 *J. Amer. Chem. Soc.* **59**, 1134.
Davies, M. M. and Sutherland, G. B. B. M. 1938*a* *Nature, Lond.*, **141**, 372.
— — 1938*b* *J. Chem. Phys.* **6**, 755, 767.
Dennison, D. M. 1931 *Rev. Mod. Phys.* **3**, 280.
Ellis, J. W. 1931 *Phys. Rev.* **38**, 693.
Errera, J. 1937*a* *Trans. Faraday Soc.* **33**, 120.
— 1937*b* *J. Chim. Phys.* **34**, 617.
Errera, J. and Mollet, P. 1936 *Nature, Lond.*, **138**, 882.
Errera, J. and Sack, H. 1938 *Trans. Faraday Soc.* **34**, 728.
Fox, J. J. and Martin, A. E. 1937 *Proc. Roy. Soc.* A, **162**, 419
— — 1938 *Proc. Roy. Soc.* A, **167**, 257.
Freudenberg, K. and Mecke, R. 1933 *Z. Phys.* **81**, 465.
Ganz, E. 1937 *Ann. Phys., Lpz.*, (5), **28**, 445.
Hibben, J. H. 1937 *J. Chem. Phys.* **5**, 166.
Johnston, H. L. and Walker, M. K. 1932 *Phys. Rev.* **39**, 535.
Kinsey, E. L. and Ellis, J. W. 1937 *Phys. Rev.* **51**, 1074.
Levin, A. and Meyer, C. F. 1928 *J. Opt. Soc. Amer.* **16**, 137.
Magat, M. 1934 *J. Phys. Radium*, **5**, 347.

Magat, M. 1936 *Ann. Phys., Paris*, **6**, 108.
Mecke, R. 1933 *Z. Phys.* **81**, 313.
Morgan, J. and Warren, B. E. 1938 *J. Chem. Phys.* **6**, 666.
Pauling, L. 1935 *J. Amer. Chem. Soc.* **57**, 2680.
Plyler, E. K. 1924 *J. Opt. Soc. Amer.* **9**, 545.
— 1932 *Phys. Rev.* **39**, 77.
Plyler, E. K. and Cravon, C. J. 1934 *J. Chem. Phys.* **2**, 303.
Plyler, E. K. and Sleator, W. W. 1931 *Phys. Rev.* **37**, 1493.
Randall, H. M., Dennison, D. M., Ginsburg, N. and Weber, L. R. 1937 *Phys. Rev.* **52**, 160.
Robertson, R. R. and Fox, J. J. 1928 *Proc. Roy. Soc.* A, **119**, 128.
Rodebush 1938 *see* Borst, Buswell & Rodebush.
Rosenbaum, C. K. and Walton, J. H. 1930 *J. Amer. Chem. Soc.* **52**, 3568.
Rubens, H. and Ladenburg, E. 1909 *Verh. dtsch. phys. Ges.* **11**, 16.
Sleator, W. W. 1918 *Astrophys. J.* **48**, 125.
Sleator, W. W. and Phelps, E. R. 1925 *Astrophys. J.* **62**, 28.
Sutherland, G. B. B. M. 1933 *Proc. Roy. Soc.* A, **141**, 535.

The specific heat of superconducting mercury, indium and thallium

By A. D. Misener, *H. H. Wills Physics Laboratory, University of Bristol*

(*Communicated by J. D. Cockcroft, F.R.S.—Received* 25 *August* 1939)

INTRODUCTION

The application of thermodynamics to the transition between the superconducting and normal states in the presence of a magnetic field yields formulae by which the entropy difference and specific heat difference of the two states may be determined from measurements of the threshold magnetic field (Gorter and Casimir 1934). These determinations involve the deduction of the first and second derivatives of the threshold field curve. They have been made for a number of superconductors (Daunt and Mendelssohn 1937; Daunt, Horseman and Mendelssohn 1939) and in the case of tin the agreement with direct specific heat measurements is good (Keesom and van Leer 1938). The usual process of differentiating twice by visually determining the tangents to the curves, however, introduces a considerable experimental error.

The work described in this paper was undertaken to determine the difference in specific heats more accurately and to investigate the variation of specific heat with temperature of superconducting mercury, indium and thallium. The threshold field curves were accurately determined. By the method of least squares, polynomials were obtained which fitted these curves within the experimental uncertainty. The derivatives were then calculated mathematically from these polynomials and the desired values computed. The results, therefore, have the accuracy of the directly measured values. The validity of the results depends upon the accuracy with which the chosen formula represents the form of the threshold field curve. This curve has no simple form. A least square polynomial taken to sufficiently many terms may lay claim to being the best representation and therefore to justify the considerable labour involved in its determination. The number of terms to be included in the polynomial is determined by the necessity of fitting the experimental data over the complete temperature range.

The formula derived for the threshold-field curves are useful also in determining the threshold values near the transition temperature of the metal where direct determinations are difficult. These values are important for calculations of the depth of field penetration in superconductors (Appleyard, Bristow, London and Misener 1939).

METHOD

The experimental arrangement is illustrated in figure 1. The specimen (S) was in the form of a long cylinder (diam./length 1/50). To prevent oxidation it was cast in a thin walled glass capillary. On this capillary was wound a double layer search coil (C) consisting of 2000–3000 turns of 50 gauge copper wire. This was connected to a ballistic galvanometer. The sensitivity was such that with the coil at liquid helium temperatures a change in field of 0·2 G produced a millimeter deflexion. The specimen was held vertical in a narrow Dewar vessel (D) filled with liquid helium. On the surface of the Dewar vessel was wound a uniform single layer solenoid (F) twice the length of the specimen. This was surrounded by the liquid nitrogen jacket (N) which fitted inside the large solenoid (G) used to provide the external longitudinal magnetic field.

To determine the threshold field, the temperature was kept constant by controlling the vapour pressure over the liquid helium in D. A small current was passed through solenoid F, sufficient to produce a field of 0·7 G. This current was reversed. When the specimen was superconducting no flux through the search coil C was observed. A larger magnetic field was then applied by passing a suitable current through G. This was gradually increased, the current in F being periodically reversed. When the sum of the two fields exceeded the threshold field large deflexions were produced by the reversal of the small field *F*. This arises from the fact that when the threshold value is passed the flux due to fields of both *G* and *F* enter the specimen. Large deflexions were observed until the difference of the fields exceeded the threshold field. Then the specimen was always in the normal state and the change of flux produced by reversal of the current in *F* was solely that produced by *F* itself.

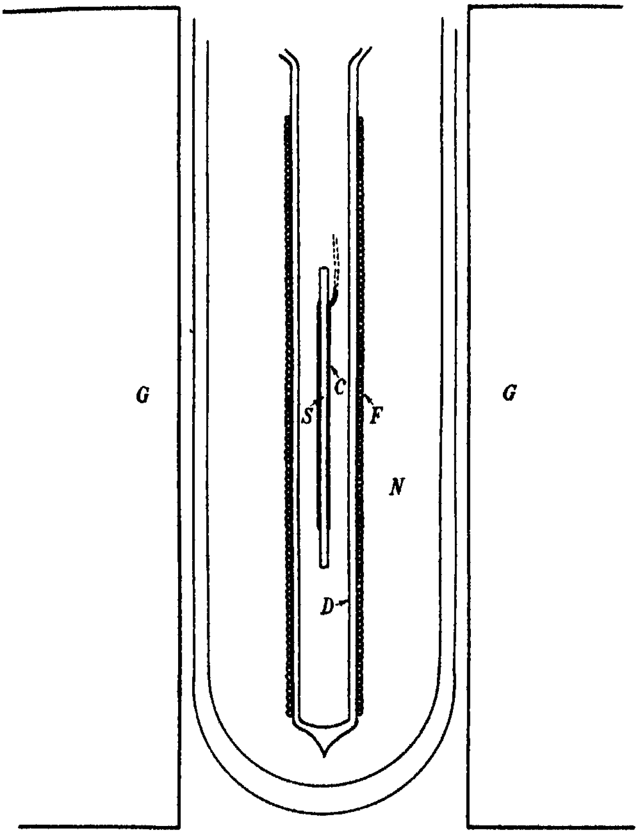

FIGURE 1

Figure 2 shows a typical set of readings taken near the transition point of the metal. The field which first penetrates the specimen is taken as the threshold field and is very accurately determined. Its value is obviously the field of *G* which first produces observable deflexions plus the field due to *F*. Correction was made for the earth's field and the small demagnetizing factor of the specimen when these were of the order of 0·1 % of the threshold field. The transition is seen to be accurately reversible. This proves the purity of the materials and is a necessary condition for the application of the thermodynamic treatment to the transition. It was tested in every case. The transition is abrupt but occupies a finite field interval. When corrected for the amplitude of the field of F this interval was never more than a few per cent of the threshold field.

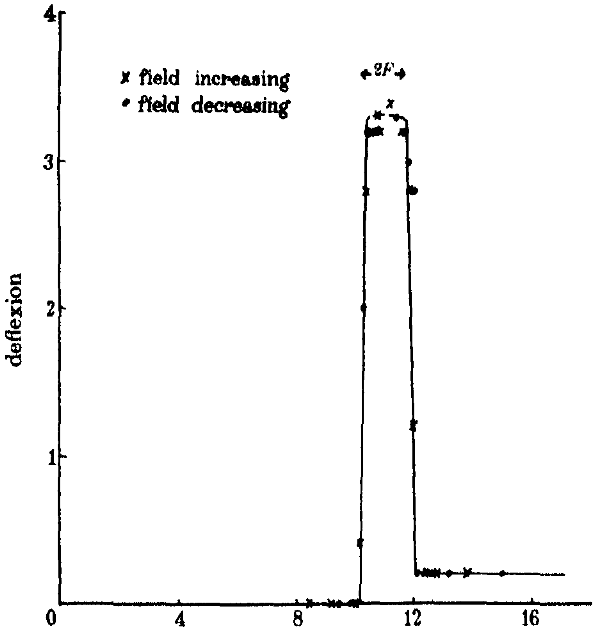

field due to solenoid G

FIGURE 2. Indium at 3·344° K

The metals were supplied by Hilger and Co. and were the purest obtainable from them. The purity as given by the manufacturer was mercury 99·999 %, thallium 99·995 %, indium 99·985 %. The fields produced by G were measured with a calibrated fluxmeter using search coils which had been compared with a standard mutual inductance. Temperatures were determined from the vapour pressures of the helium bath using the 1937 Leiden values. Vapour pressures below 4 cm. of mercury were read on a Macleod gauge.

RESULTS

Between 75 and 100 determinations of the threshold field of each metal were made at a variety of temperatures between the transition point and 1·1° K. Assuming a polynomial of the type

$$H_c = A + CT^2 + DT^3 + ET^4 + \dots$$

to fit these results, normal equations were computed from these determinations and the values of the coefficients evaluated. It was found that for mercury and thallium the terms beyond T^4 could be neglected; for indium the term in T^5 had to be included before the formula would fit all the experimental results within 0·3 G, the estimated experimental error. The formulae obtained were

Mercury: $H_c = 412{\cdot}58 - 19{\cdot}50T^2 - 2{\cdot}133T^3 + 0{\cdot}266T^4$.
Transition point = 4·167° K.

Thallium: $H_c = 170{\cdot}67 - 30{\cdot}93T^2 - 0{\cdot}193T^3 + 0{\cdot}219T^4$.
Transition point = 2·392° K.

Indium: $H_c = 269{\cdot}18 - 14{\cdot}86T^2 - 6{\cdot}840T^3 + 1{\cdot}299T^4 - 0{\cdot}015T^5$.
Transition point = 3·368° K.

Values of the critical field together with the difference in specific heat between the superconducting and the normal state calculated from these formulae are given in table 1.

The entropy difference, ΔS, between the normal and the superconducting state is calculated from

$$\Delta S = \frac{V}{4\pi} H_c \frac{dH_c}{dT},$$

where V is the atomic volume and the specific heat difference ΔC from

$$\Delta C = \frac{VT}{4\pi}\left[\left(\frac{dH_c}{dT}\right)^2 + H_c \frac{d^2H_c}{dT^2}\right)\Bigg].$$

Below 1·0° K the values must be regarded as extrapolated. They are, however, a better approximation to the actual values than is obtained by linear extrapolation from the last experimentally determined points.

The threshold field values for mercury and thallium agree well with those of Daunt and Mendelssohn (1937, 1939). Indium shows appreciably lower values. However, these agree with the values determined by resistance measurements made by the author on the same material (Misener 1938). The specific heat differences for thallium are in excellent agreement with the directly determined values of Keesom and Kok (1934) (table 2).

This agreement confirms the validity of the reasoning by which the specific heat differences have been derived from the threshold field curves. This has been previously verified only for the case of tin (Keesom and van Leer 1938).

TABLE 1

	Mercury			Indium			Thallium			
T °K	H_c gauss	ΔS 10^{-4} cal.	ΔC 10^{-4} cal.	H_c gauss	ΔS 10^{-4} cal.	ΔC 10^{-4} cal.	H_c gauss	ΔS 10^{-4} cal.	ΔC 10^{-4} cal.	T °K
0·0	412·6	—	—	269·2	—	—	170·7	—	—	0·0
0·1	412·4	−0·43	−0·41	269·0	−0·35	−0·36	170·4	−0·35	−0·34	0·1
0·2	411·8	0·87	0·79	268·5	0·71	0·72	169·4	0·69	0·68	0·2
0·3	410·8	1·33	1·14	267·7	1·07	1·00	167·9	1·02	0·99	0·3
0·4	409·3	1·79	1·46	266·4	1·43	1·37	165·7	1·34	1·26	0·4
0·5	407·5	2·25	1·74	264·7	1·78	1·63	162·9	1·65	1·49	0·5
0·6	405·1	2·72	1·98	262·5	2·13	1·96	159·5	1·98	1·66	0·6
0·7	402·4	3·19	2·18	259·9	2·48	2·30	155·5	2·20	1·76	0·7
0·8	399·1	3·66	2·34	256·7	2·73	2·63	150·9	2·44	1·77	0·8
0·9	395·4	4·12	2·45	253·0	3·07	2·94	145·6	2·64	1·70	0·9
1·0	391·2	−4·58	−2·52	248·8	−3·41	−3·28	139·8	−2·81	−1·46	1·0
1·1	386·5	5·02	2·53	244·0	3·75	3·51	133·3	2·95	1·23	1·1
1·2	381·4	5·45	2·48	238·6	4·07	3·70	126·3	3·04	0·82	1·2
1·3	375·7	5·87	2·38	232·6	4·36	3·70	118·6	3·08	−0·29	1·3
1·4	369·5	6·26	2·21	226·1	4·59	3·57	110·4	3·08	+0·39	1·4
1·5	362·9	6·64	1·98	219·1	4·83	3·12	101·5	3·03	1·20	1·5
1·6	355·7	6·98	1·67	211·3	5·02	2·73	92·1	2·92	2·16	1·6
1·7	348·0	7·30	1·30	203·2	5·17	2·11	82·2	2·76	3·28	1·7
1·8	339·8	7·60	0·84	194·5	5·28	1·33	71·6	2·53	4·54	1·8
1·9	331·0	7·85	−0·30	185·3	5·33	−0·40	60·5	2·25	5·97	1·9
2·0	321·8	−8·07	+0·32	175·3	−5·32	+0·67	48·9	−1·90	+7·55	2·0
2·1	312·0	8·25	1·03	165·0	5·26	1·89	36·7	1·49	9·29	2·1
2·2	301·8	8·39	1·84	154·1	5·13	3·28	24·0	1·02	11·18	2·2
2·3	291·0	8·49	2·71	142·7	4·96	4·83	10·8	0·49	13·23	2·3
2·4	279·6	8·54	3·75	130·9	4·72	6·36				2·4
2·5	267·8	8·54	4·86	118·7	4·39	7·83				2·5
2·6	255·5	8·49	6·08	106·1	4·07	9·78				2·6
2·7	242·6	8·39	7·41	93·1	3·67	11·43				2·7
2·8	229·3	8·23	8·86	79·8	3·22	13·37				2·8
2·9	215·4	8·01	10·45	66·2	2·72	14·90				2·9
3·0	201·1	−7·74	+12·15	52·4	−2·20	+16·67				3·0
3·1	186·3	7·40	13·98	38·3	1·62	18·92				3·1
3·2	171·0	7·01	15·95	24·1	1·03	20·40				3·2
3·3	155·2	6·56	18·05	9·8	0·43	22·47				3·3
3·4	139·0	6·04	20·29							3·4
3·5	122·3	5·46	22·68							3·5
3·6	105·2	4·82	25·21							3·6
3·7	87·6	4·11	27·88							3·7
3·8	69·6	3·34	30·71							3·8
3·9	51·2	2·51	33·71							3·9
4·0	32·3	−1·62	36·81							4·0
4·1	13·1	0·67	40·16							4·1

Table 2

Temp. ° K	ΔC 10^{-4} cal.	
	Misener	Keesom and Kok
1·4	0·39	0·4
1·5	1·20	1·4
2·0	7·55	7·5
2·1	9·29	9·25
2·2	11·18	11·2
2·3	13·23	13·3

According to Sommerfeld's theory the specific heat in the normal state, $C_n = \gamma T$, where

$$\gamma = \left(\frac{d\Delta S}{dT}\right)_{T=0} = \left(\frac{d\Delta C}{dT}\right)_{T\to 0}.$$

The γ values so obtained are given in table 3, where they are compared with those of Daunt and Mendelssohn (1937, 1939).

Table 3

	Misener	Daunt and Mendelssohn
Mercury	4·5	3·8
Indium	3·6	3·5
Thallium	3·4	2·8

The agreement for indium is good but the values for mercury and thallium are distinctly higher. The specific heat differences are shown in figure 3. There is no evidence of the inflexion in the curve for mercury found by Daunt and Mendelssohn (1937).

The specific heat of the metal in the superconductive state may be expressed as

$$C_s = \Delta C + \gamma T.$$

Curves showing the dependence of C_s on T are given in figure 4. The "reduced temperature" T/T_c (T_c = transition temperature) is used for the abscissae. The curves are seen to be of a much simpler form than those previously obtained (Daunt, Horseman and Mendelssohn 1939, Keesom and van Leer 1938). Also the specific heat is negligible only very close to the absolute zero.

By making a logarithmic plot, as in figure 5, it is seen that the specific heats of superconducting mercury and thallium follow at T^3 law with a high degree of accuracy. With indium this condition does not hold, the variation being according to T^4. This difference of behaviour may possibly be explained by difference of purity as the indium is the least pure of the metals used. Yet it seems difficult to attribute such a marked change of behaviour to 0·01 % of impurity, which was not sufficient to produce any observable hysteresis in the magnetic transition.

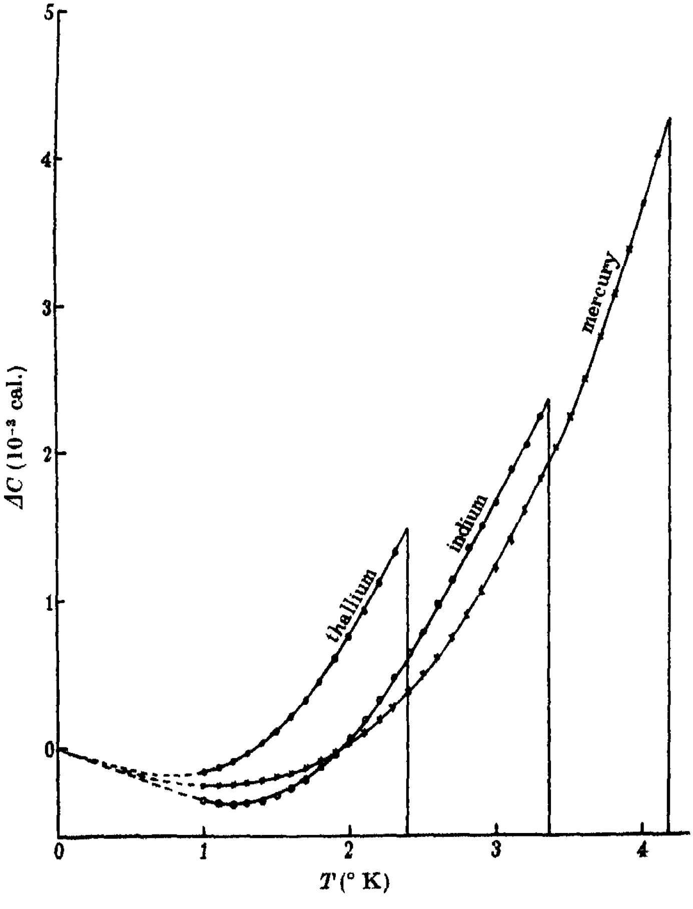

FIGURE 3

DISCUSSION

The estimated probable error of the experimental determinations of H_c is 0·3 G. The least square polynomial deduced from these values has, therefore, a probable error of less than 0·05 G. This assumes that the temperatures are accurately known. Down to 1·5° K the 1937 temperature scale is probably sufficiently accurate for the values of H_c to be correct to

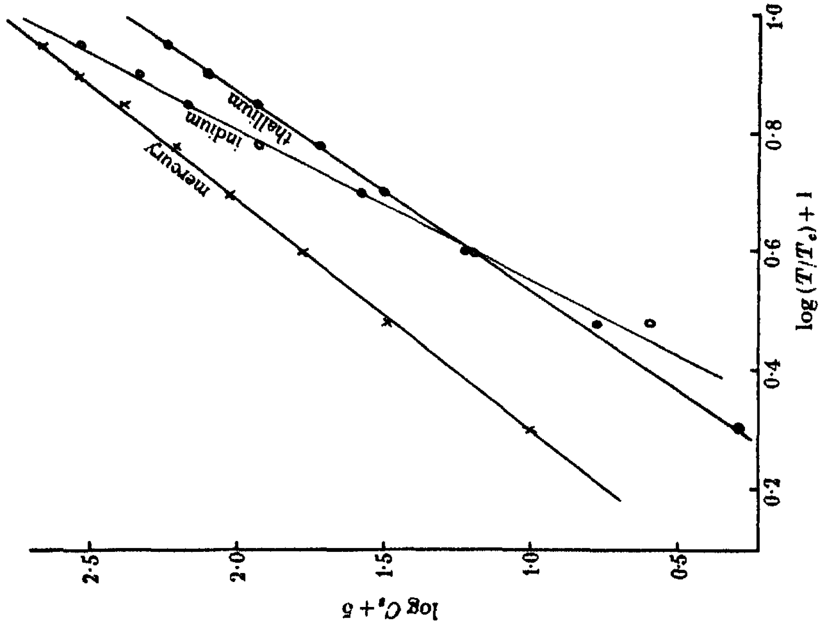

FIGURE 5

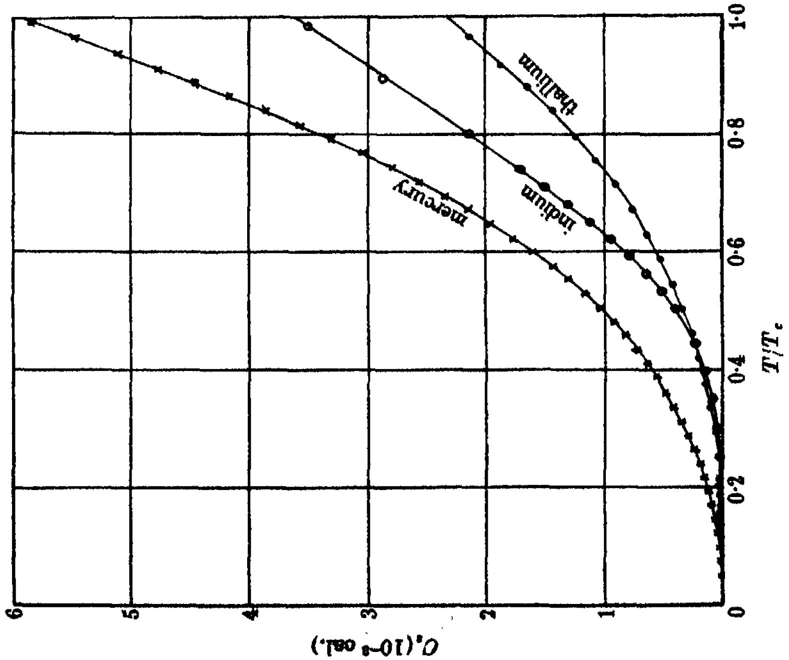

FIGURE 4

0·1 G. At lower temperatures a change of the temperature scale would change the threshold field values proportionally. A small systematic variation of temperature below, say, 1·5° K, would make no appreciable change in the coefficients of the polynomials, provided the large number of determinations above 1·5° K were made with the correct temperature scale or even with a scale subject to small random corrections. Hence a change of 0·01° K in the temperature scale at the lower temperatures would change the values of H_c, and all quantities derived therefrom, by 1 %, which may be taken as an estimate of the accuracy of the results.

Kok (1935) has fitted a polynomial to the early Leiden values of the threshold field of mercury. He obtained

$$H_c = 433{\cdot}0 - 89{\cdot}08T^2 + 60{\cdot}59T^3 - 18{\cdot}608T^4 + 1{\cdot}8774T^5.$$

The expression does not show such a satisfactory rapid decrease in the magnitude of the coefficients as the one found by the author, nor does he give any idea of the accuracy of the fit and the temperature range.

It is interesting to note that, in agreement with previous results (Daunt and Mendelssohn 1937, 1939) the total electronic entropies of mercury and indium calculated according to Sommerfeld's formula

$$S = 3{\cdot}26 \times 10^{-5} n^{\frac{1}{3}} \left(\frac{A}{d}\right)^{\frac{2}{3}} T$$

are substantially less than the observed entropy differences of the superconducting and normal states. The value for thallium is only slightly less. Table 4 is a comparison at 0·5° K where the formula might be expected to hold.

Table 4. $T = 0{\cdot}5°$ K

	n	S theor. 10^{-4} cal.	ΔS exp. 10^{-4} cal.
Mercury	2	1·18	2·25
Indium	3	1·42	1·78
Thallium	3	1·56	1·65

This work was carried out at the Royal Society Mond Laboratory, Cambridge and I wish to thank Dr J. D. Cockcroft both for placing the facilities of the laboratory at my disposal and for his advice and encouragement during the research. The late Dr E. T. S. Appleyard undertook the tedious duty of checking the computation of the polynomials. I am indebted to the Royal Commission for the Exhibition of 1851 for a scholarship during the tenure of which this work was carried out.

SUMMARY

Threshold field curves for mercury, indium and thallium were accurately determined by a magnetic method down to a temperature of 1·1° K. By least square methods, polynomials were fitted to these curves and from these the specific heat of the metals in the superconducting state was calculated using the formulae of Gorter and Casimir. The values obtained for thallium agree with the direct determinations of Keesom and Kok. The specific heat of superconducting mercury and thallium varies as T^3, that of indium as T^4.

REFERENCES

Appleyard, E. T. S., Bristow, J. R., London, H. and Misener, A. D. 1939 *Proc. Roy. Soc.* A, **172**, 540–558.
Daunt, J. G. and Mendelssohn, K. 1937 *Proc. Roy. Soc.* A, **160**, 127–136.
Daunt, J. G., Horseman, A. and Mendelssohn, K. 1939 *Phil. Mag.* **27**, 754–764.
Gorter, C. J. and Casimir, H. 1934 *Physica*, **1**, 305–320.
Keesom, W. H. and Kok, J. A. 1934 *Physica*, **1**, 175–181, 503–512, 595–608.
Keesom, W. H. and van Leer, P. H. 1938 *Physica*, **5**, 193–201.
Kok, J. A. 1935 Dissertation, Leiden.
Misener, A. D. 1938 *Proc. Roy. Soc.* A, **164**, 43.

The molecular spectrum of iodine excited by fluorescence (in the presence of nitrogen) and by active nitrogen

By A. Elliott, Ph.D., D.Sc.
Physics Department, The University of Sheffield

(*Communicated by S. R. Milner, F.R.S.—Received* 28 *September* 1939)

[Plates 12, 13]

Introduction

The fluorescence spectrum of iodine vapour in the presence of a large excess of foreign gas has been described by Oldenberg (1924) and by Duschinsky and Pringsheim (1935). Oldenberg noted a strong "continuum" with maximum intensity at about 3425 A, on which was superposed a series of diffuse bands, some weak bands about 9 A apart in the neighbourhood of 2700 A, several diffuse bands between 4900 and 4300 A, and a continuum at about 5100 A. The last, unlike the other bands, was shown to be present only when nitrogen was employed as foreign gas, and was attributed to a photochemical reaction between iodine and nitrogen. The "continuum" 3425 A (sometimes referred to as 3412 or 3460 A—the latter figure refers to the long wave-length limit of the spectrum) has often been observed in iodine spectra, e.g. in emission in a high-frequency discharge (Curtis and Evans 1933), in a Geissler tube (Konen 1898) and in absorption in iodine vapour at high temperature (Skorko 1933; Warren 1935), when it shows clear signs of structure. The diffuse band at 4300 is also well known in the literature of iodine spectra as the continuum 4300 A, and accompanies 3425 in emission spectra. It does not appear to have been observed in absorption.

Duschinsky and Pringsheim (1935*a*) photographed the 3425 A "continuum" and showed clearly that it contained sharp bands. They believed it to be made up of a genuine continuum with bands superposed on it, and doubted whether the bands and continuum formed part of the same system. At low pressures (a few cm. of mercury) of foreign gas the continuum predominates; at higher pressures the bands are relatively strong. Duschinsky and Pringsheim gave measurements of the wave numbers of the band heads, and obtained some regularity in the spacing of the heads, but did not succeed in making a satisfactory analysis. Measurements of the other bands excited by fluorescence in iodine with nitrogen present do not appear to have been made by them.

The present work is concerned with the bands near 2700 A and with the "continua" 3425 and 4300 A. Mention is also made of some new bands in the region 4630–4440 A. The "continua" are shown to consist of sharp bands when the pressure of foreign gas (nitrogen) is high, and it is extremely doubtful whether at low pressures any genuine continuum is produced. Rather the low pressure of foreign gas appears to allow the development of a large number of bands, whose overlapping gives the appearance of a continuum.

Plate 13, strips (*d*) and (*e*), shows these "continua" and bands under low dispersion. The bands near 2700 A may be seen on the high frequency side of the wave-length 2727 A, which is marked. Other wave-lengths referred to above are also indicated on plate 13.

EXPERIMENTAL

The iodine was contained in a clear quartz tube, on one end of which was sealed a quartz window. Light from an aluminium spark fell on the side of the tube, and the fluorescent light emerging from the window was examined spectroscopically. For the ultra-violet region, two quartz spectrographs were employed, namely, a Hilger E 2 instrument, and one giving a slightly greater dispersion constructed from a mounting originally intended for use with a plane grating. For the visible region, a dense flint prism was substituted for the quartz prism on this mounting. The spark was fed from a 64,000 V transformer (2 kVA output) with a bank of oil-immersed condensers in parallel with the gap.

When the quartz tube was filled with nitrogen at atmospheric pressure, and the spark operated, the green glow described by Oldenberg was observed, due to the continuum at 5100 A. After a few minutes' running, however, a fog appeared in the tube, due presumably to the formation of solid particles caused by photochemical union of iodine and nitrogen. This fog scattered the light from the spark strongly, and it was found necessary to sweep it away by streaming nitrogen through the tube continuously, otherwise the fluorescence spectrum would have had a strong aluminium spark spectrum superposed on it. It is intended to investigate the photochemical reaction at some future time.

Where the intensity of the spectrum was sufficient, Ilford thin film half-tone plates were employed; the graininess of these plates was quite negligible. For photographing the less intense portions, Ilford rapid process panchromatic plates were used. The appearance of the spectrum may be seen on reference to plate 12. The different band systems developed are considered in the following sections.

The band system 2520–2730 A

Reference to spectrum (*c*), plate 12, shows that these bands form a fairly compact system, degraded towards the red. The intensity distribution is remarkable in that the intensities of the bands fall off sharply at the long-wave end of the system, and very much less sharply at the other end. No doubt the high intensities of the bands at the long-wave end are partly spurious, due to the overlapping of bands in the sequences.

TABLE 1. WAVE-LENGTHS AND WAVE NUMBERS OF THE BAND HEADS IN THE REGION 2727–2524 A

λ in A	ν in cm.$^{-1}$	λ in A	ν in cm.$^{-1}$	λ in A	ν in cm.$^{-1}$
2727·4	36654	2646·5	37774	2586·6	38649
2720·7	36744	2644·6	37802	2583·4	38697
2714·2	36833	2642·3	37835	2580·3	38744
2704·7	36962	2637·9	37898	2577·2	38790
2703·6	36977	2635·6	37930	2574·1	38837
2702·5	36992	2633·2	37965	2570·8	38886
2696·6	37073	2626·7	38059	2567·9	38931
2695·4	37089	2624·2	38096	2564·6	38981
2694·4	37103	2622·7	38117	2561·6	39026
2687·3	37201	2617·6	38192	2558·4	39075
2686·0	37219	2614·9	38231	2555·1	39126
2679·0	37316	2611·3	38283	2552·4	39167
2677·4	37338	2608·3	38327	2548·9	39221
2668·7	37460	2605·7	38366	2545·4	39274
2665·7	37502	2601·9	38422	2543·0	39311
2664·0	37526	2599·1	38463	2539·4	39368
2660·0	37582	2596·5	38502	2533·5	39459
2655·3	37649	2592·9	38556	2524·2	39604
2651·2	37707	2589·9	38600	2513·9	39766

Wave-lengths and wave numbers of the band heads are given in table 1. The vibrational analysis is set out in the usual way in table 2 and shows satisfactory agreement between corresponding values of ω (the interval between consecutive bands in a progression). The average values of ω' vary from 96 to 93 cm.$^{-1}$, those of ω'' from 148 to 111 cm.$^{-1}$. At the short-wave end of the spectrum, the progression with $v' = 3$ can be extended to include four more bands which are, however, too faint for measurement. The v'' numbering has been assigned on the assumption that the last band observed is the 3–0 band. It is of course possible that more faint bands would be observed if the intensity of the spectrum or the time of exposure could be increased, but neither of these possibilities appeared feasible. In any case, a lower limit is set to the v'' numbering. With regard to the vibrational numbering in the upper electronic state, the progression with lowest v' is a progression of the strongest bands in the system and shows only a single maximum of intensity. It may therefore, according to the theory of Franck and Condon, be supposed to be composed of bands coming from the level $v' = 0$.

In table 2 a curve has been drawn through the strongest bands in each v'' progression (horizontal row). This curve is a Franck-Condon parabola of the "open" type corresponding to a considerable decrease in internuclear distance as a result of the change in electronic configuration, and is of the kind to be expected in a system with the vibrational frequencies $\omega' = 96{\cdot}5$ and $\omega'' = 158$ cm.$^{-1}$ (these values are obtained by extrapolation).

On plotting the interval ω between two consecutive bands in a v'' progression against the mean v'' for the two bands concerned, a graph is obtained which consists of two linear portions, with a change of slope at $v'' = 17$. Up to this value of v'', the band heads are represented by the formula

$$\nu = 39709 + 96{\cdot}5(v' + \tfrac{1}{2}) - 0{\cdot}3(v' + \tfrac{1}{2})^2 - 158(v'' + \tfrac{1}{2}) + 1{\cdot}1(v'' + \tfrac{1}{2})^2.$$

Owing to the small range of v' in the bands observed, the value 0·3 cm.$^{-1}$ for the constant $x_e\omega_e'$ must be regarded as very rough.

The band system 3450–3040 A (*the "continuum"* 3245 A)

A reproduction of the bands in this region is given in spectrum (*b*), plate 12 (fluorescence in iodine at room temperature, in the presence of nitrogen at a pressure of 1 atm.). The general distribution of intensity in the system is very similar to that in the bands described in the previous section, except that the fall in intensity from the maximum (at about 3420 A) is very much steeper. No bands have been recorded at wave-lengths greater than 3454 A, but in the other direction the system extends at least as far as 3040 A. Table 3 gives the wave-lengths, wave numbers and assignment of vibrational quantum numbers, together with the wave numbers calculated from the formula

$$\nu = 33744 + 104(v' + \tfrac{1}{2}) - 0{\cdot}2(v' + \tfrac{1}{2})^2 - 214{\cdot}26(v'' + \tfrac{1}{2}) + 0{\cdot}592(v'' + \tfrac{1}{2})^2.$$

The observations of Skorko (1933) and of Warren (1935), who have obtained some of the bands in absorption at high temperatures, made it very likely that the lower state was that of the normal iodine molecule, and the known vibrational constants for that state (Jevons 1932) have been inserted

TABLE 2. VIBRATIONAL SCHEME FOR BANDS IN THE REGION 2727–2524 A

$v' \backslash v''$	4		5		6		7		8		9		10		11		12		13		14		15		16		17		18		19		20		21		22		23		24
0									38502	136	38366	135	38231	135	38096	131	37965	130	37835	128	37707	125	37582	122	37400	122	37338	119	37219	116	37103	111	36992								
									98		97		96		96		94		95		95								97		98		97								
1									38600	137	38463	136	38327	135	38192	133	38059	129	37930	128	37802								37316	115	37201	112	37089	112	36977						
									97		93		95		91						96														96						
2	39274	148	39126	145	38981	144	38837	140	38697	141	38556	134	38422	139	38283						37898	124	37774	125	37649	123	37526								37073	111	36962				
	94		95		94		94		93		93																														
3	39368	147	39221	146	39075	144	38931	141	38790	141	38649																														36833
	91		90		92		95		96		95																														
4	39459	148	39311	144	39167	141	39026	140	38886	142	38744																														

in the formula above. The constants for the upper state have been chosen to secure the best fit with the observed wave numbers, but $x_e\omega_e'$ is subject to considerable uncertainty. Owing to the fragmentary nature of the progressions, it would not serve any useful purpose to give a scheme such as that in table 2 for these bands, but table 4 is given to show roughly the intensity

TABLE 3. WAVE-LENGTHS AND WAVE NUMBERS OF THE BAND HEADS IN THE REGION 3450–3040 A

Band	λ in A	ν obs. (cm.$^{-1}$)	ν calc. (cm.$^{-1}$)	Band	λ in A	ν obs. (cm.$^{-1}$)	ν calc. (cm.$^{-1}$)
*	3454·1	28943		*	3237·5	30879	
8–28	3448·2	28992	28988	*	3234·6	30907	
*	3441·6	29048		9–18	3229·9	30952	30954
7–27	3438·9	29071	29068	*	3224·3	31006	
*	3435·8	29097		*	3222·2	31026	
4–25	3431·4	29134	29129	8–17	3219·9	31048	31046
8–27	3427·2	29170	29169	*	3214·3	31102	
12–29	3423·6	29201	29208	*	3211·9	31125	
7–26	3418·8	29242	29250	9–17	3209·7	31147	31147
9–27	3413·3	29272	29270	8–16	3199·9	31242	31240
4–24	3409·7	29320	29314	*	3197·1	31269	
8–26	3406·3	29349	29351	9–16	3189·3	31346	31341
1–22	3403·3	29375	29378	*	3184·8	31390	
3–23	3400·6	29398	29397	12–17	3178·8	31449	31446
5–24	3397·8	29422	29416	*	3172·8	31516	
9–26	3394·7	29449	29452	11–16	3169·6	31541	31541
2–22	3391·3	29479	29482	*	3165·7	31579	
4–23	3388·9	29500	29500	12–16	3159·2	31644	31640
10–26	3382·9	29552	29552	11–15	3149·5	31742	31736
1–21	3381·2	29567	29566	*	3146·4	31773	
3–22	3379·2	29584	29584	10–14	3140·2	31836	31833
5–23	3377·0	29604	29602	*	3136·9	31869	
9–25	3374·1	29629	29635	*	3133·4	31905	
0–20	3371·6	29651	29652	11–14	3130·6	31934	31933
2–21	3369·7	29668	29670	*	3128·5	31955	
4–22	3367·6	29686	29687	*	3124·3	31998	
10–25	3362·6	29730	29735	10–13	3121·0	32032	32031
1–20	3359·9	29754	29755	11–13	3111·4	32131	32131
3–21	3357·9	29772	29772	*	3097·9	32271	
5–22	3356·0	29789	29789	*	3089·2	32361	
7–23	3354·3	29804	29804	*	3085·5	32400	
2–20	3348·1	29859	29859	*	3075·1	32510	
4–21	3346·4	29874	29875	*	3065·9	32607	
3–20	3336·5	29963	29961	*	3057·3	32699	
5–21	3334·9	29977	29977	*	3053·4	32741	
8–18	3240·6	30850	30853	*	3048·5	32794	
				*	3040·4	32881	

* Indicates that a band has not been classified.

distribution. The fact that ω'' is very nearly twice as great as ω' gives rise to a phenomenon already noted in the ${}^1\Sigma_u^+ \leftarrow {}^1\Sigma_g^+$ absorption system of iodine (Warren 1935), namely, that in part of the spectrum a number of progressions coincide more or less exactly to give the appearance of a single progression of bands, which appear diffuse if the coincidence is not exact. Measurements in the region where this occurs have not been made, as they are quite useless for the purpose of analysis; this accounts for the gap in table 3 between 29,977 and 30,850 cm.$^{-1}$, and for the omission from table 4 of the bands in the neighbourhood of a line joining 7–16 and 2–19. This fact must be kept in mind in considering the intensity distribution shown in table 4. The distribution of intensity supports Warren's suggestion that the long-wave "edge" or limit of the system can be explained in terms of the Franck-Condon theory of intensities, as was done by Loomis and Nile (1928) for the bands of Na_2. I have calculated the potential energy functions for the two I_2 electronic levels here concerned, and obtain as the locus of strong transitions the broken curve in table 4. The data employed for the upper electronic state are as follows: $\omega_e = 104$ cm.$^{-1}$, $x_e\omega_e = 0{\cdot}2$ cm.$^{-1}$, $r_e = 3{\cdot}3$ A, $D_e = 33{,}291$ cm.$^{-1}$.

TABLE 4. VIBRATIONAL SCHEME FOR BANDS IN THE REGION 3650–3040 A.

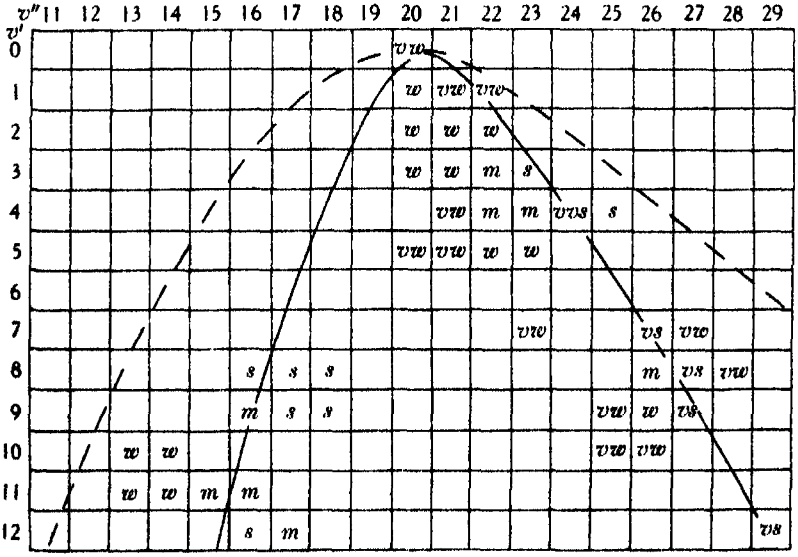

v'' v'	11	12	13	14	15	16	17	18	19	20	21	22	23	24	25	26	27	28	29
0										*vw*									
1										*w*	*vw*	*vw*							
2										*w*	*w*	*w*							
3										*w*	*w*	*m*	*s*						
4											*vw*	*m*	*m*	*vvs*	*s*				
5										*vw*	*vw*	*w*	*w*						
6																			
7													*vw*			*vs*	*vw*		
8						*s*	*s*	*s*								*m*	*vs*	*vw*	
9						*m*	*s*	*s*							*vw*	*w*	*vs*		
10			*w*	*w*											*vw*	*vw*			
11			*w*	*w*	*m*	*m*													
12						*s*	*m*												*vs*

r_e is estimated from Morse's relation $\omega_e r_e^3$ = constant. The relation does not hold exactly, for $\omega_e r_e^3$ has values 4020 and 3500 for the two states concerned in the visible absorption bands of iodine. A mean value 3700 has been used for this product. D_e is calculated on the assumption (Mulliken 1934) that the $^1\Sigma_u^+$ level here concerned dissociates to give iodine atoms in the $^2\mathrm{P}_{\frac{3}{2}}$ and $^2\mathrm{P}_{\frac{1}{2}}$ states respectively. The work of dissociation, D_e, is given by adding the energy of the products of dissociation (54,632 cm.$^{-1}$) to the work of dissociation for the normal state (12,435 cm.$^{-1}$) and subtracting the energy of electronic excitation of the $^1\Sigma_u^+$ level (33,744 cm.$^{-1}$).

The agreement in position between the theoretical locus of greatest intensity in a horizontal row and the locus of greatest observed intensities is very imperfect, though the two are of the same type, and coincide in the progression with $v' = 0$. The data available for constructing the curve for the upper state are, however, very imperfect, and it is not surprising that there should be some discrepancy between theory and observation.

The processes involved in the production of the band system under consideration appear to be as follows: Light from the aluminium spark, of wave-lengths 1854 and 1862 A, is absorbed by cold iodine vapour (most of the molecules of which have zero vibrational quantum number) and the molecules are raised to the $^1\Sigma_u^+$ level, with a very considerable amount of vibrational energy. In the absence of foreign gas, fluorescence of the ordinary type takes place (Oldenberg 1924; Duschinsky, Hirschlaff and Pringsheim 1935), and some of the molecules return to the various vibrational levels of the normal $^1\Sigma_g^+$ state. Other molecules undergo transitions which lead to the emission of the McLennan bands (McLennan 1914); the nature of these transitions is still obscure (Duschinsky and Pringsheim 1935*b*). In the presence of foreign gas, however, the excited molecules hand over some of their vibrational energy during collisions with the foreign gas molecules, and as a result there is a concentration of iodine molecules in the lower vibrational levels of the $^1\Sigma_u^+$ state; the rotational energies of these molecules will be affected by the collision processes and will, if collisions are numerous enough, be distributed more or less according to the Maxwell-Boltzmann law. Transitions will occur to that part of the $^1\Sigma_g^+$ potential energy curve lying immediately below the minimum of the $^1\Sigma_u^+$ potential energy curve; this portion corresponds to twenty quanta of vibrational energy. The resulting band spectrum, with its peculiar intensity distribution, is the one described in this section.

The mechanism described above accounts satisfactorily for the observation of Gerlach and Gromann (1923) that the "continuum" 3425 is very prominent in a discharge tube spectrum at high temperatures. At high temperatures, an appreciable number of molecules in the normal state will have vibrational energies of twenty or more quanta. Excitation of these molecules to the $^1\Sigma_u^+$ level will result in an appreciable concentration of molecules in the lower vibrational states of this level, for, according to the Franck-Condon principle, transitions will occur chiefly without change of internuclear distance. The return of the molecules to the normal state will be accompanied by emission of the 3425 "continuum". The spectrum so emitted will contain bands originating from many vibrational levels of the $^1\Sigma_u^+$ state and will therefore appear as a continuum.

The band system 4321–4041 A (*the "continuum"* 4300 A)

The appearance of this system (plate 12, spectrum (*a*)) is strikingly similar to that of the system dealt with in the preceding section, but the intensity of the whole system is very much lower. Wave-lengths and wave numbers of the band heads are given in table 5. It has not been possible to make a satisfactory analysis here, but it seems certain that in these bands, as in those of the last section, ω'' is very nearly twice as great as ω'; the difficulty of analysis is probably due to this feature. The vibrational frequencies ω' and ω'' lie between 90 and 100, and 190 and 200 cm.$^{-1}$ respectively. No doubt the peculiar intensity distribution (a very sharp fall on the long wave side, giving the appearance of an "edge") is due to the same cause as in the bands in the region 3450–3040 A. It should be pointed out that, although there appears to be a fairly long progression of strong bands in the system, the intervals between consecutive bands are sufficiently irregular to show that it is not really a single progression.

TABLE 5. WAVE-LENGTHS AND WAVE NUMBERS OF THE BAND HEADS IN THE SYSTEM 4321–4041 A

λ in A	ν in cm.$^{-1}$	λ in A	ν in cm.$^{-1}$	λ in A	ν in cm.$^{-1}$
4321·4	23134	4264·5	23443	4180·8	23912
4316·9	23158	4260·8	23463	4175·9	23940
4312·8	23180	4256·3	23488	4171·9	23963
4308·4	23204	4253·4	23504	4158·6	24040
4306·0	23217	4247·6	23536	4147·0	24107
4303·2	23232	4244·1	23555	4141·3	24140
4298·4	23258	4241·1	23572	4132·1	24194
4293·4	23285	4237·9	23590	4124·4	24239
4290·1	23303	4227·5	23648	4107·0	24342
4286·9	23320	4209·9	23747	4090·2	24442
4282·0	23347	4205·6	23771	4086·7	24463
4277·1	23374	4202·6	23788	4078·8	24510
4274·7	23387	4197·0	23820	4073·3	24543
4272·3	23400	4193·1	23842	4057·1	24641
4268·8	23419	4188·5	23868	4041·2	24738

The band system 4630–4440 A

These bands differ from all the others with which the present work is concerned in that they degrade to the violet, indicating that $\omega' > \omega''$. As may be seen from plate 12, spectrum (*a*), the system contains only a small number of heads, of which the most intense by far is situated at 4596 A. Table 6 gives the wave-lengths and wave numbers of the band heads. There are indications of a progression with successive intervals of 126 and 132 cm.$^{-1}$, with the intervals increasing towards the high-frequency end of the spectrum; hence these intervals are presumably those between successive vibrational levels of the lower electronic state concerned. The analysis is by no means clear, however, chiefly owing to the small number of bands developed under the conditions of observation. It has yet to be established whether the emitter of these bands is an iodine molecule, since they have been observed only in the presence of iodine and nitrogen.

TABLE 6. WAVE-LENGTHS AND WAVE NUMBERS OF THE BAND HEADS IN THE SYSTEM 4630–4440 A

λ in A	ν in cm.$^{-1}$	λ in A	ν in cm.$^{-1}$	λ in A	ν in cm.$^{-1}$
4630·2	21591	4576·4	21845	4523·4	22101
4622·1	21629	4569·5	21878	4515·4	22140
4613·6	21669	4556·6	21940	4503·0	22201
4609·3	21689	4549·8	21973	4495·7	22237
4601·5	21726	4542·1	22010	4446·6	22483
4596·0	21752	4530·2	22068	4440·8	22512
4589·2	21784				

The influence of excitation conditions upon the spectra produced

In an attempt to correlate the various band systems here described with the electronic levels of I_2, fluorescence spectra of iodine have been photographed using various pressures of nitrogen up to 1 atm. As far as possible, the same exposure was given for each of these spectra, which may be seen on reference to plate 13. In addition to the fluorescence spectra, the spectrum of iodine excited by active nitrogen (which was observed by Fowler and Strutt 1923) is reproduced on this plate. All these spectra were photographed on Ilford Rapid Process Panchromatic plates. A detailed photometric comparison of the intensities of the bands under various conditions of excitation would be very difficult to carry out satisfactorily, and has not been attempted. The main features revealed by visual inspection (some of which have been noted by Oldenberg 1924) are as follows:

The fluorescence band system $^1\Sigma_u^+ \rightarrow {}^1\Sigma_g^+$, which forms the 3425 "continuum", is very weak at low-nitrogen pressures, and increases in intensity with increasing nitrogen pressure up to about 2 cm. pressure (of mercury). At higher pressures still, the intensity of the higher frequency part of this system is reduced, but the intensity of the maximum increases slowly up to a pressure of at least 1 atm. of nitrogen. The individual bands in the system are easily seen in the original plate at 10 cm. nitrogen pressure, but are much clearer with a pressure of nitrogen of 1 atm. When excited by active nitrogen at a pressure of 2 cm. of mercury, the system shows the individual bands much more distinctly than does the fluorescence spectrum with the same pressure of nitrogen, though the reproduction does not show this very well, owing to the limited range of density which the bromide print can reproduce. Little trace, if any, of McLennan's diffuse bands (which appear on the fluorescence spectrum taken in pure iodine vapour) can be seen in the spectrum excited by active nitrogen at a pressure of 2 cm. of mercury, though they show quite distinctly in the fluorescence spectrum with nitrogen pressures up to 10 cm.

In fluorescence, the band system 2727–2524 A first appears distinctly at about 10 cm. pressure of nitrogen, and does not alter greatly in intensity when the pressure of nitrogen is increased to 1 atm. This system is very feeble in active nitrogen, and the individual bands of which it is composed do not show up at all clearly.

The band system 4321–4041 A (the "continuum" 4300) is situated in a region where the McLennan bands are strong, and estimates of intensity at low pressures may be falsified thereby. It is clear, however, that this system suffers a considerable reduction in intensity when the pressure of nitrogen is increased from 10 cm. of mercury to 1 atm. The system is relatively strong in the spectrum excited by active nitrogen.

The intensity of the band system 4630–4440 A increases with increasing pressure of nitrogen up to about 2 cm. pressure, after which further increase of pressure causes a diminution of intensity. What appears to be a continuation of the same system shows in the spectrum, excited by active nitrogen, as a row of nearly equally spaced diffuse bands, which can be followed nearly to 4300 A.

Besides these band systems, which have been considered in some detail, there are several apparently diffuse or continuous bands in the spectra shown on plate 13, quite apart from the McLennan bands. There are two such bands with maxima of intensity at 4740 and 4650 A respectively, which appear strongly on the spectrum excited by active nitrogen, and rather weakly in fluorescence with high pressures of nitrogen. They show no structure on the photograph from which spectrum (*a*), plate 12, was made, and may be regarded for the time being as continuous. It is not certain what relation these bands bear to the band system 4321–4041 A, which itself appears as a very diffuse band on the low dispersion photograph reproduced on plate 13. There are also three diffuse, broad bands in the spectrum excited by active nitrogen, with fairly sharp long wave limits, whose maxima of intensity lie at 2878, 2829 and 2769 A respectively. It is not unlikely that each of these apparently diffuse bands is itself really a system of bands with intensity distribution similar to that of the band system 2727–2524 A. No trace of these three bands, or systems of bands, appears in the spectra excited by fluorescence in the presence of nitrogen. Finally, there is a broad, apparently continuous band at 5100 A, which is much stronger at high pressures of nitrogen than at low pressures; this has been shown by Oldenberg to be present only when nitrogen is present, and is attributed by him to a photochemical reaction between iodine and nitrogen.

Emission "continua" of Cl_2, Br_2 *and* I_2

It now appears certain from a comparison of the emission spectra of Cl_2, Br_2 and I_2 excited by active nitrogen (Cameron and Elliott 1939, and this paper) and by an electrical discharge through the vapour (see for example Ludlam and West 1924) that the "continua" whose maxima of intensity lie at wave-lengths 2580, 2880 and 3425 A respectively are analogous, and since the present work shows that the I_2 "continuum" is a band system, very probably due to a $^1\Sigma_u^+ \rightarrow {}^1\Sigma_g^+$ transition, all these so-called continua may be assigned to the same transition; they are not really continua at all, but are band systems with an unusual distribution of intensity. The interpretation of the 2580 A "continuum" in Cl_2 suggested by Cameron and Elliott (1939) must therefore be rejected in favour of that given above.

SUMMARY

The fluorescence spectrum of iodine vapour in the presence of nitrogen at 1 atm. pressure has been photographed. The spectrum contains four separate band systems.

A vibrational analysis has been carried out for two of these systems, one of which is often referred to as the "continuum" 3425, and which is due to a $^1\Sigma_u^+ \rightarrow {}^1\Sigma_g^+$ transition.

The effect of varying nitrogen pressures on the intensities of the bands has been examined.

The spectrum of iodine vapour excited by active nitrogen has been photographed and compared with the fluorescence spectra of iodine vapour in the presence of nitrogen.

REFERENCES

Cameron, W. H. B. and Elliott, A. 1939 *Proc. Roy. Soc.* A, **169**, 463.
Curtis, W. E. and Evans, S. F. 1933 *Proc. Roy. Soc.* A, **141**, 603.
Duschinsky, F. and Pringsheim, P. 1935*a* *Physica*, **2**, 923.
— — 1935*b* *Physica*, **2**, 633.
Duschinsky, F., Hirschlaff, E. and Pringsheim, P. 1935 *Physica*, **2**, 439.
Gerlach, W. and Gromann, F. 1923 *Z. Phys.* **18**, 239.
Jevons, W. 1932 *Report on band spectra of diatomic molecules*, p. 280. London: The Physical Society.
Konen, H. 1898 *Ann. Phys., Lpz.*, **65**, 257.
Loomis, F. W. and Nile, S. W. 1928 *Phys. Rev.* **32**, 873.
Ludlam, E. B. and West, W. 1924 *Proc. Roy. Soc. Edinb.* **44** (2), 185.
Mulliken, R. S. 1934 *Phys. Rev.* **46**, 549.
Oldenberg, O. 1924 *Z. Phys.* **25**, 136.
Skorko, E. 1933 *Nature, Lond.*, **131**, 366.
Strutt, R. J. and Fowler, A. 1912 *Proc. Roy. Soc.* A, **86**, 105.
Warren, D. T. 1935 *Phys. Rev.* **47**, 1.

DESCRIPTION OF PLATES 12 AND 13

Plate 12

The plate shows the fluorescence spectrum of iodine vapour excited by the light from a condensed aluminium spark, in the presence of one atmosphere of foreign gas (nitrogen). The iodine vapour was at a temperature of about 40° C.

Owing to the sharp falling off in intensity from the maximum with increasing frequency, spectrum (*b*) could only be reproduced satisfactorily by making a composite print from several plates which had received different exposure times. Spectra (*a*) and (*c*) are each from a single plate, but the exposure given to the print (*c*) was graded to allow the weak bands at the high frequency end of the spectrum to show. Within the region covered by the spectra, all the bands listed in the tables are marked.

Plate 13

The spectra (*a*) to (*e*) inclusive are produced by fluorescence in iodine vapour at room temperature, using the light of a condensed aluminium spark for excitation. The pressure of foreign gas (nitrogen) present is indicated in cm. of mercury. As far as possible, the exposures given to these spectra were the same. Spectrum (*f*) was excited by active nitrogen (at a pressure of 2 cm. of mercury) to which was added iodine vapour at about 30° C.

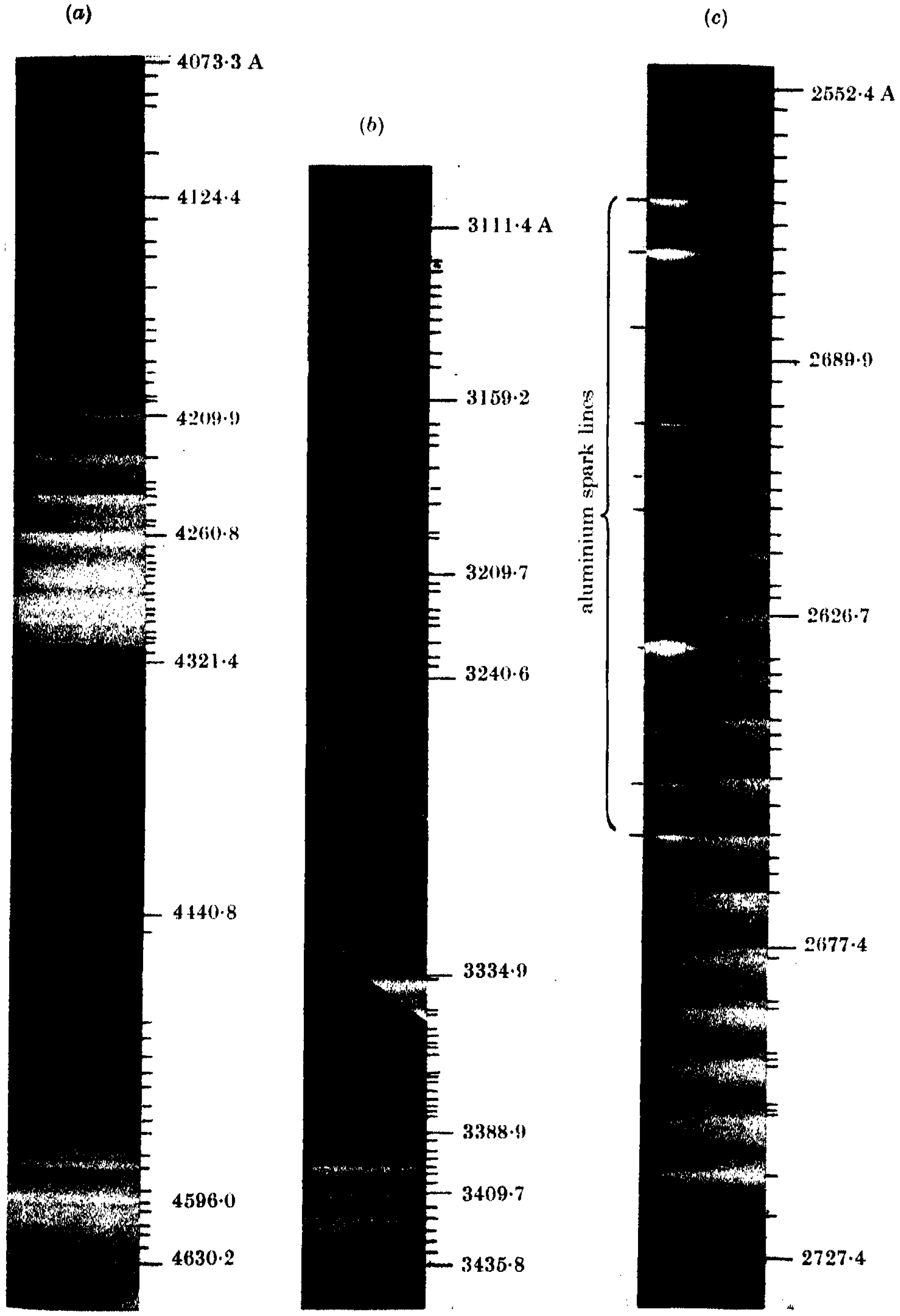

I_2 fluorescence spectra in the presence of nitrogen bands at 1 atmosphere pressure.

(*Facing p.* 286)

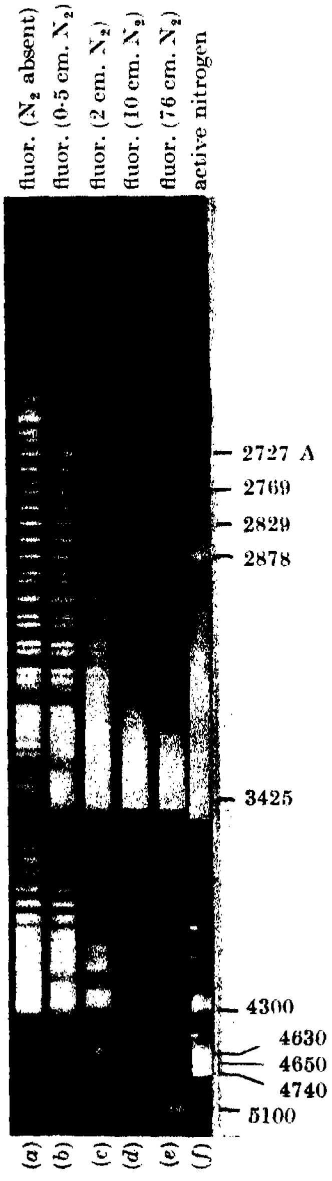

I_2 fluorescence spectra.

REFERENCES

Cameron, W. H. B. and Elliott, A. 1939 *Proc. Roy. Soc.* A, **169**, 463.
Curtis, W. E. and Evans, S. F. 1933 *Proc. Roy. Soc.* A, **141**, 603.
Duschinsky, F. and Pringsheim, P. 1935*a* *Physica*, **2**, 923.
— — 1935*b* *Physica*, **2**, 633.
Duschinsky, F., Hirschlaff, E. and Pringsheim, P. 1935 *Physica*, **2**, 439.
Gerlach, W. and Gromann, F. 1923 *Z. Phys.* **18**, 239.
Jevons, W. 1932 *Report on band spectra of diatomic molecules*, p. 280. London: The Physical Society.
Konen, H. 1898 *Ann. Phys., Lpz.*, **65**, 257.
Loomis, F. W. and Nile, S. W. 1928 *Phys. Rev.* **32**, 873.
Ludlam, E. B. and West, W. 1924 *Proc. Roy. Soc. Edinb.* **44** (2), 185.
Mulliken, R. S. 1934 *Phys. Rev.* **46**, 549.
Oldenberg, O. 1924 *Z. Phys.* **25**, 136.
Skorko, E. 1933 *Nature, Lond.*, **131**, 366.
Strutt, R. J. and Fowler, A. 1912 *Proc. Roy. Soc.* A, **86**, 105.
Warren, D. T. 1935 *Phys. Rev.* **47**, 1.

DESCRIPTION OF PLATES 12 AND 13

Plate 12

The plate shows the fluorescence spectrum of iodine vapour excited by the light from a condensed aluminium spark, in the presence of one atmosphere of foreign gas (nitrogen). The iodine vapour was at a temperature of about 40° C.

Owing to the sharp falling off in intensity from the maximum with increasing frequency, spectrum (*b*) could only be reproduced satisfactorily by making a composite print from several plates which had received different exposure times. Spectra (*a*) and (*c*) are each from a single plate, but the exposure given to the print (*c*) was graded to allow the weak bands at the high frequency end of the spectrum to show. Within the region covered by the spectra, all the bands listed in the tables are marked.

Plate 13

The spectra (*a*) to (*e*) inclusive are produced by fluorescence in iodine vapour at room temperature, using the light of a condensed aluminium spark for excitation. The pressure of foreign gas (nitrogen) present is indicated in cm. of mercury. As far as possible, the exposures given to these spectra were the same. Spectrum (*f*) was excited by active nitrogen (at a pressure of 2 cm. of mercury) to which was added iodine vapour at about 30° C.

Adsorption of lauryl sulphonic acid in the surface of its aqueous solution, and the Gibbs theorem

By JAMES W. McBAIN, F.R.S. AND LLOYD A. WOOD*
Stanford University, California

(*Received* 25 *July* 1939)

The absolute amount of adsorption per square centimetre of exposed surface of a solution may be measured with certainty and with moderate accuracy. In the microtome method (McBain and Humphreys 1932; McBain and Swain 1936; McBain, Ford and Mills 1940) the quiescent surface is cut from a solution in complete equilibrium with its vapour, collected, and analysed. In the interferometer method (Ford and McBain 1936; McBain, Mills and Ford 1940) a similar surface in equilibrium is compressed into the bulk of the liquid in the path of an interferometer beam which measures excess coming from the known surface destroyed.

Both methods applied to solutions of lauryl sulphonic acid, $C_{12}H_{25}SO_3H$, agree in showing strong positive adsorption over the whole range of concentrations.

On the other hand, the curve of surface tension with concentration is of Type III, showing very great lowering in extreme dilution, leading immediately to a minimum, followed by a definite rise to a shallow maximum, with a slight decrease of this already low value with further concentration. The Gibbs theorem demands an initial positive adsorption of the acid, followed by no adsorption at all where the surface tension is most lowered, followed by strong negative adsorption, then zero adsorption, still in dilute solution with very low surface tension, followed by slight positive adsorption.

It is evident that there is a complete contradiction between experimental observation and generally accepted theory. Throughout all these dilute solutions, which are all less than 0·012 N, the surface tensions are less than are those of the comparable pure organic liquids.

It is difficult to question the experimental evidence because all suggested sources of error have been forestalled or evaluated. About a hundred instances of Type III surface tension curves are contained in the references in McBain and Mills (1939), obtained by all the different methods of measuring surface tension. Lauryl sulphonic acid was chosen for this study on account of its stability, its indifference to carbon dioxide in the air, and for the fact that it cannot hydrolyse, being already a free acid.

---

* Shell Research Fellow.

It is unlikely that there is any mistake in the derivation of the Gibbs theorem subsequent to the assumptions made in his first equation (497), since the following steps have been carefully scrutinized by a series of authors in recent years. The primary assumptions made are that the system is actually of two components only, water and acid, and that no forms of energy other than internal, heat, surface, together with the ordinary chemical energy (μm) such as obtain within a solution, are involved.

The Gibbs theorem is commonly misunderstood as corresponding to the following statement of J. J. Thomson (1888) which conflicts with the Gibbs theorem for Type III curves. Thomson states: "Thus if the surface tension is increased by the addition of the salt there will be less salt per unit volume in the film than in the liquid in bulk, while if the surface tension is diminished by the addition of salt there will be more salt in unit volume of the film than in unit volume of the rest of the liquid." The Gibbs theorem, on the other hand, states that for a given value of activity and of slope of surface tension at that particular activity, the adsorption is independent of the nature of the chemical substances concerned and of the surface tension of the solvent, whether that be lower, higher or the same as that of the solution. Thomson's statement has the merit of intuitive appeal for all cases, including Type III curves.

The importance of the submerged double layer as a factor in determining and modifying surface tension of all aqueous surfaces was emphasized by McBain, Ford and Wilson (1937), and has been adduced by a number of authors, such as Langmuir (1938) and Evans (1937) in discussing the surface tension of dilute solutions of electrolytes (Jones and Ray 1937). The Gibbs theorem itself when applied to solutions of the fatty acids would show that, since the exterior layer of molecules is constant, the further decrease of surface tension with increasing concentration must be due to deeper layers.

X-ray examinations by Trillat (1926, 1927, 1928), Clark *et al.* (1935), Tausz *et al.* (1930, 1933) has shown that in lubricating oils orientation extends for thousands of Ångström units beneath the surface.

The curious and extended time effects recently observed with surface tension, surface potential and electrokinetic mobility show that surfaces of ordinary solutions exhibit complicated and but little understood complexities. (For example: Adam and Shute 1938; Doss 1935–8; McBain and Perry 1939; Alty 1924; Currie and Alty 1929; Florence, Myers and Harkins 1936.)

There still would be serious difficulty in accounting for the very great lowering of surface tension where the Gibbs theorem requires zero adsorption in those numerous Type III curves where surface tension is lowered in extremely dilute solution and thereafter remains at a nearly constant value without noticeable maxima or minima. It is difficult to believe that a surface layer in which 99·99 % of the molecules are water (or 99·85 % by weight) can have a surface tension 43 dynes below that of 100 % water, and 11 dynes below that of a complete monomolecular layer of a higher fatty acid on water. The actual measurements indeed show strong positive adsorption of the solute, of the order of a monomolecular layer.

EXPERIMENTAL

(1) *The microtome method*

Many detailed improvements were made in the microtome and in the procedure adopted for this work.

The trough.

The solution lies in a shallow trough of pure silver, *C*, figure 1, 83·6 cm. long, 5·1 cm. wide, containing a depth of about 5 mm. of solution. Each passage of the microtome removes 80 % of the exposed surface. Thus, any insoluble contamination is soon removed by repeated cuts. The trough is set between two rails of pure solid silver (*B*, *B*) that form the track upon which the microtome carriage slides. These are kept scraped true and level to a few ten-thousandths of an inch. The space below is closed with a subtrough of silver (*A*) containing a large reservoir of the same solution. Overhanging silver trays (*D*, *D*) also contain solution. All these help to maintain saturated aqueous vapour above the solution, and prevent evaporation. The inner enclosure containing the trough is 110 cm. in length and is closed with a sloping ceiling (*E*) to avoid any drip into the trough, and the lower surface of the overhanging troughs are similarly inclined. The trough is in contact only with three silver strips to minimize approach of any contamination. Creeping of the solution over the low ends of the trough was noticeable in measurements nos. 1–110, but was prevented in nos. 111–164 by a very thin application of dicetane to the cut edges. The solution was thoroughly stirred initially, and after each replenishment before each run, by a rod of fused silica extending the length of the trough and manipulated as required from side to side by another silica rod. No effect of such stirring on the adsorption was discernible in comparative measurements. Each end of the inner enclosure has a vertically sliding door consisting of a stainless steel frame closed with thin silver foil, through which the microtome may pass without damage when by accident the door is not opened.

The outer enclosure is of silver plated brass, 8 ft. long, 18 in. wide and 6 in. deep, with a glass ceiling and sliding automatic doors which open electrically as the door passes. This enclosure is likewise kept saturated by covering the floor with dishes containing water and by four cloth curtains suspended from the ceiling within the entrance and dipping into water, with two similar wet curtains near the exit. All crevices and joints in both enclosures were carefully sealed with clean paraffin, leaving only the crevices around the closely fitting doors.

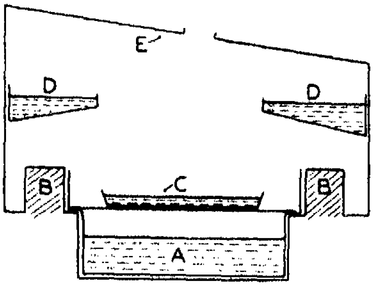

FIGURE 1. Cross-section of microtome apparatus.

The microtome.

The microtome blade was of 20% iridium, 80% platinum. A softer blade containing only 5% iridium was used for runs, nos. 1–110. The edge was ground to about 30° and was very carefully trued and levelled. The blade was permanently mounted in a cylinder of pure silver by means of Bakelite lacquer baked on at 135°. The end joints of the cylinder were also sealed with the lacquer.

The solution sliced off is thrown into the cylinder and kept there by a baffle plate of pure silver. The cylinder is mounted on bearings so that the microtome hangs in the correct position underneath for cutting, and when a pin is tripped by a flexible rubber projection, the blade and opening come on top and no solution is lost. The baffle plate when lifted out exposed the contents of the cylinder for withdrawal by a pipette. The bearings had eight adjustable screws for levelling and arranging the depth of cut. Stainless steel plates were used for runners and the brass framework was all coated with Bakelite lacquer baked on.

Materials.

The conductivity water used was redistilled in fused silica and it had a specific conductivity of about 3×10^{-7} mhos. It was stored in a silica vessel except during a run. The lauryl sulphonic acid prepared by M. E. Synerholm by the method of Noller and Gordon (1933) was used for the interferometer experiments and for the microtome experiments with 2·10 and 2·93 g./litre. A different specimen, prepared by Dr M. L. Koenig, was used for the other microtome experiments, with closely agreeing results. The equivalent weight of each by titration was within 0·05 % of theory, the balance being probably mainly water. Concentration of the stock solution was thereafter determined by titration. Solution was transferred by means of a large pipette, suction being applied through a long rubber tube.

Procedure.

It is essential to avoid loss or evaporation or contamination.

The car and rails were cleaned with pure benzene and the microtome rinsed many times with solution until the residue was of exactly the same concentration as that in the trough. The doors of the inner enclosure were then opened manually through a small hole otherwise kept covered. The car was then rinsed twice more and shot through at about 25 miles/hr., the first and last doors operating automatically. The sample was quickly transferred to the special solid silver interferometer cell, or, if it had foamed badly, stored in a tightly stoppered weighing-bottle. All this, from the opening of the inner doors, required less than a minute.

Samples of the solution in the trough were taken from both ends and the centre, and similarly stored for direct comparison with the surface sample and for evidence that the solution throughout the trough was homogeneous. The weighing bottles were kept in a saturated atmosphere where it had been established that no change in concentration took place over a period of days. Temperature was always checked at seven points with thermocouples and no measurements were made when a difference of more than 0·05° was found between opposite ends of the inner enclosure. Homogeneity of the solution in the trough was restored when necessary by repeatedly drawing it out at one end, mixing it with stock solution in a silica flask and putting it back at the opposite end. This was repeated four times, care being taken not to disturb the surface more than necessary.

Solution lost from the trough in the microtome, or by running over the end after the car, was replaced from stock.

Blanks of two kinds were run to measure concentration changes due to the experimental procedure. In the first seven, solution was shaken in the weighing bottle until well covered with froth and poured into the microtome which had just been operated as in an experiment, except that the trough solution was lowered to prevent cutting. Upon analysis the concentration of a 5 c.c. sample was increased 0·8 division on the interferometer scale. This was offset within 0·1 division by four blanks in which a solution 9·0 divisions more concentrated than the rinse solution, thus similating a surface sample, was run into the rinsed barrel as ready to operate, and on analysis showed a decrease due to total handling of 0·9 division.

Calculation.

The adsorption, Γ_g and Γ_n, is the number of grams or mols of solute per square centimetre. $\Gamma_g = 250\Gamma_n = \Delta Vk/A$, where Δ is the interferometer reading between surface layer and bulk liquid, V is the volume of the surface sample, k the interferometer constant, $1{\cdot}6 \times 10^{-6}$ g. solute/c.c. solution/interferometer division, readings being made to 0·1 division, and A the area sliced, 334 sq. cm.

Experimental results.

After the preliminary twenty-five, only those experiments are omitted which were total failures, usually due to solution not having been collected. The age of the surface is the time elapsed since the previous cut. An asterisk (*) denotes that the solution was thoroughly homogenized immediately preceding measurement, the surface presumably being fully aged. In contrast to the experience with hydrocinnamic acid and other solutions, there was no demonstrable effect of age, although no measurements were carried out before the lapse of 15 min.

In some of the experiments the surface was swept in a manner similar to that customary with the film balance, but no effect was discernible.

Table 1 gives in detail the results for 0·0113 N lauryl sulphonic acid, containing 2·82 g./l., and table 2 summarizes in minimum space the remainder of the seventy-six complete measurements. The experiments are arranged in order of age.

It is clear that every measurement showed adsorption of lauryl sulphonic acid to be positive. The same result follows from two sets of measurements with dynamic surfaces. In the first set of three, 0·012 N solution was shaken in a closed weighing bottle, and the concentration of the liquid was found to be 9·6, 10·1 and 11·2 mg./l. less concentrated than an equal volume of collapsed foam. In the second, a litre of 0·0113 N solution was placed in a vertical tube two metres high and three centimetres wide, and fine bubbles of air free from carbon dioxide were forced in through a sintered glass filter. The bubbles, drained in their slow upward passage, were collapsed in a separate receptacle by a jet of clean air. When two-thirds of the liquid had foamed over, the residue would not form stable bubbles. A repetition of the process with the liquid first collected yielded 535 c.c. of 0·023 N solution, leaving a residue of 346 c.c. of 0·0007 N. Hence, over the range from 0·0007 N to twice the original 0·012 N, the sorption on a moving bubble is positive.

Table 1. Adsorption in the surface of 0·0113 N lauryl sulphonic acid, by the microtome method

No.	Temp. °C.	Age	V c.c.	Δ	$\Gamma_g \times 10^8$	$\Gamma_n \times 10^{10}$
43	21·7	15 min.	4·1	7·4	15·1	6·0
60	21·2	15 min.	4·1	5·3	10·8	4·3
59	21·2	20 min.	4·5	6·3	14·1	5·6
58	21·2	22 min.	4·2	6·6	13·8	5·5
44	21·7	23 min.	4·9	5·2	12·8	5·1
45	21·7	27 min.	2·1	12·6	13·2	5·3
48	21·2	30 min.	3·8	8·2	15·5	6·2
56	21·2	30 min.	4·0	5·6	11·0	4·4
57	21·2	30 min.	4·3	5·6	12·0	4·8
50	21·3	30 min.	2·3	11·3	12·9	5·2
42	21·7	40 min.	1·9	15·2	14·4	5·8
41	21·7	1 hr.	4·5	4·7	11·1	4·4
54	21·3	1 hr.	4·2	5·1	11·0	4·4
51	21·3	1·75 hr.	4·1	5·3	11·5	4·6
61	21·3	4 hr.	2·2	9·9	10·8	4·3
49	21·3	23 hr.	3·3	11·6	19·3	7·6
55	21·2	*	2·8	8·6	12·0	4·8
52	21·3	*	3·6	8·3	15·1	6·0
				Average	13·1	5·2

Table 2. Adsorption in the surface of all lauryl sulphonic acid solutions, by the microtome method

Conc. g./l.	Range of Ages	Values of $\Gamma_g \times 10^8$	Mean $\Gamma_g \times 10^8$	Mean $\Gamma_n \times 10^{10}$
3·10	15–30 min.*	15, 13, 19, 17, 10, 12	14·2	5·7
2·93	20 min.–26 hr.*	13, 21, 10·8, 12·3, 14·4, 9·5, 9·8	13·0	5·2
2·82	15 min.–23 hr.*	Table I	13·1	5·2
2·16	15 min.–40 hr.	7·8, 10·5, 13·9, 5·2, 8·9, 10·4, 9·3, 12·0	9·8	3·9
2·10	12 min.–44 hr.*	1·0, 11·6, 7·4, 6·3, 19, 10·3, 4·5, 9·0, 15, 7·5, 9·0, 10·1, 10·5, 15	9·2	3·7
1·50	15 min.–3 hr.*	10·3, 14·5, 11·4, 12·0, 12·1, 15·0, 12·5, 11·4, 17·0, 17·9, 15·8, 16·0, 15·3, 15·0, 10·9	13·8	5·4
0·5	15 min.–5·3 hr.*	9·1, 6·4, 5·7, 7·1, 5·9, 2·6, 5·8, 6·9	6·7	2·7

(2) *The interferometer method*

The interferometer method is based on the assumption that the surface layer can be collected by compression by moving a barrier extending nearly a millimeter below the surface (total depth of solution usually about 3 mm.). The operation is carried out in a cell 76·6 cm. long, placed in the path of a Hilger Rayleigh interferometer. Details of the equipment have been described elsewhere (McBain, Mills and Ford 1940). Here the partition between the standard solution and that whose surface was being compressed extended to the glass ceiling to prevent intercommunication of the vapour. The liquid was not in contact with rubber and the barrier slid on a platinum wire against a platinum surface.

The solution was thoroughly stirred by tilting the cell bodily both sideways and endways until a constant reading was obtained in the interferometer. Then the barrier was drawn back, exposing fresh surface. After ageing, the barrier was run forward again until it dropped off the ends of the skids, imprisoning the liquid collected. The ends of the barrier were connected to the trough by long strips of vertical gold foil lying in the surface.

The first effect of stirring, like the first effect of pushing the barrier forward, was a distinct lowering in the interferometer reading, returning to zero in a few minutes. It was necessary to wait 2–5 hr. before the collapsed surface had diffused evenly, giving a strong positive reading. The interferometer was read to 0·2 division, the constant k being $3{\cdot}9 \times 10^{-7}$ g./c.c. The adsorption is again equal to $\Delta Vk/A$.

The interferometer method will give a change smaller than the reality if any of the surface layer is lost under the moving barrier, and it is clear that the total effect per square centimetre would asymptotically approach zero if the barrier were moved an indefinitely great distance. In practice, with lauryl sulphonic acid solution, it was found that a movement of 6 cm. gave almost as great an interferometer change as 16 cm. Thus with 16 cm. over two-thirds of the collection has escaped under the barrier. Hence 6 cm. was used but must still represent a low result. An example is given in Table 3 in which the average deviation from the mean is 16 %.

In Table 4 are given the initial values for the solution of minimum surface tension, showing that after 3 min. the adsorption attained its final value, the subsequent twenty-two measurements giving, with an average deviation of 13 %, $7{\cdot}7 \times 10^{-8}$ and $3{\cdot}1 \times 10^{-10}$ grams and mol./cm.^{2} respectively.

All ninety experiments carried out with the interferometer are summarized in table 5. Again there is no detectable influence of age of surface, after the first few minutes.

TABLE 3. ADSORPTION IN THE SURFACE OF 0·0084 N LAURYL SULPHONIC ACID (2·10 g./l.), BY THE INTERFEROMETER METHOD

No.	Age	Temp. °C	Δ	$\Gamma_g \times 10^8$	$\Gamma_n \times 10^{10}$
38	45 min.	21·0	8·8	16·4	6·5
36	2·5 hr.	21·5	5·0	9·3	3·7
40	14·5 hr.	20·8	6·9	12·9	5·2
37	15·3 hr.	20·9	8·2	15·3	6·1
39	15·5 hr.	20·9	6·6	12·2	4·9
			Average	13·2	5·3

TABLE 4. INITIAL ADSORPTION IN THE SURFACE OF 0·00062 N LAURYL SULPHONIC ACID (1·55 g./l.), BY THE INTERFEROMETER METHOD

No.	Age	Temp. °C	Δ	$\Gamma_g \times 10^8$	$\Gamma_n \times 10^{10}$
60	3 sec.	21·3	2·1	3·1	1·2
59	5 sec.	21·2	2·7	4·0	1·6
58	15 sec.	21·2	4·0	6·0	2·4
69	15 sec.	23·3	2·2	3·3	1·3
62	1 min.	21·7	3·8	5·7	2·3
66	3 min.	22·9	3·9	5·8	2·3
68	10 min.	23·1	5·3	7·9	3·2

TABLE 5. ADSORPTION IN THE SURFACE OF ALL LAURYL SULPHONIC ACID SOLUTIONS, BY THE INTERFEROMETER METHOD

g./l.	Range of ages	Mean $\Gamma_g \times 10^8$	Mean $\Gamma_n \times 10^{10}$
2·93	30–150 min.	(4·4)*	(1·8)*
2·10	45 min.–15·5 hr.	13·2	5·3
1·55	3 sec.–41 hr.	7·7	3·1
0·5	3 sec.–21 hr.	7·5	3·0

* This result is too low because the barrier was moved 15·6 cm.

(3) *The surface tension*

Such methods as drop weight and maximum bubble pressure are of little value in studying solutions whose surface tension changes slowly with time. Even the method of capillary rise used by Reed and Tartar (1936) failed to yield definite values over an extended period in their study of solutions of sodium lauryl sulphonate. We chose the du Noüy ring method, using a large platinum basin in a saturated atmosphere and a chainometric chemical balance with a magnetic damper in place of a torsion wire. To begin with, all the platinum was heated to redness. The surface of the solution was carefully swept. The ring was kept submerged except when actually in use. Measurements made in rapid succession on a surface several days or weeks old showed only a rise of 0·04 dyne after each disturbance.

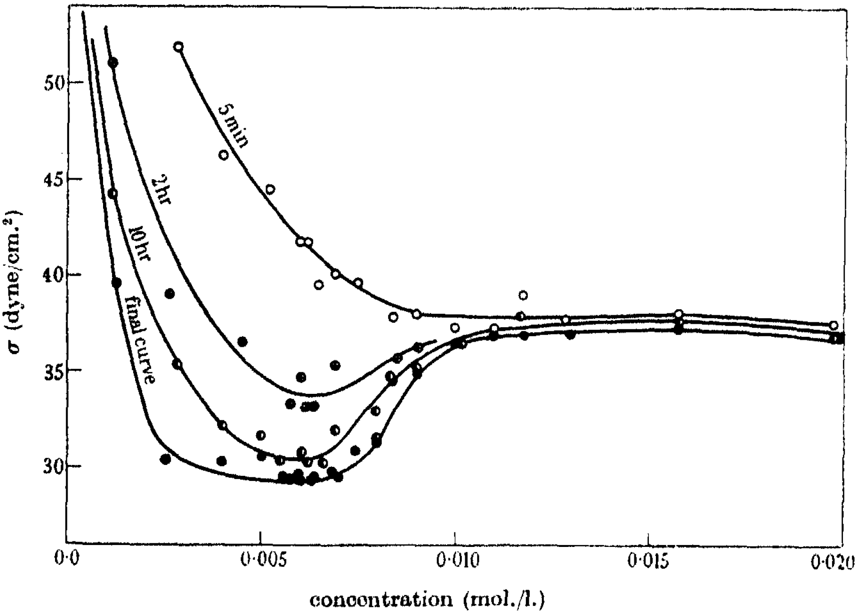

FIGURE 2. Surface tension measurements of lauryl sulphonic acid at various ages.

The surface tension of solutions of less than 0·01 N lauryl sulphonic acid decreases with time for many days as shown in figure 2 for 22°. This is confirmed by unpublished measurements by L. H. Perry using the pendant drop method of Andreas, Hauser and Tucker (1938), even after the introduction of a number of improvements such as keeping the drop in a saturated atmosphere in contact only with platinum. Similar time effects have been recorded by Adam and Shute (1938).

The shape of the Type III curve is likewise confirmed with the PLAWM trough (McBain and Vinograd 1940) and by measurements of capillary rise. A large amount of carbon dioxide had no appreciable effect upon the surface tension. Solutions were always frothed vigorously and the foam removed before beginning their study. Very similar results are reported for the corresponding sulphate by Tartar and Cadle (1939) using the sessile bubble method, and again long time effects were observed.

DISCUSSION

The adsorption was calculated for the final surface tension curve of lauryl sulphonic acid (figure 2) at 22° by the classical theorem of Gibbs in mols per square centimetre:

$$\Gamma_n = \Gamma_2' = \frac{-d\sigma}{d\mu} = \frac{-1d\sigma}{RTd\log_e a} = -d\sigma/(\nu dg + \nu gd\log_e m_2)$$

$$= -d\sigma/(di + id\log_e m_2),$$

where $\nu = 2$ and $\frac{d\log_e a}{dm_2} = \frac{\nu dg}{dm_2} + \frac{\nu g}{m_2}$ (McBain and Mills 1939).

The values of g are from freezing-point data (McBain, Dye and Johnston 1939).

The calculated results are compared with the experimental results in table 5.

It is interesting that at 0·0087 N, where the surface tension slope is upwards, the Gibbs theorem would predict a deficiency of lauryl sulphonic acid in the surface amounting to $11{\cdot}2 \times 10^{-10}$ mol./sq. cm. This is the equivalent of a surface in which there is no lauryl sulphonic acid in a top layer 12,700 A thick, or a correspondingly thicker layer if this is not pure water.

TABLE 6. CALCULATED AND ACTUALLY OBSERVED ADSORPTION Γ_n IN mol./cm.$^2 \times 10^{10}$ IN THE AIR-WATER SURFACE OF SOLUTIONS OF LAURYL SULPHONIC ACID

Concentration g./l.	Γ_n adsorption from S.T. by the Gibbs theorem	Γ_n microtome results	Γ_n Rayleigh interferometer results
0·0020	+2·4	+2·7	+3·0
0·0060	0·0	+5·4	—
0·0062	0·0	—	+3·1
0·0084	−8·7	+3·7	+5·3
0·0087	−11·2	+3·9	—
0·0113	−0·3	+5·2	—
0·0117	−0·2	+5·2	+1·8*
0·0122	−0·2	+5·7	—

* See footnote to table 5.

Preliminary experiments on solutions of sodium butyl benzene sulphonate were carried out previous to the adoption of the modifications in apparatus and technique already described. Twelve experiments with a

concentration of 35 g./l. all gave positive values averaging $\Gamma_g = +31 \times 10^{-8}$ and $\Gamma_n = +13 \times 10^{-10}$. This, however, is a concentration at which the slope of the surface tension curve is zero and for which, as for so many other detergents, the Gibbs prediction is zero adsorption.

Finally, experiments with the free butyl benzene sulphonic acid were carried out with the interferometer method, using a solution beyond the minimum of surface tension 38·4 g./l. Once again, the observed adsorption was positive, amounting to about 5 divisions or about 4×10^{-10} mol./cm.^{2}; instead of the negative value deduced from surface tension by the Gibbs equation.

SUMMARY

One hundred and sixty-six measurements made with the microtome and with the interferometer agree in showing that positive adsorption occurs in the surface of all dilute solutions of aqueous lauryl sulphonic acid. A similar result follows from dynamic measurements and from measurements with sodium butyl benzene sulphonate and butyl benzene sulphonic acid. No time effect is observable after the first few minutes.

The surface tension of solutions of lauryl sulphonic acid changes over long periods of time extending to hours or days.

Since the surface tension is at a minimum in 0·0062 N lauryl sulphonic acid, the Gibbs theorem would predict zero adsorption followed by negative adsorption, in contrast to the positive values actually fonnd. Similar predictions would follow for all the numerous known instances of Type III curves where in extreme dilution the surface tension is lowered to a fraction of that of water, thereafter passing through a minimum or remaining constant.

REFERENCES

Adam, N. K. and Shute, H. L. 1938 *Trans. Faraday Soc.* **34**, 758.
Alty, T. 1924 *Proc. Roy. Soc.* A, **106**, 315.
Andreas, J. M., Hauser, E. A. and Tucker, W. B. 1938 *J. Phys. Chem.* **42**, 1001.
Clark, G. L., Lincoln, B. H. and Sterrett, R. R. 1935 *Proc. Amer. Petr. Inst.* Sect. III, **16**, 81.
Currie, B. W. and Alty, T. 1929 *Proc. Roy. Soc.* A, **122**, 622.
Evans, A. W. 1937 *Trans. Faraday Soc.* **33**, 794.
Doss, K. S. G. 1935 *Curr. Sci.* **4**, 405.
—— 1936 *Proc. Ind. Acad. Sci.* **4**, 11, 97.
—— 1937 *Curr. Sci.* **5**, 645.
—— 1938 *Kolloidzschr.* **84**, 138.
Florence, R. T., Myers, R. J. and Harkins, W. D. 1936 *Nature, Lond.*, **138**, 405.
Ford, T. F. and McBain, J. W. 1936 *J. Amer. Chem. Soc.* **58**, 378.

Jones, G. and Ray, W. A. 1937 *J. Amer. Chem. Soc.* **59**, 187.
Langmuir, I. 1938 *Science*, **88**, 430.
McBain, E. L., Dye, W. B. and Johnston, S. A. 1939 *J. Amer. Chem. Soc.* **61**, 3210.
McBain, J. W., Ford, T. F. and Mills, G. F. 1940 Communicated to *J. Amer. Chem. Soc.*
McBain, J. W., Ford, T. F. and Wilson, D. A. 1937 *Kolloidzschr.* **78**, 1.
McBain, J. W. and Humphreys, C. W. 1932 *J. Phys. Chem.* **36**, 300.
McBain, J. W and Mills, G. F. 1939 *Reports on Progress in Physics*, **5**, for 1938, p. 30.
McBain, J. W., Mills, G. F. and Ford, T. F 1940 Communicated to *J. Amer. Chem. Soc.*
McBain, J. W. and Perry, L. H. 1939 *Industr. Engng Chem.* **31**, 35.
McBain, J. W. and Swain, R. C. 1936 *Proc. Roy. Soc.* A, **154**, 608.
McBain, J. W. and Vinograd, J. R. 1940 *J. Amer. Chem. Soc.* January.
Noller, C. R. and Gordon, J. J. 1933 *J. Amer. Chem. Soc.* **55**, 1090.
Tartar, H. V. and Cadle, R. D. 1939 Presented at 16th National Colloid Symposium. *J. Phys. Chem.* **43**, 1173.
Tausz, J. *et al.* 1930 *Z. angew. Chem.* **43**, 570.
—— 1933 *Erdöl. u. Teer*, **9**, 331.
Thomson, J. J. 1888 *Applications of dynamics to physics and chemistry*, p. 191. London: Macmillan and Co.
Trillat, J. J. 1926 *Rev. Sci.* **64**, 552; *Ann. Phys., Lpz.*, **10**, 5; *C.R. Acad. Sci., Paris*, **182**, 843.
—— 1927 *Hall aux cuirs, Suppl. Tech.* p. 137.
—— 1928 *C.R. Acad. Sci., Paris*, **187**, 168; *Mech. Eng.* **50**, 471; *Metallwirtsch.* **7**, 101.

The association of meteorological changes with variations of ionization in the F_2 region of the ionosphere

By J. Bannon, B.Sc., A. J. Higgs, B.Sc.,
D. F. Martyn, D.Sc. and G. H. Munro, M.Sc.

(*Communicated by T. H. Laby, F.R.S.—Received 4 April 1939*)

[Plate 14]

1. INTRODUCTION

Of the known regions in the ionosphere, the F_2 region shows the most erratic variations. Whereas the E and F_1 regions show ionization maxima diurnally at noon, and seasonally in midsummer, in accordance with theory (Chapman 1931), the F_2 region on the other hand frequently shows diurnal ionization maxima both in the morning and afternoon, with a minimum near noon, while the seasonal variation shows maxima near the equinoxes and minima at both midsummer and midwinter. In addition to these unusual diurnal and seasonal variations, the F_2 region is particularly subject to disturbances, most of which tend to lower its maximum ionization density. Thus Appleton and Ingram (1935) have shown that magnetic storms are frequently accompanied by a decrease in the F_2 ionization, while Martyn, Munro, Higgs and Williams (1937) have found that *all* bright hydrogen solar eruptions are accompanied by a reduction of the F_2 maximum ionization density.

In addition to these types of variation, Martyn and Pulley (1936) found some evidence that the noon F_2 ionization density correlated positively with the barometric pressure at the ground.

We have now available 19 months' continuous observations, at half-hourly intervals or less, of the maximum ionization densities of the F_2 region. It is the object of this paper to examine this material, to reject the days of magnetic and solar disturbances, and to see if the large variations found to remain in the residual observational material are associated with meteorological conditions.

In a subsequent paper the variations due to solar eruptions will be studied.

2. Experimental methods

The observations were made at the Liverpool field station of the Radio Research Board, lat. 33° 55′ S, long. 150° 59′ E, and at the Commonwealth Solar Observatory, Canberra, lat. 35° 15′ S, long. 149° 10′ E. At the former site the observations were made by a method previously referred to (Martyn *et al.* 1937). These observations were made near noon, and were particularly valuable in providing a sensitive indication of solar eruptive activity at times when the sky was overcast and spectroheliosope observations impossible. At the latter site observations were made at half-hourly intervals by the automatic variable frequency radio pulse transmitting and receiving equipment originally designed by Wood (1936). This equipment records on 35 mm. cine-film the equivalent heights and penetration frequencies of the various regions of the ionosphere. The records obtained from this apparatus (hereafter called P'-f, or equivalent path-frequency records) permit the evaluation of the maximum ionization densities in the various regions penetrated. Similar P'-f records were obtained by manual methods at Liverpool each day at noon.

The observations cover the period from 19 March 1937 to 31 October 1938.

3. Typical experimental results

Two typical P'-f records, obtained at noon respectively on 24 and 25 October 1938, are reproduced in figure 1 (plate 14). In these records the abscissae give the frequency in megacycles per second, and the ordinates the equivalent heights of the reflecting regions. A height scale is superposed on the record at unit intervals on the frequency scale. The separation between each dot on these height scales corresponds to an equivalent path of 100 km. It is seen that the penetration frequency $f^0_{F_2}$ of the upper (ordinary) component of the F_2 region echoes, which was about 8·3 Mc./sec. on the 24th, has increased to 11·0 Mc./sec. on the 25th. In other respects the two P'-f records appear similar in type to each other, as well as to the great majority of the thousands of such records which have been obtained. In particular they do not exhibit any of the peculiar characteristics associated with magnetic storms or solar eruptions, types which will be discussed elsewhere. The distribution of weather over Australia on these two days is shown in figures 2 and 3, which are tracings of the relevant features of the weather charts issued by the

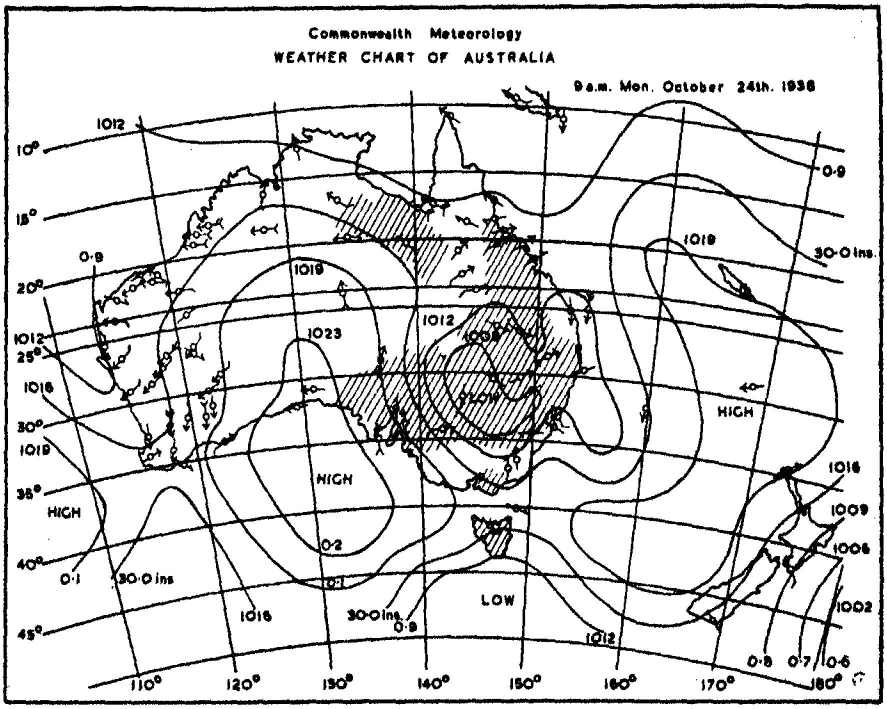

Figure 2. Weather chart of Australia 24 October 1938.

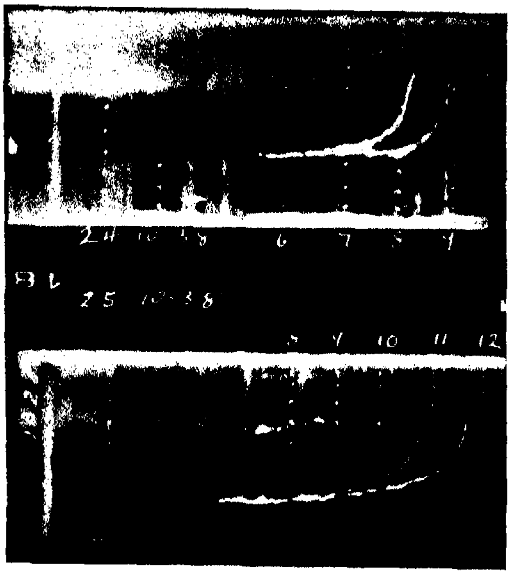

FIGURE 1. Noon P'-f records, 24 and 25 October 1938.

Commonwealth Meteorological Bureau. It is seen that while on the 24th an extensive cyclonic depression accompanied by widespread and heavy rainfall covered the whole of New South Wales, on the 25th (at 9 a.m.) the centre of this depression had passed eastwards into the Tasman Sea. The frequent occurrence of such daily variations in F_2 ionization in association with this type of meteorological condition suggested the desirability of making the detailed analysis which is given in the next section.

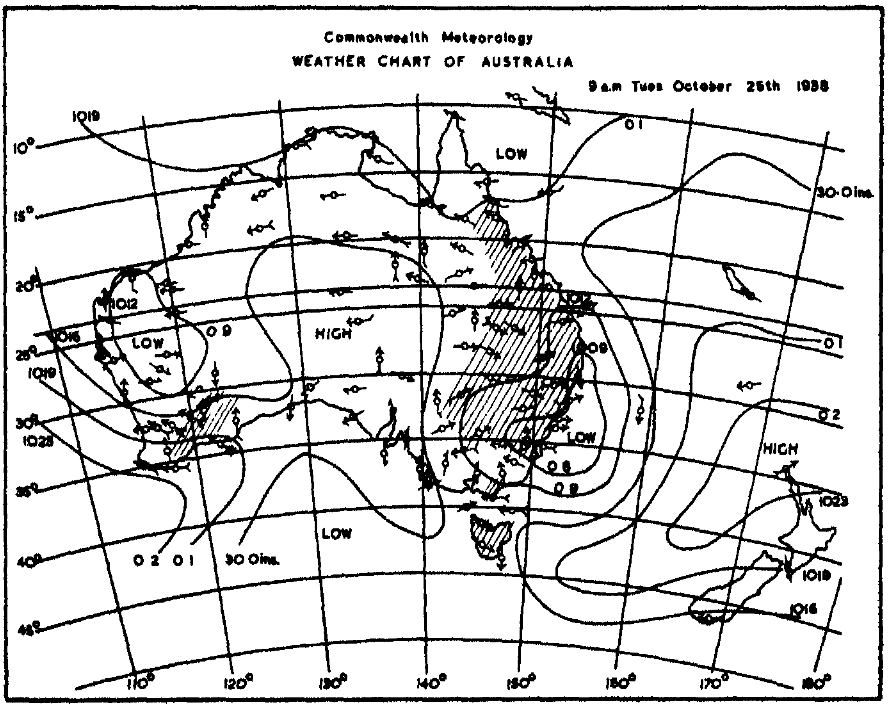

FIGURE 3. Weather chart of Australia 25 October 1938.

4. ANALYSIS OF RESULTS

The frequent occurrence of examples of F_2 ionization variation similar to that described in the previous section have indicated a possible connexion between the ionization density in the F_2 region and the meteorological conditions at the ground. In the present section, 19 months' observations are analysed to see if this relationship can be substantiated. For this purpose the observational material was treated in the following way. The noon value of $f^{0}_{F_2}$—the maximum electron density in the F_2 region is proportional to this quantity—was selected as the daily index of the maximum ionization density.

Days on which a magnetic storm occurred, or on which the P'-f records showed magnetic storm characteristics, were rejected. The total number of days rejected for this reason was 13.

The records obtained on days in which a solar eruption was occurring at noon were specially examined. As a rule the depression of critical frequency from this cause was small, being less than 0·5 Mc./sec., and it was possible to obtain an interpolated noon value from the examination of the morning and afternoon values.

We may regard Australian weather as being controlled by a succession of anticyclones which pass from west to east in fairly regular succession. The track of the centres of these anticyclones passes, on the average, approximately at the latitude of our observing stations. In the transition zone between two such successive anticyclones, there is a region of relatively sudden discontinuity in the characteristics of the air. To the east of this frontal zone the air flow is from lower latitudes where it will have been warmed and possibly charged with water vapour. To the west of this zone the winds blow from higher latitudes and the air is generally colder and drier. In this main frontal zone the phenomena elucidated by Bjerknes and others occur; tongues of warm air intrude into the cold mass and warm and cold fronts and eventually cyclonic depressions may appear. The preliminary analysis suggested that the F_2 ionization would be found to be below the average amount on occasions when this main frontal zone passed through New South Wales.

For the purpose of this analysis the various days were divided into two classes. The first class contained those days on which a main front was present in the area included between lat. 29° S and lat. 36° S, and long. 140° E and long. 156° E. The second class contained those days when no front existed in this region.

Days in the first class are referred to below as "frontal" days; those in the second class are called "non-frontal" days. The dates on which they occurred are shown in figure 4 as explained in the following section.

The days having been thus classified, the average monthly noon values of $f^{0\prime}_{F_2}$ were worked out for each class. The results are shown in tables 1 and 2, which give the values for Mount Stromlo and Liverpool (N.S.W.) respectively. In the last column in each table is shown the difference between the monthly average noon $f^{0\prime}_{F_2}$ in each class. It is seen that with the exception of August 1937 and July and August 1938, the "non-frontal" days show a higher average value of $f^{0\prime}_{F_2}$ than the "frontal" days. The difference tends to be greatest about the months of March and October, when it amounts to about 20 % at Stromlo and 11 % at Liverpool. The average difference over the whole period of observation is 11 % at Stromlo and 6 % at Liverpool.

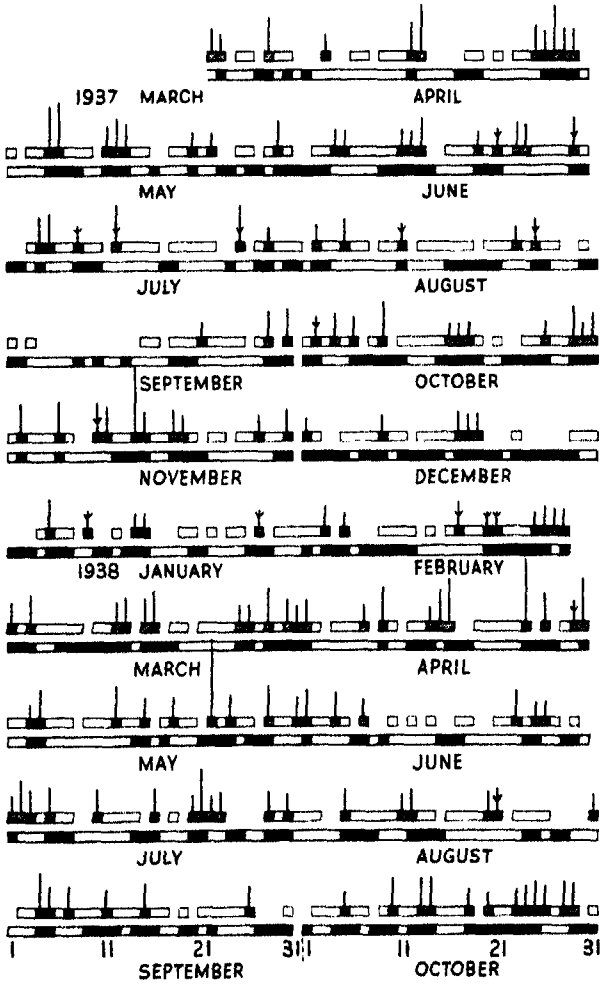

FIGURE 4. Distribution of "frontal" and "non-frontal" days from March 1937 to October 1938, together with days of significant differences between the maximum electron densities in the F_2 region above Liverpool (Sydney) and Mount Stromlo (Canberra).

It is seen that the analysis of these 530 days confirms the view that a great, and probably the major part, of the day-to-day fluctuation of F_2 ionization density is associated with meteorological changes at the ground.

5. Comparison of Liverpool and Stromlo results

A comparison of tables 1 and 2 shows that the trend of the variations at Liverpool and Stromlo is similar but not identical. The principal difference is that the magnitude of the difference between "non-frontal" and "frontal" days is greater at Stromlo. This fact is at first sight so surprising, in view of the small difference in location of these two places, that we have subjected it to special examination. The results are set out in figure 4. In the figure the "frontal" days are indicated by blocked-in squares. The unblocked squares on the same row are "non-frontal" days. Each row represents two months of days. Above each such row appears a second row of hatched or unhatched squares. Each hatched square represents a day on which there was a significant difference (> 0·4 Mc./sec.) in the values of $f^0_{F_2}$ at Stromlo and Liverpool. The unhatched squares in this row represent days on which no such signi-

Table 1. Monthly averages of $f^{0'}_{F_2}$ for "frontal" and "non-frontal" days, Mount Stromlo (Canberra)

	"Non-frontal"		"Frontal"		"Non-frontal"	"Frontal"	
Month	No. of days	Sum of squares of $f^0_{F_2}$	No. of days	Sum of squares of $f^0_{F_2}$	Average of squares of $f^0_{F_2}$	Average of squares of $f^0_{F_2}$	Difference of averages
1937							
April	20	2610	8	1033	130	129	1
May	13	1489	12	1267	115	106	9
June	17	1773	10	969	104	97	7
July	17	1834	9	897	108	100	8
August	14	1582	11	1302	113	118	−5
September	16	2166	9	1164	135	129	6
October	8	940	16	1535	118	96	22
November	15	1426	11	894	95	81	14
December	6	576	14	1169	96	84	12
1938							
January	9	652	11	744	72	68	4
February	8	698	17	1465	87	86	1
March	9	1163	20	2172	129	109	20
April	14	2087	11	1416	149	129	20
May	17	2157	10	1107	127	111	16
June	17	1495	11	948	88	86	2
July	17	1521	13	1216	89	93	−4
August	19	2095	12	1365	110	114	−4
September	13	1489	16	1698	115	106	9
October	10	1151	20	1964	115	98	17
Total	259	28904	241	24325	—	—	—
Average		112	—	101	—	—	—

ficant difference existed. On some occasions, for instrumental reasons, observations were lacking at one or other site. These days are represented by leaving gaps in the upper row. The magnitude of the difference between the values of $f^0_{F_2}$ at Stromlo and Liverpool is represented by the length of the vertical line above each hatched square. The unit length is the side of the square, and corresponds to a frequency difference of 0·33 Mc./sec. On the great majority of occasions the Liverpool value of $f^0_{F_2}$ is the greater of the two, but on a few occasions the reverse effect occurs. Such occasions, when $f^0_{F_2}$ (Stromlo) $>$ $f^0_{F_2}$ (Liverpool), are indicated by downward pointing arrowheads on the vertical strokes, which indicate the magnitude of the difference.

TABLE 2. MONTHLY AVERAGES OF $f^{0\,2}_{F_2}$ FOR "FRONTAL" AND "NON-FRONTAL" DAYS, LIVERPOOL (SYDNEY)

	"Non-frontal"		"Frontal"		"Non-frontal"	"Frontal"	
Month	No. of days	Sum of squares of $f^0_{F_2}$	No. of days	Sum of squares of $f^0_{F_2}$	Average of squares of $f^0_{F_2}$	Average of squares of $f^0_{F_2}$	Difference of averages
1937							
April	18	2559	8	1135	142	142	0
May	14	1673	15	1697	119	113	6
June	18	1941	12	1248	108	104	4
July	19	2051	11	1138	108	103	5
August	16	1862	13	1533	116	118	−2
September	10	1398	8	1106	140	138	2
October	9	1105	20	2189	123	109	14
November	15	1442	12	1123	96	94	2
December	6	589	20	1639	98	82	16
1938							
January	12	812	14	921	68	66	2
February	8	710	17	1495	89	88	1
March	9	1185	20	2398	132	120	12
April	17	2165	12	1744	154	145	9
May	17	2204	12	1450	130	121	9
June	19	1730	11	998	91	91	0
July	17	1612	14	1380	95	99	−4
August	19	2192	12	1419	115	118	−3
September	13	1591	17	1899	122	112	10
October	10	1198	20	2180	120	109	11
Total	266	30019	268	28692	—	—	—
Average		113	—	107	—	—	—

A study of the positions of the blocked and hatched squares shows that there is a strong tendency for a significant difference to occur on a "frontal" day.

In table 3 such an occurrence is called a "Hit", and the failure of such an occurrence a "Miss". Over the whole period the percentage of "Hits" recorded is 72. On a random distribution the anticipated percentage of "Hits" would be 49.

TABLE 3. STATISTICAL ANALYSIS OF "HITS" AND "MISSES" IN COINCIDENCE OF DAYS OF SIGNIFICANT DIFFERENCES (BETWEEN VALUES OF $f^0_{F_2}$ AT LIVERPOOL AND STROMLO) WITH "FRONTAL" DAYS

Month	Total no. of days	No. of "frontal" days	No. of days with significant difference	Observed "Hits"	Observed "Misses"
1937					
March (part)	7	3	3	2	1
April	18	7	8	5	3
May	23	11	8	7	1
June	27	13	10	6	4
July	24	9	6	3	3
August	24	11	5	3	2
September	15	6	3	2	1
October	26	17	11	10	1
November	26	11	10	7	3
December	20	15	5	5	0
Totals	210	103	69	50	19
1938					
January	17	7	5	4	1
February	22	15	9	8	1
March	27	19	11	11	0
April	23	9	10	7	3
May	27	10	9	6	3
June	19	6	6	3	3
July	22	11	12	7	5
August	23	9	6	2	4
September	24	12	6	4	2
October	27	17	12	10	2
Totals	231	115	86	62	24
Grand totals	441	218	155	112	43

Anticipated no. of "Hits" = 49 %.
Observed no. of "Hits" = 72 %.

6. CONCLUSIONS

It would appear that the observations here described fully confirm the conclusion (Martyn and Pulley 1936) that ionization changes in the F_2 region of the ionosphere are associated with meteorological changes at the ground. This surprising result is obviously difficult to explain theoretically. It seems clear that the constitution of the atmosphere must change from day to day in the F_2 region if these results are to be explained. At the same time the changes must occur rapidly, in a time measured in hours, in order that the association with meteorological conditions should be maintained. There are obvious, and probably insuperable, difficulties in the way of an explanation in terms of convection, while the time necessary for any process of diffusion (even from the level of the ozone region upwards) is quite prohibitive. Another possibility to be considered is an explanation based on variations in radiation from the ground and from clouds. It is known that cloud amount varies greatly among types of meteorological classifications we have employed, and it is known that any radiation process would take effect in the F_2 region in a time measured in minutes. It seems impossible, however, to conceive of any radiation which could appreciably affect the F_2 region after traversing the upper troposphere and stratosphere. Ultra-violet radiation would be completely absorbed in these regions, visible radiation would be unabsorbed in the F_2 region, and infra-red radiation could not appreciably affect the temperature.

A more probable source of explanation might be found in the variations of ozone amount, which are known to occur in the ozone region. While it seems unlikely that appreciable amounts of ozone could exist in the F_2 region itself on account of the high temperatures found there, yet changes in ozone amount at lower levels might permit changes in other constituents, notably water vapour, the products of which might find their way upwards by diffusion. Here again the difficulty would appear to be the prohibitive time required for any diffusion process below 100 km. to be effective.

It appears that the most likely explanation may be that there exist large-scale movements of air in the high atmosphere in parallel with the main air mass movements at low levels—that, for example, a large influx of tropical air at low levels is accompanied by an influx of air of special characteristics (probably high humidity and/or low ozone content) at the very high levels up to 250 km. The presence of water vapour, or its dissociation products, would be expected to have a pronounced effect on the electron density in the F_2 region.

At present, however, any such theory would necessarily be highly speculative. It appears highly desirable to study the effects described in this paper at a large number of locations. It is to be anticipated, for example, that the precise nature of the association may be different in different regions of the earth, and would depend on the peculiar meteorological features of each region. For example, it is already known (Lejay 1936) that the association of ozone with meteorological conditions is of a different nature in Shanghai from that obtaining in Europe. The difference is attributed by Lejay, probably rightly we believe, to the fact that the Siberian anticyclone to the *North* affects the Shanghai ozone, while the Azores anticyclone to the *South* affects Western European ozone.

An important consequence of the results here described would appear to be that the seasonal variation of ionization in the F_2 region over any region of the earth should be profoundly affected by *climatic* considerations. It has been generally assumed until now that the F_2 ionization would depend almost entirely on the strength of solar radiation, and so would depend only on latitude. On the other hand, the results of observations now being accumulated from many parts of the world do not appear to support this view. It is found (Berkner and Wells 1938) that the seasonal variation of F_2 ionization at places of equal latitude in opposite hemispheres is entirely different.

It appears that the results described in this paper provide an explanation of these anomalies. It is almost a necessary consequence of the results that the seasonal variations at any one location, and the differences in the seasonal variations at several locations of equal latitude, must be largely governed by climatic considerations.

7. ACKNOWLEDGEMENTS

This work has been carried out as part of the programme of the Radio Research Board of the Commonwealth Council for Scientific and Industrial Research, and of the Commonwealth Solar Observatory. The thanks of the authors are due to Sir G. C. Simpson and to the late Dr E. Kidson for the benefit of very considerable discussion concerning the meteorological problems involved, and to Mr L. V. Berkner for the benefit of discussion concerning the observations made at the Watheroo Observatory of the Carnegie Institution, Department of Terrestrial Magnetism, Washington. We have been supplied with Australian weather information by the courtesy of the Commonwealth Meteorologist, Mr W. S. Watt. It is again a pleasure to acknowledge the constant interest and support of the Chairman of the Board, Professor J. P. V. Madsen.

SUMMARY

A study has been made of the day-to-day variations in the noon values of the maximum electron density in the F_2 region of the ionosphere, at two observing stations near Sydney and Canberra. The small number of days on

which these values are affected by association with magnetic storms are excluded from the analysis. Large day-to-day fluctuations, amounting sometimes to 50 %, remain at each station. It is found that these fluctuations are associated with meteorological changes observed at the ground. Over 19 months of daily observations it is found that on days when the region between lat. 29° S and lat. 36° S, and long. 140° E and long. 156° E is free from "frontal" conditions, the values of F_2 ionization are higher on the average by 6 % near Sydney and 11 % near Canberra than on other days. A similar difference is found in the averages for each month, except in August 1937 and July and August 1938, when a small negative difference occurs at each station. The difference is greatest in the equinoctial months when it amounts to about 20 % for Stromlo. It is found that while the values of ionization density measured at Sydney and Canberra are usually equal, there is a strong tendency for the Canberra values to be lower than the Sydney values on "frontal" days. This result is considered surprising, since the observing stations are only 250 km. apart.

The theoretical difficulties in the way of an explanation of the association here found between F_2 ionization and meteorological conditions are discussed.

It is pointed out that the results suggest that current views concerning the seasonal variation of F_2 ionization in various regions of the earth may require revision. The current view regards the F_2 region ionization as normally influenced solely by the intensity of solar radiation, thus depending in magnitude solely on latitude. The results here presented suggest that local climatological factors may exert a profound influence on the magnitude, and on the seasonal and diurnal variations of F_2 ionization.

REFERENCES

Appleton and Ingram 1935 *Nature, Lond.*, **136**, 548.
Berkner and Wells 1938 *Terr. Magn. Atmos. Elect.* **43**, 15.
Chapman 1931 *Proc. Phys. Soc.* **43**, 26.
Lejay 1936 *Quart. J.R. Met. Soc.*, **62**, Ozone Suppt. 58.
Martyn, Munro, Higgs and Williams 1937 *Nature, Lond.*, **140**, 603.
Martyn and Pulley 1936 *Proc. Roy. Soc.* A, **154**, 455.
Wood 1936 *J. Instn Engnrs, Aust.*, **17**, 403.

Behaviour of the crystalline structure of brass under slow and rapid cyclic stresses

By W. A. Wood, *Physics Department*, and
P. L. Thorpe, *Engineering Department*,
National Physical Laboratory, Teddington, Middlesex

(*Communicated by G. W. C. Kaye, F.R.S.—Received* 1 *July* 1939)

[Plates 15, 16]

During X-ray tests on an annealed brass (Cu 69·43 %, Zn 30·54 %) subjected to cyclic stressing it was noted that the behaviour of the crystalline structure of the grains depended on the speed of application of the stress. The structural changes occurring under a slow cycle could be different in kind from those produced by stress cycles applied at 2200 cyc./min., the frequency associated with the fatigue-testing machine employed. The difference was not due to changes in the final external deformation of the specimens because such changes in each case were reduced to the same negligible proportions by the use of cycles of reversed direct stress, that is, by cycles symmetrical in tension and compression. The effect was especially noticed in the brass because, in contrast with a mild steel previously the subject of X-ray tests under cyclic stressing (Gough and Wood 1936), it belongs to the class of materials in which the primitive yield point under static tensile loading is *less* than the fatigue limit under cycles of reversed direct stress (as given by the amplitude S of the limiting safe stress range $\pm S$); in the brass, therefore, the stress cycles of great physical interest, which are those where the stress range just exceeds the limiting safe range, are cycles in which the stress during each repetition passes through the values corresponding to the primitive yield points in tension and also in compression. The extent of the difference between the slow and rapid cycle appeared to be such that in the latter the main structural modifications shown by previous X-ray work to be associated with transition through a yield point were entirely suppressed. It was evident that an investigation of the conditions accompanying this suppression would give useful information on the response of the internal crystalline structure of the metal to an externally applied stress; also it would afford an opportunity for distinguishing the individual parts played by the various structural changes which have been brought out by recent X-ray work on the progressive deformation of metals and on metals in different states of hardness. In the present paper therefore the X-ray observations are compared with the static and cyclic stress/extension relationships as given by mechanical measurements.

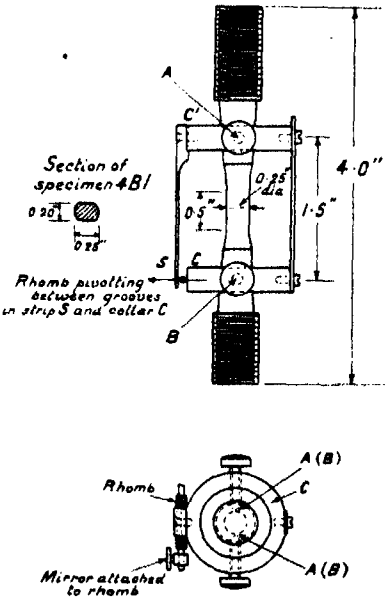

Figure 1. Fatigue specimen with extensometer attached.

Normal structural response under static tensile test

First we give the extension measurements and the behaviour of the crystalline structure under a sensitive static tensile test, because these provide what may be termed the *normal* response of the structure to an applied stress. The stress-strain data given by a Dalby Autographic Recorder showed the yield to occur at 4·5–5 tons/sq. in. and fracture at 20 tons/sq. in. This test was not sufficiently accurate for the early stages of deformation, and, for this range, a sensitive mirror extensometer was attached to the specimens in the manner shown in figure 1, which also gives the shape and dimensions of the specimens employed. The extensions thus measured were reduced to fractions of an inch by calibrating the extensometer with the help of a steel of known elastic modulus. It will be noted that the extension was measured between two points *A* and *B* which were not on the central test portion of the specimens; this was done in order to avoid damage to this surface and interference with the X-ray reflexions. As, however, the points were similarly placed on all specimens and the specimens themselves were similar, these extension measurements were entirely sufficient for the purpose of the investigation. The stress-extension curve obtained in this way from 0 to 10 tons/sq. in. is given in figure 2, curve (c); it will be seen that the material shows a quite definite yield at 4·8 tons/sq. in. The load was removed from this specimen at 6, 7, 8, 9 and 10 tons/sq. in. whilst X-ray photographs were obtained.

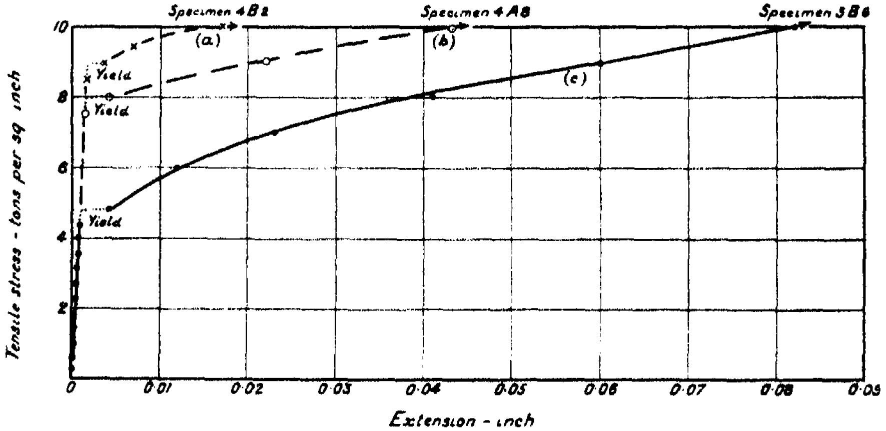

FIGURE 2. Stress-extension curves up to 10 tons/sq. in. on specimens (a) after cyclic stressing at ± 9 tons/sq. in., (b) after cyclic stressing at ± 8 tons/sq. in., (c) in initial condition.

The photographs were taken by a back reflexion technique described elsewhere in more detail (Gough and Wood 1936). An incident beam of approximately 1 mm. cross-section falls perpendicularly on the surface of the specimen and the beams reflected backwards by the grains through a large angle are recorded on a flat photographic film which is pierced with a hole at the centre to permit passage of the incident beam in a direction perpendicular to the film. The beam used in the present experiments consisted of the $K\alpha_1$, α_2 and β wave-lengths from a nickel target; the reflexion ring recorded was the (331) $\alpha_1\alpha_2$ doublet. The advantage of this technique is that the experimental conditions are most sensitive to both lattice variations and to the breakdown of the grains. The points to which it is desired to draw attention for later discussion are those described below.

The initial condition of the brass was the annealed state in which the individual grains were highly perfect, as shown by preliminary X-ray tests. After machining to shape, the surface layers cold-worked by this operation were removed by etching in a solution of ammonium persulphate. The X-ray photograph of this initial condition is given in figure 6 (plate 15) which consists of a ring of sharp isolated (331) reflexion spots, each of which is a reflexion from the atomic planes of one grain as defined by a metallographic grain boundary.

Up to the yield point the change in this type of photograph is negligible. This was confirmed by subjecting a specimen to loads of 2, 3 and 4 tons/sq. in. for 5 min. and then removing the load for the X-ray examination of the specimen. At the yield point, however, an extensive change sets in and becomes progressively more marked as plastic deformation proceeds, accelerating when the specimen necks prior to fracture. The photographs reproduced in figures 7*a*, 8*a*, 9*a* and 10*a* (plates 15, 16) are those taken after loads of 7, 8, 9 and 10 tons/sq. in., since these will be required later for comparison purposes. They suffice to show that the photographs after yield are different in type from before; after yield they are characterized by the elongation of the reflexion spots into arcs which coalesce and replace the initially separated spots by the continuous (331) $\alpha_1\alpha_2$ ring. This change means that the original grains are dispersed into independently reflecting units with crystallographic orientations varying over an angular range of many degrees; it is difficult in a polycrystalline material like the present exactly to specify these ranges because of the mutual inference of the various reflexion arcs, but other work in progress on single aluminium crystals shows that changes of 20–30° are quickly reached within one grain. The units have been termed crystallites to distinguish them from the initial metallographic grain; they are also characterized by a lower limiting size of the order of 10^{-5} cm. (Wood 1935*a*, Wood 1939). It will be noticed that the process of crystallographic re-orientation does not necessarily involve bodily re-orientation of the units of the grain; the same effect would be produced if the apparently parallel sections between the members of a pseudo-parallel system of slip lines elongated by very different amounts in the same direction, for it is well known that a crystal constrained to deform in a definite direction will do so by a change in its crystallographic orientation to an extent depending on the degree of extension. Physically, however, the units will differ as much as neighbouring grains with different crystallographic orientations. This then is the chief visible change in the X-ray photographs on transition through a yield point and gives the physical interpretation, as well as a non-destructive test, of the occurrence of a primitive yield from that point of view. In passing, it was found that these effects are as marked in the soft brass as in the previously tested mild steel (Gough and Wood 1936) with a much more pronounced yield point; the present explanation is an extension of the one given in that work.

EXTENSIONS AND X-RAY CHANGES UNDER REVERSED DIRECT STRESS CYCLES

The transition in structure occurring at the yield point under static stress is irreversible; if therefore a specimen is taken slowly through a cycle of stress symmetrical in tension and compression it is evident that this internal breakdown will set in as soon as the stress in the first half of the cycle exceeds the yield point and will be thereafter retained although the cycle may be built up in such a way as to leave no appreciable final external deformation, the external change in one half being cancelled out by that in the opposing half of the cycle. Actually it was found that the breakdown was much the same for a slow cycle of $\pm S$ as for a single static load of S tons/sq. in. The photographs already reproduced in figures 7*a*, 8*a*, 9*a* and 10*a* (plates 15, 16) therefore serve also to represent the condition after a slow cycle at ± 7, ± 8, ± 9 and ± 10 tons/sq. in. respectively.

The following specimens were subjected to the same ranges of reversed direct stress as the above, applied, however, by a standard form of electromagnetic fatigue-testing machine operating at 2200 cyc./min.; they were X-rayed in the initial condition and after the number of stress cycles shown in table 1. This number was chosen with reference to previous knowledge (Gough and Wood 1940) of the fatigue properties of the material and in the first three was such as could safely be applied without producing a fatigue crack. The fourth specimen 4B3 did finally exhibit a fatigue crack but is included as a matter of interest. The limiting safe range of the material was ± 5 to ± 5·5 tons/sq. in.

TABLE 1. SPECIMENS SUBJECTED TO CYCLES OF REVERSED DIRECT STRESS

Specimen	Stress range tons/sq. in.	No. of cycles applied	Change in diameter after test %	X-ray photograph after test
3B7	± 7	10^6	0·0	Figure 7*b*
4A8	± 8	10^5	0·2	Figure 8*b*
4B2	± 9	3×10^4	0·3	Figure 9*b*
4B3	± 10	5×10^3	*	Figure 10*b*†

* Specimen finally exhibited fine fatigue crack.

† Photographed well away from fatigue crack.

The X-ray photographs obtained after the high frequency tests at ± 7, ± 8, ± 9 and ± 10 tons/sq. in. are shown respectively in figures 7*b*, 8*b*, 9*b* and 10*b* and they are thus to be compared with figures 7*a*, 8*a*, 9*a* and 10*a* (plates 15, 16) which represent the condition of the structure after slow cyclic stresses or static loads of corresponding ranges. It will be at once evident that the two sets of photographs are radically different. The essential difference is that in the first set taken after the high frequency cycles the photographs retain the main characteristic of the initial state in that the reflexion spots, though exhibiting a slight diffusion, *are still isolated spots* and have not undergone the marked elongation which leads to the continuous ring formation characteristic of the slow cyclic or static stress. The large angular dispersal of the crystallites which physically marks the primitive yield point has therefore been suppressed or removed, although the maximum stress of the cycle in one case is practically double the initial yield stress under static tension. The changes shown by the special fractured specimen 4B3 are probably due mostly to slight plastic deformation produced when the fatigue crack occurred; even then the spectrum is very different from that under 10 tons/sq. in. static load. The difference between the slow and rapid cyclic tests is therefore that, at the end of the latter, the crystallites if formed at all retain to within a degree or so the crystallographic orientation of the parent grains and, so far as the X-rays are concerned, do not behave independently of the initial grains. It might have been possible, however, for a dispersed crystallite formation to have occurred in the initial stages and to have been removed before making the final X-ray test. This point was tested by taking a specimen in which the grains were first broken down by producing an initial permanent set under static load and then applying reversed cyclic stresses in the usual way. No recovery in respect of the crystallite formation was found. Under the rapid cyclic stressing of the above specimens this dispersal appears, therefore, to be suppressed entirely during the whole course of the tests.

It was next necessary to confirm, by mechanical measurements of the external deformation, the evident inference from the X-ray results that the specimens had not undergone a primitive yield change under the high frequency cyclic tests. This was done by simultaneous measurements of the amplitude of the strain exhibited by a given specimen as the stress cycle was built up as follows: a given cycle was reached in steps of ± 2, ± 3, ± 4, ... tons/sq. in. at the standard frequency of 2200 cyc./min., each step being held long enough to permit measurement of the amplitude of the strain as given by the mirror extensometer attached to the specimen; the final stress range was maintained for the number of cycles stated in table 1 and the cyclic stress then removed, also in measured steps. The final stress-strain relationships are given to the left of figures 3, 4 and 5, respectively, for the specimens 3B7 subjected to the range at ± 7 tons/sq. in., 4B8 to ± 8 tons/sq. in., and 4B2 to ± 9 tons/sq. in. The extensions obtained under the static loading of specimens 3B6 are also indicated for purpose of comparison in the same figures and plotted on the same scale. These curves show that under the rapid cyclic stressing the original yield point of the material has been postponed beyond the initial value of 4·8 tons/sq. in. up to the order of maximum stress of 7, 8, or 9 tons/sq. in., respectively, corresponding to the various stress cycles employed. They therefore completely confirm the conclusion from the X-ray results that, with the suppression of the dispersed crystallite formation, the primitive yield also is suppressed. Further, they prove that there is no critical external strain at which the dispersal into the crystallite sets in; in fact, there is no theoretical reason why the suppression should not be carried on and the yield postponed in this manner to stresses corresponding to the breaking point of the metal.

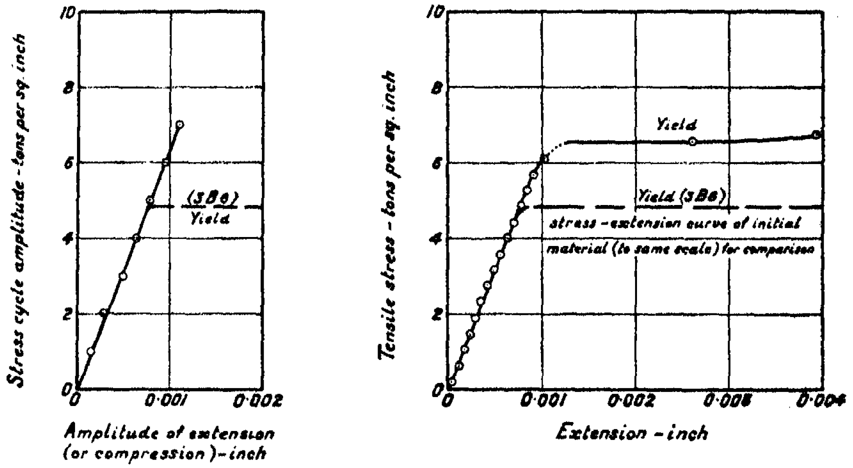

(i) (ii)

FIGURE 3. Difference between extension produced by: (i) Rapid alternating stress (± 7 tons/sq. in.). Specimen 3B7. Extension under alternating stress (after 1,000,000 cycles at ± 7 tons/sq. in.). (ii) Slow static tensile stress. Specimen 3B7. Subsequent static tensile test (showing permanent rise of yield point).

The obvious interpretation of the inhibition of the dispersal of the grains into crystallites is that under the cycles at high frequency the value of the applied stress, and the corresponding external strain, exceed the values associated with the primitive yield point for so short a time during each cycle that the structure is not allowed sufficient time to break down. This raises interesting issues with regard to the finite nature of the time required for the effective propagation of a slip movement, and it is hoped when opportunity occurs to experiment with different frequencies. This time lag is not, however, a fundamental factor because, as shown in the next

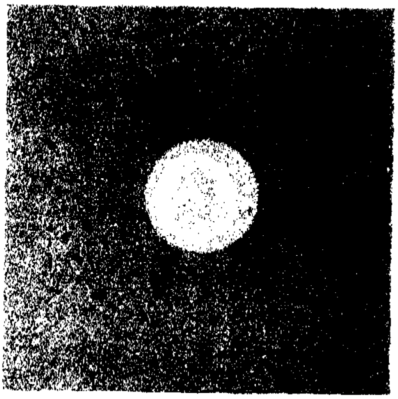

Figure 6. Initial state.

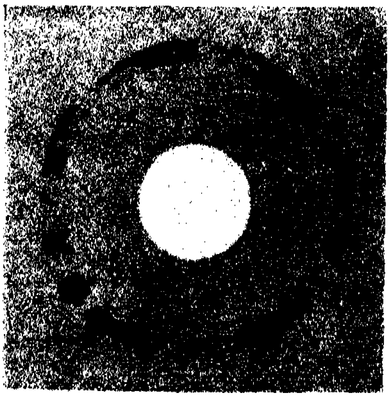

Figure 7*a*. Static $+7t/\text{in.}^2$ or slow cycle $\pm 7t/\text{in.}^2$.

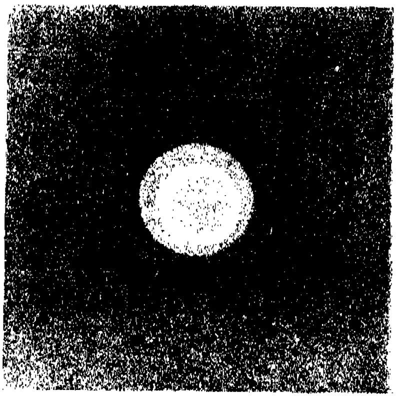

Figure 7*b*. Rapid cycle $\pm 7t/\text{in.}^2$.

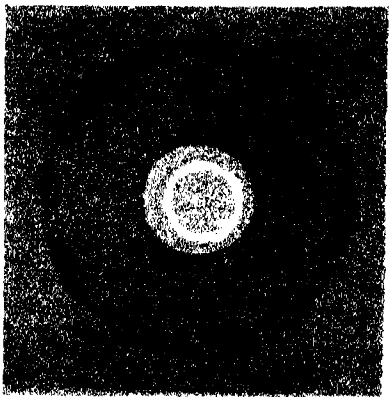

Figure 8*a*. Static $+8t/\text{in.}^2$ or slow cycle $\pm 8t/\text{in.}^2$.

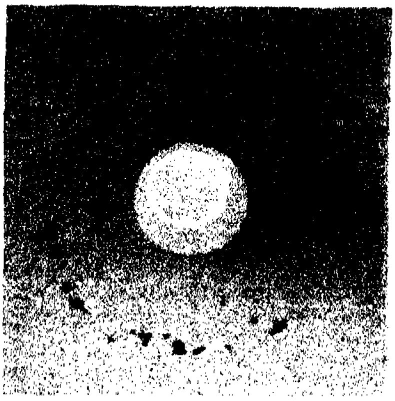

Figure 8*b*. Rapid cycle $\pm 8t/\text{in.}^2$.

FIGURE 9*a*. Static $+9t/\text{in.}^2$ or slow cycle $\pm 9t/\text{in.}^2$.

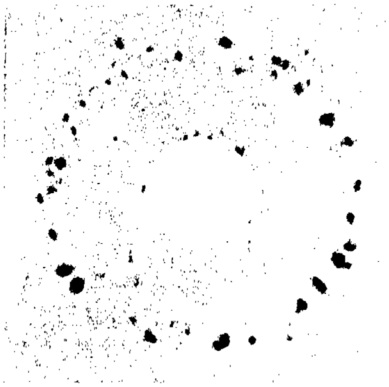

FIGURE 9*b*. Rapid cycle $\pm 9t/\text{in.}^2$.

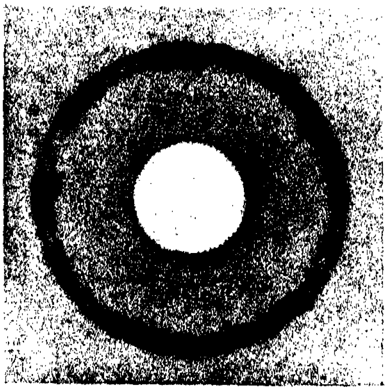

FIGURE 10*a*. Static $+10t/\text{in.}^2$ or slow cycle $\pm 10t/\text{in.}^2$.

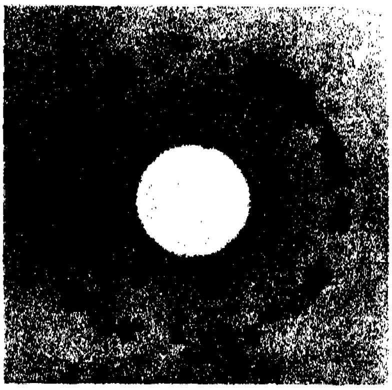

FIGURE 10*b*. Rapid cycle $\pm 10t/\text{in.}^2$ (fractured).

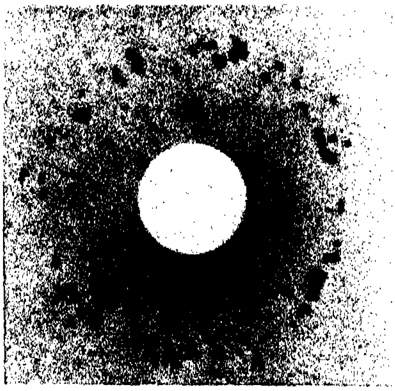

FIGURE 11. Static load $+8t/\text{in.}^2$ after prior cycles at $\pm 8t/\text{in.}^2$ (yield just beginning). This shows inhibition of breakdown of grains under rapid cyclic stressing to persist (up to maximum stress of prior cycle) when specimen is subsequently stressed statically.

section, the inhibition of the dispersed crystallite formation over the cyclic stress range employed becomes a permanent property of the material in that it also characterizes the material under subsequent application of static stress, a point which is regarded as one of the main results of the present research.

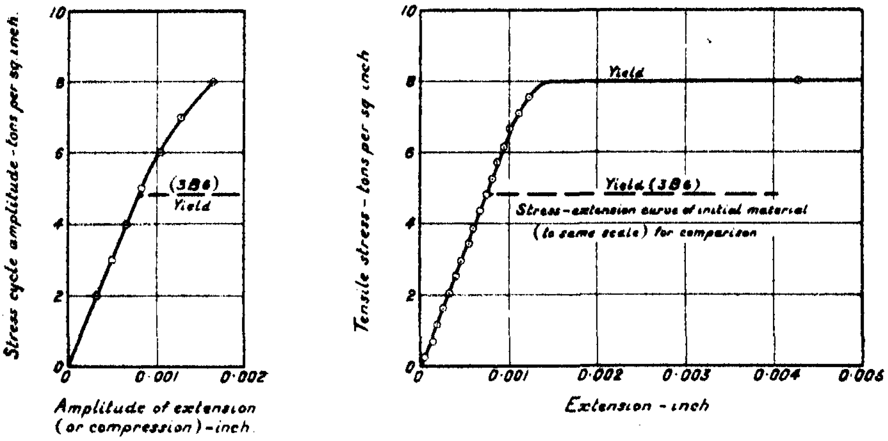

(i) (ii)

FIGURE 4. Difference between extension produced by: (i) Rapid alternating stress (± 8 tons/sq. in.). Specimen 4A8. Extension under alternating stress (after 100,000 cycles at ± 8 tons/sq. in.). (ii) Slow static tensile stress. Specimen 4A8. Subsequent static tensile test (showing permanent rise of yield point).

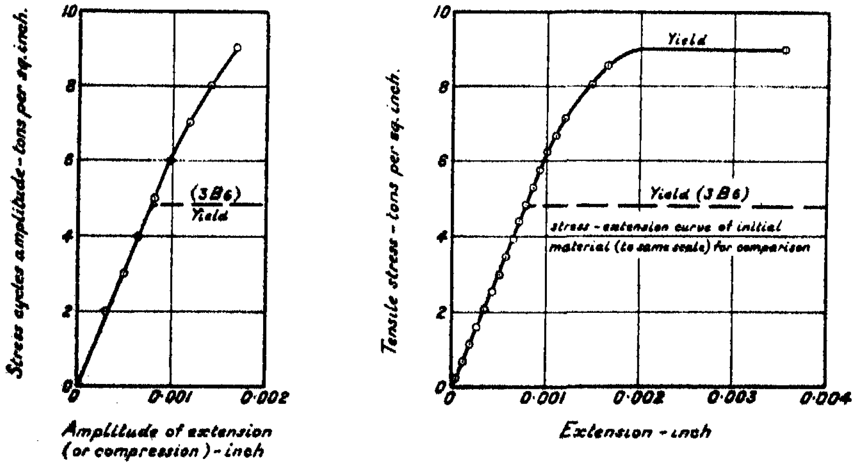

(i) (ii)

FIGURE 5. Difference between extension produced by: (i) Rapid alternating stress (± 9 tons/sq. in.). Specimen 4B2. Extension under alternating stress (after 30,000 cycles at ± 9 tons/sq. in.). (ii) Slow static tensile stress. Specimen 4B2. Subsequent static tensile test (showing permanent rise of yield point).

PERMANENT INHIBITION OF DISPERSED CRYSTALLITE FORMATION

After the cyclic history indicated in table 1, the specimens 3B7, 4A8 and 4B2, which were still far from being fractured by fatigue, were subjected to subsequent static tensile tests in which the normal stress-extension curves were obtained; also X-ray photographs were taken after appropriate loads had been applied. These photographs showed no obvious change in the nature of the reflexions until for a given specimen the load was increased beyond the original primitive yield point up to a value of the same order of magnitude as the maximum of the stress cycle employed in the prior cyclic treatment. At this latter value the grains began to exhibit the marked dispersal into crystallites already shown to define a primitive yield point, and then, on further increased loading, proceeded to break down in the manner also shown to be characteristic of plastic deformation. It will be sufficient to illustrate the point by figure 11 (plate 16) of specimen 3B7, previously subjected to the cycle ± 8 tons/sq. in. and now after the subsequent static load of 8 tons/sq. in. It will be seen that the breakdown has only just commenced, and that the condition of the structure is still very different from that shown by figure 8*a* (plate 15) which was taken after application of the same load statically to the initial annealed material. Physically, this observation shows that the previous cyclic stressing has permanently modified the crystalline structure of the grains in a precise manner depending on the amplitude of the stress cycle employed. This modification is of the nature of a work-hardening process, and the experiments clear the ground considerably, as far as X-ray work is concerned, by proving directly that the dispersal of the grains into the differently oriented crystallites has no immediate relation with this mechanism of hardening.

As was to be expected, the accompanying stress-extension curves given by the specimens in the static tensile tests confirmed the permanent rise in the primitive yield point. These curves are given for the specimens 3B7, 4A8 and 4B2 in the right-hand sections of figures 3, 4 and 5, respectively, and show directly that the initial yield point has been raised practically to the maximum of the prior stress cycle employed (the stress-extension curve of the initial material is again indicated for purposes of comparison on the same diagrams). The same stress-extension curves for 4A8 and 4B2 are also repeated for convenience in curves (*a*) and (*b*) of figure 2 which contains the stress-extension curve (*c*) of the initial material on a closer scale of abscissae and permits the extensions of those specimens occurring at the higher loads to be plotted up to 10 tons/sq. in.; this diagram thus brings out further the lag of the plastic deformation of these two specimens behind that of the initial material over the range considered.

INTERNAL LATTICE STRAINS

It will be evident from the above work that the dispersal of the grains into the differently oriented crystallites is involved, primarily, only in the mechanism by which the grains change shape during plastic deformation. The reason for the inhibition of this formation as a result of prior cyclic stressing, and for the associated rise in yield point, has still to be demonstrated experimentally. However, in view of other X-ray investigations on metals in different states of hardness which have indicated the relevance of lattice distortion as a factor in strain-hardening (Wood 1933, 1935*b*, 1939), the following further tests were made. A specimen (4 B 1) was subjected to similar reversed direct stresses at ± 8 tons/sq. in. in the fatigue-testing machine and removed from the machine at intervals for precise examination of the lattice dimensions. For these measurements the shape of the specimen was modified from the standard, two parallel flats being machined on the specimen for the length of the test portion as indicated in the cross-section drawn in figure 1. These could be brought into contact with a fixed stop on the X-ray spectrometer, and personal errors in repeating the position of the reflecting surface at successive stages of the test thus eliminated. Also the specimen was not stationary, as in the previous test, but oscillated ± 5° about an axis in the surface of the specimen perpendicular to the incident beam. By increasing the number of reflecting grains, this movement gave a ring sufficiently continuous for accurate measurement of the diameter, from which the lattice dimensions were deduced in the usual way. The rings utilized for this purpose were the (331) α and (422) β obtained with nickel K-radiation and the (420) β with cobalt radiation; these occurred at large enough diffraction angles to be sensitive to small changes in lattice openings.

The results showed first that the lattice changed to an easily measurable extent and, within the limits of measurement, that the changes appeared to be of the nature of a pure volume expansion. The results expressed in terms of a percentage change in the side of the original unit cell at the different stages of test, are as follows:

No. of cycles ($\times 10^3$)	0	50	90	150	300	636*
Lattice change (%)	—	$0{\cdot}02_0$	$0{\cdot}02_4$	$0{\cdot}02_4$	$0{\cdot}02_9$	$0{\cdot}03_5$

* Fracture stage.

The total change on the (420) β ring for example corresponded to a change in diameter of about 1 mm. which, since the measurements could be repeated to 0·1 mm. without difficulty, was well beyond experimental error. It will be noted that there is a distinct change in the first 50,000 cycles; this is followed by a practically stationary condition up to 150,000 cycles and then a final rise before fracture. These lattice changes were confirmed on a second specimen 4B4.

A further change noted was a slight but distinct radial broadening of the ring. A similar diffusion will be seen in the isolated spots in the earlier photographs from the stationary specimens (for instance, on comparison of the initial state shown by figure 6 with figures 7*b*, 8*b* or 9*b* after cyclic stressing). The same effect was obtained in the previous research, already referred to, on a mild steel and was there described as due to a "dislocation" of the grains. The present work makes it possible to extend this explanation. The preceding sections have shown that the crystallites, if formed within a grain under cyclic stressing, must possess essentially the same orientation and therefore co-operate in the reflexion from the parent grain; this rules out the possibility of the radial line broadening being due to the incomplete resolution which is known to be associated with an *independently* reflecting particle size less than about 10^{-4} cm. The diffusion is therefore to be attributed to irregularity in the above measured lattice expansion from grain to grain, or from point to point within a single grain, changes which would give rise to corresponding variations in the diffraction angle. Such slight lack of homogeneity in the lattice change is reasonably to be expected. The expansion together with the slight diffusion of the rings are therefore considered to form direct indication of the incidence of an internal strain in the atomic lattice during application of the cyclic stresses, and in view of existing evidence on the association of lattice distortion with hardening, this factor appears to be the one responsible for the changes in yield point arising from prior cyclic stressing and the observed suppression of the breakdown into the dispersed crystallite formation characteristic of normal plastic deformation.

Conclusion

The present paper has been limited to experimental observations and the immediate inferences. In view of the present incomplete understanding of strain-hardening and plastic deformation of metals it has not been thought worth while attempting to relate the results to current theories. It will be necessary first to extend the work to other metals, including brittle materials, especially in connexion with the part played by lattice distortion, and also to make X-ray tests whilst the metal is actually under load. Further work on these lines is in progress, but the results already obtained above constitute points of interest which definitely supplement existing data on the behaviour of the crystalline structure of the metallic grain under mechanical deformation, and which will require consideration in any complete theoretical treatment of the subject.

In conclusion, the authors acknowledge their indebtedness to Dr H. J. Gough, F.R.S., who collaborated in previous researches from which the above developed, to Dr G. W. C. Kaye, F.R.S., in whose department the X-ray work has been undertaken by one of us (W. A. W.), and also to Dr S. L. Smith and Dr G. A. Hankins with whom a number of points were discussed.

SUMMARY

The stress-extension relationships for an annealed α-brass have been measured for static tensile stress and for a symmetrical alternating tension-compression applied at a frequency of 2200 cyc./min., and the mechanical properties indicated by the curves have been studied in relation to the changes in crystalline structure of the grains as shown by the X-ray diffraction method. It is shown that the dispersal of the grains into widely oriented crystallites, which constitutes the physical characteristic of the change at the yield point under ordinary static or slow cyclic stress, is entirely suppressed under the same ranges of cyclic stress when applied at the high frequency, and that, after the cyclic stressing has ceased, this suppression persists up to a static load equal to the maximum of the prior stress cycle employed; the mechanical measurements indicate a corresponding inhibition of the primitive yield point. A further result is obtained by a precise comparison of the dimensions of the atomic lattice of specimens subjected to cycles of an unsafe range of stress; these show that an appreciable internal strain of the nature of a volume expansion is built up in the lattice during the rapid cyclic stressing, and it is considered that it is this distortion which is associated with the inhibition of the dispersed crystallite formation and rise in primitive static yield point.

REFERENCES

Gough, H. J. and Wood, W. A. 1936 *Proc. Roy. Soc.* A, **154**, 510.
— — 1940 Report (in preparation).
Wood, W. A. 1933 *Phil. Mag.* **16**, 719.
— 1935*a* *Trans. Faraday Soc.* **31**, 1248.
— 1935*b* *Phil. Mag.* **19**, 219.
— 1939 *Nature, Lond.*, **143**, 163.
— 1939 *Proc. Roy. Soc.* A, **172**, 231.

The equilibrium of grains on the bed of a stream

By C. M. White
Imperial College of Science and Technology, London

(*Communicated by G. I. Taylor, F.R.S.—Received* 1 *August* 1939)

Symbols

b = breadth of channel or nozzle.
c, c_1, c_2, etc. = numerical coefficients.
d = depth of liquid in channel.
g = gravitational acceleration.
i = energy head gradient.
k = diameter of sand grains.
l = length of nozzle.
p = pressure $[ML^{-1}T^{-2}]$.
Q = volume flowing per unit time.
U = velocity in main stream outside boundary layer.
$\overline{U}$ = mean velocity in main stream.
u = velocity at any point within the boundary layer.
u' = superimposed pulsation velocity.
$V_* \equiv \sqrt{(\tau/\rho)}$ (with dimensions of velocity).
x = distance down nozzle in direction of flow.
y = perpendicular distance from wall.
y_1 = shift of origin to allow for turbulent mixing among grains.
$z \equiv y/y_1$.
α = numerical coefficient in equation (2).
δ = thickness of boundary layer.
η = packing coefficient $\equiv k^2$ times number of grains per unit area.
θ = angle of tilt of bed in nozzle no. 2 in experiments nos. 7 and 9.
μ = viscosity $[ML^{-1}T^{-1}]$.
ν = kinematic viscosity $[L^2T^{-1}]$.
ρ = density of fluid $[ML^{-3}]$.
ρ' = effective density of sand grains in the fluid.
τ and $\bar{\tau}$ = mean stress on bed $[ML^{-1}T^{-2}]$, e.g. dynes per sq. cm.
ϕ = angle of repose of top layer of grains in the particular fluid.
$\chi \equiv U/2{\cdot}5V_*$, a substitution used in Appendix II.

A fluid flowing over a loose flat granular bed tends to move the grains forward, and the conditions under which movement begins depend, not only upon the speed, but also upon the nature of the motion in the stream itself: viscous steady motion, steady inviscid motion, and turbulent motion act somewhat differently, and the speed necessary to dislodge grains differs appreciably.

Like any solid boundary, the loose granular bed exerts a drag upon the fluid, and the accompanying shear stress is transmitted from bed to fluid almost wholly by the more prominent grains in the uppermost layer. Each such grain transmits a small force, and the manner in which it does so, again depends upon the type of motion, though it is now the local motion which is concerned, rather than that of the main stream. Two extreme cases may be distinguished. At slow speeds and with small grains the pressure at the front of the grain does not appreciably exceed that at its rear, and the force applied is the resultant of viscous stresses acting tangentially as in figure 2. At high speeds and with large grains such tangential drag becomes relatively unimportant compared with the drag due to pressure differences: the pressure distribution is not symmetrical but is less over the downstream half of the grain, so that when integrated it gives rise to a resultant force or form drag whose component resists the motion. Both at low speeds and at high speeds, if the main stream be turbulent, the force applied to the grain fluctuates irregularly. In the low-speed case, if the main stream be steady, the force on the grain is also steady. In the high-speed case, whatever the state of the main stream, eddies are shed from the back of the grains, and grains farther downstream are at least subjected to the cumulative effect of the pulsations from upstream.

With regard to their equilibrium as they lie on the bed, grains of diameter k usually occupy more area than k^2. A packing coefficient η, defined as k^2 times the number of grains per unit area, conveniently expresses their closeness. When a mean stress τ is applied to the bed each exposed grain transmits a horizontal force $\tau k^2/\eta$ from fluid to bed. In the high-speed case, when tangential components are negligible, the resultant force, if the grain be regarded as spherical, passes through its centre, and the forces are in equilibrium and the grain about to move when, as in figure 1,*

$$\tau = \eta \frac{\pi}{6} \rho' g k \tan\phi, \tag{1}$$

where ρ' is the effective density of the grain in the fluid, and ϕ is the angle of respose of the surface layer of grains. For the slow-speed case the corresponding force system is shown in figure 2, where it is seen that the line of action lies above the centre of gravity, and, since the height at which the force acts cannot be predicted analytically, an experimental coefficient α must be included in the equation which becomes

---

* That the force on the grain is nearly horizontal seems to be proved by an experiment described later (p. 333).

$$\tau = \alpha\eta\frac{\pi}{6}\rho' g k \tan\phi. \tag{2}$$

Equations (1) and (2) concern the equilibrium of grains just as they are about to move, and in both the value of τ is a local and instantaneous one, often considerably in excess of the time average for the whole bed, so experimental arrangements which will verify (1) or determine α in (2) are not easily found.

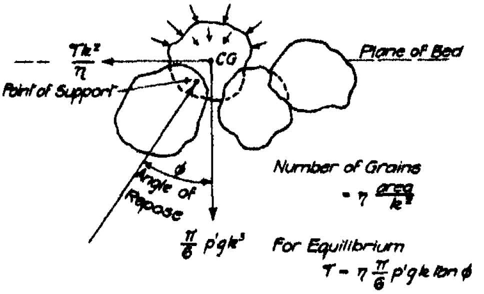

FIGURE 1. Equilibrium of an individual sand grain when the fluid acts normally to the surface and tangential stresses are negligible; $V_* k/\nu > 3{\cdot}5$ and assuming that the "lift" component is negligibly small.

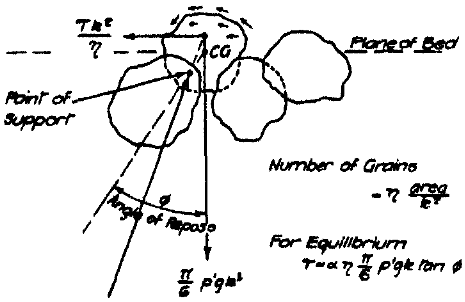

FIGURE 2. Equilibrium of an individual sand grain when the tangential stresses are of major importance; $V_* k/\nu < 3{\cdot}5$.

EXPERIMENTS AND RESULTS—AT LOW SPEEDS

From the experiments of Nikuradse (1933), considered in the light of those by Fage (1933), it is clear that viscous or tangential stresses predominate only when $V_* k/\nu$ is less than 3·5, where V_* is $\sqrt{(\tau/\rho)}$ and ν the kinematic viscosity of the fluid. This condition in an ordinary channel necessitates the use of a fluid more viscous than water: accordingly, an experiment was made with lubricating oil, $\nu = 1{\cdot}6$ cm.^{2} sec.$^{-1}$.

An open channel, 5·08 cm. wide, 100 cm. long, with a smooth bed of sand sloping at approximately 1 in 28, was arranged in the Civil Engineering Department of Imperial College, London. The oil supply to the upper end of the channel was gradually increased until the grains began to move. The drag was measured in two ways: from the product of the slope, density, and depth; and also from the mean velocity as determined by volumetric measurement of the rate of oil flow, using the relation $\tau d/\mu \overline{U} = 3$,* from which $\overline{U}$, and the equally uncertain dimension d, may be eliminated by substitution from

$$\tau = \rho g d i \quad \text{and} \quad Q = bd\overline{U}.$$

The results, summarized in table 1, show that the Aylesford sand begins to move when the drag τ is between 8 and 11 dynes/sq. cm.; the corresponding drag for Leighton Buzzard sand is 26 dynes/sq. cm. Unexpectedly this value appears to be independent of the initial closeness of packing of the grains: in experiment 2*a* the bed was rough as left by the edge of a metal strip used to level the dry sand surface, and the packing coefficient η was between 0·3 and 0·4. In experiment 2*b*, oily sand was smoothed as much as possible, and left for 2 days while surface tension completed the levelling: η was then estimated to be 0·8–1·0. Yet, despite this large variation, there was no significant difference in τ. The probable explanation is that when the top grains are far apart the resultant force is lower down, so, although in accordance with figure 2 the drag per top grain is greater, its moment about the point of support remains sensibly unchanged. It is sufficient therefore to determine the product $\alpha\eta$ in equation (2); and the values are:

PARALLEL FLOW—STEADY VISCOUS MOTION THROUGHOUT THE STREAM

Exp. no.	Sand	k mm.	tan ϕ in oil	τ dynes/sq. cm.	$\alpha\eta$
1	No. 2 Aylesford	0·21	1·4	9·5	0·37
2	No. 3 Leighton Buzzard	0·90	1·05	26	0·31

Of the two values, the second, 0·31, is the more reliable, as the individual grains of the finer sand were almost invisible in oil. With very close packing, η approximates to unity, so α is then of the order 0·3–0·4, which is consistent with the location of the forces in figure 2. Equation (2) is thus verified.

---

* The 3 is valid only for infinitely wide channels, for smaller width-depth ratios the value increases a little.

Table 1. Parallel flow—steady viscous motion throughout the stream

Exp. no.	Bed			Slope	Q c.c./sec.	ν cm.²/sec.	Average depth d cm.	τ dynes/sq. cm.		Remarks
	Sand	k mm.	Initial condition					From Q	From d	
1a	No. 2 Aylesford	0·21	Very irregular	0·0343	2·73	1·69	0·405	11·4	12·2	General bed movement
1b	,, ,,	0·21	Exceptionally smooth	0·0354	0·483	1·63	—	8·0	—	No movement
				0·0354	2·00	1·63	0·39	12·1	12·2	General movement
2a	No 3 Leighton Buzzard	0·90	Very irregular	0·0369	18·2	1·63	(0·8)	27·4	(26)	Movement begins
2b	,, ,,	0·90	Very smooth	0·0370	14·7	1·63	0·84	26·2	27·6	Very few grains move
				0·0370	34·0	1·63	1·08	34·6	35·2	1 % of top grains moving

The next experiment made with a less viscous fluid presented a difficulty. In a parallel channel with sufficient drag to move grains, the flow would be turbulent; the drag on individual grains would vary from moment to moment, and its instantaneous value would be difficult to assess. A new technique was required to meet this difficulty. Fortunately, even at quite high speeds, steady motion is possible if the fluid is made to accelerate as in a nozzle. When the form of the nozzle is known, and its wall smooth, the surface drag can be calculated by methods such as that used by Polhausen (see Howarth 1394). In general, τ varies with x along the length of the nozzle; but if the boundary layer equations are examined, it will be found that τ is constant in nozzles shaped to make U^3/x constant.* The drag is then given by

$$\frac{\tau}{\rho} = c\sqrt{\frac{\nu U^3}{x}}, \tag{3}$$

where the constant c according to Polhausen's solution should be 0·75; but some of the comparisons made by Howarth suggest that the drag is actually 25 % more, which would be more consistent with the value $c = 1{\cdot}05$ obtained by an experiment described later. Such a converging nozzle arranged horizontally is just what is needed for the sand-bed experiment: the acceleration gives a steady main stream, and the cubic form keeps the drag constant.

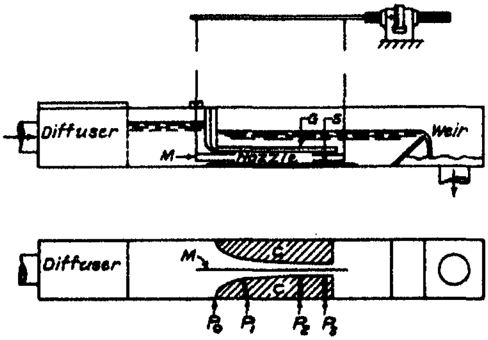

FIGURE 3. Constant-drag nozzle used in experiment 3. Suspended strip M was removed during sand experiments.

One series of experiments was made with the nozzle shown in figure 3. The brass cheeks C, of length $l = 20$ cm., were so shaped that

$$\frac{b}{l} = 0{\cdot}1\left(\frac{l}{x}\right)^{\frac{1}{3}}.$$

---

* See Appendix I.

These were covered with a glass sheet G, through which the sand-bed S could be observed. The speed was determined by using the pressure tapping holes P, and regarding the nozzle as a Venturi meter. As a direct check on the estimation of the drag, a thin metal stip M was suspended by two fine cotton threads 50 cm. long, mounted on a micrometer bar. Usually this strip was removed when testing for sand-bed movement. The water supply was increased gradually until the sand grains moved. Usually grains were scoured from all parts of the bed, so confirming that the drag was uniform. The continuous removal of sand steadily increased the cross-sectional area of the nozzle until, after an hour or so, the speed in the main stream was insufficient to remove further grains. The drag under these conditions is the maximum that the bed can resist without trace of movement. With regard to the sand, that of experiment 1 was somewhat irregular in size, and in water gave values of $V_* k/\nu$ approximately equal to, instead of less than 3·5, so another finer and more closely sieved sand was used.

After scouring to a standstill the result was:

CONVERGING FLOW. MAIN STREAM: STEADY AND INVISCID.
BOUNDARY LAYER: STEADY

Exp. no.	Sand	k mm.	Tan ϕ in water	τ dynes/sq. cm.	$\alpha\eta$
3	No. 1	0·122	1·0	3·56	0·39

Here τ was computed from the drag observed with the smooth brass strip which, after correcting for form drag, gave values 10 % greater than those predicted. Allowing for this, and for the uncertainty in k and $\tan\phi$, the value of $\alpha\eta$ is consistent with the earlier oil experiments.

Together, the oil and the water experiments extending in $V_* k/\nu$ from 0·04 to 2·1, a 50-fold range, prove that there is no significant change in $\alpha\eta$. Shields (1936) concludes otherwise, viz. that $\tau/\rho' gk$, instead of being constant, varies inversely as $V_* k/\nu$; but the present result is based on a much wider experimental range.

EXPERIMENTS AND RESULTS—AT HIGH SPEEDS

Equation (1), valid for $V_* k/\nu \gg 3{\cdot}5$, is more difficult to test. Eddies, shed from the grains, vary τ; at the moment of dislodgement τ exceeds the mean value, and it is the mean which is measured. From the work of Fage (1933) the magnitude of the pulsations can be estimated. The mean speed u at any particular distance y from the wall has superimposed upon it pulsations $\pm u'$. By ultra-microscope Fage found that near the top of pyramids on the wall of a very rough square pipe $u' = 0{\cdot}5u$, so the maximum speed was $1{\cdot}5u$, and the maximum stress presumably $2{\cdot}25\bar{\tau}$. In the present experiments, the boundary layer is relatively a little smaller than half Fage's pipe, and the opposite side of the pipe is of course absent, so the maximum stress should be somewhat less, possibly only about twice the mean, and in comparing the results with (1) this allowance must be made.

The nozzle (figure 3) used in the previous experiments was too small for larger grains, and as the proximity of the cheeks to the bed often caused secondary circulations and local scour, a larger nozzle was built with parallel sides and converging top. This arrangement, seen in figure 4, had proved very satisfactory in some earlier qualitative experiments. To give constant drag, with a turbulent boundary layer, the nozzle must converge approximately exponentially,* and the parameter depends upon the ratio of x to k, so that, strictly speaking, each size of sand requires a different nozzle: however, the differences are small, and are compensated, when a nozzle is used with an inappropriate size of sand, by the bed adjusting itself into a slightly curved form. Again, a suspended strip was used to check the mean value of the drag, but this time it was coated with sand grains similar in size and spacing to those of the bed. The nozzle was sealed to operate under pressure, so the threads supporting the strip were made very short, and the displacement measured by travelling microscope. Equation (1) includes the variables ρ', k, and $\tan\phi$, all of which were varied. Two sands, both closely sieved, and one sample of steel shot were tested, and their apparent angle of repose varied by tilting the whole apparatus.

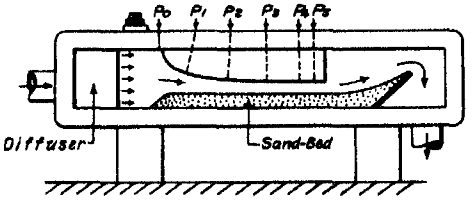

FIGURE 4. Constant-drag nozzle used for experiments 4–10.

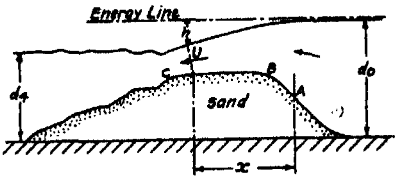

FIGURE 5. Converging flow over a naturally formed weir crest.

During the experiments the behaviour of some of the sand, which had become piled up downstream against the overflow weir, suggested that an experiment could be made with the arrangement shown in figure 5. Water was allowed to flow over a weir-like pile of sand in an ordinary glass-sided flume until the crest BC was lowered to the position of stability. In this way a converging "nozzle" was formed between the downward-sloping free surface of the water and the sand-bed BC. The velocity U was found from the head h, which was measured directly by pointer gauge. At the point C diverging flow begins, and the bed farther downstream becomes irregular. With a suitably chosen flow, the length BC was almost long enough to mask the unsatisfactory conditions in the region AB. The drag here may have differed considerably from that over the test length BC, but the only effect there would be like that due to change in the origin for x, which should accordingly be regarded as unknown. The difficulty was overcome by measuring h at two or more distances within the length BC, so that the drag could be found by trial from equation (15) of Appendix II, the unknowns being τ and the origin for x. The whole experimental arrangement was very simple, and less difficult to handle than either of the nozzles. The results obtained with it agreed with those with the nozzles. The combined results are given in table 2.

---

* See Appendix II.

As seen from the last column, the observed drag, over the wide ranges explored, main-stream speed from 38 to 2700 cm./sec., $V_* k/\nu$, from 33 to 128 and ρ'/ρ from 1·6 to 2100, was consistently one-half of that calculated from equation (1). Indeed, the very constancy of the one-half is a little perplexing. If the one-half is the result of stress fluctuations, then the slower ones of water should have far more effect than the much more rapid ones of air, yet the experiments fail to distinguish between the two. Each value is the mean of several experiments, from which admittedly some of the individual readings varied by $\pm 25\ \%$, so it is just conceivable that a difference of that order might have passed undetected. A more likely explanation is that the fluctuations are slow, more in the nature of variation with place rather than with time, just as a flame may cling to the side of one lump of coal for some time, and then, suddenly swinging over, may remain against another for a further indefinite period. However, whether this is so or not, if lift is negligible, the last column of table 2 appears to prove that in turbulent boundary layers a few grain diameters thick the stress is so irregular, either in time or place, that local maxima twice the mean are maintained for periods during which the fluid travels distances much greater than the grain diameter. Under these circumstances bed movement begins when the mean drag is one-half of that from (1). Experiments 7, 8 and 9 also support the inclusion of $\tan\phi$ in equation (1).

TABLE 2. CONVERGING FLOW. MAIN STREAM: STEADY AND INVISCID. BOUNDARY LAYER: TURBULENT

Epx. no.	Bed material	Diam. k mm.	Fluid	Main stream approximate final speed cm./sec.	Mean drag $\tau_{\text{obs.}}$ dynes/cm.^{2}	$\frac{\rho'}{\rho}$	$\frac{V_* k}{\nu}$	$\frac{\tau_{\text{obs.}}}{\rho' g k}$	$\tan\theta$	$\tan\phi$	$\frac{\tau_{\text{obs.}}}{\tau_{\text{cal.}}}$*
4	Sand no. 3	0·90	Water	38	16·9	1·6	33	0·119	0	1	0·57
5	Steel shot	0·71	Water	62	30·8	6·9	35	0·064	0	0·685	0·47
6	Sand no. 3	0·90	Air	1142	22·5	2100	80	0·098	0	1	0·47
7	Sand no. 4	5·6	Water	56	50·0	1·6	360	0·057	−0·45	1	0·54
8	Sand no. 4	5·6	Water	75	89·0	1·6	480	0·101	0	1	0·48
9	Sand no. 4	5·6	Water	91	133·0	1·6	590	0·151	0·50	1	0·54
10	Sand no. 4	5·6	Air	2700	146·0	2100	1280	0·102	0	1	0·49
										Mean	0·50$_5$

* Calculated from $\tau_{\text{cal.}} = \eta \frac{\pi}{6} \rho' g k \cos\theta(\tan\phi + \tan\theta)$ taking $\eta = 0{\cdot}4$ as determined by counting top grains.

RESULTS WITH CONVERGING, DIVERGING, AND PARALLEL FLOWS COMPARED

In open parallel flumes the drag to start movement is much less. For example, the Leighton Buzzard sand no. 3 would, according to the experiments of Casey (1935) or of the U.S. Waterways Experiment Station, start moving at 5 dynes/sq. cm. instead of the present 16·9 dynes/sq. cm.; again, sand no. 4 would start at 44 dynes/sq. cm. in a flume, instead of at 89 dynes/sq. cm. Apart from the effect of possible surface waves, the only significant difference between the two kinds of experiment is that, in converging flow, turbulence is restricted to the boundary layer, whereas in parallel flumes it extends throughout the stream. Large-scale turbulence, well away from the bed, may not materially contribute to the mean stress[*] near the bed, but it does very materially add to the maximum stress fluctuations there, and particularly to those slow ones which more easily dislodge grains. Fage's measurement of the total turbulence already referred to, which gave $u' = \frac{1}{2}u$ at the pyramid top, was made with a pipe so rough that probably the whole disturbance was generated by a local grain or two. At the other extreme, near the wall of a smooth pipe, Fage (1936) found $u' = 7V_*$. The mean speed at the top of the grains, when these are just large enough to begin to influence the motion, can be estimated from the logarithmic distribution

$$u = 5{\cdot}76V_* \log \frac{33y}{k}. \tag{4}$$

At the top of the grain, taking the origin for y to be $k/33$ below the centre line of the top layer of grains, the value of y is $(-\frac{1}{2}+\frac{1}{33})\,k$, and inserting this in equation (4), the mean speed at the top of the grain is also $u = 7V_*$. So the fluctuations here are just equal to the mean, and the speed varies from zero to $2u$. If a laminar sublayer exists, as it may if $V_* k/\nu < 3{\cdot}5$, then stress is proportional to speed, and the maximum value of the drag is twice the mean. Thus, since the wall contributes nothing, one may say that large-scale turbulence by itself doubles the maximum stress at the wall. On the other hand, if the turbulence extends up to and into the wall, as it does if $V_* k/ \gg 3{\cdot}5$, then the speed variation of 2 to 1 implies a stress variation of 4 to 1, and the maximum drag is four times the mean. As we have already seen that either large-scale turbulence or wall turbulence can individually double the stress, it is not inconsistent to find that the two together multiply it by 4. This factor must be inserted in equation (1) before it is applicable to large grains in parallel flumes. The comparison is then:

---

[*] In the Prandtl-Nikuradse theory of pipe resistance it is assumed that disturbances originating elsewhere do not appreciably influence the value of a local time-average shear-stress; but when, as in the present problem, particular instantaneous maximum values are under discussion the more distant sources of disturbance cannot be ignored.

DRAG TO START MOVEMENT

Type of flow	k mm.	By experiment dynes/cm.^{2}	Predicted from equation (1)
In converging nozzle			Turbulence factor = 2
	0·9	16·9	14·9 dynes/cm.^{2}
	5·0	89	92 dynes/cm.^{2}
In parallel flume			Turbulence factor = 4
	0·9	5	7·5 dynes/cm.^{2}
	5·6	44	46 dynes/cm.^{2}

and the agreement is good; it confirms that just one-half of the maximum stress fluctuation at the bed in a parallel flume originates in large-scale disturbances far from the bed.

In some cases such large-scale turbulence can even be the controlling factor. A nozzle twice the length of that in figure 4 was made with the upstream part converging and the downstream part diverging. The flow was increased until gentle movement occurred in the upstream part of the bed. Here, due to convergence, the drag was relatively great, whereas, due to the divergence of the downstream part, the mean drag there was zero or even slightly negative. In the converging part the main stream was steady, while in the diverging part it was strongly turbulent. The bed in the downstream part was extremely active, in spite of negligible mean drag and progressively slower speed.

LIFT

Earlier workers have attempted in other ways to explain the very large difference between flume values and the static force required to dislodge an individual grain. Jeffreys (1929) suggested that fixed particles are subject to a lift component due to the particular pressure distribution on their surface. It is self-evident that such a lifting force must exist. Fage's experiments with closely packed pyramids gave lift* as large as the drag, but the existence of open spaces in a loosely packed bed of sand grains seems to allow some equalization of pressure, since, if the present estimate of the effect of packing and of pulsations is correct, the lift component must here be negligibly small. To verify this an experiment was made in which the grains of a loosely packed bed were so cemented that they remained in place in a stream moving at more than twice the speed necessary to sweep unfixed grains away. A test grain was modelled in wax, $\rho' = 0{\cdot}05$ g./c.c., $k = 5{\cdot}6$ mm., and fastened to the end of a piece of cotton. The test grain was placed successively in typical hollows on the fixed bed, and prevented from moving downstream by the tension on the cotton which carried the whole of the horizontal force on the grain. Despite the high speed the grain did not rise, and so the lift seems less than its weight, which was only 3 % of that of an ordinary silica grain.

---

* Calculated from original data personally communicated to the author.

CONCLUSION

In conclusion it can be emphasized that despite uncertainties, often as much as ± 25 %, the experiments establish that, at low speeds, there is a wide range of $V_* k/\nu$ in which, for any one size of grain, the stress to start movement is sensibly constant. Further, they establish that, other things being constant, the stress varies directly as the grain diameter. There is some evidence also that the stress varies directly as $\tan\phi$. Rounded sand grains subjected to a steady viscous drag begin to move when

$$\tau = 0{\cdot}18\rho' g k \tan\phi.$$

This would also apply if the force were steadily applied by an inviscid fluid in the particular case when, as they usually are, the centres of the grains in the top layer are $1{\cdot}75k$ apart. Lift seems to be negligible. If this is so, then at high speeds wall turbulence reduces the mean apparent starting stress by 40 % or more. The present experimental values are at least twice those from open flumes, a difference explained by large-scale turbulence which also causes the stress at the wall to fluctuate, and to reach a maximum twice the mean. In irregular rivers this factor is much larger, and transport of grains would begin at correspondingly lower values of mean drag, were it not for the contrary action of form drag which probably transfers more than half the total drag directly to the bed without the intermediary of tangential drag. In one experiment with a divergent nozzle, large-scale turbulence was strong enough to raise clouds of grains, though at the bed itself the time average of the tangential drag was zero.

Before equations (1) and (2) can be applied to natural rivers, allowance must be made for the fact that a large fraction of their total drag is transferred to the bed directly as form drag, that large-scale turbulence is probably greatly in excess of the values here considered, and also that it is accompanied by non-uniform distribution of the time-average drag from place to place. The form drag enables the bed apparently to withstand a greater drag, while turbulence and non-uniformity have the opposite result. These opposing factors can be great or small, and in some instances they happen to neutralize each other, but this must not be interpreted as justifying the direct application of the present results to rivers.

APPENDIX I. CONSTANT DRAG NOZZLE

With non-turbulent boundary layer

The equation for steady motion

$$u\frac{\partial u}{\partial x}+v\frac{\partial u}{\partial y}+\frac{1}{\rho}\frac{\partial p}{\partial x}-\nu\frac{\partial^2 u}{\partial y^2}=0, \tag{5}$$

when applied to a boundary layer of thickness δ, outside which $u = U$ when $y \geqslant \delta$, can be satisfied within certain restrictions by the solution

$$\frac{u}{U}=f\left(\frac{y}{\delta}\right), \tag{6}$$

where the function f is independent of x.

After eliminating v in (5) by substitution from the equation of continuity

$$\frac{\partial u}{\partial x}+\frac{\partial v}{\partial y}=0, \tag{7}$$

and after eliminating p by substitution from the equation

$$\frac{\partial p}{\partial x}+\rho U\frac{\partial U}{\partial x}=0, \tag{8}$$

which is derived on the assumptions that the flow outside is irrotational, and that $\partial p/\partial y = 0$; and after integrating between the limits $y = 0$, $u = 0$ and $y = \delta$, $u = U$, equation (5) can be expressed as

$$U\frac{\partial}{\partial x}U\delta\int_0^1\frac{u}{U}\,d\left(\frac{y}{\delta}\right)-\frac{\partial}{\partial x}U^2\delta\int_0^1\left(\frac{u}{U}\right)^2 d\left(\frac{y}{\delta}\right)+U\delta\frac{\partial U}{\partial x}-\nu\frac{U}{\delta}\left[\frac{\partial(u/U)}{\partial(y/\delta)}\right]_{y=0}=0; \tag{9}$$

written in this way, each of the integrals is, in the light of (6), seen to have degenerated into a mere numerical constant.

The boundary layer thickness is a function of x, but if the drag stress at the wall is to be constant

$$\mu\left(\frac{\partial u}{\partial y}\right)_{y=0} = \text{const.}$$

or

$$\mu\frac{U}{\delta}\left(\frac{\partial(u/U)}{\partial(y/\delta)}\right)_{y=0} = \text{const.}$$

or

$$\frac{\delta}{U} = c_1 \nu \frac{\rho}{\tau}, \tag{10}$$

each side of which is independent of x. Using (10) to eliminate δ, equation (9) becomes

$$U\frac{\partial}{\partial x}c_2 U^2 - \frac{\partial}{\partial x}c_3 U^3 + U^2\frac{\partial U}{\partial x} = \frac{V_*^4}{c_1\nu}$$

or

$$\frac{U^3}{x} = \frac{V_*^4}{c_4 c_1 \nu}, \tag{11}$$

where

$$c_4 = \tfrac{2}{3}c_2 - c_3 + \tfrac{1}{3};$$

so, with steady motion, the necessary conditions can be satisfied, and the drag is constant when U is made to vary directly as $x^{\frac{1}{3}}$.

The velocity distribution arbitrarily assumed by Pohlhausen gives $\sqrt{(c_1 c_4)} = 0{\cdot}75$, whereas Blasius's distribution applied to the somewhat analogous case of the upstream face of a circular cylinder would require $\sqrt{(c_1 c_4)} = 0{\cdot}95$. The smooth strip suspended in the first nozzle gave

$$\sqrt{(c_1 c_4)} = 1{\cdot}05,$$

and this value was used in experiment no. 3.

APPENDIX II. CONSTANT DRAG NOZZLE

With turbulent boundary layer

Assuming that the motion is like that near the wall of a very rough pipe, the velocity distribution within the boundary layer is

$$u = 2{\cdot}5 V_* \log_e \frac{y}{y_1}, \tag{12}$$

where the constant y_1, in effect a shift of origin, takes into account the turbulent mixing which persists among the grains even where $u \to 0$.

This velocity distribution, when V_* is constant, implies that when $y < \delta$ the stream function is independent of x, so that the stream lines are parallel to the wall. There is a discontinuity at the edge of the boundary layer outside which the stream lines are somewhat inclined, and they therefore turn abruptly through a small angle as they enter the boundary layer (figure 6).

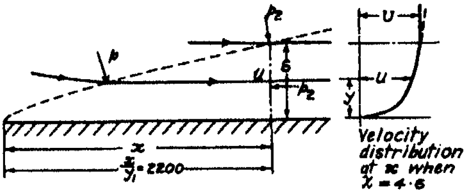

FIGURE 6. Boundary layer near rough wall with constant drag. Vertical scale is exaggerated sixfold.

With stream lines parallel in the boundary layer, the momentum in the x-direction does not change, and the mean apparent shear stress, corresponding to the last term in (5), arises entirely from pressures external to the boundary layer: and these give

$$\tau x = \int_{y_1}^{\delta} (p - p_2)\, dy. \tag{13}$$

Since p is determined by the irrotational motion outside, and, since once it has entered the boundary layer the speed of a stream line remains unchanged, (9) may be written

$$V_*^2 x = \tfrac{1}{2} \int_{y_1}^{\delta} (U^2 - u^2)\, dy, \tag{14}$$

which with (12) gives $\dfrac{x}{y_1} = \dfrac{6{\cdot}25}{2} \displaystyle\int_1^{e^\chi} (\chi^2 - \log^2 z)\, dz,$

where $\chi = U/2{\cdot}5V_*$ and $z = y/y_1$. The two limits $z = 1$ and $z = \delta/y_1$ correspond respectively to $\log z = 0$ and $\log z = \chi$ (cf. (12)); so, making the integration and inserting these limits,

$$\frac{x}{6{\cdot}25 y_1} = e^\chi(\chi - 1) - \frac{\chi^2}{2} + 1.$$

Nikuradse's closely packed grains cemented to the wall of a pipe give $y_1 = k/33$, but Schlichting's loosely packed spherical particles $1{\cdot}5k$ apart give $y_1 = k/9$ and this more nearly represents the present case. So

$$1{\cdot}5\frac{x}{k} = e^\chi(\chi - 1) - \frac{\chi^2}{2} + 1, \tag{15}$$

which, since χ varies as U, gives the relation between x and U necessary to keep τ constant.

From (15) the drag coefficient should then be

$\frac{x}{k}$	χ	$\frac{\tau}{\rho U_x^2}$
5	2·07	0·037
10	2·43	0·027
20	2·82	0·020
50	3·45	0·0134
100	3·95	0·0102
300	4·76	0·0071
1000	5·7	0·0049
3000	6·62	0·0036
10,000	7·67	0·0027
50,000	9·1	0·00194

In comparison, the hanging strip, after allowing for form drag, gave 19 % greater drag when $x/k = 45$: but as the strip was only $3{\cdot}5k$ wide, the partly exposed edges, for which no allowance was made, would account for the excess, and the tabulated values may be accepted as substantially correct.

REFERENCES

Casey, H. J. 1935 *Mitt. Vers Anst. Wasserb. u. Schiffb. Berl.* Heft 19.
Fage, A. 1933 *Rep. Memo. Aero. Res. Comm., Lond.*, p. 1585.
—— 1936 *Phil. Mag.* (7), **21**, 80.
Howarth, L. 1934 *Rep. Memo. Aero. Res. Comm., Lond.*, p. 1632.
Jeffreys, H. 1929 *Proc. Camb. Phil. Soc.* **25**, 272.
Nikuradse, J. 1933 *Forschungsh. Ver. dtsch. Ing.* no. 361.
Shields, A. 1936 *Mitt. Vers Anst. Wasserb. u. Schiffb. Berl.* Heft 26.
U.S. Waterways Exp. Sta., Vicksburg, 1936, paper 17.

The neutrons from the disintegration of fluorine by deuterons

By T. W. Bonner,* *Cavendish Laboratory, Cambridge*

(*Communicated by J. D. Cockcroft, F.R.S.—Received* 16 *October* 1939)

[Plate 17]

The emission of neutrons from a target of calcium fluoride when bombarded by 3 MeV deuterons was first reported by Lawrence and Livingston (1934). Early unpublished experiments to determine the distribution in energy of the neutrons from this reaction were made by Bonner and Brubaker in 1935 and later by Stephens and Djanab in 1937, but due to the small yield of neutrons obtained from the reaction, these experiments were not completed. The present experiment was begun because it seemed feasible to measure the energy of the neutrons from this reaction with the high voltage apparatus of the Cavendish Laboratory. A larger yield of neutrons was expected due to the large currents of high-speed deuterons which were available.

The method used to determine the energy of the neutrons is the same as that previously used (Bonner and Brubaker 1935*a, b*, 1936*a, b*; Stephens *et al.* 1937; Bonner 1938). Recoil protons or recoil helium nuclei are produced in a Wilson cloud chamber which is filled with either methane or helium. When investigating neutrons of high energy, it is advantageous to use a pressure in a cloud chamber of several atmospheres so that the protons or α-particles of high energy produced in collisions with neutrons will be completely stopped in the chamber. The energy of the recoil particle, usually a proton or α-particle, is readily determined from its range. The neutron energy may be computed from the relation

$$E_0 \cos^2\theta = E\frac{(M+1)^2}{4M},$$

where E_0 is the initial energy of the neutron, E the energy given to the nucleus in the collision, M the mass of the nucleus, and θ the angle between the initial path of the neutron and the trajectory of the nucleus which has been struck. In the case of collisions between neutrons and protons, M is 1 and

---

[*] Fellow of the John Simon Guggenheim Memorial Foundation.

so $E = E_0 \cos^2\theta$; *in the case of the collisions of neutrons with helium nuclei* $E_0 \cos^2\theta = \frac{25}{16} E$. *If recoil protons are measured which are nearly in the forward direction, they have essentially the same energy as the incident neutrons since the value of* $\cos^2\theta$ *is nearly unity for small values of* θ. Recoils at larger angles can be used to determine neutron energies if the angle θ is measured and the appropriate $\cos^2\theta$ correction applied. However, there are two objections to this second procedure. In the first place an accurate measurement of angle takes more time and is more difficult than an accurate measurement of track length. In the second place serious errors are introduced in such energy measurements by those neutrons which do not proceed directly from the source but are scattered by the material in or around the cloud chamber. Such scattered neutrons occasionally also produce recoils in the cloud chamber and lead to calculated energies of neutrons many of which are too large. In most experiments an accurate determination of the maximum energy of the neutrons is important in order that the disintegration Q value of the reaction may be calculated; hence such a method is not applicable, since a sharp end point cannot be obtained using this method. An ambiguity in the maximum energy of the neutrons will be especially marked in cases where these neutrons are not as numerous as neutrons of lower energy from the same reaction.

Experimental arrangement

The experimental arrangement for getting the high energy deuterons on the target is shown in figure 1. The ion beam falls on a tungsten shutter at A which becomes heated to a temperature of from about 800 to 1200° C. This shutter is opened for about $\frac{1}{25}$ sec., and so allows a burst of deuterons to proceed to the target at C after being deflected through 90° by the analysing magnet B. Deuteron currents between 80 and 100 μA were obtained at the target. The timing mechanism was adjusted so that no deuterons struck the target before the cloud chamber was fully expanded. Preliminary experiments were carried out with a shutter in the beam between the target and the magnetic analyser. In those experiments many old recoil tracks were observed which obscured the good tracks. These old tracks came from neutrons produced in the magnet box, presumably from the disintegration of carbon by deuterons. This difficulty was overcome by putting the shutter in the position A as shown in the diagram. With this arrangement no old recoils were observed.

The targets of either CaF_2 or KF were held in a brass cup at the end of the horizontal tube. This cup was insulated by a 3 in. section of glass tubing. The current to the target was detected by the ballistic throw of a micro-ammeter. The burst of deuterons could be observed by the fluorescence produced on the target and this was useful in aligning the tube so that the ion beam hit the centre of the target. The centre of the cloud chamber was placed 25 cm. from the target in such a position that the neutrons were observed at an angle of 90 ± 18° to the direction of the 950 kV deuterons. In most of the experiments the cloud chamber was filled with helium at an expanded pressure of 4 atm. Water vapour was used in these experiments to keep the ratio of helium atoms to hydrogen atoms as large as possible. To investigate the neutrons of low energy, methane at a pressure of 1·5 atm. was used in the chamber.

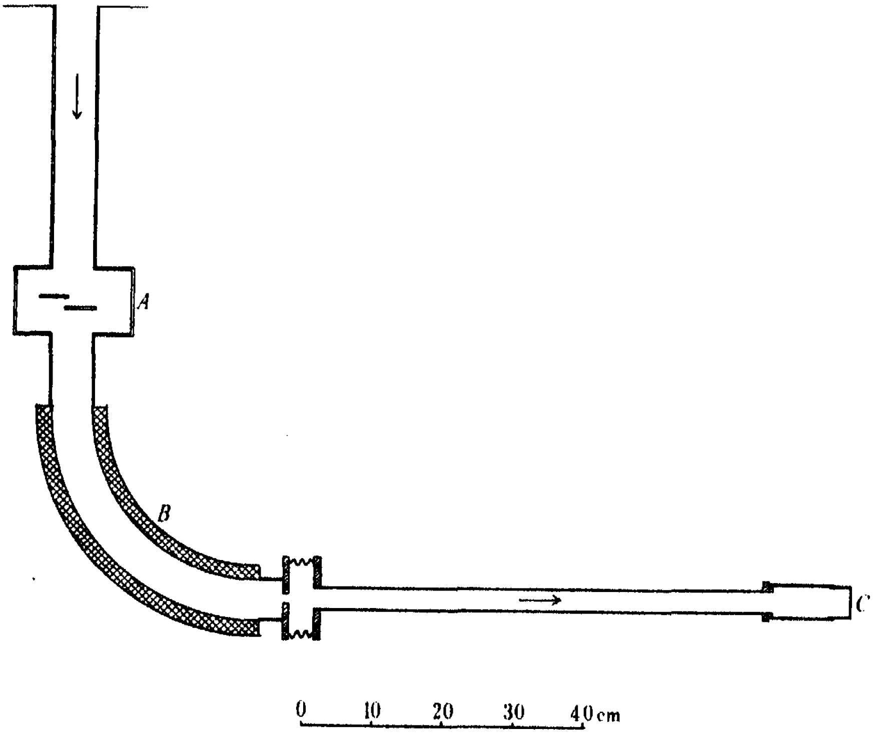

FIGURE 1. Schematic diagram of target arrangement.

Stereoscopic pictures of the cloud chamber were taken by the use of a direct and a mirror image. Both images appeared side by side on the same frame of the 35 mm. film. For measurement the cloud chamber tracks were reprojected through the same system of mirror and lens on to a white screen.

RESULTS

2300 pairs of stereoscopic pictures were taken when either targets of CaF_2 or KF were bombarded with 950 kV deuterons. 2100 of these photographs were taken with a cloud chamber filled with helium and the remaining 200 with methane in the chamber. In the first series the track lengths of 2000 helium recoils were measured which were projected in nearly the forward direction (0–12°). Sample photographs of these recoil tracks are shown on plate 17.

The stopping power of the gas in the chamber was determined by using the α-particles from Th C and Th C′ for calibration. A weak source of Th B + C + C′ was introduced into the chamber before it was filled with helium. Then photographs were taken of the two groups of α-particles from this source. The mean track lengths of the two groups were found to be $10{\cdot}45 \pm 0{\cdot}10$ and $5{\cdot}65 \pm 0{\cdot}10$ cm. The mean range of these two α-particle groups is 8·53 and 4·71 cm., so the computed stopping power is respectively 0·816 and 0·833. Within the experimental errors these measurements show the expected change of stopping power with range (Mano 1934). The stopping powers for particles of shorter ranges were computed from the theoretical variation of stopping power as given by Mano. The energies of the helium recoils were obtained from their ranges by the use of the range-energy curve of Holloway and Livingston (1938).

Figure 2 gives the distribution in energy of the helium recoils after multiplying the energy of the recoils by the factor 25/16 which converts the measurement of energy to that of the neutron. The curve of figure 2 does not give the true distribution in energy of the neutrons because no correction has been made for the variation with energy of the cross-section for collisions of neutrons with helium atoms. Also a correction needs to be applied for the different probability of measuring tracks of varying length in the cloud chamber. This correction is necessary because the longer range tracks have a greater probability of hitting a wall than do the short tracks.

The curve of figure 2 indicates that several groups of neutrons with energies of 11·1, 9·7, 7·1, 5·9, 4·1, and 2·6 MeV come from the disintegration of fluorine by deuterons. The group at 2·6 MeV is close to that expected from the reaction

$$H^2 + H^2 \rightarrow He^3 + n^1,$$

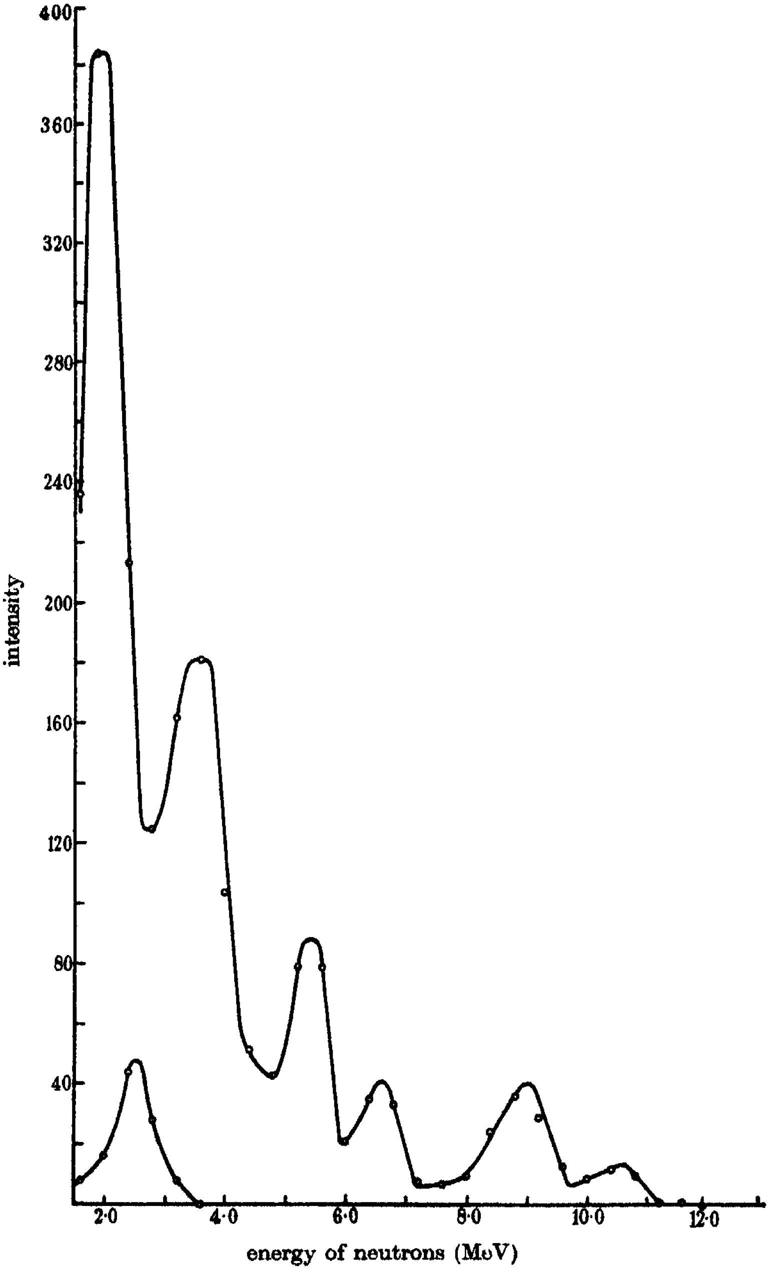

FIGURE 2. Distribution in energy of the neutrons as inferred from the energy of helium recoils.

and so a test run was made under identical conditions with a target of deuterium in place of the target of fluorine. The lower curve of figure 2 shows the distribution in energy of the neutrons from this reaction. Under these experimental conditions the neutrons from the deuteron-deuterium reaction would be expected to have a considerable spread of energy because of the high bombarding energy and because of the large angular aperture, 90 ± 18°, at which the neutrons were observed. The observed curve is consistent with the expected energy distribution and clearly shows that the 2·6 MeV group of neutrons from targets of fluorine is not due to deuterium contamination.

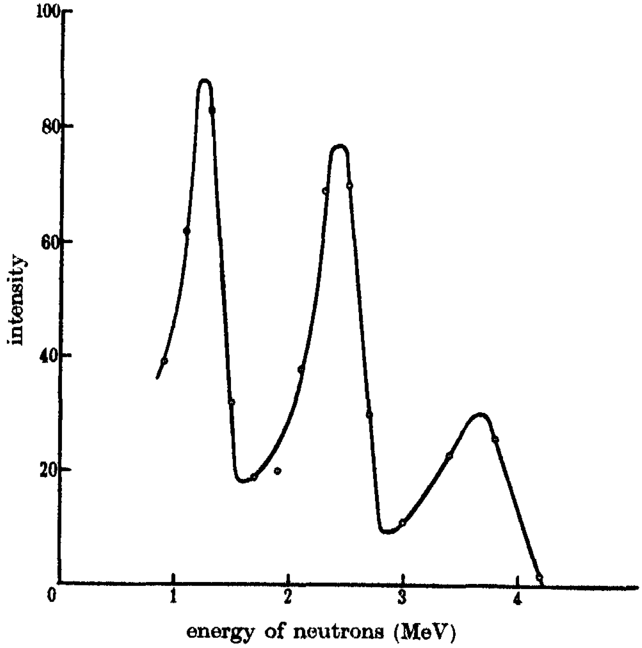

FIGURE 3. Distribution in energy of the neutrons as inferred from the energy of recoil protons.

The measurements of the energy of neutrons were extended to lower values by the results which were obtained when the cloud chamber was filled with methane. The lengths of 450 tracks of protons were measured which recoiled in the forward direction. The distribution in energy of these recoil protons, after correction for the probability of observing tracks of differing lengths, is given in figure 3. This distribution confirms the groups of neutrons at 2·6 and 4·1 MeV and shows that there is also a group of lower energy at 1·5 MeV.

The neutrons which are observed are attributed to the nuclear reaction

$$(1)\ F^{19} + H^2 \rightarrow Ne^{20} + n^1 + Q_1.$$

For a comparison with the experimental results shown in figures 2 and 3, a theoretical curve is given in figure 4 showing the distribution in energy of the recoils from the group of neutrons from fluorine with an energy of 6·0 MeV. In this calculation we have assumed an exponential excitation function, doubling every 100 kV, and spherical symmetry in centre of mass coordinates for collisions between neutrons and helium nuclei. Curve *A* gives the distribution in energy for those recoils which are measured in the forward direction (0–12°) as calculated for neutrons observed exactly at 90° to the bombarding deuterons. In curve *B* we have taken into account that neutrons were observed at an angle of 90 ± 18° and also have corrected for the pure range straggling of the recoil helium nuclei of this energy. We have further calculated from the amount of material in the cloud chamber that about 15 % of the neutrons which traverse the cloud chamber have been elastically scattered in the walls or neighbouring material and come from a random direction. The small fraction of recoils from these scattered neutrons which are measured will produce a tail on the low-energy side of the group of recoils. The inclusion of these recoils is not serious as the intensity is only

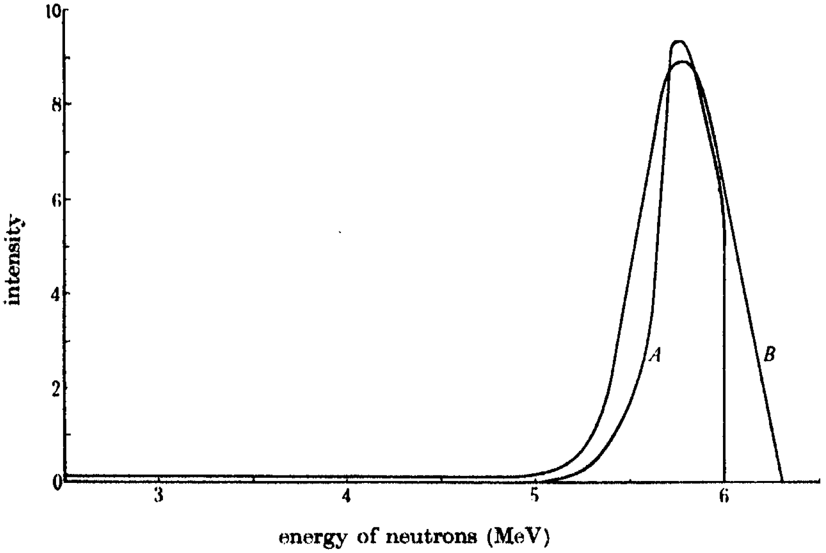

FIGURE 4. Calculated shape of a group of recoils from neutrons with an energy of 6 MeV.

approximately 1 % of the unscattered effect. Curve *B* gives approximately the shape of a group of recoils under our experimental conditions. When we compare the expected distribution with the curves of figures 2 and 3, we see that the experimental curves can be explained by discrete groups of neutrons with energies of 11·1, 9·7, 7·1, 5·9, 4·1, 2·6 and 1·5 MeV. There appears to be no evidence for a continuum of neutrons from this disintegration. Fluorine has only one isotope and so the only other reactions energetically possible for the production of neutrons are

$$(2)\quad F^{19} + H^2 \rightarrow O^{16} + He^4 + n^1 + 6\cdot 0\,\text{MeV}$$

$$(3)\quad F^{19} + H^2 \rightarrow Ne^{20*} + n^1$$
$$Ne^{20*} \rightarrow O^{16} + He^4.$$

From reaction (2) we should expect a continuous distribution in energy of the neutrons and very few neutrons with energies above about 3 MeV. If this reaction takes place it must be weak in comparison to reaction (1). The distribution in energy of the neutrons from reaction (3) in general would be quite similar to that from reaction (1) except that a group of neutrons might be broadened if the lifetime of the excited Ne^{20} is sufficiently short. A discussion of this possibility will be deferred to a later portion of this paper.

CALCULATION OF THE *Q* VALUES

The disintegration *Q* values of the reaction were determined from an integral range-number curve. Figure 5 gives the integral range-number curve for recoils in helium which have a track length greater than 2·7 cm. The extrapolated ranges of the groups of recoils were determined from the extrapolated track lengths by multiplying by the appropriate stopping power. Curves similar to that of figure 5 were made for the groups of neutrons of lower energy and a summary of the data is given in table 1. The disintegration *Q* values were calculated from the extrapolated ranges by the method of Livingston and Bethe (1937). These *Q* values are also given in table 1. The neutrons of maximum energy correspond to the case where the Ne^{20} is left in its normal state. The experimental value of $Q_1{}^\circ = 10\cdot 80 \pm 0\cdot 20$ MeV agrees quite closely with the value of $Q_1{}^\circ = 10\cdot 72 \pm 0\cdot 20$ MeV as calculated from the isotopic masses of F^{19}, H^2, Ne^{20}, and n^1. The other *Q* values correspond to excited states of Ne^{20} at 1·5, 4·2, 5·4, 7·3, 9·0 and 10·1 MeV. The dissociation energy necessary to break Ne^{20} into $O^{16} + He^4$ is only 4·73 MeV, so we see that the excited states of Ne^{20} above this energy are unstable against emission of α-particles. The highly excited states might be expected to

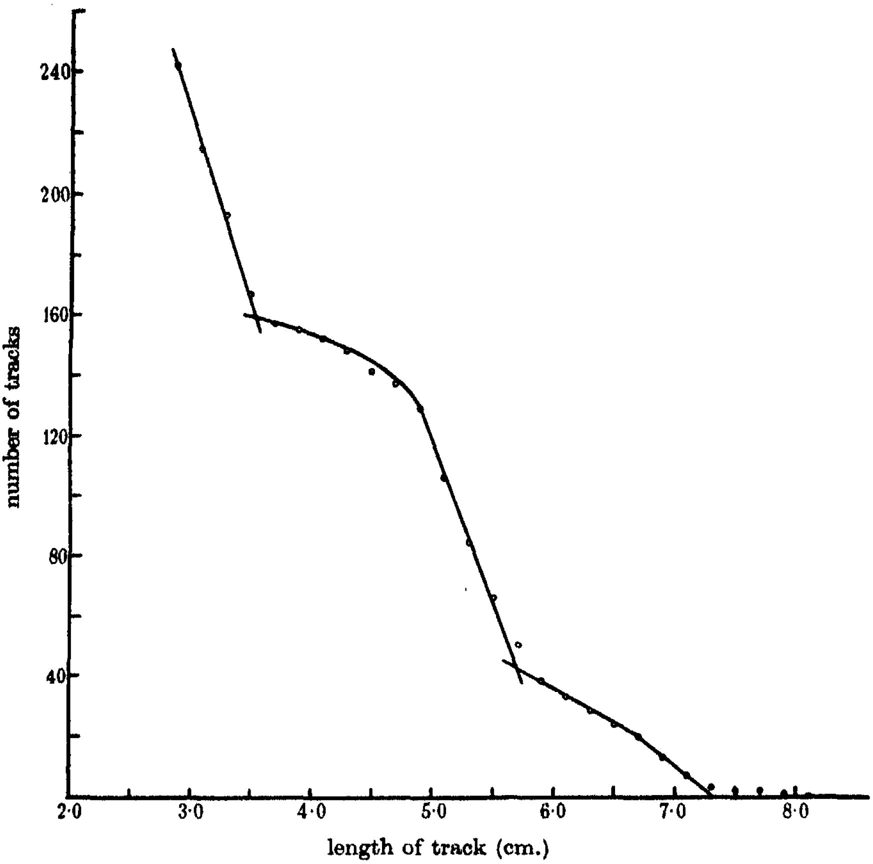

FIGURE 5. Integral range-number curve for helium recoils whose track lengths are greater than 2·7 cm.

TABLE 1

Extrapolated length cm.	Stopping power	Extrapolated range cm.	Energy of neutron at 90° MeV	Q MeV	Ne^{20*} MeV
7·30 ± 0·15	0·82	5·99 ± 0·15	11·08 ± 0·20	10·80 ± 0·20	0
5·73 ± 0·10	0·83	4·76 ± 0·12	9·67 ± 0·15	9·33 ± 0·15	1·5
3·55 ± 0·10	0·84	2·98 ± 0·12	7·09 ± 0·14	6·62 ± 0·14	4·2
2·66 ± 0·05	0·87	2·32 ± 0·12	5·93 ± 0·14	5·39 ± 0·14	5·4
1·65 ± 0·05	0·89	1·47 ± 0·13	4·15 ± 0·13	3·53 ± 0·13	7·3
8·09 ± 0·20	1·34	10·83 ± 0·50	2·57 ± 0·08	1·84 ± 0·10	9·0
3·18 ± 0·10	1·37	4·35 ± 0·30	1·49 ± 0·08	0·74 ± 0·10	10·1

break up before a γ-ray is emitted, unless we invoke selection rules to prohibit the disintegration of Ne^{20*} into $O^{16}+He^{4}$.

The experimental results indicate that the level in Ne^{20} at 10·1 MeV is not wider than 0·2 or 0·3 MeV. We can get a rough idea of this expected width from the uncertainty relation

$$\Delta E \, . \, \Delta T \approx \hbar,$$

where ΔE is the width of the nuclear level and ΔT is the time the excited Ne^{20} exists before breaking up into $O^{16}+He^{4}$. Since an α-particle in such an excited Ne^{20} is very near the top of the coulomb barrier, the lifetime can be estimated from the relation

$$\Delta T \approx R/v,$$

where v is the velocity of the α-particle in the Ne^{20*} and R is the nuclear radius. If we take a value of $R = 5{\cdot}4 \times 10^{-13}$ cm. and assume an α-particle velocity of 1/20 that of the velocity of light, we get a value of $\Delta E \approx 1{\cdot}6$ MeV. Since this value may be considered only as a rough upper limit to the value of ΔE, it does not seem to make necessary the use of selection rules forbidding the disintegration into $O^{16}+He^{4}$. It is reasonable that the actual width is smaller than the estimated since the estimate does not take into account the internal rearrangements necessary for the formation of the α-particle. The level in Ne^{20} at 10·1 MeV may be much narrower than the limit set by experiment and, if this be true, selection rules must prevent the disintegration into $O^{16}+He^{4}$.

In view of the considerations given above, it would be especially interesting to investigate the γ-rays and α-particles from this reaction so that one could tell whether a γ-ray or an α-particle is emitted by the excited Ne^{20}. Burcham and Smith (1938) have found five groups of α-particles from the disintegration of fluorine by deuterons, but from energy considerations it is apparent that these α-particles were correctly attributed to the reaction

$$F^{19}+H^{2} \rightarrow O^{17}+He^{4}+10{\cdot}1\ \text{MeV}.$$

They also found a group of α-particles with a range of 2·8 cm. which they attributed to carbon contamination. This is just the range of α-particles which would be produced if the Ne^{20}, excited to the 10·1 MeV level, broke up into $O^{16}+He^{4}$. Further experiments are needed to see if this 2·8 cm. group is partly due to fluorine.

A highly excited level in Ne^{20} has been observed in a different type of experiment. A resonance in the scattering of 5·8 MeV α-particles in oxygen has been observed independently by Brubaker (1938) and by Devons (1939).

FIGURE 7. A cloud-chamber photograph in helium at 4 atm. showing about eighty recoil helium tracks. There were four measurable tracks (0–12°) on this picture. The longest one points almost directly at the source of neutrons which appears to be above the cloud chamber and was projected by a 10·8 MeV neutron. The other three measurable tracks were produced by neutrons with energies of 2·3, 2·4 and 5·8 MeV. The bright object in the lower right-hand part of the cloud chamber is the holder for the Th source of α-particles.

FIGURE 8. The recoil track in the centre of the chamber is due to a head-on collision since it points towards the source as does the shorter tracks in the upper right-hand part of the chamber. The long faint track in the centre of the chamber is a proton which started at the top of the chamber and continued across the chamber. Note that there are no definite ends to this track since it went out of the illuminated portion of the chamber.

An excited level in Ne^{20} at about 9·5 MeV is indicated by these experiments. The energy of this level is not very accurate and it may reasonably be assumed to correspond to either the 9·0 or 10·1 MeV level which was found in our experiments.

The true distribution in energy of the neutrons has been computed by using the known variation with energy of the cross-section for the collision of neutrons in helium and hydrogen (Staub and Stephens 1939; Bethe and Bacher 1936). Such a corrected distribution is shown in figure 6. This curve shows that the most probable groups of neutrons from the reaction are those at 2·6 and 4·1 MeV. The distribution curve seems to decrease in intensity for both larger and smaller energies, and one naturally thinks that this most probable energy may be related to the nuclear temperature of the highly excited intermediate Ne^{21}. For a comparison with the experimental distribution, a curve of the form

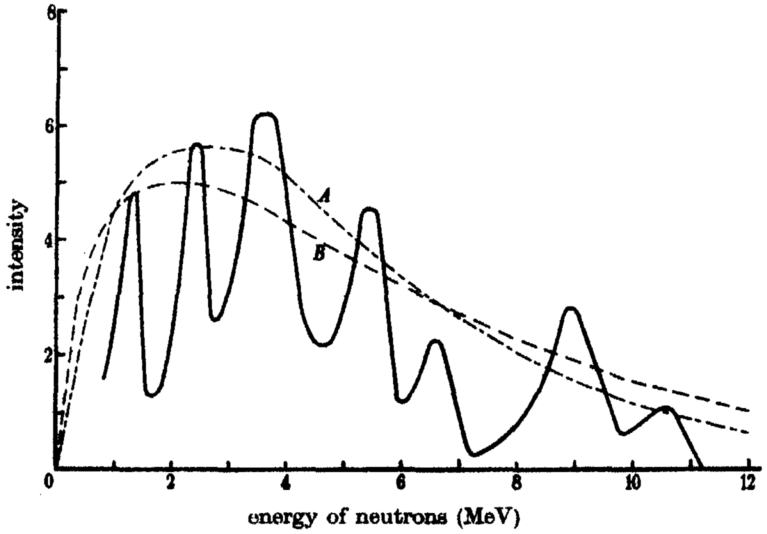

FIGURE 6. Corrected curve showing the true distribution in energy of the neutrons. The dotted curves are theoretical distribution.

$$N\,dE = e^{-E/\tau}\,E\,dE$$

is used. This relation was derived by Weisskopf (1937) for the distribution in energy of neutrons for closely spaced nuclear levels. This assumption is not satisfied in the present case. Nevertheless, the general idea of temperature advanced by Bohr may apply and the presence of an exponential factor in the energy distribution may be expected since energy levels which are not too widely spaced should approximate the picture of closely spaced levels. The best fit was obtained for a value of the nuclear temperature $\tau = 2{\cdot}5$ MeV and this distribution is that of curve *A* in figure 6. Although good agreement with the experimental curve is obtained with a value of $\tau = 2{\cdot}5$ MeV, we think that this nuclear temperature should not be taken too seriously, because it is uncertain whether this theoretical distribution should be applied to the experimental distribution which appears to be composed of discrete groups of neutrons. A reasonable fit can also be obtained by a distribution of the form

$$NdE = e^{-E/\tau}(E)^{\frac{1}{2}}\,dE.$$

The best fit for this distribution was obtained for a value of $\tau = 4$ MeV and the resulting curve is shown as *B* of figure 6. The fact that agreement is obtained in both these cases shows that agreement with experiment is not very dependent on the power of E assumed, showing that the exact mechanism of escape is not very important for the fit. Of course, a different nuclear temperature is obtained depending on the power of E which is used.

The writer is deeply indebted to Mr P. I. Dee, Dr C. W. Gilbert, Dr W. E. Burcham and many others in the High Voltage Laboratory for their generous help and assistance throughout the course of these experiments. Thanks are also due to Professor G. Breit for discussions on the theoretical aspects of the problem.

SUMMARY

The neutrons from the disintegration of fluorine by deuterons have been investigated by the method of observing helium or hydrogen recoils in a high pressure cloud chamber. When targets containing fluorine were bombarded with 950 kV deuterons, several groups of neutrons were observed. The disintegration Q values computed from the energies of the neutron groups are 10·80, 9·33, 6·62, 5·39, 3·53, 1·84 and 0·74 MeV. The nuclear reaction appears to be (F^{19}, H^2, Ne^{20}, n^1). The disintegration value $Q = 10{\cdot}80 \pm 0{\cdot}20$ MeV corresponds to a transition to the ground state of Ne^{20} and smaller Q values indicate excited states in Ne^{20} at 1·5, 4·2, 5·4, 7·3, 9·0 and 10·1 MeV. Only a small fraction of the neutrons belong to the group of maximum energy. The excited states in Ne^{20} at 5·4, 7·3, 9·0 and 10·1 MeV are unstable against α-particle emission and so they may break up into O^{16} and an α-particle. The experimental width of the level in Ne^{20} at 10·1 MeV appears to be not greater than about 0·2 or 0·3 MeV.

REFERENCES

Bethe, H. A. and Bacher, R. F. 1936 *Rev. Mod. Phys.* **8**, 117.
Bonner, T. W. 1938 *Phys. Rev.* **53**, 711.
Bonner, T. W. and Brubaker, W. M. 1935*a* *Phys. Rev.* **47**, 910.
— — 1935*b* *Phys. Rev.* **48**, 742.
— — 1936*a* *Phys. Rev.* **49**, 19.
— — 1936*b* *Phys. Rev.* **50**, 308.
Brubaker, G. 1938 *Phys. Rev.* **54**, 1011.
Burcham, W. E. and Smith, C. L. 1938 *Proc. Roy. Soc.* A, **168**, 176.
Devons, S. 1939 *Proc. Roy. Soc.* A, **172**, 559.
Holloway, M. G. and Livingston, M. S. 1938 *Phys. Rev.* **54**, 18.
Lawrence, E. O. and Livingston, M. S. 1934 *Phys. Rev.* **45**, 220.
Livingston, M. S. and Bethe, H. A. 1937 *Rev. Mod. Phys.* **9**, 289.
Mano, G. 1934 *J. Phys. Radium*, **5**, 628.
Staub, H. and Stephens, W. E. 1939 *Phys. Rev.* **55**, 131.
Stephens, W. E. and Bonner, T. W. 1937 *Phys. Rev.* **52**, 527.
Stephens, W. E., Djanab, K. and Bonner, T. W. 1937 *Phys. Rev.* **52**, 1079.
Weisskopf, V. 1937 *Phys. Rev.* **52**, 295.

The transfer of excitation energy from uranium ions in solution

BY ALFRED H. CARTER AND JOSEPH WEISS
University of Durham, King's College, Newcastle-upon-Tyne

(*Communicated by G. R. Clemo, F.R.S.—Received* 23 *October* 1939
—*Revised* 29 *November* 1939)

1. INTRODUCTION

The transfer of electronic excitation energy between molecules and atoms has attracted a good deal of attention during recent years. In the case of gases, this subject has been studied mainly by physicists, and important contributions have been made by J. Franck and his school in particular. In condensed systems, the transfer of excitation energy (absorbed primarily from an external light source) and the behaviour of excited molecules form the basis for all types of photosensitized reactions. These reactions are of considerable importance for the various types of biological photosynthesis and for many technical problems.

From a theoretical standpoint these reactions are interpreted by the hypothesis of collisions of the second kind put forward by Klein and

Rosseland (1921). Although their theory is based on a thermodynamical argument without giving a detailed picture of the actual mechanism, it has been assumed frequently that a direct transfer of a quantum of light energy can take place from the excited molecule to another molecule which under the influence of this acquired energy undergoes a chemical change.

West, Müller and Jette (1928), in an attempt to study collisions of the second kind in solution, investigated the photosensitized decomposition of oxalic acid by uranium salts. They arrived at the important conclusion that this sensitized photodecomposition goes parallel with the quenching of the uranium fluorescence by the oxalic acid. The elementary process of the quenching of the fluorescence was thus recognized as the primary process in this photosensitized reaction, a result in agreement with similar results obtained by Gaffron (1926) and Noack (1927) from a study of various photosensitized oxidations.

In agreement with the views then accepted about the quenching of fluorescence in solution, West *et al.* (1928) suggested a mechanism based on the direct transfer of energy from the light-absorbing uranium salt to the oxalic acid as mentioned above. They considered this mechanism to be proved when they were able to show that substances (such as I^-, Br^-) which themselves strongly quenched the fluorescence of uranium salts, did actually inhibit the decomposition of oxalic acid. However, Rollefson (1935) and Pringsheim (1937) pointed out that a difficulty still existed. Iodide ions in a concentration of about 1/1000 M, which are sufficient to bring about a considerable quenching of the uranium fluorescence, do not decelerate the decomposition of oxalic acid, and a concentration about 100 times greater is necessary in order to inhibit the rate of decomposition perceptibly. In order to overcome this difficulty the latter author assumed the formation of a complex between the uranium salt and the oxalic acid which would be stable towards the influence of iodide ions. As evidence for this complex he adduced the comparatively slight changes in the absorption spectra in the visible, which manifest themselves when oxalic acid is added to a uranium salt.

The idea that a simple transfer of the absorbed energy is responsible for the photosensitized decomposition can be ruled out immediately by energy considerations alone. The quantum of energy absorbed by the uranium salt in the visible (blue) region of the spectrum cannot possibly suffice, in itself, to bring about the photolysis of oxalic acid which requires the absorption of an ultra-violet light quantum for its decomposition (Allmand and Reeve 1926).

As we shall show further on in this paper, it is possible to obtain more detailed information about the mechanism of the energy transfer by investigating this reaction in the presence of substances which can act as quenchers of the uranium fluorescence. We have undertaken, therefore, to study this reaction in the absence and presence of iodide and bromide ions.

A considerable amount of work has been devoted to the study of the photosensitized decomposition of oxalic acid and this reaction is also used in photometry. Previous investigators have mostly been satisfied by a measure of the total oxalic acid decomposed. Although we possess some investigations of Bruner and Kozak (1911) and Büchi (1924) who have shown that formic acid and uranous salt are formed during the reaction, these facts have been more or less disregarded and the net reaction has often been represented, according to: $H_2C_2O_4 = CO_2 + CO + H_2O$.

Our own investigations have shown, in fact, that even in the most favourable cases, only about 50% of the oxalic acid decomposition takes place in accordance with the above reaction.

If the original conception of a simple transfer of excitation energy or of the formation of a stable complex between the oxalic acid and the uranium salt is correct, we would expect further that the addition of quenching substances would result in a decrease in the reaction velocity without any appreciable change in the reaction products. The same effect should result from the addition of hydrogen ions unless an exceptionally great stability of this complex towards hydrogen ions is assumed.

In the course of our study, we have reinvestigated also the quenching of the fluorescence of uranium salts by iodide ions, as no detailed information is given in the literature, and we were able to demonstrate experimentally the nature of the elementary reaction of this quenching process.

2. EXPERIMENTAL

(a) *Experimental arrangement*

The method consisted essentially of irradiating the solutions in an oxygen-free atmosphere, collecting the evolved carbon monoxide, and analysing the solutions to determine the amount of oxalic acid decomposed, and the amounts of uranous salt and formic acid formed. It is essential to exclude completely the oxygen for two reasons: (i) to prevent the reoxidation of the uranous salt formed, (ii) to prevent a photosensitized oxidation of the iodide or bromide ions in the solution.† We have excluded all air by bubbling through the solutions a stream of air-free carbon dioxide, prepared by the methods used in micro-analysis (Pregl.).

---

† In the experiments of West *et al.* (1928) these precautions were not taken and according to their own account some free iodine was formed in the reaction mixture, a fact which must introduce some ambiguity.

The reaction vessels consisted of two glass bottles (15 × 8 × 5 cm.) fitted with rubber stoppers carrying two capillary tubes, one reaching nearly to the bottom of each vessel and the other just through the stopper. The bottles were fixed in a thermostat maintained at a temperature of $25^\circ \pm 0{\cdot}1^\circ$ C. The carbon dioxide was passed into the reaction vessels and the evolved gases were collected in two nitrometers filled with specially prepared caustic potash solutions. The light source consisted of a 1000 W projection lamp fixed in a suitable cover and placed in front of the glass window of the thermostat. The intensity of illumination was adjusted until both vessels appeared to be equally illuminated and checked by carrying out a blank experiment with the same solution in both vessels.

(b) *Methods of analysis*

(i) *Original solution*

The concentration of the original oxalic acid or sodium oxalate was determined by direct titration with 1/10 N potassium permanganate.

(ii) *Solution after experiment.*

(i) *Carbon monoxide.* This was obtained by a direct measurement of the collected gas.

(ii) *Uranous salt.* In the solutions without iodide the uranous salt was determined by direct titration with 1/10 N potassium permanganate after cooling in ice.

For solutions containing iodide the uranous salt was determined in most cases by difference, the results being confirmed in some experiments by the use of two other methods.

In the first method, the iodide was precipitated by silver sulphate. The total uranous and oxalic acid were determined by titration with 1/10 N potassium permanganate and the amount of uranous salt obtained by subtracting the oxalic acid from this total.

The second method employed an apparatus specially designed for the purpose, which permitted the precipitation of the uranous salt (with NaOH) and the complete separation of it from the other substances present in an atmosphere of oxygen-free nitrogen. The precipitate was then dissolved in dilute sulphuric acid in the nitrogen atmosphere and titrated with 0·1 N permanganate.

(iii) *Formic acid.* 50 c.c. portions of the solution were made just alkaline with caustic soda solution. After standing to allow the uranous salt to be completely oxidized, an excess of mercuric chloride was added and the formic acid determined as calomel, the latter being determined by addition of excess 0·05 N iodine and the excess back-titrated by 0·05 N thiosulphate.

(iv) *Residual oxalate.* In the solutions without iodide the oxalate was determined after the uranous salt by heating the solution and titrating with 0·1 N potassium permanganate.

For the solutions with iodide the oxalate was precipitated by calcium chloride and the precipitate filtered and washed free from iodide and chloride. It was then dissolved in dilute sulphuric acid, heated and titrated with 0·1 N potassium permanganate.

(c) *Photochemical reaction between* U^{VI} *and* I^-

200 c.c. portions of 1/60 M uranium sulphate were placed in two flasks and connected to a purified nitrogen supply. The flasks were placed in a trough of water and a stream of nitrogen passed through. They were then illuminated by a mercury arc lamp, the nitrogen stream being maintained throughout. The amount of iodine liberated was then determined by titration with 0·05 N sodium thiosulphate.

3. RESULTS

As has been mentioned already in the experimental part, experiments were carried out with oxalic acid, with oxalic acid acidified with sulphuric acid, and with sodium oxalate. The reaction mixture in the case of sodium oxalate had a $pH \sim 5$ (measured colorimetrically). In table 1 we have given the total oxalic acid decomposed in a given time ($-\Delta$ Ox) in the absence of the inhibitor and the deceleration ($-\Delta(\Delta \text{Ox})$) in the presence of various concentrations of iodide.

In the case of oxalic acid our results are in fair agreement with the previous measurements of West *et al.* (1928), although for reasons already stated (I_2 formation), their results are not wholly reliable. In our experiments carbon dioxide entirely free from air was used, and we tested separately after each experiment for free iodine with negative results in all cases except those employing M/10 and 1 M sulphuric acid. However, even in these cases this was not due to free oxygen but to the photochemical reduction of U^{VI} by I^- in the more strongly acid solutions. As will be seen, the inhibition increases rather strongly with increasing hydrogen-ion concentration.

We wish to compare with the above results our measurements of the quenching of the fluorescence of uranium ions by iodide ions (KI), which we give in figure 1.

TABLE 1. THE RELATION BETWEEN REACTION VELOCITY AND IODIDE CONCENTRATION

No. of experiment	Time in hours	Conc. of Ox in mol./l. $\times 10^2$ [Ox]	Conc. of I^- in mol./l. $\times 10^2$ $[I^-]$	Ratio $\frac{[I^-]}{[Ox]}$	Ox decomp. in the absence of I^- $-\Delta Ox$ $\times 10^3$	Decrease in Ox decomp. in the presence of I^- $-\Delta(\Delta Ox)$ $\times 10^3$	Percentage deceleration $\frac{-\Delta(\Delta Ox)}{\Delta Ox}$ $\times 10^2$	Remarks
17*a*	6	3·334	0·1	0·030	4·06	0·02	0·5	[Ox] = oxalic acid
1	6	3·285	1·0	0·305	3·92	0·10	2·6	
18	6	3·350	1·0	0·298	6·37	0·17	2·7	
9	8	3·390	1·0	0·295	5·00	0·14	2·8	
3	6	3·300	3·33	1·007	2·83	0·40	14·1	
11	8	3·333	5·0	1·500	4·69	0·90	19·2	
4	6	3·090	10	3·085	2·68	0·10	37·3	
15*a*	8	3·366	10	2·971	4·40	1·65	37·5	
23_b^a	6	3·320	5 10	1·500 3·010	4·60	0·90	19·5	
23*b*	6	3·320	10	3·010	6·37	2·40	37·7	
6	6	3·300	0·33	0·100	4·35	0	0	[Ox] = sodium oxalate
13	8	3·333	1·0	0·303	4·90	0·13	2·7	
13*a*	8	3·293	1·0	0·303	4·00	0·11	2·8	
22	6	3·290	1·0	0·304	5·45	0·20	2·7	
8	6	3·333	2·49	0·748	4·20	0·20	4·8	
7	6	3·315	4·97	1·500	4·40	0·60	13·6	
14*b*	8	3·333	10	3·000	5·40	1·80	33·3	
25_b^a	6	3·333	7·5 10	2·250 3·000	5·71	0·71	12·4	
10	7	3·383	1·0	0·296	4·35	0·30	6·9	[Ox] = oxalic acid + M/100 H_2SO_4 (α)
19	6	3·350	1·0	0·299	6·10	0·40	6·6	
12	8	3·333	5·0	1·500	4·32	1·11	25·7	
20	6	3·333	1·0	0·299	1·62	0·30	18·5	+ M H_2SO_4 (β)
21	6	3·333	1·0	0·299	4·15	0·82	19·8	+ M/10 H_2SO_4 (γ)

The experiments were carried out with uranium nitrate solution (approx. M/10) employing a photoelectrical apparatus similar to that used by Rabinovitch and Weiss (1937). On account of the comparatively low intensity of fluorescence of the uranium salt solution, these results cannot be regarded as very accurate, but they will suffice for the present purpose. In fact, our curve showing the dependence of the fluorescence upon the iodide-ion concentration, can be represented fairly well by the hyperbolic relation, viz.

$$\frac{I}{I_a} = \frac{1}{1 + 5 \times 10^3 (I^-)} \qquad (1)$$

(I_a = maximum intensity of fluorescence; I = intensity at a given I^- concentration).

It follows from the above results that an iodide-ion concentration sufficient to cause considerable quenching of the uranium fluorescence has practically no effect on the decomposition reaction.

We have mentioned previously that it should be possible to obtain more direct information about the mechanism of the reaction from a study of the reaction products under various conditions. The results of such investigations are given in the following tables. The experiments were carried out as before with oxalic acid, oxalic acid with various concentrations of sulphuric acid, and with sodium oxalate.

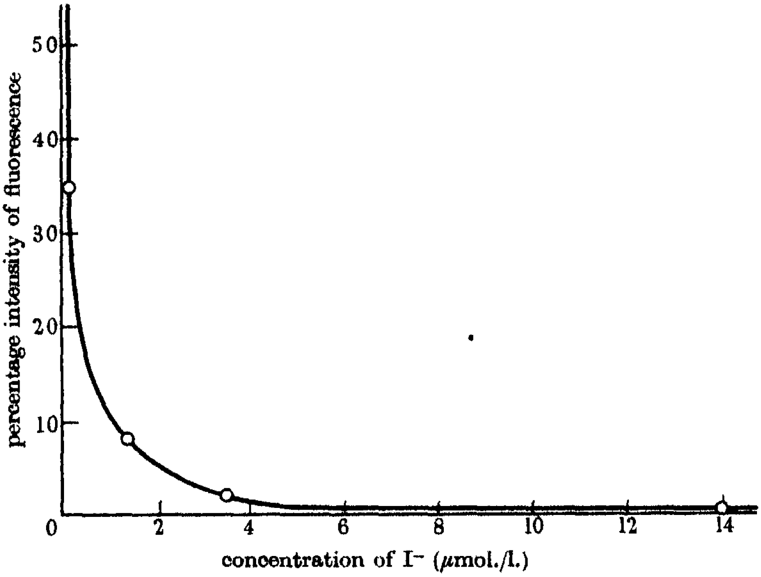

FIGURE 1. *Quenching of the fluorescence of uranium ions by iodide ions (KI).*

The results of these experiments show that the total loss in oxalic acid or oxalate can be represented by the following three stoichiometric equations:

(*a*) Decomposition to carbon monoxide:

$$H_2C_2O_4 = CO + CO_2 + H_2O.$$

(*b*) Decomposition to formic acid:

$$H_2C_2O_4 = HCOOH + CO_2.$$

(*c*) Oxidation to carbon dioxide with the formation of a corresponding amount of uranous salt:

$$H_2C_2O_4 + U^{VI} = H_2O + 2CO_2 + U^{IV}.$$

Tables 2*a*, 3*a* and 4*a* give the results of our experiments without iodide, and also indicate the degree of reproducibility of the results. Tables 2*b*, 3*b* and 4*b* contain the results of experiments obtained with varying concentrations of iodide ions.

Table 5 shows the variation in the amounts of the reaction products with the amount of free sulphuric acid.

If any of the previously advanced theories are correct the relative amounts of the reaction products should *not* depend on any inhibitor present, but this is not in agreement with our experiments.

In the case of oxalic acid, the carbon monoxide formed, originally 51 %, falls to 42 % at an iodide concentration of 10^{-1} mol./l. and the formic acid from about 44 to 42 %. For sodium oxalate the carbon monoxide is only changed by about 4 %, whereas the formic acid changes from 71 to 56 %. Similar results are obtained with oxalic acid acidified with sulphuric acid. The presence of sulphuric acid introduces very marked changes in the relative amounts of the reaction products, even in the absence of iodide, although the absolute rate of reaction (as has been found by previous workers) is not very strongly affected. In fact, for the strongest acid used (1 M), the course of the reaction is completely changed, as no formic acid could be detected either in the absence or presence of iodide. Some free iodine was liberated in the latter case.

These results are not specific for iodide ions as similar results were obtained with bromide ions, as will be seen from table 6.

DISCUSSION

There are three independent facts which render untenable the previous theories for the mechanism of the energy transfer in the photosensitized reaction. (1) The energy of the light quantum primarily absorbed is in itself insufficient to bring about the photochemical decomposition by transference of the light quantum from the uranium salt to the oxalic acid, (2) there is no inhibiting effect by iodide ions in a concentration sufficient to quench the uranium fluorescence, and (3) the change in the relative amounts of the reaction products with varying concentration of the inhibitors (I^-, Br^-, etc.).

The first reason is not specific for the reaction in question, but arises similarly for every type of photosensitized reaction. The second has already been pointed out by Rollefson (1935) and Pringsheim (1937), while the third is the new experimental fact put forward in this paper.

In order to explain the difficulty arising out of (2), Rollefson (1935) and

TABLE 2*a*. THE DECOMPOSITION PRODUCTS OF OXALIC ACID IN THE ABSENCE OF IODIDE

No. of experiment	Time in hours	Conc. of Ox acid mol./l. [Ox] × 10^3	Ox acid decomp. mol./l. $-\Delta$Ox × 10^3	CO formed mol./l. $+\Delta$CO × 10^3	Uranous salt formed mol./l. $+\Delta U^{IV}$ × 10^3	HCOOH formed mol./l. $+\Delta$HCOOH × 10^3	% HOx decomposed into CO	% HOx decomposed into HCOOH
1	6	3·285	3·92	1·99	0·20	1·73	50·7	44·1
2	6	3·500	3·60	1·84	0·20	1·59	51·1	44·0
3	6	3·300	2·73	1·38	0·10	1·20	50·6	44·0
4	6	3·090	2·68	1·37	0·10	1·21	51·1	45·0
9	8	3·393	5·00	2·56	0·20	2·24	51·2	44·8
11	8	3·333	4·69	2·42	0·10	2·17	51·0	44·0
17	8	3·315	3·45	1·76	0·15	1·54	51·0	44·6
17*a*	6	3·334	4·06	2·07	0·20	1·79	51·0	44·1
17*b*	6	3·334	5·76	2·91	0·30	2·55	50·5	44·3
18	6	3·353	6·37	3·29	0·25	2·83	51·7	44·4
						Mean percentages	51·0	44·3

TABLE 2*b*. THE PERCENTAGE CHANGE OF THE REACTION PRODUCTS WITH THE IODIDE CONCENTRATION

(Substrate: oxalic acid)

No. of experiment	Time in hours	Conc. of Ox acid mol./l. [Ox] × 10^3	Conc. of iodide mol./l. [I^-] × 10^3	Ratio [I^-]/[Ox]	HOx decomp. mol./l. $-\Delta$Ox × 10^3	CO formed mol./l. $+\Delta$CO × 10^3	Uranous salt formed mol./l. $+\Delta U^{IV}$ × 10^3	HCOOH formed mol./l. $+\Delta$HCOOH × 10^3	% HOx decomposed into CO	% HOx decomposed into HCOOH
17*a*	6	3·334	0·1	0·030	4·04	2·04	0·20	1·80	50·5	44·5
17	8	3·315	0·1	0·030	5·42	2·71	—	—	50·0	—
15*a*	8	3·366	0·33	0·098	4·40	2·25	0·20	1·95	51·1	44·3
2	6	3·500	0·33	0·097	3·40	1·72	0·20	1·50	50·6	44·1
18	6	3·353	1·0	0·298	6·26	3·13	0·25	2·88	50·0	44·2
27*a*	6	3·350	2·5	0·750	5·15	2·52	0·30	2·33	48·9	43·3
3	6	3·330	3·3	1·007	2·27	1·09	0·20	0·98	48·0	43·2
11	8	3·333	5	1·500	3·59	1·61	0·40	1·55	44·9	43·0
24*a*	6	3·353	5	1·490	4·85	2·14	—	—	44·1	—
27*b*	6	3·350	7·5	2·250	4·76	2·05	0·45	2·04	43·0	42·9
4	6	3·090	10	3·085	1·77	0·75	0·34	0·72	42·3	40·7
15*b*	8	3·366	10	2·971	2·40	1·01	0·45	0·99	42·0	41·3
24*b*	8	3·353	10	3·000	4·24	1·78	0·45	1·80	42·0	42·4

TABLE 3*a*. THE DECOMPOSITION OF SODIUM OXALATE IN THE ABSENCE OF IODIDE

No. of experiment	Time in hours	Conc. of NaOx mol./l. $[Ox] \times 10^2$	NaOx decomp. mol./l. $-\Delta Ox \times 10^3$	CO formed mol./l. $+\Delta CO \times 10^3$	Uranous salt formed mol./l. $+\Delta U^{IV} \times 10^3$	HCOOH formed mol./l. $+\Delta HCOOH \times 10^3$	% NaOx decomposed into CO	% NaOx decomposed into HCOOH
6	6	3·330	4·35	0·992	0·25	3·108	22·8	71·4
7	6	3·315	4·20	0·937	0·25	3·013	22·4	71·7
8	6	3·333	3·90	0·828	0·30	2·770	21·3	71·0
13	8	3·333	4·90	1·090	0·30	3·510	22·2	71·6
13*a*	8	3·293	4·00	0·914	0·25	2·836	22·9	70·9
22	6	3·290	5·45	1·257	0·30	8·893	23·1	71·4
						Mean percentages	22·5	71·3

TABLE 3*b*. THE PERCENTAGE CHANGE OF THE REACTION PRODUCTS WITH THE IODIDE CONCENTRATION

(Substrate: sodium oxalate)

No. of experiment	Time in hours	Conc. of NaOx mol./l. $[Ox] \times 10^2$	Conc. of iodide mol./l. $[I^-] \times 10^2$	Ratio $[I^-]/[Ox]$	NaOx decomp. mol./l. $-\Delta Ox \times 10^3$	CO formed mol./l. $+\Delta CO \times 10^3$	Uranous salt formed mol./l. $+\Delta U^{IV} \times 10^3$	HCOOH formed mol./l. $+\Delta HCOOH \times 10^3$	% NaOx decomposed into CO	% NaOx decomposed into HCOOH
6	6	3·300	0·33	0·10	4·15	0·922	0·30	2·93	22·2	70·6
14*a*	8	3·333	0·33	0·10	4·90	1·084	0·40	3·40	22·1	69·4
13	8	3·333	1·0	0·30	3·60	0·758	0·40	2·45	21·0	68·0
13*a*	8	3·293	1·0	0·30	2·90	0·632	0·40	1·95	21·8	67·2
22	6	3·290	1·0	0·30	5·25	1·163	0·55	3·54	22·1	67·4
8	6	3·333	2·49	0·75	3·80	0·698	0·80	2·32	18·4	63·2
7	6	3·315	4·97	1·50	3·60	0·643	0·85	2·12	17·9	59·0
25*a*	6	3·333	7·5	2·25	5·70	1·090	1·30	3·31	19·0	58·1
25*b*	6	3·333	10	3·00	5·00	0·920	1·40	2·80	18·4	56·0
14*b*	8	3·333	10	3·00	3·00	0·550	0·80	1·68	18·3	56·0

TABLE 4*a*. THE DECOMPOSITION PRODUCTS OF OXALIC ACID ($+$M/100 H_2SO_4) IN THE ABSENCE OF IODIDE

No. of experiment	Time in hours	Conc. of HOx mol./l. $[Ox] \times 10^2$	HOx decomp. mol./l. $-\Delta Ox \times 10^3$	CO formed mol./l. $+\Delta CO \times 10^3$	Uranous salt formed mol./l. $+\Delta U^{IV} \times 10^3$	HCOOH formed mol./l. $+\Delta HCOOH \times 10^3$	% HOx decomposed into CO	% HOx decomposed into HCOOH
10	7	3·383	4·35	2·43	0·30	1·62	55·9	37·2
12	8	3·333	4·32	2·41	0·30	1·61	55·8	37·3
19	6	3·350	6·25	3·50	0·40	2·35	56·0	37·9
						Mean percentages	55·9	37·5

TABLE 4*b*. THE PERCENTAGE CHANGE OF THE REACTION PRODUCTS WITH THE IODIDE CONCENTRATION

(Substrate: oxalic acid + M/100 H_2SO_4)

No. of experiment	Time in hours	Conc. of Ox acid mol./l. $[Ox] \times 10^2$	Conc. of iodide mol./l. $[I^-] \times 10^2$	Ratio $[I^-]/[Ox]$	HOx decomp. mol./l. $-\Delta Ox \times 10^3$	CO formed mol./l. $+\Delta CO \times 10^3$	Uranous salt formed mol./l. $+\Delta U^{IV} \times 10^3$	HCOOH formed mol./l. $+\Delta HCOOH \times 10^3$	% HOx decomposed into CO	% HOx decomposed into HCOOH
16	8	3·363	0·33	0·10	6·33	3·48	0·52	2·33	55·0	36·8
10	7	3·383	1·0	0·30	3·60	1·96	0·34	1·30	54·4	36·1
19	6	3·350	1·0	0·30	5·96	3·24	0·55	2·17	54·4	36·4
26*a*	6	3·353	2·5	0·75	5·05	2·62	0·60	1·83	51·9	36·2
12	8	3·333	5	1·50	3·20	1·51	0·57	1·12	47·2	35·0
26*b*	6	3·353	7·5	2·25	5·10	2·20	1·10	1·76	43·0	34·3
16*a*	8	3·363	10	2·98	4·00	1·51	1·30	1·37	37·8	34·2

TABLE 5. THE DECOMPOSITION PRODUCTS OF OXALIC ACID IN THE PRESENCE OF HYDROGEN IONS

(Variation in H_2SO_4 concentration)

No. of experiment	Time in hours	H_2SO_4 conc. molarity	Conc. of I^- mol./l. and ratio $[I^-]/[Ox]$	Conc. of HOx mol./l. $[Ox] \times 10^2$	HOx decomp. mol./l. $-\Delta Ox \times 10^3$	CO formed mol./l. $+\Delta CO \times 10^3$	Uranous salt formed mol./l. $+\Delta U^{IV} \times 10^3$	HCOOH formed mol./l. $+\Delta HCOOH \times 10^3$	% HOx decomposed into CO	% HOx decomposed into HCOOH
19	6	M/100	Without iodide	3·350	6·25	3·50	0·40	2·35	56·0	37·9
21	6	M/10		3·333	4·15	3·14	0·45	0·56	75·7	13·5
20	6	M/1		3·333	1·62	0·86	0·75	0	53·4	0
19	6	M/100	$[I^-]=10^{-2}$ $[I^-]/[Ox]=0·299$	3·350	5·96	3·24	0·55	2·17	54·4	36·4
21	6	M/10		3·333	3·33	2·50	0·45	0·38	75·1	11·4
20	6	M/1		3·333	1·31	0·45	0·85	0	34·4	0

TABLE 6. THE PERCENTAGE CHANGE OF THE REACTION PRODUCTS WITH THE BROMIDE CONCENTRATION (KBr)

(Substrate: oxalic acid)

No. of experiment	Time in hours	Conc. of Ox acid mol./l. $[Ox] \times 10^2$	Conc. of bromide mol./l. $[Br^-] \times 10^2$	Ratio $[Br^-]/[Ox]$	HOx decomp. mol./l. $-\Delta Ox \times 10^3$	CO formed mol./l. $+\Delta CO \times 10^3$	Uranous salt formed mol./l. $+\Delta U^{IV} \times 10^3$	HCOOH formed mol./l. $+\Delta HCOOH \times 10^3$	% HOx decomposed into CO	% HOx decomposed into HCOOH
28*a*	6	3·35	1·0	0·30	5·80	2·90	0·60	2·30	50·0	39·6
28*b*	6	3·35	5·0	1·50	5·05	2·25	0·60	2·20	44·5	43·6
29*a*	6	3·32	5·0	1·50	5·20	2·30	0·60	2·30	44·2	44·2
29*b*	6	3·32	10·0	3·00	4·50	1·98	0·60	1·92	44·0	42·7

Pringsheim (1937) postulated the formation of a complex between the uranium ions and oxalic acid. There is no *a priori* reason why the manner in which this complex decomposes should be influenced by the mere presence of iodide or hydrogen ions, but not its stability. It would be expected, rather, that the stability of the complex would be influenced by hydrogen ions in particular, and thereby the rate of the decomposition should be decreased. On the contrary, however, in agreement with the work of previous authors, we have found that the rate of the reaction (above a certain limit) is not appreciably affected by hydrogen ions, but that the reaction products are. Furthermore, an increase in the iodide concentration beyond the region of practically complete quenching of the fluorescence steadily inhibits the reaction. Obviously this could not be the case if a stable complex was the only deciding factor, as in such a case the rate must approach a constant value with increasing iodide concentration.

In order to obtain a closer understanding of this reaction it is necessary to consider the elementary process of quenching of fluorescence which is the primary process in all photosensitized reactions.

The quenching of the fluorescence of uranium ions by iodide ions follows the general scheme (Weiss 1939):

$$D^* + Acc \rightleftharpoons D^- + Acc^+; \tag{2}$$

D^* represents the excited molecule or ion which has absorbed primarily the light energy, and Acc the quenching molecule or ion.

The quenching process consists of an electron transfer from the quenching acceptor to the excited molecule or ion. The conditions for this non-adiabatic change have been discussed in detail in a previous paper (Weiss 1939). They can be summarized by saying that for a non-adiabatic electron transfer, the potential curves must be such that the energetic distance ΔV between the curves should change by an amount comparable to its own magnitude, during a time equal to the period associated with this energy difference. This period is $\frac{h}{\Delta V}$ and during this time the nuclei move by $v\frac{h}{\Delta V}$, where $v = \frac{\partial x}{\partial t}$ is the nuclear velocity, and hence the condition becomes (h = Planck's constant):†

$$v\frac{\partial \Delta V}{\partial r}\frac{1}{\Delta V} \geqslant \frac{\Delta V}{h}.$$

---

† We are indebted to Professor R. Peierls (private communication) for this expression.

On the basis of a quantum mechanical interpretation of reaction (2), it can be seen that the decreased zero-point energy of the electron in the transition state ($[D^*Acc] \rightleftarrows [D^-Acc^+]$) results in a binding force between the reacting molecules or ions. This explains immediately a sort of complex formation manifested through the absorption spectrum, which goes parallel to the quenching, such as has been observed by Rollefson (1935) and Pringsheim (1937) in the case of the uranium salt-oxalic acid mixture, and by Hellström (1936) in the quenching of the fluorescence of methylene blue by ferrous ions.

The quenching of uranium fluorescence by iodide is now represented by the following reactions:

Light absorption: $$UO_2^{++} + h\nu_1 \rightarrow UO_2^{++*} \tag{3}$$

Emission of fluorescence:

$$UO_2^{++*} \rightarrow UO_2^{++} + h\nu_2. \tag{4}$$

Quenching of fluorescence:

$$UO_2^{++*} + I^- \rightarrow UO_2^{+} + I. \tag{5}$$

For the stationary state it follows, as shown previously (Weiss 1938):

Intensity of fluorescence:

$$I = k_4[UO_2^{++*}]_{\text{stat.}} = \frac{k_4 I_a}{k_4 + k_5[I^-]},$$

and for the relative intensity of fluorescence (I/I_a) an equation similar to equation (1), where I_a = absorbed light intensity per sec. (in general equivalent to the maximum fluorescence intensity in the absence of any quenching substances) and $\tau = 1/k_4 \sim 10^{-4}$ sec. represents the mean life period of the excited uranium ion (in the absence of quenching substances), and the value of which is given according to the measurements of Perrin and Delorme (1928) and Wawilow and Lewschin (1928).

In the experiments reported above we have found the value of the product: $\tau k_5 \sim 5 \times 10^3$. From this we obtain for the reaction constant of equation (5) the value $k_5 \sim 0{\cdot}5 \times 10^8$ sec.$^{-1}$ (mol./l.)$^{-1}$.

In reaction (5) we have postulated the formation of a UO_2^+ radical which is derived from a pentavalent uranium salt. This appears as a consequence of the fact that in all these electron transfer processes only *one* electron is transferred in each elementary process. We should expect UO_2^+ to be rather unstable and to have the properties of a free radical. However, there is also sufficient evidence in the literature for a pentavalent uranium salt to assume its existence (Ruff and Heinzelmann 1911; Oechsner de Conick and Camo 1901; Schwarz 1920).

The above reactions are probably followed by

Recombination: $$2\mathrm{I} = \mathrm{I}_2, \tag{6}$$

Dismutation: $$2\mathrm{UO}_2^{+} \rightleftarrows \mathrm{UO}_2^{++} + \mathrm{UO}_2, \tag{7}$$

$$(\mathrm{UO}_2 + 2\mathrm{H}_2\mathrm{O} \rightleftarrows \mathrm{U}^{4+} + 4\mathrm{OH}^-). \tag{8}$$

Under normal conditions the reoxidation of the uranous salt or of UO_2^+ radical by iodine molecules or atoms is sufficiently rapid so that no formation of either of these can be observed when the light is switched off and the original state thus restored. If, however, conditions can be found when this reoxidation process is inhibited, molcular iodine and uranous salts should be formed during or even after irradiation of a solution containing a uranium salt and iodide ions. It is well known (McCoy and Bunzel 1909) that in the presence of a sufficient amount of free acid (e.g. sulphuric), oxidation of the uranous salt by oxygen is appreciably retarded.† This can also be shown to be true for oxidation with iodine. We have irradiated, therefore, a mixture of uranium sulphate and iodide ions in the presence of sulphuric acid (in the complete absence of any oxygen). The result is that molecular iodine and uranous salt are formed in equivalent concentrations. There was no difference in the amounts formed if the reaction was stopped (by addition of a measured excess of sodium thiosulphate solution) during or after illumination (see table 7). Also the photosensitized oxidation of iodide ions by molecular oxygen in the presence of uranium salts is now easily understood, and we have the following cycle:

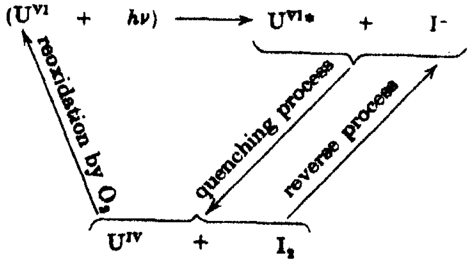

---

† McCoy and Bunzel (1909) have found that the rate of oxidation is inversely proportional to the square of the hydrogen-ion concentration. They have suggested that this might be due to the fact that not U^{4+} but $\mathrm{U(OH)}_2^{++}$ enters into the rate-determining oxidation process. There is, however, in addition, the possibility that U^{5+} which will be formed from the U^{4+} (by every oxidizing agent) will again take up an electron unless it is stabilized through a reaction with OH^- forming, for instance, $\mathrm{U(OH)}_2^{3+}$ which may decompose into UO_2^+ and H^+ ions.

The photochemical decomposition of oxalic acid is represented by the following sequence of reactions:
(Elementary process of quenching = photochemical primary process)

$$UO_2^{++*} + HC_2O_4^- \rightarrow UO_2^+ + HC_2O_4, \tag{9}$$

and

$$HC_2O_4 \rightarrow CO_2 + COOH. \tag{10}$$

This can be followed by a further decomposition of the COOH radical, according to:

$$COOH \rightarrow CO + OH, \tag{11}$$

with the formation of *carbon monoxide* which is liberated.

TABLE 7. THE PHOTOCHEMICAL REACTION BETWEEN URANIUM SALTS AND IODIDE IONS

Solution: uranium sulphate: $1\cdot66 \times 10^{-2}$ mol./l.; potassium iodide: $1\cdot5 \times 10^{-2}$ mol./l.

Time of experiments: one hour

No. of exp.	Conc. of H_2SO_4 mol./l.	Conc. of I_2 formed mol./l. × 10^3	Conc. of U^{IV} salt formed mol./l. × 10^3	Remarks
1	No free acid	0·00	0·00	—
2*a*	1·0	0·125	0·15 ± 0·05	—
2*b*	2·0	0·250	0·300 ± 0·05	—
3	2·0	0·250	—	No difference in (I_2) during and after illumination

The OH radical being a strong oxidizing agent will oxidize any penta- or tetravalent uranium salt present according to

$$UO_2^+ + OH = UO_2^{++} + OH^-, \tag{12}$$

or

$$U^{4+} + OH = U^{5+} + OH^-, \tag{13}$$

$$\left.\begin{aligned} U^{5+} + 2H_2O &\rightleftharpoons UO_2^+ + 4H^+, \\ U^{5+} + 2OH^- &\rightleftharpoons UO_2^+ + 2H^+, \end{aligned}\right\} \tag{14}$$

or else the COOH radical can be reduced by UO_2^+ (or U^{4+}), according to

$$\left.\begin{aligned} COOH + UO_2^+ &\rightarrow COOH^- + UO_2^{++} \\ COOH + U(OH)_2^{++} &\rightarrow COOH^- + UO_2^+ + H^+ \end{aligned}\right\}, \tag{15}$$

with the formation of formic acid; thus:

$$COOH^- + H^+ \rightleftarrows HCOOH. \tag{16}$$

The above sequence of reactions describes the photosensitized decomposition of oxalic acid as a "true" catalytic process, without apparent change of the uranium salt.

However, the fact that the uranium salt passes through a state of lower valency in the course of the reaction is proved by the photoxidations of various organic substances with uranium salts in which the corresponding stoichiometric amount of uranous salt has actually been observed (cf. Weiss 1938).

According to the results in this paper it is formed also in the photochemical reaction between uranium ions and iodide ions. Even in the photosensitized decomposition of oxalic acid, there is always some uranous salt formed, the amount of which would again be expected to increase with increasing concentration of free acid. This is in agreement with our results and those of Büchi (1924). In this case the hydroxyl radicals do not disappear, then, through reactions (12) or (13), but may react with oxalic acid or COOH radical, according to

$$COOH + OH \rightarrow CO_2 + H_2O. \tag{17}$$

The fact that the anion ($HC_2O_4^-$) appears in the actual primary process (reaction (9)) must be concluded from the dependence of the reaction velocity on the hydrogen-ion concentration (cf. also Rollefson 1935; McGinnis 1935).

The fact that small quantities of iodide ions do not inhibit the reaction can now be explained quite easily. The iodine atoms formed primarily in the quenching of the fluorescence, from excited uranium ions and iodide ions, according to reaction (5), attack the oxalate ion in exactly the same way as the excited uranium ion, viz.

$$I + HC_2O_4^- \rightarrow I^- + HC_2O_4. \tag{18}$$

The reaction product is identical with that of reaction (9), and it makes here no difference whether iodine atoms or the (UO_2^{++*}) excited ions bring about the formation of the HC_2O_4 radical. For low concentrations of iodide ions, therefore (although sufficiently high for quenching the fluorescence), no inhibition of the actual reaction takes place, in agreement with experiment. The above reaction (18) has been studied independently by various authors (Berthoud and Bellenot 1924; Allmand and Young 1931; Griffith, McKeown and Winn 1933) in the photochemical interaction between molecular iodine and oxalate. In this case the iodine atoms are formed by a direct photochemical splitting of the iodine molecules.

If, however, the ratio $(I^-)/(Ox)$ is increasing, the iodine atoms formed primarily will not be available to react only with the anions of oxalic acid (reaction (18)), because they will then also reoxidize the uranous ions formed primarily, as would be the case if no oxalate was present. This means a loss of the active iodine atoms with the degradation of light energy into heat and consequently the inhibition of the oxalic acid decomposition.

From the work of the above authors we must conclude further that increasing iodide concentration inhibits the photochemical reaction between iodide ions and oxalate, and this is a further reason why with increasing iodide concentration the net reaction is decelerated.

Similar conditions hold in the case of bromine. The photochemical reaction between bromine atoms and oxalic acid and oxalate has been studied particularly by Griffith *et al.* (1933).

The change of the relative amounts of reaction products formed with changing iodide or bromide concentrations is an important new qualitative result which cannot be explained on the previously advanced theories.

We have seen that free acid has an inhibiting effect on the reducing power of uranous salt, so that, in this case, with increasing hydrogen-ion concentration, reaction (15) is obviously almost completely inhibited, and the COOH radicals are oxidized to carbon dioxide and water (reaction (17)) without the formation of any formic acid. At low *p*H values, a considerable amount of formic acid (up to 72% in the case of the sodium oxalate mixture ($p\text{H} \sim 5$) is formed. There must be a simultaneous decrease in the amount of uranous salt formed with decreasing hydrogen-ion concentration, a conclusion in agreement with experiment.

The decrease in the amount of formic acid is also accompanied by an increase in the amount of carbon monoxide formed, because the monomolecular decomposition of COOH radicals (reaction (11)) can compete successfully with the bimolecular oxidation reaction with the OH radicals (reaction (17)).

It has already been pointed out with regard to the speed of the reaction at low concentrations of iodide ions, that the latter will likewise not influence the reaction products appreciably. However, with increasing iodide-ion concentrations, we should expect a decrease in the amounts of carbon monoxide and formic acid formed, and an increased oxidation of oxalic acid or oxalate to carbon dioxide, because in this case the oxidation by iodine atoms, according to

$$\text{COOH} + \text{I} \rightarrow \text{CO}_2 + \text{HI}, \tag{19}$$

and the direct oxidation of HC_2O_4 radicals or the corresponding $C_2O_4^-$ anions by iodine molecules, thus

$$C_2O_4^- + I_2 \rightarrow 2CO_2 + I^- + I, \tag{20}$$

will become more important.

This reaction occurs in the photochemical reaction between iodine and oxalic acid—in our case the iodine is formed by the recombination of two iodine atoms. Again, of course, there will be competition for the iodine atoms between the uranous ions and the oxalic acid, and the relative amounts of reaction products formed must depend on the relative velocities of these processes.

We have confined ourselves to giving a qualitative discussion in which the main features of the reaction are brought out very well. A quantitative study would necessarily involve an independent knowledge of the reaction constants which we do not possess and a number of arbitrary assumptions would be necessary. However, all the kinetic data available can be derived from the mechanism presented above. As pointed out before, similar considerations apply to the reaction between bromine and oxalic acid.

It will be seen that the experimental facts can be explained by a dynamical theory, and not by the formation of a complex between the uranium salt and the oxalic acid. However, the theory indicates the formation of a complex arising through the quantum mechanical resonance in the photochemical primary process, but this is only a secondary effect.

Our thanks are due to Professor G. R. Clemo, F.R.S., for his interest in this work.

SUMMARY

1. The transfer of electronic excitation energy in solution has been investigated in the case of the photosensitized decomposition of oxalic acid by uranium ions, and more detailed information about the mechanism of the energy transfer has been obtained by studying the reaction in the presence of substances (I^-, Br^-) which can act as quenchers of the uranium fluorescence.

2. New experimental facts are presented which cannot be explained by any of the previously advanced theories. In particular widely different relative amounts of the products of decomposition (CO, CO_2, $HCOOH$) have been observed with varying concentration of the quenching substances and hydrogen ions present in the solution.

3. A theory is discussed based on the electron transfer process between

excited uranium ions and oxalate ions. The observed complex formation between the reacting ions is interpreted on the basis of a quantum mechanical resonance in the elementary process of quenching.

4. In connexion with the above investigation the quenching process of the uranium fluorescence by I^- has been investigated and the elementary processes involved have been studied experimentally and discussed on a similar theoretical basis.

REFERENCES

Allmand, A. J. and Reeve, L. 1926 *J. Chem. Soc.* p. 2834.
Allmand, A. J. and Young, K. W. 1931 *Trans. Faraday Soc.* **27**, 515.
Berthoud, A. and Bellenot, H. 1924 *Helv. Chim. Acta*, **7**, 307.
Bruner, L. and Kozak, J. 1911 *Z. Electrochemie*, **17**, 354.
Büchi, P. F. 1924 *Z. phys. Chem.* **111**, 269.
Gaffron, H. 1926 *Biochem. Z.* **179**, 167.
Griffith, R. O., McKeown, A. and Winn, A. G. 1933 *Trans. Faraday Soc.* **29**, 369.
Hellström, H. 1936 *Naturwissenschaften*, **24**, 76.
Klein, O. and Rosseland, S. 1921 *Z. Phys.* **4**, 46.
McCoy, H. N. and Bunzel, H. H. 1909 *J. Amer. Chem. Soc.* **31**, 367.
McGinnis 1935 Thesis, University of California.
Noack, K. 1927 *Biochem. Z.* **183**, 144.
Oechsner de Conick and Camo 1901 *Bull. Acad. Belg. Cl. Sci.* **321**.
Perrin, F. and Delorme, R 1928 *C.R. Acad. Sci., Paris*, **186**, 428.
Pregl, F. *Quantitative organic micro-analysis*, 2nd English ed., pp. 89–92.
Pringsheim, P. 1937 *Physica*, **4**, 733.
Rabinovitch, E. and Weiss, J. 1937 *Proc. Roy. Soc.* A, **162**, 251.
Rollefson, G. K. 1935 *Chem. Rev.* **17**, 425.
Ruff, O. and Heinzelmann, A. 1911 *Z. anorg. Chem.* **72**, 63.
Schwarz, R. 1920 *Helv. Chim. Acta*, **3**, 330.
Wawilow, S. J. and Lewschin, W. L. 1928 *Z. Phys.* **48**, 397.
Weiss, J. 1938 *Trans. Faraday Soc.* **34**, 451.
— 1939 *Trans. Faraday Soc.* **35**, 48. General Discussion on Luminescence.
West, W., Müller, R. H. and Jette, E. 1928 *Proc. Roy. Soc.* A, **121**, 294, 317.

Rotational analysis of the first negative band spectrum of oxygen. II

By Thomas E. Nevin
University College, Dublin

(*Communicated by A. W. Conway, F.R.S.—Received* 30 *October* 1939)

In a previous paper (Nevin 1938)[*], the author has given an analysis of the (0, 1) λ 6438, (0, 0) λ 6026, and (1, 0) λ 5632 bands of the first negative band spectrum of oxygen and has shown that the system is due to a transition $^4\Sigma_g^- \rightarrow {}^4\Pi_u$. The present paper contains an analysis of the (0, 2) λ 6856 and (2, 0) λ 5295 bands.

Using the method described in (I) to excite the spectrum, a discharge through helium containing a small amount of oxygen, the plates of the band λ 6856 taken in the second order of the grating could be measured only as far as λ 6720 on account of the large number of ghosts and the blackening produced below this point by the enormously over-exposed helium line λ 6678. To photograph the remainder of the band it was necessary to use a hollow cathode discharge through commercial oxygen as described by Frerichs (1926). This source is considerably less intense than the discharge through helium the exposures with which, in the case of the present band, were between 12 and 18 hr. with Ilford Astra III plates. To reduce the exposures to a reasonable time a cylindrical lens made by Hilger, 15 cm. long and 5 cm. wide with a focal length of 30 cm., was mounted at right angles to the axis of the spectrograph between the grating and the plate as described by Oldenberg (1932). The lens was mounted so that its axis could be adjusted exactly perpendicular to the slit and the grating rulings, a point of the highest importance if the definition is not to be impaired. As far as could be judged there was no loss of resolving power over the length of plate covered by the lens. Satisfactory exposures of a range of 180A were obtained in about 6 hr. with the hollow cathode discharge taking a current of 0·8 amp. The plates were measured with respect to third order iron standards.

The λ 5295 band had already been photographed in the second order at the same time as the bands analysed in (I). However, to complete the analysis it was found necessary to take a third order plate, and to save time the arrangement described above was used, the entire band being obtained on a single plate with an exposure of 5 hr. The resolving power attained on this plate with sharp lines was about 200,000. The theoretical resolving power of the grating in this order is 250,000, so the reduction caused by the lens must have been very small.

---

[*] Referred to as (I) throughout this paper.

DATA

The wave numbers and intensities of the lines of the (2, 0) and (0, 2) bands have been tabulated, and the eight tables containing them deposited for reference in the archives of the Royal Society. With the cylindrical lens the astigmatism varies along the length of the plate, so the intensity estimates for the (0, 2) band can be relied on only over a narrow range. In the case of the (2, 0) band the intensity estimates are mainly from second order plates taken without the lens.

To save space the combination differences which check the assignment of the lines to the branches have been omitted. They can be calculated readily with the aid of the combination relations at the heads of the columns of tables 13–19 in (I). The assignment of the bands to the vibrational transitions (2, 0) and (0, 2) is confirmed by the fact that the combination differences for the final state of the former band agree with the combination differences for the final state of the (0, 0) and (1, 0) bands while a similar relation holds good for the initial state of the latter band and the initial state of the (0, 0) and (0, 1) bands.

Unassigned lines are most numerous in the case of the (2, 0) band which is to be expected from the fact that this band according to Bozoky and Schmid (1935) is the first of the sequence $v' - v'' = 2$, the second band of which (3, 1) to judge from the vibrational intensity distribution to be expected should be at least as intense as (2, 0). Up to the point at which the (3, 1) band commences unassigned lines are relatively few. In the (0, 2) band, the only band of the sequence $v' - v'' = -2$ observed by Bozoky and Schmid the number of unassigned lines is small, though to judge from their position the (1, 3) band is present with low intensity.

The number of times each line has been used in the analysis is indicated in the tables by a suffix to the wave number. The letters which appear in some cases after the intensity figure have the following meanings: *b*, blend of two or more lines which appears comparatively sharp; *d*, diffuse line; *c*, line confused with another line which may affect both the wave-length and the intensity; *v*, line shaded towards shorter wave-lengths; *r*, line shaded towards longer wave-lengths.

THE $^4\Pi$ STATE

It was shown in (I) for the $^4\Pi$ levels $v'' = 0$ and $v'' = 1$ that the separations $\Delta F''_{21}(J) = F''_2(J) - F''_1(J)$ and $\Delta F''_{43}(J) = F''_4(J) - F''_3(J)$ did not agree with the separations calculated from the theoretical formulae of Brandt and Budó ((I), equations (4)). A similar disagreement occurs in the level $v'' = 2$. In all three bands, however, the separations are in good agreement with the values given by the following formulae:

$$\left.\begin{aligned}
F_1(J) &= B_v[J(J+1) - \tfrac{3}{2}\{y_1 + 4J(J+1)\}^{\frac{1}{2}}] + D_v(J-\tfrac{3}{2})^2(J-\tfrac{1}{2})^2,\\
F_2(J) &= B_v[J(J+1) - \tfrac{1}{2}\{y_1 + 4J(J+1)\}^{\frac{1}{2}}] + D_v(J-\tfrac{1}{2})^2(J+\tfrac{1}{2})^2,\\
F_3(J) &= B_v[J(J+1) + \tfrac{1}{2}\{y_1 + 4J(J+1)\}^{\frac{1}{2}}] + D_v(J+\tfrac{1}{2})^2(J+\tfrac{3}{2})^2,\\
F_4(J) &= B_v[J(J+1) + \tfrac{3}{2}\{y_1 + 4J(J+1)\}^{\frac{1}{2}}] + \alpha + \beta J + D_v(J+\tfrac{3}{2})^2(J+\tfrac{5}{2})^2,
\end{aligned}\right\}\quad (1)$$

where $y_1 = Y(Y-4)$ with $y = A/B_v$ and α and β are constants. The formulae differ from those of Brandt and Budó in the omission of a term

$$-2B_v\frac{y_2 - 2J(J+1)}{y_1 + 4J(J+1)}$$

from the expressions for $F_1(J)$ and $F_4(J)$ and a term

$$+2B_v\frac{y_2 - 2J(J+1)}{y_1 + 4J(J+1)}$$

from the expressions for $F_2(J)$ and $F_3(J)$. In addition, the terms $\alpha + \beta J$ have been added to the expression for $F_4(J)$. From these equations it follows that

$$\left.\begin{aligned}
\Delta F_{21}(J) &= F_2(J) - F_1(J) = B_v[y_1 + 4J(J+1)]^{\frac{1}{2}} + 4D_v(J-\tfrac{1}{2})^3,\\
\Delta F_{32}(J) &= F_3(J) - F_2(J) = B_v[y_1 + 4J(J+1)]^{\frac{1}{2}} + 4D_v(J+\tfrac{1}{2})^3,\\
\Delta F_{43}(J) &= F_4(J) - F_3(J) = B_v[y_1 + 4J(J+1)]^{\frac{1}{2}} + \alpha + \beta J + 4D_v(J+\tfrac{3}{2})^3.
\end{aligned}\right\}\quad (2)$$

Samples of the agreement between the values of the term differences calculated from these expressions and the values calculated from the branches as described in (I) are shown in table 1. That the agreement is not exact, however, is shown by the fact that the value of A from $\Delta F_{21}(J)$ is not exactly the same as the value derived from $\Delta F_{32}(J)$. As the formulae have no theoretical basis it is hardly worth while attempting to modify them to make the agreement exact. They do, however, give a first approximation to the form which theoretical formulae, to explain the structure of the levels, must take.

TABLE 1. OBSERVED AND CALCULATED VALUES OF $\Delta F_{21}(J)$, $\Delta F_{32}(J)$ AND $\Delta F_{43}(J)$

$v'' = 0$

J	$\Delta F_{21}(J)$		$\Delta F_{32}(J)$		$\Delta F_{43}(J)$	
	Obs.	Calc.	Obs.	Calc.	Obs.	Calc.
5·5	51·78	51·81	51·82	51·81	51·12	51·12
10·5	55·63	55·59	55·63	55·58	55·08	55·09
15·5	61·09	61·11	61·11	61·09	60·81	60·78
20·5	67·89	67·91	67·88	67·88	67·78	67·75
25·5	75·61	75·61	75·59	75·57	75·60	75·61
30·5	83·92	83·95	83·96	83·90	—	—
35·5	92·77	92·72	92·63	92·64	—	—

$\alpha = -0{\cdot}99\ \text{cm.}^{-1}$; $\beta = +0{\cdot}038\ \text{cm.}^{-1}$.

$$A\begin{cases}\text{From } \Delta F_{21}(J) = -47{\cdot}95\ \text{cm.}^{-1}.\\ \text{From } \Delta F_{32}(J) = -47{\cdot}99\ \text{cm.}^{-1}.\end{cases}$$

$v'' = 1$

J	$\Delta F_{21}(J)$		$\Delta F_{32}(J)$		$\Delta F_{43}(J)$	
	Obs.	Calc.	Obs.	Calc.	Obs.	Calc.
5·5	51·68	51·72	51·66	51·72	51·09	51·20
10·5	55·38	55·41	55·40	55·41	55·10	55·02
15·5	60·77	60·80	60·76	60·78	60·51	60·53
20·5	67·39	67·44	67·43	67·41	67·32	67·28
25·5	74·92	74·98	74·98	74·95	74·99	74·92
30·5	—	—	83·16	83·10	—	—
35·5	—	—	—	—	—	—

$\alpha = -0{\cdot}66\ \text{cm.}^{-1}$; $\beta = +0{\cdot}027\ \text{cm.}^{-1}$.

$$A\begin{cases}\text{From } \Delta F_{21}(J) = -47{\cdot}93\ \text{cm.}^{-1}.\\ \text{From } \Delta F_{32}(J) = -47{\cdot}99\ \text{cm.}^{-1}.\end{cases}$$

$v'' = 2$

J	$\Delta F_{21}(J)$		$\Delta F_{32}(J)$		$\Delta F_{43}(J)$	
	Obs.	Calc.	Obs.	Calc.	Obs.	Calc.
5·5	51·47	51·65	51·68	51·65	51·04	51·05
10·5	55·15	55·24	55·18	55·23	54·81	54·82
15·5	60·42	60·47	60·52	60·46	60·20	60·20
20·5	66·90	66·96	66·97	66·93	66·86	66·84
25·5	74·32	74·34	74·40	74·30	74·38	74·37
30·5	82·37	82·33	82·40	82·27	82·48	82·49
35·5	—	—	—	—	—	—

$\alpha = -0{\cdot}75\ \text{cm.}^{-1}$; $\beta = +0{\cdot}034\ \text{cm.}^{-1}$.

$$A\begin{cases}\text{From } \Delta F_{21}(J) = -47{\cdot}92\ \text{cm.}^{-1}.\\ \text{From } \Delta F_{32}(J) = -48{\cdot}01\ \text{cm.}^{-1}.\end{cases}$$

It is easy to show from equations (1) that the relation

$$\Delta_2 F''_m(J) = 4B''_v(J+\tfrac{1}{2})+8D''_v(J+\tfrac{1}{2})^3,$$

used in (I) to calculate B''_v and D''_v, holds to a high degree of approximation so justifying the method used to calculate these constants. The values of $\Delta_2 F''_i(J)$ calculated from (1) are in exact agreement with the observed values derived from the branches.

The Λ-type doubling for the level $v''=2$ calculated as explained in (I) is shown in figure 1. In agreement with the results for the levels $v''=0$ and $v''=1$ the doubling is very small in the ${}^4\Pi_{\frac{5}{2}}$ and ${}^4\Pi_{\frac{3}{2}}$ states while in the ${}^4\Pi_{\frac{1}{2}}$ state it again increases more or less linearly with J. In the ${}^4\Pi_{\frac{1}{2}}$ state $v''=0$ and $v''=1$ the doubling increased at first and finally decreased for the highest values of J. In the level $v''=2$ a maximum is not observed up to the highest observed value of J. Apart from this point there is a close similarity in the results for the three levels, the doubling in ${}^4\Pi_{\frac{1}{2}}$ and ${}^4\Pi_{-\frac{1}{2}}$ increasing systematically with v''.

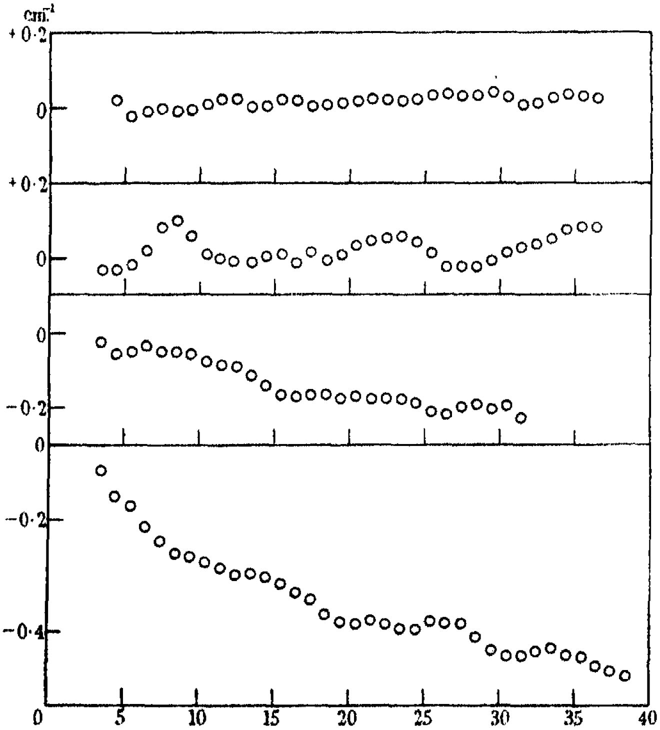

FIGURE 1. Λ-type doubling in the ${}^4\Pi$ state; $v''=2$.

MOLECULAR CONSTANTS

The analysis of the two bands in the present paper makes possible a calculation of the vibrational constants of the system. Writing the R branches in the form

$$R_i(J) = \nu_0 + F'_i(J+1) - F''_i(J),$$

and the corresponding expressions for the P and Q branches it is easy to show with the aid of equations (1) and (2) of (I) for the initial state and equations (1) of the present paper for the final state that when the Λ-doubling is neglected

$$\Sigma R_i(J) + \Sigma P_i(J) = 8\nu_0 + 18B'_v + 8(B'_v - B''_v)J(J+1),$$

and

$$\Sigma Q_i(J) = 4\nu_0 + 5B'_v + 4(B'_v - B''_v)J(J+1),$$

apart from small terms in higher powers of $J(J+1)$. A nearly linear relation exists, therefore, between the sum of the wave numbers of corresponding lines of the R and P branches and $J(J+1)$ and the sum of the wave numbers of corresponding lines in the Q branches and $J(J+1)$. A short extrapolation in the first case gives $8\nu_0 + 8B'$ and in the second case $4\nu_0 + 5B'$ so the origin of each band is obtained.

In calculating the sums on the left-hand side of these equations it was necessary to calculate by interpolation the alternate missing lines of each of the branches. In the R_3 and P_2 branches which are not observed for low values of J the positions of the lines were calculated from the ${}^RQ_{43}$ and ${}^PQ_{12}$ branches respectively. The agreement between the two ν_0 values for each band was satisfactory and the average of the two values for the five bands analysed is given in table 2.

TABLE 2. BAND ORIGINS

v' \ v''	0	1	2
0	16666·74	15651·82	14657·67
1	17829·34		
2	18957·77		

The origins are represented by the formula

$$\nu = 16587{\cdot}88 + 1196{\cdot}77u' - 17{\cdot}09u'^2 - 1035{\cdot}69u'' + 10{\cdot}39u''^2,$$

where $u = v + \frac{1}{2}$.

The constants of the O_2^+ molecule in the initial ${}^4\Sigma$ and final ${}^4\Pi$ states for the levels $v = 0$, 1 and 2 are given in table 3. The values of B and D have been calculated by the method of least squares which should give a better result than the graphical method used in (I). The probable error of B differs somewhat for the different levels but it is approximately $\pm 0{\cdot}00005$ cm.$^{-1}$. The probable error of D is about $\pm 0{\cdot}09 \times 10^{-6}$ cm.$^{-1}$.

TABLE 3. MOLECULAR CONSTANTS

		$^4\Sigma$ state		$^4\Pi$ state	
$v=0$	B'_0	$= 1{\cdot}27626$ cm.$^{-1}$	B''_0	$= 1{\cdot}09681$ cm.$^{-1}$	$Y \sim -43{\cdot}74$ cm.$^{-1}$
	D'_0	$= -5{\cdot}91 \times 10^{-6}$ cm.$^{-1}$	D''_0	$= -4{\cdot}83 \times 10^{-6}$ cm.$^{-1}$	$A \sim -47{\cdot}97$ cm.$^{-1}$
$v=1$	B'_1	$= 1{\cdot}25420$ cm.$^{-1}$	B''_1	$= 1{\cdot}08099$ cm.$^{-1}$	$Y \sim -44{\cdot}36$ cm.$^{-1}$
	D'_1	$= -6{\cdot}07 \times 10^{-6}$ cm.$^{-1}$	D''_1	$= -4{\cdot}73 \times 10^{-6}$ cm.$^{-1}$	$A \sim -47{\cdot}96$ cm.$^{-1}$
$v=2$	B'_2	$= 1{\cdot}23213$ cm.$^{-1}$	B''_2	$= 1{\cdot}06531$ cm.$^{-1}$	$Y \sim -45{\cdot}02$ cm.$^{-1}$
	D'_2	$= -6{\cdot}28 \times 10^{-6}$ cm.$^{-1}$	D''_2	$= -4{\cdot}64 \times 10^{-6}$ cm.$^{-1}$	$A \sim -47{\cdot}96$ cm.$^{-1}$
	B'_e	$= 1{\cdot}28729$ cm.$^{-1}$	B''_e	$= 1{\cdot}10466$ cm.$^{-1}$	
	D'_e	$= -5{\cdot}81 \times 10^{-6}$ cm.$^{-1}$	D''_e	$= -4{\cdot}88 \times 10^{-6}$ cm.$^{-1}$	
	α'_e	$= 0{\cdot}02206$ cm.$^{-1}$	α''_e	$= 0{\cdot}01575$ cm.$^{-1}$	
	β'_e	$= -0{\cdot}185 \times 10^{-6}$ cm.$^{-1}$	β''_e	$= +0{\cdot}095 \times 10^{-6}$ cm.$^{-1}$	
	I'_e	$= 21{\cdot}693 \times 10^{-40}$ g. cm.^{2}	I''_e	$= 25{\cdot}279 \times 10^{-40}$ g. cm.^{2}	
	r'_e	$= 1{\cdot}2731$ A	r''_e	$= 1{\cdot}3743$ A	
	w'_e	$= 1196{\cdot}77$ cm.$^{-1}$	w''_e	$= 1035{\cdot}69$ cm.$^{-1}$	
	$x'_e w'_e$	$= 17{\cdot}09$ cm.$^{-1}$	$x''_e w''_e$	$= 10{\cdot}39$ cm.$^{-1}$	

The values of ϵ and γ, the fine-structure constants of the $^4\Sigma$ state, are given in table 4 for the levels $v' = 0$, 1 and 2. They have been calculated separately from equations (7) of (I):

$$\Delta f'_{21}(K) = 3\epsilon - 3\gamma - 2\gamma K,^{*}$$

$$\Delta f'_{34}(K) = 3\epsilon - \gamma + 2\gamma K,$$

by the method of least squares.

TABLE 4. SPIN FINE-STRUCTURE CONSTANTS FOR THE $^4\Sigma$ STATE

	$\Delta f_{21}(K)$	
v	3ϵ	γ
0	$0{\cdot}4258 \pm 0{\cdot}0018$ cm.$^{-1}$	$-0{\cdot}0005 \pm 0{\cdot}0001$ cm.$^{-1}$
1	$0{\cdot}4333 \pm 0{\cdot}0019$ cm.$^{-1}$	$-0{\cdot}0007 \pm 0{\cdot}0001$ cm.$^{-1}$
2	$0{\cdot}4247 \pm 0{\cdot}0037$ cm.$^{-1}$	$-0{\cdot}0003 \pm 0{\cdot}0002$ cm.$^{-1}$

	$\Delta f_{34}(K)$	
v	3ϵ	γ
0	$0{\cdot}4448 \pm 0{\cdot}0023$ cm.$^{-1}$	$-0{\cdot}0003 \pm 0{\cdot}0001$ cm.$^{-1}$
1	$0{\cdot}4476 \pm 0{\cdot}0032$ cm.$^{-1}$	$-0{\cdot}0001 \pm 0{\cdot}0002$ cm.$^{-1}$
2	$0{\cdot}4265 \pm 0{\cdot}0047$ cm.$^{-1}$	$+0{\cdot}0002 \pm 0{\cdot}0003$ cm.$^{-1}$

---

* There is a misprint in (I) where the third term is given as $3\gamma K$.

For the levels $v' = 0$ and 1 though $\Delta f_{21}(K)$ and $\Delta f_{34}(K)$ depend linearly on K the difference between the two values of 3ϵ considerably exceeds the probable error and Budó's formulae appear to hold only to a first approximation. For $v'' = 2$ the formulae appear to represent the observed structure in a satisfactory manner.

SUMMARY

In continuation of previous work the (0, 2) and (2, 0) bands of the first negative system of oxygen due to the transition ${}^4\Sigma_g^- \rightarrow {}^4\Pi_u$ have been photographed in the second order of a 21 ft. grating and an analysis of the bands is given.

The ${}^4\Pi$ level $v'' = 2$ exhibits the same structure as the previously analysed levels $v'' = 0$ and 1 failing to agree with the theoretical structure predicted by Brandt and Budó. An empirical formula is given which represents the observed structure reasonably well.

A complete table of the molecular constants of five bands of the system is given.

REFERENCES

Bozoky, L. and Schmid, R. 1935 *Phys. Rev.* **48**, 465.
Frerichs, R. 1926 *Z. Phys.* **35**, 683.
Nevin, T. E. 1938 *Phil. Trans.* A, **237**, 471.
Oldenborg, O. 1932 *J. Opt. Soc. Amer.* **22**, 441.

The combustion of aromatic and alicyclic hydrocarbons

III. Ignition and cool-flame characteristics

By J. H. Burgoyne, T. L. Tang and D. M. Newitt
Department of Chemical Technology, Imperial College, London

(*Communicated by A. C. Egerton, Sec.R.S.—Received* 22 *November* 1939)

Introduction

In a previous communication (Burgoyne 1937), attention was drawn to certain apparently anomalous features of the slow combustion of *n*-butyl benzene, and it was shown, *inter alia*, that the observed irregularities in the temperature coefficient of the reaction could be accounted for by the occurrence of cool-flame ignitions of the same type as those exhibited by the higher aliphatic hydrocarbons (Townend and Chamberlain 1936).

These circumstances suggested that a general survey of the ignition characteristics of the aromatic hydrocarbons would be desirable as an aid to elucidating the mechanism of their combustion; and the present paper embodies the results for the series previously studied, together with two members of the alicyclic series which have been included to serve as a connecting link with the paraffins and olefines.

Owing to the wide variations in reactivity towards oxygen of the compounds in question, it was found impracticable to employ the same experimental technique throughout the series; for whilst the ignitions of the more reactive members could safely be studied in silica and glass vessels, the remainder involved high pressures and required the use of steel apparatus. Comparative experiments, however, showed that no essential alteration in the ignition characteristics resulted from the substitution of one material for the other.

Apparatus and experimental method

The low-pressure apparatus has been described in Part I (Burgoyne 1937). The method of determining ignition temperatures was to prepare a stock of the hydrocarbon-oxygen or hydrocarbon-air mixture in a 2 l. glass bulb maintained at a temperature sufficiently high to ensure that the hydrocarbon would remain in the vapour phase. Measured quantities of the mixture were then admitted to an evacuated silica vessel, of capacity *ca.* 500 c.c., contained in an electric furnace heated to the desired reaction temperature.

The high-pressure apparatus was similar in arrangement to the above and requires no special description.

The occurrence of cool-flame and true ignitions were indicated in both apparatus by the readings of a suitable pressure gauge attached to the reaction vessel, and the progress of the reactions preceding and following ignition could be followed by measuring the rate of pressure change, by analysis of "snap" samples of the reacting medium and of the products, and, in some instances, by direct visual observation through a window let into the side of the furnace. The actual ignition temperatures recorded are limiting values defined as the lowest temperature to which the reaction vessel had to be heated for ignition ultimately to occur at the given pressure.

RESULTS

The data summarized below include (1) the determination of the influence of initial pressure upon the ignition ranges of selected mixtures of the various combustibles with oxygen or air, and (2) the analysis of the products from reactions in the several combustion zones. The results of (1) are shown by means of a series of diagrams (figures 1–4), in which the limiting ignition temperatures are plotted against pressure for constant mixture composition, and of (2) by means of carbon or oxygen "balances" in which an attempt is made to account for all the carbon or oxygen originally present in the reacting medium. The low- and high-pressure experiments are dealt with separately.

I. EXPERIMENTS AT LOW PRESSURES IN THE SILICA APPARATUS

(*a*) *Cyclohexane* (*hexahydrobenzene*).

Curve *A*, figure 1, relates to an equimolecular cyclohexane-oxygen mixture ignited in a silica vessel.

The curve will at once be recognized as resembling in all essential features the corresponding curve for any of the higher paraffin hydrocarbons and, in particular, that of *n*-hexane which is shown inset in the figure. There are, for example, two well-defined ignition ranges, the one characterized by a progressive fall of ignition temperature with increasing pressure, from 630° at 45 mm. to 395° at 210 mm. pressure, and the other by the occurrence of two pressure minima at 325° (160 mm.) and 275° (175 mm.), respectively. At pressures above 200 mm. the slope of the ignition curve diminishes and the ignition temperature tends to become independent of the pressure. It is to be noted that ignition is preceded, in all cases, by an induction period or time "lag" which varies with pressure.

Attention may also be drawn to a region on the low-pressure side of the ignition curve, below 395° (the shaded area adjacent to the curve), within which cool-flame ignition followed by slow combustion takes place, and phenomena are observed similar to those which have been described for some of the higher paraffin hydrocarbons (Newitt and Thornes 1937). Thus, on traversing the region from low to high pressures, there is a zone near the lower limit, in which as many as four or five successive feeble ignitions may be observed. As the pressure is raised these coalesce into a single ignition, the intensity of which increases with pressure. The cool-flame combustion uses up only a small proportion of the available oxygen, the remainder contributing to a subsequent slow oxidation. As the true ignition curve is approached the rate of this secondary oxidation increases until eventually a second cool-flame ignition occurs, which ultimately gives place to a true ignition. The time lags during these successive stages show a progressive diminution.

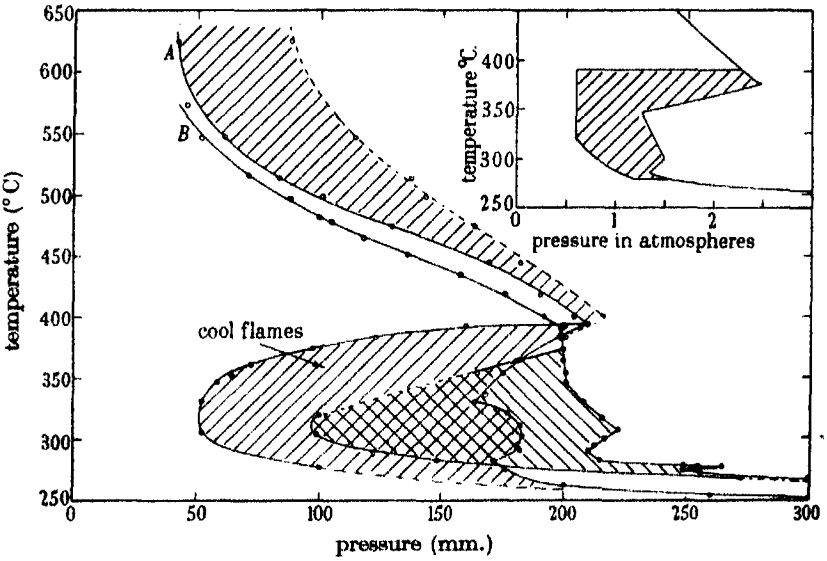

FIGURE 1

In the upper ignition region, above 400°, there is an area to the left of the limiting ignition curve, in which slow combustion takes place accompanied by luminescence but no cool-flame formation. On traversing this region in the direction of increasing pressure, the rate of combustion increases until eventually inflammation occurs. Combustion is not, however, complete in the first instance, ignitions near the limit being succeeded by a period of slow combustion. The approximate pressures at which this after-combustion is no longer detectable are indicated in the diagram by the broken line to the right of the ignition curve. The time lags in the upper ignition region diminish progressively with fall of temperature from about 5 sec. at 550° to less than 1 sec. at 390°. In the lower region, on the other hand, they increase with fall of temperature, at first slowly from 390° down to 275°, and then rapidly, until at 262·5° the lag is as much as 70 min. In this neighbourhood the values are very sensitive to small changes of temperature, as may be seen from the following data which relate to points on the lower branch of the ignition curve:

Ignition temperature (° C)	271	268	265·5	262·5
Time lags (min.)	2·5	7·8	17·5	70

The determination of the ignition temperature in this region is, therefore, a tedious operation, and the probable errors are greater than in other parts of the curve.

(*b*) *Cyclohexene* (*tetrahydrobenzene*).

Curve *B*, figure 1, is for an equimolecular cyclohexene-oxygen mixture, also in the silica vessel. In this instance we have a ring compound containing one unsaturated linkage which might be expected to confer on it a greater immunity to oxygen attack than was found for the corresponding fully saturated cyclohexane (Beatty and Edgar 1934). Reference to the curve will show that this expectation is only partially fulfilled.

There are, as before, two distinct ignition regions meeting at 390° and 200 mm., and a third pressure minimum at 278° (250 mm.). There is also a region, of lesser extent, in which cool flames are observed. The cool flames are less intense than with cyclohexane, and the pressure pulse accompanying them is so feeble as to render difficult the exact delimitation of the upper boundary.

The time lags vary in much the same way as those of cyclohexane, but they are of shorter duration, particularly at the lower temperatures where they are measured in minutes rather than in hours.

(*c*) *Aromatic hydrocarbons.*

Although *n*-propylbenzene proved to be considerably more reactive towards oxygen than the lower members of the aromatic series, it was found impracticable to determine the complete ignition curve of an equimolecular mixture in the silica apparatus owing to the comparatively high pressures involved. Data were obtained, however, for the upper part of the curve (curve *F*, figure 2), together with a portion of the cool-flame zone (*F′*), indicating the existence of a lower ignition system.

The upper parts of the ignition curves of equimolecular mixtures with oxygen of benzene, toluene and ethylbenzene in the silica apparatus are given for comparison (curves *C*, *D* and *E*).

With *n*-butylbenzene the complete curve (curve *G*) was found to lie within the pressure limits of the apparatus, and, although carbon was deposited during the ignition reaction, no difficulty was experienced in obtaining data for the lower ignition system.

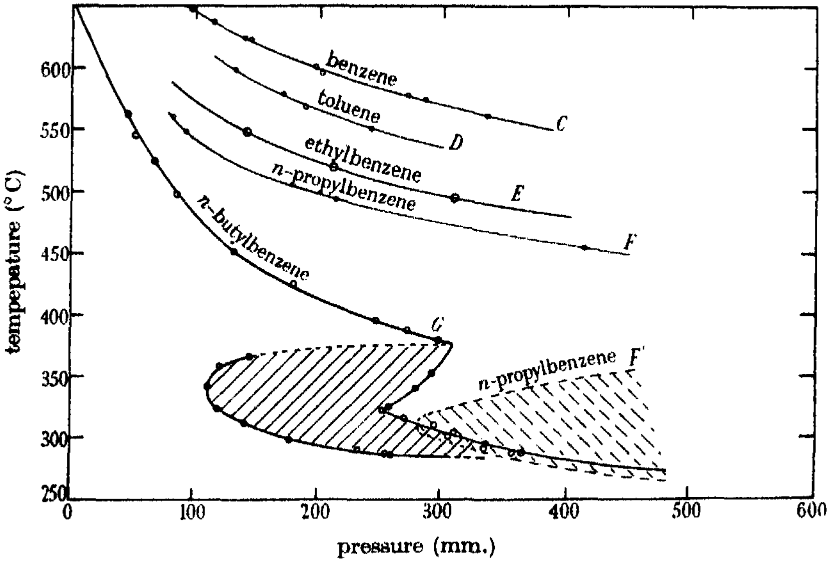

FIGURE 2

It will be seen that the curve *G* resembles in many respects the corresponding curve for the two alicyclic hydrocarbons and for the higher paraffins, although there are some minor differences. In the upper region, for example, the curve is almost identical with that of cyclohexene, both lying on the low-pressure side of the cyclohexane curve; but below 420° the curves "fan out" and their location with respect to pressure indicates a considerable variation in reactivity, cyclohexane being by far the most reactive and *n*-butylbenzene the least so. The latter, however, has only one clearly defined pressure minimum, at 323° (250 mm.). Such variations might be expected from the structural differences between the aromatic and the alicyclic compounds.

The actual mechanism by which oxidation takes place in the three cases has not been fully elucidated, but there is reason to believe that ignition in the lower region is conditioned by the relative stability of one or more of the intermediate products of combustion which, by their thermal decomposition or further oxidation, give rise to active centres in the reacting medium (Neumann and Aivazov 1935; cf. Egerton and Ubbelohde 1935). If this be so, it may be concluded from a comparison of the three curves that, whilst similar processes are probably concerned in the earlier stages of the oxidation, their rates would by no means be identical.

II. EXPERIMENTS AT HIGH PRESSURES IN THE STEEL APPARATUS

In the case of the aromatic hydrocarbons equimolecular combustible-oxygen mixtures are not very suitable for experimenting in the ignition region, since copious carbon deposition invariably accompanies inflammation and the reaction vessel has, in consequence, to be "burnt out" after each experiment. In seeking to compare the behaviour of a series of such compounds, therefore, air has been substituted for oxygen, and standard mixtures containing 1·85 times the theoretical amount of hydrocarbon for complete combustion to carbon dioxide and water have been employed. The actual percentages of combustible substance are as follows: benzene 5, toluene 4·3, ethylbenzene and the xylenes 3·5 and *n*-propylbenzene and mesitylene 3·2 %. The substitution of air for oxygen necessitates the use of much higher pressures and silica and glass apparatus can no longer safely be employed.

(*a*) *Benzene and its mono-alkyl derivatives.*

In figure 3 the ignition data for the standard mixtures with air of benzene, toluene, ethylbenzene and *n*-propylbenzene are shown graphically together with the corresponding data for a 15 % methane-air mixture for reference purposes. It will be noted that the curves fall into the accepted order of reactivity of the four hydrocarbons (Burgoyne 1937), and that, with the exception of *n*-propylbenzene, the ignition temperatures fall progressively with increase in pressure, the points lying on smooth curves.

Benzene, as might be expected from its structure, ignites with more difficulty than any of its derivatives or methane, its ignition temperature at any given pressure within the range of the present experiments being upwards of 100° higher than that of toluene.

n-Propylbenzene shows characteristics which we now associate with the higher paraffin hydrocarbons. It has an upper and lower ignition range, and the latter includes a pressure minimum at 340° (5 atm.). There is also evidence of feeble cool-flame inflammation in the neighbourhood of the pressure minimum, although the recording apparatus was not sufficiently sensitive to enable the boundaries of the cool-flame zone to be defined.

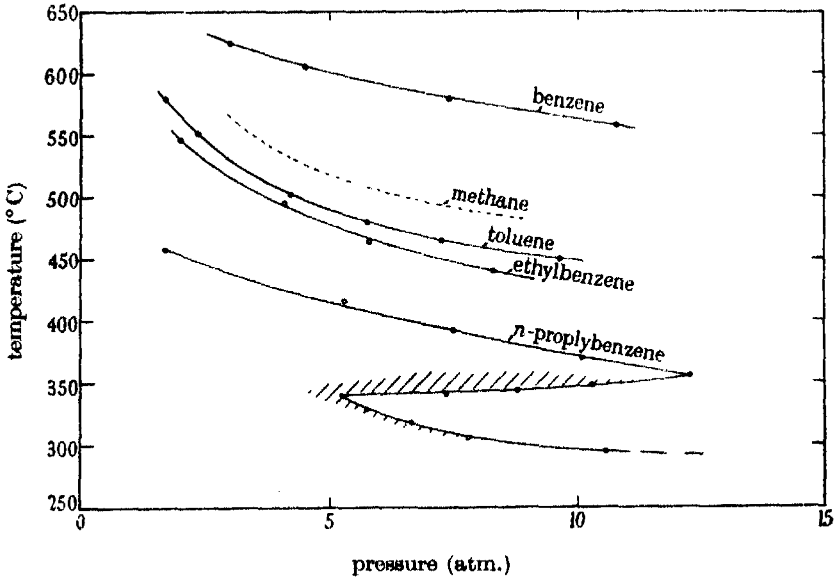

FIGURE 3

In the case of benzene the time lags before ignition do not exceed 1 or 2 sec. at any pressure, and are comparable with the time taken to introduce the combustible mixture into the reaction vessel. For the remaining compounds the lags are of longer duration and at first increase with pressure, reaching a maximum, in the case of toluene, at about 5 atm. In general they diminish as the series is ascended, as shown by the following figures which relate to ignitions at 5 atm. pressure:

Hydrocarbon	Ignition temperature °C	Time-lag sec.
Toluene	490	23
Ethylbenzene	480	4
n-Propylbenzene	418	2

(*b*) *The three xylenes and mesitylene.*

From the point of view of the relation between structure and reactivity it is of interest to compare, as in figure 4, the ignition characteristics of *o*-, *m*- and *p*-xylene one with another and with their isomer ethylbenzene. The order of increasing reactivity is para-, meta-, ortho-, which is also the order adduced from the slow-combustion experiments previously described (Burgoyne 1937). The lower ignition regions of the ortho- and meta-xylenes have each two pressure minima and well-defined cool-flame zones, whilst that of para-xylene has only one pressure minimum at an unusually high temperature and there are no detectable cool-flame ignitions.

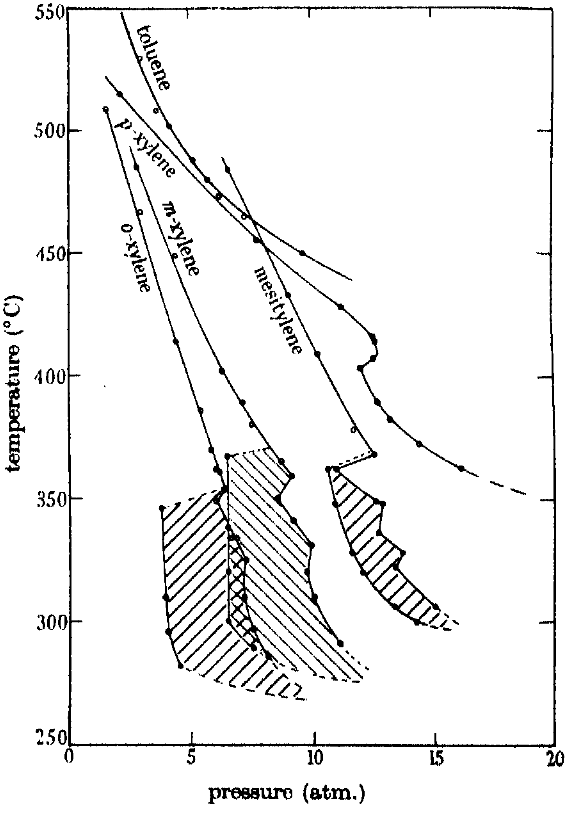

FIGURE 4

On comparing the ignition curves of *p*-xylene, ethylbenzene and toluene, it appears as though the effect of two symmetrically placed side-chains upon the reactivity of the benzene nucleus is little if at all greater than that of one side-chain of the same length. Mesitylene, which is also symmetrical, has, likewise, a comparatively high resistance to oxidation. There are three pressure minima in the lower ignition region at 362° (11·5 atm.), 338° (12·9 atm.) and 322° (13·5 atm.), and a well-defined but restricted cool-flame zone. As might be expected, it is somewhat more reactive than *p*-xylene but less so than the *o*- or *m*-derivatives. Attention may also be drawn to the unusually long time lags in the lower ignition range.

THE PRODUCTS OF OXIDATION IN THE SLOW-COMBUSTION AND COOL-FLAME REGIONS

In the high-pressure experiments, owing to the increased quantity of reactants concerned, it was possible not only to analyse the gaseous products, but also to carry out an analysis of the condensable substances formed. In the latter connexion, estimations were made of the total acid, aldehyde, phenol and alcohol radicles resulting from slow and cool-flame combustions of typical hydrocarbons.

Under the prevailing conditions of experiment, it was not possible to take "snap" samples of the reacting medium, and in all cases the combustion was allowed to proceed to completion before analysis. In subsequent experiments in the low-pressure apparatus, which are to be reported in a later communication, it was possible to follow the various combustion processes analytically throughout their whole course; and it was shown that certain factors which are not evident in the ultimate reaction products play an important part intermediately, and, in particular, the formation and decomposition of peroxides are closely associated with the propagation of cool flames.

In the case of the higher derivatives, it was possible only to assess the distribution of oxygen in the products, but with lower members (e.g. toluene) a more complete knowledge of the combustion chemistry (Newitt and Burgoyne 1936) permitted an estimate also to be made of the distribution of the carbon involved in reaction.

(1) *Toluene-air medium*

In table 1, the results relative to a 4·3 % toluene-air mixture at 8 atm. and three different temperatures are shown. Such a mixture ignites at about 445° C, so that the high-temperature experiment approaches limit conditions closely. To this fact may be attributed the elevation of the ratio CO/CO_2 and the falling off of the "acid" and "phenol" figures.

As demonstrating the influence of mixture composition, it is interesting to compare the results of the above experiments with those of some earlier ones in the same reaction vessel, using considerably richer mixtures (Newitt and Burgoyne 1936). This comparison is made in table 2, where the distribution of reacted carbon is the basis. The relationship between a high proportion of oxygen and ring rupture is very marked, as is also the tendency of the side-chain to appropriate oxygen at the expense of the nucleus in rich mixtures.

TABLE 1. DISTRIBUTION OF OXYGEN IN PRODUCTS OF 4·3 % TOLUENE-AIR MIXTURE AT 8 ATMOSPHERES (SLOW COMBUSTION)

Temp. ° C ...	340	400	440
Percentage oxygen as:			
Phenols	25·3	44·8	24·7
Alcohols	39·6	10·4	27·3
Aldehydes	29·6	31·0	40·5
Acids	5·5	13·8	7·5
Ratio CO/CO_2	0·23	0·15	0·28
Percentage oxygen appearing as products of:			
(1) Ring rupture	81·8	94·2	95·6
(2) Side-chain oxidation	13·6	3·2	3·3
(3) Nuclear oxidation	4·6	2·6	1·1

TABLE 2. INFLUENCE ON PRODUCTS OF TOLUENE CONCENTRATION, IN SLOW COMBUSTION AT 400° C

Mixture:			
Toluene	0·35 atm.	20·0 atm.	42·8* atm.
Oxygen	1·6 ,,	1·0 ,,	1·5 ,,
Nitrogen	6·05 ,,	4·0 ,,	5·7 ,,
Percentage carbon burnt in products as:			
CO_2	54·0	14·7	4·2
CO	16·3	4·2	3·9
C_6H_5COOH	4·2	8·1	9·7
C_6H_5CHO	8·7	30·1	31·0
$C_6H_5CH_2OH$	3·0	31·1	16·6
$C_6H_4(OH)_2$	13·1	10·2	9·3
$HCHO$	0·7	—	—
Ratio CO/CO_2	0·15	0·28	0·93
Percentage oxygen appearing as products of:			
(1) Ring rupture	94·2	68·0	60·9
(2) Side-chain oxidation	3·2	27·5	33·8
(3) Nuclear oxidation	2·6	4·5	5·3

* At 391° C.

(2) *Xylene-air media*

In all cases, 5 % xylene-air mixtures were employed, the temperature being so adjusted as to give different types of slow combustion and (where possible) cool flames, at the same pressure.

In table 3 are the results for *o*-xylene, relating to a cool-flame reaction at 340° C and to a slow combustion at 400° C, the initial pressure being 4·6 atm. in each case. The 5 % mixture ignites at 5 atm. and 400° C, so that the conditions for the latter reaction approached the ignition limit closely, and the ratio CO/CO_2 is therefore unusually high. The "phenol" figure is not lowered, however, as was the case with toluene.

TABLE 3. DISTRIBUTION OF OXYGEN IN PRODUCTS OF REACTION OF 5 % *o*-XYLENE-AIR MEDIUM AT 4·6 ATM.

Temp. ° C ...	340	400
Nature of combustion	Cool flame	Slow combustion
Percentage oxygen as:		
Phenol	9·3	20·7
Alcohol	18·6	36·2
Aldehyde	18·6	22·6
Acid	53·5	20·5
Ratio CO/CO_2	0·08	5·03
Percentage oxygen appearing as products of:		
(1) Ring rupture	95·7	98·1
(2) Side-chain oxidation	3·9	1·5
(3) Nuclear oxidation	1·4	0·4

If the behaviour of toluene at 340 and 400° C is compared, it is seen that the substitution of the methyl group in the ortho position brings about an increased appropriation of oxygen to the side-chain carbon atoms. With *m*-xylene (table 4), however, more oxygen goes to the nucleus, presumably

TABLE 4. DISTRIBUTION OF OXYGEN IN PRODUCTS OF OXIDATION OF 5 % *m*-XYLENE-AIR MIXTURE AT 6·5 ATM.

Temp. ° C ...	300	342	402
Nature of combustion	Cool flame	Cool flame	Slow combustion
Percentage oxygen as:			
Phenol	28·9	30·0	52·0
Alcohol	12·9	18·4	23·0
Aldehyde	18·2	28·4	19·5
Acid	40·0	23·4	5·5
Ratio CO/CO_2	0·29	0·17	0·07
Percentage oxygen appearing as products of:			
(1) Ring rupture	79·1	94·0	98·3
(2) Side-chain oxidation	14·9	4·2	0·8
(3) Nuclear oxidation	6·0	1·8	0·9

because this molecule is more symmetrical and does not possess a point of such great vulnerability as is caused by the juxtaposition of methyl groups in the ortho derivative. In this connexion, *p*-xylene (table 5) is more akin to *m*-xylene than might have been expected, and it is evident that, as regards the attraction of oxygen to the side-chains, it is of little significance whether one or two nuclear hydrogen atoms separate them so long as they are not, in fact, adjacent.

TABLE 5. DISTRIBUTION OF OXYGEN IN PRODUCTS OF SLOW COMBUSTION OF 5 % *p*-XYLENE-AIR MIXTURE

Temp. ° C ...	340*	340	401
Pressure, atm. ...	14·4	9	9
Percentage oxygen as:			
Phenol	31·0	29·2	45·4
Alcohol	21·2	1·0	9·1
Aldehyde	18·2	33·8	41·0
Acid	29·6	36·0	4·5
Ratio CO/CO_2	0·21	0·14	0·02
Percentage oxygen appearing as products of:			
(1) Ring rupture	94·0	97·1	97·8
(2) Side-chain oxidation	4·1	2·0	1·2
(3) Nuclear oxidation	1·9	0·9	1·0

* 3·5 % mixture.

When the results for the three xylenes are compared it is perhaps surprising, at first sight, to observe that the distinction between the cool-flame reactions of the ortho and meta derivatives and the slow combustion at the same temperature of the para derivative is not very marked. Thus, in each case, lowering the reaction temperature causes increases in the figures for "acid" and "oxygen in side-chain" and decreases in "phenol", "alcohol", "aldehyde", "oxygen in nucleus" and "oxygen in breakdown products". Turning to the results for a 4 % mesitylene-air mixture (table 6), it will be seen that the ultimate products of the slow-combustion and cool-flame reactions at 304° C are strikingly similar, and the only substantial difference is in the aldehyde-acid distribution. There is strong evidence, then, that the final reaction products are much the same at a given temperature whether a cool flame has been propagated or not. This, in turn, suggests that the mechanism is the same in the two cases and that a cool flame is merely an intensification by pressure of a stage of the slow combustion at the same temperature.

It will be observed in table 6 that there is a marked falling off in the "acid" and "phenol" figures near the ignition limit (experiment at 385° C) as in the case of toluene.

TABLE 6. DISTRIBUTION OF OXYGEN IN PRODUCTS OF REACTION OF 4 % MESITYLENE-AIR MIXTURE

Temp. ° C ...	304	304	340	385
Pressure, atm. ...	11·5	14	11·5	9·2
Nature of reaction ...	Slow combustion	Cool flame	Cool flame	Slow combustion
Percentage of oxygen as:				
Phenol	33·2	32·0	32·4	19·4
Alcohol	13·2	13·4	2·3	24·6
Aldehyde	11·8	17·4	21·0	42·0
Acid	42·5	37·2	44·3	14·0
Ratio CO/CO_2	0·21	0·26	0·15	0·21
Percentage of oxygen appearing as products of:				
(1) Ring rupture	84·7	85·0	95·7	93·5
(2) Side-chain oxidation	10·2	10·2	2·9	5·2
(3) Nuclear oxidation	5·1	4·8	1·4	1·3

DISCUSSION

In view of the fact that experiments bearing upon other aspects of the low-temperature combustion of the aromatic hydrocarbons have yet to be reported, it is hardly profitable at the present juncture to discuss in detail the chemical processes underlying the phenomena already described. There is a clear analogy, however, between the ignition curves of the aromatic and aliphatic hydrocarbons, modified by significant differences which may be briefly summarized. Since the benzene derivatives under consideration have, in all cases, saturated side-chains, it is to the paraffins that attention must be directed for purposes of comparison (cf. Townend and co-workers 1933, 1934, 1936). Indeed, an examination of the respective ignition curves will quickly reveal that the relationship between the olefines and the aromatic hydrocarbons is but slight. With benzene, toluene and ethylbenzene we are not at present concerned, since, as in the case of methane, no evidence has so far been adduced to show that they have a low-temperature ignition system at all.

The main differences between the higher paraffins and those aromatic hydrocarbons which propagate cool flames seem to be associated with the transition between the high- and low-temperature systems of ignition, which occurs at a lower temperature in the latter class. Thus, whereas with the paraffins the main pressure maximum in the true ignition curve is invariably located at 390–400°, with the aromatic hydrocarbons it occurs between 350 and 370°. Moreover, the point of inflexion in the ignition curve, where the influence of the low-temperature mechanism upon the high-temperature kinetics is first manifest, is situated upwards of 450° for all aliphatic hydrocarbons, but is not encountered until about 390° with the higher homologues of benzene. The upper temperature limit of the cool-flame zone, too, is some 30° lower in the latter case than the former. As for the other prominent features of the curves, namely, pressure minima of ignition and the lower cool-flame boundary it is not possible to generalize, since these vary considerably, even within the same series, according to the nature of the fuel.

With regard to the alicyclic hydrocarbons examined, the transitional character is not very marked, and it may be said that the cyclic structure has little effect upon aliphatic characteristics. Cyclohexane indeed is in all respects a typical paraffin, and although little is known directly of the ignition characteristics of the 6-carbon olefines, tetrahydrobenzene appears to conform closely excepting that the location of the cool-flame zone is abnormally low. Neither of the olefines examined by Kane and Townend (1937) (up to and including amylene) showed a definite pressure minimum of ignition, although a second point of inflexion in the true ignition curve was located, as in the present case of tetrahydrobenzene (*ca.* 375°).

The occurrence of cool-flame ignitions in hydrocarbon combustions is generally considered to be associated with the accumulation and subsequent reaction, by oxidation or decomposition, of some intermediate of high intrinsic energy. If this explanation be accepted, it follows that, while this intermediate in the case of aromatic combustions may be analogous in its structure and mode of production to the aliphatic counterpart, it, or a predecessor in its formation, is certainly comparatively unstable thermally. As a consequence, the low-temperature systems of the aromatic hydrocarbons fail to persist to such high temperatures as in the case of the higher paraffins and the pressure extent of the cool-flame zone is generally less in the former instance: thus, for example, the cool flame of *n*-propylbenzene is ill-defined as compared with that of propane.

It is of interest to note, in this connexion, that the higher aromatic aldehydes are known to be comparatively unstable thermally, decomposing at quite low temperatures to the next lower hydrocarbon:

$$C_6H_5.CH_2...CH_2CHO = C_6H_5.CH_2...CH_3 + CO.$$

In the light of the known participation of higher aldehydes in the low-temperature combustion system (Newitt and Thornes 1937), this type of reaction is probably significant in determining differences of behaviour between the aromatic and aliphatic hydrocarbons.

ACKNOWLEDGEMENTS

The authors are indebted to the Department of Scientific and Industrial Research for a grant to one of us (J. H. B.) during the tenure of which part of the investigation here described was carried out.

SUMMARY

The general ignition characteristics of eleven aromatic and alicyclic hydrocarbons have been investigated, and previous conclusions regarding their relative reactivity to oxygen are confirmed.

While benzene, toluene, and ethylbenzene show smooth ignition curves within the limits of pressure available, the other hydrocarbons examined exhibit low-temperature ignition systems and, except in the case of *p*-xylene, cool flames are propagated.

Cyclohexane behaves as a typical paraffin, but tetrahydrobenzene, while resembling the olefines in most respects, has cool-flame limits characteristic of the aromatic series.

Chemical analyses of the ultimate products of slow combustion and cool-flame reactions show that the two types of combustion yield similar results at the same temperature. The low-temperature systems of the aromatic hydrocarbons are similar to those of the paraffins, and what differences occur appear to be conditioned merely by the relative stability of analogous intermediate products.

REFERENCES

Beatty and Edgar 1934 *J. Amer. Chem. Soc.* **56**, 102, 107, 112.
Burgoyne 1937 *Proc. Roy. Soc.* A, **161**, 48.
Egerton and Ubbelohde 1935 *Nature, Lond.*, **135**, 997.
Kane and Townend 1937 *Proc. Roy. Soc.* A, **160**, 174.
Neumann and Aivazov 1935 *Nature, Lond.*, **135**, 655.
Newitt and Burgoyne 1936 *Proc. Roy. Soc.* A, **153**, 448.
Newitt and Thornes 1937 *J. Chem. Soc.* pp. 1656, 1669.
Townend and Chamberlain 1936 *Proc. Roy. Soc.* A, **154**, 95.
Townend, Cohen and Mandelekar 1934 *Proc. Roy. Soc.* A, **146**, 113.
Townend and Mandelekar 1933 *Proc. Roy. Soc.* A, **141**, 484.

The combustion of aromatic and alicyclic hydrocarbons

IV. The kinetics of the slow combustion of benzene and its mono-alkyl derivatives at low temperatures

By J. H. Burgoyne, Ph.D.
Department of Chemical Technology, Imperial College, London

(*Communicated by A. C. Egerton, Sec.R.S.—Received* 22 *November* 1939)

Introduction

In previous papers of this series the ignition and slow-combustion reactions of a number of aromatic hydrocarbons have been examined, mainly from the kinetic standpoint. In the present and following communications it is proposed further to consider benzene and its single side-chain derivatives, in relation particularly to the oxidation reactions occurring below 400° C, and to correlate this mode of combustion by kinetic and analytical observations with the types previously examined.

The hydrocarbons to which attention is chiefly directed are benzene, toluene, ethylbenzene, *n*-propylbenzene and *n*-butylbenzene.

Apparatus and experimental methods

The apparatus employed has been described in Part I, and the methods of procedure in observing reaction rates and determining ignition and cool-flame limits have been indicated. The reaction vessel used throughout the present work was, except where otherwise stated, the same as that used for the low-pressure determination of ignition limits in Part III, and the kinetic and analytical experiments may be referred to the curves in figure 2 of that paper.

n-Propylbenzene

Experiments in the unpacked bulb

In carrying out experiments upon the rate of oxidation below 400° of benzene and its alkyl derivatives, the field is limited by two considerations. With the lower members, especially with benzene itself, the rate of reaction is very slow at the maximum pressure available (rather less than 1 atm.), and there is little scope to examine the effect of varying concentrations. With butylbenzene on the other hand, the intervention of cool flames at quite low pressures (*ca.* 100 mm.) again limits the opportunity for kinetic measurements. Intermediately, *n*-propylbenzene proves to be a good subject for investigation, and since it has been possible to study this hydrocarbon in some detail, it will be convenient to consider it first in describing the experimental results.

p-Δp relationships. The combustion of an equimolecular propylbenzene-oxygen mixture between 250 and 400° has been examined. The method of experiment was to observe the rate of reaction at specified temperature intervals and various pressures by means of the pressure increase. It was observed that at given temperatures above 290° the final pressure increment (Δp) bore a linear relationship to the initial total pressure (p) of the medium, and that the graphs passed approximately through the origin of co-ordinates. Below 290°, the extrapolated line cut the axis of p at a positive value, indicating a tendency for Δp to increase abnormally with increasing initial pressure. With this reservation, the results suggested that the course of the reaction was unaffected by variations of pressure at a given temperature, and that the manometric method of measuring the reaction rate was therefore justified. In the series of experiments in which the partial pressure of oxygen alone was varied, the Δp-p graph was again linear and passed through the origin provided that the concentration of hydrocarbon was sufficient to react with all the oxygen. It was thereby concluded that the course of the reaction was not changed by varying the oxygen concentration, and that the variations observed in Δp were entirely due to differences in the amount of hydrocarbon oxidized.

The "order of reaction". It has been shown in Part I that the rate of oxidation of propylbenzene above 400° is governed by the relationship

$$\frac{1}{t_{20-60}} = Kp^n, \tag{1}$$

where p is the initial pressure of the combustible mixture and n has a constant value of 2·1. The present investigation has shown that, while the "order of reaction" varies considerably at temperatures below 400°, the equation (1) still holds good at any given temperature. Some values of n are given in table 1.

The early stages of the reactions are governed by a relationship similar to equation (1), namely,

$$\frac{1}{t_{0-20}} = K'p^{n'}, \tag{2}$$

and corresponding values of n' are included in table 1. It will be seen that while the general trend of the indices is the same, n' is greater than n at the lower temperatures but becomes relatively less above 350° C.

TABLE 1. VALUES OF n AND n' FOR AN EQUIMOLECULAR n-PROPYLBENZENE-OXYGEN MIXTURE

Temp. (° C)	n	n'
259	1·2	1·7
272	1·5	1·9
278	1·3	2·1
290	2·3	3·0
303	3·5	3·1
311	4·3	4·1
320	4·2	—
327	3·9	4·0
354	3·6	3·3
360	3·4	—
366	3·4	3·1
394	2·1	1·9
438	2·1	—

The influence of the reaction temperature. Referring again to Part I, it will be recalled that at high temperatures, reactive propylbenzene-oxygen media adhere to the equation of Arrhenius. The graph relating log t_{20-60} with the reciprocal of the absolute temperature is therefore linear and the energy of activation was found to be 39 kg.cal./g.mol. Below 400°, however, a difference is again noticeable.

In figure 1, the log t_{20-60}-$1/T$ relationship is shown for equimolecular propylbenzene-oxygen mixtures at certain specified pressures (full lines). Commencing at the high temperature (left-hand) end of the graphs and proceeding in the direction of decreasing temperature, it is seen that there is a departure from the constant value of E which, in fact, decreases to a considerable negative figure. A reverse change then sets in and at low temperatures E again assumes a positive value which appears ultimately to become steady. The negative temperature coefficient observed with propane (Pease 1929, 1938; Newitt and Thornes 1937), and in the case of other aliphatic hydrocarbons is thus exemplified by n-propylbenzene.

With regard to the influence of the total pressure on this phenomenon, reference to figure 1 shows that the negative temperature coefficient becomes greater in magnitude and extent and persists to higher temperatures as the initial pressure is increased, i.e. as the zone of cool-flame propagation is approached.

If the rate of the initial stages of the reaction is also examined by plotting log t_{0-20} against $1/T$, a somewhat similar result is obtained (broken lines in figure 1), but the stated influences of the total pressure on the extent of the negative temperature coefficient become much more pronounced, and at the lowest pressure considered (100 mm.) the range in which E has a definitely negative value is almost obliterated.

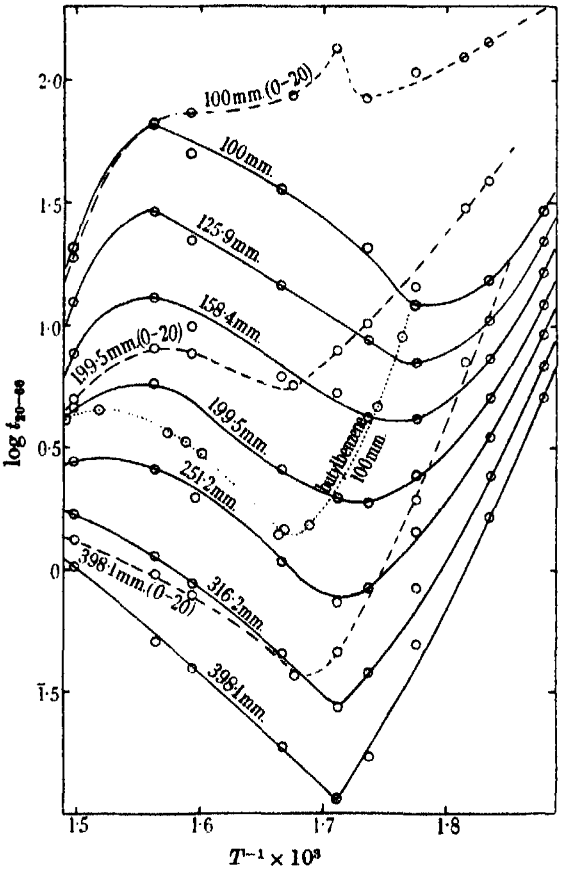

FIGURE 1

In figure 2 will be found a curve relating the final pressure increment for equimolecular propylbenzene-oxygen mixtures (expressed as a percentage of the initial total pressure) to the reaction temperature. In this case the initial pressure was 100 mm., but since $\Delta p/p$ has a constant value at given temperatures, the curve should apply equally well to any equimolecular propylbenzene-oxygen mixture. Above 400°, the graph is linear, indicating a uniform course of reaction, and such appears also to be the case below about 310°. Intermediately, however, a transition occurs which results at about 350° in a tendency for Δp to be unaffected by the reaction temperature.

The influence of individual reactant concentrations. At temperatures above 400°, the partial pressure of oxygen has a negligible influence on the rate of combustion of propylbenzene: this is substantially true at lower temperatures also. Thus at 275° the value of n with respect to the oxygen concentration is less than 0·1, and at 311°, where the overall value of n is 4·3, the "contribution" of oxygen is only 0·6. Corresponding values of n' with respect to the oxygen concentration are 0·1 (at 275°) and 0·8 (at 311°).

The influence of dilution with nitrogen. In table 2 are shown the results of experiments in which a mixture of 100 mm. propylbenzene and 100 mm. oxygen was allowed to react at three different temperatures in the presence of various amounts of nitrogen. Results relating to the period of maximum velocity (t_{20-60}) and to the initial stages (t_{0-20}) are given.

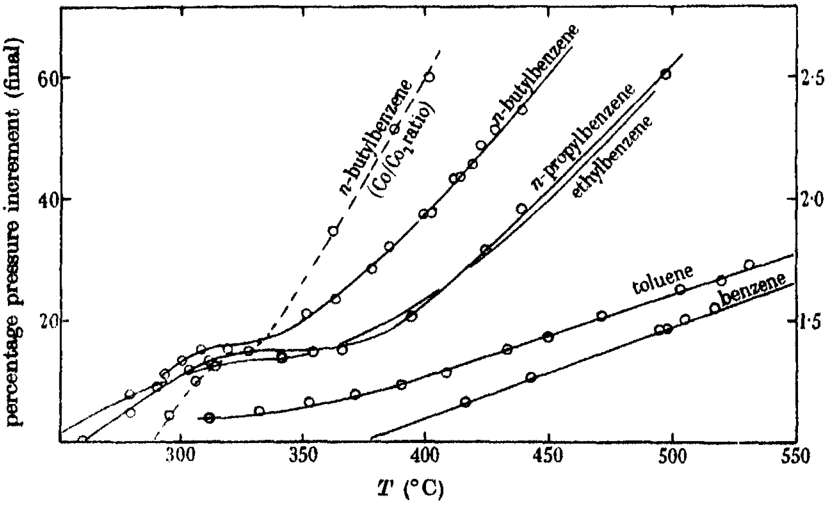

FIGURE 2

At 403° progressive dilution, after causing a preliminary retardation, considerably accelerates the main reaction (cf. Burgoyne 1937). The initial stage is also accelerated but to a less extent.

At 307° the main reaction is again accelerated but only slightly, whereas the accelerating effect of dilution on the initial stage is very marked. This somewhat unexpected reversal of the state of affairs at high and low temperatures has been confirmed by an independent series of experiments.

At 275° progressive dilution has only a small effect on the kinetics, the main reaction being retarded and the initial stage accelerated.

Influence of the condition of the vessel walls. The influence of the history and condition of the reaction vessel upon the rate of the combustion is similar at high and low temperatures. A reaction in a vessel which has stood full of air at the reaction temperature for a period is rather slower and its "induction period" is substantially increased as compared with one which follows a mere evacuation of a previous mixture. To allow the vessel to stand evacuated at the reaction temperature also produces a retarding effect, though less quickly than when air is present. The effect of "oxidizing" the surface can be simulated by washing out the bulb with an organic solvent, when a brownish substance is dissolved which evidently cannot be removed by prolonged evacuation.

TABLE 2. INFLUENCE OF NITROGEN DILUTION ON THE RATE OF REACTION OF A 100 MM. n-PROPYLBENZENE + 100 MM. OXYGEN MIXTURE

Main reaction

Temp. °C	Relative values of $\frac{1}{t_{20-60}}$ in the presence of x mm. of nitrogen, where x is				
	0	100	200	300	400
275	1·00	0·89	0·80	0·86	0·73
307	1·00	—	0·88	1·14	1·22
403	1·00	—	1·04	1·14	1·33

Initial stages

Temp. °C	Relative values of $\frac{1}{t_{0-20}}$ in the presence of x mm. of nitrogen, where x is				
	0	100	200	300	400
275	1·00	1·14	1·21	1·26	1·31
307	1·00	—	1·14	1·55	1·70
403	1·00	—	1·06	1·20	1·22

Experiments in the packed bulb

The results so far described refer to reactions in a cylindrical quartz vessel of normal design. When this was replaced by one of similar dimensions filled with small pieces of silica, significant differences in the reaction kinetics were observed.

p-Δp relationships. The relationship of the pressure increment to the initial total pressure did not suggest any important variation in the course of the reaction at a given temperature. Contrary to observations made with the unpacked vessel, however, Δp tended to increase *less* with increasing values of p than a linear law would allow.

The "order of reaction". Experiments to determine the "order of reaction" at specified temperatures showed that packing did not affect the trend of n to a maximum value at about 310°, but the high-order reaction was found to persist to higher temperatures than normally. n' showed a marked divergence, however, for while it was greater than n at the lowest temperature it fell off almost to zero at 400° and was in all cases less than in the unpacked vessel. Values of n and n' are given in table 3.

TABLE 3. VALUES OF n AND n' FOR AN EQUIMOLECULAR n-PROPYLBENZENE-OXYGEN MIXTURE IN THE PACKED BULB

Temp. (° C)	n	n'
279	1·2	1·5
311·5	4·2	1·8
404	3·2	Very low
434	2·1	Very low

The influence of the reaction temperature. The increased surface-volume ratio brought about a considerable retardation of the reaction at all temperatures. In figure 3 curves are given showing the relationship between log t_{20-60} and $1/T$ at specified pressures: corresponding curves for the unpacked vessel are shown as broken lines. The range in which the temperature coefficient is negative is seen to be generally shifted to lower temperatures by packing, and to decrease considerably in extent with increasing pressure. It is therefore limited by packing at high pressures and extended at low.

The initial stages of the reaction also show a negative temperature coefficient in the packed bulb.

Reference to figure 3 shows that t_{20-60} is increased by packing at all temperatures, but that the increase is most marked in the region of the negative temperature coefficient. This is also true of the initial stages of the reaction, but to a less degree.

The influence of the condition of the vessel walls. Whereas with the ordinary vessel a "first reaction" is retarded at all stages, in the packed bulb, the reverse is the case. In the latter circumstances the initial stage is accelerated to a greater extent than the main reaction.

n-BUTYLBENZENE

Although the combustion reactions of butylbenzene have received less detailed study than those of propylbenzene, a general analogy is apparent. Thus, the curves in figure 2 relating the pressure increment to the reaction temperature in the two cases, follow similar courses, and the corresponding log t_{20-60}-$1/T$ graphs (see figure 1) bear a marked resemblance one to the other. In the figure an equimolecular butylbenzene-oxygen mixture at 100 mm. may be compared with like propylbenzene-oxygen media at 100 mm. and 251·2 mm. initial pressure. Reference to the ignition curves in Part III (figure 2) will show that the 100 and 250 mm. ordinates are similarly placed relative to the respective cool-flame zones of the two hydrocarbons.

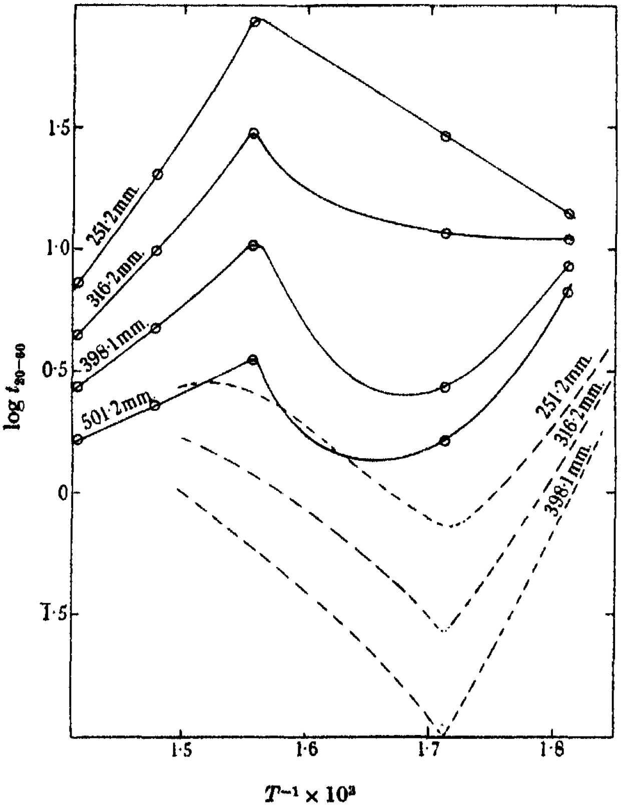

FIGURE 3

BENZENE, TOLUENE AND ETHYLBENZENE

The results described in Part III (cf. figure 3) gave no indication of the existence or otherwise of low-temperature ignition systems with the three lowest aromatic hydrocarbons. It becomes a matter of interest, therefore, to see how far the low-temperature isothermal reactions of these fuels present kinetic analogies with propyl- and butyl-benzene, whose slow combustion reaction below 400° can be definitely related to ignition systems in the same temperature region.

In figure 2, $\Delta p/p$-t curves are shown relating to equimolecular mixtures with oxygen of ethylbenzene, toluene and benzene. The inflexion which was noted in the case of propylbenzene is seen to persist, but with decreasing magnitude, in the first two curves and to disappear with benzene. The evidence of the corresponding $\log t_{20-60}$-$1/T$ graphs (broken lines in figure 4), which relate to equimolecular mixtures at 650 mm. initial pressure, is similar. Thus, in these curves, the deflexion associated with the negative temperature coefficient becomes progressively less pronounced on descending the series and in the case of benzene no deviation from the linear law is evident. In the latter instance, however, the results are inconclusive since, in the material region of temperature, benzene becomes extremely unreactive towards oxygen. Thus a mixture at 650 mm. and 379° gave no perceptible pressure change in 24 hr. and a similar mixture at 323·5°, even after 4 days, gave no manometric evidence of combustion. In the latter case, the ultimate gaseous products (benzene-free) had the following composition:

CO_2	1·45 %	C_2H_4	0·80 %
O_2	96·85 %	CO	0·90 %

and washings from the reaction bulb gave negative tests with Schiff's reagent, Schryver's reagent, bromine water and lead acetate.

Toluene and ethylbenzene, on the other hand, showed distinct analogies with propylbenzene. Thus, apart from the evidence of the negative temperature coefficient demonstrated in figure 4, the "order of reaction" was shown to be increased between 300 and 350°. In the case of toluene, n had values at 315° of 3·0, 1·6 and 1·3, relative respectively to the total hydrocarbon and oxygen concentrations. The corresponding figures above 400° are 2·0, 0·9 and 1·0 (see Part I) from which it is evident that the increase in the overall "order of reaction" at the lower temperature is again due mainly to the hydrocarbon factor.

In table 4, values of n and n' are given, relating to the total pressure of an equimolecular ethylbenzene-oxygen medium at specified temperatures. Although these figures increase below 400° they do so less rapidly than in the case of propylbenzene and the increase in n is seen to persist even below 300°. That the changes are due chiefly to the hydrocarbon concentration factor is demonstrated by the fact that at 314°, n and n' have values of 0·5 and 0·1 respectively, relative to the partial pressure of oxygen.

TABLE 4. VALUES OF n AND n' FOR AN EQUIMOLECULAR ETHYLBENZENE-OXYGEN MIXTURE

Temp. (° C)	n	n'
279	3·0	2·0
309	2·8	2·1
314	2·8	2·2
341	2·7	2·6
362	2·4	1·6*
382	2·1	1·8*
438	2·0	—

* Mean values: the log p-log t curve is not exactly linear.

DISCUSSION

In view of the evidence now brought forward, the necessity of distinguishing more than one temperature zone of reaction in connexion with the combustion of aromatic hydrocarbons becomes increasingly apparent. Whether benzene is in conformity with its homologues in this respect is, however, not yet clear, and while this combustible must tentatively be classed with methane and ethylene, in the case of higher members of the series the existence of a low-temperature combustion system is no longer in doubt. The evidence regarding toluene and ethylbenzene is, as yet, of an indirect character and they may, like ethane, be considered as merely potentially capable of cool-flame propagation.

Hitherto, the recognition of the low-temperature combustion system in the aromatic series has rested on ignition data (Part III), but further grounds of distinction now come to light, which may be summarized under the following six headings:

(i) the "order of reaction",
(ii) the temperature coefficient of combustion,
(iii) the pressure increment,
(iv) the influence of dilution on the reaction rate,
(v) the influence of surface factors on the reaction rate, and
(vi) the induction period.

In neither class can the evidence be reconciled with normal temperature effects, without the assumption of some fundamental change of reaction mechanism, and to facilitate discussion it will be convenient to postulate two modes of combustion, of which one is predominant above about 400° and one below 300°, whilst in the intervening range of temperature the two mechanisms co-exist. Proceeding on such lines then, we may compare the characteristics of the high- and low-temperature reactions, as exemplified by propylbenzene, utilizing the headings already detailed.

Throughout the entire range of reaction temperature, the rate of oxidation is almost exclusively determined by the concentration of hydrocarbon. The "order of reaction", which in such complex types of chemical change must be regarded as a somewhat formal term, is less below 300° than above 400°, and intermediately (at 310–320°) increases to double the high-temperature value. The fact that oxygen plays so little part under any conditions can only be adequately explained by invoking a chain mechanism.

Consideration of activation energy data also points to the participation of chains in both high- and low-temperature reactions: thus, the respective values of E are 39, and upwards of 50 kg.cal./g.mol., which are unusually high figures for a bimolecular change. Intermediately, a low level of about -17 kg.cal./g.mol. is reached at *ca.* 330°, the actual temperature and value of E depending to a small extent on the pressure of the reacting medium.

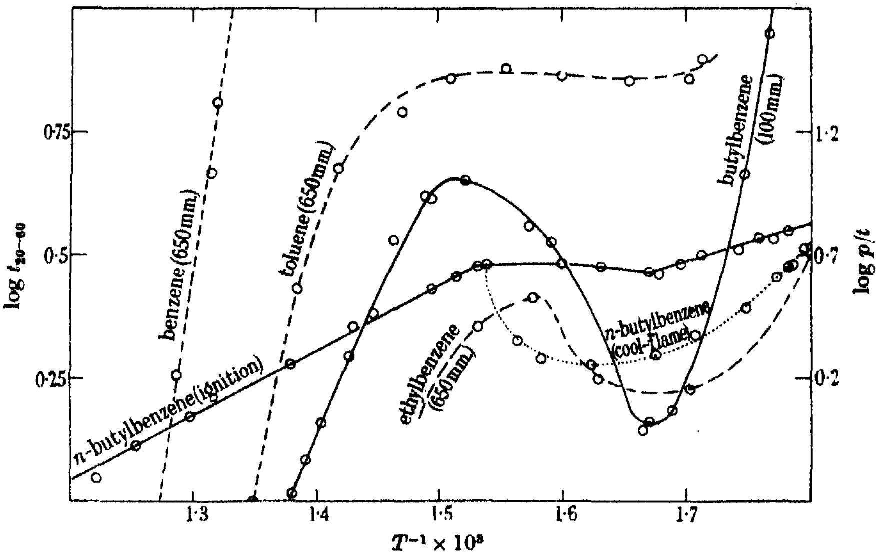

FIGURE 4

It is of interest in this connexion to consider also the case of *n*-butylbenzene, in which full data are available relating to slow combustion and ignition reactions in the same reaction vessel (cf. Part III, figure 2, and present communication, figure 1). In figure 4 (full-line curve) which refers to an equimolecular mixture with oxygen, $\log_{10} t_{20-60}$ (slow combustion) and $\log_{10} p/T$ (ignition) are plotted on the same base of reciprocal absolute temperature, throughout the complete combustion range, the $\log p/T$-$1/T$ curve for the cool-flame boundary being shown as a broken line. It will be seen that the corresponding turning-points of the two main curves occur at similar temperatures, namely 380° C ($1/T = 1{\cdot}53$) and 325° C ($1/T = 1{\cdot}67$); and that the minimum in the cool-flame graph coincides with the minimum gradient (i.e. least value of E) of the other curves at 344° C ($1/T = 1{\cdot}62$). According to the slow-combustion data, the energy of activation is 28 kg. cal./g.mol. at high temperatures, and 65 at low temperatures, whilst intermediately the least value is -14.

As has been observed previously (Burgoyne 1939), it is not possible to calculate E from ignition data without a complete knowledge of the underlying kinetics. We may, however, compare the factors $E/(n+1)$ (from slow combustion) and $AR/\log_{10} e$ (from ignition, A being the gradient of the $\log p/T$-$1/T$ curve), which should be equal if the underlying combustion mechanism is not changed when the isothermal reaction develops into ignition. From the figures given in table 5, it is seen that at high temperatures, the relationship is normal, as judged by similar data for ethylbenzene and propylbenzene (Burgoyne 1939); and in the present instance it is evident that chain branching plays some part in the high-temperature ignition of butylbenzene, although its role is less important than with the lower homologues. In the region of the negative temperature coefficient the correspondence of values appears to be fairly good, but at low temperatures, $E/(n+1)$, while being about double $RA/\log e$ (ignition), corresponds well with $RA/\log e$ (cool flame) at the same temperature. Until a clearer conception of the significance of the negative temperature coefficient is obtained, it would be premature to associate the slow combustion and ignition data in the corresponding temperature range, but in the lower zone it appears that the slow reaction bears a kinetic relationship to the cool-flame ignition somewhat similar to that existing between slow combustion and true ignition at high temperatures.

Table 5. Values of the ratio $E/(n+1)$

Zone of combustion	$E/(n+1)$ from slow combustion data	$RA/\log_{10} e$ from ignition data	
		True ignition	Cool flame
Above 400°	9·0	12·0	—
300–400°	*ca.* $-2{\cdot}6$	$-2{\cdot}4$	Varies continuously from -58 at 375° to $+13$ at 290°
Below 300°	*ca.* 14·5	7·1	

The normal steady decrease with falling temperature of the final pressure increment in the slow combustion of propylbenzene and other hydrocarbons is probably mainly associated with the corresponding decrease in the ratio CO/CO_2, since the formation of CO results in a much greater increase of volume than does the formation of CO_2 (Burgoyne 1937). It is shown in figure 2 that the pressure increment in the low-temperature zone is greater than would be forecast by extrapolation of the high-temperature Δp-t graph, whilst a curve relating the CO/CO_2 ratio to the temperature in the case of butylbenzene, which is shown in the same diagram, is seen to have a transitional inflexion similar to that of the corresponding Δp-t curve. This matter will be discussed more fully in the light of a more detailed examination of the products formed at various stages of combustion.

The effects of dilution and surface factors upon the reaction rates are preferably considered together, since they both bear on the relationship of chain rupture at the walls and in the gas phase. The experimental data is clarified by tabulation, thus:

	Dilution causes	Packing causes
In the high-temperature zone	Acceleration	Retardation
In the intermediate zone	Less acceleration	Considerable retardation
In the low-temperature zone	Retardation	Retardation

The facts are readily explained if it is assumed that in the high-temperature reaction chain rupture at the walls predominates, whilst in the low-temperature zone deactivation in the gas phase is predominant. In the former case, inert molecules will impede diffusion to the surface, but in the latter instance deactivation takes place both in the gas phase and at the walls, so that when the processes are superposed, as in the intermediate zone, the two types of surface deactivation become additive while the opposing effects of the inert gas molecules counteract one another. At low temperatures energy chains are likely to be concerned, but in the high-temperature zone the effect of the walls is probably to catalyse some chain-breaking process of a chemical character.

In so far as nitrogen has the effect of de-energizing chains, oxygen may also have a similar influence. That the latter acts as a deactivating medium is clear from the fact that the oxygen concentration has very little effect on the reaction velocity in any circumstances. Since the rate of the initial act of oxidation must be proportional at least to the first power of this factor, subsequent chain-breaking activity is indicated, although the operation of oxygen in this connexion, as contrasted with nitrogen, may be not only of a physical but also of a chemical nature. The latter type of mechanism is evidently more significant in the high- than in the low-temperature zone.

Above 400°, the induction period is always of very short duration, but as the reaction temperature is lowered it becomes progressively longer. The rate of the initial stages of combustion may itself be considered from four aspects, namely,

(i) the order of reaction,
(ii) the temperature coefficient,
(iii) dilution effects,
(iv) surface effects.

With regard to the first, there is no apparent reason to dissociate the initial stages of the reaction from the main combustion, since the effect of temperature on the order of reaction and the relative influence of the reactants on the rate are similar in the two cases. The same is true of the respective temperature coefficients, for although insufficient data are available to determine the energy of activation in the initial stages above 400°, in the low-temperature zone E' has a value of 58 kg.cal./g.mol. and intermediately the minimum value (*ca.* 337° C) is $-18{\cdot}0$.

The influence of addition of an inert gas on the rate of the induction reaction is, however, characteristic below 400°; and in contrast with conditions obtaining above this temperature, the initial stage is accelerated to a greater extent than the main reaction by the same degree of dilution. At the same time, the retarding effect of surface is diminished at all temperatures, particularly in the transitional zone. Taken in conjunction, these results suggest that in the low and intermediate temperature regions the induction reaction is modified in two respects by comparison with the main combustion, namely:

(i) by the appearance of a catalytic surface effect, and
(ii) by decreased deactivation in the gas phase, chain rupture at the surface remaining the same.

An important anomaly of the induction period is shown in the packed bulb (see table 3) when, at high temperatures, its duration becomes independent of the pressure. This characteristic is reflected in the transitional zone where (*ca.* 310°) the value of n' is much less than that of n, although below 300° they are similar. In this case, it is probable that the large increase of surface due to packing has fundamentally changed the induction mechanism, possibly by introducing a surface decomposition of low order. Further evidence, pointing in this direction, lies in the reversal, on packing, of the effect of "sensitization" of the surface by use, a feature which is especially marked in the initial stages of combustion. It is noteworthy in this connexion, however, that packing causes no change in the "order" of the main combustion reaction at high temperatures.

In the foregoing, the existence of two modes of combustion has been tacitly assumed for purposes of discussion. It is possible, however, to give a more precise interpretation to the experimental results on the basis of theories of the two-stage process of hydrocarbon combustion.

Kane (1938) and, independently, Belov and Neumann (1938), have made the suggestion that at low temperatures, the combustion of aliphatic hydrocarbons consists essentially of two parallel chain reactions:

$$A \xrightarrow{K_1} B \xrightarrow{K_2} C, \tag{3}$$

$$A \xrightarrow{K_3} C, \tag{4}$$

where A and C represent the initial and final states of the reacting medium, and B is a more or less stable intermediate which controls the processes giving rise to cool flames and is also capable of promoting the direct oxidation (4). The two-stage process persists so long as a certain concentration of B is maintained, but at high pressures the single-stage combustion is so promoted by B as to become predominant. At sufficiently high temperatures too, when B is decomposed more rapidly than it is formed, the two-stage process ceases to exist; at the same time the disappearance of B causes a retardation in reaction (4) which outweighs the normal effect of temperature on K_3 and brings about a reversal in the sign of the temperature coefficient.

It is now evident that in the "high-temperature zone" process (4) and in the "low-temperature zone" (3) are respectively predominant, whilst intermediately the two processes co-exist, with the added complication that B may now become sufficiently active and concentrated to initiate the independent cool-flame reaction.

In the case of propylbenzene, the direct process $A \rightarrow C$ is characterized by short chains of a chemical nature, which are ruptured at the walls; and the two-stage process $A \rightarrow B \rightarrow C$ involves long chains, including energy chains which become deactivated both in the gas phase and at the surface. There is every reason to suppose that a similar state of affairs exists with both lower and higher members of the series, although with toluene and ethylbenzene the decreased order of reaction in the intermediate zone, as compared with propylbenzene, is possibly an indication of the absence, under the existing conditions of experiment, of the process by which the intermediate B initiates cool flames. In the case of benzene there is as yet no evidence of the existence of a two-stage process.

The author is indebted to Dr D. M. Newitt for his continued interest in this investigation, and to the Department of Scientific and Industrial Research for a grant, during the tenure of which the work here described was carried out.

SUMMARY

The kinetics of the combustion of benzene and the four simplest monoalkyl derivatives have been studied in the temperature range between 250 and 400° C, and the results compared with those previously obtained relating to the region above 400°.

It is concluded that, excepting in the case of benzene itself, the oxidation of these fuels consists of two co-existent chain reactions, as is thought to be the case with the aliphatic hydrocarbons also. Of these processes, one is predominant below 300° and the other above 400°, whilst in the intervening range of temperature the two mechanisms proceed on terms of approximate equality. The low-temperature reaction, on intensification gives rise to cool flames, while from the high-temperature mechanism a chain-thermal ignition results. The kinetic characteristics of the two processes are demonstrated and compared.

In the intermediate temperature zone (300–400°), the prominence of the process of cool-flame initiation is thought to be the partial cause of the observed increase in the "order of reaction", and it is suggested that the negative temperature coefficient is due to the mutual interaction of the co-existent chain reactions.

REFERENCES

Belov and Neumann 1938 *C.R. Acad. Sci. U.R.S.S.* **18**, 333.
Burgoyne 1937 *Proc. Roy. Soc.* A, **161**, 48.
— 1939 *Proc. Roy. Soc.* A, **171**, 421.
Kane 1938 *Proc. Roy. Soc.* A, **167**, 62.
Newitt and Thornes 1937 *J. Chem. Soc.* pp. 1656, 1669.
Pease 1929 *J. Amer. Chem. Soc.* **51**, 1839.
— 1938 *J. Amer. Chem. Soc.* **60**, 2244.

The thermal decomposition of nitrogen iodide

By F. R. Meldrum

Bristol University

(*Communicated by W. E. Garner, F.R.S.—Received* 27 *November* 1939)

Bunsen (1852) was the first to suggest that the formula of nitrogen iodide was $NH_3.NI_3$, although this was disputed later on account of the fact that any attempts made to remove the ammonia resulted in complete decomposition. An alternative formula, $NH_2I.NHI_2$, which took account of this fact, was, however, disproved by Silberrad (1905), who prepared triethylamine by the action of zinc ethyl on nitrogen iodide.

Eggert (1921) investigated the thermal decomposition of nitrogen iodide and showed that the following equation represented the changes occurring during detonation, thermal or photochemical decomposition: (1) $8NH_3.NI_3 \rightarrow 5N_2 + 6NH_4I + 9I_2$. The primary step (also suggested by Chattaway and Orton (1900) for the photochemical decomposition) was supposed to be: (2) $NH_3.NI_3 = N_2 + 3HI$, followed by either or both of the following reactions: (3) $5HI + NH_3.NI_3 \rightarrow 2NH_4I + 3I_2$; (4) $3HI + 7NH_3.NI_3 = 4N_2 + 6NH_4I + 9I_2$. These results were obtained when the products were allowed to accumulate up to atmospheric pressures. The present investigation has shown that the decomposition takes a different course if the products are removed in high vacua.

The properties of the substance when subjected to mechanical shock are well known. Under the impact of a small falling weight it detonates even at liquid-air temperatures (Eggert 1921). Eggert states that the detonation of this substance occurs under the action of pressure alone (at 5000 atm.) even when the substance is wet. Garner and Latchem (1936) showed that the substance detonates in a hard vacuum immediately it is dry, an observation which was confirmed by Belajev and Chariton (1936). The decomposition proceeds quietly at -10° C if the pressure of the gas above the crystals be not allowed to fall below 2×10^{-3} cm., the reaction slowing up as the products accumulate and coming to a standstill before all of the iodide is decomposed. It was suggested by Garner and Latchem that one of the products acted as a retarding agent stabilizing the solid. It was thought that the retarding agent was iodine, but this has been shown by the present investigation to be incorrect.

In spite of the large volume of experimental research on nitrogen iodide, the details of the kinetics of its decomposition are still very obscure. Neither the activation energy nor the heat liberated in its decomposition is known, and there has been no extended investigation into its sensitivity to heat or to shock. It has been the object of this investigation to obtain information along these lines and also to throw some light on the initiation of detonation generally.

EXPERIMENTAL

Preparation of nitrogen iodide. The method described by Garner and Latchem was employed (1936). 10 c.c. of 880 ammonia was added to 2 c.c. of 0·7 N iodine in N-KI solution. The nitrogen iodide was washed three times by decantation with N/100 ammonia, and filtered, using a special hard smooth paper (Whatman No. 52). The precipitate could then be removed from the paper wet and transferred to a small glass bucket and dried under vacuum. In order to make the conditions for each experiment as nearly as possible the same, the procedure was standardized as regards times of settling and amounts of washing liquid. The solid was given 3 min. to settle before decantation, and the washing was carried out each time with 25 c.c. of liquid. The operations were carried out in a dark room.

The glass bucket containing the nitrogen iodide was lowered into the reaction vessel by a glass winch and the substance was allowed 10 min. to acquire the temperature of the reaction vessel before pumping was begun. At 0° C detonation occurred almost immediately after attaining a hard vacuum, which was about 12 min. from the commencement of the pumping. At $-13°$ C it was possible to dry the substance without detonation and to determine the pressure-time curves, which were similar in shape to those previously reported by Garner and Latchem.

Effect of iodine vapour on the reaction. Iodine vapour was found not to retard appreciably the detonation at 0° C, and had no marked effect on the rate of reaction at $-13°$ C. The pressure of iodine vapour employed was that in equilibrium with solid iodine at $-13°$ C. From these experiments it was clear that iodine was not the product responsible for the phenomena described by Garner and Latchem, and that there was some unsuspected volatile product which was responsible. It was therefore decided to make a complete analysis of the products of the slow decomposition of nitrogen iodide at low gas pressures.

Analysis of the products of reaction. From experiments carried out with a Pirani gauge it was found that the permanent gas evolved in the decomposition of nitrogen iodide possessed a thermal conductivity similar to that of nitrogen. A sample of the permanent gas was therefore collected and analysed and found to be nitrogen, in agreement with the conclusions of Eggert. A qualitative test indicated that ammonia was one of the products of the reaction. This gas, the nitrogen, and the iodine produced from a known weight of nitrogen iodide were then determined quantitatively.

The apparatus used in the analysis consisted of a reaction vessel fitted with a glass winch and placed in series with three glass traps and a McLeod gauge. The nitrogen iodide was introduced into the reaction vessel in a moist state and almost completely dried by pumping, the water vapour being collected in the trap farthest away from the reaction vessel, the other traps being kept at room temperature. The pumps were then cut off and the drying completed in a closed space which contained the McLeod gauge. The nitrogen produced was measured, and the iodine liberated was collected in the first trap which was surrounded with solid carbon dioxide and alcohol and the ammonia collected in the second trap, which was surrounded with liquid air. The traps were connected to one another with ground joints, and after admission of dry air were disconnected from one another, and their contents separately analysed.

The iodine was washed out of the first trap with potassium iodide solution and titrated with N/100 thiosulphate. It was found to contain a small amount of ammonia which was estimated by distilling with alkali and treatment with Nessler solution. The second trap contained most of the ammonia, and this was estimated by passing into N/100 H_2SO_4 and titration of the resulting solution with N/100 NaOH.

The bulk of the nitrogen iodide was decomposed, a small residue left undecomposed being determined by weighing and by decomposition with sulphuric acid and the titration of the iodine by N/100 thiosulphate.

The analytical figures are given in the following table:

Millimols of			Ratio	
Nitrogen	Ammonia	Iodine	NH_3/N_2	I_2/N_2
0·0320	0·061	0·095	1·91	2·97
0·0380	0·082	0·113	2·16	2·98
0·0198	0·051	0·0614	(2·58)	3·10
0·0194	—	0·0579	—	2·98
0·0180	0·0357	0·0510	1·98	2·84
0·0197	0·0425	0·0598	2·16	3·03
0·0190	0·0415	0·0570	2·18	3·00
		Average	2·08	2·99

The results correspond very closely to the equation

$$2NH_3.NI_3 = N_2 + 2NH_3 + 3I_2,$$

which is the simplest possible reaction. It should be pointed out that the results of Eggert (1921), which show that ammonium iodide is one of the main products of the reaction, were obtained under such conditions that the gaseous products were at much higher pressures than those obtaining in the present work. It is, however, certain that nitrogen iodide decomposes quantitatively at low pressures into nitrogen, ammonia and iodine. The fact that ammonia is liberated supports the Bunsen formula for nitrogen iodide, which is thus an ammoniate or ammine.

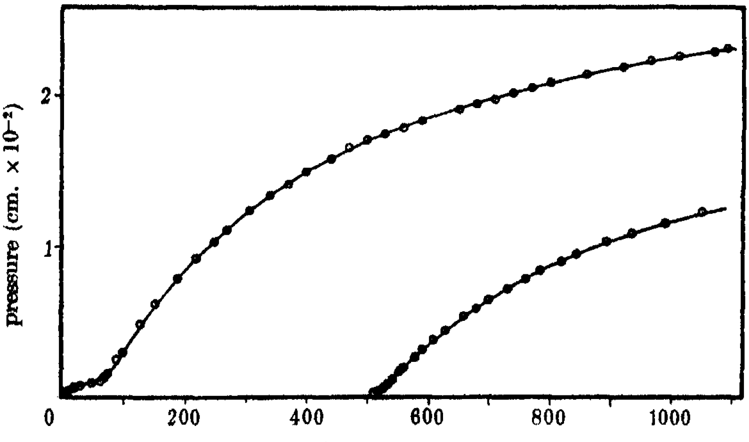

FIGURE 1

The pressure-time curves. During the previous experiments the opportunity was taken of following the progress of the reaction over a long period (20 hr.). The general characteristics of the curves can be seen from figure 1. After a period of pumping, and the reaction system has been isolated, a comparatively quick initial rise of pressure is observed. This is probably due to the decomposition of isolated crystals which have dried quickly. A very slow reaction follows, almost corresponding to an induction period. The length of this period varies with the temperature and time of pumping, but usually lasts 1–2½ hr. At the end of this period the rate increases, sometimes attaining a steady value within 3 min. The rate falls off with time and at four-fifths decomposition at approx. 2×10^{-2} cm. it is very slow.

For the analysis of the p/t curves, it was necessary to know the p_∞ values corresponding to complete decomposition. This was calculated from the last pressure measured and the weight of the residue. It was found that the plot of $\log dp/dt$ against $\log(p_\infty - p)$ gave a straight line. The slopes of the lines were not, however, constant, but varied between 1·25 and 2·12 for five experiments (see table 1). This relationship was found to be useful for obtaining the values of dp/dt at the beginning of the reaction proper, when attempts were made to derive the activation energy. It has, however, no theoretical basis (see later).

TABLE 1

T° C	$p_\infty \times 10^{-4}$ cm.	n
− 12·5	295	1·55
− 14·0	293	1·58
− 15·0	232	1·25
− 17·0	253	1·82
− 19·0	245	2·12

Retardation of the reaction by ammonia and water. The effect of known pressures of ammonia and water vapour on the rate of decomposition was studied. As sources of ammonia, solid ammonia, $2AgCl.3NH_3$ and $AgCl.NH_3$ at − 79° C were employed with pressures of 3·76, $1{\cdot}8 \times 10^{-2}$ and $1{\cdot}9 \times 10^{-3}$ cm. respectively. The effect of ammonia was studied by isolating the reaction vessel from the liquid oxygen trap and McLeod gauge during the initial stages of the reaction and opening it to a vessel containing the source of ammonia. The amount of reaction that occurred during the period of isolation from the McLeod gauge was measured after the removal of the ammonia. Corrections had to be made for the amount of permanent gases passing into the vessel containing the ammonia source. The first experiments made with solid ammonia as a source showed that the reaction was completely stopped and that it could be started again only with difficulty. It was also found with the lower ammonia pressures that it was possible to slow down the reaction, and that the original rate did not at once reappear after the ammonia had been removed. This observation was checked by following the action of ammonia with a Pirani gauge, by means of which it was shown that the reaction could be stopped by approximately 4×10^{-3} cm. of ammonia and that on removing the ammonia there was a lag before the reaction started again (figure 2). The pronounced dip in the p/t curves is due to a diffusion-pump effect during the condensation of ammonia. The lag is probably due to the time necessary for the building up of the equilibrium concentration of nitrogen iodide molecules on the surface (see later).

Water vapour has a retarding effect during the period of its application, but the rate returns to its former value immediately after the removal of the water vapour. Ice at −35° C was used as a source, with a vapour pressure of $16{\cdot}7 \times 10^{-3}$ cm.

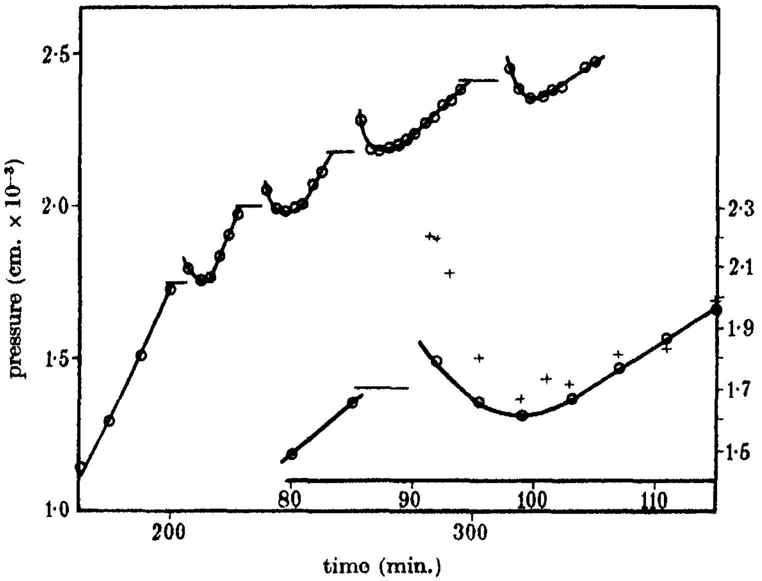

FIGURE 2

○ McLeod readings; + Pyrani readings; – period over which ammonia was applied.

Effect of pressure. This was measured by either adding or subtracting nitrogen whilst the reaction was proceeding. There was a distinct retarding effect on increasing the pressure. The experimental values are given by the equation

$$k_p = k_0(1 - 2{\cdot}23p + 3{\cdot}17p^2 - 1{\cdot}55p^3),$$

where k_0 is the rate in vacuum and k_p is the value at a pressure p from $0\text{–}1{\cdot}0 \times 10^{-2}$ cm. The ratio of the rate at different pressures to the rate in vacuum is given below:

Pressure × 10^{-2} cm.	0	0·10	0·20	0·30	0·50	0·90
Ratio	1·0	0·81	0·68	0·58	0·49	0·43

The retardation with increasing pressure is probably due to the effect of gas pressure on the rate of escape of ammonia molecules from the gas film adjacent to the surface.

Determination of energy of activation. On account of the variation of surface area of different batches of crystals, it was necessary to determine the temperature coefficient from the changes in the rate of reaction which occurred on changing the temperature during a run on one batch of crystals. This method had been used previously by Garner and Marke (1936) and Colvin and Hume (1929). Use was made of the fact that over the initial portion of the p/t curve, the rates of reaction are practically constant. The changes in rate were made both for a rise and a fall in temperature, and in some cases several changes were made (see figure 3). The time taken in attaining temperature equilibrium on changing the bath was only a matter of seconds. The results are summarized in table 2.

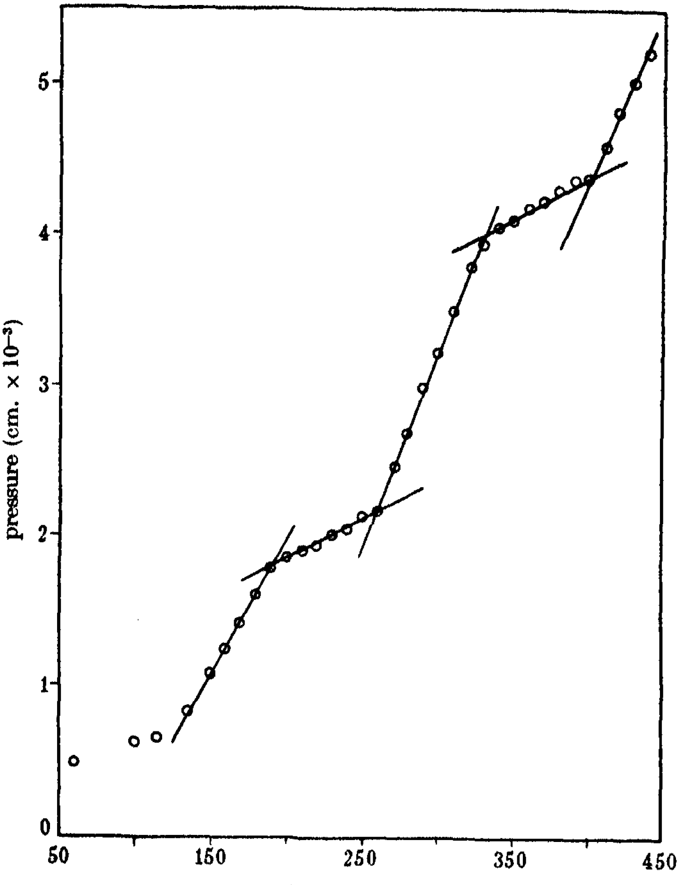

FIGURE 3

k_1 and k_2 are the slopes of the p/t curves before and after the change of temperature. The activation energy cannot be determined very accurately owing to the small range of temperatures over which measurements could safely be made. The mean value is 19·0 ± 1·3 kcal.

TABLE 2

Exp.	T_1	T_2	k_1	k_2	E	Mean
2	−11·0	−20·5	0·671	0·135	22·2	—
3	−11·0	−21·5	0·632	0·143	18·5	—
13	−15·4	−24·3	0·378	0·092	20·0	—
20	−20·6	−28·5	0·353	0·086	21·8	18·3
	−28·5	−21·2	0·086	0·234	16·8	
21	−20·5	−27·5	0·296	0·081	22·4	18·2
	−27·5	−20·9	0·081	0·192	16·0	
22	−20·5	−29·0	0·236	0·068	17·8	16·9
	−29·0	−20·9	0·068	0·195	15·9	
23	−20·6	−29·5	0·178	0·052	16·8	18·8
	−29·5	−20·2	0·052	0·259	20·8	
	−20·2	−29·5	0·259	0·056	19·4	19·0
	−29·5	−20·6	0·056	0·220	18·7	

Determination of particle size. In the study of solid decomposition it is normally the area of the reacting surface which is of importance rather than the mass or volume of the substance. This question is of particular interest in the case of nitrogen iodide because of the suggestion of Roginski (1938) that the reaction is not confined to the surface of the solid but occurs throughout the lattice. This possibility can be tested by the application of the Polanyi-Wigner equation to the experimental results, since the rates of solid reactions occurring at the interface between the product and the reactant or on the surface of a solid have been shown, in many cases, to be in agreement with rates calculated from this equation within one or two powers of ten. In order to be able to make use of this equation, it is necessary to determine the surface area of a batch of crystals.

The particles of nitrogen iodide as prepared in these experiments are extremely small and could not be measured by means of a micrometer eyepiece and a microscope objective 1/5. Their size could only be estimated by microphotography. The nitrogen iodide was suspended in paraffin and photographed, using 1/5 objective. In prints with a magnification of 300, the diameters of apparently individual particles were estimated to lie between 0·5 and 1·5 mm. This gives a mean radius of approximately $1{\cdot}8 \times 10^{-4}$ cm.

With glycerine as a mounting liquid the nitrogen iodide decomposed to give bubbles of gas, probably nitrogen. The bubbles were never seen to coalesce even when in contact, so that it was thought that a bubble arose from each crystal of nitrogen iodide. If that were true, the particle size could be estimated from the gas bubble rather more accurately than from the particles themselves. The mean radius was found to be $12{\cdot}5 \times 10^{-4}$ cm. Assuming that the gas is nitrogen, since ammonia and iodine are soluble in glycerine, and making allowance for the dependence of pressure on the diameter of the bubble, the average radius of a spherical particle of nitrogen iodide is found to be $2{\cdot}8 \times 10^{-4}$ cm. This is of the same order as that determined by microphotography of the crystals, and it is sufficiently accurate for the purpose in view.

Application of the Polanyi-Wigner equation. According to this equation, the rate of reaction $= N\nu e^{-E/RT}$, where N is the number of molecules per sq. cm. of interface and ν is the lattice vibration. Taking the density of nitrogen iodide as 3·5, the number of molecules per sq. cm. $2{\cdot}9 \times 10^{14}$ and a frequency of 10^{13}, the activation energies may be directly calculated from the measured rates of reaction expressed in molecules per sq. cm. per sec. The results are summarized in table 3. The activation energy derived by this method is in good agreement with that previously calculated from the temperature coefficient of the reaction. This shows that the Polanyi-Wigner equation is applicable and that the reaction is very probably limited to the surfaces of the crystals, contrary to Roginski's suggestion with regard to this decomposition. A chain reaction, unless the chains are very short, appears to be ruled out.

TABLE 3

Area cm.^{2}	Rates × 10^{13} mol./sec. cm.^{2}	E kcal.
56	1·64	17·3
57	1·79	18·8
45	1·73	18·9
51	1·39	20·2
48	1·37	16·9
	Mean	18·4

The decomposition appears to be an evaporation reaction, the nitrogen iodide giving only gaseous products. Thus there can be no question of nuclei formation as in a decomposition where one of the products is a solid. The reaction is thus analogous to the initial step in the reaction occurring when the alkali azides are heated in vacuum where the products are also gaseous. In the case of alkali azides, however, the evaporation reaction passes into an autocatalytic reaction after an induction period. There was, however, no evidence that an autocatalytic reaction occurs in the case of nitrogen iodide.

Calculation of self-heating. If the reacting substance is assumed to lose heat only by radiation to the walls of the vessel, the self-heating can be calculated from the expression

$$\gamma \frac{dm}{dt} = \sigma s(T_1^4 - T_2^4),$$

where γ = heat change per mol., dm/dt = no. of mol. decomposing in unit time, σ = Stefan's constant, $5{\cdot}73 \times 10^{-5}$ ergs/cm.$^{-2}$ sec.$^{-1}$ (° K)$^{-4}$ if the radiator be taken as a black body.

At $-19°$ C, with a rate of 2×10^{-8} mol./sec. and an area of 1 sq. cm. and taking $\gamma = 25$ kcal., which is probably an upper limit to the value of the heat given to the solid by the reaction,* the self-heating = 0·4° C.

The value will be reduced considerably by loss of heat owing to conduction by the gas, for at 10^{-3} cm. the rate of loss by conduction is considerably greater than that by radiation. It may therefore be presumed that in experiments with gas present, self-heating was negligible.

The detonation of nitrogen iodide. The research on the conditions under which nitrogen iodide detonates is not complete so that the results obtained will only be mentioned briefly. It was found that the detonation almost always occurs in a vacuum at $-11°$ C with quite short time lags and that the occurrence of detonation obeys the laws of chance. The average time lag decreases with increase in temperature and at 0° C it is already too short to measure.

DISCUSSION

From the analytical work it is clear that the overall reaction proceeding during the thermal decomposition is relatively simple, viz. $2NH_3.NI_3 = 2NH_3 + N_2 + 3I_2$. It has been established that the ammonia, which had not been previously detected amongst the products of decomposition, acts as a negative catalyst for the reaction. Water vapour also exerts a retarding influence and the rate of reaction depends on the pressure of nitrogen present. At temperatures below $-6°$ C the rates of the thermal decomposition can be studied, since the substance does not immediately detonate at the low pressures, 10^{-5} cm., obtained during drying and evacuation. There is an induction period, which is probably the period during which the water evaporates, during which the reaction is very slow. At the end of this period, the reaction attains immediately its maximum rate, there being no acceleration similar to that observed with many explosives.

---

* See following paper.

The activation energy of the reaction as determined from the temperature coefficient and from the application of the Polanyi-Wigner equation is 18–19 kcal., and the heat of formation of the substance from its elements has been shown to be -35 kcal.*

The constitutional formula of nitrogen iodide. The three ammines of nitrogen iodide, $NI_3 12NH_3$, $NI_3 3NH_3$, $NI_3 2NH_3$, have been prepared by Hugot (1900) and Ruff (1900), and it was shown that these substances were stable only at low temperatures, and that all of the amines lose ammonia to yield $NI_3.NH_3$ as a final product. Attempts to remove the last ammonia molecule result in the complete break-up of the molecule. The fact, however, that the ammonia in this compound can be recovered quantitatively as such if the decomposition be allowed to occur in a hard vacuum, provides definite proof that nitrogen iodide is nevertheless an ammine.

If the overall reaction is $2NH_3.NI_3 \rightarrow 2NH_3 + N_2 + 3I_2$, it is natural to assume that the first step in the reaction is the removal of ammonia from the ammoniate and that the deammoniated compound NI_3, being very unstable, breaks down immediately to give nitrogen and iodine. This, of course, implies that nitrogen iodide can have no separate existence, in contradiction to the statement of Cremer and Duncan (1930). Biltz (1925) has suggested that the stabilization of unstable chemical compounds can be brought about by means of energy-producing supplementary reactions and, among the examples, he quotes the stabilization of NI_3 by the action of ammonia, the system being stabilized by the loss of the heat of ammoniation. That the removal of ammonia is the first stage in the decomposition is supported by the fact that substances which combine with ammonia (e.g. acids) decompose nitrogen iodide instantly. Nitrogen iodide is then to be considered as nitrogen tri-iodide monoammine.

The activation energy. If the above simple explanation of the reaction be correct, then the rate-controlling reaction is the loss of ammonia, and the measured activation energy will be that of the removal of the ammonia. In the case of carbonates, Zawidski and Breitschneider (1935) show that the activation energy for the removal of carbon dioxide is equal to the heat of the corresponding reverse reaction. Although this is probably not generally true for endothermic dissociation in the solid state, a sufficient number of cases has been found where it holds to make it worth while to consider whether or not it can be true for ammines. Biltz has shown that the stability of an ammine varies very much with the "Teilbildungswärme", which is the heat liberated by the addition of ammonia to the lesser ammoniated compound. The "Teilbildungswärme" varies from about 37 to 7 kcal. per molecule of ammonia, and there is a considerable variation in stability. An interesting example is indium tri-iodide, which, according to Klemm, has a covalent character and forms a series of ammines. In $I_3.5NH_3$ ("Teilbildungswärme" = 15 kcal./mol.), which evolves three molecules of ammonia, has a dissociation pressure at 156° C of only 26 mm. It may be concluded from the comparative stability of nitrogen iodide considered as an ammine, that the heat of ammoniation is of the order of 15–20 kcal.

---

* This refers to heat of formation of nitrogen tri-iodide.

A further argument which has weight in such cases, is that reactions which occur between the surface of a solid and a gas with a liberation of a heat < 20 kcal., do not take place in the reverse direction at appreciable rates in a hard vacuum at room temperatures. This is borne out by experiment and can be deduced also from the Polanyi-Wigner equation. It therefore follows that in the case of nitrogen iodide which decomposes rapidly at room temperature, at a rate governed by the above equation, the heat of ammoniation cannot exceed 20 kcal. Since the activation energy is 19 kcal., this means that the activation energy is approximately the same as the heat of reaction.

If nitrogen iodide be considered as an ammine, it must have a definite dissociation pressure, always assuming that there are three phases present. Making this assumption, and taking the heat of ammoniation as 19 kcal., the dissociation at any temperature may be calculated from the Nernst equation,

$$\log p(\text{atm.}) = \frac{\Delta H_0}{4{\cdot}57T} + 1{\cdot}75 \log T + aT + C,$$

for a molecule in which only one gaseous product is formed. For monoammine Biltz and Huttig (1920) find empirically that a has a value of $-0{\cdot}0017$, and that ΔH_0 can be replaced fairly accurately by ΔH, the calorimetric value at room temperature. On this basis, the dissociation pressure of nitrogen iodide at $-13°$ C is 1×10^{-7} cm. and at $-19°$ C is $0{\cdot}4 \times 10^{-7}$ cm.

The retarding effect of ammonia. The fact that ammonia has a pronounced retarding effect on the reaction means that one possible mechanism of the reaction can be disregarded. If the first stage in the reaction were the decomposition of an NI_3 group, then there could be no retarding effect by the ammonia.

From the rate at which ammonia is produced in the solid reaction and the dimensions of the tubes leading to the liquid air trap, the stationary concentration of ammonia at the surface of the solid can be found. At −19° C, with a pressure of nitrogen of 2×10^{-3} cm., the concentration of ammonia is found to be 4×10^{-5} cm. This is greater than the dissociation pressure calculated for $NI_3.NH_3$ at this temperature, viz. $0{\cdot}4 \times 10^{-7}$ cm. Since the pressure of ammonia at the surface is so much greater (approximately 1000 times) than the dissociation pressure of the ammine, it may be concluded that the conditions for the application of the phase rule cannot apply, in the sense that there are not two phases present. The rapid dissociation of the free NI_3 molecules on the surface would explain the considerable excess of ammonia pressure over the dissociation pressure since the majority of the NI_3 molecules will decompose before there is a chance of an ammonia molecule returning to the surface, with the result that the rate of evaporation of ammonia is always greater than the rate of condensation on the surface.

The experiments on the addition of ammonia to the system containing decomposing iodide, have shown that a pressure of 1×10^{-3} cm. ammonia will stop the reaction. Since with this pressure, the rate of collision with the surface is $5{\cdot}5 \times 10^{18}$ mol. sec.$^{-1}$ cm.^{2}, the number of ammonia molecules colliding with each surface molecule is 2×10^4 per sec. This can only mean that the average life of an NI_3 molecule is about 10^{-4} sec. and that it requires an activation energy for its decomposition. From the Polanyi-Wigner equation this activation energy is seen to be $\sim 4{\cdot}5$ kcal.

The effect of inert gas on the rate of reaction. The primary effect of gas pressure must be to slow down the rate of diffusion of ammonia away from the reaction surface and thereby increase the stationary concentration of ammonia at this surface. This effect will depend in a complicated fashion on the rate of reaction, the pressure, and on the dimensions of the apparatus. It is then very difficult to discuss the forms of the pressure-time curves for the reaction. The pressure varies with time, and the back reaction with the formation of ammine is affected in a complicated fashion by the total pressure. If the particles of nitrogen iodide were spheres and there were no effect of pressure on the reaction velocity, the following equation, $dp/dt = k(p_\infty - p)^{\frac{2}{3}}$ should hold. Actually, the experimental curve could be fitted to $dp/dt = k(p_\infty - p)^n$, where n varies from 1·25 to 2·1. This high value of n must be due to the retarding effect of ammonia, which increases with increase in pressure, but it is not practicable to calculate precisely the effect of this on the $p-t$ curves.

Mechanism of the decomposition of NI_3 *after the removal of ammonia.* If we consider the reactions which can possibly occur with a low activation energy, we are limited to:

(1) $2NH_3.NI_3 = 2NH_3 + N_2 + 2I_2 + 2I + 14$ kcal.

(2) $2NH_3.NI_3 = 2NH_3 + N_2 + 3I_2 + 49{\cdot}1$ kcal.

(3) $NI_3 + NH_3.NI_3 = NH_3 + N_2 + 2I_2 + 2I + 33{\cdot}1$ kcal.

(4) $NI_3 + NH_3.NI_3 = NH_3 + N_2 + 3I_2 + 68{\cdot}1$ kcal.

(5) $2NI_3 = N_2 + 3I_2 + 87$ kcal.

These all involve two molecules; other reactions involving the production of nitrogen atoms are not considered because the energy required for the production of a nitrogen atom is so great. In order that the reaction be exothermic, nitrogen must be formed in the molecular state. Bowen (1923) has pointed out that the photochemical decomposition of NCl_3 must involve two molecules for the same reason.

On account of the retarding influence of ammonia, reactions (1) and (2) can be eliminated. Reaction (5) can also be disregarded since according to the assignment of 19 kcal. for the heat of ammoniation, the activation energy of the overall reaction would be 38 kcal. The reaction following the removal of ammonia can only be accounted for by equations (3) or (4). No definite decision can be arrived at as between these two mechanisms, but on account of the complex reaction products formed at high pressures, it is possible that iodine atoms are produced as in (3) which react further with ammonia to give ammonium iodide according to the overall equation,

$$8NH_3 + 6I \rightarrow 6NH_4I + N_2.$$

This is a question which requires further investigation.

The author wishes to express his thanks for the Michael Hiatt Baker Scholarship awarded him by the University of Bristol, and to Imperial Chemical Industries and the Colston Research Society for grants for the purchase of apparatus.

SUMMARY

The thermal decomposition of nitrogen iodide has been studied at low pressures and the reaction shown to be $2NH_3.NI_3 \rightarrow 2NH_3 + N_2 + 3I_2$. The activation energy from the temperature coefficient and from calculations made with the aid of the Polanyi-Wigner equation is 18–19 kcal. The

reaction is retarded by ammonia and water and also by an increase in pressure over the solid.

The mechanism of the reaction is discussed in the light of the above results and of the calorimetric results quoted in the following paper.

REFERENCES

Belajev and Chariton 1936 *Acta Phys. U.S.S.R.* **5**, 763.
Biltz 1925 *Nachr. Ges. Wiss. Göttingen*, 193.
Biltz and Huttig 1920 *Z. anorg. Chem.* **109**, 111.
Bowen 1923 *J. Chem. Soc.* **123**, 1199.
Bunsen 1852 *Liebigs Ann.* **84**, 1.
Chattaway and Orton 1900 *Amer. Chem. J.* **24**, 159.
Colvin and Hume 1929 *Proc. Roy. Soc.* A, **125**, 635.
Cremer and Duncan 1930 *J. Chem. Soc.* p. 2750.
Eggert 1921 *Z. Elektrochem.* **27**, 547.
Garner and Latchem 1936 *Trans. Faraday Soc.* **32**, 567.
Garner and Marke 1936 *J. Chem. Soc.* p. 657.
Hugot 1900 *Ann. Chim. Phys.* (7), **21**, 5.
Roginski 1938 *Trans. Faraday Soc.* **34**, 960.
Ruff 1900 *Ber. dtsch. Chem. Ges.* **33**, 3025.
Silberrad 1905 *J. Chem. Soc.* **87**, 55.
Zawidski and Breitschneider 1935 *Z. Elektrochem.* **41**, 215.

The heat of formation of nitrogen iodide

By F. R. Meldrum

Bristol University

(*Communicated by W. E. Garner, F.R.S.—Received* 27 *November* 1939)

The reaction chosen for the determination was the decomposition of nitrogen iodide in dilute hydriodic acid according to the equation (with excess hydriodic acid present)

$$2NH_3.NI_3 + 5HI = 2NH_4I + 3HI_3.$$

This reaction has the advantage that it is unnecessary to prepare the nitrogen iodide in the dry state, a difficulty met with in the method involving the detonation of the substance in some form of bomb calorimeter, quite apart from the complexity of the reaction products in that case. The reaction with hydriodic acid proceeds rapidly, and appears to be quantitative (Chattaway and Orton 1899). A difficulty was encountered when analyses were made of the final products, as it was found that the amount of ammonia obtained was greater than that corresponding to the composition $NH_3.NI_3$. Since the excess varied quite considerably from sample to sample, it was considered to be adsorbed or loosely combined ammonia, such as is frequently met with in compounds containing ammonia. The existence of higher ammines of NI_3 lends support to this view.

To overcome the difficulty introduced by this excess of which the state of combination and heat content were unknown, and which it was not considered correct to treat as free ammonia, advantage was taken of the fact that the proportion of excess ammonia could be varied quite considerably. The experiments were considered in pairs, the effect of the excess ammonia being eliminated between them.

EXPERIMENTAL

The nitrogen iodide was freshly prepared before each experiment by the method already described (Garner and Latchem 1936), being washed with N/100 ammonia and filtered. About 0·5 g. was transferred wet to a thin walled bulb at the end of a tube fitted with a ground joint and glass hooks for attachment to a joint supported in the lid of the calorimeter. The bulb could be pierced by a glass rod when required.

The calorimeter (see figure 1) consisted of a large Dewar vessel (20 × 7·5 cm.) closed with a bung through which passed a Beckmann thermometer, a glass screw stirrer, the support for the tube containing the substance, and a tube for the insertion of a pipette. The stirrer was driven by a small electric motor through bevel gearing to give constant speed. It was found necessary to use rather violent stirring in order to prevent the heavy nitrogen iodide (density 3·5) from settling to the bottom of the calorimeter, so that the rate of temperature rise due to the stirring was greater than ordinarily used. On account of this, the addition of heat due to the stirring considerably exceeded that lost by other means so that very accurate control of the surrounding temperature was not attempted. The calorimeter was merely immersed in a bath at about 19° C.

About 330 ml. 0·092 N hydriodic acid obtained by dilution of a fresh sample of B.D.H. "Analar" hydriodic acid (constant boiling) was placed in the calorimeter, adjusted to 18° C and allowed to come to equilibrium with the calorimeter. A 25·0 ml. sample was withdrawn and titrated for iodine with N/100 thiosulphate. Stirring was commenced and temperature readings taken every minute for 10 min. (see figure 2*b*). The bulb containing the nitrogen iodide was then broken and readings continued for a further 10 min. At the end of that time the iodine was titrated with N/5 thiosulphate, and the ammonia in solution determined by distillation with 20 % NaOH into sulphuric acid, and titration of the excess sulphuric acid with carbonate-free NaOH. The weight of solution taken was determined by weighing the calorimeter and contents.

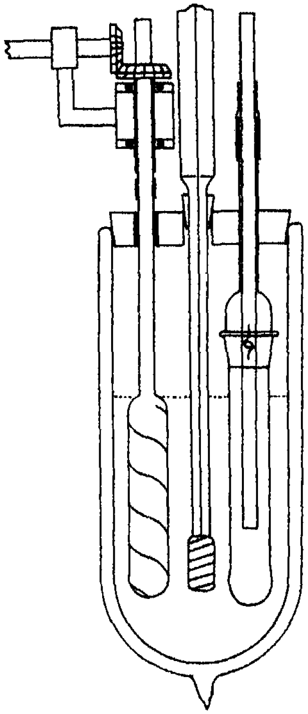
FIGURE 1

In order to determine the water equivalent of the calorimeter under conditions as nearly comparable as possible with those of the experiment, the heat of solution of potassium iodide crystals in water was used, taking the value for the heat of solution at 18° C, −5·11 kcal. (Landolt-Börnstein 1923) (see figure 2*a*). Heat capacity data for potassium iodide solutions were available (*International Critical Tables* 1929*a*). The mean of a number of determinations when reduced to a common basis for the weight of the

Pyrex bulb, was 27·1 g., with a maximum variation from the mean of 1·3 g.

Blank experiments were made to show that there was no detectable heat effect due to the breaking of the glass bulb and that the oxidation of hydriodic acid during the period of an experiment was negligible.

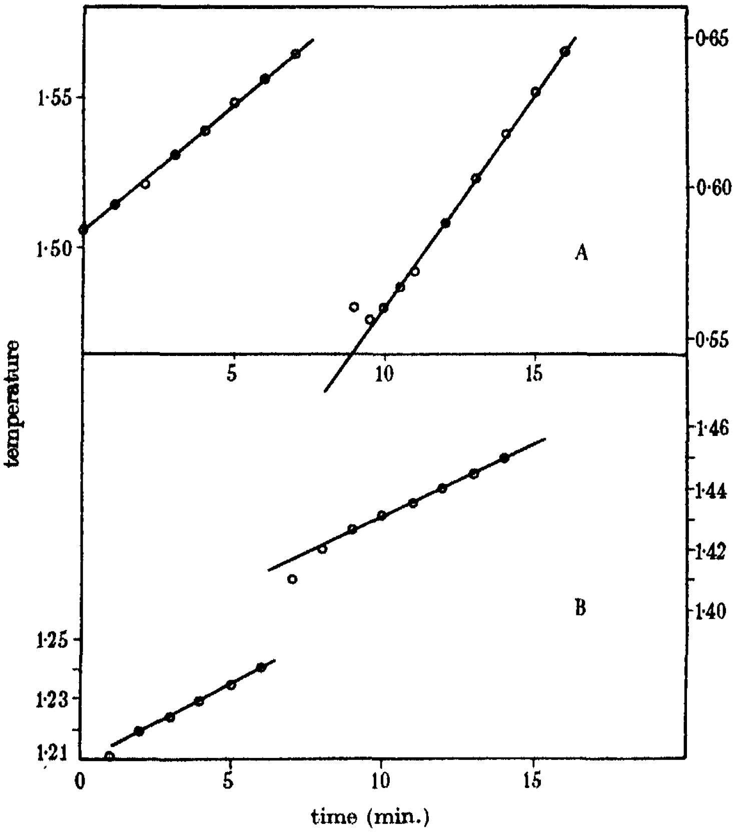

FIGURE 2

The type of temperature/time curves obtained is shown in figure 2. The extrapolation to time of mixing is a straight line, due to the relatively high input of heat through stirring.

From the iodine titre minus a small correction for iodine unavoidably present in the hydriodic acid solution, the amount of nitrogen iodide ($NH_3.NI_3$) used was determined (6 ml. N-thiosulphate = 1 millimol $NH_3.NI_3$). The difference between the ammonia actually found and that expected from the amount of nitrogen iodide (1 millimol gives 2 millimols of ammonia) was taken as adsorbed ammonia. It will be seen that the ratio of the nitrogen iodide to the excess ammonia varies quite considerably (table 1).

For the calculation of the heat produced during the reaction, the heat capacity of 0·092N HI was determined by interpolation between the heat capacities of pure water and a 6·7 % solution of hydriodic acid ($c_m = 0{\cdot}9213$ cal. over a range 16–20° C) (*International Critical Tables*, 1929*c*). This interpolation appears to be justifiable judging by the data of Randall and Ramage for hydrochloric acid (1927). Since the interpolated point is close to that for pure water, the error is probably small. Owing to the large excess of hydriodic acid, it can be shown that practically all of the iodine is present in the form of I_3' ions, and since the concentration of this was small, the solution was treated as HI. The same applies to the ammonium iodide present.

The results of the experiments are given in table 1.

TABLE 1

Exp.	Temp. rise ° C	Water equiv. g.	Wt. of solution g.	Heat produced cal.	Millimols $NH_3.NI_3$	Millimols excess NH_3	$\dfrac{NH_3.NI_3}{\text{excess } NH_3}$
8	0·167	26·4	312·2	55·86	0·85	1·05	0·81
9	0·170	26·3	310·3	57·00	0·93	0·42	2·21
10	0·172	26·2	309·5	57·04	0·94	0·39	2·41
11	0·150	26·6	313·1	50·34	0·815	0·56	1·46
12	0·196	26·3	309·9	65·04	1·11	0·48	2·31
13	0·228	26·4	308·7	75·55	1·29	0·40	3·22
14	0·130	26·3	300·6	41·98	0·68	0·34	2·00
15	0·148	26·0	308·3	48·85	0·785	0·25	3·14
16	0·082	26·1	321·5	27·83	0·50	0·84	0·60
17	0·182	25·8	314·0	61·10	0·985	0·59	1·67
18	0·178	26·2	313·0	59·65	0·97	0·47	2·06
19	0·173	26·2	319·5	59·03	0·98	0·31	3·16
20	0·149	25·9	316·3	50·36	0·88	0·30	2·93
21	0·184	25·8	313·4	61·68	1·01	0·37	2·73

These results were treated as follows. From each experiment an equation can be obtained,

$$Ax + By = C,$$

where A = no. of millimols of $NH_3.NI_3$,

B = no. of millimols of excess ammonia,

x = heat produced by reaction of 1 millimol of $NH_3.NI_3$ with 0·092N HI,

y = heat produced by reaction of 1 millimol excess NH_3 with 0·092N HI.

These equations may be taken in pairs and solved for x and y. Obviously equations in which the ratio A/B differs as much as possible will be likely to give the most accurate values of x and y. Certain pairs give very uncertain values of x and y because their ratios A/B were too close, and these pairs were therefore not considered any further. In table 2 are given (*a*) in the top right-hand section the values of x obtained from the best pairs, (*b*) in the bottom left-hand section, the corresponding values of y.

TABLE 2

Exp.	8	9	10	11	14	17	18	19	21
8	—	58·8	58·2	56·8	59·0	58·6	58·8	58·4	59·1
9	5·6	—		60·4	57·1	59·0			
10	6·1		—	56·5	55·7	57·6	55·8		
11	7·2	2·0	10·1	—	61·5		60·9		
14	5·4	9·3	12·0	0·4	—	60·2		57·7	59·2
17	5·8	5·1	7·4		3·1	—	59·2	58·2	59·6
18	5·6		11·8	1·3		4·7	—	57·9	59·8
19					8·6	6·4	7·4	—	
21	5·2				5·1	4·0	3·5		—

The mean value of x is 58·7 cal. and of y, 6·0 cal. The final value for x was obtained by substituting the mean value for y in all the equations, and taking the mean. The values obtained are all quite consistent apart from experiment 16, which is rejected for experimental reasons.

TABLE 3

Exp.	x (cal.)	Exp.	x (cal.)
8	58·3	15	60·3
9	58·6	16	(45·6)
10	58·2	17	58·4
11	57·6	18	58·6
12	56·0	19	58·3
13	56·7	20	55·2
14	58·7	21	58·9

The mean value (excluding experiment 16) is 58·0 ± 1·3 cal. Since the number of experiments was quite large, it may be taken that this value is reasonably accurate. Therefore

$$NH_3NI_3(s) + 8HI(aq.) = 2NH_4I(aq.) + 3HI_3(aq.).\quad \Delta H = -58{\cdot}0 \text{ cal.}$$

Calculation of the heat of formation of nitrogen iodide.

(1) $\tfrac{1}{2}(H_2) + [I] = HI_{aq.}\quad \Delta H = -13{\cdot}35$ cal. (i)

(*International Critical Tables*, 1929*b*.)

(2) $\tfrac{1}{2}(N_2) + 2(H_2) + [I] = NH_4I_{aq.}\quad \Delta H = -45{\cdot}6$ cal.

(*International Critical Tables*, 1929*d*.)

(3) $\tfrac{1}{2}(H_2) + 3[I] = HI_3$ aq.

According to *International Critical Tables* (5th vol.), which uses data given by Washburn and Strachan (1913), $\Delta H = -21{\cdot}76$ cal. This value appears to be in error. Their calculation is as follows:

(*a*) The heat of solution of iodine in water. $2[\mathrm{I}] = \mathrm{I}_2$ aq. Washburn and Strachan calculate the mean value of ΔH over the range 25–60° from solubility data of Sammet (1905), using the formula

$$\Delta H = R \ln \frac{s_2}{s_1} \Big/ \left(\frac{1}{T_1} - \frac{1}{T_2}\right)$$

as $-6{\cdot}39$ cal. Data for a range of temperatures between 0 and 55° C are given by Hartley and Campbell (1908) and there appears to be no reason for neglecting the lower temperature data, particularly as corresponding values are consistent with those of Sammet. It is found that ΔH increases with temperature, e.g.

	15–20°	18–25°	25–35°	35–45°	45–55°
ΔH	$+4{\cdot}8$	$+5{\cdot}1$	$+5{\cdot}8$	$+6{\cdot}4$	$+7{\cdot}4$ cal.

so that Washburn and Strachan's value is too high for use at 25° C. At 18° C, the value has been taken as $+4{\cdot}8$ cal.

$$2[\mathrm{I}] = \mathrm{I}_2 \text{ aq.} \quad \Delta H = +4{\cdot}8 \text{ cal.} \tag{ii}$$

(*b*) I_2 aq. $+ \mathrm{I}'$ aq. $= \mathrm{I}_3'$ aq. Washburn and Strachan using earlier data on equilibrium constants calculate $\Delta H = -3{\cdot}8$ cal. From the data of Jones and Kaplan (1928), the mean value over the range 0–25° C is now calculated to be $-4{\cdot}33$ cal. This agrees with the value for the range 15–25° C of 4·24 cal. calculated from data of Fedstieff (1910) and Jakowkin (1894; 1896). The value at 18° C has been taken as $-4{\cdot}3$ cal.

$$\mathrm{I}_2 \text{ aq.} + \mathrm{I}' \text{ aq.} = \mathrm{I}_3' \text{ aq.} \quad \Delta H = -4{\cdot}3 \text{ cal.} \tag{iii}$$

Combining equations (i), (ii) and (iii),

$$\tfrac{1}{2}(\mathrm{H}_2) + 3[\mathrm{I}] = \mathrm{HI}_3 \text{ aq.} \quad \Delta H = -12{\cdot}85 \text{ cal.}$$

(4) Heat of formation of $\mathrm{NH}_3.\mathrm{NI}_3$:

$$[\mathrm{NH}_3.\mathrm{NI}_3]s + 8\mathrm{HI} \text{ aq.} = 2\mathrm{NH}_4\mathrm{I} \text{ aq.} + 3\mathrm{HI}_3 \text{ aq.} \quad \Delta H = -\ 58{\cdot}0 \text{ cal.}$$

Therefore $(\mathrm{N}_2) + 3/2(\mathrm{H}_2) + 3[\mathrm{I}] = [\mathrm{NH}_3.\mathrm{NI}_3]$. $\Delta H = 35{\cdot}0$ cal.

DISCUSSION

The method cannot be considered to yield a very accurate value for the heat of formation of nitrogen iodide, but in view of the entire lack of data on the subject in question, the results obtained were considered of some interest. From the well-known explosive nature of nitrogen iodide, it would be expected that the substance itself would be highly endothermic. The heat of formation may be compared with that of nitrogen trichloride, 53(?) cal. The combination of ammonia with nitrogen tri-iodide must liberate energy, so that the heat of formation of nitrogen tri-iodide (if indeed it exists in the free state) must be of the same order as that of nitrogen trichloride. There is some evidence that the heat of ammoniation of NI_3 is 19 kcal., so that the heat of formation of NI_3 is -65 kcal., and the high value for such a simple molecule is in accord with its explosive character.

The value for y, 6·0 cal., gives the heat of neutralization of "excess" ammonia (NH_3^*) by hydriodic acid:

$$NH_3^* + HI\ \text{aq.} = NH_4I\ \text{aq.}\quad \Delta H = -6{\cdot}0\ \text{cal.}$$

This ammonia is bound to the solid nitrogen iodide ammine and if it is assumed that the "heat of solution" of the ammoniated nitrogen iodide does not differ appreciably from that of nitrogen iodide, the heat of ammoniation of nitrogen iodide ammine can be seen to be approximately 7 cal., since

$$NH_3\ \text{aq.} + HI\ \text{aq.} = NH_4I\ \text{aq.}\quad \Delta H = -13{\cdot}3\ \text{cal.}$$

$$NH_3(g) + NH_3.NI_3(s) = NH_3^*.NH_3.NI_3.\quad \Delta H = -7{\cdot}0\ \text{cal.}$$

The only suggestion which has been made regarding the value of the heat of formation of nitrogen tri-iodide is that of Pauling (1932), when he put forward a value for the energy of the N : I bond. This value was derived from the "additivity of covalencies" and from the electronegativity map deduced from it. The value of the map appears to be reduced considerably by changes in the accepted values for the energies of certain bonds, and it is doubtful if the values predicted for such bonds as the N : I bond have any value now. According to this value, NI_3 would have a very small heat of formation, which is hardly in accord with the explosive character of $NH_3.NI_3$, a substance of even lower energy.

The author wishes to express his thanks for the Michael Hiatt Baker Scholarship awarded him by the University of Bristol, and to Imperial Chemical Industries and the Colston Research Society for grants for the purchase of apparatus.

SUMMARY

From measurements of the heat of reaction of nitrogen iodide with excess of aqueous hydriodic acid, it is shown that the heat of formation of nitrogen iodide from the elements is − 35 kcal./mol.

REFERENCES

Chattaway and Orton 1899 *Chem. News*, **79**, 90.
Fedstieff 1910 *Z. anorg. Chem.* **69**, 22.
Garner and Latchem 1936 *Trans. Faraday Soc.* **32**, 567.
Hartley and Campbell 1908 *J. Chem. Soc.* **93**, 741.
International Critical Tables 1929*a* **5**, 124.
— 1929*b* **5**, 177.
— 1929*c* **5**, 122.
— 1929*d* **5**, 179.
Jakowkin 1894 *Z. phys. Chem.* **13**, 541.
— 1896 *Z. phys. Chem.* **20**, 19.
Jones and Kaplan 1928 *J. Amer. Chem. Soc.* **50**, 1845.
Landolt-Börnstein 1923 (5th edition), Hw., 1549.
Pauling 1932 *J. Amer. Chem. Soc.* **54**, 3570.
Randall and Ramage 1927 *J. Amer. Chem. Soc.* **49**, 93.
Sammet 1905 *Z. Phys. Chem.* **53**, 641.
Washburn and Strachan 1913 *J. Amer. Chem. Soc.* **35**, 708.

On the natural frequencies of vibrating [illegible]

By R. V. Southwell, F.R.S.

(*Received* 15 *November* 1939)

Introduction and Summary

1. The basic problem of Vibration Theory is to calculate for a given system the modes and associated frequencies of its "normal" free oscillations. These are components into which the whole motion can be resolved when the system vibrates freely, and through *small* distances, about its position of equilibrium. Each one is wholly independent of every other, and has its own (in general) distinct phase and frequency, which are common to all parts of the system. Relatively to one another the amplitudes of different parts are invariant, but the phase and magnitude of a normal oscillation are not (in theory) restricted.

Exact calculation is difficult even when attention is confined to the gravest (i.e. lowest) natural frequency, and on that account great value attaches to a theorem of Lord Rayleigh whereby a close estimate of this frequency can be based on a comparatively rough assumption in regard to the corresponding mode. It is known that the result will err, if at all, in the direction of *over-estimation*: if then by equally simple calculations it were possible to obtain a second figure close to it and known to be an *under-estimate*, such knowledge would for practical purposes be very nearly as useful as an exact result.

It sometimes happens that either the "masses" or the "elasticities" of a system* can be separated into parts for which (if they operated severally) frequencies could be calculated exactly, and then it is easy to construct both upper and lower limits to the gravest frequency of the complete system.† But although an appropriate extension of Rayleigh's method has been given by Temple and Bickley (1933), in general the finding of close lower limits is difficult, whereas close upper limits can be obtained with ease.

Part I of the present paper is concerned with this problem of lower limits. It is based on a second theorem of Lord Rayleigh (apparently less well known) which relates to the effect on the natural frequencies of altering the masses of a system, and it utilizes that theorem in combination with the concepts of the "Relaxation Method" to develop rules* whereby from any trial solution both upper and lower limits can be deduced. In essence the treatment is identical with a "Comparison Method" of which Temple and Bickley take cursory notice in their book (1933, § 1.5): they however make no appeal to Rayleigh's second theorem, apparently regarding the Comparison Method as justified by intuition. Being concerned solely with continuous systems governed by differential equations, and with a method of their own which yields a lower limit closer to the correct value, it was not to be expected that they would pursue the Comparison Method further; but in relation to systems of limited but considerable freedom (N finite but large), and especially when applied as an extension of the "relaxation" technique, that method appears to greater advantage. The need for more detailed consideration is felt when it is applied to determine lower limits to frequencies higher than the fundamental, and it is then that the value of Rayleigh's second theorem is apparent; for although it is intuitively obvious that any increase of flexural rigidity will raise the "Euler load" of a rod used as a compression member, it is less evident that it will raise *every one* of the natural frequencies of transverse vibration.

---

* That is, of an *elastic* system. But everything in this paper will apply (e.g.) to *electrical* vibrations, if "masses" and "elasticities" are replaced by analogous quantities.

† Cf. (e.g.) Temple and Bickley 1933, Chap. 6 ("Comparison and synthetic theorems").

2. In this paper, for brevity, the relaxation procedure is not described in detail, therefore continuous systems have to be taken as examples and the trial solutions are algebraic functions; consequently our rule for lower limits is useful only in relation to gravest frequencies, owing to difficulties which arise at nodal points (cf. §§ 10, 21). The restriction hardly matters in a method which is not intended primarily for the treatment of continuous systems, more especially since satisfactory (though more elaborate) methods have been propounded by Temple and Bickley (cf. § 1), also by Duncan and Lindsay (1939) in a paper circulated (in typescript) by the Aeronautical Research Committee at a time when this paper was nearly completed. The last was held to justify suppression of a section dealing with higher modes and frequencies:† instead, a method is suggested (§§ 16–20) whereby specially close estimates of gravest frequency can be made if required.

3. Corresponding with the theorem of which notice has been taken in § 1, Lord Rayleigh propounded similar theorems relating to the effect of a change in the "elasticities" and (as a particular case) to the effects of con-

---

* Stated in (17) and (18) of § 12.

† The method though not identical had some similarity with the first of two alternative methods suggested by Duncan and Lindsay.

straints. He showed that the imposition of a constraint will cause every frequency to increase unless (in particular instances) the effect is *nil* because the point constrained would in any event be nodal (i.e. stationary) in the free vibration.

Now from this result it would seem to follow that the frequencies of a bar completely free are lower than those of the same bar when its ends are held stationary. But in fact for a uniform bar the natural frequencies have the same values *whether both ends are clamped or both completely free*, and lower values obtain when both ends are simply supported. Thus in this instance the imposition of supports (which are constraints preventing terminal displacement) has the consequence of *lowering* the frequencies of a bar initially free. A paradox is presented, and to resolve it is the second purpose of this paper (Part II).

Acknowledgement should be made here of help received from Miss A. Pellew and Mr D. G. Christopherson, in the computations of §§ 13–15 and 21–23 and in the construction of figures 1 and 2.

I. ON THE CALCULATION OF UPPER AND LOWER LIMITS TO NATURAL FREQUENCIES

The governing equations

4. Lagrange's equations, typified by

$$\frac{d}{dt}\left(\frac{\partial \mathfrak{T}}{\partial \dot{q}_k}\right)-\frac{\partial \mathfrak{T}}{\partial q_k}+\frac{\partial \mathfrak{V}}{\partial q_k}=Q_k, \tag{1}$$

where $\mathfrak{V}$ denotes the potential and $\mathfrak{T}$ the kinetic energy, govern the motion of any mechanical or elastic system. Their number (N) is equal to the number of co-ordinates which suffices for the specification of every possible configuration. To every "generalized co-ordinate", typified by q_k, there corresponds a "generalized component of velocity", typified by $\dot{q}_k$, and a "generalized component of external force", typified by Q_k.

In the absence of external forces all the Q's are zero, and without loss of generality we may assume the co-ordinates to be measured in relation to the equilibrium configuration as datum, so that $\mathfrak{V}$ is a homogeneous quadratic function of their instantaneous values. Moreover in the case of *small vibrations* about a configuration of stable equilibrium $\mathfrak{T}$ can be expressed as a homogeneous quadratic function of the generalized velocities, with coefficients which (to a first approximation) have values independent of the co-ordinates: then equation (1) takes the simpler form

$$\frac{d}{dt}\left(\frac{\partial \mathfrak{T}}{\partial \dot{q}_k}\right)+\frac{\partial \mathfrak{V}}{\partial q_k}=0. \tag{2}$$

If now we assume that every co-ordinate fluctuates with the same frequency and phase, so as to be expressible in the form

$$q_k = a_k \sin(pt+\epsilon) \quad (a_k \text{ constant}), \tag{3}$$

then we may write

$$\mathfrak{V}=\mathsf{V}\sin^2(pt+\epsilon), \quad \mathfrak{T}=\mathsf{T}p^2\cos^2(pt+\epsilon), \tag{4}$$

where V and T are *both* homogeneous quadratic functions of the a's, *essentially positive*. The type-equation (2) reduces to

$$\frac{\partial \mathsf{V}}{\partial a_k}-p^2\frac{\partial \mathsf{T}}{\partial a_k}=0, \tag{5}$$

and because (by a familiar property of quadratic forms)

$$\left.\begin{aligned} 2\mathsf{V} &= a_1\frac{\partial \mathsf{V}}{\partial a_1}+a_2\frac{\partial \mathsf{V}}{\partial a_2}+\ldots+a_k\frac{\partial \mathsf{V}}{\partial a_k}+\ldots,\\ 2\mathsf{T} &= a_1\frac{\partial \mathsf{T}}{\partial a_1}+a_2\frac{\partial \mathsf{T}}{\partial a_2}+\ldots+a_k\frac{\partial \mathsf{T}}{\partial a_k}+\ldots,\end{aligned}\right\} \tag{6}$$

from the N equations of type (5) we deduce that

$$\mathsf{V}=p^2\mathsf{T}. \tag{7}$$

Alternatively we can derive (7) as a consequence of the assumption (3) applied to the equation

$$\mathfrak{V}+\mathfrak{T}=\text{const.}, \tag{8}$$

which (for conservation of energy) must hold in the absence of external forces which do work on the system.*

"*Rayleigh's principle*"

5. It is easy to show (and was observed by Lagrange) that the N equations of type (5) are the conditions for a stationary value of p^2 as calculated from (7). For if $p_2=\mathsf{V}/\mathsf{T}$ is stationary, then

$$\delta(\mathsf{V}/\mathsf{T})=\delta\mathsf{V}/\mathsf{T}-\mathsf{V}\,\delta\mathsf{T}/\mathsf{T}^2=(\delta\mathsf{V}-p^2\delta\mathsf{T})/\mathsf{T}$$

---

* The qualification is needed, in order that external forces due to *constraints* may not be excluded.

must vanish for all possible variations, therefore for any variation δa_k occurring singly. On this result Lord Rayleigh based his well-known "principle" whereby the gravest (or lowest) natural frequency may be estimated from (7) on the basis of an assumed form for the corresponding mode: An error of the first order made in regard to the mode will, by reason of the stationary property, entail an error of the second order of small quantities in regard to p^2; and in regard to the gravest value p_1^2 (which, being the smallest of the stationary values, must be an absolute *minimum*) the estimate will err, if at all, on the side of *excess*.

The practical application of Rayleigh's principle is too widely known to call for illustration here.

Rayleigh's theorem regarding the effect of added mass

6. A further application of the stationary property, also due to Lord Rayleigh (1896, vol. 1, §88), seems on the other hand to be less familiar. This relates to the effect on the natural frequencies of a change made in the masses of an elastic system: Excepting cases in which the effect is *nil* (as when mass is added at a nodal point) *any increase of mass will lower every natural frequency, and* vice versa.

To prove the theorem we conceive the change to be made in a series of infinitesimal steps, and it is here that use is made of the stationary property. Any change made in the mass of a system will (in general) alter both the mode and the associated frequency of every free vibration: therefore the whole effect on any frequency of an infinitesimal change may be regarded as consisting (i) of the effect as calculated without allowance for the accompanying change in the mode and (ii) of the effect of this latter alteration. But, in virtue of the stationary property (§5), an infinitesimal change in the mode will entail a change of the second order in p^2; consequently in any one of the infinitesimal steps, and therefore in the integrated result of all such steps, (ii) is negligible in comparison with (i). Now the sign of (i) can be deduced from (6), since *if the mode is unaltered* $\mathbf{T}$ must be increased (and $\mathbf{V}$ left unchanged) by any increase of mass. Hence we have the theorem stated.

Use of the theorem as complementary to "Rayleigh's principle"

7. In practical applications (having regard to the uncertainty of physical data) it is not essential that frequencies be calculable exactly, but it is on the other hand desirable that estimates should have known margins of error. From this standpoint "Rayleigh's principle" as originally presented (§5) has one drawback in that it provides only an upper limit to the gravest

frequency, and extensions have been made by Temple and Bickley (1933) to remove this disability. We now develop an alternative procedure for the finding of a lower limit, based on the theorem of §6. Fundamentally it is identical with the "Comparison Method" of which (cf. §1) Temple and Bickley take cursory notice in their first chapter; but it gains in practical convenience when stated (as here) in terms of the standard concepts of "relaxation" theory.

Detailed discussion of the relaxation treatment is reserved with a view to brevity, and accordingly in this paper only continuous systems have been taken as examples. They serve better than systems of restricted freedom to illustrate the essentials of the Comparison Method, but of necessity they fail to exhibit its potentialities, for the reason that the choice of trial solutions is restricted (when they are treated by orthodox methods) by the need of determining maxima and minima.* Better results are obtained when systems are in effect given restricted freedom by the use of finite-difference approximations; but even so it is not easy to find lower limits as close as the upper limits afforded by "Rayleigh's principle" (§5). The real value of the Comparison Method is revealed only when advantage is taken of the relaxation technique, with its power to amend a trial solution locally. Of necessity this presumes a system of restricted freedom, and on that account N has been taken as finite (but not otherwise restricted) in the argument of this paper. Such treatment has the authority of Lord Rayleigh.

Introduction of the notion of "constraints". The physical basis of "Rayleigh's principle"

8. Let us suppose that constraints are operative which permit the maintenance of any specified displacements whether steady or oscillatory, and that we use them to maintain a trial solution in which the N displacements of type q_k all vary in accordance with (3). Now writing

$$\left.\begin{array}{c} F_k = p^2 T_k - V_k, \\ \text{where } T_k \text{ and } V_k \text{ (for brevity) replace} \\ \dfrac{\partial \mathrm{T}}{\partial a_k} \text{ and } \dfrac{\partial \mathrm{V}}{\partial a_k}, \end{array}\right\} \qquad (9)$$

we can interpret $F_k \sin(pt+\epsilon)$ as the force, corresponding with the generalized displacement q_k, which comes upon the constraint controlling q_k;

---

* A "relaxation" technique for continuous systems was described in a recent paper (Bradfield, Christopherson and Southwell 1939, §§13–31).

and then, disregarding the common time-factor $\sin(pt+\epsilon)$, we may think of F_k as the force corresponding with a displacement a_k.

Multiplying (9) throughout by $\frac{1}{2}a_k$, and summing the N equations which can be obtained in this way, we have in virtue of (6)

$$\tfrac{1}{2}\Sigma_N[F_k \cdot a_k] = p^2\mathsf{T} - \mathsf{V}, \tag{10}$$

whence equation (7) results provided that $\Sigma_N[F_k \cdot a_k] = 0$. Observing that F_k according to (9) and (6) is a linear function of the a's, so that $\frac{1}{2}\Sigma_N[F_k \cdot a_k]$ measures the total work done by the forces on the constraints in virtue of the a-displacements, we find in this result a physical interpretation of Rayleigh's use of (7) for the estimation of p^2 on the basis of an assumed mode (§5): Unless the assumed mode is correct, forces will be needed to maintain it, and the magnitudes of those forces will depend upon the frequency of their fluctuation; but for some particular frequency the forces *on the whole* will do no work, and this is Rayleigh's estimate of the natural frequency.

Imposition by the "Comparison Method" of lower limits to the natural frequencies

9. In an exact solution (p^2 having its correct value) every F is zero in accordance with (5): in a trial solution, any one force can be made to vanish by a suitable choice of frequency, but a different value (in general) is required for each of the several forces. On the other hand, whatever value be attached to p^2 we can make F_k zero by suitably altering the value of $T_k (= \partial\mathsf{T}/\partial a_k)$, and this alteration will not affect the other forces if it is made by merely changing the coefficient of a_k^2 in the quadratic expression for T. Increasing that coefficient we shall be adding mass to the system, and vice versa. The added mass will increase the kinetic energy when, and only when, $\dot{q}_k$ is non-zero.

If when every F has been brought to zero every mass has been either left unaltered or increased, then the chosen value of p^2 will be exact as regards a system modified by *addition* of mass and therefore (by the theorem of §6) it will *underestimate* the frequency of the unmodified (i.e. the given) system: in other words, it will furnish a lower limit to the required value $\mathbf{p}^2$. Now an increase made in the mass associated with $\dot{q}_k$ will entail a positive increase in the value of $a_k . T_k$ and therefore, by (9), a positive increase in the value of $a_k . F_k$: consequently only positive or zero additions of mass will be needed to bring all F's to zero *provided that every product of the type* $a_k . F_k$ *is negative or zero*, and on that understanding we may assert that p^2 in (9) has a value less than $\mathbf{p}^2$.

10. The highest value of p^2 which can with certainty be termed a lower limit is the highest value which makes one of the $a.F$ products zero and all the others negative. Now according to (9) the value of $a_k.F_k$ changes sign when

$$p^2 = V_k/T_k, \tag{11}$$

and higher values of p^2 will make $a_k.F_k$ positive provided that $a_k.T_k$ is positive. If then $(V/T)_S$ denotes *the smallest value of* V_k/T_k *which corresponds with a positive product* $a_k.T_k$, we may assert that

$$\mathbf{p}^2 \nless (V/T)_S, \tag{12}$$

but no higher value can be imposed (by our argument) as a lower limit.

This result will of course be nugatory unless the ratio $(V/T)_S$ is positive, since we know *a priori* that $\mathbf{p}^2$ cannot be negative: therefore negative values of $a_k.T_k$ call for consideration only when associated with negative values of $a_k.V_k$. If $a_k.V_k$ and $a_k.T_k$ are both negative, $a_k.F_k$ will change sign *from positive to negative* as p^2 increases through the value given by (11), and (12) will be invalidated unless that value is *less* than $(V/T)_S$ as defined above. The method becomes too complicated to have practical value when negative values of $a_k.V_k$ and $a_k.T_k$ are thus taken into account, and these in relation to gravest modes will not usually occur if the trial solution is reasonably correct. (Both products must for the most part be positive, because $\Sigma_N[a_k.V_k] = 2\mathsf{V}$ and $\Sigma_N[a_k.T_k] = 2\mathsf{T}$ are essentially positive functions.)

11. Equation (12) states the Comparison Method in a form appropriate to continuous systems and to orthodox methods. We now deduce a form more convenient for use with the relaxation technique.

Adopting that procedure we shall systematically modify both the mode and the assumed frequency with the aim of making all the F's negligible. At any stage in the calculations we can by Rayleigh's principle impose an upper limit p_R^2 on the required value $\mathbf{p}^2$, choosing p_R^2 so that

$$\Sigma_N[a_k.F_k] = 0 \tag{13}$$

(cf. §8). So it remains to devise a rule for the imposition of a lower limit.

Suppose that for some trial value p^2 all products of the type $a_k.F_k$ have been calculated, and now let p^2 be altered to $(p^2+\Delta p^2)$. By (9), the value of $a_k.F_k$ will be altered to

$$a_k(F_k+\Delta p^2.T_k), \tag{14}$$

and this altered value will be zero if

$$\Delta p^2 = -\frac{F_k}{T_k}. \tag{15}$$

An algebraically greater value of Δp^2 will make the altered value positive provided that $a_k . T_k$ is positive. If then $(F/T)_L$ denotes *the algebraically largest value of F_k/T_k which corresponds with a positive product $a_k . T_k$*, we may assert that

$$\mathrm{p}^2 \nless p^2 - \left(\frac{F}{T}\right)_L, \tag{16}$$

but no higher value can be imposed (by our argument) as a lower limit.

Provided that "liquidation" has been continued until all the F's are small, the lower limit given by (16) will always be positive: it may happen that $(F/T)_L$ is negative because too low a value has been assumed for p^2, but the formula will not be invalidated on that account. Negative values of $a_k . T_k$ must be contemplated, and when $a_k . T_k$ is negative $a_k . F_k$ will change sign *from positive to negative* as Δp^2 increases through the value given by (15), therefore (16) will be invalidated unless F_k/T_k is algebraically *greater* than $(F/T)_L$ as defined above. But negative values of $a_k . T_k$ will occur only in the neighbourhood of nodal points, and there (for practical purposes) they may be neglected.

Procedure for the imposition of upper and lower limits on the gravest frequency

12. The converse theorem to that of § 9 (that p^2 in (9) may be regarded as an upper limit when every product of the type $a_k . F_k$ is zero or *positive*) can be established and applied in similar fashion; but its practical value is small, in that the upper limit imposed by Rayleigh's principle is lower and therefore preferable. (We have proved this in § 8, where it was shown that the "Rayleigh upper limit" makes $\Sigma_N[a_k . F_k]$ zero; for when that condition is realized one or more products of the type $a_k . F_k$ will evidently be negative, unless the trial solution happens to be exact.)

In relation to continuous systems, then, the rule for imposing upper and lower limits on p_1^2 is

$$(V/T)_S < p_1^2 < p_R^2, \tag{17}$$

where p_R^2 is calculated from (13). Alternatively, if by relaxation methods all products of the type $a_k . F_k$ have been calculated for some trial value p^2, then according to (14) the upper limit allowed to Δp^2 by Rayleigh's principle is given by

$$\Sigma_N[a_k . F_k] + \Delta p^2 . \Sigma_N[a_k . T_k] = 0,$$

and combining this result with (16) we have the rule

$$p^2 - \left(\frac{F}{T}\right)_L < p_1^2 < p^2 - \frac{\Sigma_N[a_k . F_k]}{\Sigma_N[a_k . T_k]}. \tag{18}$$

Examples: (1) *Estimation of the fundamental frequency of a clamped bar and disk*

13. In illustration of (17) we now apply that rule to two continuous systems which have been studied by Temple and Bickley (cf. § 7). For such systems the N separate equations of type (5) are replaced by a single governing equation which holds for all values of the independent variable (or variables) within a specified range, together with special conditions which must be satisfied at the ends of the range or at all points of some specified boundary. Thus the governing equation of a uniform bar vibrating transversely has the form

$$B\frac{d^4y}{dx^4} = mp^2y, \tag{19}$$

and at both ends, if these are "clamped", the conditions

$$y = \frac{dy}{dx} = 0 \tag{20}$$

must be satisfied. The gravest frequency corresponds with a value p_1^2 where

$$p_1^2ml^4/B = \mu_1^4 = (4{\cdot}7300408)^4 = 500{\cdot}5639. \tag{21}$$

Temple and Bickley (§ 5.4), using Rayleigh's method with an assumed form*

$$y/y_c = 16x^2(l-x)^2/l^4 \tag{22}$$

(for ends at 0 and l), obtained an estimate in which the correct value of μ_1^4 is replaced by 504; and using an iterative method for improving the assumption they showed that for the form*

$$y/y_c = \frac{256}{163}\{9l^4x^2(l-x)^2 + 4l^2x^3(l-x)^3 + 3x^4(l-x)^4\}/l^8 \tag{23}$$

the estimated figure is reduced to 500·567.... This value is still too high (in conformity with § 5), but it is very close to the correct value.

14. Writing in conformity with (9) of § 8

$$F = p^2T - V = mp^2y - B\frac{d^4y}{dx^4}, \tag{24}$$

---

* In (22) and (23) y_c stands for the central deflexion.

we may regard F as a distributed loading which measures the accuracy of an assumed mode (y) and frequency (p^2). Then corresponding with $\Sigma[a_k . F_k]$ we have the definite integral $\int_0^l yF\,dx$, and "Rayleigh's principle" gives for an upper limit to p_1^2 (cf. §11) the equation

$$0 = \int_0^l yF\,dx = mp^2\int_0^l y^2\,dx - B\int_0^l \left(\frac{d^2y}{dx^2}\right)^2 dx, \tag{25}$$

in virtue of the terminal conditions (20). To obtain a lower limit we have merely to calculate (cf. §10) the smallest values of the quotient

$$V/T = B\frac{d^4y}{dx^4}\bigg/ my, \tag{26}$$

since in this instance $yT(=my^2)$ is necessarily positive.

Using (25) we confirm the results of Temple and Bickley cited in §11. From (26), assuming y to have the form (22), we have

$$(V/T)_S = [24B/mx^2(l-x)^2]_S = 384B/ml^4,$$

so that in this instance (17) becomes

$$384 < \frac{mp_1^2 l^4}{B} < 504. \tag{27}$$

When on the other hand y is assumed to have the form (23), then according to (26)

$$\begin{aligned}(V/T)_S &= [5040B/m\{9l^4 + 4l^2x(l-x) + 3x^2(l-x)^2\}]_S \\ &= 5040 \times \tfrac{16}{163}\, B/ml^4 = 494{\cdot}724B/ml^4,\end{aligned}$$

and (17) gives a much closer "bracket", namely

$$494{\cdot}724 < \frac{mp_1^2 l^4}{B} < 500{\cdot}567. \tag{28}$$

The extreme range of numerical uncertainty is 5·843, so that the assumption of a mean value (497·645) entails an error in p^2 lying within the range ± 2·93, i.e. ± 0·59 %. The percentage error in frequency is only half as great (less than 0·3 %).

15. As a second example we consider transverse vibrations of a uniform disk clamped at all points of a circle of radius a. The true value of the gravest frequency is given by

$$p_1^2 = 104{\cdot}362_5 D/ma^4, \tag{29}$$

D denoting the flexural rigidity and m the mass per unit area. In the gravest mode the deflexion w is a function only of the radial distance.

Writing in conformity with (9) of §8*

$$F = p^2T - V = mp^2w - D\left[\frac{d^2}{dr^2}+\frac{1}{r}\frac{d}{dr}\right]^2 w, \tag{30}$$

we have corresponding with $\Sigma[a_k . F_k]$ the definite integral $2\pi\int_0^a wFr\,dr$, so "Rayleigh's principle" gives for an upper limit to p_1^2 (cf. §11) the equation

$$0 = \int_0^a wFr\,dr = mp^2\int_0^a w^2r\,dr - D\int_0^a \frac{1}{r}\left\{\frac{d}{dr}\left(r\frac{dw}{dr}\right)\right\}^2 dr, \tag{31}$$

in virtue of the boundary conditions at $r=0$ and $r=a$. The product $wT(=mw^2)$ is necessarily positive, so to obtain a lower limit we have only to calculate (cf. §10) the smallest value of the quotient

$$V/T = D\left[\frac{d^2}{dr^2}+\frac{1}{r}\frac{d}{dr}\right]^2 w/mw. \tag{32}$$

Taking as an assumed form for the deflexion

$$w = c(a^3 - 3ar^2 + 2r^3), \tag{33}$$

Temple and Bickley (§5.5) obtained by Rayleigh's method

$$p_R^2 = 105D/ma^4. \tag{34}$$

This result is confirmed by (31). From (32) we have

$$(V/T)_S = [18D/mr(a^3 - 3ar^2 + 2r^3)]_S = 69{\cdot}238D/ma^4,$$

so that in this instance (17) becomes

$$69{\cdot}238 < \frac{ma^4p^2}{D} < 105. \tag{35}$$

The much closer bracket

$$102{\cdot}431_5 < \frac{ma^4p^2}{D} < 104{\cdot}364_5 \tag{36}$$

was obtained by taking in place of (33), as an assumed form for the deflexion,

$$w = c\left\{\frac{437}{7}a^7 - \frac{717}{5}a^5r^2 + 105a^3r^4 - 35ar^6 + \frac{384}{35}r^7\right\}. \tag{37}$$

The mean of the two limits in (36) gives p with an error certainly less than 0·5 %.

---

* Cf. (e.g.) Southwell 1936, §243, equation (41).

Improved approximations to a gravest mode and frequency

16. The iterative method employed by Temple and Bickley (cf. §13) substitutes an approximation to the wanted mode in the inertia terms of the governing equation, then solves this to obtain a new and closer approximation. E.g. the substitution (22), made for y on the right of (19), leads (except for a nugatory multiplying constant) to the closer approximation (23), and a substitution from (33) leads in the same way to (37). It will now be shown that two successive approximations to the first mode, thus related, can be made to yield a still closer approximation to the first mode and frequency, together with a reasonably good approximation to some higher frequency, —usually the second.

17. Let y_A, y_B stand for the displacement at x in two distinct modes A, B, both satisfying the terminal conditions but otherwise (for the moment) not restricted. Let V and T have the same significance as before, and let V_A, T_A and V_B, T_B denote their values corresponding with y_A and y_B. Let V and T, conformably with (9), replace (for brevity) $\partial\mathsf{V}/\partial y$ and $\partial\mathsf{T}/\partial y$, and for the two modes A and B let these "forces" be distinguished similarly by suffixes A and B. We now combine A and B in a third mode C by writing

$$y_C = y_A - \alpha . y_B, \tag{38}$$

α being arbitrary; and we trace the effect of α on the frequency as calculated on Rayleigh's principle for the mode y_C.

Since V and T are homogeneous quadratic functions of the displacements, we have according to (38)

$$\left.\begin{aligned} \mathsf{V}_C &= \mathsf{V}_A - 2\alpha\mathsf{V}_{AB} + \alpha^2\mathsf{V}_B, \\ \mathsf{T}_C &= \mathsf{T}_A - 2\alpha\mathsf{T}_{AB} + \alpha^2\mathsf{T}_B, \end{aligned}\right\} \tag{39}$$

where $2\mathsf{V}_{AB}$ stands for the sum or integral of such products as $y_A . V_B$ or $y_B . V_A$,* and T_{AB} has a similar significance. By Rayleigh's principle we have

$$p_A^2 = \mathsf{V}_A/\mathsf{T}_A, \quad p_B^2 = \mathsf{V}_B/\mathsf{T}_B, \quad p_C^2 = \mathsf{V}_C/\mathsf{T}_C \tag{40}$$

for the frequencies corresponding with modes A, B and C.

As given by (39) and (40) p_C^2 is stationary in respect of variations in α provided that

$$\frac{\mathsf{V}_{AB} - \alpha\mathsf{V}_B}{\mathsf{T}_{AB} - \alpha\mathsf{T}_B} = p_C^2 = \frac{\mathsf{V}_A - 2\alpha\mathsf{V}_{AB} + \alpha^2\mathsf{V}_B}{\mathsf{T}_A - 2\alpha\mathsf{T}_{AB} + \alpha^2\mathsf{T}_B} = \frac{\mathsf{V}_A - \alpha\mathsf{V}_{AB}}{\mathsf{T}_A - \alpha\mathsf{T}_{AB}}. \tag{41}$$

---

* These have the same sum, by the Reciprocal Theorem.

Eliminating p_C^2 from these equations we obtain a quadratic equation in α, giving two values which make p_C^2 stationary; eliminating α, a quadratic equation in p_C^2 of which the two roots are the wanted stationary values. The equation in α may be written as

$$\alpha^2 - \alpha \frac{\mathsf{T}_A}{\mathsf{T}_{AB}} \frac{p_A^2 - p_B^2}{p_{AB}^2 - p_B^2} + \frac{\mathsf{T}_A}{\mathsf{T}_B} \frac{p_A^2 - p_{AB}^2}{p_{AB}^2 - p_B^2} = 0, \tag{42}$$

and the equation in p_C^2 as

$$(p_C^2 - p_A^2)(p_C^2 - p_B^2) = \frac{\mathsf{T}_{AB}^2}{\mathsf{T}_A \cdot \mathsf{T}_B} (p_{AB}^2 - p_C^2)^2, \tag{43}$$

where

$$p_{AB}^2 = \mathsf{V}_{AB}/\mathsf{T}_{AB}. \tag{44}$$

18. Suppose now that the modes A, B (as yet unrestricted) are "T-orthogonal" in the sense that $\mathsf{T}_{AB} = 0$. If they are also "V-orthogonal" in the sense that $\mathsf{V}_{AB} = 0$, then the roots of (42) are 0 and ∞, those of (43) are p_A^2 and p_B^2: this means that p_B^2 increases or decreases steadily from p_A^2 to p_B^2 as α is increased from 0 to ∞, i.e. as the mode is altered from A to B.

When on the other hand A and B are "T-orthogonal" but *not* "V-orthogonal", (42) reduces to

$$\alpha^2 - \alpha \frac{\mathsf{T}_A}{\mathsf{V}_{AB}} (p_A^2 - p_B^2) - \frac{\mathsf{T}_A}{\mathsf{T}_B} = 0, \tag{45}$$

and (43) to

$$(p_C^2 - p_A^2)(p_C^2 - p_B^2) = \frac{\mathsf{V}_{AB}^2}{\mathsf{T}_A \cdot \mathsf{T}_B}. \tag{46}$$

The two roots in α have opposite signs, and of the two roots in p_C^2 neither lies between p_A^2 and p_B^2 (otherwise the left-hand side of (46) would be negative). This means that by one combination of A and B we can obtain a mode C which (since p_C^2 is less than either of p_A^2, p_B^2) is a closer approximation than either to the gravest mode; from another combination we can deduce a value of p_C^2 which is higher than either of p_A^2, p_B^2 and (being stationary in respect of variations in α) should be a good approximation to some higher frequency.

19. Now A and B can always be combined to give a mode which is "T-orthogonal" to B, since we have from (38)

$$\mathsf{V}_{BC} = \mathsf{V}_{AB} - \alpha \mathsf{V}_B, \quad \mathsf{T}_{BC} = \mathsf{T}_{AB} - \alpha \mathsf{T}_B, \tag{47}$$

whence $\mathsf{T}_{BC} = 0$ if $\alpha = \mathsf{T}_{AB}/\mathsf{T}_B$. (We observe that the same value will not make C also "V-orthogonal" to B unless $p_{AB}^2 = p_B^2$.) Evidently this combined mode may be substituted for A in the above discussion: therefore without requiring A and B to be orthogonal we can combine them to obtain a closer approximation to the gravest mode and a good approximation to some higher frequency.

Equations (42) and (43) must then be used *without modification*. That is to say, the sum of the roots in p_C^2 will be

$$\left.\begin{aligned} &\left(p_A^2+p_B^2-2\frac{\mathsf{V}_{AB}\cdot\mathsf{T}_{AB}}{\mathsf{T}_A\cdot\mathsf{T}_B}\right)\bigg/\left(1-\frac{\mathsf{T}_{AB}^2}{\mathsf{T}_A\cdot\mathsf{T}_B}\right), \\ &\text{and their product will be} \\ &\left(p_A^2\cdot p_B^2-\frac{\mathsf{V}_{AB}^2}{\mathsf{T}_A\cdot\mathsf{T}_B}\right)\bigg/\left(1-\frac{\mathsf{T}_{BB}^2}{\mathsf{T}_A\cdot\mathsf{T}_B}\right). \end{aligned}\right\} \quad (48)$$

20. In particular we may use these results in conjunction with the iterative process of Temple and Bickley, which (cf. § 16) is expressed by*

$$V_B=T_A \qquad (49)$$

and makes B a closer approximation than A to the wanted first mode (i.e. $p_A^2>p_B^2>p_1^2$). It is easy to deduce from (49) that

$$\mathsf{V}_{AB}=\mathsf{T}_A, \quad \mathsf{T}_{AB}=\mathsf{V}_B, \qquad (50)$$

and making these substitutions in (42) we find that the wanted values of α are the roots of

$$\alpha^2-\alpha(p_A^2-p_B^2)/(1-\mathsf{V}_B^2/\mathsf{T}_A\cdot\mathsf{T}_B)+\frac{\mathsf{V}_A\cdot\mathsf{V}_B-\mathsf{T}_A^2}{\mathsf{T}_A\cdot\mathsf{T}_B-\mathsf{V}_B^2}; \qquad (51)$$

making them in (48) we find that the sum of the roots in p_C^2 is given by

$$\left.\begin{aligned} &(p_A^2-p_B^2)\bigg/\left(1-\frac{\mathsf{V}_B^2}{\mathsf{T}_A\cdot\mathsf{T}_B}\right) \\ \text{and their product by}\quad &\left(p_A^2\cdot p_B^2-\frac{\mathsf{T}_A}{\mathsf{T}_B}\right)\bigg/\left(1-\frac{\mathsf{V}_B^2}{\mathsf{T}_A\cdot\mathsf{T}_B}\right). \end{aligned}\right\} \quad (52)$$

Comparing these expressions with the sum and product of the roots of (51), we observe that *the two wanted values of α are also the two wanted values of p_C^2*. The same result can be obtained by substitution from (50) in (41), and then it appears that the larger root in p_C^2 is associated with the smaller root in α, and vice versa. I.e. we have

$$p_{C'}^2/\alpha''=1=p_{C''}^2/\alpha',$$

single and double dashes being used to distinguish associated quantities.

---

* The form of (49) though not dimensionally consistent is legitimate, because the amplitudes of the modes A, B are not restricted. It simplifies the formulae of § 20, but it leads to unfamiliar and "dimensionally incorrect" forms for T_A, T_B, V_B (cf. § 21).

As shown above the smaller value will be closer than either p_A^2 or p_B^2 to the wanted value of p_1^2, and the larger should yield a fair approximation to some higher frequency (usually the second: this can be decided by inspection of the plotted mode y_C). In this way, without much added labour, additional information can be derived from results like those of §§ 13–15. The calculations must be *exact*, since we shall be working with two approximations A and B which are nearly identical, and on that account the method is restricted (in practice) to continuous systems. We now apply it to the calculations of §§ 13–15.

Examples: (2) *Estimation of the gravest mode and frequency for a clamped bar and disk*

21. From the governing equation (19) we have

$$V_B = B\frac{d^4 y_B}{dx^4} = m y_A = T_A \tag{53}$$

as the form of (49) appropriate to a uniform bar vibrating transversely. Hence, taking

$$y_A = x^2(l-x)^2/l^4$$

in accordance with (22), we obtain

$$By_B = \frac{m}{7!}\{9l^4x^2(l-x)^2 + 4l^2x^3(l-x)^3 + 3x^4(l-x)^4\}/l^4, \tag{54}$$

in conformity with (23). The quantities which appear in (52) are now given by

$$\left.\begin{aligned}
2\mathsf{T}_A &= \int_0^l y_A T_A\,dx = m\int_0^l y_A^2\,dx = \frac{ml}{630},\\
2\mathsf{T}_B &= \int_0^l y_B T_B\,dx = m\int_0^l y_B^2\,dx = \frac{3911 m^3 l^9}{24310\times(5040)^2 B^2},\\
2\mathsf{V}_A &= \int_0^l y_A\,.\,B\frac{d^4 y_A}{dx^4}\,dx = 24\frac{B}{l^4}\int_0^l y_A\,dx = \frac{4B}{5l^3},\\
2\mathsf{V}_B &= \int_0^l y_B V_B\,dx = m\int_0^l y_B\cdot y_A\,dx = \frac{2879 m^2 l^5}{180180\times 5040 B},
\end{aligned}\right\} \tag{55}$$

so that

$$\left.\begin{aligned}
p_A^2 &= \mathsf{V}_A/\mathsf{T}_A = 504\frac{B}{ml^4},\\
p_B^2 &= \mathsf{V}_B/\mathsf{T}_B = \frac{680\times 2879 B}{3911 ml^4} = 500\cdot567\,.\,.\,\frac{B}{ml^4},
\end{aligned}\right\} \tag{56}$$

as in §14. Therefore according to (52) the sum of the stationary values of $p_{\mathcal{C}}^2$ is

$$\frac{B}{ml^4} \times \frac{13424 \times 140936796}{3911 \times 29899}$$

and their product is

$$\frac{B^2}{m^2l^8} \times \frac{6511680 \times 140936796}{3911 \times 29899}.$$

Accordingly the stationary values of $p_{\mathcal{C}}^2$ are

$$(6712 \pm \sqrt{39648215{\cdot}61}) \times \frac{140936796}{3911 \times 29899} \frac{B}{ml^4}$$

$$= 500{\cdot}56413 \frac{B}{ml^4} \quad \text{and} \quad 15678{\cdot}815 \frac{B}{ml^4}, \tag{57}$$

and these (cf. §20) are also the wanted values of α. The lower value of $p_{\mathcal{C}}^2$ corresponds with the higher value of α, i.e. with a mode in which according to (38)

$$y \propto \frac{x^2(l-x)^2}{l^4}\left[1 - \frac{15678{\cdot}815}{7!}\left\{9 + \frac{4x(l-x)}{l^2} + \frac{3x^2(l-x)^2}{l^4}\right\}\right]. \tag{58}$$

For this

$$(V/T)_S = 498{\cdot}33150 \frac{B}{ml^4}, \tag{59}$$

so that we have in place of (28)

$$498{\cdot}33150 < \frac{ml^4 p_1^2}{B} < 500{\cdot}56413, \tag{60}$$

—a still closer "bracket". The correct value (cf. §24) is

$$(4{\cdot}7300408)^4 = 500{\cdot}5639.$$

The larger value of $p_{\mathcal{C}}^2$ corresponds with the smaller value of α, i.e. with a mode in which according to (38)

$$y \propto \frac{x^2(l-x)^2}{l^4}\left[1 - \frac{500{\cdot}56413}{7!}\left\{9 + \frac{4x(l-x)}{l^2} + \frac{3x^2(l-x)^2}{l^4}\right\}\right], \tag{61}$$

and this when plotted is seen (from the number of its nodal points) to be an approximation to the second symmetrical mode. Because the "V-force" and "T-force" do not vanish for the same value of x (as they would if the mode were correct), strictly speaking our rule cannot be used to calculate a lower limit to the frequency.

If by some stretching of the argument of §10 it is considered justifiable to neglect (V/T) in the neighbourhood of points of inflexion, then

$$(V/T)_S = 9874{\cdot}157 \frac{B}{ml^4}, \tag{62}$$

and our approximation (61) to the second symmetrical mode gives the "bracket"

$$9874{\cdot}157 < \frac{ml^4p_3^2}{B} < 15678{\cdot}815. \tag{63}$$

But this, as was to be expected, is rather wide. The correct value (cf. § 24) is

$$(10{\cdot}9956078)^4 = 14617{\cdot}6299, \tag{64}$$

so the upper (Rayleigh) limit in (63) is the nearer of the two.

22. In relation to the clamped disk (§ 15), equation (49) has the form*

$$D\left[\frac{d^2}{dr^2}+\frac{1}{r}\frac{d}{dr}\right]^2 w_B = mw_A,$$

and taking

$$w_A = a^3 - 3ar^2 + 2r^3 \tag{65}$$

in conformity with (33) we deduce that

$$Dw_B = \frac{m}{64\times 105}\{\tfrac{437}{7}a^7 - \tfrac{717}{5}a^5r^2 + 105a^3r^4 - 35ar^6 + \tfrac{384}{35}r^7\}, \tag{66}$$

in conformity with (37). Then

$$\left.\begin{aligned}
\mathsf{T}_A &= \pi\int_0^a w_A\,.\,T_A\,.\,r\,dr = \pi m\int_0^a w_A^2\,.\,r\,dr = \tfrac{3}{35}\pi m a^8,\\
\mathsf{T}_B &= \pi m\int_0^a w_B^2\,.\,r\,dr = \frac{\pi m^3a^{16}}{D^2}\,.\,\frac{1524239}{193729536000},\\
\mathsf{V}_A &= \pi D\int_0^a rw\left[\frac{d^2}{dr^2}+\frac{1}{r}\frac{d}{dr}\right]^2 w_A\,dr = 9\pi Da^4,\\
\mathsf{V}_B &= \pi\int_0^a w_B\,.\,V_B\,.\,r\,dr = \pi m\int_0^a w_A\,.\,w_B\,.\,r\,dr = \frac{\pi m^2a^{12}}{D}\,\frac{25493}{31046400},
\end{aligned}\right\} \tag{67}$$

so that

$$p_A^2 = \mathsf{V}_A/\mathsf{T}_A = \frac{105D}{ma^4}, \quad p_B^2 = \mathsf{V}_B/\mathsf{T}_B = \frac{104{\cdot}364_5D}{ma^4}, \tag{68}$$

as in § 15. According to (52) the sum and product of the stationary values of p_C^2 are

$$\frac{1937550\times 2772}{1771379}\,\frac{D}{ma^4} \quad\text{and}\quad \frac{195249600\times 2772}{1771379}\,\frac{D^2}{m^2a^8}$$

respectively; so the stationary values are

$$104{\cdot}36361D/ma^4 \quad\text{and}\quad 2927{\cdot}67448D/ma^4, \tag{69}$$

and these are also the wanted values of α (cf. § 17).

---

* Cf. equation (32), § 15. w replaces y in §§ 13–17.

The lower value of p_0^2 corresponds with the higher value of α, i.e. with a mode in which

$$w \propto (a-r)^2\left[a+2r-\frac{2927\cdot67448}{105\times64}\{\tfrac{437}{7}(a^5+2a^4r)\right.$$
$$\left.+\tfrac{1}{35}(1536a^3r^2-1298a^2r^3-457ar^4+384r^5)\}\right]. \quad (70)$$

The larger corresponds with the smaller value of α, i.e. with a mode in which

$$w \propto (a-r)^2\left[a+2r-\frac{104\cdot36361}{105\times64}\{\tfrac{437}{7}(a^5+2a^4r)\right.$$
$$\left.+\tfrac{1}{35}(1536a^3r^2-1298a^2r^3-457ar^4+384r^5)\}\right]. \quad (71)$$

In neither instance does our rule for lower limits provide a useful result, owing to infinities at $r=0$ and at $r=a$ which characterize (V/T) as deduced from (33). These being positive do not affect the lower limits given in (35) and (36), and similar infinities do not characterize (V/T) as deduced from (37); but because the value of α is positive in (70) and (71), in both instances

$$(V/T)_S = -\infty \quad (72)$$

and the lower limit is nugatory in accordance with §10. The origin of the difficulty is to be found in the choice by Temple and Bickley (cf. §15) of a starting assumption (33) which is the static solution for a *concentrated* central force. When it is desired to find a lower limit in the manner here suggested, a mode should be assumed for which the V-force is everywhere finite.

All then that we can derive from (70) and (71) is an upper (Rayleigh) limit to p_1^2, viz.

$$\frac{ma^4p_1^2}{D} < 104\cdot36361, \quad (73)$$

which is extremely close to the correct value (29), and an upper limit to p_2^2, viz.

$$\frac{ma^4p_2^2}{D} < 2927\cdot67448, \quad (74)$$

which (as was to be expected) is much less satisfactory. The correct value as determined with the aid of a table of Bessel functions* is

$$1581\cdot73_5. \quad (75)$$

---

* Cf. (e.g.) Southwell 1936, §244, equation (47).

II. ON A PARADOX PRESENTED BY RAYLEIGH'S SECOND THEOREM

Rayleigh's theorem regarding the effect of a constraint

23. In §6 we presented "Rayleigh's second theorem" as relating solely to the effect of added mass; but an exactly similar argument can be employed to show that (except in cases where the effect is *nil*) any increase made in the stiffness of a system will have the effect of *raising* every natural frequency. Lord Rayleigh in fact presented both conclusions as a single theorem (*loc. cit.* §6), and added that this "may sometimes be used for tracing the effects of a constraint; for if we suppose that the potential energy of any configuration violating the condition of constraint gradually increases, we shall approach a state of things in which the condition is observed with any desired degree of completeness. During each step of the process every free vibration becomes (in general) more rapid, and a number of the free periods (equal to the degrees of liberty lost) become infinitely small. The same practical result may be reached without altering the potential energy by supposing the *kinetic* energy of any *motion* violating the condition to increase without limit. In this case one or more periods become infinitely large, but the finite periods are ultimately the same as those arrived at when the potential energy is increased, although in one case the periods have been throughout increasing, and in the other diminishing. This example shows the necessity of making the alterations by steps; otherwise we should not understand the correspondence of the two sets of periods."

This exposition serves to explain the fact, at first sight paradoxical in the light of Rayleigh's second theorem, that a "constraint" may be regarded as the limit either of an added elasticity or of an added mass;* but it does not as it stands explain a further paradox which is presented in the theory of transverse vibrations of bars. As Lord Rayleigh remarked (but without further comment),† the natural frequencies of a uniform bar of which both ends are "clamped" (i.e. constrained both in position and direction) are identical with the natural frequencies of the same bar when both ends are completely free: the first four are given by

$$l\sqrt{\frac{mp^2}{B}} = \mu = 4{\cdot}7300408,\quad 7{\cdot}8532046,\quad 10{\cdot}9956078,\quad 14{\cdot}1371655 \qquad (76)$$

---

* "Whether the constraint is effected by making infinite the kinetic energy of any motion, or the potential energy of any displacement, which violates it, makes no difference to the vibrations which remain. In the first case one vibration becomes infinitely slow and in the second case one becomes infinitely quick." (Rayleigh, 1896, §92*a*.)

† Rayleigh (1896, §172).

(l denoting the length of the bar, B its flexural rigidity, and m its mass per unit length), whereas in the case where both ends are "simply supported" (i.e. fixed in position but not in direction) they are given by

$$\mu = \pi \times (1, 2, 3, 4) = 3\cdot14159, \quad 6\cdot28318, \quad 9\cdot42477, \quad 12\cdot56637. \tag{77}$$

Thus the effect of imposing terminal supports (preventing displacement) on a bar initially free has been (apparently) to *lower* the frequencies from (76) to (77).

24. If in the manner of Lord Rayleigh we picture a continuous modification whereby the simply supported bar is converted into one of which both ends are clamped, his explanation quoted above will serve to explain the change of frequencies from (77) to (76). For by opposing an increasing elastic resistance to the terminal slopes we shall raise all frequencies in accordance with the theorem stated at the beginning of § 23, whereas by adding at each end an increasing rotatory inertia we shall lower all frequencies in accordance with § 6: in the first instance two of the initial frequencies will have become infinite, and in the second instance two will have become zero, when conditions of complete clamping have been attained and two degrees of freedom have accordingly been lost. Both processes are in fact easy to follow in calculation. Figure 1 relates the frequency parameter μ with (a) the terminal elastic resistance and (b) the added rotational inertia, the relevant formulae being

$$\left.\begin{aligned}
&\text{in } (a)\\
&\frac{4B}{Kl} = -(\tan\alpha + \tanh\alpha)/\alpha \text{ for the first, third, ... etc. (symmetrical) modes,}\\
&\qquad = (\cot\alpha - \coth\alpha)/\alpha \text{ for the second, fourth, ... etc. (anti-symmetrical) modes,}\\
&\text{in } (b)\\
&\frac{ml^3}{4I} = \alpha^3(\tan\alpha + \tanh\alpha) \text{ for the first, third, ... etc. (symmetrical) modes,}\\
&\qquad = -\alpha^3(\cot\alpha - \coth\alpha) \text{ for the second, fourth, ... etc. (anti-symmetrical) modes,}
\end{aligned}\right\} \tag{78}$$

where $\alpha = \frac{1}{2}\mu$ as defined in (76) and (77), and K is the elastic restoring couple per radian of terminal slope. Abscissae represent μ and ordinates the corresponding values of Kl/B and I/ml^3 as calculated from (78).

25. If on the other hand we picture a continuous modification whereby a bar with both ends free is converted into one of which both ends are simply supported, then (according to §23) the argument would seem to run as follows: Terminal displacements may be opposed either (*a*) by an increasing elastic resistance or (*b*) by increasing inertia, and in either method the terminal slopes are left unrestrained: adopting (*a*) we shall raise every frequency until two have become infinite, adopting (*b*) we shall lower every

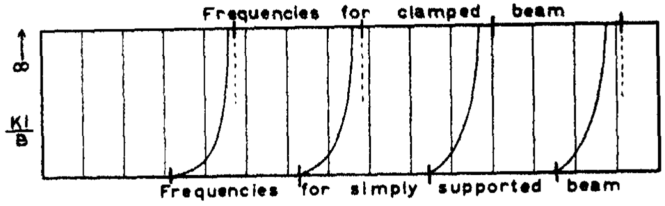

FIGURE 1(*a*)

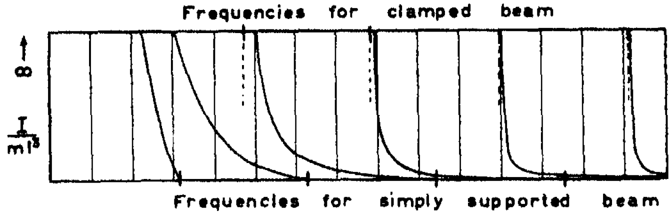

FIGURE 1(*b*)

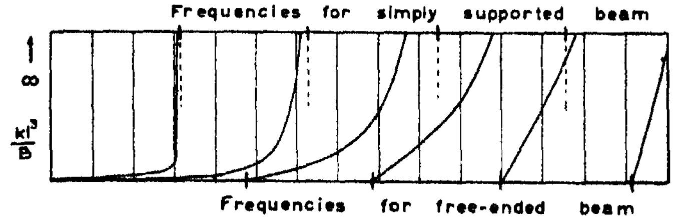

FIGURE 2(*a*)

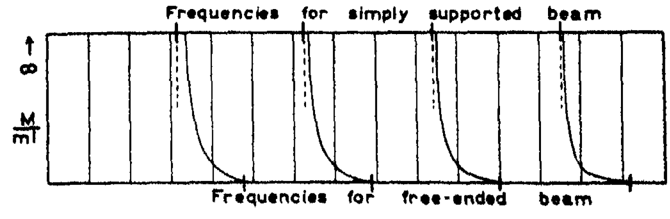

FIGURE 2(*b*)

frequency until two have become zero, by the time that conditions of complete "support" have been attained and two degrees of freedom have been lost. When however we test this argument by calculation, we find in fact that no frequencies are brought to zero under conditions of simple support. Figure 2 relates the frequency parameter μ with (a) the elastic resistance and (b) the added inertia, the relevant formulae being

$$\left.\begin{aligned}
&\text{in } (a)\\
&\frac{kl^3}{4B} = \alpha^3(\tan\alpha + \tanh\alpha) \text{ for the first, third, ... etc. (symmetrical) modes,}\\
&\qquad = -\alpha^3(\cot\alpha - \coth\alpha) \text{ for the second, fourth, ... etc. (anti-symmetrical) modes,}\\
&\text{in } (b)\\
&\frac{4M}{ml} = -(\tan\alpha + \tanh\alpha)/\alpha \text{ for the first, third, ... etc. (symmetrical) modes,}\\
&\qquad = (\cot\alpha - \coth\alpha)/\alpha \text{ for the second, fourth, ... etc. (anti-symmetrical) modes,}
\end{aligned}\right\} \quad (79)$$

where $\alpha = \frac{1}{2}\mu$ as before. M denotes the (*non-rotatory*) terminal inertia, and k the elastic restoring force per unit of terminal displacement.*

26. Thus the argument of §25 fails in relation both to (a) and (b). As to (a), it is the fact that all frequencies increase steadily with the terminal elastic resistance, but what makes this possible is the appearance of two new frequencies which vanish with the spring constant k and so (apparently) should be added to the sequence (76); and as to (b), although with increasing terminal inertia all frequencies decrease steadily, yet none come to zero as predicted, therefore none (in Rayleigh's sense) are "lost".

This last result is not surprising, because strictly speaking the freedom of a system is not altered by a mere addition of mass; and it can be reconciled with figure 2 (a), because there the loss of two frequencies which become infinite is offset by the introduction of two that have no counterpart in figure 2 (b). But before this can be taken as an explanation it must be shown that the new frequencies are in fact excluded by the conditions of figure 2 (b). If they are, then by opposing elastic resistance to terminal displacement we have merely replaced one type of restriction by another, and it will follow that the bar has a like degree of freedom whether its ends be simply supported or entirely free. The conclusion will be acceptable, since it evidently can make no difference to the final conditions whether they have been attained by process (*a*) or (*b*).

---

* We observe that m/I in figure 1 equals k/B in figure 2, K/B in figure 1 equals m/M in figure 2.

27. When α is made very small in (79), the expressions for $kl^3/4B$ tend to equality with $2\alpha^4$ and $2\alpha^4/3$, respectively, for the first and second mode: this means that very weak springs permit vibrations in which (α being small) the bar is almost unstrained. But in the absence of spring constraints such vibrations are excluded for the reason that *they are incompatible with the conservation of momentum.* Here then we have the two restrictions,* operative when the bar is free, which under the conditions of figure 1 (*a*) are exchanged for two restrictions of another type (zero terminal slope). Preventing terminal displacements, we reduce the number of displacements which remain to be varied; but (because constraints entail external forces) we are no longer required to satisfy the momentum equations, and on that account the two lost "freedoms" are restored.

28. Reverting to § 23, it seems permissible to conclude that the paradox there presented is due to a neglect in Lord Rayleigh's argument of the principle of momentum. Being based solely on the energy equation (7), his generalized treatment of vibrations disregards that principle throughout: yet it is easy to see (by considering a system of restricted freedom) that conservation of momentum implies one relation between the displacements, conservation of angular momentum another. *Any relation imposed on the displacements will restrict the freedom of a system, therefore according to Rayleigh's principle will tend to raise the frequencies*; and it happens that the relations which are imposed by momentum conditions in the case of a uniform bar completely free have exactly the same effect as the relations imposed by "clamps" which prohibit terminal slopes.

SUMMARY

On the basis of a theorem due to Lord Rayleigh and relating to the effect on the natural frequencies of an added mass, methods are developed whereby lower limits can be imposed upon the frequencies of a specified system. Since upper limits can be imposed on the basis of "Rayleigh's principle", information so obtained is for practical purposes of equal value with an exact solution.

---

* Both linear and angular momentum must be conserved in the motion of a bar completely free.

The methods can be applied as an extension of the "relaxation" technique, and it is then that their value is revealed most clearly. In this paper attention is confined to continuous systems governed by differential equations, and for these, incidentally, a method is developed whereby specially close estimates of the fundamental frequency can be made if desired.

The concluding section of the paper is concerned with the resolution of a paradox presented by Lord Rayleigh's theorem regarding the effect of a constraint.

REFERENCES

Bradfield, K. N. E., Christopherson, D. G. and Southwell, R. V. 1939 *Proc. Roy. Soc.* A, **169**, 289–317.

Duncan, W. J. and Lindsay, D. D. 1939 *Aero. Res. Comm.* typed report no. 4207: *Methods for calculating the frequencies of overtones.*

Rayleigh, Lord 1896 *Theory of sound*, 2nd ed. Macmillan and Co.

Southwell, R. V. 1936 *Introduction to the theory of elasticity.* Oxford Univ. Press.

Temple, G. and Bickley, W. G. 1933 *Rayleigh's principle.* Oxford Univ. Press.

The lattice spacings of the primary solid solutions of silver, cadmium and indium in magnesium

BY GEOFFREY VINCENT RAYNOR

(*Communicated by W. Hume-Rothery, F.R.S.—Received* 27 *September* 1939)

1. INTRODUCTION

In 1934 Hume-Rothery, Mabbott and Channel-Evans discussed the factors affecting the formation of primary solid solutions in silver and copper, and concluded that the predominant factors were the atomic diameters and valencies of the solvent and solute elements. In a later paper (Hume-Rothery and Raynor 1938) it was shown that the same considerations applied to the formation of solid solutions in magnesium, provided that due allowance was made for the highly electropositive nature of this metal.

In the case of copper and silver alloys, where general valency effects are marked (Hume-Rothery *et al.* 1934), Hume-Rothery, Lewin and Reynolds (1936) carried out an investigation of the mean lattice spacings of primary solid solutions of cadmium, indium, tin and antimony in silver, and of zinc, gallium and germanium in copper. It was found that, to a high degree of accuracy, equal percentages of cadmium, indium, tin and antimony expanded the lattice of silver by amounts proportional to 2 : 3 : 4 : 6 respectively. Zinc, gallium and germanium in equal atomic concentration in copper expanded the copper lattice by amounts proportional to 3 : 4 : 4·8. These factors have been confirmed by Owen and Roberts (1939) and shown also to apply at high temperatures. The factor for germanium in copper was, however, given as 5.

In the present paper, an investigation has been made of the mean lattice spacings of the primary solid solutions of silver, cadmium and indium in magnesium. The solute elements are all of favourable size factor with regard to magnesium, and, though not in the same period as the solvent, are themselves in one period.

Particular interest attaches to the present series in so far as silver and indium have respectively one less and one more valency electron per atom than magnesium, while the valency of cadmium is the same as that of magnesium. The effect of a diminution of electrons on the lattice spacing may therefore be compared with the effect of an increase.

A further point of interest is that, whereas in the work of Hume-Rothery *et al.* (1936) on copper and silver alloys the mean lattice distortions corresponded with an expansion, the lattice of magnesium is contracted by silver, cadmium and indium.

In this paper the term "mean lattice distortion" is used to denote the differences between the lattice constants of the solid solution and the solvent metals as measured by the ordinary powder methods of X-ray analysis. The X-ray methods, as is well known, give the mean lattice distortions, while more or less intensely localized regions of distortion may occur without preventing the formation of sharp diffraction lines. The data described below refer to the mean lattice spacings only.

2. GENERAL EXPERIMENTAL PROCEDURE

A satisfactory technique for the preparation of filings of reactive metals and alloys has been described elsewhere (Raynor and Hume-Rothery 1939). For the present purpose a modification of this method was employed, which gave filings for which the totals of the two constituents determined by analysis were satisfactory. Alloys were annealed for a sufficient time in the lump form to ensure the attainment of equilibrium, after which filings were prepared in an atmosphere of argon and sealed up in an evacuated hard glass tube without exposure to the atmosphere at any point. The filings were annealed in the evacuated tube to relieve the mechanical strain introduced by filing, and the tube rapidly cooled in air.* The tube was broken in an atmosphere of argon and the fine filings separated by sieving through a 250-mesh gauze. The filings in the sieve were well agitated in order to secure a representative sample. After sufficient fine filings had collected, the remainder were sealed up in an evacuated glass tube for analysis and the fine filings tipped immediately into a watch-glass containing Canada balsam dissolved in xylol. The whole operation up to the release of the fine filings was carried out in argon or *in vacuo*, so that there was no exposure to the atmosphere. Tests showed that the compositions by analysis of the sieved and unsieved filings were identical, so that in general the unsieved residues were used for analysis.

In the analyses both metals were always determined as a check on contamination. The figures given are based, therefore, on the analysis of the filings after all annealing treatments had been completed, that is, in the condition in which they were used in the X-ray experiments, and not on analyses of the alloy in lump form. In view of the volatility of magnesium during annealing, and of possible segregation effects, such precautions are essential to obtain reproducible results.

The lattice constants were determined from Debye-Scherrer photographs obtained with a 19 cm. camera of the type, though on a larger scale, used by Bradley and Jay (1932), in conjunction with a demountable X-ray tube made by the Metropolitan Vickers Electrical Co., Ltd.

The temperature of the camera during an exposure of 2–3 hr. duration was accurately controlled by the use of currents of air, and remained constant.

The camera was standardized against quartz as recommended by Bradley and Jay (1933), whose $\cos^2\theta$ extrapolation method was used throughout the work in order to eliminate errors due to absorption, film shrinkage, eccentricity of the specimen, etc. For the standardization copper radiation was used, since this radiation was to be used for the alloy experiments; the values of the wave-lengths assumed were $\mathrm{Cu}_{K\alpha1}$ 1·537395 A and $\mathrm{Cu}_{K\alpha2}$ 1·541232 A. The fundamental constants assumed in the calibration for quartz at 27° C were $a = 4{\cdot}24653$ A and $c/a = 1{\cdot}09996(5)$. The standard angle of the camera, as given by shadows of the fixed knife-edges, corresponded with an angle of 84·302° in the Bragg equation.

The films were measured on an accurately calibrated measuring microscope which read directly to 0·01 mm. and allowed estimation to

---

* For the magnesium-silver alloys the procedure was different, and is described later.

0·001 mm. Duplicate photographs of the same specimen gave results agreeing within 0·0001 A when allowance had been made for the differences in temperature of the exposures. For this purpose it was assumed that the coefficients of expansion in the dilute alloys were the same as those of magnesium. The values of the lattice spacing quoted in the paper have been reduced to a common temperature of 20° C.

Copper radiation was chosen for the alloy experiments because it gave a very suitable combination of high-angle lines, which are important for the accurate spacing determinations. In general, the lattice spacing determinations were based upon the measurement of the seven outermost lines, the line with the highest angle of reflexion being due to the (11·0) 2 reflexion, and independent of axial ratio. From the first line, therefore, was obtained an accurate and invariant first point on the Bradley-Jay extrapolation curve. The (10·6) and (20·5) reflexions with high values of "l" are very sensitive to slight variations in the axial ratio; a difference of 0·0001 in the axial ratio produces a very marked difference in the points for these lines on the extrapolation curve. Thus, by a process of successive approximation, the value of c/a for a particular film was established to a high degree of accuracy; it is estimated that the extreme error involved in the determination of the axial ratio is ± 0·0001.

The values of the "a" parameter deduced directly from the extrapolation curves are accurate to within ± 0·0001 A, so that the values obtained for the "c" parameter, involving the determination of c/a, are accurate to within ± 0·0003 A.

3. MATERIALS USED

The magnesium was presented by the National Physical Laboratory and was 99·95 % pure, the chief impurities being iron (0·03 %), silicon (0·01 %) and aluminium (0·01 %). The silver was chemically pure, and was supplied by Messrs Johnson, Matthey and Co., Ltd., while spectroscopically pure cadmium was presented by the National Smelting Co., Avonmouth. The indium, supplied by the Indium Corporation of America, was refined by Messrs Johnson, Matthey and Co., Ltd., after which no impurities could be detected by chemical means.

4. EXPERIMENTAL RESULTS

(a) *Pure magnesium*

Four separate determinations of the lattice spacings of pure magnesium gave the axial ratio at 20° C as 1·6237, while the values of the "a" parameter were respectively 3·20250, 3·20253, 3·20250 and 3·20258 A. During a previous investigation of the thermal expansion of magnesium (Raynor and Hume-Rothery 1939), the values of "a" at room temperature (20° C) obtained lay between the limits 3·20253 and 3·20263 A. The results of the two investigations, carried out using two different cameras which were separately calibrated, are therefore in complete agreement, while both are in agreement with the value 3·2030 A at 25° C (= 3·20258 at 20° C) obtained by Jette and Foote (1935).

(*b*) *Magnesium-silver*

The alloys were prepared under flux by melting together the constituent metals, and, after thorough stirring, pouring into a heavy copper mould. Owing to the restricted solid solubility of silver in magnesium at low temperatures, the general procedure was modified. The ingots were annealed to equilibrium at 468° C, which is near to the eutectic temperature, and quenched. The filings, prepared as already described, were sealed for the strain-relieving anneal into *silica* bulbs, with a wall thickness of ⅓ mm., and again annealed at 468°, and quenched in water. The lines on the photographs were sharp, showing that 1 hr. annealing at 468° C was sufficient to relieve the mechanical strain. The results are shown in table 1 and the "a" parameters plotted graphically in figure 1. The points lie on a smooth curve from which no point differs by more than 0·0002 A; the curve is definitely not linear, the mean lattice contraction as the percentage of silver is increased, becoming less than that required by a linear relation.

TABLE 1

Alloy no.	Composition		Lump anneal	"a" spacing in A at 20° C	c/a at 20° C	"c" spacing in A at 20° C
	Wt. % Ag	At. % Ag				
1	3·19	0·74	10 days 468° C	3·1980 (0)	1·6238	5·1929 (1)
2	6·89	1·67	10 days 468° C	3·1916 (5)	1·6223	5·1778 (1)
3	9·49	2·31	10 days 468° C	3·1893 (3)	1·6217	5·1721 (4)
4	13·45	3·38	10 days 468° C	3·1842 (6)	1·6210	5·1616 (9)

The axial ratio for this system appears to increase slightly in very dilute solution, this increase being followed by a very rapid fall in c/a. The film for alloy 1 was of a high quality, and the increase in axial ratio from that of magnesium, though slight, is definite. The "c" parameters and the volume of the unit cell are plotted in figures 2 and 3 respectively.

(c) *Magnesium-cadmium*

Alloys were prepared by melting the constituent metals under flux and casting into copper moulds. Since the solubility of cadmium in magnesium is wide, quenching was unnecessary, and the tubes of annealed filings were cooled in air. To remove filing-strain the filings were in general annealed for 10–12 hr. at 310° C; the subsequent X-ray photographs gave sharp diffraction lines.

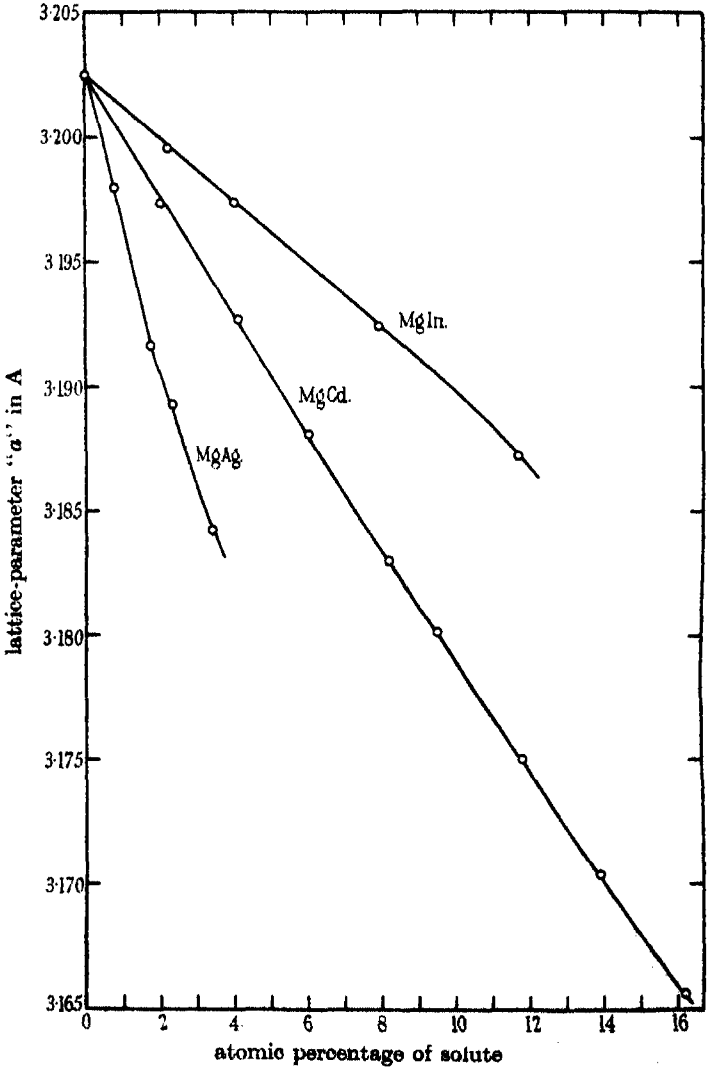

FIGURE 1

The results obtained are given in table 2 and plotted in figures 1–3. It will be seen in figure 1 that a smooth curve may be drawn through the points, from which no point differs by more than 0·0002 A. Again the curve is definitely not linear, although the linearity of the initial portion persists up to comparatively high concentrations of cadmium. Above 10 atomic %, however, the curve shows that the contraction is progressively less than that corresponding with a linear relation.

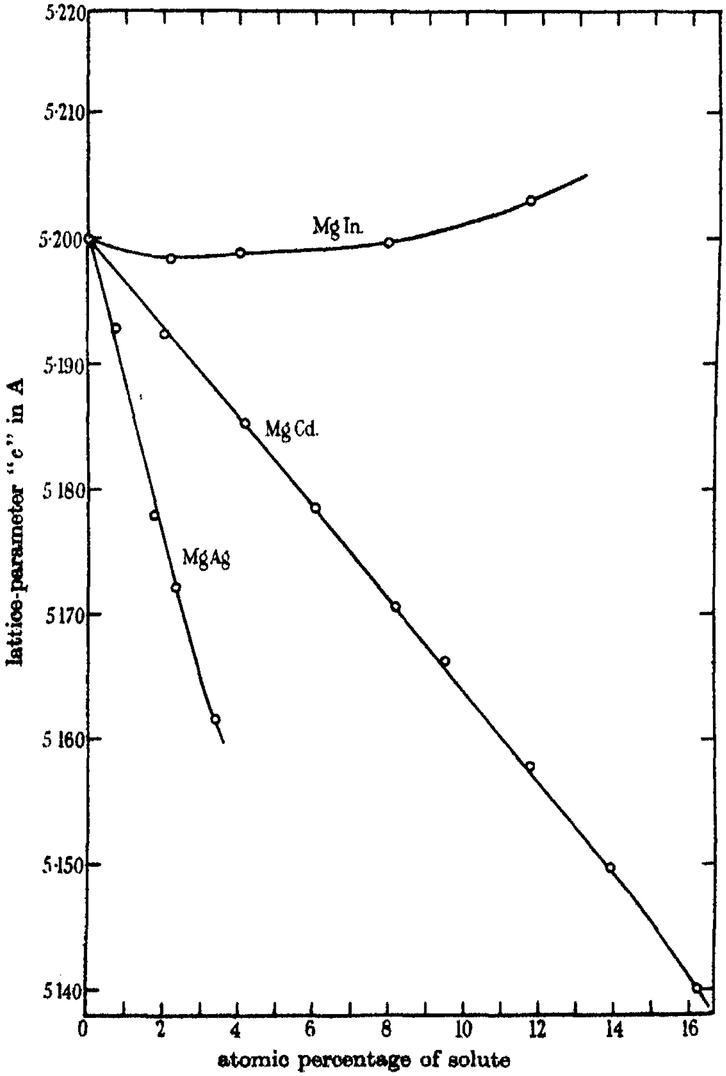

FIGURE 2

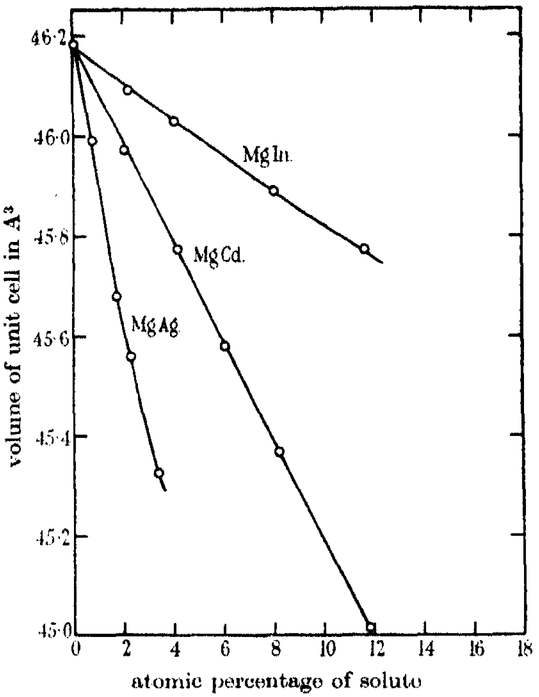

FIGURE 3

TABLE 2

Alloy no.	Composition		Lump anneal	"*a*" spacing in A at 20° C	*c*/*a* at 20° C	"*c*" spacing in A at 20° C
	Wt. % Cd	At. % Cd				
1	8·52	1·98	11 days 494° C	3·1972 (8)	1·6239	5·1920 (6)
2	16·71	4·16	11 days 494° C	3·1927 (2)	1·6241	5·1852 (9)
3	22·89	6·04	13 days 501° C	3·1880 (8)	1·6243	5·1784 (0)
4	29·24	8·205	11 days 494° C	3·1829 (7)	1·6245	5·1707 (3)
5	32·67	9·50	13 days 501° C	3·1801 (5)	1·6246	5·1664 (7)
6	38·16	11·78	11 days 494° C	3·1750 (5)	1·6245	5·1578 (7)
7	42·73	13·90	17 days 501° C	3·1704 (2)	1·6243	5·1497 (1)
8	47·20	16·20	18 days 494° C	3·1656 (0)	1·6237	5·1399 (8)

Previous investigators (Natta 1928; Dehlinger 1930) have suggested that the axial ratio of the structure for the magnesium-rich alloys is constant. The present work, however, in which small variations in the axial ratio are accurately determinable, shows that there is a regular though slight increase in the axial ratio until a composition of 10 atomic % is reached. After this there is a marked fall in c/a, until at 16 atomic % the axial ratio for magnesium has again been reached. This behaviour is probably connected with the existence of the superlattice Mg_3Cd. The work of Grube and Schiedt (1930) on the equilibrium diagram of the system shows that the area occupied by this superlattice extends, on the magnesium-rich side of Mg_3Cd, to 16 atomic % cadmium at 100° C. Although no superlattice lines could be detected on the photographs in the present work, other work has shown that the superlattice rearrangement occurs at room temperature. It is probable that the ordering process is beginning to occur in the region 10–16 atomic % cadmium, with a consequent diminution in the strain attendant on solid solution of cadmium in magnesium. As the strain is diminished, the axial ratio would be expected to revert towards that of magnesium.

TABLE 3

Alloy no.	Composition Wt. % Cd	 At. % Cd	"a" spacing at 353° C	c/a at 353° C	"c" spacing at 353° C
1	8·52	1·98	3·2280 (0) A	1·6243	5·2432 (4) A
2	16·71	4·16	3·2242 (0) A	1·6244	5·2373 (9) A

Two alloys, during the course of the work, were exposed in a high temperature camera at 353° C, and the results are shown in table 3. The lattice-constants of magnesium at 353° C are $a = 3{\cdot}2320$ (0) A and $c/a = 1{\cdot}6242$ (4), so that, at 353° C, both the lattice spacing and the axial ratio changes are less marked than at room temperature.

(*d*) *Magnesium-indium*

The alloys for this investigation were prepared by the addition of magnesium to stock alloys, richer in indium, which had been prepared in connexion with previous work. As before, the newly prepared alloys were cast in copper moulds.

To remove the strain introduced by filing, the filings were annealed before use for 10–12 hr. at 310° C, and the tube cooled in air.

The results of the work are shown in table 4 and graphically in figures 1–3. Again it will be seen that a smooth curve may be drawn in figure 1 such that no point differs from it by more than 0·0001 A. The curve appears to be at first linear and then to fall very slightly. The change of axial ratio with composition is in this case large, compared with the effects in the magnesium-silver and magnesium-cadmium systems, and in contrast to these systems the "c" parameter first decreases slightly and then rises.

TABLE 4

Alloy no.	Composition Wt. % In	Composition At. % In	Lump anneal	"a" spacing in A at 20° C	c/a at 20° C	"c" spacing in A at 20° C
1	9·45	2·16	11 days 497° C	3·1995 (5)	1·6247	5·1983 (1)
2	16·46	4·01	11 days 497° C	3·1973 (7)	1·6260	5·1989 (2)
3	29·04	7·98	11 days 497° C	3·1924 (5)	1·6287	5·1995 (4)
4	38·35	11·65	11 days 497° C	3·1872 (4)	1·6325	5·2031 (7)

(e) *Analysis*

In all cases the actual filings were submitted for analysis. The analyses were all made by Messrs Johnson, Matthey and Co., Ltd., and satisfactory totals of the two constituents were reported.

5. DISCUSSION

The curves of figure 1 indicate that a definite valency effect exists for the contraction of the "a" parameter of magnesium by silver, cadmium and indium. At equiatomic compositions decreasing the valency of the solute increases the lattice distortion in the basal plane.

The atomic percentages of indium and cadmium in alloys of equal lattice distortion vary as $1 : \frac{1}{2}$. In the case of silver, owing to the restricted solubility in magnesium, the test is less satisfactory, but the corresponding factor is very close to $\frac{1}{5}$. This implies that, in dilute solution where the lattice spacing-composition curves may be taken as straight lines, the lattice distortions per atom of indium, cadmium and silver are in the ratio of 1 : 2 : 5. Thus, if the lattice spacings of the three alloy systems are plotted against the atomic percentages of the solutes multiplied by the above factors, the points should lie on a single curve. This has been done in figure 4, where each point is represented by a rectangle whose height is equivalent to 0·0004 A and the width to 0·1 atomic %. These limits represent errors of about ± 1 part in 20,000 for the lattice spacing and ± 0·05 atomic % on the composition axis. The agreement with the whole number relation for cadmium and indium in dilute solution is therefore very exact, although separation occurs later owing to the downward curvature of the curve for magnesium-indium.

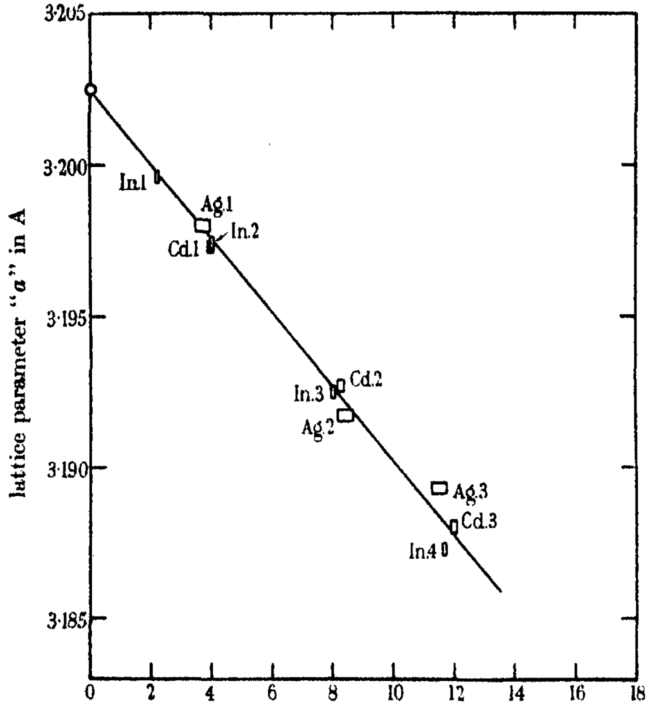

FIGURE 4

For silver, in dilute solution only, the factor 5 is within the limits of the experimental error. Assuming the factor for indium to be 1, those for cadmium and silver cannot lie outside the limits 2·1 and 1·9 or 5·2 and 4·9 respectively, without producing marked separation of the points.

The closest distances of approach of the atoms in the crystals of metallic cadmium and indium are closely similar when allowance is made for incomplete ionization of indium in the elementary state, so that if we accept the views of Hume-Rothery *et al.* (1934), the size factors for these metals in magnesium $\left(\text{i.e. } \frac{\text{A.D. solute} - \text{A.D. magnesium}}{\text{A.D. magnesium}}\right)$ are almost identical.* Thus it is improbable that size effects greatly influence the relative lattice distortions produced by cadmium and indium; the difference in behaviour may be attributed to the higher valency of indium. We may regard the substitution of indium for cadmium, involving the addition of 1 electron per atom, as causing a lattice expansion in the basal plane relative to the magnesium-cadmium distortion curve. Similarly, the substitution of silver for cadmium, involving the subtraction of one electron per atom, causes an additional contraction relative to the magnesium-cadmium curve. This confirms a principle deduced from studies of copper and silver alloys, that the distortion produced is the resultant of a size effect, which may be an expansion or contraction according to the relative atomic diameters of solute and solvent, and of an electronic effect in which an increase in the solute valency causes an expansion.

---

* The work of Hume-Rothery *et al.* showed that, from the point of view of solid solution formation, the interatomic distances in the crystals of the elements furnished a better correlation than the Goldschmidt atomic radii.

The factors may be expressed as $1 + (3 - \text{valency of solute})^2$.

Figure 2 shows that the same tendency affects the curves for the "c" parameters, but that the regularity is absent. The "c" parameter for the magnesium-silver alloys is contracted more than that in the magnesium-cadmium alloys; for the magnesium-indium system the "c" parameter falls slightly in very dilute solution and then rises, so that there is a marked distinction between the alloys in which the number of electrons per atom is equal to or less than two, and those in which the number exceeds two.

The curves of the volume of the unit cell plotted against composition (figure 3) show that the contraction of the cell at equiatomic percentages of indium, cadmium and silver are approximately in the ratio of 1 : 3 : 9. These factors may be expressed as $1 + 2\,(3 - \text{valency of solute})^2$.

The effects in the magnesium series of alloys may be interpreted qualitatively in terms of the electron energy distribution in the crystals. The form of the first Brillouin zone for the close-packed hexagonal structure has been derived by Jones (1934) and is shown in figure 5. There is an energy discontinuity across each of the bounding planes A, B and C, but the discontinuity vanishes for electrons moving with velocities in certain directions along edges such as PQ. The complete first zone is therefore made up of the figure bounded by planes of the type A, B and C with the addition of a small truncated prism, as shown on one A face, on each of the six A faces. The number of electrons per atom contained in the incomplete zone bounded by A, B and C type planes is 1·743 for magnesium. Since magnesium is divalent, there must be overlap into higher zones; the theory indicates that this overlap takes place at A and at corners such as QP. With two electrons per atom there is no overlap at the B positions.

Jones (1934) has considered the effect of an internal stress in crystals due to a small number of electrons lying beyond a plane of energy discontinuity in k-space. Essentially, the theory predicts that electrons lying beyond such a plane produce a stress, perpendicular to the plane and proportional to the number of overlapping electrons, tending to displace the plane towards the origin of k-space. Since the value of k at such a plane is inversely proportional to the lattice parameter in the corresponding direction in the crystal, this results in a tendency to expand the lattice in this direction.

If we now consider the distortion curves for the magnesium-cadmium system as standards depending mainly on size effects, and not on valency, we may interpret the magnesium-indium curves. Substitution of a trivalent atom for a divalent atom increases the number of electrons per atom for the structure. This leads to an increased overlap round the sides of the zone. The stress in a direction perpendicular to the hexagonal axis is thus increased, leading to a lattice expansion in the basal plane relative to the size effect. In very dilute solution "c" also decreases less than in the magnesium-cadmium system. It is possible that, as the number of electrons per atom increases, overlap begins at B, and that this is responsible for the subsequent increased expansion of the "c" parameter as shown in figure 2, and for the relatively rapid rate at which the axial ratio rises in the magnesium-indium alloys.

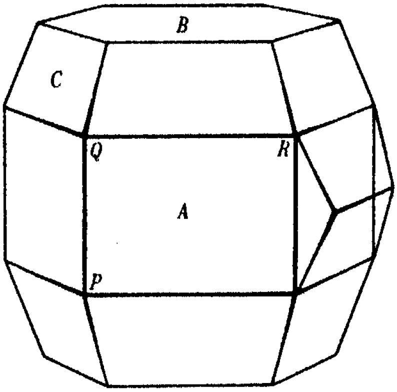

FIGURE 5

Similarly, for magnesium-silver the overlap of electrons is decreased, so that the stresses in the basal plane are reduced, leading to a contraction of the "a" parameter as compared with the standard contraction in the magnesium-cadmium system.

It is probable that the fact that the valency of the solute affects mainly the overlap of electrons round the sides of the Brillouin zone (perpendicular to the hexagonal axis), and not the overlap at the B position (parallel to the hexagonal axis), accounts for the observance of clear numerical factor effects for the "a" parameter and not for the "c" parameter.

The equation given by Jones relating the strain produced to the increase in the number of electrons per atom gives results of the right order for the η-phase in the system copper-zinc, but for magnesium solid solutions it would indicate a much greater expansion for the magnesium-indium alloys relative to the magnesium-cadmium system than actually occurs.

This is probably due to the fact that, for a system such as copper-zinc, where the number of electrons per atom for the structure is less than two, the overlap perpendicular to the hexagonal axis probably occurs mainly in the A positions. For magnesium-indium, however, where the number of electrons per atom increases from two, the increase in overlap is probably confined mainly to the overlap into the second zone along the six edges such as PQ, and the stress conditions will be different from the case considered by Jones.

The author expresses his gratitude to Professor C. N. Hinshelwood, F.R.S., for his kindness in providing laboratory accommodation; to Dr W. Hume-Rothery, F.R.S., in whose laboratory the work was carried out, for helpful criticism; and to the Department of Scientific and Industrial Research for a Senior Research Award. Grateful acknowledgement is also made to the Government Grants Committee of the Royal Society for a grant towards the expenses of analysis, and to the Aeronautical Research Committee and The Imperial Chemical Industries, Ltd., for other assistance. Thanks are also due to Mr A. R. Powell of Messrs Johnson, Matthey and Co., Ltd., for his care in connexion with the analytical work.

SUMMARY

Accurate measurements have been made of the lattice spacings of the primary solid solutions of silver, cadmium and indium in magnesium. At equiatomic compositions, decreasing the valency of the solute increases the lattice distortion in the basal plane. In dilute solution, indium, cadmium and silver contract the "a" parameter by amounts proportional to 1 : 2 : 5 respectively, while the volume of the unit cell is contracted by amounts proportional to 1 : 3 : 9 respectively. The "a"-parameter factors may be expressed as $1+(3-\text{valency})^2$ and the volume factors as $1+2(3-\text{valency})^2$. There is no such regularity for the "c" parameters.

The results may be interpreted qualitatively in terms of the Brillouin zone theory of metals.

REFERENCES

Bradley, A. J. and Jay, H. 1932 *Proc. Phys. Soc.* **44**, 563.
— — 1933 *Proc. Phys. Soc.* **45**, 507.
Dehlinger, U. 1930 *Z. anorg. Chem.* **194**, 223.
Grube, G. and Schiedt, E. 1930 *Z. anorg. Chem.* **194**, 190.
Hume-Rothery, W., Mabbott, G. W. and Channel-Evans, K. M. 1934 *Phil. Trans.* A, **233**, 1.
Hume-Rothery, W., Lewin, G. F. and Reynolds, P. W. 1936 *Proc. Roy. Soc.* A, **157**, 167.
Hume-Rothery, W. and Raynor, G. V. 1938 *J. Inst. Metals*, **63**, 227.
Jette, E. R. and Foote, F. 1935 *J. Chem. Phys.* **3**, 605.
Jones, H. 1934 *Proc. Roy. Soc.* A, **147**, 400.
Natta, G. 1928 *Ann. Chim. Appl.* **18**, 135.
Owen, E. A. and Roberts, E. W. 1939 *Phil. Mag.* (7) **27**, 294.
Raynor, G. V. and Hume-Rothery, W. 1939 *J. Inst. Metals*, **65** (in the Press).

The equilibrium and lattice-spacing relations in the system magnesium-cadmium

BY W. HUME-ROTHERY, F.R.S., AND G. V. RAYNOR

(*Received* 23 *November* 1939)

1. INTRODUCTION

The alloys of magnesium and cadmium are of great interest, since both metals have the same valency, and almost the same atomic volume, but the axial ratios of their close-packed hexagonal structures differ markedly, being 1·885(2) for cadmium, and 1·6237 for magnesium. The equilibrium diagram of the system has always attracted great interest, and very conflicting results have been obtained by different investigators. The earlier investigations led to the conclusion that the liquidus and solidus curves were very close together, and fell continuously from the melting point of magnesium to that of cadmium, so that, at the higher temperatures, a continuous solid solution was formed, which, at low temperatures, underwent a transformation in the region of 50 atomic % of cadmium, owing to the supposed existence of a compound MgCd. The work of Hume-Rothery and Rowell (1927) confirmed the existence of this transformation, and later work (Grube and Schiedt 1930; Dehlinger 1930; Riederer 1937) showed that this transformation corresponded to the formation of a superlattice based on the composition MgCd, and that at low temperatures two other superlattices, based on the compositions $MgCd_3$ and Mg_3Cd, were also formed. These low temperature transformations were securely established, and all investigations indicated the existence of wide solid solutions in both magnesium and cadmium, but the remainder of the system has been in great dispute. According to Hume-Rothery and Rowell, magnesium could hold approximately 60 atomic % of cadmium in solid solution, and cadmium could dissolve approximately 24 atomic % of magnesium, whilst, between these two solid solutions, a compound $MgCd_2$ of fixed composition was formed by a peritectic reaction. Grube and Schiedt (1930) qualitatively confirmed the limits of the primary solid solutions, but not the existence of the compound $MgCd_2$, and, apart from the superlattice transformations, their equilibrium diagram showed the two primary solid solutions separated by a two-phase region. Dehlinger (1930) stated that his X-ray investigations confirmed the diagram of Grube and Schiedt, but a careful examination of his powder photographs shows that they are really inconclusive, since, with varying compositions, lines appear and disappear in a way which is consistent with the existence of $MgCd_2$. Riederer (1937) concluded that the diagram of Hume-Rothery and Rowell represented stable equilibrium, and that of Grube and Schiedt metastable equilibrium. The present investigation has succeeded in explaining these apparent inconsistencies, and has also shown interesting relations between the two types of crystal structure, which may be interpreted in terms of the Brillouin zone theories.

2. MATERIALS USED

The magnesium used in the present investigation was kindly presented by the National Physical Laboratory, and was of 99·95 % purity, the principal impurities being iron (0·03 %), silicon (0·01 %), and aluminium (0·01 %). The cadmium was spectroscopically pure, and was from two batches of metal kindly presented by the New Jersey Zinc Company and the National Smelting Company Ltd., respectively.

3. MICROSCOPIC INVESTIGATION

The part of the diagram in dispute was in the region 60–80 atomic % of cadmium, and in the first part of the present work a series of thirteen alloys was prepared in the range 58–78 atomic % cadmium. These alloys were melted under flux, and cast into heavy copper moulds, so as to give cylindrical ingots ¼ in. in diameter, which were at once sealed in evacuated glass tubes, and annealed for 1 month at 310° C. The tubes were then cooled in a blast of air, since the experience of Hume-Rothery and Rowell suggested that quenching in water was responsible for the development of cracks. After this treatment, alloys 58 and 60,* on etching with dilute alcoholic nitric acid, showed large homogeneous crystals, and a similar structure was shown by alloys 76 and 78, the structure of these last two alloys being developed by mere exposure to the atmosphere. Alloys 62, 66, 67, 68, 70 and 71 were also attacked by the atmosphere, and their microstructures showed large homogeneous crystals with localized patches of a substance which at first appeared grey upon a light background, but on further exposure underwent a colour reversal, and became the lighter constituent against a dark background. This substance existed mainly at the surface of the specimen, and in the vicinity of cracks, and was undoubtedly the supposed compound "$MgCd_2$" of Hume-Rothery and Rowell, who explicitly noted the curious reversal of colour contrast. In spite of the long time of annealing, alloy 67 only showed relatively small amounts of this substance, in contrast to the results of Hume-Rothery and Rowell, who, with shorter times of annealing, obtained an almost complete conversion of their alloy 66·6 into the supposed compound $MgCd_2$, which, however, always contained numerous cracks and holes. In order to examine the matter further, a sample of alloy 67 was kept in an ordinary corked tube for 7 weeks, when microscopic examination showed that the outside shell of the specimen had been completely converted into the grey substance, although the inside was still unchanged. On standing for a further 6 weeks in a corked tube, the alloy completely crumbled to powder. In contrast to this, a specimen kept for 12 months in a sealed evacuated tube showed no change from the original microstructure. It was further shown that, on annealing specimens which had been partly converted into the grey substance by exposure to air, the grey substance penetrated the alloy along grain boundaries, and also along cleavage planes, with the production of a Widmanstätten type of structure, similar to that illustrated by Hume-Rothery and Rowell. The phenomenon was examined in great detail with the conclusion that the supposed compound $MgCd_2$ was formed to an increasingly smaller extent as the alloys were more stringently kept out of contact with air. To examine the matter further, a series of alloys in this range was cast in an atmosphere of argon, using a modification of the method of Hume-Rothery (1928). These alloys were sealed in evacuated glass tubes with the minimum exposure to the atmosphere, and after annealing for 4 weeks at 300° C were almost homogeneous, with only very occasional traces of the grey material.

---

* For abbreviation an alloy containing 60 atomic % of cadmium is referred to as alloy 60.

The experiments described above show clearly that the supposed compound $MgCd_2$ is not an equilibrium constituent of the magnesium-cadmium system, but is formed only in alloys which have been attacked by the air. Hume-Rothery and Rowell's conclusion that the compound $MgCd_2$ grew on annealing was presumably due partly to the penetration effect described above, and partly to the fact, that, in general, as their annealing experiments continued, they used specimens which had stood for longer periods in corked tubes, so that what was really the result of progressive attack by the air was mistaken for growth during the annealing process. The present experiments also show that X-ray investigations, using filings prepared in air, will almost certainly lead to erroneous conclusions in this part of the diagram, and Riederer's conclusion that $MgCd_2$ was a true constituent of the stable system is readily understood, since the longer filings are annealed, the more the grey material will tend to penetrate the grains.* In the present work it was shown quite conclusively that alloys in the region of 67 atomic % cadmium are much more readily attacked by air than any other alloys in the system, and there is a striking resemblance between this phenomenon and that observed in the system nickel-chromium, where the work of Jenkins *et al.* (1937) showed that needle markings (Widmanstätten structure) appeared on annealing some alloys. This effect was traced to contamination by nitrogen and on annealing in air, an additional phase was produced most readily when the alloy contained one atom of nickel to two of chromium. The occurrence of a maximum rate of attack in each case at the 2 : 1 atomic ratio appears most significant.

4. THE LIQUIDUS AND SOLIDUS CURVES AND THE ABSENCE OF A TWO-PHASE REGION

The work described above showed clearly that the supposed compound $MgCd_3$ has no existence, but further annealing experiments with alloys cast in argon, and also with alloys cast under flux, but protected from atmospheric attack, failed to reveal any signs of the two-phase region required by the diagram of Grube and Schiedt. The alloys were examined in great detail after an annealing treatment of 4 weeks at 300° C, and 2½ and 4 weeks at 200° C. The details of this work have been deposited with the Royal Society, and the conclusion reached was that the comparatively wide two-phase region shown in the diagram of Grube and Schiedt did not exist. As this conclusion was quite unexpected, the liquidus and solidus curves were redetermined.

---

* It is interesting to note that Riederer's X-ray work with filings was not in agreement with his work on massive metal in this region.

For the determination of the liquidus curves, the two metals were melted in crucibles lined with fluorspar and alumina, the weight used varying from 30 g. for the magnesium-rich alloys to 100 g. for the cadmium-rich alloys. The crucibles were heated in a closed glass tube filled with argon, and a covering of flux was used for alloys melting above 500° C in order to minimize loss by volatilization. The rate of cooling was from 0·7 to 1·4° C/min., and all the precautions described by Hume-Rothery and Raynor (1938) were taken. In one series of experiments the composition of the melt was determined by the analysis of a small sample extracted by suction through an alumina tube shortly before the arrest point. In another series, the tube was allowed to cool rapidly after the arrest was established, and the whole ingot dissolved for analysis. For the cadmium-rich alloys the compositions determined by analysis agreed so closely with those calculated from the weights of metals used that it was thought justifiable to analyse some of the ingots only, and to use the synthetic compositions for the remainder.

The exact details of the liquidus determinations are in table 2 of the collected tables deposited with the Royal Society, and the results are shown in figure 1, which also summarizes the results of the annealing experiments. The liquidus curve is smooth and continuous, and there is no sign of irregularity in the region 60–80 atomic % cadmium as would be required by the diagram of Grube and Schiedt. No secondary arrests corresponding to a peritectic reaction were observed, and the liquidus curve is typical of a system with a continuous solid solution.*

The solidus curve was determined by both quenching and heating-curve methods. For the quenching experiments, alloys melting below 450° C were cast in the argon apparatus, whilst the remaining alloys were melted under flux, and cast into ¼ in. diameter copper moulds. The heating-curve alloys were melted under flux, and cast into ½ in. diameter iron moulds, the heating curves being carried out in closed tubes as described by Hume-Rothery and Raynor (1937), at a heating rate of 0·6–1·0° C/min. All alloys were made homogeneous by a long preliminary anneal, before being used either for the heating-curve or quenching experiments.

---

* The bend in the liquidus curve shown by Hume-Rothery and Rowell in the region of 70 atomic % cadmium was not confirmed, and may have been due to atmospheric contamination.

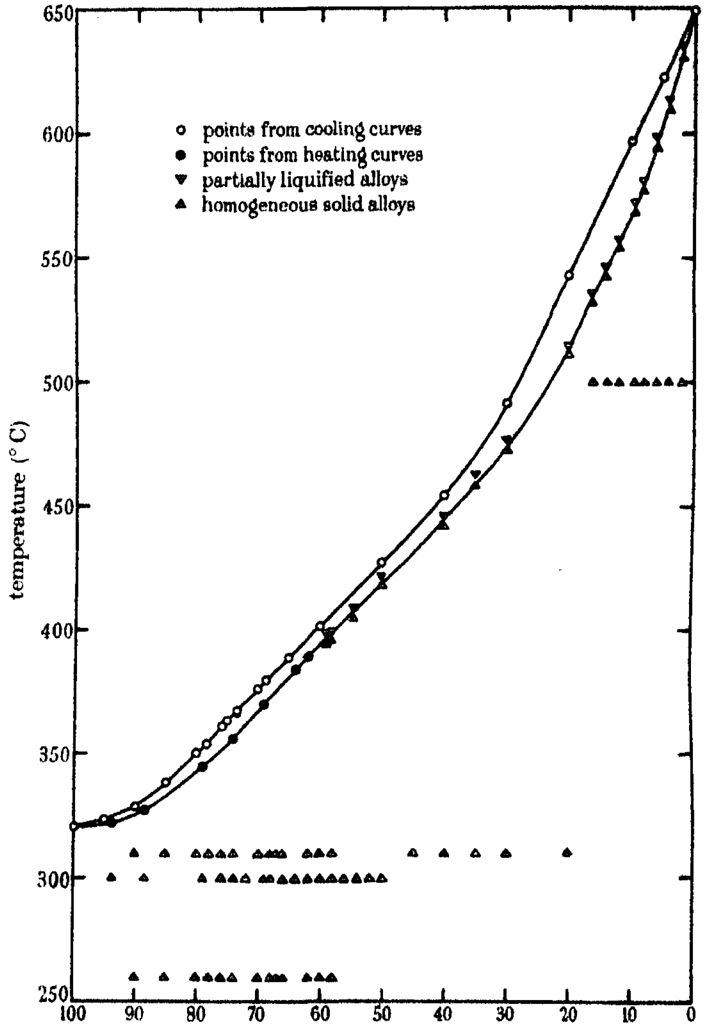

FIGURE 1

The exact details of the solidus experiments are given in table 3 of the tables deposited with the Royal Society, and the results are shown in figure 1, from which it will be seen that the solidus curve, like the liquidus curve, is smooth and continuous, and gives no indication of a two-phase region. For the magnesium-rich alloys, the present solidus curve is slightly lower than that of Hume-Rothery and Rowell, but is in good agreement with values obtained by the extrapolation of the results of Haughton and Payne (1935) on ternary magnesium-aluminium-cadmium alloys.

The liquidus, solidus and microscopic work are therefore in complete agreement as to the absence of a two-phase region at high temperatures, and, in view of the marked difference in the axial ratios of magnesium and cadmium, a complete investigation was made of the lattice-spacing relations.

5. X-RAY INVESTIGATION OF THE SOLID ALLOYS

The results previously described clearly suggested that a continuous series of solid solutions existed at the higher temperature. In view of the widely differing axial ratios of magnesium and cadmium this appeared rather improbable, and the problem was therefore examined by X-ray crystal analysis. Examination showed that, with quenched alloys, the superlattice transformations took place on keeping the alloys at room temperatures, and X-ray powder photographs were therefore taken at 310° C, using the high-temperature camera of Hume-Rothery and Reynolds (1938). For this purpose the alloys were first annealed in lump form for 2–4 weeks at 300–310° C, and filings were prepared in an atmosphere of argon, using the apparatus of Raynor and Hume-Rothery (1939), by means of which the whole process of filing, sieving, and sealing into a silica capillary is accomplished without exposure to the air at any stage. The specimens were then annealed for periods up to 24 hr. in the high temperature camera, and subsequently exposed for 2–3 hr. using copper K_α radiation. During the anneals and exposures the temperature was controlled by hand to an accuracy of ± 0·4° C, or by a Foster Temperature Controller to an accuracy of ± 1° C.

The resulting films were then measured accurately by means of a specially calibrated travelling microscope, and the lattice spacings deduced by the $\cos^2\theta$ extrapolation method of Bradley and Jay (1932). For the magnesium-rich alloys the outermost lines are in order (11.0)2, (12.4), (10.6), (20.5), and (12.3). Since the outermost line is of the form (*hk*.0), its spacing is independent of the axial ratio, and since the (10.6) and (20.5) reflexions are very sensitive to changes in the axial ratio, a process of trial and error enables the latter to be obtained to a high degree of accuracy. For the magnesium-rich alloys the side of the unit cell, *a*, was determined to within ± 0·0002 A, and the axial ratio *c*/*a* to within ± 0·0002.* With increasing cadmium content the results became less accurate, because the contraction in the lattice spacing causes the (11.0)2 line to move off the film, and at the same time the alloys become increasingly nearer to the melting point. Experience has shown that in this, and other alloy systems, as the melting point is approached, the general X-ray scattering at a given fraction of the absolute melting point is much more pronounced with solid solutions than with pure metals, so that the films cannot be measured so accurately. Thus, for alloys containing more than about 65 atomic % cadmium, *c*/*a* is accurate to within ± 0·0005. At 310° C, alloy 94·35 is within 10° C of its melting point, and for this alloy the accuracy is only ± 0·0005 A for *a*, and ± 0·001 for *c*/*a*.

Table 1

Alloy no.	Composition at % Cd	Preliminary annealing	Annealing of filings in camera at 310° C hr.	Axial ratio *c*/*a*	*a* in A	*c* in A
Pure Cd	100·00	—	—	1·900	2·9913	5·6835
1	94·35	16 days 310° C	4	1·870	3·0115	5·6315
2	87·26	18 days 310° C	2	1·820	3·0330	5·5200
3	82·04	16 days 310° C	4	1·771	3·0565	5·4131
4	77·94	4 weeks 300° C	4½	1·743	3·0700	5·3510
5	76·26	4 weeks 310° C	2	1·735	3·0761	5·3370
6	74·57			1·726	3·0850	5·3247
7	72·51			1·710	3·0945	5·2916
8	71·25	4 weeks 300° C		1·702	3·0980	5·2728
9	69·00	4 weeks 310° C		1·694(0)	3·1000	5·2514
10	63·75	4 weeks 300° C		1·665(0)	3·1195	5·1940
11	60·85	4 weeks 310° C	24	1·6578	3·1240	5·1790
12	59·43			1·6515	3·1290	5·1675
13	58·40	4 weeks 300° C	2	1·6515	3·1288	5·1672
13	58·40		24	1·6515	3·1290	5·1675
14	59·09		2	1·6515	3·1290	5·1675
14	59·09		24	1·6515	3·1290	5·1675
15	54·67		3	1·6437	3·1310	5·1464
16	51·49			1·6420	3·1385	5·1534
17	50·56		2	1·6400	3·1410	5·1512
18	45·80	6 days 403° C + 3 days 310° C	20	1·6349	3·1475	5·1459
19	40·00			1·6320	3·1554	5·1496
20	35·00			1·6291	3·1640	5·1544
21	30·00			1·6280	3·1705	5·1616
22	20·00		17	1·6262	3·1880	5·1843
Pure Mg	0·00	—	—	1·6235	3·2275	5·2398

---

* For pure magnesium the corresponding degrees of accuracy were ± 0·0001 A for *a* and ± 0·0001 for *c*/*a*.

The results of these experiments are given in table 1 and figure 2, and are of considerable interest. The addition of cadmium to magnesium causes a contraction in the lattice spacing *a* but only a very slight increase in the

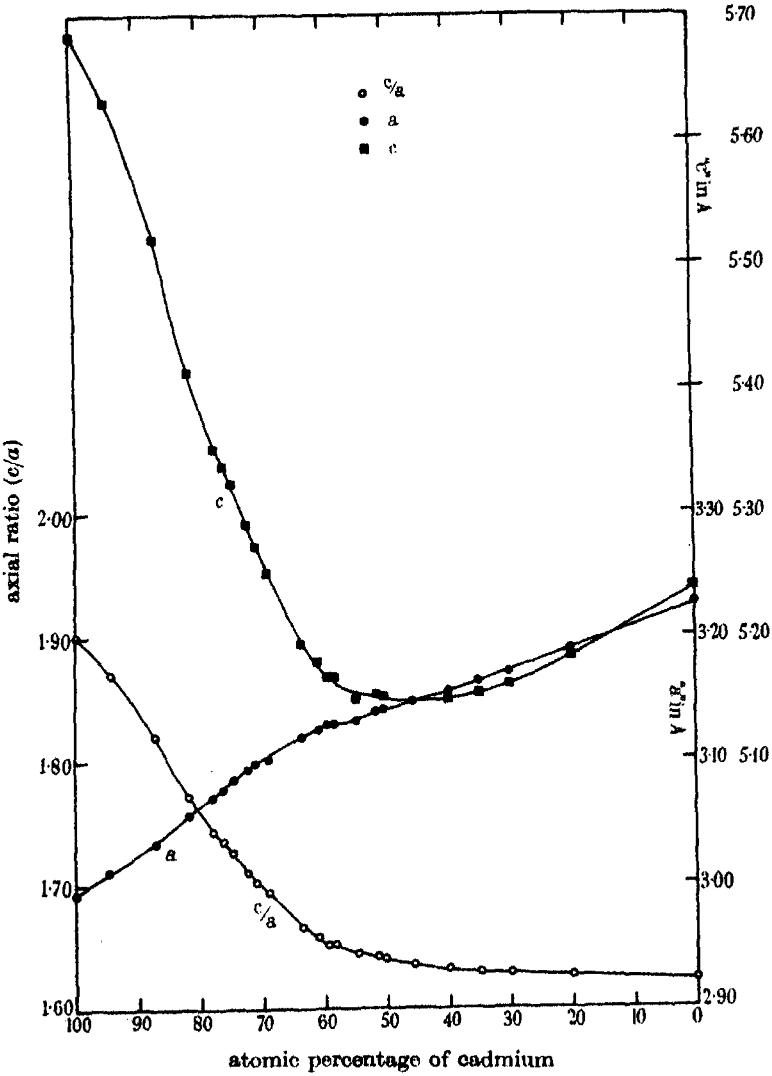

FIGURE 2

axial ratio; so that the lattice constant *c* decreases in almost the same proportion as *a*. In contrast to this, the addition of magnesium to cadmium causes an expansion of the lattice constant *a*, but at the same time the axial ratio decreases so markedly that the lattice spacing c contracts rapidly with increasing magnesium content, and each metal contracts the c spacing of the other. The two branches of the curves connecting a, c and c/a with composition for the magnesium and cadmium solid solutions approach one another rapidly but, instead of intersecting at points, there is a very short horizontal section in each curve in the region 58·5–60·0 atomic % cadmium. The three alloys concerned were examined very carefully, and all were analysed, and as will be seen from table 1 the lattice spacings are identical. It must be emphasized that the phenomenon is not that of two alloys of different structures or different lattice spacings existing in equilibrium over a range of compositions of the alloy as a whole, but is one in which the two solid solutions have merged into a structure of fixed lattice dimensions, which persist over a narrow range of composition. This effect appears to be quite new, and it is not possible to say whether a two-phase region exists. We have been able to examine microscopically the three alloys from which the X-ray specimens were prepared, and there was no indication of a two-phase structure, whilst the work previously described has shown that there is no indication of a peritectic horizontal, or of any discontinuity in the liquidus and solidus curves. Since the grain sizes of those three alloys were all large, the evidence on the whole favours the view that no two-phase region exists, but, as pointed out by Bradley (1938), it is doubtful whether any methods would distinguish between phases of identical lattice spacing and almost identical composition.

6. DISCUSSION

The previous sections have shown why the diagram of Hume-Rothery and Rowell was in error. In the work of Grube and Schiedt the specimens were annealed and cooled to room temperature, and, after this treatment, the electrical conductivities were measured while the rods were heated at a rate of 1° C/min. Our own work shows that the superlattice transformations take place when the alloys are kept at room temperature, and examination of the curves of Grube and Schiedt makes it clear that in some cases their rate of heating was too rapid for equilibrium to be reached, and this may account for the breaks in their conductivity/composition curves which led to the erroneous conclusion of a two-phase region.

The chief interest in the present work lies in the curious lattice-spacing relationships, and for these interpretations may be offered from two points of view, each representing part of the truth.* We may adopt first the Brillouin zone theory of Mott and Jones (1936), according to which the energy characteristics of electrons in a close-packed hexagonal crystal depend to a great extent on the axial ratio. From this point of view we shall regard the lattice-spacing relationships as due to two factors: (1) a normal size effect, resulting in a contraction of the lattice as the smaller cadmium atoms replace the larger magnesium atoms, and (2) an electronic effect, superimposed on the normal size effect.

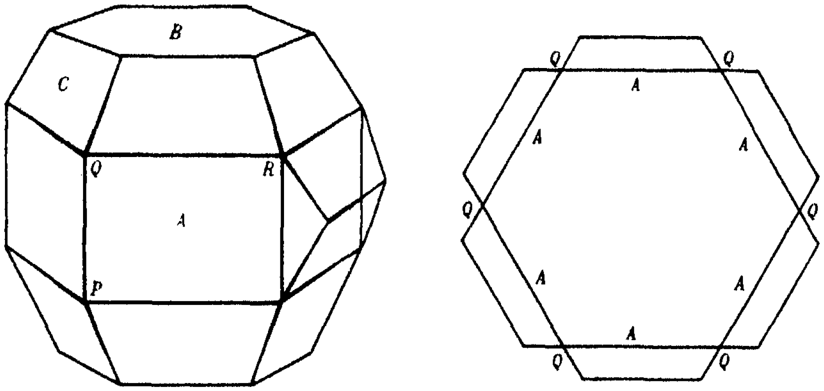

FIGURE 3

The first Brillouin zone of the close-packed hexagonal structure is shown in figure 3, and, within this zone, the energy of an electron varies continuously in all directions. There is a discontinuity across each of the bounding planes, but the calculations of Jones (1934) indicate that the energy discontinuity for electrons moving in certain directions vanishes along certain edges, such as *PQ* and *QR*, so that the smallest volume in k-space surrounded everywhere by an energy discontinuity for electrons with velocities in all directions is that enclosed by the original figure with the addition, on each of the *A* faces, of a small truncated prism. This complete zone, surrounded everywhere by an energy discontinuity, contains exactly two electrons per atom. Since magnesium and cadmium are conductors of electricity, there must be an overlap into a second zone, and two types of overlap have to be considered:

(1) Overlap from the incomplete first zone across the faces *A* into the small truncated prisms. This will be termed the *A* overlap.

---

* The position here is rather like that met with in the structure of the diamond, in which the Brillouin zone theory gives the best picture of the electrical properties, whilst the conception of co-valent bonds gives an indication of the density of the electron cloud in space, and explains the tetrahedral structure.

(2) **Overlap from the complete first zone into a second outer zone.** Mott and Jones (1936) have shown that this may occur either at B (figure 6*a*), or at the re-entrant corners (points Q) in figure 6*b*. These may be termed the B and Q overlaps respectively.

The calculations of Mott and Jones show that for magnesium, with axial ratio 1·6237, the A overlaps take place first, followed by the Q overlaps, but with two electrons per atom there is no overlap at B, and the $N(E)$ curve is of the form shown in figure 4, where the shaded portion represents two electrons per atom. For cadmium, with axial ratio 1·885, the first overlap occurs at B, followed by the A overlap, but with two electrons per atom there is no overlap at Q, and the resulting $N(E)$ curve is of the form shown in figure 5. In both figures 4 and 5, the $N(E)$ curve for the Q overlap, after the vertically rising initial portion has been passed, rises more steeply away from the energy axis than that for the B overlaps, because the overlaps at Q concern electrons moving with velocities in six directions, whereas the overlap at B concerns electrons moving with velocities in only two directions (Hume-Rothery and Raynor 1938).

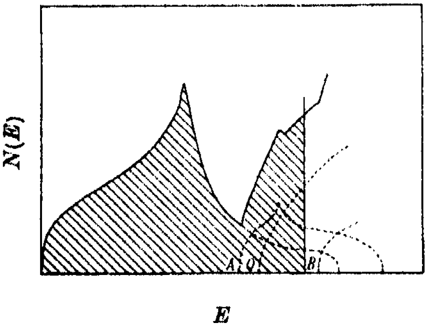

FIGURE 4

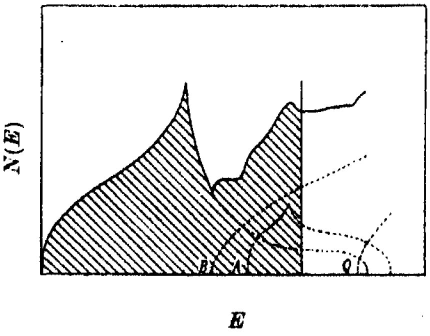

FIGURE 5

Jones (1934) has shown that the effect of a small overlap outside the boundary of a zone is to compress the Brillouin zone in k-space, and hence to expand the crystal in the direction concerned in real space.

Referring to figures 4 and 5, it will be seen that the passage from magnesium to cadmium changes the overlaps from the order AQB to BAQ, and we have to consider how this will affect the lattice spacings. The change may be divided into the stages shown in figure 6. In the stage (1)–(2), B approaches Q, and since there are two electrons per atom B must reach the shaded zone before Q. The formulae of Mott and Jones show that the total number of electrons overlapping from the first incomplete zone is only slightly affected by the axial ratio, and hence in stage

(1)–(2) the electronic change affects mainly the number of electrons in the A and Q zones, and since both these concern electrons with velocities at right angles to the principal axis, there will be relatively little effect on the axial ratio, and both the a and c parameters will show the normal contraction. In stage (2)–(3) the B overlap begins, and, if the Jones theory is accepted, this overlap will tend to expand the lattice in the c direction, and the normal contraction in this direction will now be opposed by the expansion produced by the increasing B overlap. As will be seen from figure 2, this is what has been observed experimentally. At the end of stage (2)–(3), B and Q coincide, as shown in figure 6(c), and it is here that

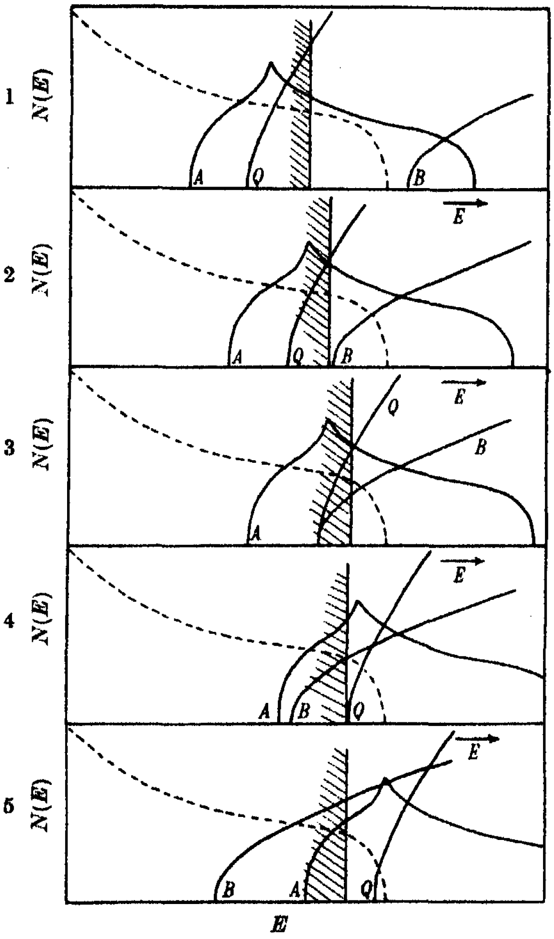

FIGURE 6

interesting effects may be expected in passing through the next stage (2)–(4). Exact details cannot be given until the curves are known more accurately, but since the Q curve rises more steeply than the B curve, the relative movement of B to the left, and Q to the right, will result in the removal of more electrons from the Q overlap than are introduced at the B overlap, and these excess electrons will have to be accommodated in the A zone, and in the first zone. Since the presence of electrons in the A zone produces an expansion of the a parameter, the normal contraction of both a and c parameters may be opposed by electronic effects in this range, in which case the increase in axial ratio will be less marked. Finally, in the last stage (4)–(5), where the Q overlap no longer occurs, the B overlap grows and the A overlap diminishes, with the result that the c parameter expands, whilst the a parameter diminishes more rapidly than at first. The zone theory, therefore, when combined with a general size effect, enables us to predict that the addition of cadmium to magnesium will result first in a general contraction without much alteration of axial ratio, and that this will be followed by an increase in axial ratio, an interval in which effects may compensate each other, and then a final range in which the axial ratio increases markedly, and the a parameter diminishes more rapidly. This is in good agreement with the facts.

The Brillouin zone theory considers the electrons as moving in a periodic field, and takes no account of the nature of the ions, or the distribution of the electron cloud in space. It is well known from the work of Jauncey and Bruce (1937) and McNatt (1939) that in zinc and cadmium the electron clouds of the atoms are anisotropic (spheroidal), although in certain alloys they are spherical. In view of the strongly polarizing nature of magnesium we should therefore regard the solution of cadmium in magnesium as involving the attraction of the electrons out of the anisotropic cadmium configuration, so that the cadmium atoms dissolve as spheres, with little effect on the axial ratio of magnesium. With increasing cadmium content there is an increasing tendency for the cadmium-like configuration to be taken up, since adjacent cadmium atoms become more common. From figure 2 it will be seen that with increasing cadmium content, the break in the curves occurs at the composition 58·2 atomic % cadmium, i.e. 7 cadmium atoms out of 12 $(100\times\frac{7}{12}=58\cdot3)$. In a survey of other alloys (Hume-Rothery, Raynor and Reynolds 1939) it has been shown that there is much indirect evidence for the existence of short-range order in concentrated solid solutions. If we accept this point of view, we can understand the tendency for the solid solution to assume a cadmium-like nature when there are 7 cadmium atoms to 5 magnesium atoms, since in the close-packed structure each atom has 12 neighbours, and when $\frac{7}{12}$ of the total number of atoms are of cadmium, a structure involving short-range order will enable the great majority of cadmium atoms to have more neighbours of cadmium than of magnesium. From this point of view we can therefore understand the position of the break in the curve, and the short region of constant lattice spacing is also comprehensible, since, when ordered structures are involved, lattice spacings are often anomalous. The complete theory must clearly involve both the zone characteristics, and the electron density in space, and it is satisfactory to note that both conceptions agree with the facts.

The authors must express their indebtedness to Professor C. N. Hinshelwood, F.R.S., for laboratory accommodation, and many other facilities which have greatly encouraged the present research. Grateful acknowledgement is also made to the Council of the Royal Society, the Department of Scientific and Industrial Research, the British Non-Ferrous Metals Research Association, and the Curators of the Leigh Fund of the University of Oxford for financial assistance, and to the Imperial Chemical Industries Ltd. for the loan of apparatus. The work has been carried out during the tenure of a Royal Society Warren Research Fellowship, and a Fellowship at Magdalen College, Oxford, by one of the authors (W. H.-R.), and of a D.S.I.R. Senior Research Award by the other author (G. V. R.).

SUMMARY

The equilibrium diagram of the system magnesium-cadmium has been investigated by thermal, microscopic and X-ray methods. The liquidus and solidus curves pass smoothly from the melting point of magnesium to that of cadmium, with no indication of a discontinuity characteristic of a peritectic reaction. Microscopic methods show no indication of a two-phase region above the temperatures of the superlattice transformations. The supposed compound $MgCd_2$ of Hume-Rothery and Rowell is not a true constituent of the system magnesium-cadmium, but is an oxide-nitride complex formed when the alloys are exposed to the atmosphere. It is formed most readily when the composition of the alloy corresponds with the formula $MgCd_2$; a somewhat similar effect has been noted in the system nickel-chromium. The two-phase region claimed by Grube and Schiedt is not confirmed.

The lattice spacings of a complete series of alloys at 310° C have been measured with a high-temperature X-ray camera. The first additions of

cadmium to magnesium cause a contraction of the *a* parameter of the unit cell, but have little effect on the axial ratio, so that the *c* parameter contracts in almost the same proportion. With further additions of cadmium the axial ratio increases slightly. The addition of magnesium to cadmium causes an expansion of the *a* parameter, but, at the same time, the axial ratio decreases so markedly that the *c* parameter diminishes, so that each metal decreases the *c* parameter of the other. A stage is then reached at which the solid solutions derived from magnesium and cadmium acquire identical lattice spacings which persist unchanged over a narrow range of compositions. These effects are discussed, and are shown to be in agreement with the Brillouin zone theory developed by Jones.

REFERENCES

Bradley, A. J. 1938 Discussion to paper by Gayler and Sutherland. *J. Inst. Met.* **63**, 142.

Bradley, A. J. and Jay, H. 1932 *Proc. Phys. Soc.* **44**, 573.

Dehlinger, U. 1930 *Z. anorg. Chem.* **194**, 223.

Grube, G. and Schiedt, E. 1930 *Z. anorg. Chem.* **194**, 190.

Haughton, J. L. and Payne, R. J. M. 1935 *J. Inst. Met.* **57**, 287.

Hume-Rothery, W. 1928 *J. Inst. Met.* **40**, 65.

Hume-Rothery, W. and Raynor, G. V. 1937 *J. Inst. Met.* **61**, 205.

— — 1938 *J. Inst. Met.* **63**, 201.

Hume-Rothery, W. and Reynolds, P. W. 1938 *Proc. Roy. Soc.* A, **167**, 25.

Hume-Rothery, W. and Rowell, S. W. 1927 *J. Inst. Met.* **38**, 137.

Jauncey, G. E. M. and Bruce, W. A. 1937 *Phys. Rev.* **51**, 1067.

Jenkins, C. H., Bucknell, E. H., Austin, C. R. and Mellor, G. A. 1937 *J. Iron Steel Inst.* **136**, 187.

Jones, H. 1934 *Proc. Roy. Soc.* A, **147**, 400.

McNatt, E. M. 1939 *Phys. Rev.* **56**, 406.

Mott, N. F. and Jones, H. 1936 *The theory of the properties of metals and alloys.* Oxford.

Raynor, G. V. and Hume-Rothery, W. 1939 *J. Inst. Met.* (advance copy).

Riederer, K. 1937 *Z. Metallk.* **29**, 423.

The dehydration of crystals of chrome alum

By J. A. Cooper and W. E. Garner, F.R.S.

(*Received* 27 *December* 1939)

[Plate 18]

The loss of water from a salt hydrate can occur with or without changes in the lattice structure. Thus, the water of crystallization of zeolites can be removed without the collapse of the original lattice; whereas in many other hydrates, such as the alums or copper sulphate pentahydrate, the removal of water is associated with changes in the structure of the solid and the production of a new solid phase. In the latter an interface is formed separating the two solid phases, and it is at this interface that the dehydration occurs. The water liberated at the interface passes through a superposed layer of product before it reaches open space. The rate of liberation of water may be dependent on the thickness of the superposed layer of product, as is seen in the case of the dehydration in vacuum of copper sulphate pentahydrate (Garner and Tanner 1930; Smith and Topley 1931). This effect was called "impedance" by Smith and Topley, and they showed that the "impedance" practically vanishes if the dehydration is studied in water-vapour pressures lower than the dissociation pressure of the salt hydrate. Since water vapour accelerates the rate of crystallization of the product (Colvin and Hume 1938) it is clear that it is the degree of crystallization of the product that determines whether impedance will occur or not.

The two processes, (1) the loss of water from the interface and (2) the subsequent reorganization of the lattice, do not appear to be very closely linked, since the solid product in many examples undergoes considerable shrinkage subsequent to the loss of water (see plate 18A, for chrome alum). The following model of the dehydration process serves to indicate the possibilities. I represents the solid reactant, and II is a transition layer derived from I by the loss of water either without lattice change or by a collapse of the original lattice. III is the product undergoing slow crystallization, and IV is the open space which may be a hard vacuum or may contain water vapour.

The velocity of the dehydration at the transition layer is usually measured by determining the rate at which the interface penetrates the solid from the loss of weight of a crystal of salt hydrate suspended on a silica spring in a hard vacuum (Garner and Tanner 1930; Topley and Smith 1931). Dehydration has also been followed by measuring the rate of growth of nuclei (Bright and Garner 1934). If there is impedance to the rate of flow of water across III then, in order to obtain the maximum rate at the transition layer, it is necessary to extrapolate back to zero thickness.

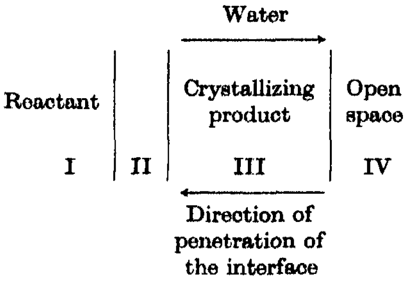

FIGURE 1

The rate of loss of water across the transition layer will obviously depend on its thickness and therefore upon the speed of crystallization of the product. The rate of crystallization of the product will be modified by changes in the temperature at which the dehydration is carried out and also by the presence of water vapour in the open space. These considerations have to be taken into account in any study of the temperature coefficient of the dehydration process.

The experimental work bearing on the above discussion is somewhat scanty. The dehydration of copper sulphate pentahydrate has been fairly thoroughly investigated. The activation energy from the temperature coefficient is 16–18 kcal. (Smith and Topley 1931; Bright and Garner 1934) and the heat of dissociation (Carpenter and Jette 1923) is 12·6 kcal. The difference between these two values, 3–6 kcal., may be real, but on the other hand may be due to a decrease in the thickness of layer II with rise in temperature. The rates of dehydration calculated from the Polanyi-Wigner equation, $dr/dt = \nu N e^{-E/RT}$, where N is the number of water molecules per sq. cm., are 50–100 times greater than the experimental rates and this divergence from theory may also be due to changes in II with temperature. Water vapour in the open space causes a decrease in the rate of dehydration and the rates in the presence of water vapour decrease in the manner given by curve 1 in figure 2. On the other hand, manganous oxalate bihydrate (Smith and Topley 1935; Volmer and Seidel 1937) gives curve II with both a minimum and a maximum. It was shown by the latter two authors, by X-ray measurements, that the product was amorphous when the dehydration was carried out in vacuum and crystalline when carried out in the presence of water vapour. The initial fall in rate is probably due to the retarding effect of water vapour on the diffusion through a relatively thick transition layer II, and the intermediate rise in rate to a decrease in the thickness of this layer by crystallization of the product. Unfortunately, in this case there are no measurements on the temperature coefficient of the reaction.

In the present investigation, the dehydration of chrome alum has been studied with a view to throwing light on the phenomena occurring at the interface between the two solid phases. An earlier investigation (Cooper and Garner 1936) has shown that spherical nuclei are formed, which increase in size at a linear rate after an initial induction period, and that the number of nuclei formed increases approximately linearly with time. This investigation has now been extended.

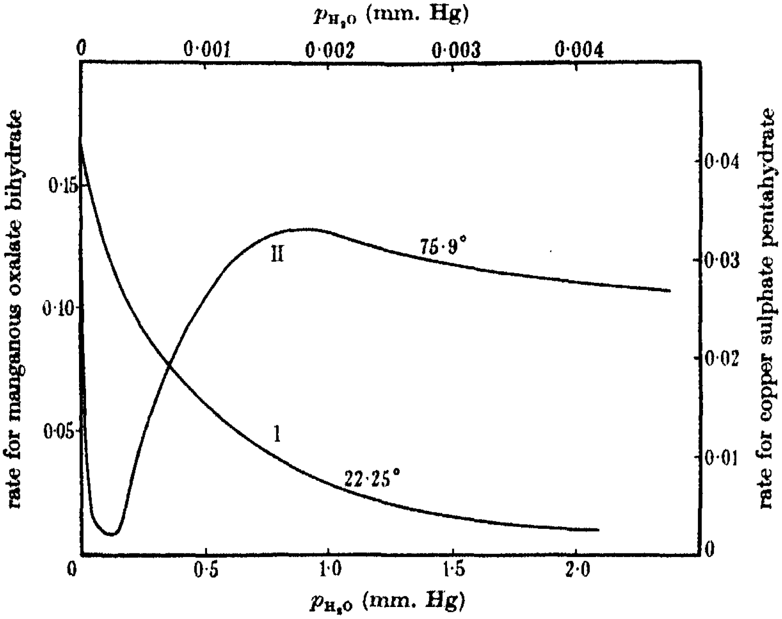

FIGURE 2

The temperature coefficient of the rate of nuclear growth and of the rate of penetration of the interface have been determined. This has necessitated measurements of the self-cooling which occurs when the crystals undergo dehydration, and in the course of this work values have been obtained for the heat of dissociation of the alum which have been compared with those derived directly from the temperature coefficient of the dissociation pressure. The effects of water vapour on the rate of dehydration have also been studied, and it has been shown that in this respect the dehydration of chrome alum forms a case intermediate between those of copper sulphate pentahydrate and manganous oxalate bihydrate (see figure 2).

EXPERIMENTAL

The apparatus used for observing the nuclei and the measurement of nuclear growth is depicted in figure 3. It consists of a double-walled vessel, provided with windows for illumination and observation. That for observation consisted of a plane window in the form of a hollow joint *B* which was ground into the double walls of the reaction vessel. The dimensions of this were such that the lens of a microscope could be inserted nearly as far as the inner wall of the reaction vessel. The crystal was suspended at *F*, and the water liberated on decomposition was removed through wide tubing into a U-tube *C* which was surrounded by a CO_2-

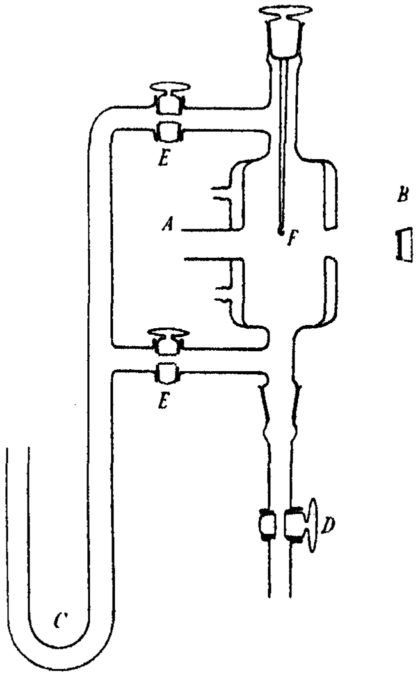

FIGURE 3

alcohol mixture. A ground joint with a tap *D* was placed at the bottom of the vessel so that at any time air could be admitted to the reaction vessel only, and any crystals which fell from the suspension could easily be removed. Tube *A* was for the introduction of a constant vapour pressure of water vapour. The crystal was illuminated with a 100 c.p. Pointolite lamp shining through a cell containing water, and the crystal was observed with a Winkel cathetometer, and, when needed, photographs taken on a Zeiss film camera attachment. Water was pumped between the walls of the hollow reaction vessel from a large tank fitted with a heater and a refrigerator. Temperatures between 0 and 40° C could be obtained and maintained constant to within 0·01° C. The vacuum in the reaction vessel was tested from time to time with a McLeod gauge.

A saturated solution of Kahlbaum's "Puriss" chrome alum was made in distilled water and allowed to crystallize in a dust-free air thermostat over caustic potash. Crystals were removed from the solution, and then immersed for one or two seconds in distilled water to remove the film of saturated solution adhering to the crystals. They were then placed in contact with a piece of soft filter paper which ensured drying without scratching. After this process they were stored over powdered chrome alum in a desiccator.

Nuclei. Two types of nuclei are found (see plate) and these are distinguished both by the intensity of the reflected light and by their structure under the microscope. The commonest type is slightly pink in colour which, as they grow, develop radial cracks, with a star-shaped hole in the centre. This is evidently due to a crystallization of the product which occurs with a contraction in volume. The second type is considerably whiter in colour and does not develop radial cracks. The plate, B, C and D shows both types of nuclei at two different stages of growth. The second type of nucleus is obviously unstable compared with the first, since, on coming into contact, the second type passes into the first, as is shown in C and D. The rate of growth of the unstable nuclei is about one-third of that of the common type, and it occurs more frequently on crystals dehydrated below 20° than at higher temperatures. The colour of the unstable nuclei, their slow rate of growth, and occurrence at the lower temperatures indicate that they are more microcrystalline than the common nuclei. They may consist of a different hydrate but no evidence has been obtained which bears on this point.

Rates of nuclear growth. There were found to be anomalies in the rates of growth when the nuclei were small. In figure 4 is given a number of typical cases of growth on the same crystal face. 1, 2, 3, 4 and 7 represent the increase in nuclear size with time for type I, and 5 and 6 for type II. Some nuclei show a period of slow growth in the beginning, e.g. 4 and 7; others grow uniformly, e.g. 6, and yet others start to grow rapidly at first and then slow down, e.g. 1, 2 and 5. In all cases, however, the rate of growth settles down to the same constant value for the same kind of nuclei. The initial anomalies must depend on the treatment of the crystal surface, since in a large number of cases studied in the earlier investigation (Cooper and Garner 1936) only one of the above types of behaviour was

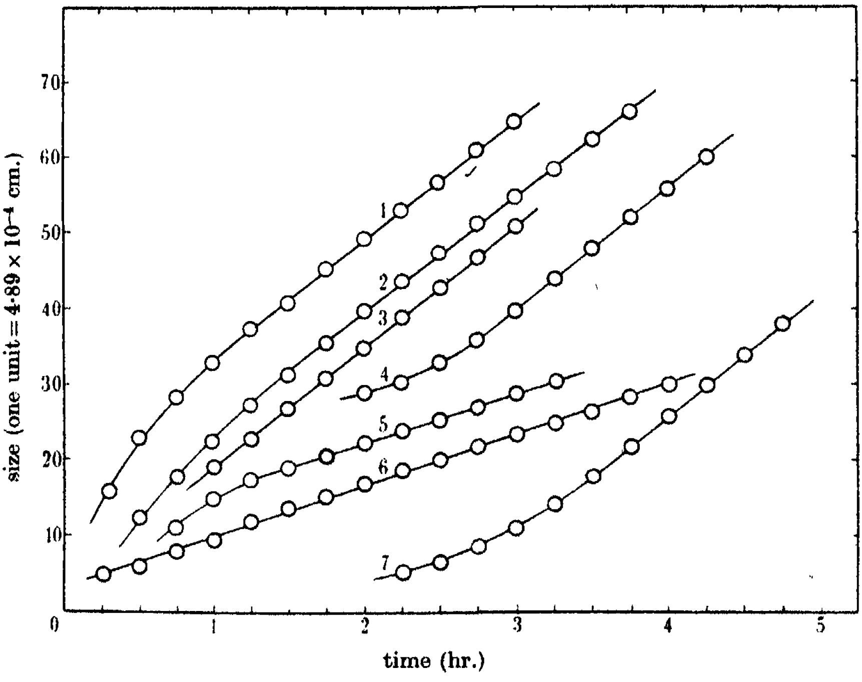

Figure 4

found, viz. an initial slow rate of growth. It is possible that the rapid initial growth of some nuclei is due to dislocation of the surface due to handling. In considering these curves it should not be overlooked that the crystal cools as the dehydration proceeds, and the linear rate of growth may not set in until a constant temperature has been attained.

A table of the rates of growth of the nuclei at different temperatures is given below. The values given are the averages of approximately ten nuclei at each temperature. The temperatures are uncorrected for self-cooling.

Although there is good agreement between the rates of growth for different nuclei on the same crystal, the degree of reproducibility from crystal to crystal is not very high. The average values have been taken in the calculation of the activation energy. (see figure 8).

TABLE 1

	Type I		Type II	
Temp. °C	Increase in diam. × 10^5 cm./sec.	Average radial growth × 10^6 cm./sec.	Increase in diam. × 10^6 cm./sec.	Average radial growth × 10^6 cm./sec.
30	1·139	5·27	4·51	2·25
	1·033			
	0·991			
25	0·781	3·68	2·97	1·67
	0·739		3·72	
	0·744			
	0·683			
20	0·411	2·03	1·82	0·892
	0·388		1·75	
	0·422			
15	0·221	1·10	1·07	0·523
14	0·207	1·03	1·02	
10	0·111	0·554	0·597	0·295
			0·582	

Measurement of the rate of decomposition by the loss in weight method. A crystal of chrome alum was suspended on a silica balance in a double-walled vessel similar to that described in figure 3, and the rate of loss of weight followed in a hard vacuum. The surfaces of the crystal were thoroughly scratched beforehand in order to speed up the nucleation and to ensure that the reaction penetrated the crystal in parallel planes. It was found that the reaction came to a standstill when 12·1–12·3 mol. of water were lost out of the twenty-four originally attached to the compound, $K_2SO_4 . Cr_2(SO_4)_3, 24H_2O$.

Calculations were made from the loss in weight curve, of the volume of undecomposed material present at various times, assuming that 12 mol. of water were lost and that the whole of the reaction occurred at the interface between the reactant and its product. A curve was constructed, *A*, showing the change in the volume of the undecomposed material with time. Next, curve *B* was drawn showing the relationship between depth of penetration and the undecomposed volume. The latter was calculated from the dimensions of the crystal. The crystals chosen for experiment possessed a large and well-formed upper face which was parallel with the surface on which the crystal was grown. Only 111 faces were present and of the eight faces, six lay on the sides of the crystal and two formed the top and bottom surfaces. From the geometry of the crystal, its volume can be calculated from the product of the area of the top face and the thickness. Volumes calculated in this way always agreed within 2–3 % with those derived from the mass and density of the crystal.

From curves *A* and *B*, a graph of the depth of penetration against time was constructed. Typical graphs for 30° are shown in figure 5. Straight lines are obtained up to about two-thirds of the decomposition, and the rate of penetration of the interface is constant. The values for the rates of penetration at a number of temperatures are given in table 2.

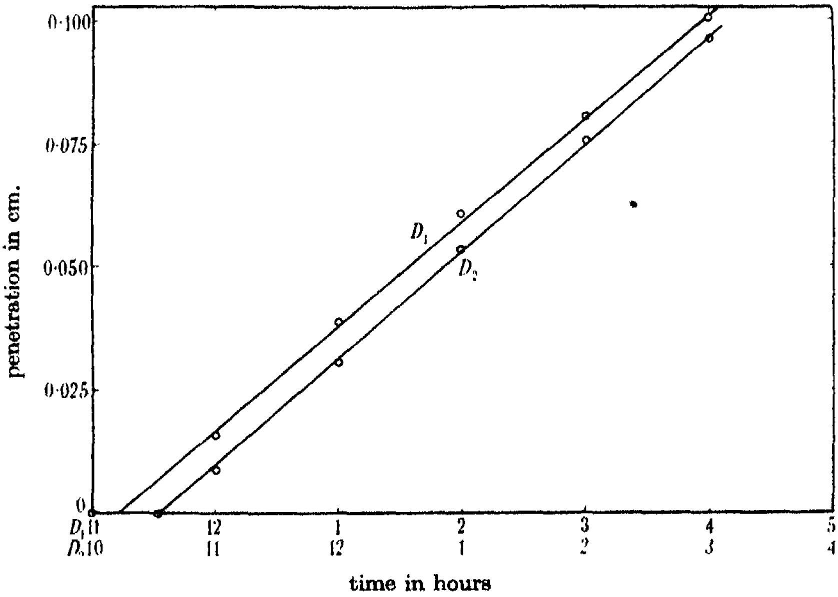

FIGURE 5

TABLE 2

Temp. ° C	35	30	25	20	15
Penetration in cm./sec.	8·64	6·04	4·03	2·22	1·20
$\times 10^6$	8·89	5·85	3·84	2·22	1·11

In order to check the assumption that the loss of water was confined to the interface, the depth of penetration was measured in two cases by breaking a partially dehydrated crystal and measuring the depth under a microscope. It was not possible to do this very accurately on account of the nature of the fracture. The rates determined by this method at 35 and 30° C were 7·8 and $5{\cdot}9 \times 10^{-6}$ cm./sec. respectively. These were sufficiently near the values obtained in table 2 to warrant the assumption made.

The values for the rate of penetration of the interface are a little greater than those obtained for the linear growth of the nuclei (table 1), but the temperature coefficient is the same in the two cases (see figure 8).

The fact that the rate of penetration is independent of the depth is of some interest. In the instance of copper sulphate, both Garner and Tanner (1930) and Smith and Topley (1931) found that the rate of penetration falls off with the extent of penetration. This the latter two authors ascribe to an "impedance" to the escape of water vapour from the interface and to the establishment of a pressure gradient in the product between the interface and the surrounding space. The existence of this pressure gradient is regarded as being responsible for a reduction in the rate of reaction as the thickness of the product increases. The absence of any retardation of the reaction due to the thickness of the superimposed product in the dehydration of chrome alum speaks for the absence of "impedance" to the loss of water, and for a loosely packed and somewhat coarsely crystalline product. The absence of impedance is also confirmed by the close correspondence between the rate of spread of the reaction on the surface and the rate of penetration into the crystal. This argument would, however, be invalidated were it not shown later that the temperature of the interface remained constant during the period for which the constant rate of penetration was measured (see later).

Self-cooling of the crystals. In order to be able to calculate the activation energies of these processes, it is necessary to know accurately the temperature of the crystals during the dehydration in hard vacuum. This was measured experimentally in the apparatus shown in figure 6. Two crystals, about 1½–2 cm. broad, corresponding as closely as possible in shape, were cemented on to a thin copper-constantan thermocouple, *D*, by means of durofix. The length of each thermocouple lead immersed in the crystals was approximately 4–5 cm. The changes in temperature of the crystals during the dehydration were measured by means of a Moll galvanometer. By scratching the crystals beforehand, it was ensured that the reaction penetrated the crystals in parallel planes and the durofix prevented dehydration between the two crystals. Since from table 2 the rate of penetration was known, it was possible to correlate the temperature of the crystal at any time with the area of interface and with a known rate of reaction.

It was shown that the amount of self-cooling remained constant for a considerable fraction of the decomposition and, in fact, it was more nearly constant than could be accounted for in view of the decreasing area of interface. The conclusion was reached that this was due to the product being a poor conductor of heat, so that although the amount of heat liberated decreases with time, this was balanced by a decreased loss of energy from the surface of the crystal. Table 3 shows the average values for self-cooling. From these values, and assuming that Wien's Law holds, it is possible to calculate the heat of reaction. The equation which applies is $\lambda\delta\Delta = K\Delta_0(T_1^4 - T_0^4)$, where Δ_0 is the original area from which radiation occurs, and Δ is the interfacial area at any time. In the initial stages, $\Delta_0 = \Delta$. λ is the heat of crystallization per g., δ is the rate of reaction in

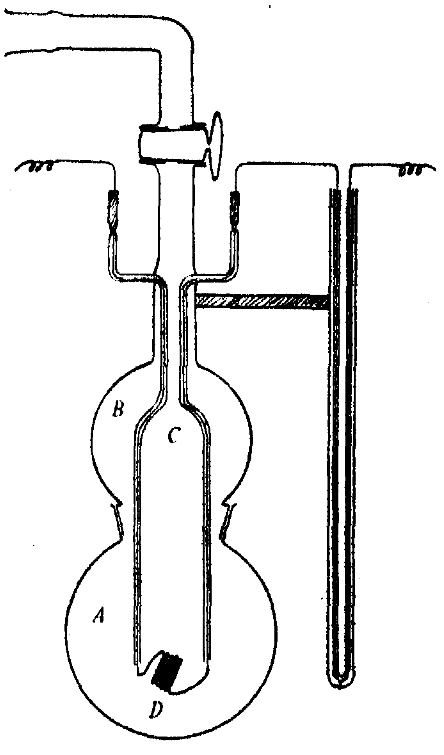

FIGURE 6

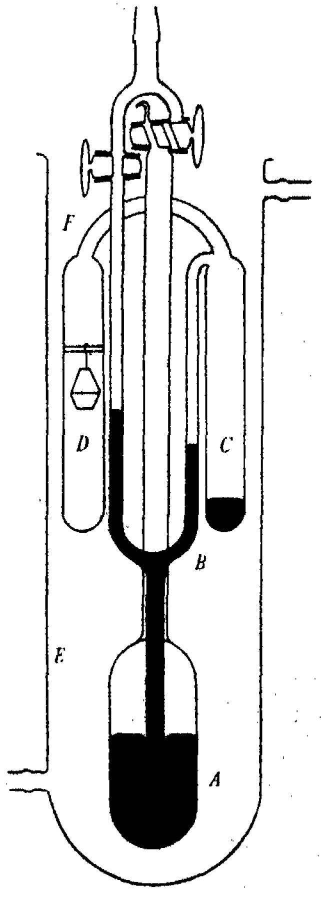

FIGURE 7

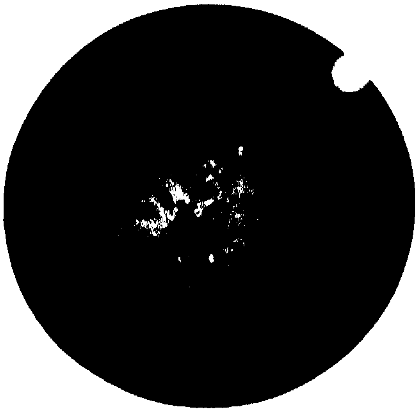

A

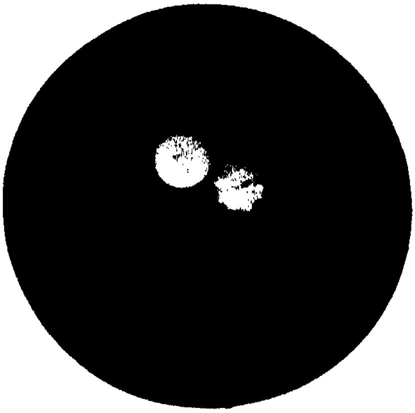

B

F

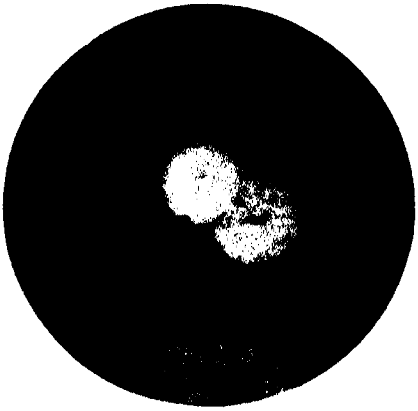

C

E

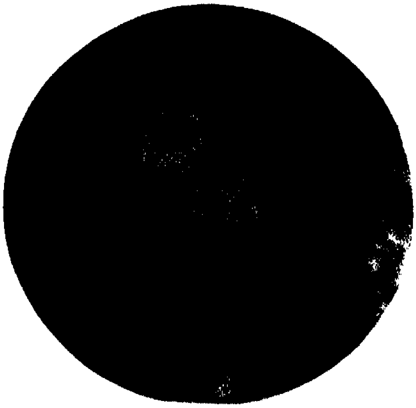

D

g. per sec. per sq. cm. and K is Planck's constant. The heats per gram mol. were calculated for the initial stages of the reaction only, when the interface was situated very close to the crystal surface. This minimized any error due to the poor conductivity of the product.

TABLE 3

Thermostat temp., ° C	35	30	25	20	15	10
Cooling	11·8	8·8	6·2	4·1	2·3	(1·3)*

* Extrapolated.

TABLE 4

Temp., ° C	35	30	25	20	15
Heat per g. mol., cal.	11,980	11,690	10,250	9632	9443

The heats of reaction so calculated decrease steadily with decrease in temperature and this decrease is probably real, for even if black-body conditions be not strictly applicable the constant K should not vary appreciably with temperature. The fall in the heat of reaction with decrease in temperature indicates that the product becomes more amorphous in character the lower the temperature. This is in accord with the changes in the microscopical appearance of the nuclei over the above range of temperatures. In connexion with the above experiments, the specific heat of chrome alum has been determined at room temperature and found to be 0·274 cal./g.

In order to determine how closely the above values agreed with the heat of reaction obtainable from the temperature coefficient of the dissociation pressures, a single crystal was suspended in the apparatus shown in figure 7, and dehydrated so as to give a thin film of product on the surface. Conditions were chosen so as closely to approach those employed in the determination of self-cooling. Starting at 20° C, the dissociation pressure was measured on the manometer over a range of temperatures. Care was taken that at no time was the crystal subjected to water vapour pressures greater than the dissociation pressure. If this were exceeded by no more than a millimetre, the approach to equilibrium was exceedingly slow, and equilibrium could not be attained in several days. Equilibrium could only be approached with certainty from below. The following values were obtained for the dissociation pressures:

TABLE 5

Temp., ° C	20	25	30	35
Pressure, mm. Hg	9·33	13·30	17·77	24·41

from which $Q = 10{,}030$ cal./mol. This is in fairly close agreement with the average values of table 4, showing that Planck's constant can be successfully applied to this case.

The lack of reversibility in the dissociation equilibrium has not been exhaustively investigated although it is an important matter for study. The dissociation pressure will obviously depend on the state of aggregation of the product, and possibly on the direction of the approach to equilibrium or pseudo-equilibrium.

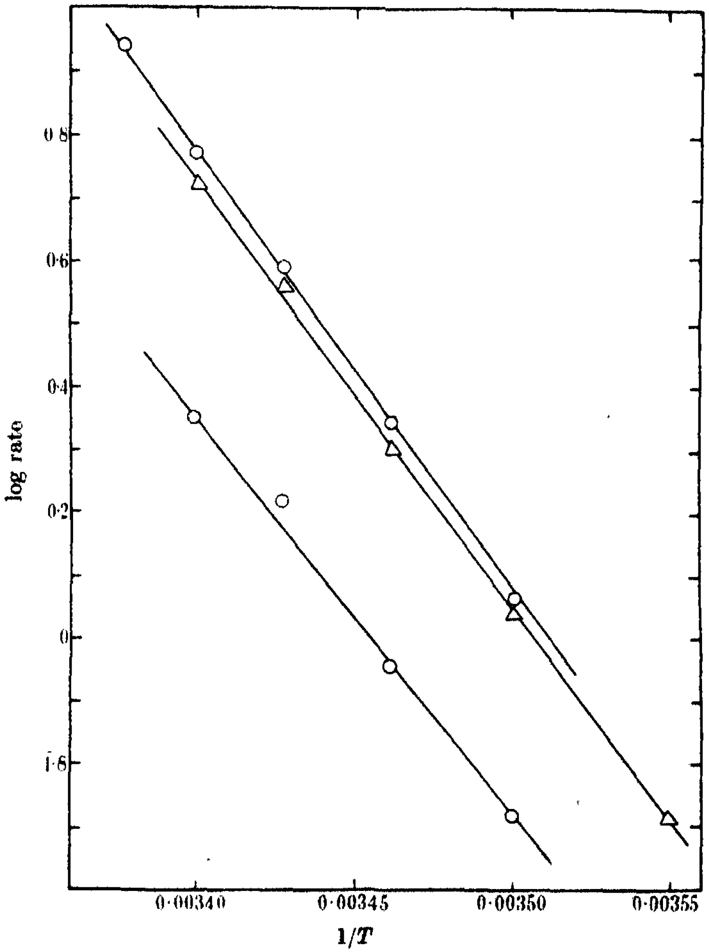

FIGURE 8. ○ Rates of growth of nuclei. △ Rate of penetration.

Activation energy of the dehydration processes. After correction of the temperatures of the crystals for self-cooling, figure 8 was constructed by plotting log rates of reaction against $1/T$. These gave straight lines from which the following activation energies were obtained. The first two values

Penetration of the crystal	Rate of growth of nuclei of type I	Rate of growth of nuclei of type II
31,240	30,780	28,500 cal.

which refer to the production of the same crystalline product should give the same activation energies, which is the case within experimental error. The divergence is greater for the nuclei of the second type, but here the experimental error is greater and possibly the value obtained is, within the experimental error, the same as for the other two values.

These activation energies are very high for processes occurring at such low temperatures.

Effects of water vapour on the velocity of dehydration. The velocity of growth of the nuclei (type I) was measured in the apparatus shown in figure 1. The crystals were heated in a hard vacuum with the thermostat at 20° C, until the nuclei formed were sufficiently large to be measured accurately. They were then exposed to the action of water vapour. A reservoir of distilled water kept at constant temperature served as a source of water vapour and the vapour pressures employed ranged from 0·008 to 8 mm. The experimental results are shown in figure 9 and table 6, from which it will be observed that the rate of growth at first increases as the pressure increases, reaches a maximum and then falls to zero as 8 mm. is approached.

TABLE 6

mm. H_2O	9·1	7·75	6·55	5·50	4·55	3·0	1·95	1·55
Radial growth $\times 10^6$ cm./sec.	0·0	0·167 0·0	0·041	0·290	0·543	0·978	1·36	1·51
mm. H_2O	1·24	0·78	0·48	0·29	0·096	0·030	0·008	0
Radial growth $\times 10^6$ cm./sec.	1·88	2·28 2·29 2·08	2·38 2·43 —	2·63 2·45 —	2·32 2·42 —	2·03 — —	1·94 — —	2·21 2·05 1·94

In order to test whether the initial rise in the rate of growth was due to a modification of the temperature of the crystal caused by the introduction of water vapour, measurements of self-cooling were made at a number of water vapour pressures. This was done in the apparatus shown in figure 6. After the crystals, undergoing dehydration in a hard vacuum, had attained a constant self-cooling, water vapour was introduced and a new value for the self-cooling determined. Equilibrium was obtained within a few minutes. The water vapour was then removed and the self-cooling for hard vacuum determined. No difficulty was experienced in obtaining reproducibility. The following values for the self-cooling, with the thermostat temperature at 20° C, were obtained:

Pressure H_2O, mm.	5·50	4·55	3·0	1·95	1·24	0·776	0·475	0·285	0·00
Self-cooling, ° C	0·5	1·1	1·85	2·4	2·9	3·3	3·8	3·9	4·1

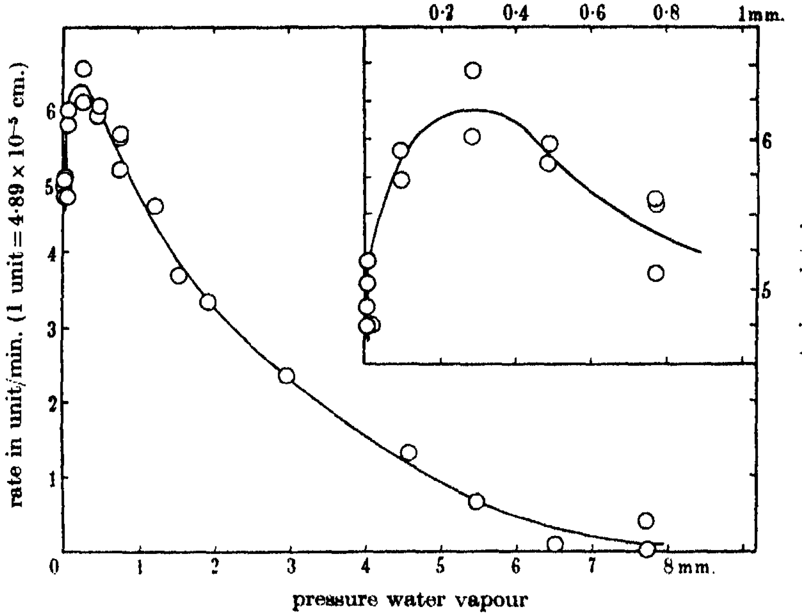

FIGURE 9

For water vapour pressures below 0·3 mm., the self-cooling was very nearly that occurring in a hard vacuum, and since the maximum in figure 9 occurs at about 0·3 mm., it is clear that the maximum cannot be a secondary effect due to self-cooling.

The values recorded in figure 9 suffer from the disadvantage that, although in all cases the thermostat temperature was 20°, the actual temperature of the crystal was 15·9° in a hard vacuum and increases as the water vapour pressure is increased. It is possible to convert the rates of growth to those appertaining to 20° C if it be assumed that the activation energy in the presence of water vapour be the same as that in hard vacuum.

This calculation has been made in order to determine the effect on the curves recorded in figure 9. No essential difference was found so that the curves are not recorded.

A few measurements were carried out at 25° C, to determine if the maximum persisted at this temperature. The results are shown below:

mm. H_2O	13·30	1·95	0·776	0·285	0
Radial growth × 10^6 cm./sec.	0	2·75	8·06	3·92	3·92

The maximum is even more marked at 25 than at 20° C. The character of the nuclear growth was found to be markedly affected by water vapour. In plate 1 are shown photographs of nuclei observed at 0·78 mm. H_2O (*E*) and at 1·95 mm. H_2O (*F*). At the lower vapour pressure the nuclei are scalloped, each scallop being contained between two radial cracks. At the higher pressure, the growth is very compact and structureless. The centre portions of the nuclei in *F* were grown in a hard vacuum and only the outer rim at a vapour pressure of 1·95 mm.

DISCUSSION

The rate of dehydration of crystals of chrome alum is not appreciably affected by the thickness of the superposed layer of the product. This means that the rate of flow through layer III, figure 1, is much faster than that of the liberation of water at the transition layer. Since the heat of dissociation is 10 kcal., and since the activation energy for the whole process is of the order of 31 kcal., it is clear that diffusion across layer III should have but a slight effect on the rate.

It has been shown that the dehydration occurs to a preponderating extent in the transition layer and that the final product has a composition, $K_2SO_4.Cr_2(SO_4)_3, 12H_2O$. There is, however, a recrystallization of the product after the water is lost, as is shown by the shrinkage which occurs in the nuclei (plate 1). The "self-cooling" has been measured and the results have been shown to be consistent with the view that chrome alum behaves as a black-body. Smith and Topley (1931) assumed that this was the case in correcting their results with copper sulphate pentahydrate for "self-cooling". The heats of dissociation can be calculated from the self-cooling assuming black-body radiation, and it is shown that the heat of dissociation increases with rise in temperature. This may be taken to mean that the extent to which the collapsed lattice undergoes crystallization increases with rise in temperature, which view is supported by the microscopical observations.

The activation energy for nuclear growth on the surface of crystals of chrome alum, and the rate of penetration of the interface into the body of the crystal is of the order of 31 kcal. This is considerably greater than that of the heat dissociation, viz. 10 kcal. The activation energy is abnormally high for a reaction occurring in the neighbourhood of room temperature. As a general rule, solid reactions with an activation energy > 20 kcal. are very slow at room temperature. Normally, the Polanyi-Wigner equation, $dr/dt = N\nu e^{-E/RT}$ is obeyed within one or two powers of ten for exothermic and endothermic solid reactions. When applied to the dehydration of chrome alum, using the experimental value of $E = 31$ kcal., the calculated value of ν is $1 \cdot 2 \times 10^{25}$, which is 10^{12} times greater than the normal frequency of activation. The dehydration of copper sulphate pentahydrate is approximately normal, but there are other abnormal cases of hydrate decomposition where the Polanyi-Wigner equation gives too high a value for the frequency of activation, notably the dissociation of calcium carbonate hexahydrate (Hume and Topley 1928) where the discrepancy is 10^{23}. Hume and Colvin (1929) also obtain a high value of $E = 40$ kcal. for the dissociation of potassium oxalate hemihydrate for which the above equation also gives too high a value for ν. In the light of the model (figure 1), it will be seen that such high activation energies are probably to be explained as due to effects of temperature on the transition layer. Since there is no evidence from figure 8 that E changes with temperature, the effect in question is possibly a decrease in the thickness of the transition layer with increase in temperature.

The effect of the thickness of the transition layer can be visualized as follows. If there be "impedance" to the flow of water through the collapsed lattice of the transition layer, II, then in the molecular layers adjacent to the lattice of the reactant, water molecules will be present in concentrations which will vary with the temperature. If x be the fraction of spaces in the collapsed lattice unoccupied by water molecules, then the rate of dehydration will be $dr/dt = N\nu x e^{-E/RT}$, where N is the number of water molecules per cm.^{2} of the original lattice. Since x has a temperature coefficient, calculation of the activation energy from the temperature coefficient of the rate of growth of nuclei will give a value which may be considerably greater than E.

As far as the effects of water vapour are concerned, chrome alum behaves in an intermediate fashion to copper sulphate pentahydrate and manganous oxalate bihydrate. There is no minimum on the rate-vapour pressure curve, only a maximum. This maximum at low vapour pressures is to be explained as due to a decrease in the thickness of the transition layer II as a consequence of the catalysis of the crystallization of the product, and the fall after the maximum to an increasing concentration of water vapour molecules in the transition layer which causes a reversal of the reaction. It would appear that the form taken by the rate-vapour pressure curves depends in a complex fashion on the properties of the collapsed lattice in the transition layer and on its rate of crystallization. This affects the temperature coefficient of the reaction and if the properties of the transition layer change appreciably with temperature, there may occur anomalously high temperature coefficients.

One of us (J. A. C.) wishes to express his indebtedness to the Department of Scientific and Industrial Research for a maintenance grant. The authors are also grateful to Imperial Chemical Industries Ltd. and to the Colston Research Society for grants for the purchase of apparatus.

SUMMARY

Measurements have been made of the rate of growth of dehydration nuclei over the 111 surfaces of crystals of chrome alum for a range of temperatures. These rates have been compared with the rates of penetration into the crystal. The self-cooling of the crystals has been measured and the heat of dissociation calculated both from the self-cooling and the temperature coefficient of the dissociation pressure. The heat of dissociation, 10 kcal., is much less than the calculated activation energy for the dehydration, viz. 31 kcal. An explanation is advanced for the abnormally high activation energy.

It is shown that small pressures of water vapour cause an acceleration of the rate of dehydration.

REFERENCES

Bright and Garner 1934 *J. Chem. Soc.* p. 1872.
Carpenter and Jette 1923 *J. Amer. Chem. Soc.* **45**, 583.
Colvin and Hume 1938 *Trans. Faraday Soc.* **34**, 1739.
Cooper and Garner 1936 *Trans. Faraday Soc.* **32**, 1739.
Garner and Tanner 1930 *J. Chem. Soc.* **132**, 47.
Hume and Colvin 1929 *Proc. Roy. Soc.* A, **125**, 635.
Hume and Topley 1928 *Proc. Roy. Soc.* A, **120**, 211.
Topley and Smith 1931 *Proc. Roy. Soc.* A, **134**, 224.
— 1935 *J. Chem. Soc.* p. 321.
Volmer and Seidel 1937 *Z. phys. Chem.* **179**, 153.

The repulsive forces between isotopic molecules

By R. P. Bell

(*Communicated by C. N. Hinshelwood, F.R.S.—Received* 2 *August* 1939)

It is usually assumed that the forces of attraction and repulsion between two molecules depend only on their electronic structures and are independent of the nuclear masses. While this assumption is undoubtedly true to a first approximation it fails to take into account the zero-point energy associated with the nuclear vibrations, which will modify the charge distribution both of the nuclei and of the electronic shells. Since the zero-point energy depends upon the nuclear mass, this may lead to differences between the behaviour of a pair of isotopic molecules such as H_2 and D_2. If the restoring force of the nuclear vibration is not directly proportional to the displacement of the nuclei from their mean position, then the mean internuclear distance will be different for the two isotopes. The magnitude of this anharmonic effect can be calculated from spectrum data, and it is found that for H_2 and D_2 the difference is less than 10^{-11} cm., and hence negligible. However, the energy of interaction of two molecules will not be a linear function of the internuclear distance within the molecules, so that even for harmonic oscillations the observed interaction will depend upon the magnitude of the zero-point energy. Both the attractive and the repulsive intermolecular forces will be affected in this way, but it is difficult to treat the former owing to the absence of any exact treatment of exchange forces between molecules. The problem is more easily attacked in the case of the Coulomb forces (which have a net repulsive effect), and the present paper constitutes an attempt to estimate the isotope effect for this type of force.

It will be necessary to neglect the mutual deformation of the charge distributions caused by the approach of the two molecules. This assumption is usually made in dealing with Coulomb forces, and it is unlikely to introduce serious error in calculating the isotopic difference. The total Coulomb interaction between two molecules can then be written as

$$G = G_n + G_{ne} + G_e, \qquad (1)$$

where G_n is the interaction between the nuclei of the two molecules, G_{ne} the interaction between the nuclei of one molecule and the electron shell of the other, and G_e the interaction between the two electron shells. The principles involved are most easily seen by considering G_n for two diatomic molecules.

On the assumption that all directions of approach are equally probable, if the zero-point energy is neglected the nuclear charge may be regarded as being distributed over an infinitely thin spherical shell of diameter equal to the internuclear distance r_0. If $Z\epsilon$ is the total nuclear charge for one molecule and R the distance between the centres of mass of the two molecules, then provided that $R > r_0$, G_n is given by

$$G_n = \frac{Z^2\epsilon^2}{R}. \tag{2}$$

If, on the other hand, we take into account the zero-point energy, the thin spherical shell must be replaced by a spherical charge distribution which has its maximum charge density at $r = \frac{1}{2}r_0$ and which falls away on either side of this in accordance with the law

$$\rho \propto e^{-(r-\frac{1}{2}r_0)^2/b^2}, \tag{3}$$

where $b = (h/4\pi^2\mu\nu)^{\frac{1}{2}}$ is the amplitude of a classical harmonic oscillation of energy $\frac{1}{2}h\nu$. The value of G_n is then obtained by calculating the interaction between two such distributions when their centres are distant R apart. Without carrying out the calculation it is readily seen that for values of R which occur in practice G_n will differ negligibly from the value given by equation (1), since it is only the overlapping portions of the charge distributions which will lead to such differences. Thus for a hydrogen molecule $r_0 = 0{\cdot}75$ A, $b = 0{\cdot}09$ A, and the charge density at a distance of 1 A from the centre has fallen to 10^{-20} of its maximum value.

The same principles apply to the interactions involving the electrons, though in this case the effects are much greater. The ordinary electronic wave functions represent the probability distribution of the electrons for fixed nuclei, and we must superimpose upon this a second probability distribution corresponding to the zero-point energy of the nuclei. Thus the complete wave function (supposed real) for the electrons of one diatomic molecule can be written $\psi_1 = \psi_1(\tau_1, x_1)$, where τ_1 represents spatial co-ordinates referred to the centre of mass and x_1 is a co-ordinate for the nuclear vibration. The interaction between the electron shells of two such molecules is then given by

$$G_e = Z_1 Z_2 \epsilon^2 \int \frac{1}{r_{12}} \psi_1^2 \psi_2^2 \, d\tau_1 \, d\tau_2 \, dx_1 \, dx_2, \tag{4}$$

where the integrations with respect to τ_1 and τ_2 are over all space, and those with respect to x_1 and x_2 from $-\infty$ to $+\infty$. In the same way the interaction between the nuclei of molecules (1) and the electron shell of molecule (2) is given (for not too small intermolecular distances) by

$$G_{ne} = Z_1 Z_2 \epsilon^2 \int \frac{1}{r_1} \psi_2^2 \, d\tau \, dx_2, \tag{5}$$

where we neglect as before the effect of the zero-point energy on the charge distribution of the nuclei themselves, but allow for its effect on the electron shells. The usual expressions for the Coulomb interaction correspond to equations (4) and (5) without integration over x_1 and x_2.

An exact evaluation of the expressions for G_e and G_{ne} is not possible even for the simplest diatomic molecule, since we have no knowledge of the exact electron distribution or of its dependence upon the nuclear separation. We can, however, carry out the calculation for a simple model, which should be adequate to estimate the difference between pairs of isotopes. This model consists of a point positive charge $Z\epsilon$ surrounded by a spherical distribution of negative electricity of equal charge represented by a hydrogen-like wave function. The effect of the zero-point energy is introduced by supposing that the radius of maximum electron density (which is determined by the effective nuclear charge Z') is not fixed, but that its distribution about a mean value is described by the wave function of a harmonic oscillator. The total wave function can then be written as $\psi_1 = \psi_1(r_1)\,\phi_1(x_1)$, where

$$\left.\begin{aligned}
\psi_1(r_1) &= \left\{\frac{Z_1'^3}{\pi a_0^3}\right\}^{\frac{1}{2}} e^{-Z_1' r_1/a_0},\\
\phi_1(x_1) &= \left(\frac{1}{\pi^{\frac{1}{2}} b}\right)^{\frac{1}{2}} e^{-\frac{1}{2}x_1^2/b^2},\\
Z_1' &= Z_0'/(1 + Z_0' x_1/a_0),\\
Z_0' &= \text{mean effective nuclear charge},\\
b &= \text{classical amplitude of zero-point energy},\\
a_0 &= \text{radius of Bohr orbit for hydrogen} = 0{\cdot}529\ \text{A.}
\end{aligned}\right\} \tag{6}$$

The interaction between two molecules thus represented can be evaluated as an expansion in powers of $Z_0' b/a_0$. It is first necessary to calculate the Coulomb interaction G_0 between two spherical distributions with fixed effective nuclear charges Z_1' and Z_2'; this is equivalent to integrating first with respect to τ_1 and τ_2 in equations (4) and (5). We have

$$G_0 = Z^2\epsilon^2 \left\{\frac{1}{R} + \int \psi_1^2(r_1)\,\psi_2^2(r_2)\,\frac{1}{r_{12}}\,d\tau_1\,d\tau_2 - \int \psi_1^2(r_1)\,\frac{1}{r_2}\,d\tau - \int \psi_2^2(r_2)\,\frac{1}{r_1}\,d\tau\right\}, \tag{7}$$

where R is the distance between the centres of the two distributions. This can be evaluated by the usual methods, using confocal elliptic co-ordinates, and gives after reduction

$$G_0 = \frac{Z^2\epsilon^2e^{-2\Lambda}}{64\lambda^3R}\Big\{e^{2\Lambda\lambda}(1-\lambda)^3\,[3(1+\lambda)^2\,(1-\lambda)-(1-\lambda)^3-2\Lambda(1+\lambda)^4$$
$$+3\Lambda(1-\lambda^2)^2-\Lambda(1-\lambda)^4]-e^{-2\Lambda\lambda}(1+\lambda^3)\,[3(1+\lambda)\,(1-\lambda)^2$$
$$-(1+\lambda)^3-2\Lambda(1-\lambda)^4+3\Lambda(1-\lambda^2)^2-\Lambda(1+\lambda)^4]\Big\}, \qquad (8)$$

where
$$\Lambda = \frac{R}{2a_0}(Z_1'+Z_2').$$

The observed value of G is then given by

$$G = \int_{-\infty}^{+\infty}\int_{-\infty}^{+\infty} G_0\phi_1^2(x_1)\,\phi_2^2(x_2)\,dx_1dx_2. \qquad (9)$$

For present purposes we can expand G_0 in powers of λ, giving

$$G_0 = \frac{Z^2e^2e^{-2\Lambda}}{R}\{1+\tfrac{5}{8}\Lambda-\tfrac{3}{4}\Lambda^2-\tfrac{1}{6}\Lambda^3$$
$$-\lambda^2(\tfrac{3}{4}\Lambda+\tfrac{11}{8}\Lambda^2-\tfrac{21}{8}\Lambda^3+\tfrac{1}{2}\Lambda^4+\tfrac{1}{15}\Lambda^5)+O(\lambda^4)\}. \qquad (10)$$

Equation (9) is then expanded in powers of $Z_0'x/a_0$, noting that only even powers in the integrand contribute to G. Writing $\Lambda_0 = RZ_0'/a_0$ we obtain

$$G = \frac{Z^2\epsilon^2e^{-2\Lambda_0}}{\pi Rb^2}\int_{-\infty}^{+\infty}\int_{-\infty}^{+\infty}\Big\{1+\tfrac{5}{8}\Lambda_0-\tfrac{3}{4}\Lambda_0^2-\tfrac{1}{6}\Lambda_0^3$$
$$-\frac{(Z_0')^2}{a_0^2}(x_1^2+x_2^2)\,(\tfrac{7}{8}\Lambda_0+\tfrac{55}{32}\Lambda_0^2-\tfrac{67}{32}\Lambda_0^3+\tfrac{1}{12}\Lambda_0^4+\tfrac{1}{10}\Lambda_0^5)$$
$$+O\Big(\frac{(Z_0')^4x^4}{a_0^4}\Big)\Big\}\,e^{-(x_1^2+x_2^2)/b^2}\,dx_1dx_2$$
$$= \frac{Z^2\epsilon^2e^{-2\Lambda_0}}{R}\Big\{1+\tfrac{5}{8}\Lambda_0-\tfrac{3}{4}\Lambda_0^2-\tfrac{1}{6}\Lambda_0^3$$
$$-\frac{(Z_0')^2b^2}{a_0^2}(\tfrac{7}{8}\Lambda_0+\tfrac{55}{32}\Lambda_0^2-\tfrac{67}{32}\Lambda_0^3+\tfrac{1}{12}\Lambda_0^4+\tfrac{1}{10}\Lambda_0^5)+O\Big(\frac{(Z_0')^4b^4}{a_0^4}\Big)\Big\}. \qquad (11)$$

We shall now use equation (11) to estimate the isotope effect for the molecules H_2 and D_2, where $Z = 2$. The equations given by Lennard-Jones (1931) for the repulsion between two hydrogen molecules are fitted fairly well for $R = 2$–3 A if we put $b = 0$ and $Z_0' = 0{\cdot}97$ in equation (11). The vibrational spectrum of hydrogen gives $b(H_2) \sim 0{\cdot}090$ A and $b(D_2) \sim 0{\cdot}075$ A, so that it is clear that further terms in equation (11) are negligible. Table 1 gives some approximate values calculated from equation (11). ΔG is the difference between the repulsive energies for the two isotopes (the value for hydrogen being the greater), ΔR is the difference between the distance at which the energies of repulsion are the same for the two isotopes, and T is the temperature at which $G(H_2) = kT$.

TABLE 1

R cm. × 10^8	$G(H_2)$ ergs × 10^{14}	ΔG ergs × 10^{14}	ΔR cm. × 10^8	T °K
2·25	21·1	0·34	0·007	1540
2·50	10·1	0·33	0·009	740
2·75	5·4	0·26	0·012	390
3·00	2·5	0·19	0·017	180
3·25	1·00	0·13	0·026	73
3·50	0·30	0·08	0·048	22

The isotopic differences are thus appreciable, being 2–25 % in G and 0·3–1·4 % in R in the range investigated. In view of the crudeness of the model it is not claimed that these calculations can do more than indicate the order of magnitude of the isotope effect, but they do suggest that such an effect would be detectable by experiment. The most probable means of detecting it would be by measurements of the second virial coefficients of hydrogen and deuterium. It should, however, be remembered that there are two other factors which will contribute to an isotopic difference in the virial coefficients. In the first place the exchange forces between the molecules will be effected by the zero-point energy of the nuclei in the same way as the repulsive forces. In the second place it is strictly necessary to use quantum theory in deriving the equation of state of a gas from the intermolecular forces, and hence for light molecules there will be some dependence on the mass even when the forces of attraction and repulsion are identical. The first effect could be largely eliminated by making measurements at fairly high temperatures, where the attractive forces become relatively less important. On the other hand, calculation appears to show (Uhlenbeck and Beth 1936; De Boer and Michels 1938) that the quantum effect will lead to isotopic differences which are at all temperatures considerably greater than those due to the difference in repulsive fields. The only measurements for H_2 and D_2 at present available (Schaefer 1937, 1938) are in the range 23–45° K. It is possible that measurements for H_2, D_2 and HD over a range of temperatures would make it possible to disentangle the various effects.

SUMMARY

It is pointed out that the charge distribution in a diatomic molecule will be a function of the zero-point energy of the nuclear vibration, and hence that the forces of attraction and repulsion between two such molecules will depend upon the nuclear masses. In the case of the Coulomb repulsion the magnitude of this effect is estimated by the quantitative treatment of a simple model. Calculated numerical data are given which indicate that this effect of the nuclear mass should lead to a measurable difference between the second virial coefficients of hydrogen and deuterium, though there are several other factors which would also contribute to the observed difference.

REFERENCES

De Boer, J. and Michels, A. 1938 *Physica*, **5**, 945
Lennard-Jones, J. E. 1931 *Proc. Phys. Soc.* **43**, 461.
Schaefer, K. 1937 *Z. phys. Chem.* **36** B, 85; 1938, **38** B, 187.
Uhlenbeck, G. and Beth, E. 1936 *Physica*, **3**, 729.

On the statistical method in nuclear theory

By K. Fuchs
Carnegie Research Fellow, University of Edinburgh

(*Communicated by M. Born, F.R.S.—Received* 2 *November* 1939)

1. INTRODUCTION

The calculation of the energies of heavy nuclei presents a many-body problem with a very large number of particles. For the treatment of this problem the statistical method seems to be indispensable.

But the statistical method, as applied hitherto in nuclear physics, has some serious drawbacks. It proceeds from the Hartree approximation, each particle being supposed to move in the average field of the other particles. With this approximation the total wave function can be represented by a determinant of independent wave functions. The calculation of the energy then leads to expressions containing the wave functions only in the form of densities or mixed densities

$$\rho(r) = \sum_i \phi_i^*(r)\,\phi_i(r); \quad \rho(r,r') = \sum_{i \neq j} \phi_i^*(r)\,\phi_j^*(r')\,\phi_i(r')\,\phi_j(r), \qquad (1\cdot 1)$$

where the summation extends over all independent wave functions.

In nuclear physics it is not permissible to replace the actual field by the average field and the objections against this method are well known (cf. Bethe and Bacher 1936, p. 150).

But the assumption of independent wave functions is not essential for a statistical treatment. In this paper I shall develop the general theory of a statistical method without making use of any such assumption. This is possible by a generalization of the determinantal expression of the total wave function, which leads to a generalization of the density functions. Expressions for the energy due to various types of nuclear forces are derived.

2. The nuclear forces

In the meson theory of nuclear forces the neutron and the proton are regarded as two states of the same particle. This is done by introducing a new variable, the "particle variable", which can have two values corresponding to the neutron and the proton state. The "particle wave function" has therefore two components, similar to the spin function.

Let $n(i)$ and $p(i)$ be the particle functions representing a pure neutron or pure proton state respectively of the ith particle. They are the proper functions of the neutron and proton operator N_i and P_i, such that

$$\left.\begin{aligned} P_i p(i) &= p(i), & N_i p(i) &= 0, \\ P_i n(i) &= 0, & N_i n(i) &= n(i). \end{aligned}\right\} \qquad (2\cdot1)$$

$n(i)$ and $p(i)$ are mutually orthogonal and normalized. They may be represented by the matrices

$$n(i) = \begin{pmatrix} 1 \\ 0 \end{pmatrix}, \quad p(i) = \begin{pmatrix} 0 \\ 1 \end{pmatrix}, \quad N_i = \begin{pmatrix} 1 & 0 \\ 0 & 0 \end{pmatrix}, \quad P_i = \begin{pmatrix} 0 & 0 \\ 0 & 1 \end{pmatrix}.$$

Introduce the operators V_i and W_i which change a neutron into a proton and vice versa

$$\left.\begin{aligned} V_i p(i) &= n(i), & W_i p(i) &= 0, \\ V_i n(i) &= 0, & W_i n(i) &= p(i). \end{aligned}\right\} \qquad (2\cdot2)$$

The matrix representation of these operators is obviously

$$V_i = \begin{pmatrix} 0 & 1 \\ 0 & 0 \end{pmatrix}, \quad W_i = \begin{pmatrix} 0 & 0 \\ 1 & 0 \end{pmatrix}.$$

The exchange operators can now be defined as

$$U_{ik} = V_i W_k. \tag{2·3}$$

With (2·2) the effect of these operators is

$$\left.\begin{aligned} &U_{ik}p(i)\,n(k) = n(i)\,p(k),\\ &U_{ik}n(i)\,n(k) = U_{ik}n(i)\,p(k) = U_{ik}p(i)\,p(k) = 0.\end{aligned}\right\} \tag{2·4}$$

Thus U_{ik} exchanges the ith and kth particle, if the former is a proton and the latter a neutron. The total exchange operator, exchanging the two particles, if they are unlike particles, is $U_{ik} + U_{ki}$.

Further define the spin operator

$$S_{ik} = \tfrac{1}{2}(\sigma_i . \sigma_k + 1), \tag{2·5}$$

where σ is the Pauli spin vector. It can easily be verified that

$$\left.\begin{aligned} &S_{ik}\alpha(i)\,\alpha(k) = \alpha(i)\,\alpha(k), \quad S_{ik}\beta(i)\,\alpha(k) = \alpha(i)\,\beta(k),\\ &S_{ik}\alpha(i)\,\beta(k) = \beta(i)\,\alpha(k), \quad S_{ik}\beta(i)\,\beta(k) = \beta(i)\,\beta(k).\end{aligned}\right\} \tag{2·6}$$

The operator S_{ik} can therefore be regarded as exchanging the spin co-ordinates of the ith and kth particle. Here α and β are the two spin functions representing upward and downward spin.

With the help of these operators the potentials corresponding to the Majorana, Heisenberg, Bartlett and Wigner forces can be defined:

$$\left.\begin{aligned} M_{ik} &= J^m(r_{ik})\,S_{ik}(U_{ik} + U_{ki}),\\ H_{ik} &= J^h(r_{ik})\,(U_{ik} + U_{ki}),\\ B_{ik} &= J^b(r_{ik})\,S_{ik},\\ W_{ik} &= J^w(r_{ik}).\end{aligned}\right\} \tag{2·7}$$

It will be noted that the Majorana operator exchanges particle and spin co-ordinates, whereas the Heisenberg operator exchanges the spin co-ordinates only. In the original definition the Majorana operator exchanges the spatial co-ordinates only, and the Heisenberg operator the spatial and spin co-ordinates. This of course amounts to practically the same. But in the original definition it must be stated expressly that the operator operates only between unlike particles, whereas with the definition (2·7) this is automatically the case. In any case, the operator "exchange of co-ordinates" is so abstract that it seems preferable to reduce it to simpler operators arising naturally from the meson theory.

The forces between like particles are only of the Bartlett and Wigner type, operating indiscriminately between neutrons and protons. But if the neutral meson exists, there should also be forces acting between two like particles, but not between neutrons and protons. Such a potential may be represented by the operators

$$\left.\begin{aligned} K_{ik} &= J^k(r_{ik})\,S_{ik}(P_{ik}+N_{ik}), & P_{ik} &= P_i P_k, \\ L_{ik} &= J^l(r_{ik})\,(P_{ik}+N_{ik}), & N_{ik} &= N_i N_k. \end{aligned}\right\} \tag{2·8}$$

These forces correspond to Bartlett and Wigner forces, operating only between like particles.

3. THE WAVE FUNCTION

Consider now a nucleus with a total number A of particles. Let ν, μ be the numbers of neutrons with spin α, β respectively and κ, λ the corresponding numbers of protons. Assuming that the spin and particle functions can be separated, we might take the total wave function as a product of the individual spin and particle functions multiplied into a general spatial function

$$\begin{aligned} \Phi(1,2,\ldots,\nu;\nu+1,\ldots;\nu+\mu+1,\ldots;\nu+\mu+\kappa+1,\ldots,A)\,n(1)\,\alpha(1)\ldots \\ \ldots n(\nu+1)\,\beta(\nu+1)\ldots p(\nu+\mu+1)\,\alpha(\nu+\mu+1)\ldots \\ \ldots p(\nu+\mu+\kappa+1)\,\beta(\nu+\mu+\kappa+1)\ldots. \end{aligned} \tag{3·1}$$

But we must ensure that the total wave function is antisymmetric in the co-ordinates of all particles. This can be done by summing (3·1) over all possible permutations, adding a + or − sign according as the permutation is even or odd. This summation can again be written in the form of a determinant. The simplest way of doing so is by means of the symbolic method. We split the wave function symbolically into a number of factors:

$$\begin{aligned} \Phi(1,2,\ldots,A) = \phi_1(1)\ldots\phi_\nu(\nu)\,\psi_1(\nu+1)\ldots \\ \ldots\chi_1(\nu+\mu+1)\ldots\omega_1(\nu+\mu+\kappa+1)\ldots. \end{aligned} \tag{3·2}$$

Here each factor by itself has no meaning. Only the total product is defined by (3·2); the single factors are only symbolic quantities introduced for the purpose of abbreviated notation.

With this notation the total wave function may be written in the form

$$\Psi = \frac{1}{\sqrt{A!}}\begin{vmatrix} \phi_1(1)\,n(1)\,\alpha(1) & \ldots & \omega_\lambda(1)\,p(1)\,\beta(1) \\ \vdots & & \vdots \\ \phi_1(A)\,n(A)\,\alpha(A) & \ldots & \omega_\lambda(A)\,p(A)\,\beta(A) \end{vmatrix} \tag{3·3}$$

where the ith row contains the following elements:

$$\begin{gathered}\phi_1(i)\,n(i)\,\alpha(i),\\ \phi_2(i)\,n(i)\,\alpha(i),\ldots,\phi_\nu(i)\,n(i)\,\alpha(i),\\ \psi_1(i)\,n(i)\,\beta(i),\ldots,\psi_\mu(i)\,n(i)\,\beta(i),\\ \chi_1(i)\,p(i)\,\alpha(i),\ldots,\chi_\kappa(i)\,p(i)\,\alpha(i),\\ \omega_1(i)\,p(i)\,\beta(i),\ldots,\omega_\lambda(i)\,p(i)\,\beta(i).\end{gathered}$$

Taking for example the diagonal term in the determinant and substituting for the product of wave functions according to (3·2) the term (3·1) is obtained. The other terms in the determinant obviously give all the permutations of this diagonal term.

For shortness I shall assume the language of independent wave functions, wherever convenient. Thus I shall say that in the term (3·1) the first particle is in the first neutron state with spin α or the first $n\alpha$-state, etc.

It is clear that the wave function Φ cannot be symmetric in the co-ordinates of two particles of the same type—say two neutrons with spin α for then the total wave function would vanish identically. But it can be symmetric in the co-ordinates of two particles of different types.

The wave function is normalized so that

$$\int \Psi^* \Psi \, d\tau = 1, \tag{3·4}$$

where the integration includes summation over all spin and particle variables.

Since the total wave function (3·3) is now of the same form as in the independent particle picture, we might simply take over the equations derived in that picture, and substitute for the density functions the generalized expressions. Indeed, apart from a complication to be mentioned presently, this would give the correct results. However, in order to obtain the correct generalization of the density functions, it is necessary to go more closely into the calculation. Furthermore, as far as I am aware, no calculations have been made taking into account separately the two spin directions. Such calculation seems desirable in order to obtain the energies of nuclei with uneven numbers of neutrons and protons. This calculation might be expected to be rather tedious. However, by another application of the symbolic method it can be greatly reduced.

The complication mentioned above arises from the orthogonality relations. In the independent particle picture we have the relations

$$\int \phi_i(1)\,\phi_k(1)\,d\tau_1 = 0, \quad \text{if } i \neq k, \tag{3·5}$$

and similar relations for the other functions. With the generalized wave function (3·1) these relations are not in general correct, but constitute a specialization of the problem. In the form (3·5) of course they are only symbolic equations; their real meaning is obviously

$$\int \Phi^*\left(\ldots \overset{i}{\times} \ldots \times \ldots; \ldots; \ldots; \ldots\right) \Phi\left(\ldots \times \ldots \overset{i}{\times} \ldots; \ldots; \ldots; \ldots\right) d\tau_i = 0. \quad (3·6)$$

Here Φ^* is any term in the development of the determinant (3·3) and Φ any other term, such that the ith particle is in two different $n\alpha$-states (indicated by the two crosses). The expression (3·6) is a measure of the exchange probability between the two $n\alpha$-states. Owing to the saturation effect this probability will be small for two states of the same type. I shall therefore assume that the orthogonality relations are satisfied; the generalization to the case for which this is not so can be made without much difficulty.

From (3·6) together with the orthogonality relations for the spin and particle functions it follows that in the normalizing integral (3·4) only square terms contribute. These all give the same contribution. Therefore (3·4) can be reduced to

$$\int \Phi^* \Phi \, d\tau = 1. \quad (3·7)$$

For later use I shall now develop the determinant (3·3) with respect to the first two rows. In order to avoid the collection of too many indices it is convenient to introduce the indices n, m, p, q referring respectively to $n\alpha$-, $n\beta$-, $p\alpha$, $p\beta$-states. Denote by D_{ij}^{nm} the subdeterminant obtained by omitting the first two rows, the ith $n\alpha$-column and the jth $n\beta$-column. The subdeterminant is to be taken with its proper sign so that

$$D_{ij}^{nm} = -D_{ji}^{mn}. \quad (3·8)$$

The other subdeterminants will be denoted correspondingly by D_{ij}^{nn}, D_{ij}^{np}, etc.; if the upper and lower indices are both equal, I define

$$D_{ii}^{nn} = 0. \quad (3·9)$$

Applying the symbolic method again, the subdeterminants can be split into two factors

$$D_{ij}^{nm} = d_i^n d_j^m. \quad (3·10)$$

In view of the antisymmetry of the subdeterminants, the d anticommute

$$d_i^n d_j^m = -d_j^m d_i^n. \quad (3·11)$$

With the help of these symbolic quantities, the desired expansion of the determinant (3·3) can be written down in the form

$$\Psi = \frac{1}{\sqrt{A!}} F(1)\, F(2), \tag{3·12}$$

$$\begin{aligned} F(1) = n(1)\left\{\alpha(1) \sum_{i=1}^{\nu} \phi_i(1)\, d_i^n + \beta(1) \sum_{i=1}^{\mu} \psi_i(1)\, d_i^m\right\} \\ + p(1)\left\{\alpha(1) \sum_{i=1}^{\kappa} \chi_i(1)\, d_i^p + \beta(1) \sum_{i=1}^{\lambda} \omega_i(1)\, d_i^q\right\}. \end{aligned} \tag{3·13}$$

Let us consider now some integrals over the products of two subdeterminants. In view of the orthogonality relations most of these vanish; thus

$$\int D_{ij}^{*nn} D_{kl}^{nn}\, d\tau_{12} = \int d_i^{*n} d_j^{*n} d_k^n d_l^n\, d\tau_{12} = 0, \quad \text{unless} \quad \begin{cases} i=k \\ j=l \end{cases} \text{or} \quad \begin{matrix} i=l, \\ j=k. \end{matrix} \tag{3·14}$$

Here the integration $d\tau_{12}$ extends over all co-ordinates except those of the first and second particle. Also

$$\int D_{ij}^{*nm} D_{kl}^{nm}\, d\tau_{12} = \int d_i^{*n} d_j^{*m} d_k^n d_l^m\, d\tau_{12} = 0, \quad \text{unless} \quad \begin{cases} i=k, \\ j=l, \end{cases} \tag{3·15}$$

and corresponding integrals for the other combinations of upper indices. All products of four d-factors, which do not also contain along with every d the corresponding d^*, give vanishing integrals. For example,

$$\int D_{ij}^{*nm} D_{kl}^{np}\, d\tau_{12} = \int d_i^{*n} d_j^{*m} d_k^n d_l^p\, d\tau_{12} = 0. \tag{3·16}$$

4. THE GENERALIZED DENSITIES

In this section I shall consider those integrals over products of two subdeterminants which do not vanish. They lead to the generalized densities. In order to define these I introduce first auxiliary densities

$$\begin{aligned} f_{ij}^{nm}(i', j'; i, j) = \int \Phi^*(1, 2, \ldots, i', \ldots; \ldots j' \ldots; \ldots; \ldots) \\ \times \Phi(1, 2, \ldots, i, \ldots; \ldots j \ldots; \ldots; \ldots)\, d\tau_{ij}. \end{aligned} \tag{4·1}$$

Here the indices i, j indicate the ith $n\alpha$-state and the jth $n\beta$-state. The integration extends over the co-ordinates of all particles except those of the particles in these two states.

$f_{ij}^{nm}(1, 2; 1, 2)$ is the average probability of finding a particle in the ith $n\alpha$-state at the point 1 and a particle in the jth $n\beta$-state at the point 2. $f_{ij}^{nm}(1, 2; 2, 1)$ is the corresponding exchange probability. Summation over all $n\alpha$-states and $n\beta$-states gives the probability or exchange probability respectively for a particle in any $n\alpha$-state at the point 1 and a particle in any $n\beta$-state at the point 2. These I define as the generalized densities

$$\left.\begin{aligned} \rho^{nm}(1,2;\,1,2) &= \sum_{i=1}^{\nu}\sum_{j=1}^{\mu} f_{ij}^{nm}(1,2;\,1,2), \\ \rho^{nm}(1,2;\,2,1) &= \sum_{i=1}^{\nu}\sum_{j=1}^{\mu} f_{ij}^{nm}(1,2;\,2,1). \end{aligned}\right\} \tag{4·2}$$

The densities for all other upper indices are defined correspondingly. (In the case of equal indices we have to add the definition $f_{ii}^{nn} = 0$.)

Integrating once more the average density of neutrons with spin α multiplied into the number μ of neutrons with spin β is obtained,

$$\int \rho^{nm}(1,2;\,1,2)\,d\tau_2 = \mu\rho_n(1). \tag{4·3}$$

But for equal indices

$$\int \rho^{nn}(1,2;\,1,2)\,d\tau_2 = (\nu-1)\,\rho_n(1). \tag{4·4}$$

This is a consequence of the Pauli principle, since in the summation over the auxiliary densities the summation for the second particle excludes the state in which the first particle is ($f_{ii}^{nn} = 0$).

Consider now the integral (3·15) for the case $i = k$, $j = l$. In view of the orthogonality relations only square terms contribute, and these give the auxiliary density f_{ij}^{nm}, if multiplied with the missing wave functions of the first and second particle. Summation over all i and j yields the densities

$$\left.\begin{aligned} \frac{1}{(A-2)!}\int \sum_i \sum_j \phi_i^*(1)\,\psi_j^*(2)\,D_{ij}^{*nm}\phi_i(1)\,\psi_j(2)\,D_{ij}^{nm}\,d\tau_{12} &= \rho^{nm}(1,2;\,1,2), \\ \frac{1}{(A-2)!}\int \sum_i \sum_j \phi_i^*(1)\,\psi_j^*(2)\,D_{ij}^{*nm}\phi_i(2)\,\psi_j(1)\,D_{ij}^{nm}\,d\tau_{12} &= \rho^{nm}(1,2;\,2,1). \end{aligned}\right\} \tag{4·5}$$

In view of (3·15) these expressions can also be written as fourfold sums:

$$\left.\begin{aligned} \frac{1}{(A-2)!}\int \sum_i \phi_i^*(1)\,d_i^{*n} \sum_j \psi_i^*(2)\,d_j^{*m} \sum_k \phi_k(1)\,d_k^n \sum_l \psi_l(2)\,d_l^m\,d\tau_{12} &= \rho^{nm}(1,2;\,1,2), \\ \frac{1}{(A-2)!}\int \sum_i \phi_i^*(1)\,d_i^{*n} \sum_j \psi_j^*(2)\,d_j^{*m} \sum_k \phi_k(2)\,d_k^n \sum_l \psi_l(1)\,d_l^m\,d\tau_{12} &= \rho^{nm}(1,2;\,2,1). \end{aligned}\right\} \tag{4·6}$$

I therefore define the symbolic quantities

$$\frac{1}{\{(A-2)!\}^{\frac{1}{2}}}\int \sum \phi_i(1)\,d_i^n(d\tau_{12})^{\frac{1}{2}} = \rho^n(1). \tag{4·7}$$

Here $(d\tau_{12})^{\frac{1}{4}}$ indicates that we are dealing only with a symbolic integration, which has a meaning only if four such integrals are multiplied, giving together one integral over $d\tau_{12}$. With (4·7), (4·6) reduces to the simple equation

$$\left.\begin{aligned}\rho^{*n}(1)\,\rho^{*m}(2)\,\rho^{n}(1)\,\rho^{m}(2) &= \rho^{nm}(1,2;\,1,2),\\ \rho^{*n}(1)\,\rho^{*m}(2)\,\rho^{n}(2)\,\rho^{m}(1) &= \rho^{nm}(1,2;\,2,1).\end{aligned}\right\} \qquad (4\cdot 8)$$

Corresponding equations hold for other indices.

From the definition (4·7) it follows that the ρ obey the same commutation laws as the d; two ρ's anticommute, but ρ commutes with ρ^* (the commutability of ρ and ρ^* is a matter of convenience and has no further significance):

$$\rho^n\rho^m = -\rho^m\rho^n; \quad \rho^n\rho^{*m} = \rho^{*m}\rho^n. \qquad (4\cdot 9)$$

Corresponding to the equations (4·8), (3·16) gives in exactly the same way

$$\rho^{*n}(1)\,\rho^{*m}(2)\,\rho^{n}(1)\,\rho^{p}(2) = 0, \qquad (4\cdot 10)$$

and all similar products vanish which do not contain along with every ρ the corresponding $\rho^*(1)$ or $\rho^*(2)$.

Consider now the case that all indices are equal. For example,

$$\rho^{*n}(1)\,\rho^{*n}(2)\,\rho^{n}(1)\,\rho^{n}(2).$$

This might be expected to be equal to $\rho^{nn}(1,2;\,1,2)$. But exchanging the last two factors, it could equally well be $-\rho^{nn}(1,2;\,2,1)$. I shall prove that it is equal to the sum of both

$$\rho^{*n}(1)\,\rho^{*n}(2)\,\rho^{n}(1)\,\rho^{n}(2) = \rho^{nn}(1,2;\,1,2) - \rho^{nn}(1,2;\,2,1). \qquad (4\cdot 11)$$

Introducing the definition (4·7) the left-hand side is

$$\frac{1}{(A-2)!}\sum_{ijkl}\int \phi_i^*(1)\,d_i^{*n}\phi_j^*(2)\,d_j^{*n}\phi_k(1)\,d_k^n\,\phi_l(2)\,d_l^n\,d\tau_{12}.$$

With (3·14) this is equal to

$$\frac{1}{(A-2)!}\sum_{ij}\int \phi_i^*(1)\,d_i^{*n}\phi_j^*(2)\,d_j^{*n}\{\phi_i(1)\,d_i^n\phi_j(2)\,d_j^n + \phi_j(1)\,d_j^n\phi_i(2)\,d_i^n\}\,d\tau_{12}$$

$$= \frac{1}{(A-2)!}\sum_{ij}\int \phi_i^*(1)\,\phi_j^*(2)\,D_{ij}^{*nn}\{\phi_i(1)\,\phi_j(2) - \phi_j(1)\,\phi_i(2)\}\,D_{ij}^{nn}\,d\tau_{12}.$$

This expression easily reduces to (4·11) which is therefore proved.

Consider now an integral of the form

$$J = \int \Psi^* O_{12} \Psi\, d\tau_{12}, \qquad (4\cdot 12)$$

where O_{12} is an operator acting only on the co-ordinates of the first and second particle. Introducing (3·12) this integral is

$$J = \frac{1}{A!}\int F^*(1)\,F^*(2)\,O_{12}\,F(1)\,F(2)\,d\tau_{12}.$$

Now split this integral into four symbolic integrals,

$$J = \frac{1}{A(A-1)}\,G^*(1)\,G^*(2)\,O_{12}\,G(1)\,G(2), \tag{4·13}$$

where
$$G(1) = \frac{1}{\{(A-2)!\}^{\frac{1}{2}}}\int F(1)\,(d\tau_{12})^{\frac{1}{2}}.$$

Introducing the expression (3·13) for F, the integrals (4·7) are obtained

$$G(1) = n(1)\{\alpha(1)\rho^n(1)+\beta(1)\rho^m(1)\}+p(1)\{\alpha(1)\rho^p(1)+\beta(1)\rho^q(1)\}. \tag{4·14}$$

5. THE MAJORANA ENERGY

The Majorana potential (2·7) contains the operator $J^m_{12}S_{12}U_{12}$. There are altogether $A(A-1)$ such operators, all giving obviously the same contribution to the energy. The total Majorana energy is therefore

$$E_M = A(A-1)\int \Psi^* J^m_{12}S_{12}U_{12}\Psi\,d\tau. \tag{5·1}$$

The integration over the co-ordinates of all particles except those of the first and second particle yields an integral of the form (4·12). Introducing the expression (4·13) for this integral, (5·1) reduces to

$$\int G^*(1)\,G^*(2)\,J^m_{12}S_{12}U_{12}\,G(1)\,G(2)\,d\tau_1\,d\tau_2. \tag{5·2}$$

Now, with (2·4), (2·6) and (4·14)

$$S_{12}U_{12}\,G(1)\,G(2) = n(1)\,p(2)\{\alpha(2)\rho^p(1)+\beta(2)\rho^q(1)\}\{\alpha(1)\rho^n(2)+\beta(1)\rho^m(2)\}.$$

Since the particle functions $n(1)$ and $p(1)$ are orthogonal, we obtain therefore in (5·2) a contribution only from those terms in $G^*(1)$ and $G^*(2)$ which are proportional to $n(1)$ or $p(2)$. The summation over the particle variables gives therefore

$$E_M = \int J^m_{12}\{\alpha(1)\rho^{*n}(1)+\beta(1)\rho^{*m}(1)\}\{\alpha(2)\rho^{*p}(2)+\beta(2)\rho^{*q}(2)\}$$
$$\times\{\alpha(2)\rho^p(1)+\beta(2)\rho^q(1)\}\{\alpha(1)\rho^n(2)+\beta(1)\rho^m(2)\}\,d\tau_1\,d\tau_2. \tag{5·3}$$

In order to sum over the spin variables, multiply the first bracket into the last and the second into the third. In doing so the last two brackets are commuted giving a − sign. Only square terms in the spin functions give a contribution. Thus

$$E_M = -\int J^m_{12}\{\rho^{*n}(1)\rho^n(2)+\rho^{*m}(1)\rho^m(2)\}\{\rho^{*p}(2)\rho^p(1)+\rho^{*q}(2)\rho^q(1)\}\,d\tau_1 d\tau_2,$$

or with (4·8)

$$E_M = -\int J^m_{12}\{\rho^{np}(1,2;\,2,1)+\rho^{nq}(1,2;\,2,1)+\rho^{mp}(1,2;\,2,1)+\rho^{mq}(1,2;\,2,1)\}\,d\tau_1 d\tau_2. \qquad (5\cdot4)$$

6. The Heisenberg energy

The Heisenberg potential (2·7) differs from the Majorana potential only in the fact that the operator S_{12} is absent. It leads therefore to the same equation (5·3) except that the spin variables in the last two brackets should not be interchanged:

$$E_H = \int J^h_{12}\{\alpha(1)\rho^{*n}(1)+\beta(1)\rho^{*m}(1)\}\{\alpha(2)\rho^{*p}(2)+\beta(2)\rho^{*q}(2)\} \times\{\alpha(1)\rho^p(1)+\beta(1)\rho^q(1)\}\{\alpha(2)\rho^n(2)+\beta(2)\rho^m(2)\}\,d\tau_1 d\tau_2. \qquad (6\cdot1)$$

In order to sum over the spin variables, multiply the first bracket into the third and the second into the fourth. For this purpose we need only commute ρ and ρ^* and no change of sign occurs. The result is

$$E_H = \int J^h_{12}\{\rho^{*n}(1)\rho^p(1)+\rho^{*m}(1)\rho^q(1)\}\{\rho^{*p}(2)\rho^n(2)+\rho^{*q}(2)\rho^m(2)\}\,d\tau_1 d\tau_2. \qquad (6\cdot2)$$

In order to obtain the factors in the correct order, commute $\rho(1)$ with $\rho(2)$ and obtain a − sign. With (4·8) and (4·10) it follows that

$$E_H = -\int J^h_{12}\{\rho^{np}(1,2;\,2,1)+\rho^{mq}(1,2;\,2,1)\,d\tau_1 d\tau_2. \qquad (6\cdot3)$$

7. The Bartlett energy

There are $A(A-1)/2$ Bartlett potentials of the type (2·7). Corresponding to (5·2) the Bartlett energy is therefore

$$E_B = \frac{1}{2}\int G^*(1)\,G^*(2)\,J^b_{12}S_{12}G(1)\,G(2)\,d\tau_1 d\tau_2. \qquad (7\cdot1)$$

With (2·6) and (4·14) it follows that

$$S_{12}G(1)\,G(2) = [n(1)\{\alpha(2)\,\rho^n(1)+\beta(2)\,\rho^m(1)\}+p(1)\{\alpha(2)\,\rho^p(1)+\beta(2)\,\rho^q(1)\}] \\ \times[n(2)\{\alpha(1)\,\rho^n(2)+\beta(1)\,\rho^m(2)\}+p(2)\{\alpha(1)\,\rho^p(2)+\beta(1)\,\rho^q(2)\}]. \quad (7{\cdot}2)$$

Multiply the first bracket into $G^*(1)$ and sum over the particle variables; the result is

$$\{\alpha(1)\,\rho^{*n}(1)+\beta(1)\,\rho^{*m}(1)\}\{\alpha(2)\,\rho^n(1)+\beta(2)\,\rho^m(1)\} \\ +\{\alpha(1)\,\rho^{*p}(1)+\beta(1)\,\rho^{*q}(1)\}\{\alpha(2)\,\rho^p(1)+\beta(2)\,\rho^q(1)\}. \quad (7{\cdot}3)$$

The second bracket in (7·2) multiplied into $G^*(2)$ gives the same expression with 1 and 2 interchanged. Now multiply these two expressions with each other and insert them in (7·1). In order to sum over the spin indices, we have to commute two anticommuting expressions. Therefore

$$E_B = -\frac{1}{2}\int J^b_{12}\left\{\begin{aligned} &[\rho^{*n}(1)\,\rho^n(2)+\rho^{*m}(1)\,\rho^m(2)]\,[\rho^n(1)\,\rho^{*n}(2)+\rho^m(1)\,\rho^{*m}(2)] \\ &+[\rho^{*n}(1)\,\rho^p(2)+\rho^{*m}(1)\,\rho^q(2)]\,[\rho^n(1)\,\rho^{*p}(2)+\rho^m(1)\,\rho^{*q}(2)] \\ &+[\rho^{*p}(1)\,\rho^n(2)+\rho^{*q}(1)\,\rho^m(2)]\,[\rho^p(1)\,\rho^{*n}(2)+\rho^q(1)\,\rho^{*m}(2)] \\ &+[\rho^{*p}(1)\,\rho^p(2)+\rho^{*q}(1)\,\rho^q(2)]\,[\rho^p(1)\,\rho^{*p}(2)+\rho^q(1)\,\rho^{*q}(1)] \end{aligned}\right\} d\tau_1 d\tau_2. \tag{7·4}$$

Here the second term is identical with the third, as follows by exchange of the integration variables 1 and 2. In the same way in the first and last term the two cross-products are identical. Omitting all terms which vanish according to (4·10) and using (4·8) and (4·11), the Bartlett energy is

$$E_B = \frac{1}{2}\int J^b_{12}\left\{\begin{aligned} &\rho^{nn}(1,2;\,1,2)+\rho^{mm}(1,2;\,1,2)+\rho^{pp}(1,2;\,1,2)+\rho^{qq}(1,2;\,1,2) \\ &-\rho^{nn}(1,2;\,2,1)-\rho^{mm}(1,2;\,2,1)-\rho^{pp}(1,2;\,2,1)-\rho^{qq}(1,2;\,2,1) \\ &-2\rho^{nm}(1,2;\,2,1)-2\rho^{pq}(1,2;\,2,1) \\ &+2\rho^{np}(1,2;\,1,2)+2\rho^{mq}(1,2;\,1,2) \end{aligned}\right\} d\tau_1 d\tau_2. \tag{7·5}$$

8. The Wigner energy

The Wigner energy is

$$\frac{1}{2}\int G^*(1)\,G^*(2)\,J^w_{12}\,G(1)\,G(2)\,d\tau_1 d\tau_2. \tag{8·1}$$

Multiplying $G^*(1)$ into $G(1)$ and summing over the particle and spin variables gives

$$\rho^{*n}(1)\,\rho^n(1)+\rho^{*m}(1)\,\rho^m(1)+\rho^{*p}(1)\,\rho^p(1)+\rho^{*q}(1)\,\rho^q(1).$$

Insert this expression and the corresponding expression for the second particle in (8·1). This leads to

$$E_W = \frac{1}{2}\int J^{w}_{12}\left\{\begin{array}{l}\rho^{nn}(1,2;\,1,2)+\rho^{mm}(1,2;\,1,2)+\rho^{pp}(1,2;\,1,2)+\rho^{qq}(1,2;\,1,2)\\ \quad -\rho^{nn}(1,2;\,2,1)-\rho^{mm}(1,2;\,2,1)-\rho^{pp}(1,2;\,2,1)-\rho^{qq}(1,2;\,2,1)\\ \quad +2\rho^{nm}(1,2;\,1,2)+2\rho^{np}(1,2;\,1,2)+2\rho^{nq}(1,2;\,1,2)\\ \quad +2\rho^{mp}(1,2;\,1,2)+2\rho^{mq}(1,2;\,1,2)+2\rho^{pq}(1,2;\,1,2)\end{array}\right\}d\tau_1 d\tau_2. \tag{8·2}$$

9. THE ENERGIES BETWEEN LIKE PARTICLES

The forces between like particles (2·8) can of course be treated in the same way. But it is much simpler to observe that the whole effect of the operator $N_{ik}+P_{ik}$ is to cancel all terms containing an interaction between unlike particles. Thus we need only omit these terms in the equations (7·5) and (8·2) for the Bartlett and Wigner energies. The result is

$$E_K = \frac{1}{2}\int J^{k}_{12}\left\{\begin{array}{l}\rho^{nn}(1,2;\,1,2)+\rho^{mm}(1,2;\,1,2)+\rho^{pp}(1,2;\,1,2)+\rho^{qq}(1,2;\,1,2)\\ \quad -\rho^{nn}(1,2;\,2,1)-\rho^{mm}(1,2;\,2,1)-\rho^{pp}(1,2;\,2,1)-\rho^{qq}(1,2;\,2,1)\\ \quad -2\rho^{nm}(1,2;\,2,1)-2\rho^{pq}(1,2;\,2,1)\end{array}\right\}d\tau_1 d\tau_2, \tag{9·1}$$

$$E_L = \frac{1}{2}\int J^{l}_{12}\left\{\begin{array}{l}\rho^{nn}(1,2;\,1,2)+\rho^{mm}(1,2;\,1,2)+\rho^{pp}(1,2;\,1,2)+\rho^{qq}(1,2;\,1,2)\\ \quad -\rho^{nn}(1,2;\,2,1)-\rho^{mm}(1,2;\,2,1)-\rho^{pp}(1,2;\,2,1)-\rho^{qq}(1,2;\,2,1)\\ \quad +2\rho^{nm}(1,2;\,1,2)+2\rho^{pq}(1,2;\,1,2)\end{array}\right\}d\tau_1 d\tau_2. \tag{9·2}$$

10. CONCLUSIONS

The equations obtained for the various energies are of the same form as those obtained in the independent particle picture. The reason for this is to be found in the orthogonality relations (3·6) between states of the same type, which can be supported by the fact that the exchange probability between such states can be expected to be small. It seems to me that this fact largely explains the fair success which the independent particle picture has had in the calculation of nuclear energies.

But even with this assumption there is one very important difference between the results of the independent particle picture and the results obtained in this paper. Here the density functions depend on two variables, and it must be expected that they are rather larger than in the independent particle picture, if two attracting particles are near each other, thereby giving a larger energy. In the independent particle picture this effect must be balanced by assuming larger constants in the expressions for the potentials, in order to obtain the correct energies. Indeed the constants obtained by numerical calculations have always been much larger than those obtained for the smaller nuclei by exact methods (cf. Bethe and Bacher 1936, p. 157).

Expressions for the nuclear energies have been derived taking into account separately the two spin directions. This makes it possible to differentiate between the "even" and "odd" nuclei and to investigate the stability breadth. In the following paper by B. Spain the nuclear energies are calculated, assuming independent wave functions but taking into account the spin terms, and the stability of nuclei is considered.

SUMMARY

A generalization of the statistical method for the calculation of nuclear energies is given, which makes it possible to dispense with the Hartree approximation of independent wave functions.

The two directions of the spin are considered separately and general expressions for the energy of nuclei with any spin are derived.

REFERENCES

Bethe, H. A. and Bacher, R. F. 1936 *Rev. Mod. Phys.* **8**, 82.
Spain, B. 1940 *Proc. Roy. Soc.*, A, **174**, 523.

Calculation of nuclear energies and stability by the statistical method

By B. Spain

University of Edinburgh

(*Communicated by M. Born, F.R.S.—Received* 2 *November* 1939)

1. Introduction

Leaving out of consideration those nuclei of small atomic number it is possible to develop a statistical theory of nuclei. Bethe and Bacher (1936, p. 149), as well as many other writers, have treated this subject in great detail starting from the Hartree approximation.

All these investigations were mainly concerned with the binding energy, and not much attention has been paid so far to the stability of nuclei according to the statistical theory, except the determination of the most stable nucleus with a given atomic number: this is due to the fact that previous investigators have always neglected to distinguish between quantum states with opposite spin, thereby losing the distinction between "odd" and "even" nuclei, which is essential for stability considerations.

In this paper the statistical theory is generalized by treating the two spin directions according to the method introduced by Fuchs (1940). The four different types of nuclear forces are taken into account: for simplicity it is assumed that the non-saturation combination of Wigner and Bartlett forces vanishes, i.e. the Bartlett force is double the Wigner force.

The types of interaction potential investigated up to the present have usually been the error function or the simple exponential function. The meson theory indicates a potential proportional to $(a/r)\exp(-r/a)$. For reasons indicated in the next section, I have taken a linear combination of the meson potential and the simple exponential function.

With this potential I have calculated the total energy (§§ 3–7). The constants occurring have been determined from four experimental results for ${}_{16}\mathrm{S}^{32}$ and ${}_{80}\mathrm{Hg}^{200}$ (§ 8).

The results are applied to the calculation of nuclear energies and radii. Satisfactory agreement with experiment is obtained (§ 9).

Finally, the stability of nuclei is investigated. The results are satisfactory for odd nuclei: for even nuclei, on the other hand, the region of stability obtained is too small. This seems to indicate that the statistical model does not emphasize sufficiently the difference between even and odd nuclei (§§ 10–11).

2. The nuclear forces

The potentials corresponding to the various interaction forces are defined by (F. 2·7).* For the purpose of this paper it is necessary to make some assumption about the explicit form of the various J. There is no justification (except mathematical convenience) for use of either of the interaction potentials $B\exp(-r^2/a^2)$ or $B\exp(-r/a)$ which are usually assumed in the statistical model. There is evidence from the theory of the meson (Kemmer 1938) that the correct form of the interaction potential is $B(a/r)\exp(-r/a)$. I have attempted to develop the statistical theory according to the Hartree method with this form of the potential, but the result of fitting the model to the nucleus ${}_{80}\mathrm{Hg}^{200}$ gives a value of a much larger than that deduced from the meson theory. With the potential $B\exp(-r/a)$ Bethe and Bacher (1936, p. 160) find that the corresponding value of a is smaller than the meson value. I have, therefore, taken a potential which is a linear combination of the ordinary exponential and meson potential, i.e. $B(k+a/r)\exp(-r/a)$, and fixed a from the meson theory, leaving the absolute numerical constant k to be derived from the model. Yukawa (1935) has deduced the relation $a=\hbar/M_0c$, where M_0 is the mass of the meson. The most reliable data give $M_0=170m_0$, where m_0 is the mass of the electron. With this value I obtain $a=2{\cdot}26\times10^{-13}$ cm. It is of interest to note that for values of r much smaller than a, the meson potential is the more important term.

Explicitly the assumptions are:

$$\left.\begin{aligned} J^m(r_{ik}) &= m(k+a/r)\exp(-r/a),\\ J^h(r_{ik}) &= h(k+a/r)\exp(-r/a),\\ J^b(r_{ik}) &= b(k+a/r)\exp(-r/a),\\ J^w(r_{ik}) &= w(k+a/r)\exp(-r/a),\end{aligned}\right\} \tag{2·1}$$

where m, h, b, w are unknown constants of energy dimension, determining the strengths of the various forces.

3. Wave function and densities

I now introduce the usual assumption that each particle in the nucleus moves independently and its eigenfunction is that of a free particle, i.e.

---

* Frequent reference is made to equations of Fuchs (1940). The notation (F. 2·7) means equation (2·7) of his paper.

a plane wave. The total wave function Ψ is taken to be the determinantal form (F. 3·3), where now the various ϕ_r and ψ_s represent plane waves.

The calculation of the densities and mixed densities in this case is well known (Bethe and Bacher 1936, p. 153). Since I distinguish between the two spin directions, I here introduce four maximum wave numbers:

$$\left.\begin{aligned} p_{n\alpha} &= \left(\frac{9\pi N_\alpha}{2}\right)^{\frac{1}{3}} R^{-1}, \quad p_{n\beta} = \left(\frac{9\pi N_\beta}{2}\right)^{\frac{1}{3}} R^{-1}, \\ p_{p\alpha} &= \left(\frac{9\pi P_\alpha}{2}\right)^{\frac{1}{3}} R^{-1}, \quad p_{p\beta} = \left(\frac{9\pi P_\beta}{2}\right)^{\frac{1}{3}} R^{-1}, \end{aligned}\right\} \qquad (3{\cdot}1)$$

where N_α, N_β, P_α, P_β are the numbers of neutrons and protons with spin α, β respectively, and R is the radius of the nucleus.

Then the densities are given by*

$$\left.\begin{aligned} \rho^{n\alpha,p\alpha}(1,2;\,1,2) &= N_\alpha P_\alpha/V^2, \text{ etc.,} \\ \rho^{n\alpha,n\alpha}(1,2;\,1,2) &= N_\alpha(N_\alpha-1)/V^2, \text{ etc.,} \\ \rho^{n\alpha,p\alpha}(1,2;\,2,1) &= \frac{1}{4\pi^4}\frac{1}{r_{12}^6}\{\sin p_{n\alpha}r_{12} - p_{n\alpha}r_{12}\cos p_{n\alpha}r_{12}\} \\ &\qquad \times \{\sin p_{p\alpha}r_{12} - p_{p\alpha}r_{12}\cos p_{p\alpha}r_{12}\}, \\ \rho^{n\alpha,n\alpha}(1,2;\,2,1) &= \frac{1}{4\pi^4}\frac{1}{r_{12}^6}\{\sin p_{n\alpha}r_{12} - p_{n\alpha}r_{12}\cos p_{n\alpha}r_{12}\}^2 - \frac{N_\alpha}{V^2}, \end{aligned}\right\} \qquad (3{\cdot}2)$$

where $V = \frac{4}{3}\pi R^3$ is the volume of the nucleus.

4. INTERACTION ENERGIES

(*a*) *Majorana energy*

From (F. 5·4) the first term in the Majorana energy is

$$-\int J_{12}^m \rho^{n\alpha,p\alpha}(1,2;\,2,1)\,d\tau_1\,d\tau_2$$

$$= -\frac{m}{4\pi^4}\int\left(k+\frac{a}{r_{12}}\right)\frac{e^{-r_{12}/a}}{r_{12}^6}\{\sin p_{n\alpha}r_{12} - p_{n\alpha}r_{12}\cos p_{n\alpha}r_{12}\}$$
$$\times \{\sin p_{p\alpha}r_{12} - p_{p\alpha}r_{12}\cos p_{p\alpha}r_{12}\}\,d\tau_1\,d\tau_2.$$

Now the integral over $d\tau_1 d\tau_2$ can be replaced by an integral over $d\tau_1 d\tau_{12}$, where $d\tau_{12}$ means integration over the relative co-ordinates, i.e. first integrate over the co-ordinates of particle 2 keeping particle 1 fixed. Since the value of the integrand drops rapidly to zero as r_{12} increases, the range of integration of the relative co-ordinate r_{12} can be extended to infinity. The integration over $d\tau_1$ gives a factor equal to the volume of the nucleus. Integrating also over the angular co-ordinates and introducing the dimensionless quantities

---

* The notation differs here slightly from Fuchs (1940). See paragraph following (F. 3·7).

$$x_{n\alpha}=ap_{n\alpha},\quad x_{n\beta}=ap_{n\beta},\quad x_{p\alpha}=ap_{p\alpha},\quad x_{p\beta}=ap_{p\beta}, \tag{4·1}$$

$$r_{12}=ar, \tag{4·2}$$

the above term takes the value

$$-\frac{4}{3\pi^2}\frac{mR^3}{a^3}\int_0^\infty\left(\frac{k}{r^4}+\frac{a}{r^5}\right)e^{-r}\{\sin x_{n\alpha}r-x_{n\alpha}r\cos x_{n\alpha}r\}\{\sin x_{p\alpha}r-x_{p\alpha}r\cos x_{p\alpha}r\}\,dr.$$

Introduce now the function $I_n(x,y)$ by

$$I_n(x,y)=\int_0^\infty\frac{e^{-r}}{r^n}\{\sin xr-xr\cos xr\}\{\sin yr-yr\cos yr\}\,dr. \tag{4·3}$$

Then
$$-\int J^m_{12}\rho^{n\alpha,p\alpha}(1,2;\,2,1)\,d\tau_1\,d\tau_2=-\frac{4}{3\pi^2}\frac{mR^3}{a^3}f(x_{n\alpha},x_{p\alpha}),$$

where
$$f(x,y)=kI_4(x,y)+I_5(x,y). \tag{4·4}$$

The values of I_4 and I_5 are calculated in Appendix A. From (F. 5·4) the total Majorana energy is

$$E_M=-\frac{4}{3\pi^2}\frac{mR^3}{a^3}\{f(x_{n\alpha},x_{p\alpha})+f(x_{n\alpha},x_{p\beta})+f(x_{n\beta},x_{p\alpha})+f(x_{n\beta},x_{p\beta})\}. \tag{4·5}$$

(*b*) *Heisenberg energy*

From (F. 6·3) the total Heisenberg energy is

$$E_H=-\frac{4}{3\pi^2}\frac{hR^3}{a^3}\{f(x_{n\alpha},x_{p\alpha})+f(x_{n\beta},x_{p\beta})\}. \tag{4·6}$$

(*c*) *Bartlett energy*

From (F. 7·5) it is seen that the Bartlett energy in addition also involves integrals over the ordinary densities. These lead to the following expressions:

$$\zeta=\eta+k\bar{\eta}, \tag{4·7}$$

$$\eta=\frac{1}{a^2}\int_0^R re^{-r/a}\,dr=1-(1+R/a)\,e^{-R/a}, \tag{4·8}$$

$$\bar{\eta}=\frac{1}{a^3}\int_0^R r^2e^{-r/a}\,dr=2\{1-(1+R/a+\tfrac{1}{2}R^2/a^2)\,e^{-R/a}\}. \tag{4·9}$$

Then the total Bartlett energy is

$$E_B = -\frac{2}{3\pi^2}\frac{bR^3}{a^3}\{f(x_{n\alpha}, x_{n\alpha}) + f(x_{n\beta}, x_{n\beta}) + f(x_{p\alpha}, x_{p\alpha}) + f(x_{p\beta}, x_{p\beta}) + 2f(x_{n\alpha}, x_{n\beta}) + 2f(x_{p\alpha}, x_{p\beta})\} + \frac{3ba^3}{2R^3}\{(N_\alpha + P_\alpha)^2 + (N_\beta + P_\beta)^2\}\zeta. \quad (4\cdot 10)$$

(*d*) *Wigner energy*

Similarly from (F. 8·2) the total Wigner energy is

$$E_W = \frac{2}{3\pi^2}\frac{wR^3}{a^3}\{f(x_{n\alpha}, x_{n\alpha}) + f(x_{n\beta}, x_{n\beta}) + f(x_{p\alpha}, x_{p\alpha}) + f(x_{p\beta}, x_{p\beta})\} - \frac{3wa^3}{2R^3}(N_\alpha + N_\beta + P_\alpha + P_\beta)^2\zeta. \quad (4\cdot 11)$$

(*e*) *Coulomb energy*

Since the two different spin directions are distinguished, the total Coulomb energy is

$$E_C = \frac{3}{5}\frac{e^2}{R}(P_\alpha + P_\beta)^2 - \frac{3}{2}\frac{e^2}{R}(P_\alpha^{4/3} + P_\beta^{4/3}). \quad (4\cdot 12)$$

(*f*) *Kinetic energy*

Obtaining the average densities $\rho_{n\alpha}$, etc. from (F. 4·3), and using the Fermi-Dirac expression for the kinetic energy (distinguishing between the two spin directions) the total kinetic energy is

$$E_T = \frac{3^{5/3}\hbar^2\pi^{4/3}2^{5/3}}{20M}\frac{1}{R^2}\{N_\alpha^{5/3} + N_\beta^{5/3} + P_\alpha^{5/3} + P_\beta^{5/3}\}. \quad (4\cdot 13)$$

5. SURFACE EFFECT

In calculating the integrals occurring in the interaction energies, we have extended the range of integration over the relative co-ordinate of the two interacting particles to infinity, neglecting in consequence the fact that particles near the surface interact with a smaller number of particles than do particles in the interior of the nucleus. Also the boundary of the nucleus cannot be sharply defined, as this would mean an infinite derivative of all particle wave functions leading to an infinite kinetic energy. The surface layer of the nucleus, where the density of particles drops very rapidly, must be spread out over a small region. It is obvious that if this surface layer is increased, the kinetic energy decreases and the potential energy increases. Thus for some intermediate surface layer there exists a minimum of the energy. The amount by which the energy is increased by the existence of the surface layer can be called the surface energy.

Weizsäcker (1937) attempts to set up a quantitative method of estimating the surface energy. If the density ρ is not constant he has derived the following expression for the kinetic energy:

$$\int\left\{\frac{\hbar^2}{5\pi M}\left(\frac{3\rho}{8\pi}\right)^{\frac{5}{3}}+\frac{\hbar^2}{8M}\frac{(\operatorname{grad}\rho)^2}{\rho}\right\}d\tau. \tag{5·1}$$

Using this expression instead of (4·13) the correct form of ρ ought to be deduced from the minimum condition

$$\delta\int\{\text{The total energy}\}\,d\tau=0. \tag{5·2}$$

This variational equation gives rise to a non-linear differential equation of the second order which can only be solved numerically, but this procedure would be troublesome if not impossible owing to the existence as yet of so many unknown constants.

Weizsäcker assumes that the density ρ is

$$\left.\begin{aligned}\rho &= \rho_0\{1-\tfrac{1}{2}e^{\lambda(r-R)/R}\}^2 \qquad & r\leqslant R,\\ \rho &= \tfrac{1}{4}\rho_0 e^{-2\lambda(r-R)/R} \qquad & r\geqslant R.\end{aligned}\right\} \tag{5·3}$$

The parameter λ introduced is then determined from a minimum condition, and thus the surface energy is obtained.

I have attempted to estimate the surface energy similarly with the density distribution (5·3) and also with several others. Expressing the kinetic and potential energies as power series in the parameter λ and minimizing it gives λ. Substituting to find the surface energy, I find that the series representing the energy is not convergent. The reason probably is that the correct solution of the variational equation is not easily approximated to by simple analytical functions. Weizsäcker avoided this difficulty by adopting a numerical method of solution, but this is impossible here with the large number of unknown constants.*

I have, therefore, had recourse to the semi-empirical method, i.e. a term is added involving an unknown constant to account for the surface energy. It is known that the surface energy for large nuclei ought to be proportional to $A^{\frac{2}{3}}$, where A is the total number of particles. Also we know that approximately $R = A^{\frac{1}{3}}$, so that a suitable term for the surface energy is

---

* For a criticism of Weizsäcker's method see Bethe and Bacher (1936, p. 164).

$$E_s = \frac{\omega A^{\frac{4}{3}}}{R^2}, \qquad (5\cdot 4)$$

where ω is the unknown constant introduced.

The semi-empirical term has the unsatisfactory features that it introduces a new arbitrary constant and fails to give any indication of the influence of the surface effect on the portion of the energy due to the spin.

6. Total energy

Introducing $\quad N_\alpha + N_\beta + P_\alpha + P_\beta = A = \lambda^3, \quad R = r\lambda, \qquad (6\cdot 1)$

$$N_\alpha = n_\alpha A, \quad N_\beta = n_\beta A, \quad P_\alpha = p_\alpha A, \quad P_\beta = p_\beta A, \qquad (6\cdot 2)$$

it follows from (3·1) and (4·1) that

$$x_{n\alpha} = \left(\frac{9\pi}{2}\right)^{\frac{1}{3}} n_\alpha^{\frac{1}{3}} \frac{a}{r}, \text{ etc.} \qquad (6\cdot 3)$$

Introducing the constants

$$c_m = \frac{4m}{3\pi^2 a^3}, \quad c_h = \frac{4h}{3\pi^2 a^3}, \quad c_b = \frac{2b}{3\pi^2 a^3}, \quad c_w = \frac{2w}{3\pi^2 a^3}, \qquad (6\cdot 4)$$

$$e_1 = \frac{3}{20} e^2, \quad e_2 = \frac{3}{2^{\frac{1}{3}}} e^2, \quad e_3 = \frac{3^{\frac{7}{3}} \hbar^2 \pi^{\frac{2}{3}}}{40M}, \qquad (6\cdot 5)$$

the total energy is expressed in the form

$$\begin{aligned} E = {} & -c_m r^3\lambda^3\{f(x_{n\alpha}, x_{p\alpha}) + f(x_{n\alpha}, x_{p\beta}) + f(x_{n\beta}, x_{p\alpha}) + f(x_{n\beta}, x_{p\beta})\} \\ & - c_h r^3\lambda^3\{f(x_{n\alpha}, x_{p\alpha}) + f(x_{n\beta}, x_{p\beta})\} \\ & - c_b r^3\lambda^3\{f(x_{n\alpha}, x_{n\alpha}) + f(x_{n\beta}, x_{n\beta}) + f(x_{p\alpha}, x_{p\alpha}) + f(x_{p\beta}, x_{p\beta}) \\ & \qquad + 2f(x_{p\alpha,p\beta}) + 2f(x_{n\alpha,n\beta})\} + \frac{3ba^3}{2r^3\lambda^3}\{(N_\alpha + P_\alpha)^2 + (N_\beta + P_\beta)^2\}\zeta \\ & + c_w r^3\lambda^3\{f(x_{n\alpha}, x_{n\alpha}) + f(x_{n\beta}, x_{n\beta}) + f(x_{p\alpha}, x_{p\alpha}) + f(x_{p\beta}, x_{p\beta})\} \\ & \qquad - \frac{3w}{2}\frac{a^3}{r^3\lambda^3}(N_\alpha + N_\beta + P_\alpha + P_\beta)^2 \zeta \\ & \qquad + \frac{4e_1}{r\lambda}(P_\alpha + P_\beta)^2 - \frac{2^{\frac{1}{3}} e_2}{r\lambda}(P_\alpha^{\frac{4}{3}} + P_\beta^{\frac{4}{3}}) \\ & \qquad + \frac{2^{\frac{4}{3}} e_3}{r^2\lambda^2}(N_\alpha^{\frac{5}{3}} + N_\beta^{\frac{5}{3}} + P_\alpha^{\frac{5}{3}} + P_\beta^{\frac{5}{3}}) + \frac{\omega\lambda^2}{r^2}. \end{aligned} \qquad (6\cdot 6)$$

7. EXPANSION OF THE ENERGY

The energy (6·6) takes the simplest form if the numbers of neutrons and protons with the two different spin values are all equal, i.e.

$$n_\alpha = n_\beta = p_\alpha = p_\beta. \tag{7·1}$$

All stable nuclei lie more or less in the neighbourhood of the line (7·1), and thus the energy is expanded near this line. To do this introduce

$$\left.\begin{aligned} \delta &= n_\alpha + n_\beta - p_\alpha - p_\beta, \\ s &= n_\alpha - n_\beta + p_\alpha - p_\beta, \\ t &= n_\alpha - n_\beta - p_\alpha + p_\beta, \end{aligned}\right\} \tag{7·2}$$

and since obviously

$$n_\alpha + n_\beta + p_\alpha + p_\beta = 1, \tag{7·3}$$

it follows that

$$\left.\begin{aligned} n_\alpha &= \tfrac{1}{4}(1+\delta+s+t), \quad n_\beta = \tfrac{1}{4}(1+\delta-s-t), \\ p_\alpha &= \tfrac{1}{4}(1-\delta+s-t), \quad p_\beta = \tfrac{1}{4}(1-\delta-s+t). \end{aligned}\right\} \tag{7·4}$$

From (6·3) it easily follows on expanding that

$$\left.\begin{aligned} x_{n\alpha} &= x(1+\delta\nu_\alpha), \quad x_{n\beta} = x(1+\delta\nu_\beta), \\ x_{p\alpha} &= x(1+\delta\mu_\alpha), \quad x_{\mu\beta} = x(1+\delta\mu_\beta), \end{aligned}\right\} \tag{7·5}$$

where

$$x = \left(\frac{9\pi}{8}\right)^{\frac{1}{3}} \frac{a}{r}. \tag{7·6}$$

and

$$\left.\begin{aligned} \delta\nu_\alpha &= \tfrac{1}{3}(\delta+s+t) - \tfrac{1}{9}(\delta+s+t)^2, \\ \delta\nu_\beta &= \tfrac{1}{3}(\delta-s-t) - \tfrac{1}{9}(\delta-s-t)^2, \\ \delta\mu_\alpha &= \tfrac{1}{3}(-\delta+s-t) - \tfrac{1}{9}(-\delta+s-t)^2, \\ \delta\mu_\beta &= \tfrac{1}{3}(-\delta-s+t) - \tfrac{1}{9}(-\delta-s+t)^2. \end{aligned}\right\} \tag{7·7}$$

Now proceed to insert (7·5) into the function $f(x, y)$ introduced in (4·4). By Taylor's theorem for two variables it is easily seen, since $f(x, y)$ is symmetrical in x and y, that

$$\left.\begin{aligned} f(x_{n\alpha}, x_{n\alpha}) &= f(x) + \tfrac{2}{3}xf_x(\delta+s+t) + \tfrac{1}{9}f_1(\delta+s+t)^2, \\ f(x_{n\beta}, x_{n\beta}) &= f(x) + \tfrac{2}{3}xf_x(\delta-s-t) + \tfrac{1}{9}f_1(\delta-s-t)^2, \\ f(x_{p\alpha}, x_{p\alpha}) &= f(x) + \tfrac{2}{3}xf_x(-\delta+s-t) + \tfrac{1}{9}f_1(-\delta+s-t)^2, \\ f(x_{p\beta}, x_{p\beta}) &= f(x) + \tfrac{2}{3}xf_x(-\delta-s+t) + \tfrac{1}{9}f_1(-\delta-s+t)^2, \end{aligned}\right\} \tag{7·8}$$

where

$$f(x) = f(x, x), \tag{7·9}$$

$$f_x = [\partial f(x,y)/\partial x]_{x=y}, \tag{7·10}$$

and $$f_1 = [x^2 \partial^2 f(x,y)/\partial x^2 + x^2 \partial^2 f(x,y)/\partial x \, \partial y - 2x f_x]_{x=y}. \tag{7·11}$$

Introduce $$f_2 = [x^2 \partial^2 f(x,y)/\partial x^2 - x^2 \partial^2 f(x,y)/\partial x \, \partial y - 2x f_x]_{x=y}. \tag{7·12}$$

Then the other f-functions are similarly

$$\left.\begin{aligned}
f(x_{n\alpha}, x_{n\beta}) &= f(x) + \frac{2x}{3} f_x \delta + \tfrac{1}{9} f_1 \delta^2 + \tfrac{1}{9} f_2 (s+t)^2, \\
f(x_{p\alpha}, x_{p\beta}) &= f(x) - \frac{2x}{3} f_x \delta + \tfrac{1}{9} f_1 \delta^2 + \tfrac{1}{9} f_2 (s-t)^2, \\
f(x_{n\alpha}, x_{p\alpha}) &= f(x) + \frac{2x}{3} f_x s + \tfrac{1}{9} f_1 s^2 + \tfrac{1}{9} f_2 (\delta+t)^2, \\
f(x_{n\alpha}, x_{p\beta}) &= f(x) + \frac{2x}{3} f_x t + \tfrac{1}{9} f_1 t^2 + \tfrac{1}{9} f_2 (\delta+s)^2, \\
f(x_{n\beta}, x_{p\alpha}) &= f(x) - \frac{2x}{3} f_x t + \tfrac{1}{9} f_1 t^2 + \tfrac{1}{9} f_2 (\delta-s)^2, \\
f(x_{n\beta}, x_{p\beta}) &= f(x) - \frac{2x}{3} f_x s + \tfrac{1}{9} f_1 s^2 + \tfrac{1}{9} f_2 (\delta-t)^2.
\end{aligned}\right\} \tag{7·13}$$

The expansion of the other terms in the energy (6·6) is simple; introduce (7·8) and (7·13) in (6·6) then

$$E = E_0(r) + E_1(r)\,\delta + E_2(r)\,\delta^2 + E_s(r)\,s^2 + E_t(r)\,t^2 + E_{st}(r)\,st, \tag{7·14}$$

where

$$\left.\begin{aligned}
E_0(r) &= -r^3\lambda^3\{4c_m + 2c_h + 8c_b - 4c_w\} f(x) + \frac{3a^3\lambda^3}{4r^3}(b-2w)\,\zeta \\
&\qquad + \frac{e_1\lambda^5 - e_2\lambda^3}{r} + \frac{e_3\lambda^3 + \omega\lambda^2}{r^2}, \\
E_1(r) &= -\frac{2e_1\lambda^5}{r} + \frac{4}{3}\frac{e_2\lambda^3}{r}, \\
E_2(r) &= -\frac{r^3\lambda^3}{9}\{(4c_m + 2c_h) f_2 + (8c_b - 4c_w) f_1\} + \frac{e_1\lambda^5}{r} - \frac{2}{9}\frac{e_2\lambda^3}{r} + \frac{5}{9}\frac{e_3\lambda^3}{r^2}, \\
E_s(r) &= -\frac{r^3\lambda^3}{9}\{(2c_m + 2c_h + 4c_b - 4c_w) f_1 + (2c_m + 4c_b) f_2\} \\
&\qquad + \frac{3}{4}\frac{a^3\lambda^3}{r^3} b\zeta - \frac{2}{9}\frac{e_2\lambda^3}{r} + \frac{5}{9}\frac{e_3\lambda^3}{r^2}, \\
E_t(r) &= -\frac{r^3\lambda^3}{9}\{(2c_m + 4c_b - 4c_w) f_1 + (2c_m + 2c_h + 4c_b) f_2\} \\
&\qquad - \frac{2}{9}\frac{e_2\lambda^3}{r} + \frac{5}{9}\frac{e_3\lambda^3}{r^2}, \\
E_{st}(r) &= \frac{4}{9}\frac{e_2\lambda^3}{r}.
\end{aligned}\right\} \tag{7·15}$$

Consider now the energy E_0 which is the actual energy when (7·1) is satisfied. Disregarding the Coulomb energy, the surface energy and the term involving ζ, it can be expressed in the form $E_0 = \lambda^3 F(r)$, where F is independent of λ. It follows immediately that the energy at the equilibrium radius r is proportional to the number of particles. This is of course due to the saturation character of the nuclear forces. This rough approximation is well known and the slight variations can be attributed to the Coulomb energy and the surface effect. The term in ζ depends explicitly on λ, i.e. on the total number of particles, and on that account the law of the proportionality of the energy to the total number of particles would be disturbed unless this term gives a small contribution. This means that $b-2w$ is small. Therefore, I shall assume from now on that $b=2w$. This means that all the nuclear forces (except the Coulomb force) show saturation. Some support for this assumption is obtained from Volz (1937).

Introducing

$$\left.\begin{aligned} u &= 4c_m + 2c_h + 12c_w, \\ v &= 4c_m + 2c_h, \\ w_s &= -2c_h + 4c_w, \\ w_t &= 2c_h + 4c_w, \end{aligned}\right\} \tag{7·16}$$

where only three of these four combinations are now independent, it then follows that

$$\left.\begin{aligned} E_0(r) &= -ur^3\lambda^3 f(x) + \frac{e_1\lambda^5 - e_2\lambda^3}{r} + \frac{e_3\lambda^3 + \omega\lambda^2}{r^2}, \\ E_1(r) &= -2\frac{e_1\lambda^5}{r} + \frac{4}{3}\frac{e_2\lambda^3}{r}, \\ E_2(r) &= -\frac{r^3\lambda^3}{9}\{uf_1(x) - vf_3(x)\} + \frac{e_1\lambda^5}{r} - \frac{2}{9}\frac{e_2\lambda^3}{r} + \frac{5}{9}\frac{e_3\lambda^3}{r^2}, \\ E_s(r) &= -\frac{r^3\lambda^3}{18}\{uf_4(x) - w_s f_3(x)\} + \frac{3ba^3\lambda^3}{2r^3}\zeta - \frac{2}{9}\frac{e_2\lambda^3}{r} + \frac{5}{9}\frac{e_3\lambda^3}{r^2}, \\ E_t(r) &= -\frac{r^3\lambda^3}{18}\{uf_4(x) - w_t f_3(x)\} - \frac{2}{9}\frac{e_2\lambda^3}{r} + \frac{5}{9}\frac{e_3\lambda^3}{r^2}, \\ E_{st}(r) &= \frac{4}{9}\frac{e_2\lambda^3}{r}, \end{aligned}\right\} \tag{7·17}$$

where

$$f_3 = f_1 - f_2, \quad f_4 = f_1 + f_2. \tag{7·18}$$

The functions f_1, f_2, f_3, f_4 are given in Appendix B.

8. DETERMINATION OF THE CONSTANTS

For the purpose of numerical calculation I introduce the following units:
Length: the electron radius $2 \cdot 8 \times 10^{-13}$ cm.
Energy: the mass unit.

All numerical values in this and the following sections are expressed in these units, unless otherwise stated. Numerical calculation gives

$$a = 0 \cdot 808, \tag{8·1}$$

$$e_1 = 0 \cdot 825 \times 10^{-4}, \quad e_2 = 2 \cdot 598 \times 10^{-4}, \quad e_3 = 39 \cdot 22 \times 10^{-4}, \tag{8·2}$$

and from (7·6)

$$xr = 1 \cdot 23. \tag{8·3}$$

There are now five unknown constants, k, ω, u, v and w_s or w_t. To determine these from the model itself, five experimental results are required.

For nuclei with $n_\alpha = n_\beta$ and $p_\alpha = p_\beta$, obviously $s = t = 0$, and in this case only the four constants k, ω, u and v are involved in the energy. It may seem desirable to select nuclei having, in addition, an equal number of neutrons and protons, as then the energy reduces to E_0 which only involves the three constants k, ω and u. Thus these three constants could be determined from only three experimental data. But the largest nucleus of this type is ${}_{20}\mathrm{Ca}^{40}$; in order to obtain three experimental data one more nucleus must be chosen. If this nucleus is too small, the statistical method cannot be expected to apply. If another nucleus is taken in the neighbourhood of ${}_{20}\mathrm{Ca}^{40}$, incidental irregularities, which are not expressed in the statistical model, will influence the results unduly. For these reasons one nucleus is chosen with equal numbers of neutrons and protons and another large nucleus. The nuclei selected are ${}_{16}\mathrm{S}^{32}$ and ${}_{80}\mathrm{Hg}^{200}$, and the following data are used:

1. The atomic weight of ${}_{16}\mathrm{S}^{32}$ is 31·9823.
2. The atomic weight of ${}_{80}\mathrm{Hg}^{200}$ is 200·016.
3. The nuclear radius of ${}_{80}\mathrm{Hg}^{200}$ is 9×10^{-13} cm.
4. The most stable nucleus of atomic number 200 is ${}_{80}\mathrm{Hg}^{200}$.

Data (1) and (2) are due to Aston. Datum (3) is to some extent speculative. Bethe and Bacher (1936, p. 158) assume this radius to be 8×10^{-13} cm. Their justification is that the nucleus has an atomic weight just below that of the radioactive nuclei and it, therefore, seems reasonable to assume a radius slightly smaller than those of the radioactive nuclei. Bethe (1937, p. 166) has redetermined the radioactive nuclear radii according to the many-body theory of α-decay, and he finds values which average about $3 \cdot 5 \times 10^{-13}$ cm. larger than the former values. Allowing about $2 \cdot 5 \times 10^{-13}$ cm.

for the radius of the helium particle emitted in the course of the α-decay, I take the radius to be 9×10^{-13} cm. Datum (4) is justified because there is only the one nucleus (${}_{80}\mathrm{Hg}^{200}$) with the atomic weight 200.

In addition, to calculate the nuclear energies, I take the corrected values of Livingston and Bethe (1937, p. 373) for the atomic weights of hydrogen and neutron, 1·00813 and 1·00897 respectively.

Since $s=t=0$ for ${}_{16}\mathrm{S}^{32}$ and ${}_{80}\mathrm{Hg}^{200}$, it follows from (7·14) that

$$E = E_0(r)+E_1(r)\,\delta+E_2(r)\,\delta^2. \tag{8·4}$$

The radius r is determined from the equilibrium condition

$$\frac{dE}{dr} \equiv \frac{dE_0}{dr}+\frac{dE_1}{dr}\,\delta+\frac{dE_2}{dr}\,\delta^2 = 0. \tag{8·5}$$

The stability condition is

$$\frac{dE}{d\delta} \equiv E_1(r)+2E_2(r)\,\delta = 0. \tag{8·6}$$

For ${}_{16}\mathrm{S}^{32}$, $\lambda=3{\cdot}175$, $\delta=0$, $E=-0{\cdot}2913$, whilst for ${}_{80}\mathrm{Hg}^{200}$, $\lambda=5{\cdot}848$, $r=0{\cdot}552$, $\delta=0{\cdot}2$, $E=-1{\cdot}7108$. By substitution two equations are obtained for ${}_{16}\mathrm{S}^{32}$ from (8·4) and (8·5) and for ${}_{80}\mathrm{Hg}^{200}$ three equations from (8·4), (8·5) and (8·6). In all there are five equations for the five unknowns k, ω, u, v and r. This value of r determines the radius of ${}_{16}\mathrm{S}^{32}$. These equations can be solved numerically and the solution is

$$\left.\begin{aligned} u = 2{\cdot}85\times10^{-2},\quad & v = (1{\cdot}43)\times10^{-2},\\ \omega = 4{\cdot}45\times10^{-3},\quad & k = 1{\cdot}5,\\ r = 0{\cdot}566. & \end{aligned}\right\} \tag{8·7}$$

Using (6·4) and (7·16) the force constants are obtained

$$\left.\begin{aligned} 2c_m+c_h = 7{\cdot}15\times10^{-3},\quad & c_w = (1{\cdot}18)\,10^{-3},\\ 2m+h = 2{\cdot}79\times10^{-2},\quad & w = (0{\cdot}92)\,10^{-2}. \end{aligned}\right\} \tag{8·8}$$

It is of interest to compare the values of $2m+h$ with the corresponding values derived by Bethe and Bacher (1936) for the deuteron. Denote by large letters the corresponding quantities in the theory of the deuteron: $M=30$ MeV and $H=5$ MeV. Thus

$$\frac{2m+h}{2M+H} = 0{\cdot}40. \tag{8·9}$$

Owing to the fact that the potential is now proportional to

$$(k+a/r)\exp(-r/a),$$

the above ratio should have a value approximately equal to $1/(k+a/r)$, when r is the mean distance between the interacting particles. This value of r is at most the value of r for the nucleus. From figure 1, r can be taken as approximately 0·55. From (8·1), $a = 0{\cdot}808$. Thus $1/(k+a/r) = 0{\cdot}34$. Thus the true relation between the force constants ought to be

$$\frac{2m+h}{2M+H} < 0{\cdot}34. \qquad (8{\cdot}10)$$

Thus the forces are at least about 20 % too large, in full agreement with the remarks of Bethe and Bacher (1936, p. 158).

In order to determine the constants completely, the numerical value of w_s or w_t is still required. From (7·17) it can be seen that they only occur in the spin terms. For medium and large nuclei, s and t are small in comparison with δ, and numerical calculation shows that the spin contribution is negligible. It is therefore not possible to determine the last constant from energy considerations.

As c_h has only a small influence on the spin terms of the energy, the calculations carried out later on stability considerations are not materially altered by a reasonable choice of c_h. Assuming that the ratio c_m/c_h is the same for the model and the deuteron, it follows that

$$m = 1{\cdot}29\times10^{-2}, \quad h = 0{\cdot}21\times10^{-2}. \qquad (8{\cdot}11)$$

9. NUCLEAR ENERGIES AND RADII

For convenience of numerical computation I adopt the following method of procedure: first, develop the radius r in the form

$$r = r_0 + r_1\delta + r_2\delta^2 + r_s s^2 + r_t t^2 + r_{st}st. \qquad (9{\cdot}1)$$

The radius is determined from the equilibrium condition

$$E'(r) \equiv E_0'(r) + E_1'(r)\,\delta + E_2'(r)\,\delta^2 + E_s'(r)\,s^2 + E_t'(r)\,t^2 + E_{st}'(r)\,st = 0. \qquad (9{\cdot}2)$$

Substitute the expression (9·1) for r in (9·2), then on expansion by Taylor's theorem

$$\begin{aligned} &E_0'(r_0) + \delta[E_1'(r_0) + r_1E_0''(r_0)] + \delta^2[E_2'(r_0) + r_1E_1''(r_0) + \tfrac{1}{2}r_1^2E_0'''(r_0) + r_2E_0''(r_0)] \\ &\quad + s^2[E_s'(r_0) + r_sE_0''(r_0)] + t^2[E_t'(r_0) + r_tE_0''(r_0)] + st[E_{st}'(r_0) + r_{st}E_0''(r_0)] = 0. \end{aligned} \qquad (9{\cdot}3)$$

This condition is to be true for all values of δ, s and t, thus

$$\left.\begin{aligned} &E_0'(r_0) = 0, \\ &E_1'(r_0) + r_1 E_0''(r_0) = 0, \\ &E_2'(r_0) + r_1 E_1''(r_0) + \tfrac{1}{2} r_1^2 E_0'''(r_0) + r_2 E_0''(r_0) = 0, \\ &E_s'(r_0) + r_s E_0''(r_0) = 0, \\ &E_t'(r_0) + r_t E_0''(r_0) = 0, \\ &E_{st}'(r_0) + r_{st} E_0''(r_0) = 0. \end{aligned}\right\} \tag{9·4}$$

Now solve for the various r and substitute in the expression (7·14) for the energy and in (9·1) for the radius obtaining

$$E = E_0(r_0) + \delta E_1(r_0) + \delta^2 \bar{E}_2(r_0) + s^2 E_s(r_0) + t^2 E_t(r_0) + st E_{st}(r_0), \tag{9·5}$$

$$\begin{aligned} r = r_0 - \delta \frac{E_1'(r_0)}{E_0''(r_0)} + \delta^2 \left[\frac{-E_2'(r_0)}{E_0''(r_0)} + \frac{E_1'(r_0)\, E_1''(r_0)}{(E_0''(r_0))^2} - \frac{1}{2} \frac{E_0'''(r_0)\,(E_1'(r_0))^2}{(E_0''(r_0))^3} \right] \\ - s^2 \frac{E_s'(r_0)}{E_0''(r_0)} - t^2 \frac{E_t'(r_0)}{E_0''(r_0)} - st \frac{E_{st}'(r_0)}{E_0''(r_0)}, \end{aligned} \tag{9·6}$$

where

$$\bar{E}_2(r_0) = E_2(r_0) - \frac{1}{2} \frac{(E_1'(r_0))^2}{E_0''(r_0)}. \tag{9·7}$$

Now the procedure is to solve the equation $E_0'(r_0) = 0$ for a given nucleus, obtaining a value r_0 and by substitution in (9·5) and (9·6) determine the energy and radius respectively of the nucleus. In the actual calculations the spin terms have been completely neglected. This is justified because s and t are small in comparison with δ.

Figure 1 gives both r and R plotted against A. It is seen that r decreases rapidly as A increases, there being a minimum at about $A = 130$. Then, as A increases further, there is a gradual increase of r. This is due to the opposing effects of the Coulomb energy and the surface effect. We also see that the actual nuclear radius R shows a steady increase with A.

Figure 2 gives the binding energy per particle $-E/A$ plotted against A. The crosses denote experimental values. The theoretical and experimental values have been made to fit at $A = 32$ and at $A = 200$. It is, therefore, not very remarkable that the curve fits very closely to the experimental values in the range 32–200. It is remarkable that the theoretical values agree well with the experimental values as far down as $A = 14$.

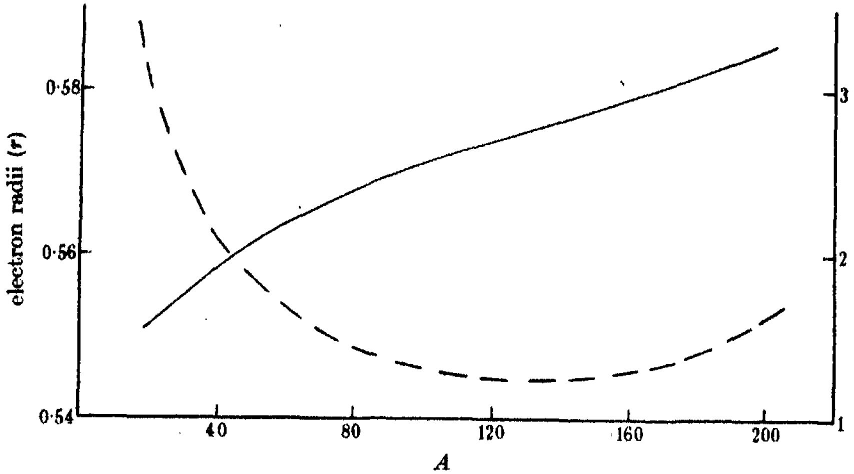

FIGURE 1. The radius R, and r (the broken curve) the radius divided by the cube root of the atomic number as functions of A. The scale on the right refers to R and that on the left to r.

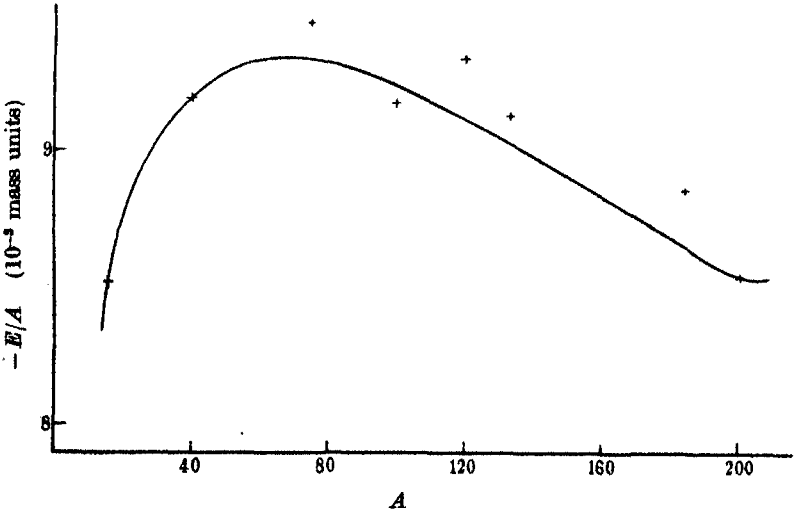

FIGURE 2. The binding energy per particle $-E/A$ as function of A. The crosses indicate experimental values.

APPLICATIONS TO STABILITY

10. ISOTOPIC NUMBERS

For the purpose of this section it will be more convenient to introduce Δ, S and T, where

$$\Delta = A\delta, \quad S = As, \quad T = At. \tag{10·1}$$

From (6·2), (7·2) and (10·1) we have

$$\left.\begin{aligned} \Delta &= N_\alpha + N_\beta - P_\alpha - P_\beta, \\ S &= N_\alpha - N_\beta + P_\alpha - P_\beta, \\ T &= N_\alpha - N_\beta - P_\alpha + P_\beta. \end{aligned}\right\} \tag{10·2}$$

The composition of a nucleus is determined if the total number of particles A and the isotopic number Δ is given. S and T define different quantum states of the nucleus, $\frac{1}{2}S$ giving the total spin, whilst T has no such immediate physical interpretation. The energy of the nucleus determined by A, Δ, S and T will be denoted by $E(A, \Delta, S, T)$.

(a) *Stability conditions*

Disregarding α-disintegration, a nucleus may disintegrate (1) because the nucleus emits an electron, (2) because the nucleus captures an electron (or emits a positron).

When Δ is the isotopic number for the original nucleus, then after disintegration the isotopic numbers become $\Delta - 2$ or $\Delta + 2$ according to case (1) or (2) respectively.

Denoting the rest mass of the electron by μ, the conditions of stability are

$$\left.\begin{aligned} E(A, \Delta, S, T) &< E(A, \Delta - 2, S', T') + \mu, \\ E(A, \Delta, S, T) &< E(A, \Delta + 2, S', T') - \mu. \end{aligned}\right\} \tag{10·3}$$

(Cf. equation (9) of Fuchs 1939. The difference is due to E denoting binding energies there, whereas here it denotes the actual energy.)

(b) *Nuclear spin*

For a given nucleus S and T are not yet determined. The lowest state is here involved; consequently S and T must be chosen in such a way that the energy due to the spin terms is a minimum. From (9·5) and (10·1) this energy is

$$\frac{1}{A^2}\{S^2E_s(r_0)+T^2E_t(r_0)+STE_{st}(r_0)\}. \tag{10·4}$$

Numerical calculation shows that $E_s > E_t$ on account of the term involving ζ and that E_{st} arising only from the Coulomb exchange energy is small. Since N_α, N_β, P_α, P_β are integers, (10·2) restrict the possible values of S and T to integers.

The four possible types of nuclei must be distinguished:

(1) The total numbers of both neutrons and protons are even. It is easy to see that both S and T must be even with the restriction $S+T=4m$, where m is an integer or zero. Thus the minimum of the spin terms (10·4) of the energy is obviously given by

$$S=T=0. \tag{10·5}$$

(2) The total numbers of both neutrons and protons are odd. It is easy to see that both S and T must be even with the restriction $S+T=4m+2$. Thus the minimum is given by (since $E_s > E_t$)

$$S=0, \quad T=\pm 2. \tag{10·6}$$

(3) The total number of neutrons is even and of protons is odd. It is easy to see that both S and T must be odd with the restriction $S+T=4m$. Thus the minimum is given by

$$S=-T=\pm 1. \tag{10·7}$$

(4) The total number of neutrons is odd and of protons is even. It is easy to see that both S and T must be odd with the restriction $S+T=4m+2$. Thus the minimum is given by

$$S=T=\pm 1. \tag{10·8}$$

Thus the statistical model gives all nuclei with an even number of particles zero spin in complete agreement with experiment. The only exceptions are of type (2), but they are so low in the atomic scale that we cannot expect the statistical model to apply to them. The exceptions are ${}_1H^2$, ${}_3Li^6$, ${}_7N^{14}$, all with unit spin. The statistical model gives all nuclei with an odd number of particles the spin $\frac{1}{2}$. Thus the model fails to account for the fact that besides the spin $\frac{1}{2}$, odd nuclei can have spins up to $\frac{9}{2}$.

(c) *Stability breadths*

For nuclei of type (1) ($S = T = 0$), the neighbouring nucleus of comparison in (10·3), is of type (2) with $S = 0$, $T = \pm 2$. Using (9·5) the stability conditions (10·3) become

$$E_0(r_0) + \frac{\varDelta}{A} E_1(r_0) + \frac{\varDelta^2}{A^2} \bar{E}_2(r_0) < E_0(r_0) + \frac{\varDelta - 2}{A} E_1(r_0) + \frac{(\varDelta - 2)^2}{A^2} \bar{E}_2(r_0) + \frac{4E_t(r_0)}{A^2} + \mu$$

and

$$E_0(r_0) + \frac{\varDelta}{A} E_1(r_0) + \frac{\varDelta^2}{A^2} \bar{E}_2(r_0) < E_0(r_0) + \frac{\varDelta + 2}{A} E_1(r_0) + \frac{(\varDelta + 2)^2}{A^2} \bar{E}_2(r_0) + \frac{4E_t(r_0)}{A^2} - \mu.$$

Combining I obtain the inequality

$$\frac{-E_1(r_0)\,A}{2\bar{E}_2(r_0)} + 1 + \frac{E_t(r_0)}{\bar{E}_2(r_0)} + \frac{A^2\mu}{4\bar{E}_2(r_0)} > \varDelta > \frac{-E_1(r_0)\,A}{2\bar{E}_2(r_0)} - 1 - \frac{E_t(r_0)}{\bar{E}_2(r_0)} + \frac{A^2\mu}{4\bar{E}_2(r_0)}. \tag{10·9}$$

Corresponding to any even value of the atomic number A, there is therefore a maximum and a minimum value of the isotopic number, within which limits the nucleus is stable. I shall denote these by $\max \varDelta$ and $\min \varDelta$, and call the difference $\max \varDelta - \min \varDelta$ the stability breadth. Thus for nuclei of type (1) the stability breadth is

$$2\{1 + E_t(r_0)/\bar{E}_2(r_0)\}. \tag{10·10}$$

It follows in a similar way that for nuclei of type (2) the stability breadth is

$$2\{1 - E_t(r_0)/\bar{E}_2(r_0)\}. \tag{10·11}$$

For nuclei of type (3) ($S = -T = \pm 1$) the neighbouring nucleus has $S = T = \pm 1$, and it then easily follows that for nuclei of type (3) the stability breadth is

$$2\{1 + E_{st}(r_0)/\bar{E}_2(r_0)\}. \tag{10·12}$$

For nuclei of type (4) the stability breadth is

$$2\{1 - E_{st}(r_0)/\bar{E}_2(r_0)\}. \tag{10·13}$$

Numerical calculation shows that $E_{st}/\bar{E}_2$ is about 10^{-2}, and thus this ratio can be neglected. Also $E_t/\bar{E}_2$ is approximately unity.

From (10·10) it is seen that the stability breadth for nuclei of type (1) is approximately four, thus allowing in general one or two stable isobars.

From (10·11) the stability breadth for nuclei of type (2) is approximately zero; thus there are no stable nuclei of this type. Apart from the few exceptions for small nuclei, which hence do not come within the scope of a statistical model, this is in agreement with experiment. This result is well known and can be explained simply without the model.

From (10·12) and (10·13) the stability breadths for nuclei of types (3) and (4) are practically two, allowing thus only one stable nucleus in general for a given value of A. Since the stability breadths are almost equal, one would expect that there are about equal numbers of both types (3) and (4). This is verified by the experimental data.

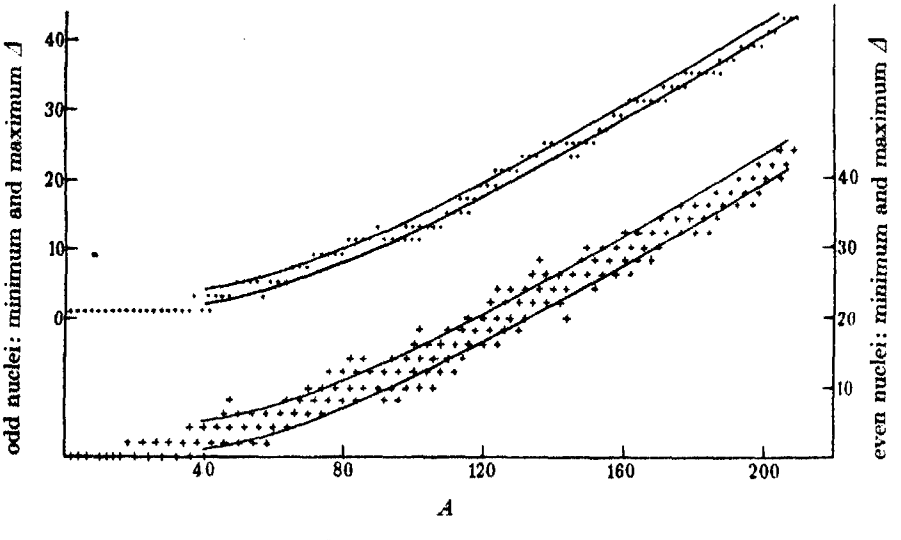

FIGURE 3. The maximum and minimum values of the isotopic number Δ for even and odd nuclei as functions of A. The scale on the right refers to even nuclei and that on the left to odd nuclei. The crosses indicate experimental stable nuclei.

The graph in figure 3 gives both max Δ and min Δ against A for the cases of nuclei with even and odd numbers of particles respectively. In addition, all the known stable nuclei (Gregoire 1938) have been indicated by crosses.

The values of the constants occurring in the model were chosen in such a way that the stability condition for $_{80}\mathrm{Hg}^{200}$ was satisfied. One would therefore expect that the mid-point of max Δ and min Δ should be 40 for $A = 200$. Actually the mid-point is about $1\frac{1}{4}$ units higher. This is almost entirely due to the fact that in calculating the numerical constants the rest mass of the electron in the stability condition has been neglected (this accounts for a discrepancy of 1·2 units). A small error is also introduced by using the expansion (9·5) in terms of r_0, instead of introducing the correct radius r, as done in the calculation of the numerical constants.

From the experimental results for even nuclei, the region of stability should be somewhat greater, as only a little over half of the stable nuclei of even atomic number lie in the region between the two curves. For odd nuclei, the greatest number of stable nuclei do lie in the region between the two curves.

As expected, the statistical model does not give the dips in the experimental curves which can be visualized by looking at figure 3.

11. THE n-CURVES

For some purposes it is more convenient to consider the n-curves introduced by Fuchs (1939). As in that paper we shall introduce the symbol (m, n, p) to represent the nucleus, where m is the total number of α-particles which can be formed from the nucleus, n is the number of surplus neutrons and p is the number of surplus protons. (Clearly p can only have the value 0 or 1.) Thus the isotopic number Δ has the value n or $n-1$ according as p has the value 0 or 1.

Fuchs defines numbers n_i, where $i = 1, 2, 3, 4$ corresponding to a *given* value of m as follows:

n_1 and n_3 are the solutions of the equation

$$E(m, n-1, 1) = E(m+1, n-4, 0) + \mu, \tag{11·1}$$

when n is even or odd respectively.

n_2 and n_4 are the solutions of the equation

$$E(m, n, 0) = E(m, n-1, 1) + \mu, \tag{11·2}$$

when n is odd or even respectively.

The various n_i then determine the scheme of stable nuclei to be found in Fuchs (1939).

To find n_1 note that $(m, n-1, 1)$ is a nucleus of type (2) having $S = 0$, $T = \pm 2$, whereas $(m+1, n-4, 0)$ is of type (1) having $S = T = 0$; hence, by using the expansion of the energy, (11·1) yields on reduction

$$2E_1(4m+n_1) + E_2(4n_1-12) + 4E_t = \mu(4m+n_1)^2,$$

where $A = 4m+n_1$. Splitting $(4m+n_1)^2$ into its two factors $A(4m+n_1)$, a linear equation for n_1 is obtained of which the solution is

$$n_1 = \frac{12\bar{E}_2 - 8mE_1 - 4E_t + 4mA\mu}{2E_1 + 4\bar{E}_2 - A\mu}. \tag{11·3}$$

Here all the terms are to the first order proportional to A, so that the right-hand side does not change rapidly with A. Thus this equation can be solved approximately and better approximations obtained by repeated substitution.

Similarly
$$n_2 = \frac{4\bar{E}_2 - 8mE_1 - 2E_{st} + 4mA\mu}{2E_1 + 4\bar{E}_2 - A\mu}, \tag{11·4}$$

$$n_3 = \frac{12\bar{E}_2 - 8mE_1 + 2E_{st} + 4mA\mu}{2E_1 + 4\bar{E}_2 - A\mu}, \tag{11·5}$$

$$n_4 = \frac{4\bar{E}_2 - 8mE_1 + 4E_t + 4mA\mu}{2E_1 + 4\bar{E}_2 - A\mu}. \tag{11·6}$$

Note that m is fixed and $A = 4m+n_i$. Since the values of n_i change slowly with A we may assume the same value of A in all four equations. Thus

$$n_3 - n_2 = \frac{8\bar{E}_2 + 4E_{st}}{2E_1 + 4\bar{E}_2 - A\mu}, \tag{11·7}$$

and
$$n_4 - n_1 = \frac{8(E_t - \bar{E}_2)}{2E_1 + 4\bar{E}_2 - A\mu}, \tag{11·8}$$

$n_3 - n_2$ measures the isotopic breadth for odd nuclei, and numerical calculation shows a steady increase from 2 to 2½ as m increases. Experimentally the number of stable isotopes is always 1 or 2, thus $n_3 - n_2$ must lie between 2 and 4. Thus there is a fair agreement here with experiment.

$n_4 - n_1$ measures the region in which stable isobars can exist, and numerical calculation shows a decrease from 0·2 to $-0·1$ passing through the value zero for m about 30. Experimentally this value should fluctuate between 3 and 7. Thus there is here no agreement with experiment.

Conclusion

The results obtained from the model give good agreement with experiment for the binding energies as can be seen from figure 3.

The stability results for odd nuclei are satisfactory, except that the model only gives stable nuclei the spin ½. On the other hand, for even nuclei the spin is correctly given as zero, but the region of stability is too small as can be seen from figure 4 (or from $n_4 - n_1 \sim 0$ which amounts to the same thing).

It is possible that other interaction potentials than (2·1) would give better agreement as far as the stability considerations are concerned, but it seems more probable that the disagreement is due to the statistical model not being powerful enough to emphasize sufficiently the difference between odd and even particles.

I wish to thank Dr K. Fuchs for the helpful advice, valuable suggestions and interest which he has taken in the progress of this paper.

APPENDIX A

Here we proceed to calculate I_4 and I_5. Now

$$I_0(x,y) = \int_0^\infty e^{-br}[\sin xr - xr\cos xr]\,[\sin yr - yr\cos yr]\,dr.$$

This integral is evaluated by expressing the circular functions in exponential form and then splitting it into four terms, each of which can be evaluated by repeated integration by parts. Then by repeatedly integrating from ∞ to b with respect to b, we obtain I_1, I_2, I_3, etc. The final result is

$$\begin{aligned} I_4(x,y) = {} & \tfrac{1}{6}(x^3+y^3)\tan^{-1}(x+y) - \tfrac{1}{6}(x^3-y^3)\tan^{-1}(x-y) \\ & - \tfrac{1}{24}\{1+3(x^2+y^2)\}\log\frac{1+(x+y)^2}{1+(x-y)^2} + \tfrac{1}{6}xy, \end{aligned}$$

$$\begin{aligned} I_5(x,y) = {} & \tfrac{1}{24}\{\tfrac{1}{4}+\tfrac{3}{2}(x^2+y^2)-\tfrac{3}{4}(x^2-y^2)^2\}\log\frac{1+(x+y)^2}{1+(x-y)^2} \\ & - \tfrac{1}{6}(x^3+y^3)\tan^{-1}(x+y) + \tfrac{1}{6}(x^3-y^3)\tan^{-1}(x-y) - \tfrac{1}{24}xy + \tfrac{1}{8}xy(x^2+y^2). \end{aligned}$$

APPENDIX B

Simple calculations give

$$f_1 = -\tfrac{1}{8}x^2\log(1+4x^2) + \tfrac{1}{2}x^4 + k\left\{\tfrac{1}{4}x^2\log(1+4x^2) - \frac{x^4}{1+4x^2}\right\},$$

$$f_2 = -\tfrac{1}{8}x^2(1+4x^2)\log(1+4x^2) + \tfrac{1}{2}x^4 + k\{\tfrac{1}{4}x^2\log(1+4x^2) - x^4\},$$

$$f_3 = \tfrac{1}{2}x^4\log(1+4x^2) + k\left\{x^4\left(1-\frac{1}{1+4x^2}\right)\right\},$$

$$f_4 = -\tfrac{1}{4}x^2(1+2x^2)\log(1+4x^2) + x^4 + k\left\{\tfrac{1}{2}x^2\log(1+4x^2) - x^4\left(1+\frac{1}{1+4x^2}\right)\right\},$$

$$\begin{aligned} f = {} & \tfrac{1}{96}(1+12x^2)\log(1+4x^2) - \tfrac{1}{3}x^3\tan^{-1}2x - \tfrac{1}{24}x^2 + \tfrac{1}{4}x^4 \\ & + k\{\tfrac{1}{3}x^3\tan^{-1}2x - \tfrac{1}{24}(1+6x^2)\log(1+4x^2) + \tfrac{1}{6}x^2\}. \end{aligned}$$

SUMMARY

Nuclear energies and radii are calculated using the statistical method, taking into account the two possible spin directions; the interaction potentials of the various nuclear forces are assumed to be proportional to $(k+a/r)\exp(-r/a)$. The results obtained are in good agreement with experiment.

The stability of nuclei is also investigated, giving satisfactory agreement with experiment for odd nuclei, but for even nuclei the results are not so satisfactory. This seems to indicate that the statistical method does not emphasize sufficiently the difference between odd and even nuclei.

REFERENCES

Bethe, H. A. 1937 *Rev. Mod. Phys.* **9**, 69.
Bethe, H. A. and Bacher, R. F. 1936 *Rev. Mod. Phys.* **8**, 82.
Fuchs, K. 1939 *Proc. Camb. Phil. Soc.* **35**, 242.
— 1940 *Proc. Roy. Soc.* A, **174**, 509.
Gregoire, R. 1938 *J. Phys. Radium*, **9**, 419.
Kemmer, N. 1938 *Proc. Roy. Soc.* A, **166**, 127.
Livingston, M. S. and Bethe, H. A. 1937 *Rev. Mod. Phys.* **9**, 245.
Volz, H. 1937 *Z. Phys.* **105**, 537.
Weizsäcker, C. F. 1937 *Z. Phys.* **96**, 431.
Yukawa, H. 1935 *Proc. Phys.-Math. Soc. Japan*, **17**, 48.

Some measurements of γ-ray energies

By S. C. Curran,* P. I. Dee and J. E. Strothers

(*Communicated by J. D. Cockcroft, F.R.S.—Received* 2 *November* 1939)

The measurement of the quantum energies of γ-radiation has presented serious difficulties. Crystal diffraction is capable of high resolution and accuracy, but is at present applicable only when strong sources are available and for quantum energies of less than about $1\cdot0 \times 10^6$ eV. When dealing with weaker sources the absorption method affords a convenient means of determining the energy of γ-radiation if this should consist of a single line, but is unsatisfactory for the analysis of a more complex spectrum. A somewhat more reliable method is found in the determination of the energies of Compton recoil electrons produced by the radiation. Results obtained by simple absorption methods are again unsatisfactory in the case of complex spectra, but by obtaining curved trajectories in a magnetic field, the energies of the Compton recoil electrons may be more accurately estimated, and hence a knowledge of the quantum energies and relative intensities of the component radiations may be acquired. The recoil electrons may be detected in an expansion chamber or by Geiger-Müller counters. Of these, the counters have the great advantage of being practically continually "sensitive", whereas the cloud chamber is sensitive only over a relatively short interval, and the difficulty of reducing the statistical fluctuations in the number of particles of different energies observed is correspondingly greater. The following paper describes results which have been obtained by the use of a "γ-ray spectrograph" in which the magnetically focused recoil electrons are detected by a system of Geiger-Müller counters.

CONSTRUCTION OF THE SPECTROGRAPH

The method of semicircular focusing of electrons has been applied to the measurement of γ-ray spectra, and where such work has depended upon internal conversion a high precision of measurement has been possible. In the absence of this internal conversion spectra have been produced by photoelectric or Compton processes in the material surrounding the source and in these instances serious difficulties arise from the broadening of the β-ray lines due to straggling and other effects (Ellis and Aston 1932). By the use of very thin foils as the source of secondary electrons, this difficulty may be, to a very large extent, obviated, but the technique necessitates a correspondingly large increase in source strength. At the present time, radioactive sources of the required intensity can seldom be produced, so that in most instances the less satisfactory method of employing thick emitters has to be rendered capable of sufficiently high resolution.

---

* Senior Caird Scholar.

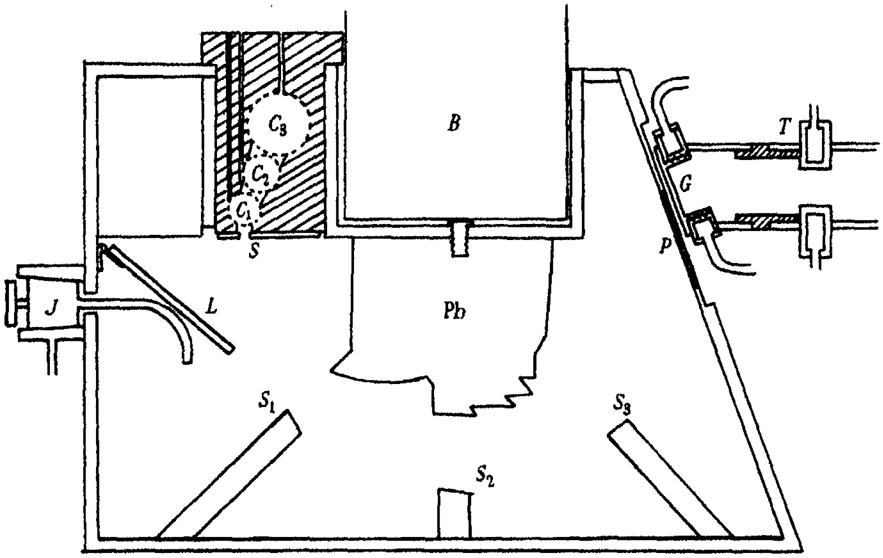

FIGURE 1

Figure 1 is a diagram of a γ-ray spectrograph which has been found to function successfully in the study of various sources of γ-radiation. The emitting surface is an aluminium plate P, at an angle of 20° to the vertical, and the electron beam produced here is focused on the slit S, which is from 2 to 3 mm. wide and 3 cm. long. Behind S are placed three very thin-walled counters C_1, C_2, C_3, of diameters 0·8, 1·2 and 2·0 cm., which are arranged in such a way that the whole of the focused beam originating at P is just included within their volume. Three slits S_1, S_2, S_3 help to define the angular spread of the beam and the lead core *Pb* is cut in such a way that it is impossible for a beam of secondary electrons emitted from any point, other than the plate P, to be focused at S. The slit S_2 is about 2·1 cm. high and the total width of the box is 4·0 cm.; with the magnet available this allows electrons of energies up to 16×10^6 eV to be bent into a semicircle of radius 6·8 cm. The counters C_1, C_2 and C_3 are made of aluminium foil 0·0008 cm. thick, and are supported in a block of Perspex: they are coupled to a set of three amplifiers and the coincidences are fed into a scale-of-two counter. The details of these circuits have been published elsewhere (Curran and Petrzilka 1939). The whole box is filled with a mixture of argon and alcohol, the total pressure being generally about 7 cm. The box could be exhausted through the tap J, which is also designed to operate a lead shutter L placed in the path of the electron beam. A lead block B outside the spectrograph shields the counters from the direct action of the γ-radiator. The source of γ-radiation G is placed immediately above the focal line in the plate P. The steep inclination of this plate is convenient when the γ-ray source is produced by the bombardment of elements with a horizontal magnetically resolved proton beam, in which case the target tube T (figure 1) is designed to fit accurately against P. At the same time the tilt of the plate permits of an increased area of secondary electron emission without loss in sharpness of focus.

EXPERIMENTAL RESULTS

(*a*) *Thorium C″*. As a test of the efficiency of the spectrograph, the spectrum of the secondary electrons produced from aluminium by the γ-radiation from the active deposit of thorium was investigated. In this case the radiation consists mainly of a strong line at $2{\cdot}65 \times 10^6$ eV and some much softer components. The experimental results are put forward in figure 2, where it is seen that the spectrum rises gradually to a maximum and then falls away steeply to a sharp end-point. Beyond the end-point there is detected a slowly decreasing number of electrons, but the break in the curve at the end-point may be very accurately determined, and corresponds to a quantum energy of $(2{\cdot}65 \pm 0{\cdot}05) \times 10^6$ eV. The agreement with the known value is entirely satisfactory. A search coil, fixed in the field gap beside the box, was used to determine the field strength at each setting of the field current; the error in the measurement of field strength by means of the attached fluxmeter was less than 1 %, and the inhomogeneity of the field over the useful area of the box was less than 2 %. It is evident from the curve of figure 2*a* that the absorption of the electrons by the contained gas and the walls of the counters has seriously reduced the intensity of the soft components of the radiation. A lower limit to the electron energy which may be measured by the spectrograph is about $0{\cdot}4 \times 10^6$ eV. The peak formed by the secondaries produced by the high energy radiation of ThC″ is broad and this is mainly due to the fact that the electrons are produced in a thickness of aluminium greater than their range. Two major factors which prevent the sharpening of this peak by decreasing the thickness of the emitter are (*a*) the necessity of using much stronger sources of γ-radiation, and (*b*) the emission of β-radiation from the source itself. The inhomogeneity of the Compton recoil electrons projected within the useful solid angle of the spectrograph is of the order of 5 % and does not contribute much to the breadth of the peak. Collimation of the γ-ray beam falling on the plate *P* would help to sharpen the peak, but this again necessitates stronger sources than are at present available. It will be pointed out later that in the analysis of the curves obtained with the spectrograph for sources emitting complex radiation, the thorium curve in figure 2 is used as a standard, and that for this purpose a plot of $N/H\rho$ as ordinate instead of the intensity N is more useful. Figure 2, curve *b*, shows this ratio $N/H\rho$ as a function of $H\rho$, and this curve will be used subsequently in the analysis of the radiations of ^{24}Na, ^{38}Cl and ^{56}Mn. It can be separated into three components. The major part is ascribed to the line of energy $2{\cdot}65 \times 10^6$ eV, a second peak can be observed for an energy of $1{\cdot}68 \times 10^6$ eV, and this is in agreement with previous work (Ellis 1934). A third component has an upper limit of $1{\cdot}1 \times 10^6$ eV, but it is obvious that this part of the radiation is complex. Known nuclear energy levels suggest

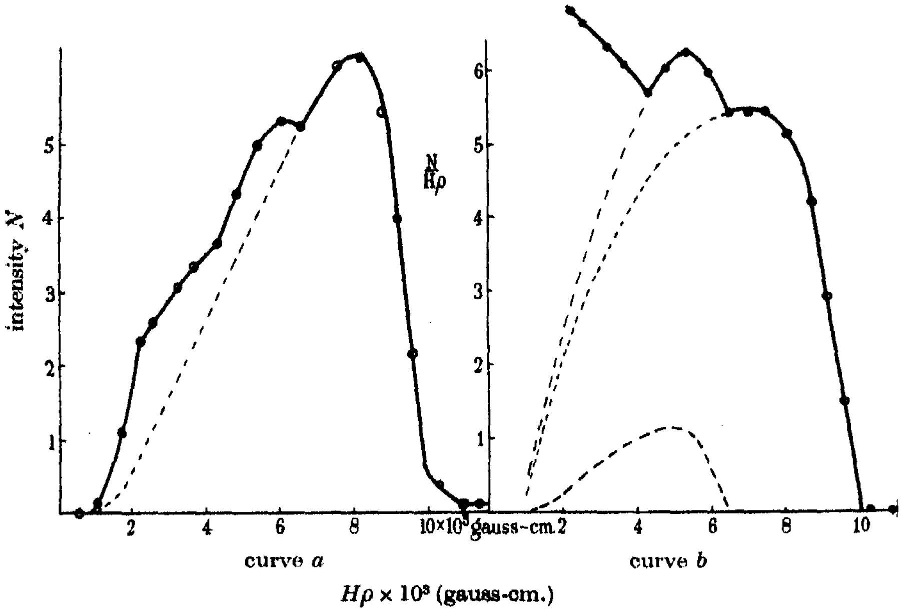

FIGURE 2

that radiation of energy 1·1 × 10^6 eV might be emitted by active thorium deposit. If the areas under the curves for the 1·68 and 2·65 × 10^6 eV lines are divided by the ranges of the recoil electrons produced by the radiations and the Compton scattering coefficients, the ratio 0·15 : 1 is obtained for the relative intensities of the lines. This is in satisfactory agreement with the previous estimate of 0·12 : 1 (Ellis 1934) and supports the use of this method of estimating intensity.

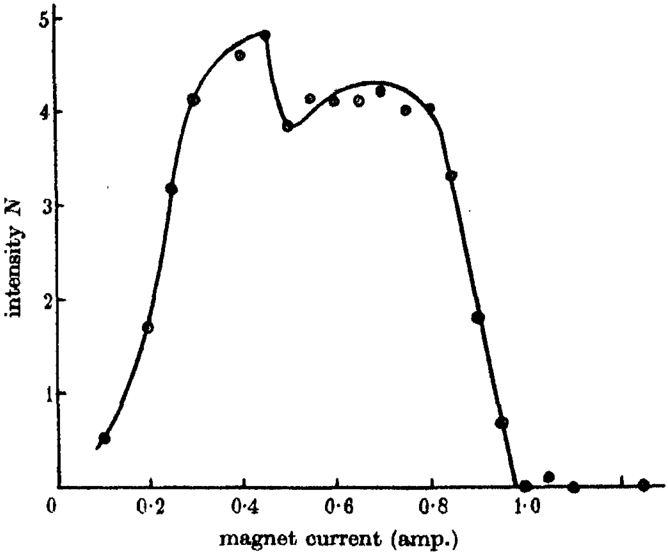

Figure 3

(*b*) *Radio-sodium* ^{24}Na. The γ-radiation from this source has been investigated by Richardson and Kurie using the expansion chamber (Richardson and Kurie 1936), and they report the existence of three lines of quantum energies 1·01, 2·04 and 3·00 ± 0·05 × 10^6 eV of relative intensities 1·05, 0·95 and 0·65. More recently Kikuchi *et al.* (1939) have investigated the γ-ray spectrum using a magnetic spectrograph and their results indicate the presence of two strong lines at (1·49 ± 0·05) × 10^6 eV and (2·97 ± 0·07) × 10^6 eV, with a doubtful weaker line at 0·8 × 10^6 eV. Our results are in good agreement with these later observations. The secondary electron spectrum is shown in figure 3 and the quantum energies of the two outstanding components are 1·46 ± 0·04 × 10^6 eV and 3·03 ± 0·05 × 10^6 eV.

An attempt has been made to measure the relative intensities of the components by using the shape of the ThC″ curve in figure 2 as a standard for a single γ-ray line of energy about 2·5–3·0 × 10^6 eV. With this assumption, the curve which would have been obtained had there been present only the $3 \cdot 03 \times 10^6$ eV radiation was constructed, and by combining this with the experimental curve, it became apparent that besides the γ-ray line at $1 \cdot 46 \times 10^6$ eV there was also a small quantity of radiation of energy in the region of $2 \cdot 0 \times 10^6$ eV. The relative intensities of the three components may be estimated from the area under each of the separate curves, but as pointed out in the case of ThC″ there are three corrections to be made: (1) variation in the Compton scattering coefficient with quantum energy, (2) variation in the effective thickness of the emitter with electron-range, and (3) decrease in the "acceptance" of the spectrograph with increasing field strength. The most convenient method of dealing with (3) is to replot the experimental curves of intensity N against $H\rho$, with $N/H\rho$ as ordinate in place of N. This is done in figure 4, and after correction for the variations (1) and (2) the relative intensities obtained are as shown in table 1.

TABLE 1

Quantum energy $\times 10^6$ eV	1·46	2·00	3·03
Intensity	1·17	0·27	1·00

Feather and Dunworth (1938) have suggested that following the β emission of ^{24}Na, de-excitation of the ^{24}Mg nucleus usually occurs in two stages from the level at $4 \cdot 49 \times 10^6$ eV (previously determined as 4×10^6 eV by Richardson), by the emission of successive γ-quanta of energy $1 \cdot 46 \times 10^6$ eV and $3 \cdot 03 \times 10^6$ eV, and more rarely by the emission of two quanta of energy about 2×10^6 eV. According to this picture it would be expected that the intensities of the $1 \cdot 46 \times 10^6$ eV and $3 \cdot 03 \times 10^6$ eV radiations would be equal. The experimental value of 1·17 for the ratio of these intensities is in fair agreement with this. The sum of the intensities of the quanta of energy about $2 \cdot 0 \times 10^6$ eV is of the order of 25 % of that of the two stronger lines, a value not at all in agreement with that given by Richardson (1938), whose results indicated a much higher yield of this radiation. However, Kikuchi *et al.* (1939) failed to observe the presence of any radiation of energy between $1 \cdot 5 \times 10^6$ eV and $3 \cdot 0 \times 10^6$ eV, but it is possible that they might fail to observe it should the intensity be as low as the above analysis indicates. In connexion with the excitation level of the ^{24}Mg nucleus at $4 \cdot 49 \times 10^6$ eV, it is of interest to note that preliminary results obtained by the use of the spectrograph in the examination of the capture γ-radiation emitted during bombardment of sodium with protons of energy $0 \cdot 85 \times 10^6$ eV (as in equation (1))

$$^{23}\mathrm{Na} + {}^{1}\mathrm{H} \rightarrow {}^{24}\mathrm{Mg} + h\nu \tag{1}$$

indicate the presence of radiation of about $4{\cdot}45 \times 10^6$ eV energy. The emission of quanta of lower energy is suggested by our results, but a more detailed investigation is necessary for the determination of their energies and intensities. From investigations upon ^{24}Na, the transitions from the

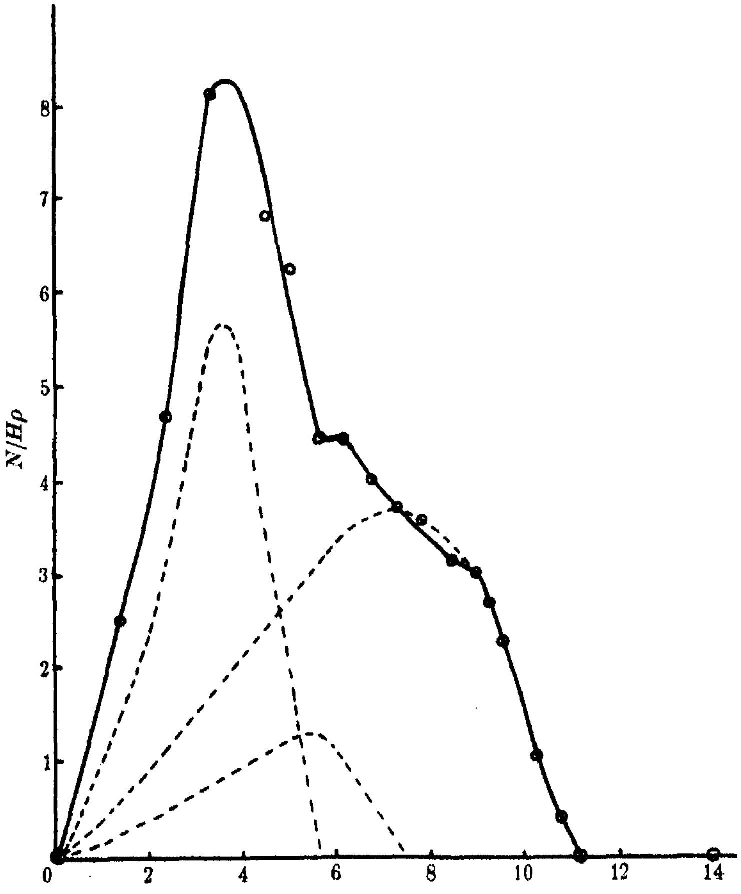

FIGURE 4

$4{\cdot}49 \times 10^6$ eV level in the excited ^{24}Mg nucleus would appear to be forbidden and yet this radiation appears in the case of proton capture by ^{23}Na. The upper limit to the quantum energy release in equation (1) with $0{\cdot}850 \times 10^6$ eV protons is about $11{\cdot}2 \times 10^6$ eV (Curran and Strothers 1939), and hence it may be that the excited ^{24}Mg nucleus returns to the ground state by the successive emission of two γ-ray quanta of energies $4{\cdot}5 \times 10^6$ eV and

$(11{\cdot}2-4{\cdot}5)\times 10^6$ eV; this would require the existence of an excitation level at $7{\cdot}3\times 10^6$ eV in the ^{24}Mg nucleus.

Another possible explanation would be found in the existence of a double level at $4{\cdot}5\times 10^6$ eV in the ^{24}Mg nucleus.

(*c*) ^{56}Mn. Sources of the radioactive isotope of manganese, ^{56}Mn, prepared in the Cambridge cyclotron by the bombardment of pure manganese dioxide with 2–4 μA hr. of deuterons of energy 9×10^6 eV proved to be sufficiently strong to permit us to investigate the spectrum of the γ-radiation emitted by the element. The half-life of the activity was checked during the experiment and was found to be 2·6 hr. in agreement with the known value. Previous investigations of this γ-radiation by the absorption method (Livingood and Seaborg 1938) have shown that its average energy is $1{\cdot}2\times 10^6$ eV, and the half-value thickness for the absorption of the secondary electrons has given the value of $1{\cdot}65\times 10^6$ eV (Mitchell and Langer 1937). More recently Dunworth (1939) has shown that the γ-rays are not homogeneous and his results indicate the presence of γ-rays of energy 1·7 and $0{\cdot}6\times 10^6$ eV. A typical curve obtained by means of the spectrograph is shown in figure 5.

It is seen that two γ-rays of energies $(0{\cdot}91\pm 0{\cdot}05)\times 10^6$ eV and $(2{\cdot}03\pm 0{\cdot}05)\times 10^6$ eV are present. By carrying out an analysis similar to that described in the case of ^{24}Na (figure 4), and making the necessary corrections, the relative intensities of the two lines are found to be 1·4 : 1. This ratio probably indicates too low a value for the intensity of the soft radiation, since the slower electrons are more strongly absorbed by the counter walls and the gas in the spectrograph. An attempt has been made to estimate the correction to be applied in order to allow for this effect and the corrected ratio of the intensities of the two components is approximately 2·1 : 1·0. Considering the rather large corrections to be made, this estimate of the relative intensities is not inconsistent with Dunworth's (1939) ratio of 2·5 : 1. The upper energy limit of the radiation has also been investigated by an absorption method, the recoil electrons producing coincidences in two thin-walled Geiger-Müller counters being gradually absorbed out by aluminium sheets placed between the counters. A precise measurement was not possible as a well-defined end-point could not be obtained, but the result was in fair agreement with the value of $(2{\cdot}02\pm 0{\cdot}05)\times 10^6$ eV given above. Recent measurements carried out in this laboratory by Townsend* have shown that the difference in the upper energy limits of the β-ray spectra (Alichanian, Alichanow and Dzelepow 1935; Brown and Mitchell 1936; Gaerttner and Crane 1936) of ^{56}Mn is in close enough agreement with our value from the γ-ray measurements to support the view that the hard γ-rays follow the emission of the soft β-rays.

---

* In course of publication.

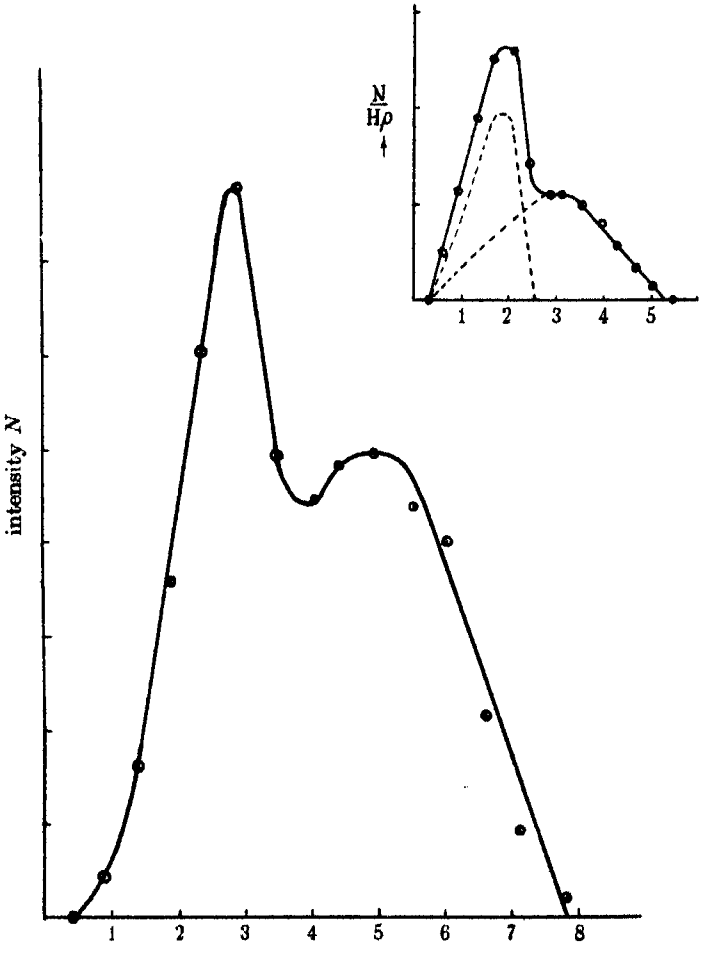

FIGURE 5

(*d*) *Fluorine.* The radiation emitted from fluorine during proton bombardment has been the subject of several investigations. Early experiments (Delsasso, Fowler and Lauritsen 1939) failed to decide whether the γ-radiation consisted of a single line, or was more complex, but more recently Halpern and Crane (1939) have stated that there is a single line at $5 \cdot 8 \times 10^6$ eV. By the method of γ-γ coincidences we have been able to show that the radiation is in fact homogeneous. The energy spectrum of the secondary electrons produced by the γ-radiation has been investigated by means of the spectrograph, and the results are shown in figure 6.

The form of the curve is precisely that which would be expected if the radiation consists of a single line, and the quantum energy of the γ-ray is determined as $(6\cdot5 \pm 0\cdot2) \times 10^6$ eV. To carry out this experiment targets of barium or calcium fluoride were deposited upon the target head of the tube *T* shown in figure 1, and were bombarded with a magnetically resolved proton beam. It was found that slight fluctuations in the position and intensity of this beam, though too slight to be recorded by the usual current measuring meter, caused a considerable change in the strength of the effective γ-ray source, and to overcome this difficulty a subsidiary Geiger counter was employed. This was placed close to the target head and was enclosed in an iron box to ensure efficient magnetic shielding. Using two scale-of-two counting meters, a count in the single counter was obtained over the same period as the triple coincidence count, and by plotting the ratio of these two counts as a function of $H\rho$, the change in the source strength during the experiment was largely eliminated. It is this ratio which is plotted as the ordinate in figure 4, where the energy of the bombarding protons is 7×10^5 eV.

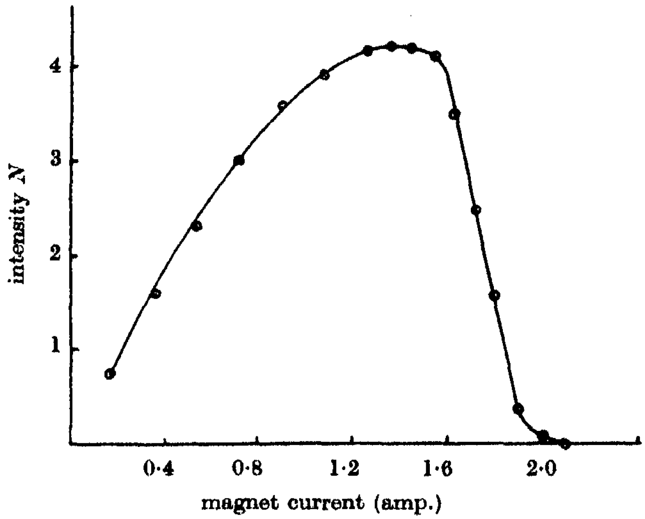

FIGURE 6

It was shown also by means of the spectrograph that the quantum energy of the radiation remained unaltered when the bombarding proton energy was changed, and it was therefore suggested (Dee, Curran and Strothers 1939) that the radiation arises in the process

$$^{19}F + ^{1}H \rightarrow (^{20}Ne) \rightarrow ^{16}O^{*} + ^{4}He \qquad (2)$$

In the case of fluorine the analysis of the radiation by means of the spectrograph was greatly facilitated by the high yield, and if sufficiently intense radiations can be obtained from other capture reactions it will also be possible to investigate their energy spectra rapidly and with accuracy.

(*e*) *Chlorine*. The γ-radiation from radio-chlorine, ^{38}Cl, has been investigated by Richardson (1936), who reported the presence of a weak line of energy $2{\cdot}5 \times 10^{6}$ eV and a strong line of energy $2{\cdot}0 \times 10^{6}$ eV. The experimental upper limit of the β-ray spectrum (Kurie, Richardson and Paxton 1936) is $4{\cdot}8 \times 10^{6}$ eV, but analysis of the spectrum shows that it consists of two components whose upper energy limits differ by about $3{\cdot}7 \times 10^{6}$ eV so that the emission of radiation of total energy equivalent to this amount is to be expected. The sum of the energies of the two lines reported by Richardson ($4{\cdot}5 \times 10^{6}$ eV) does not agree with the known energy difference of the β-ray limits ($3{\cdot}7 \times 10^{6}$ eV), although agreement is obtained if the K.-U. limits* of the β-spectra are employed. However, the assumption that the γ-rays are emitted in cascade implies that their intensities should be equal, in disagreement with his measurements. The energy spectrum of the γ-radiation has been measured by means of our spectrograph and the results are shown in figure 7. The source of ^{38}Cl was prepared by bombardment of KCl with 1 μA hr. of deuterons of energy $9{\cdot}0 \times 10^{6}$ eV. The radio-chlorine was chemically separated and the period, determined simultaneously with the results of figure 7, was found to be 37·5 min. This was taken as adequate evidence of the purity of the radioactive preparation. The ordinates of figure 7 represent the ratio of triple coincidences to γ-ray counts obtained simultaneously with a standard counter, correction for decay being thus eliminated. The statistical fluctuation is less than 5 % for each of the points.

From figure 7 we find that two strong γ-ray lines are present, the energies being $(1{\cdot}65 \pm 0{\cdot}05) \times 10^{6}$ eV and $(2{\cdot}15 \pm 0{\cdot}05) \times 10^{6}$ eV. A plot of $N/H\rho$ against $H\rho$ shows that the relative intensities of the two lines are 3 : 4, and at the same time it reveals the presence of some softer radiation. These facts are in better agreement with the β-ray data. The sum of the two quantum energies $3{\cdot}76 \times 10^{6}$ eV is approximately equal to the difference in the experimental values of the upper energy limits of the β-ray spectra.*

---

* The K.-U. limits of the spectrum are 6·1 and $1{\cdot}5 \times 10^{6}$ eV, and the emission of quantum energy of $4{\cdot}6 \times 10^{6}$ eV, which is appreciably larger than the value obtained from our measurements, is therefore to be expected. However, the K.-U. limit of $6{\cdot}1 \times 10^{6}$ eV is very much greater than the observed limit of $4{\cdot}8 \times 10^{6}$ eV.

The approximate equality of intensity of the two γ-rays agrees with the assumption that they are emitted in cascade. A very small intensity of radiation of energy $2{\cdot}6 \times 10^6$ eV is seen to be present.

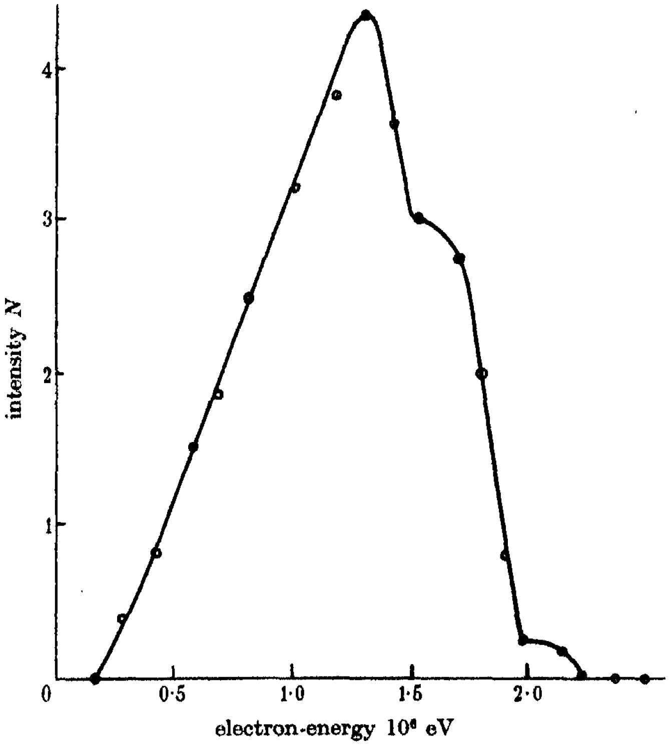

FIGURE 7

We are indebted to those in charge of the Cambridge cyclotron for the preparation of the radioactive sources. One of us (J. E. S.) is indebted to the Department of Scientific and Industrial Research and to Newnham College for the award of grants.

SUMMARY

Using the method of semicircular magnetic focusing of secondary electrons, it has been possible to construct an instrument which is suitable for the measurement of the quantum energies of γ-radiation between the limits of about 0·5 and $16{\cdot}0 \times 10^6$ eV, and which is capable of giving a reliable estimate of the relative intensities of the components of such radiation.

The detecting system consists of three thin-walled Geiger-Müller counters coupled to an amplifying system which records triple coincidences. The construction of the apparatus is such that it may be used for the analysis of γ-radiation emitted during the bombardment of light elements by protons, as well as that emitted by radioactive sources.

The apparatus was standardized by using the γ-radiation from the active deposit of thorium. Its accuracy having been thus established, it was used in the investigation of the γ-radiation from the sources ^{24}Na, ^{56}Mn and ^{38}Cl, and also the radiation emitted during the bombardment of fluorine by high-energy protons. The results are tabulated below:

Source	Quantum energies $\times 10^6$ eV	Relative intensities
^{24}Na	1·46; 2·0; 3·03	1·17 : 0·27 : 1·0
^{56}Mn	0·91; 2·03	2·1 : 1·0
^{38}Cl	1·65; 2·15	3 : 4
^{19}F + ^{1}H	6·5	—

REFERENCES

Alichanian, Alichanow and Dzelepow 1935 *Nature, Lond.*, **136**, 257.
Brown and Mitchell 1936 *Phys. Rev.* **50**, 593.
Curran and Petrzilka 1939 *Proc. Camb. Phil. Soc.* **35**, 309.
Curran and Strothers 1939 *Proc. Roy. Soc.* A, **172**, 72.
Dee, Curran and Strothers 1939 *Nature, Lond.*, **143**, 759.
Delsasso, Fowler and Lauritsen 1939 *Phys. Rev.* **51**, 527.
Dunworth 1939 *Nature, Lond.*, **143**, 1065.
Ellis 1934 *Rep. Internat. Conf. Phys.*
Ellis and Aston 1932 in Rutherford, Chadwick and Ellis, *Radiations from Radioactive Substances.*
Feather and Dunworth 1938 *Proc. Camb. Phil. Soc.* **34**, 442.
Gaerttner and Crane 1936 *Phys. Rev.* **49**, 793.
Halpern and Crane 1939 *Phys. Rev.* **55**, 206.
Kikuchi *et al.* 1939 *Proc. Phys. Math. Soc. Jap.* **21**, 260.
Kurie, Richardson and Paxton 1936 *Phys. Rev.* **49**, 368.
Livingood and Seaborg 1938 *Phys. Rev.* **54**, 391.
Mitchell and Langer 1937 *Phys. Rev.* **52**, 137.
Richardson 1936 *Phys. Rev.* **49**, 203.
— 1938 *Phys. Rev.* **53**, 124.
Richardson and Kurie 1936 *Phys. Rev.* **50**, 999.

Reciprocity failure of photographic materials at short exposure times*

By W. F. Berg

(*Communicated by C. E. K. Mees, F.R.S.—Received* 28 *November* 1939)

Recent work in which photographic materials were exposed at low temperatures (Berg and Mendelssohn 1938; Webb and Evans 1938; Berg 1939*a*; Evans and Hirschlaff 1939) has given results which can be explained by the assumption that an electronic and an ionic process occur in the formation of the latent image (Trivelli 1928; Gurney and Mott 1938). At low enough temperatures these two processes are separated because the ionic mobility is reduced to zero and the ionic process is postponed until the emulsion is warmed up prior to development, whereas the electronic mobility is but little affected.

It should be possible to separate these two processes even at room temperature, because the electrons are much more mobile than the ions, and thus for sufficiently brief exposures the electronic process should be over before the heavier ions have moved appreciably. If this were correct, no difference would be found between exposures sufficiently short to make certain of this separation, and shorter exposures still. In other words, reciprocity failure, the occurrence of which has been accounted for by the electronic and ionic processes taking place side by side (Gurney and Mott 1938), should disappear. The shape of the reciprocity curve is well represented by a catenary over the range hitherto investigated (Webb 1935). According to the present argument the catenary-like curve would be expected to bend over and become horizontal at its short exposure end. The longest exposure on the horizontal part of the curve should then bear some relation to the mobility and concentration of movable silver ions, and, in so far as these properties depend on temperature, the position of the "bend-over point" should depend on temperature also. Experiments on these lines are reported below.

---

* Communication No. 746H from the Kodak Research Laboratories, Harrow, Middlesex.

EXPERIMENTAL

(1) *The apparatus*

The apparatus used may be described as an intensity-scale sensitometer, the general lay-out of which is shown in figure 1. Exposures are made through a photographic step-wedge on film having a range of densities from 0 to 4, to the image of the ball of a 100 c.p. Pointolite lamp La. The image, 7·5 mm. in diameter, is projected on to the wedge and film by means of a lens of 5 cm. focal length and aperture $F/1{\cdot}9$. The wedge is wrapped around the periphery of a drum D; the wedge itself, the drum, and thin spacers between them form a pocket into which the film to be exposed is inserted. That part of the drum around which the film is placed forms a chamber C, which can be filled with a cooling medium. The drum is rotated by a gearless synchronous motor M_1 ("Saja" gramophone cutting) giving speeds of 78 and 33⅓ r.p.m., simply by operating a switch. In some experiments the drum was also rotated at a slower rate by a small synchronous motor driving the periphery of the turntable by means of a small rubber disk.

The exposure time is determined either by the speed of the drum and the width of a slit diaphragm just in front of the drum or by a fast sector shutters. In the latter case, the exposure consists of a series of small patches, one for each revolution of the sector, each patch being an image of the pointolite ball. In order to ensure that at least one of the exposed areas is clear of the dividing line between the steps of the wedge, the dimensions and the speed of drum, sector, and wedge, are so chosen that, on the average, two such exposures fall into each step of the wedge. Thus, the drum and sector motors need not be exactly synchronized, and to expose a film it is only necessary to open an auxiliary shutter *Sh* for about one revolution of the drum. This is done by hand, the position of the drum in the dark being indicated by a small pilot lamp attached to it.

The sector itself is made from cardboard for reasons of safety and carries several apertures, the edges of which consist of strips of black paper. The width of the narrow apertures is determined on a travelling microscope, the angle subtended by the large ones being determined directly. The accuracy is ± 2 % for the smallest aperture, and rather better than this for the larger ones. The sector is situated about 3 mm. away from the drum, and is rotated by a series-wound D.C. motor M_2 which is designed to go up to 10,000 r.p.m. The speed was not specially controlled but turned out to be constant to within ± 2 %. The various apertures of the sector are brought into action one after the other by sliding the lamp and the optical projecting system, which form one unit, along a kinematic slide in the direction of the double-headed arrow in figure 1.

By these various means, a range of exposure times of from 1/3rd to 1/300,000th sec. could be covered.

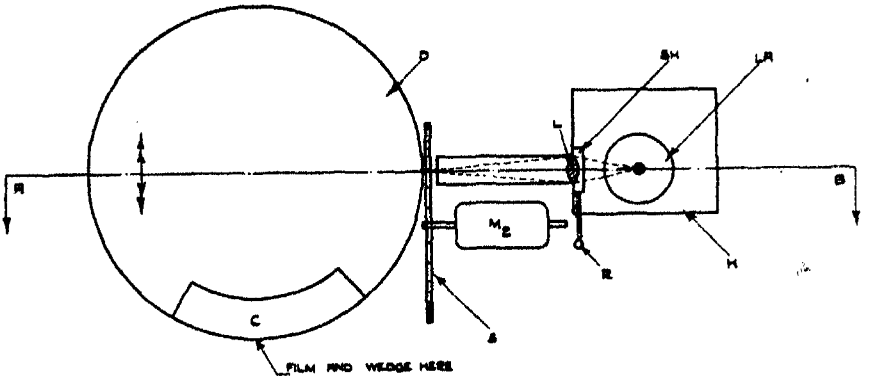

SECTION ON 'X-Y'

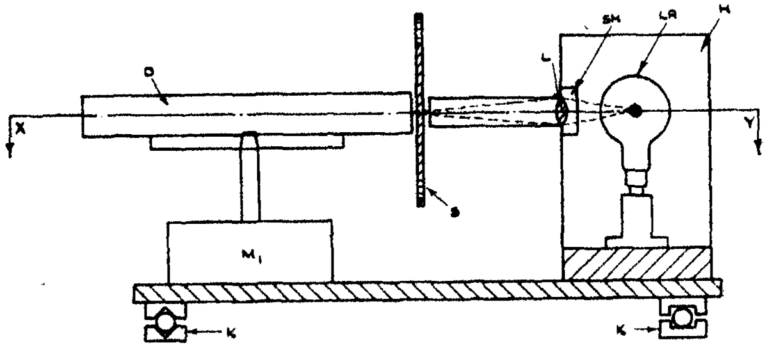

SECTION ON 'A-B'

FIGURE 1

(2) *Procedure*

It was found that the Pointolite lamp could not be relied upon to give a constant output from one experiment to the next, although the supply voltage was controlled. For this reason, a constant control exposure was made with every exposure. To make this possible the sector had an aperture of constant angle close to every aperture, and these apertures were so arranged with respect to the image of the pointolite ball that one-half of that image was exposed through the control aperture, the other half through the other aperture. In the case of the diaphragm exposures, all the diaphragms had a control aperture separated from the other aperture by a narrow strip of black paper to avoid irradiation effects. In the evaluation of the results corrections were made if the individual control exposures deviated from the average control exposure, which itself contributes one of the points on the reciprocity curve. Further corrections were applied if the speed of the sector varied, as was verified by measuring the distances between the exposed areas on each piece of film.

The lens aperture was occasionally altered to change the level of intensity incident on the wedge, but the accuracy of this adjustment was not high enough to vary the intensity in a reproducible fashion and was therefore only used to extend the range of the wedge. If this was done it was usually arranged that several points on the two sections of reciprocity curve obtained at the two aperture settings overlapped so that the two curves could be fitted to each other properly.

In order to obtain reciprocity curves from the measured densities, the photographic density of the wedge had to be accurately known, since the wedge was here the only means of varying the intensity on the film in a known manner. The density readings as obtained on a densitometer cannot be expected to represent exactly the changes in intensity on the film under working conditions, and the wedge was therefore calibrated photographically, using the method described by Toy (1925).

A serious source of error lies in the inefficiency of the shutter for the very shortest exposure times. For the exposure to be defined accurately, the shutter should be effectively in contact with the film. If this condition is not fulfilled, there will be a gradual rise in intensity up to the full value, which is maintained for a time shorter than the nominal exposure time followed by a similar fall in intensity. The total exposure is not affected, but the effective exposure time cannot be defined properly, and the total time is longer than the nominal time of exposure. For the shortest exposure used here the logarithm of the total exposure time is equal to the nominal exposure time + 0·4; for the next longer + 0·15. A similar correction applies for the shortest diaphragm exposures. For the longer exposure times in both cases the corrections become negligible. The experimental points on the curves are drawn as ellipses elongated to cover the range of exposures from the nominal to the total exposure time. No corrections have been made to allow for the possibility that the effective exposure time might be shorter than the nominal time, because any objection against the present results could only be based on the assumption that the effective time was longer than the nominal time.

For the experiments at reduced temperatures, no attempts have been made to control the temperature of the film within close limits. The film was in contact with the metal drum, the metal itself being in contact with solid carbon dioxide. The step wedge was covered by an additional piece of clear film base in order to protect the wedge from condensed moisture. This piece of base would ice up considerably during any one experiment, but it was not necessary to remove the ice, since the change in intensity occasioned by this circumstance was taken care of by the control exposure. The ice would, however, cause the intensity level incident on the wedge to be different at room and low temperatures, so that the absolute ordinates of the reciprocity curves obtained at the two temperatures cannot be compared. The reproducibility was fairly satisfactory and showed that, although the temperature of the film was not actually that of the carbon dioxide, a definite equilibrium temperature must have been reached. This was checked by thermocouple measurements which showed the temperature to be about − 40° C, equilibrium being reached 30 sec. after the film was inserted into the pocket.

All the films belonging to one experiment were processed together in a normal metol-hydroquinone developer.

RESULTS

Figures 2, 3, 4 and 5*a* show reciprocity curves of (I) a blue-sensitive, coarse grain, high-speed film at various densities, (II) of a blue-sensitive, fine grain, medium-speed film at two densities, and (III) and (IV) of two panchromatic medium grain, high-speed films. All these were exposed at room temperature. These emulsions were chosen because of their widely varying reciprocity characteristics. It is clear that reciprocity failure does disappear for all these emulsions at sufficiently short exposure times. The

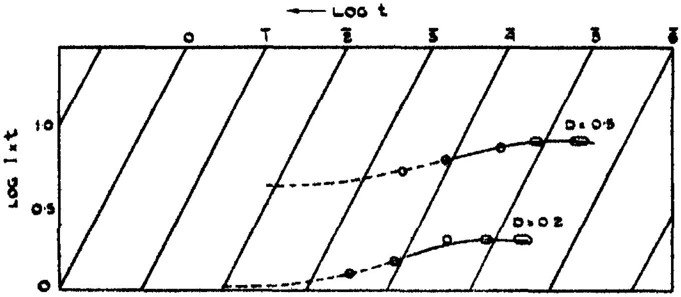

FIGURE 2

point where the curves bend over into the horizontal is, within the limits of accuracy, always at the same exposure time of about 4×10^{-5} sec., and independent of the type of emulsion or the density. The position of the bend-over point does, however, depend on temperature, as is shown by

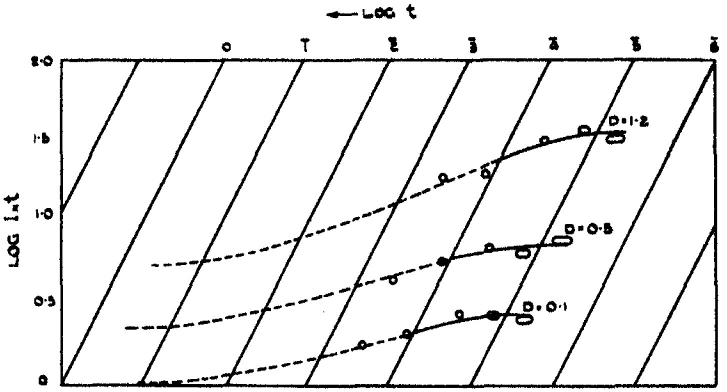

FIGURE 3

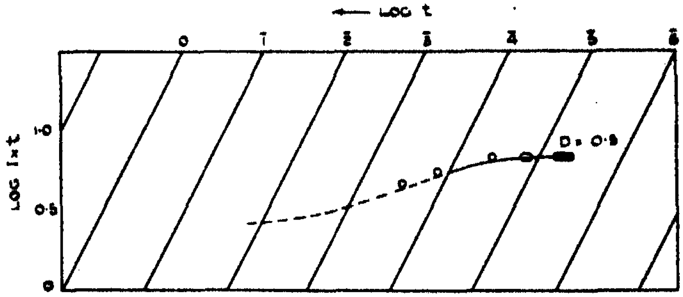

FIGURE 4

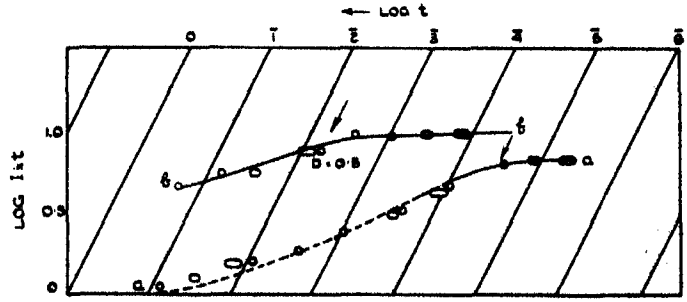

FIGURE 5

curve *b* of figure 5, which gives the reciprocity curve for film IV at −40° C. The bend-over point shifts towards longer exposures with decreasing temperature.

DISCUSSION

The order of magnitude of the time of exposure at which the bend-over point occurs can be estimated theoretically in the following way.

It is assumed that at any point on the horizontal portion of the reciprocity curve the sensitivity speck acquires a charge of N electrons before the first ion reaches the speck. This charge attracts N interstitial silver ions and neutralizes them, forming a mass of metallic silver large enough to make the grain developable (Gurney and Mott 1938). If the number of silver ions in interstitial positions per unit cell is C, these N ions are contained within a sphere of radius l, given by

$$\frac{l^3}{N} = \frac{3}{4\pi}\frac{p^3}{C}, \tag{1}$$

where p is the lattice constant, $p = 5{\cdot}78 \times 10^{-8}$ cm. The time t for the farthest ion to travel, assuming that the charge of the speck does not alter, is given by

$$t = \int_0^l \frac{kr^2}{mNe}\,dr = \frac{1}{3}\frac{k}{me}\frac{l^3}{N}, \tag{2}$$

where m is the ionic mobility, k the dielectric constant ($k = 13$), and r the distance between the charge Ne and the ion. Thus finally

$$t = \frac{1}{4\pi}\frac{p^3k}{Cme}, \tag{3}$$

or since Cme/p^3 is the ionic conductivity (K) in e.s.u. due to the interstitial ions,

$$t = \frac{k}{4\pi K}. \tag{4}$$

Measurements of the ionic mobility and of the concentration of ions in interstitial positions over a limited range of temperatures on pure silver bromide melts, have been reported by Koch and Wagner (1937). The logarithms of mobility (1) and of the concentration (2) are plotted against $1/T$ in figure 6. The equations given by Koch and Wagner have been used for the purposes of extrapolation. Curve 3 in figure 6 gives the conductivity as the product of mobility and concentration, curve 4 the conductivity from measurements by Toy and Harrison (1930) on silver bromide melts, and curve 5 similar measurements on single crystals by Lehfeld (1933) over a wider range of temperatures. All the conductivities except 5 are plotted in relative units and the curves can thus only be used for comparing the slopes, i.e. the temperature coefficients. The absolute values of conductivity depend to a large extent on the history and state of purity of the material, and have not been determined at all by Toy and Harrison. Curve 5 covers the widest range of temperatures and shows a sudden bend at about room temperatures. The high temperature branch is parallel to the conductivity curve 3 as determined at high temperature by Koch and Wagner. The low temperature branch is parallel to the ionic mobility curve 1 and fits fairly well to curve 4 by Toy and Harrison, which was also obtained at low temperatures. The obvious conclusion is that the ionic concentration does not change at temperatures below a certain critical point at about room temperature. This may be explained in two ways. Lehfeld (1933) suggests the change in his curve to be due to impurities which would cause surplus ions to be present, the number of which would be independent of temperature. Another explanation is that the number of interstitial ions is higher than that corresponding to the equilibrium temperature because the crystal has not been kept at that temperature sufficiently long for equilibrium to be reached (Koch and Wagner 1937).

These data make it possible to evaluate equations (1) and (4). The distance l over which the farthest ions travel is of the order of 10^{-6} cm., if N is assumed to be equal to 1, and 10^{-5} cm., for $N = 1000$, taking the value for C from curve 2 in figure 6 at room temperature ($C = 8{\cdot}3 \times 10^{-6}$). This result is significant because it shows that the ions travel over distances which are much smaller than the average emulsion grain. In all ordinary emulsions, therefore, the grain size itself will not influence the position of the bend-over point.

To evaluate equation (4), the value of the conductivity as determined by Lehfeld is the most reliable, viz. 9×10^{3} abs. units. This total conductivity is about twice that due to the interstitial ions, since according to Koch and Wagner about one-half of the conductivity is due to the mobility of the holes left on the lattice when the interstitial ions are formed. Inserting, therefore, $4{\cdot}5 \times 10^{-3}$ in equation (4), the time at which the bend-over should occur, is found to be $t = 2 \times 10^{-4}$ sec. It is to be noted that this figure is only an approximation since the assumptions on which the calculation is based are somewhat artificial. Further, the conductivity of the iodo-bromide emulsion grains is probably higher than that of Lehfeld's preparation. This would tend to decrease the time and bring it nearer to the experimental figure of 4×10^{-5} sec. Since N, the number of ions forming the latent image, does not appear in equation (4), the time at which the bend-over occurs should be independent, or substantially independent, of the sensitivity of the grains. This accounts for the fact that materials of different type and at different densities all have the bend-over points at the same time of exposure.

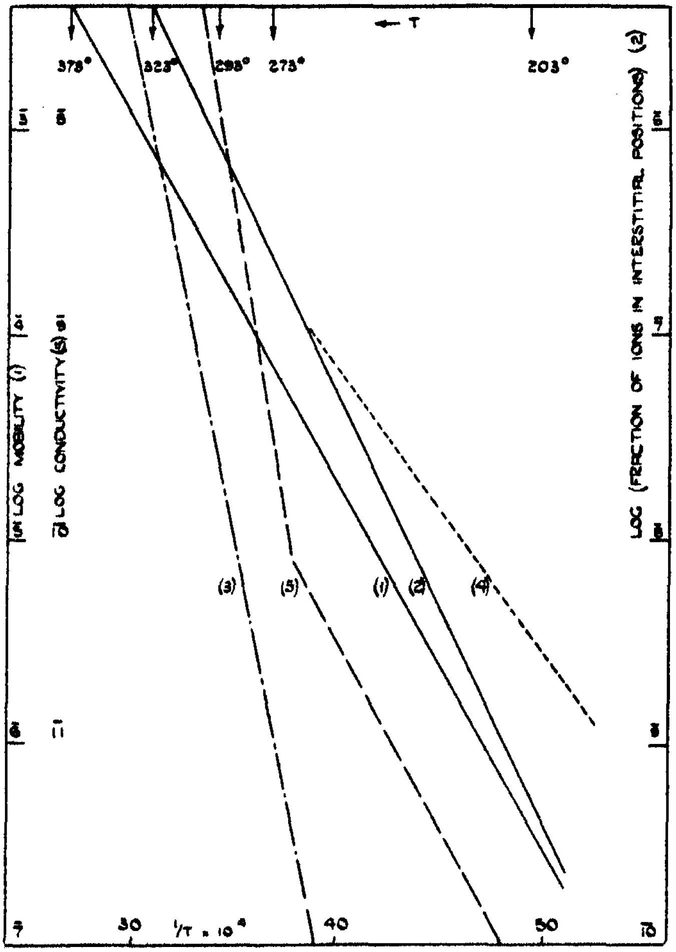

FIGURE 6

It follows from the considerations given above that the shift of the bend-over point for temperatures below room temperature should depend on the ionic mobilities only. The ratio of the mobilities at the two temperatures + 20° C and − 40° C is 1/120, and the ratio of the times for the bend-over points in figures 5*a* and 5*b* is 1/180. The agreement is satisfactory.

The fact that reciprocity failure disappears for sufficiently short exposures is consistent with the earlier result (Berg and Mendelssohn 1938), that reciprocity failure disappears at 90° K over the whole range of exposure times used. At that temperature the bend-over would be expected to occur at 10^9 sec. This was explained (Berg 1939*a*) by comparing the exposures at low temperatures with very brief exposures at room temperature and the present experiments are to be considered as confirming that suggestion. The loss in sensitivity at low temperature was thought to be brought about essentially by the low capacity of the sensitivity specks (Webb and Evans 1938) which was made responsible for any further electrons being repelled and trapped elsewhere (Berg 1939*a*). Whether trapping of electrons outside the sensitivity specks also occurs at room temperature cannot be determined from these experiments. Evidence that this trapping does occur has been provided by other means (experiments by Brentano, see Berg 1939*b*).

The author wishes to put on record his thanks for the assistance with the experiments given by Mr S. E. Brett and Mr L. J. Sumner, and with the theoretical considerations given by Mr E. W. H. Selwyn.

SUMMARY

Experiments at very high intensities and at various temperatures show that for sufficiently short exposures reciprocity failure disappears. The bend-over point in the reciprocity failure curve is shown to be connected with the mobility and concentration of the interstitial Ag^+ ions, and below room temperature varies with temperature as the mobility. These results provide further confirmation that the latent image is formed by the aggregation and neutralization of silver ions on sensitivity specks.

REFERENCES

Berg 1939*a* *Trans. Faraday Soc.* **35**, 445.
— 1939*b* *Nature, Lond.*, **144**, 356.
Berg and Mendelssohn 1938 *Proc. Roy. Soc.* A, **168**, 168.
Evans and Hirschlaff 1939 *J. Chem. Soc. Amer.* **29**, 164.
Gurney and Mott 1938 *Proc. Roy. Soc.* A, **164**, 151.
Koch and Wagner 1937 *Z. Phys. Chem.* B, **38**, 295.
Lehfeld 1933 *Z. Phys.* **85**, 717.
Toy 1925 *Photogr. J.* **65**, 164.
Toy and Harrison 1930 *Proc. Roy. Soc.* A, **127**, 613.
Trivelli 1928 *Photogr. J.* **68**, 14.
Webb 1935 *J. Chem. Soc. Amer.* **25**, 4.
Webb and Evans 1938 *J. Chem. Soc. Amer.* **28**, 249.

INDEX TO VOLUME 174 (A)

Absorption spectra of conjugated dienes in the vacuum ultra-violet (1) (Price and Walsh), 220

Absorption spectra of ethylene, deutero-ethylene and some alkyl-substituted ethylenes in the vacuum ultra-violet (Price and Tutte), 207.

Adsorption of lauryl sulphonic acid (McBain and Wood), 286.

Aliphatic chain molecules, torsional flexibility (Müller), 137.

Atmospherics, wave form, energy and reflexion by the ionosphere (Laby, McNeill, Nicholls and Nickson), 145.

Awbery, J. H. and Griffiths, E. The thermal capacity of pure iron, 1.

Bannon, J., Higgs, A. J., Martyn, D. F. and Munro, G. H. The association of meteorological changes with variations of ionization in the F_2 region of the ionosphere, 298.

Bell, R. P. The repulsive forces between isotopic molecules, 504.

Berg, W. F. Reciprocity failure of photographic materials at short exposure times, 559.

Bonner, T. W. The neutrons from the disintegration of fluorine by deuterons, 339.

Brass, crystalline structure under slow and rapid cyclic stresses (Wood and Thorpe), 310.

Burgoyne, J. H. The combustion of aromatic and alicyclic hydrocarbons. IV. The kinetics of the slow combustion of benzene and its mono-alkyl derivatives at low temperatures, 394.

Burgoyne, J. H., Tang, T. L. and Newitt, D. M. The combustion of aromatic and alicyclic hydrocarbons. III. Ignition and cool-flame characteristics, 379.

Carter, A. H. and Weiss, J. The transfer of excitation energy from uranium ions in solution, 351.

Chao, S. H. and Taylor, W. H. The lamellar structure of potash-soda felspars, 57.

Chrome alum, dehydration of crystals (Cooper and Garner), 487.

Combustion of aromatic and alicyclic hydrocarbons. III. (Burgoyne, Newitt and Tang), 379.

Combustion of aromatic and alicyclic hydrocarbons. IV. (Burgoyne), 394.

Cooper, J. A. and Garner, W. E. The dehydration of crystals of chrome alum, 487.

Critical and co-operative phenomena, V. (Devonshire), 102.

Curran, S. C., Dee, P. I. and Strothers, J. E. Some measurements of γ-ray energies, 546.

Davoud, J. G. and Hinshelwood, C. N. Kinetics of the thermal decomposition of fully deuterated diethyl ether, 50.

Dee, P. I. *See* Curran and others.

Devonshire, A. F. Critical and co-operative phenomena. V. Specific heats of solids and liquids, 102.

Drinkwater, J. W., Richardson, Sir Owen and Williams, W. E. Determination of the Rydberg constants, *e*/*m*, and the fine structures of H_α and D_α by means of a reflexion echelon, 164.

Eddington, Sir Arthur. A new derivation of the quadratic equation for the masses of the proton and electron, 16.
Eddington, Sir Arthur. The masses of the neutron and mesotron, 41.
Elliott, A. The molecular spectrum of iodine excited by fluorescence (in the presence of nitrogen) and by active nitrogen, 273.

Felspars, potash-soda, lamellar structure (Chao and Taylor), 57.
Fowler, R. H. and Guggenheim, E. A. Statistical thermodynamics of superlattices, 189.
Fox, J. J. and Martin, A. E. Investigations of infra-red spectra, 234.
Fröhlich, H., Heitler, W. and Kahn, B. The photodisintegration of the deuteron in the meson theory, 85.
Fuchs, K. On the statistical method in nuclear theory, 509.

γ-ray energies, some measurements (Curran, Dee and Strothers), 546.
Garner, W. E. *See* Cooper and Garner.
Grains on the bed of a stream, equilibrium (White), 322.
Griffiths, E. *See* Awbery and Griffiths.
Guggenheim, E. A. *See* Fowler and Guggenheim.

Heitler, W. *See* Fröhlich, Heitler and Kahn.
Higgs, A. J. *See* Bannon and others.
Hinshelwood, C. N. *See* Davoud and Hinshelwood.
Hume-Rothery, W. and Raynor, G. V. The equilibrium and lattice-spacing relations in the system magnesium-cadmium, 471.
Hurst, D. G., Latham, R. and Lewis, W. B. On the production of radium E and polonium produced by deuteron bombardment of bismuth, 126.
Hydrocarbon flames, emission spectrum (Smith), 110.

Infra-red spectra investigations (Fox and Martin), 234.

Kahn, B. *See* Fröhlich, Heitler and Kahn.

Laby, T. H., McNeill, J. J., Nicholls, F. G. and Nickson, A. F. B. Wave form, energy and reflexion by the ionosphere, of atmospherics, 145.
Latham, R. *See* Hurst, Latham and Lewis.
Lattice-spacing of the primary solid solutions of silver, cadmium and indium in magnesium (Raynor), 457.
Lattice-spacing relations and equilibrium in the system magnesium-cadmium (Hume-Rothery and Raynor), 471.
Lewis, W. B. *See* Hurst, Latham and Lewis.

McBain, J. W. and Wood, L. A. Adsorption of lauryl sulphonic acid in the surface of its aqueous solution, and the Gibbs theorem, 286.
McNeill, J. J. *See* Laby and others.

Martin, A. E. *See* Fox and Martin.
Martyn, D. F. *See* Bannon and others.
Meldrum, F. R. The heat of formation of nitrogen iodide, 424.
Meldrum, F. R. The thermal decomposition of nitrogen iodide, 410.
Mesotrons, scattering in metal plates (Wilson), 73.
Meteorological changes, association with ionization in the F_2 region (Bannon and others), 298.
Misener, A. D. The specific heat of superconducting mercury, indium and thallium, 262.
Molecular spectrum of iodine excited by fluorescence (in the presence of nitrogen) and by active nitrogen (Elliott), 273.
Müller, A. The torsional flexibility of aliphatic chain molecules, 137.
Munro, G. H. *See* Bannon and others.

Neutron and mesotron masses (Eddington), 41.
Neutrons from the disintegration of fluorine by deuterons (Bonner), 339.
Nevin, T. E. Rotational analysis of the first negative band spectrum of oxygen. II, 371.
Newitt, D. M. *See* Burgoyne and others.
Nicholls, F. G. *See* Laby and others.
Nickson, A. F. B. *See* Laby and others.
Nitrogen iodide, heat of formation (Meldrum), 424.
Nitrogen iodide, thermal decomposition (Meldrum), 410.
Nuclear energies and stability, calculation (Spain), 523.
Nuclear theory, statistical method (Fuchs), 509.

Photodisintegration of the deuteron in the meson theory (Fröhlich, Heitler and Kahn), 85.
Photographic materials at short exposure times, reciprocity failure (Berg), 559.
Price, W. C. and Tutte, W. T. The absorption spectra of ethylene, deutero-ethylene and some alkyl-substituted ethylenes in the vacuum ultra-violet, 207.
Price, W. C. and Walsh, A. D. The absorption spectra of conjugated dienes in the vacuum ultra-violet (1), 220.
Proton and electron, quadratic equation for the masses (Eddington), 16.

Radium E and polonium produced by deuteron bombardment of bismuth (Hurst, Latham and Lewis), 126.
Raynor, G. V. The lattice spacings of the primary solid solutions of silver, cadmium and indium in magnesium, 457.
Raynor, G. V. *See also* Hume-Rothery and Raynor.
Repulsive forces between isotopic molecules (Bell), 504.
Richardson, Sir Owen. *See* Drinkwater, Richardson and Williams.
Rydberg constants, e/m, and the fine structures of H_α and D_α, determination by means of a reflexion echelon (Drinkwater, Richardson and Williams), 164.

Smith, E. C. W. The emission spectrum of hydrocarbon flames, 110.
Southwell, R. V. On the natural frequencies of vibrating systems, 433.

Spain, B. Calculation of nuclear energies and stability by the statistical method, 523.
Spectrum of oxygen, first negative band (Nevin), 371.
Strothers, J. E. *See* Curran and others.
Superconducting mercury, indium and thallium specific heat (Misener), 262.
Super-lattices, statistical thermodynamics (Fowler and Guggenheim), 189.

Tang, T. L. *See* Burgoyne and others.
Taylor, W. H. *See* Chao and Taylor.
Thermal capacity of pure iron (Awbery and Griffiths), 1.
Thermal decomposition of fully deuterated diethyl ether (Davoud and Hinshelwood), 50.
Thorpe, P. L. *See* Wood and Thorpe.
Tutte, W. T. *See* Price and Tutte.

Uranium ions in solution, transfer of excitation energy (Carter and Weiss), 351.

Vibrating systems, natural frequencies (Southwell), 433.

Walsh, A. D. *See* Price and Walsh.
Weiss, J. *See* Carter and Weiss.
White, C. M. The equilibrium of grains on the bed of a stream, 322.
Wood, L. A. *See* McBain and Wood.
Williams, W. E. *See* Drinkwater, Richardson and Williams.
Wilson, J. G. The scattering of mesotrons in metal plates, 73.
Wood, W. A. and Thorpe, P. L. Behaviour of the crystalline structure of brass under slow and rapid cyclic stresses, 310.

END OF THE ONE HUNDRED AND SEVENTY-FOURTH VOLUME (SERIES A)

ABSTRACTS

OF PAPERS COMMUNICATED TO THE ROYAL SOCIETY OF LONDON

In accordance with a resolution of Council, summaries or abstracts of papers are to be published as soon as practicable. The publication of such abstracts in no way indicates that the papers have been accepted for publication in any fuller form. These abstracts are issued for convenience with the "Proceedings of the Royal Society of London" but do not form a part of the "Proceedings".

NOTE—The pagination of the "Abstracts" will be consecutive through the year and independent of the "Proceedings". To avoid any confusion with the "Proceedings", the page numbers will be preceded by the letter S (*i.e.* Summary).

---

12 JANUARY 1940

On the photon component of cosmic radiation and its absorption coefficient.

By B. ROSSI and L. JÁNOSSY. (*Communicated by P. M. S. Blackett, F.R.S.—Received* 17 *November* 1939.)

Photons, unlike ionizing particles, cannot be observed directly with counters. Owing to this difficulty very few investigations dealing with the photon component of cosmic radiation have been carried out. In the present paper a simple method is described which is suitable for the observations of cosmic-ray photons. The transition effect of photon-initiated showers in lead has been measured. The result is in agreement with the predictions of the cascade theory of Bhabha and Heitler as extended by Arley. The absorption coefficients of cosmic-ray photons have been measured in lead iron and aluminium and they agree with the theoretical values as given by Bethe and Heitler. The lower limit for the total flux of cosmic-ray photons, above 10^7 eV, has been found to be 10 % of the ionizing component of the cosmic-ray beam.

The combustion of aromatic and alicyclic hydrocarbons. III. Ignition and cool-flame characteristics.

By J. H. BURGOYNE, D. M. NEWITT and T. L. TANG. (*Communicated by A. C. Egerton, Sec.R.S.—Received* 22 *November* 1939.)

The general ignition characteristics of eleven aromatic and alicyclic hydrocarbons have been investigated, and previous conclusions regarding their relative reactivity to oxygen are confirmed.

While benzene, toluene, and ethylbenzene show smooth ignition curves within the limits of pressure available, the other hydrocarbons examined exhibit low-temperature ignition systems and, except in the case of *p*-xylene, cool flames are propagated.

Cyclohexane behaves as a typical paraffin, but tetrahydrobenzene, while resembling the olefines in most respects, has cool-flame limits characteristic of the aromatic series.

Chemical analyses of the ultimate products of slow combustion and cool-flame reactions show that the two types of combustion yield similar results at the same temperature. The low-temperature systems of the aromatic hydrocarbons are similar to those of the paraffins and what differences occur appear to be conditioned merely by the relative stability of analogous intermediate products.

The combustion of aromatic and alicyclic hydrocarbons. IV. The kinetics of the slow combustion of benzene and its mono-alkyl derivatives at low temperatures.

By J. H. BURGOYNE, PH.D. (*Communicated by A. C. Egerton, Sec.R.S.—Received* 22 *November* 1939.)

The kinetics of the combustion of benzene and the four simplest mono-alkyl derivatives have been studied in the temperature range between 250 and 400° C, and the results compared with those previously obtained relating to the region above 400° C.

It is concluded that, excepting in the case of benzene itself, the oxidation of these fuels consists of two co-existent chain reactions, as is thought to be the case with the aliphatic hydrocarbons also. Of these processes, one is predominant below 300° C and the other above 400° C, whilst in the intervening range of temperature the two mechanisms proceed on terms of approximate equality. The low-temperature reaction on intensification gives rise to cool flames, while from the high-temperature mechanism a chain-thermal ignition results. The kinetic characteristics of the two processes are demonstrated and compared.

In the intermediate temperature zone (300–400° C), the prominence of the process of cool-flame initiation is thought to be the partial cause of the observed increase in the "order of reaction", and it is suggested that the negative temperature coefficient is due to the mutual interaction of the co-existent chain reactions.

The equilibrium and lattice-spacing relations in the system magnesium-cadmium.

By W. HUME-ROTHERY, F.R.S. and G. V. RAYNOR. (*Received* 23 *November* 1939.)

The equilibrium diagram of the system magnesium-cadmium has been investigated by thermal, microscopic, and X-ray methods. The liquidus and solidus curves pass smoothly from the melting point of magnesium to that of cadmium, with no indication of a discontinuity characteristic of a peritectic reaction. Microscopic methods show no indication of a two-phase region above the temperatures of the superlattice transformations. The supposed compound $MgCd_2$ of Hume-Rothery and Rowell is not a true constituent of the system magnesium-cadmium, but is an oxide-nitride complex formed when the alloys are exposed to the atmosphere. It is formed most readily when the composition of the alloy corresponds with the formula $MgCd_3$; a somewhat similar effect has been noted in the system nickel-chromium. The two-phase region claimed by Grube and Schiedt is not confirmed.

The lattice spacings of a complete series of alloys at 310° C have been measured with a high-temperature X-ray camera. The first additions of cadmium to magnesium cause a contraction of the a parameter of the unit cell, but have little effect on the axial ratio, so that the c parameter contracts in almost the same proportion. With further additions of cadmium, the axial ratio increases slightly. The addition of magnesium to cadmium causes an expansion of the a parameter, but, at the same time, the axial ratio decreases so markedly that the c parameter diminishes, so that each metal decreases the c parameter of the other. A stage is then reached at which the solid solutions derived from magnesium and cadmium acquire identical lattice spacings, which persist unchanged over a narrow range of composition. These effects are discussed, and are shown to be in agreement with the Brillouin Zone theory developed by Jones.

A current-meter for measuring turbulence. By A. T. DOODSON, F.R.S. (*Received* 25 *November* 1939.)

The measurement of tidal currents presents many difficulties, and many types of apparatus have been designed with special objects in view. These types are reviewed and the advantages of instruments of universal type, capable of recording tidal currents moment by moment, are emphasized. Instruments for recording turbulence need to be very sensitive, yet robust, and the lack of suitable instruments led to the development of an electrically operated current meter which has been constructed with the aid of grants from the Government Grant Committee of the Royal Society. The apparatus is described in detail. It is highly sensitive to weak currents, has a scale practically linear with the velocity of current, and it gives records as frequently as at intervals of 15 sec. If required, velocities only can be registered continuously on a very open time scale. It has been used at sea for many weeks, and has given much satisfaction in performance.

The thermal decomposition of nitrogen iodide. By F. R. MELDRUM. (*Communicated by W. E. Garner, F.R.S.—Received* 27 *November* 1939.)

The thermal decomposition of nitrogen iodide has been studied at low pressures and the reaction shown to be $2NH_3.NI_3 \rightarrow 2NH_3 + N_2 + 3I_2$. The activation energy from the temperature coefficient and from calculations made with the aid of the Polanyi-Wigner equation is 18–19 kcal. The reaction is retarded by ammonia and water, and also by an increase in pressure over the solid.

The mechanism of the reaction is discussed in the light of the above results and of the calorimetric results quoted in the following paper.

The heat of formation of nitrogen iodide. By F. R. Meldrum. (*Communicated by W. E. Garner, F.R.S.—Received* 27 *November* 1939.)

From measurements of the heat of reaction of nitrogen iodide with excess of aqueous hydriodic acid, it is shown that the heat of formation of nitrogen iodide from the elements is -34 kcal./mol.

The reciprocity failure of photographic materials at short exposure times. By W. F. Berg. (*Communicated by C. E. K. Mees, F.R.S.—Received* 28 *November* 1939.)

According to recent conceptions on the formation of the photographic latent image, electric and ionic movements occur side by side. For sufficiently short times of exposure, the electronic process should be over before the less mobile ions move appreciably. Thus, for a range of short exposure times up to a certain maximum, the latent image should be formed in essentially the same manner. Electronic and ionic processes are then completely separated, and reciprocity failure, which is explained by the simultaneous occurrence of these two processes, should disappear. This is found to be the case, and the maximum time at which reciprocity failure begins to occur is found to be of the order of 4×10^{-5} sec. at room temperature for four different emulsions, and irrespective of the density. This maximum time can be calculated from data on ionic conductivity and agrees reasonably well with the above figure and also with the variation of the maximum with temperature. This is in agreement with the earlier result that at very low temperatures reciprocity failure was absent over the whole range of exposure times investigated.

The effect of unilateral castration on the production of spermatozoa. By Joseph Edwards. (*Communicated by J. Hammond, F.R.S.—Received* 29 *November* 1939.)

The effect of unilateral castration in the sexually mature rabbit on the production of spermatozoa has been studied quantitatively by means of semen exhaustion tests.

The frequency of collection is shown to have kept pace with the rate of production of spermatozoa by the testis. Contrary to what occurs in the ovary, there is no hypertrophy of spermatogenic function or of weight of testis following unilateral castration. There is a highly significant positive relationship between the weight of the testicular substance and the numbers of spermatozoa which it produces. The passage of spermatozoa through the epididymis may be accomplished in 4–7 days.

ABSTRACTS

OF PAPERS COMMUNICATED TO THE ROYAL SOCIETY OF LONDON

In accordance with a resolution of Council, summaries or abstracts of papers are to be published as soon as practicable. The publication of such abstracts in no way indicates that the papers have been accepted for publication in any fuller form. These abstracts are issued for convenience with the "Proceedings of the Royal Society of London" but do not form a part of the "Proceedings".

---

1 FEBRUARY 1940

The measurement of tides by means of the Favé pressure gauge. By R. H. CORKAN, A. T. DOODSON, F.R.S., and J. PROUDMAN, F.R.S. (*Received* 13 *December* 1939.)

The measurements and analyses described in this paper were made with the object of calculating the variable parts of the components of the horizontal gradients of pressure in the sea. For such a purpose, and in the part of the Irish Sea considered, the principal harmonic constituent of the tidal elevation must have its amplitude determined to the nearest cm. and its phase determined to the nearest 0·3°.

The instruments used were three models of the *marégraphe plongeur* Favé. Though this instrument has been described in great detail by its designer, very little has been previously published on results obtained with it. Our greatest difficulties were in connexion with the calibration of the instruments.

The results obtained from the records taken at sea may be regarded as giving a good determination of the principal harmonic constituent of the tides at the stations considered, but not sufficiently good for a reliable calculation of the horizontal pressure gradients.

The investigation has given us very valuable experience, and when opportunity next occurs we intend to make further measurements.

The dynamic constants of human muscle. By A. V. HILL, SEC.R.S. (*Received* 14 *December* 1939.)

The characteristic equation of muscle is modified to meet the case of a constant mass accelerated instead of a constant force overcome at uniform speed.

The theory is compared with experimental results obtained on human arm muscles with an inertia wheel. The agreement is good.

The value of the dynamic constant b is deduced. Its order of size is muscle length per second. P_0/a cannot be very far from 4, its mean value in frogs' muscle.

The maximum speed of shortening (unloaded) is determined experimentally. This is of the order of size $P_0 b/a$ deduced from theory.

The mechanical efficiency, the optimum speed, the possibility of reflex inhibition during rapid shortening, certain practical applications and some proposals for further research are discussed.

The photolysis of ammonia. By E. A. B. Birse and H. W. Melville.

(*Communicated by J. Kendall, F.R.S.—Received* 15 *December* 1939.)

The anomalously low stationary hydrogen atom concentration during the photodecomposition of ammonia is due either to the fact that the primary photochemical efficiency is not unity or that the hydrogen atoms are removed at an abnormally fast rate. It is shown by utilizing the para-hydrogen conversion that photodecomposing ammonia has no effect on the stationary hydrogen atom concentration of the conversion and therefore the low concentration of the ammonia photolysis must be due to inefficiency of the primary process. The primary efficiency is determined by a careful comparison of the mercury sensitized and the ammonia sensitized conversion of para-hydrogen. A method is developed for measuring accurately the rate of production of hydrogen atoms, which method is essential to the foregoing determination. This primary efficiency is found to be 0·58.

A method is also developed for measuring the lifetime of amine radicals.

Similar experiments with trideuteroammonia are also described. The primary efficiency is 0·28.

A revised and simplified scheme for the ammonia photolysis is given as a result of these new experiments.

The reaction of atomic hydrogen with hydrazine. By E. A. B. Birse and H. W. Melville.

(*Communicated by J. Kendall, F.R.S.—Received* 15 *December* 1939.)

The efficiency of the reaction of atomic hydrogen with hydrazine has been measured in the temperature range 20–200° C by comparison with that of the hydrogen atom sensitized conversion of para-hydrogen. A static system is employed, the hydrogen atoms being produced by excited mercury atoms. The energy of activation is nearly the same as that of the para-hydrogen conversion, namely *ca.* 7 kcal. and the steric factor is *ca.* 10^{-2}. From these results it is shown that hydrazine is not responsible for the low stationary hydrogen atom concentration in the photolysis of ammonia as has hitherto been supposed.

Although the hydrogen atoms react with hydrazine very efficiently the quantum efficiency of this reaction is only 0·4 instead of the expected value of 2. An explanation of this result is suggested.

It is also shown that photodecomposing hydrazine converts para-hydrogen. This is taken to mean that the primary decomposition is represented by

$$N_2H_4 + h\nu = N_2H_3 + H.$$

The quantum efficiency of the mercury sensitized decomposition of hydrazine has been found to be 0·37. An explanation of this unexpectedly low value is given.

A new simplified method of analysing the ternary mixture $p\text{-}H_2—n\text{-}H_2—N_2$ is described.

The phosphorescence of various solids. By J. T. RANDALL and M. H. F. WILKINS. *(Communicated by M. L. E. Oliphant, F.R.S.—Received* 18 *December* 1939.)

A complete understanding of luminescence phenomena in solids involves the study of such properties as emission and absorption spectra, decay laws of phosphorescence, and photoconductivity. In this paper accurate results on the decay laws of phosphorescence of a number of solids are given together with corresponding observations on photoconductivity. Measurements of the phosphorescence of pure and impure solids have been carried out by two methods. In the first and more accurate method the intensity of phosphorescence of an annulus of powder on a rotating disk was measured by means of a vacuum photocell and d.c. amplifier of the electrometer triode type. In the second method an intermittent beam of ultra-violet radiation falls on a stationary specimen; during the illumination period the intensity of luminescence rises to an equilibrium value, afterwards decaying when the ultra-violet radiation is cut off. By allowing the varying luminescence radiation to fall on the primary cathode of an electron multiplier coupled with an oscillograph, rise and decay curves of various solids can be obtained on the oscillograph screen and photographed for measurement.

In general the results are not simple for compounds activated with impurity. Pure uranyl salts, however, give a simple exponential decay $I = I_0 e^{-\alpha t}$; moreover, the salts are not photoconductors. The results confirm the idea that the luminescence of these salts is a property of excitation states within the co-ordination group of the uranyl ion. The time of decay suggests that forbidden transitions are involved. Tungstates on the other hand are slightly photoconducting in the pure state, and have a very fast decay.

A number of inorganic solids containing manganese impurity have also been examined; these include cadmium chlorophosphate, zinc mesodisilicate, cadmium silicate, cadmium borate, zinc beryllium silicates and zinc orthosilicate. In all these solids the initial decay is approximately exponential with a slight curvature of the semi-log plot convex with respect to the time axis. In the zinc beryllium silicates and in zinc orthosilicate this curvature is more pronounced, and in the latter case develops into a long phosphorescent tail. In all cases, however, the slope is a function of time and not of phosphorescence intensity, thus showing that the decays are not of the bimolecular type. The photoconduction results show that the pure non-fluorescent compounds and the impure fluorescent ones conduct in general to the same extent. We are inclined to the view that the photoconduction arises from secondary causes such as lattice defects or interstitial matrix atoms. In the solids cadmium chlorophosphate, zinc mesodisilicate, cadmium silicate, and cadmium borate, we suggest that the decay law is of the type $I = \Sigma I_0 e^{-\alpha t}$; such a result can easily arise from the non-equivalent positions of impurity atoms in various parts of the crystal. From the slope of the semi-log plot the lifetime of the excited manganese ion may be calculated.

The long tail observed for most zinc orthosilicates can best be explained by supposing that the absorption process first sets free the excited electrons. This is followed by electron trapping probably in the neighbourhood of the manganese ions. The free electrons recombine with manganese ions very rapidly; these electrons, however, remain in the excited state an appreciable time, thus giving rise to the initial exponential decay. The phosphorescent tail depends only on the rate at which electrons are released thermally from trapped positions.

Comparison of the acceleration due to gravity at the National Physical Laboratory, Teddington, and the Bureau of Standards, Washington. By B. C. Browne and E. C. Bullard. (*Communicated by Sir Gerald Lenox-Conyngham, F.R.S.—Received* 20 *December* 1939.)

The values of the acceleration due to gravity at the points used for the recent absolute determinations at the National Physical Laboratory, Teddington, and at the National Bureau of Standards, Washington, D.C., have been compared. The difference found is $1{\cdot}096_9$ cm./sec.^{2}. The difference between the two absolute determinations is $1{\cdot}101_6$ cm./sec.^{2}, whilst that deduced from previous indirect relative connexions is $1{\cdot}095_8$ cm./sec.^{2}. The agreement is within the uncertainties of the measurements, and leaves little doubt that the hitherto accepted value at Potsdam is some seventeen parts in a million too great.

The kinetics of decarboxylation in solution. By P. Johnson and E. A. Moelwyn-Hughes. (*Communicated by R. G. W. Norrish, F.R.S.—Received* 21 *December* 1939.)

The kinetics of the decarboxylation of trichloracetic tribromacetic, and trinitrobenzoic acids have been studied over extended temperature ranges in aqueous solution. The results conflict with the formula of Arrhenius, and conform better to an equation of the type

$$\ln k = c + \frac{J}{R}\ln T - \frac{E}{RT}.$$

The experimental values of J are found to be negative. Decarboxylation reactions thus come into line with catalysed and uncatalysed hydrolyses in aqueous solution.

Certain theoretical considerations are advanced to account for the observations.

ABSTRACTS

OF PAPERS COMMUNICATED TO THE ROYAL SOCIETY OF LONDON

In accordance with a resolution of Council, summaries or abstracts of papers are to be published as soon as practicable. The publication of such abstracts in no way indicates that the papers have been accepted for publication in any fuller form. These abstracts are issued for convenience with the "Proceedings of the Royal Society of London" but do not form a part of the "Proceedings".

---

8 MARCH 1940

Crystal boundaries in tin. By B. CHALMERS. (*Communicated by E. N. da C. Andrade, F.R.S.—Received* 2 *December* 1939.)

A new technique is described for preparing specimens of tin consisting of two crystals of controlled orientation, of such a size and shape that a tension can be applied transversely to the boundary. It is found that the temperature at which the crystals separate under tension is below the melting point of the crystalline material, and that the difference is independent of the angle between the crystal axes of the two crystals and of impurity providing this does not exceed about 0·02 %. The mechanism of boundary formation is considered, a distinction being drawn between two types of boundary described as "columnar" and "segregational". The structure of the boundary is discussed in the light of the new experimental evidence, which favours a "transitional lattice" rather than an "amorphous layer" theory.

The paedogenetic male cycle in *Salmo salar* L. By J. W. JONES and J. H. ORTON. (*Communicated by C. T. Regan, F.R.S.—Received* 11 *December* 1939.)

In a further study of the male sex phases throughout the year in salmon parr—accompanied by histological investigation of the gonad—the earlier observations have been confirmed. Some 2790 parr and smolts, captured mainly by rod and line from English and Welsh rivers, have been examined; 50 % of these were male. All the females are immature virgins; the males exhibit a seasonal sexual cycle in which the gonad develops in the summer, becomes mature in the autumn and is spent in winter. After spawning, a high proportion of the male parr migrate to sea as smolts. All the male smolts examined, i.e. 490, had quiescent testes, being either spent or immature and virgin. It is hereby established that two types of male smolts migrate to sea. The gradual disappearance of ripe male parr during the spawning season (beginning about November) and the correlated appearance and increase of males with spent gonads renders it virtually certain that the ripe male parr spawn on the salmon redds.

The temperature ranges in the rivers during the development of the male gonad is noted.

The finding of only 60 % spent amongst the migrating smolt males as against 75 % ripe spending and spent male parr in the preceding spawning period, November and December, may be an indication of a slight mortality among the spawning males.

The sex records given herein, along with those of ripe parr in the literature, leave no doubt that paedogenesis in the male of the Atlantic salmon occurs throughout its geographical range.

The remarkable paucity of males amongst the younger classes of immigrating salmon noted by Hutton on the Wye may be general and be compensated biologically by the abundant paedogenetic males.

Histological changes in the testis in the sexual cycle of male salmon parr.

By J. W. Jones. *(Communicated by C. T. Regan, F.R.S.—Received* 11 *December* 1939.)

Over 2500 salmon parr and smolts have been examined for condition of the gonad. The male gonads were classified according to the nomenclature of the International Council. All female gonads were immature, and the development of the male gonad was found to be seasonal. Spermatogenetic development begins from late May to July, and ripe sperm was first noticed in late September. The greatest percentage of ripe testes was taken in late October and November (the adult spawning time), during which period ripe sperm was extruded on the application of slight pressure to the abdomen. From November–December to June–July spent testes in various stages were found.

The ripening and spending of the testes may be followed macroscopically. The youngest testes sampled are paired thread-like bodies extending the length of the body cavity. As development proceeds the testes widen anteriorly; such widening extends backwards with increase in size. The ripe testes occupy almost all available space in the body cavity. The rosy pink colour of the thread-like immature testes changes to the greasy white of the almost ripe condition (stages IV and V), and eventually the milky white of a ripe testis.

As spawning proceeds a general collapse of the testes takes place, accompanied by a correlated series of colour changes. When almost all the sperm had been extruded the testes were similar in size to the II and II + developmental stages, but were of a peachy pink colour with white spots of relict sperm, and often with much relict sperm in the wide collapsed ducts. In the last stage in spending which could be ascertained macroscopically the testis was of a fawny colour with faint longitudinal striae, and had a rather wide duct.

Spermatogenic changes in the tube-like stage I were confined to an inward migration of the germ cells and their transformation into germ mother cells. These cells are large with lightly staining nuclei and cytoplasm and one or two plasmosomes; in the I+ stage they are more numerous and begin producing occasional spermatogonia. Further increase in size of the gonads is correlated with an increase in the number of the later spermatogenic products. Sperm appears in the larger II+ stages and is fairly abundant in the stage III gonads. Sperm increased in number at the expense of the earlier germ cells. In the almost ripe stage V testis and the ripe stage VI the testicular crypts are full of sperm with a few spermatids: secondary spermatocytes occur in the very tenuous crypt walls.

With the collapse of the testes due to extrusion of the sperm the outer testicular tunica becomes thicker and folded, the crypt walls become more pronounced, and the crypt cavity decreases in size. Germ mother cells reappear in the emptied testes; it is thus possible that the testes may develop more than once in the river.

No actively developing testes were found in the migrating fish.

The dehydration of crystals of chrome alum.

By J. A. COOPER and W. E. GARNER, F.R.S. (*Received* 27 *December* 1939.)

Measurements have been made of the rate of growth of dehydration nuclei over the 111 surfaces of crystals of chrome alum for a range of temperatures. These rates have been compared with the rates of penetration into the crystal. The self-cooling of the crystals has been measured and the heat of dissociation calculated both from the self-cooling and the temperature coefficient of the dissociation pressure. The heat of dissociation, 10 kcal., is much less than the calculated activation energy for the dehydration, viz. 31 kcal. An explanation is advanced for the abnormally high activation energy.

It is shown that small pressures of water vapour cause an acceleration of the rate of dehydration.

Investigations of infra-red spectra. Determination of C—H frequencies (~3000 cm.$^{-1}$) in paraffins and olefins, with some observations on "polythenes".

By J. J. FOX and A. E. MARTIN. (*Communicated by Sir Robert Robertson, F.R.S.—Received* 3 *January* 1940.)

The infra-red absorption spectra of some twenty hydrocarbons in carbon tetrachloride solution have been studied in the region 2·6–3·8 μ with the following results:

$=CH_2$ groups in ethylene and higher olefins give rise to two CH frequencies with mean values 3079 and 2978 cm.$^{-1}$, corresponding, respectively, to unsymmetrical and symmetrical valency vibrations of the CH_2 group.

$\gg\mathrm{CH}$ groups in olefins have usually a single CH valency frequency close to 3019 cm.$^{-1}$, i.e. almost half-way between the two bands of the $=\mathrm{CH_2}$ group. The $>\!\!\!-\mathrm{CH}$ frequency in saturated compounds is 2890 cm.$^{-1}$.

$>\mathrm{CH_2}$ groups have normally two CH valency vibrations with mean values 2926 and 2853 cm.$^{-1}$, corresponding, respectively, to the unsymmetrical and symmetrical vibrations within the CH_2 group. In long-chain paraffins the position of these bands and their intensity per CH_2 group remain remarkably constant from one compound to another. As found previously, bands additional to these two may occur in some cases.

CH_3 groups also have two main CH valency frequencies, corresponding to unsymmetrical and symmetrical vibrations within the CH_3 group. These frequencies are close to 2962 and 2872 cm.$^{-1}$, respectively, when the methyl group is attached to another carbon atom, but in methyl bromide the frequencies are 3049 and 2958 cm.$^{-1}$, i.e. 87 and 86 cm.$^{-1}$ higher. The CH force constant in methyl bromide is almost exactly the same as in methane, and this indicates that the CH internuclear distance does not differ from that in methane by as much as 0·001 A. The CH force constant in a CH_3 group attached to a carbon atom is nearly 6 % lower than in methane and methyl bromide. In saturated hydrocarbons the position of the methyl bands and their intensity per CH_3 group remain fairly constant, but when a methyl group is adjacent to a double bond, as in propylene, the positions and intensities of the bands vary greatly from one compound to another for comparatively small changes in the molecule. The band near 2872 cm.$^{-1}$ is split in these compounds, the mean position of the two components being close to 2872 cm.$^{-1}$. The total area of all the bands attributable to CH_3 groups in the unsaturated molecules, although somewhat lower than in saturated compounds, is still, however, approximately proportional to the number of CH_3 groups present.

Identification of the *cis* and *trans* forms of 2-butylene is readily carried out by examination of the infra-red spectra. A striking resemblance exists between the spectrum of the *trans* form and that of propylene.

Two samples of a polythene (condensed ethylene resinoid) have been examined and have spectra similar to those of long-chain normal paraffins. A band at 2960 cm.$^{-1}$ characteristic of the methyl group is found in all cases and the proportion varies from 1 CH_3 : 8 CH_2 for the most soluble part of the polythenes to 1 CH_3 : $>$ 0 CH_2 for the whole sample. The significance of these results in relation to X-ray examination is briefly discussed.

CH force constants are given for eleven varieties of CH bond, and mean integrated absorption areas are given for $\gg\mathrm{CH}$, $>\!\!\!-\mathrm{CH}$, $=\mathrm{CH_2}$, $>\mathrm{CH_2}$ and CH_3 groups.

I. A. R. I. 75.

INDIAN AGRICULTURAL RESEARCH
INSTITUTE LIBRARY
NEW DELHI.

Date of issue.	Date of issue.	Date of issue

S. C. P.—1/8/47 P. J.-3-5-48-2000